frontiers | Research Topics

The role of toll-like receptors and their related signaling pathways in viral infection and inflammation

Edited by
Ralf Kircheis and Oliver Planz

Published in
Frontiers in Immunology

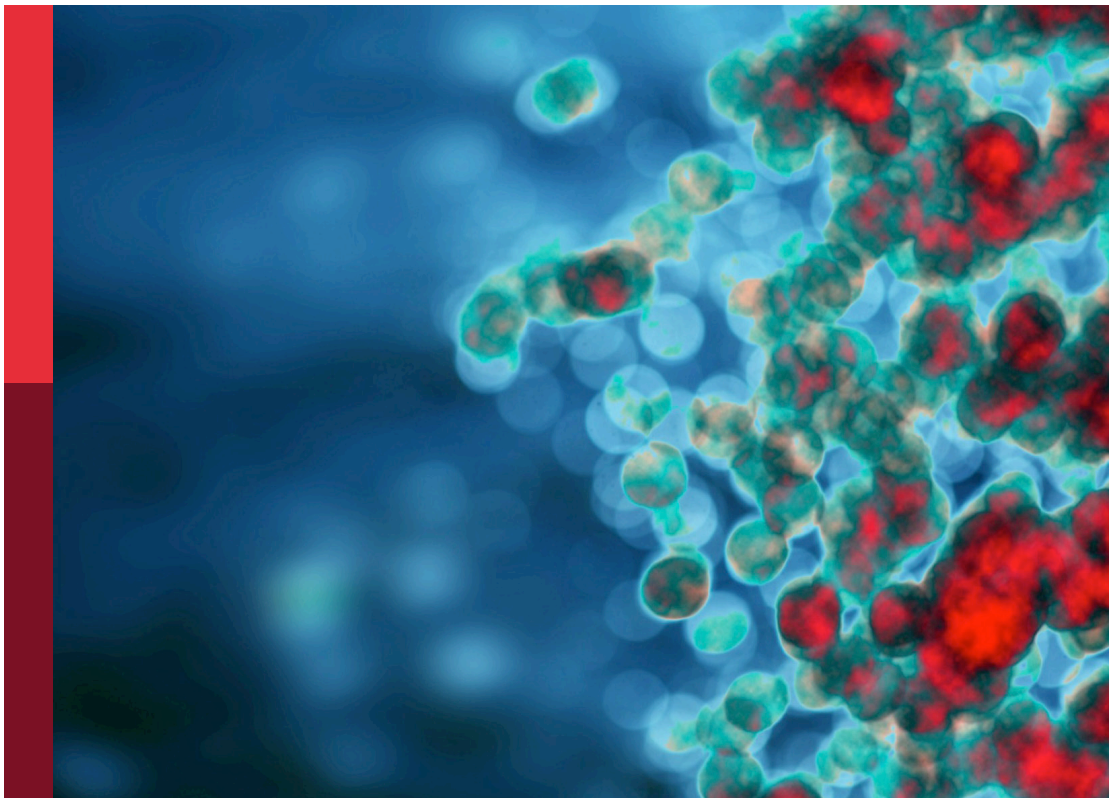

ISSN 1664-8714
ISBN 978-2-8325-4402-0
DOI 10.3389/978-2-8325-4402-0

About Frontiers

Frontiers is more than just an open access publisher of scholarly articles: it is a pioneering approach to the world of academia, radically improving the way scholarly research is managed. The grand vision of Frontiers is a world where all people have an equal opportunity to seek, share and generate knowledge. Frontiers provides immediate and permanent online open access to all its publications, but this alone is not enough to realize our grand goals.

Frontiers journal series

The Frontiers journal series is a multi-tier and interdisciplinary set of open-access, online journals, promising a paradigm shift from the current review, selection and dissemination processes in academic publishing. All Frontiers journals are driven by researchers for researchers; therefore, they constitute a service to the scholarly community. At the same time, the *Frontiers journal series* operates on a revolutionary invention, the tiered publishing system, initially addressing specific communities of scholars, and gradually climbing up to broader public understanding, thus serving the interests of the lay society, too.

Dedication to quality

Each Frontiers article is a landmark of the highest quality, thanks to genuinely collaborative interactions between authors and review editors, who include some of the world's best academicians. Research must be certified by peers before entering a stream of knowledge that may eventually reach the public - and shape society; therefore, Frontiers only applies the most rigorous and unbiased reviews. Frontiers revolutionizes research publishing by freely delivering the most outstanding research, evaluated with no bias from both the academic and social point of view. By applying the most advanced information technologies, Frontiers is catapulting scholarly publishing into a new generation.

What are Frontiers Research Topics?

Frontiers Research Topics are very popular trademarks of the *Frontiers journals series*: they are collections of at least ten articles, all centered on a particular subject. With their unique mix of varied contributions from Original Research to Review Articles, Frontiers Research Topics unify the most influential researchers, the latest key findings and historical advances in a hot research area.

Find out more on how to host your own Frontiers Research Topic or contribute to one as an author by contacting the Frontiers editorial office: frontiersin.org/about/contact

The role of toll-like receptors and their related signaling pathways in viral infection and inflammation

Topic editors

Ralf Kircheis — Syntacoll GmbH, Germany

Oliver Planz — University Hospital and Faculty of Medicine, University of Tübingen, Germany

Citation

Kircheis, R., Planz, O., eds. (2024). *The role of toll-like receptors and their related signaling pathways in viral infection and inflammation*. Lausanne: Frontiers Media SA. doi: 10.3389/978-2-8325-4402-0

Table of contents

05 Editorial: The role of toll-like receptors and their related signaling pathways in viral infection and inflammation
Oliver Planz and Ralf Kircheis

08 Innovation in Nucleotide-Binding Oligomerization-Like Receptor and Toll-Like Receptor Sensing Drives the Major Histocompatibility Complex-II Free Atlantic Cod Immune System
Xingkun Jin, Bernat Morro, Ole K. Tørresen, Visila Moiche, Monica H. Solbakken, Kjetill S. Jakobsen, Sissel Jentoft and Simon MacKenzie

22 Identification of the Association Between Toll-Like Receptors and T-Cell Activation in Takayasu's Arteritis
Yixiao Tian, Biqing Huang, Jing Li, Xinping Tian and Xiaofeng Zeng

49 Toll-Like Receptor-Induced Immune Responses During Early Childhood and Their Associations With Clinical Outcomes Following Acute Illness Among Infants in Sub-Saharan Africa
Luke S. Uebelhoer, Agnes Gwela, Bonnie Thiel, Sophie Nalukwago, John Mukisa, Christopher Lwanga, Justine Getonto, Emily Nyatichi, Grace Dena, Alexander Makazi, Shalton Mwaringa, Ezekiel Mupere, James A. Berkley and Christina L. Lancioni on behalf of the Childhood Acute Illness & Nutrition (CHAIN) Network

61 Estrogen May Enhance Toll-Like Receptor 4-Induced Inflammatory Pathways in People With HIV: Implications for Transgender Women on Hormone Therapy
Aaren Kettelhut, Emily Bowman, Janelle Gabriel, Brittany Hand, Namal P. M. Liyanage, Manjusha Kulkarni, Frances Avila-Soto, Jordan E. Lake and Nicholas T. Funderburg

74 Case Report: mRNA vaccination-mediated STAT3 overactivation with agranulocytosis and clonal T-LGL expansion
Julia R. Hirsiger, Alexandar Tzankov, Ilaria Alborelli, Mike Recher, Thomas Daikeler, Stefani Parmentier and Christoph T. Berger

81 Critical role of TLR activation in viral replication, persistence, and pathogenicity of Theiler's virus
Byung S. Kim

90 Sperm activate TLR2/TLR1 heterodimerization to induce a weak proinflammatory response in the bovine uterus
Alireza Mansouri, Mohamed Samy Yousef, Rasoul Kowsar, Nonoka Usui, Ihshan Akthar and Akio Miyamoto

102 Imidazoquinolines with improved pharmacokinetic properties induce a high IFNα to TNFα ratio *in vitro* and *in vivo*
Manuel Keppler, Simon Straß, Sophia Geiger, Tina Fischer, Nadja Späth, Thilo Weinstein, Anna Schwamborn, Jamil Guezguez, Jan-Hinrich Guse, Stefan Laufer and Michael Burnet

116 Oral prednisolone suppresses skin inflammation in a healthy volunteer imiquimod challenge model
Salma Assil, Thomas P. Buters, Pieter W. Hameeteman, Charlie Hallard, Nicoline Treijtel, Tessa Niemeyer – Van der Kolk, Marieke L. de Kam, Edwin F. I. I. I. Florencia, Errol P. Prens, Martijn B. A. van Doorn, Robert Rissmann, Naomi B. Klarenbeek, Manon A. A. Jansen and Matthijs Moerland

127 MyD88-dependent Toll-like receptor 2 signaling modulates macrophage activation on lysate-adsorbed Teflon™ AF surfaces in an *in vitro* biomaterial host response model
Laura A. McKiel, Laurel L. Ballantyne, Gian Luca Negri, Kimberly A. Woodhouse and Lindsay E. Fitzpatrick

144 TLR7 promotes chronic airway disease in RSV-infected mice
Mark A. Miles, Stella Liong, Felicia Liong, Madison Coward-Smith, Gemma S. Trollope, Osezua Oseghale, Jonathan R. Erlich, Robert D. Brooks, Jessica M. Logan, Shane Hickey, Hao Wang, Steven Bozinovski, John J. O'Leary, Doug A. Brooks and Stavros Selemidis

165 Application of toll-like receptors (TLRs) and their agonists in cancer vaccines and immunotherapy
Samik Chakraborty, Juan Ye, Herui Wang, Mitchell Sun, Yaping Zhang, Xueyu Sang and Zhengping Zhuang

184 Dexamethasone impairs the expression of antimicrobial mediators in lipopolysaccharide-activated primary macrophages by inhibiting both expression and function of interferon β
John D. O'Neil, Oliwia O. Bolimowska, Sally A. Clayton, Tina Tang, Kalbinder K. Daley, Samuel Lara-Reyna, Jordan Warner, Claire S. Martin, Rahul Y. Mahida, Rowan S. Hardy, J. Simon C. Arthur and Andrew R. Clark

frontiers | Frontiers in Immunology

TYPE Editorial
PUBLISHED 19 January 2024
DOI 10.3389/fimmu.2024.1363958

OPEN ACCESS

EDITED AND REVIEWED BY
Francesca Granucci,
University of Milano-Bicocca, Italy

*CORRESPONDENCE
Oliver Planz
oliver.planz@uni-tuebingen.de
Ralf Kircheis
rkircheis@syntacoll.de

RECEIVED 31 December 2023
ACCEPTED 08 January 2024
PUBLISHED 19 January 2024

CITATION
Planz O and Kircheis R (2024) Editorial: The role of toll-like receptors and their related signaling pathways in viral infection and inflammation.
Front. Immunol. 15:1363958.
doi: 10.3389/fimmu.2024.1363958

Editorial: The role of toll-like receptors and their related signaling pathways in viral infection and inflammation

Oliver Planz[1]* and Ralf Kircheis[2]*

[1]Institute for Immunology, Eberhard Karls University Tuebingen, Tuebingen, Germany, [2]Department of R&D, Syntacoll GmbH, Saal an der Donau, Germany

KEYWORDS

TLR - toll-like receptor, viral infection, innate immunity, inflammation, signaling pathway

Editorial on the Research Topic
The role of toll-like receptors and their related signaling pathways in viral infection and inflammation

The Research Topic addresses the role of Toll-like receptors (TLRs) and their associated signaling pathways in viral infections and inflammation. The focus is on how these receptors and pathways contribute to protecting the body against viruses and their involvement in associated inflammatory processes. The present Research Topic encompasses 13 studies shedding light on the role of TLRs in viral infections and inflammation from various perspectives.

The impact of TLRs on viral infections has been elucidated in three studies, effectively illustrating the dual nature of TLR activation in viral infection – both necessary for immune protection and contributing to virus-triggered immunopathology (1–3). Miles et al. demonstrated that TLR7 supports chronic respiratory disease after RSV infection in mice. This study unveils a previously unknown molecular mechanism of lower respiratory tract pathogenesis by RSV, emphasizing the potential of TLR7 modulation to confine RSV pathology to the upper respiratory tract. This restriction prevents its spread to the lower respiratory tract and results in a significant reduction in clinical symptoms.

Theiler's Virus, known for its ability to infect the central nervous system of mice and trigger an inflammatory reaction, is commonly utilized as a model in research to investigate the mechanisms of virus infections and the course of inflammatory reactions in the brain (4–6). In this study, Kim reviewed the role of TLRs in the mouse model of Theiler's Virus infection, concluding that the state of TLR activation in the host plays a crucial role in the initial virus replication and persistence.

The use of estrogens in feminizing hormone therapy (FHT) can elevate inflammatory reactions and the risk of cardiovascular mortality in transgender women (TW), who are at an increased risk for both human immunodeficiency virus (HIV) and cardiovascular diseases (CVD) (7–9). Kettelhut et al. demonstrate that *in vitro* data suggest estrogen exposure can enhance the activation of the innate immune system in FHT. The authors discuss the complex interactions of FHT, HIV, and CVD in TW, emphasizing the need for further research to fully understand these

interactions and determine optimal FHT regimens or complementary treatments aiming to reduce excessive immune activation.

Lipopolysaccharide (LPS), a TLR4 agonist, is used as a stimulus in many *in vitro* and *in vivo* models (10, 11). O'Neill et al. investigated the impact of dexamethasone on the expression of antimicrobial mediators in LPS-activated primary macrophages, demonstrating the inhibition of both the expression and function of interferon-β. Interferon-β plays a crucial role in the early antiviral immune response.

In a study with healthy volunteers using an imiquimod (IMQ) model, Assil et al. showed that orally administered prednisolone suppresses skin inflammation induced by IMQ, a topical agent that triggers local inflammation through TLR7.

Resiquimod, an imidazoquinoline compound with antiviral and antitumor activity, functions as a TLR7/TLR8 agonist (12, 13). In their work, Keppler et al. point out that clinical use is limited to topical application. Systemic applications of TLR ligands like Resiquimod have failed due to side effects restricting dose and efficacy. Therefore, the authors developed TLR7/8-agonistic imidazoquinolines designed to distribute via endosomes using a macrolide carrier. The substances were designed to distribute to cellular compartments where the target receptor and a specific combination of signaling molecules relevant for IFNα release are present.

The immune reaction to biomaterial implants, known as the foreign body reaction, poses a significant challenge in biomedical engineering, as it can lead to chronic inflammatory reactions to the implanted material (14). McKiel et al. demonstrate that damage-associated molecular patterns (DAMPs) and other intracellular proteins easily adsorb to biomaterial surfaces in competition with plasma proteins. Adsorbed DAMPs in adherent macrophages trigger an inflammatory reaction mediated by the MyD88-dependent TLR2 signaling pathway.

The TLR-2 signaling pathway is also involved in the inflammatory reaction triggered by sperm in the uterus during fertilization, but the precise molecular mechanism remains unknown. According to ligand specificity, TLR2 forms a heterodimerization with TLR1 or TLR6, respectively, as the initial step to mediate intracellular signaling and induce a specific type of immune response. Mansouri et al. aimed to identify the active TLR2 heterodimer (TLR2/1 or TLR2/6) involved in the immunological interaction between sperm and the uterus in cattle. Overall, the results show that sperm utilize the heterodimerization of TLR2/1, but not TLR2/6, to trigger a weak physiological inflammatory reaction in the bovine uterus. This could be the mechanism to remove excess dead sperm remaining in the uterus without tissue damage and create an ideal uterine environment for the uptake and implantation of the early embryo.

In the present Research Topic, there are three publications with a direct clinical relevance. In a case report by Hirsiger et al., the occurrence of agranulocytosis within a few days after the first dose of an mRNA-1273 vaccine against COVID-19 in a previously healthy older adult is described. The patient was diagnosed with large granular lymphocytic T-cell leukemia (T-LGL) of STAT3 wild type. The mRNA-1273 vaccine activated TLR-3, leading to TLR-mediated IL-6/STAT3 pathway activation. The authors changed the vaccination strategy and used a vector vaccine, and neutropenia did not recur. Tian et al. investigated the association between TLRs and the activation and differentiation of T-cells in Takayasu arteritis (TAK). They analyzed the mRNA frequency of 29 target genes in peripheral blood mononuclear cells (PBMCs) from 27 TAK patients and 10 healthy controls. They found increased mRNA levels of TLR2 and TLR4 in TAK patients. Furthermore, this study revealed a novel connection between TLRs and T-cells in the pathogenesis of autoimmune diseases. Another study by Uebelhoer et al. examines how malnutrition and acute illnesses affect immune responses in young children in low- and middle-income countries and which aspects of immunity are relevant in this particularly vulnerable population. Overall, the results show exaggerated innate immune responses to pathogen-associated molecules, especially TLR-4 and TLR-7/8, in acutely ill young children, persisting during recovery. Exaggerated innate immune responses to TLR ligands can contribute to chronic systemic inflammation and dysregulated responses to subsequent infection challenges.

Their ability to stimulate immunity makes TLR attractive targets for expanding numerous immunotherapeutic approaches to combat cancer (15). These immunotherapeutic strategies include the use of TLR ligands/agonists as monotherapy or in combined therapeutic approaches (16). In a review, Chakraborty et al. attempt to provide a comprehensive discussion of significant TLR agonists and their application, as well as the challenges in integrating them into cancer immunotherapy approaches, with a particular emphasis on the use of TLR agonists as functional adjuvants for cancer vaccines. They present the translational potential of an autologous cancer vaccine, as well as the immune-inducing potential of TLR agonists as a potential immunotherapy in various types of cancer.

In another study, Jin et al. show that the unique immune system of the Atlantic cod offers an unprecedented opportunity to explore the evolutionary history of pattern recognition receptor (PRR)-based signaling in the immune defense of vertebrates. The absence of major histocompatibility complex class II antigen presentation and several pathogen recognition receptors in the Atlantic cod has not impaired the immune response.

Overall, this Research Topic effectively illustrates the dual role of Toll-like receptors (TLRs) and their associated signaling pathways in viral infections, as well as in a broad variety of inflammatory processes. It highlights the two facets of TLR activation: one contributing to immune protection and the other to immunopathology.

Author contributions

OP: Writing – original draft, Writing – review & editing. RK: Writing – original draft, Writing – review & editing.

Conflict of interest

Author RK was employed by the company Syntacoll GmbH.

The remaining author declares that the research was conducted in the absence of any commercial or financial relationships that could be construed as a potential conflict of interest.

Publisher's note

References

1. Thompson JM, Iwasaki A. Toll-like receptors regulation of viral infection and disease. *Adv Drug Delivery Rev* (2008) 60:786–94. doi: 10.1016/j.addr.2007.11.003

2. Rouse BT, Sehrawat S. Immunity and immunopathology to viruses: what decides the outcome? *Nat Rev Immunol* (2010) 10:514–26. doi: 10.1038/nri2802

3. Duan T, Du Y, Xing C, Wang HY, Wang RF. Toll-like receptor signaling and its role in cell-mediated immunity. *Front Immunol* (2022) 13:812774. doi: 10.3389/fimmu.2022.812774

4. DePaula-Silva AB, Hanak TJ, Libbey JE, Fujinami RS. Theiler's murine encephalomyelitis virus infection of SJL/J and C57BL/6J mice: Models for multiple sclerosis and epilepsy. *J Neuroimmunol* (2017) 308:30–42. doi: 10.1016/j.jneuroim.2017.02.012

5. So EY, Kim BS. Theiler's virus infection induces TLR3-dependent upregulation of TLR2 critical for proinflammatory cytokine production. *Glia* (2009) 57:1216–26. doi: 10.1002/glia.20843

6. Gern OL, Mulenge F, Pavlou A, Ghita L, Steffen I, Stangel M, et al. Toll-like receptors in viral encephalitis. *Viruses 13* (2021) 13:2065–98. doi: 10.3390/v13102065

7. Nguyen HB, Chavez AM, Lipner E, Hantsoo L, Kornfield SL, Davies RD, et al. Gender-affirming hormone use in transgender individuals: impact on behavioral health and cognition. *Curr Psychiatry Rep* (2018) 20:110. doi: 10.1007/s11920-018-0973-0

8. Baral SD, Poteat T, Stromdahl S, Wirtz AL, Guadamuz TE, Beyrer C. Worldwide burden of HIV in transgender women: a systematic review and meta-analysis. *Lancet Infect Dis* (2013) 13:214–22. doi: 10.1016/S1473-3099(12)70315-8

9. Streed CG Jr., Beach LB, Caceres BA, Dowshen NL, Moreau KL, Mukherjee M, et al. Assessing and addressing cardiovascular health in people who are transgender and gender diverse: A scientific statement from the american heart association. *Circulation* (2021) 144:e136–48. doi: 10.1161/CIR.0000000000001003

10. Chow JC, Young DW, Golenbock DT, Christ WJ, Gusovsky F. Toll-like receptor-4 mediates lipopolysaccharide-induced signal transduction. *J Biol Chem* (1999) 274:10689–92. doi: 10.1074/jbc.274.16.10689

11. Ciesielska A, Matyjek M, Kwiatkowska K. TLR4 and CD14 trafficking and its influence on LPS-induced pro-inflammatory signaling. *Cell Mol Life Sci* (2021) 78:1233–61. doi: 10.1007/s00018-020-03656-y

12. Ma F, Zhang J, Zhang J, Zhang C. The TLR7 agonists imiquimod and gardiquimod improve DC-based immunotherapy for melanoma in mice. *Cell Mol Immunol* (2010) 7:381–8. doi: 10.1038/cmi.2010.30

13. Miller RL, Meng TC, Tomai MA. The antiviral activity of Toll-like receptor 7 and 7/8 agonists. *Drug News Perspect* (2008) 21:69–87. doi: 10.1358/dnp.2008.21.2.1188193

14. Anderson JM, Rodriguez A, Chang DT. Foreign body reaction to biomaterials. *Semin Immunol* (2008) 20:86–100. doi: 10.1016/j.smim.2007.11.004

15. Urban-Wojciuk Z, Khan MM, Oyler BL, Fahraeus R, Marek-Trzonkowska N, Nita-Lazar A, et al. The role of TLRs in anti-cancer immunity and tumor rejection. *Front Immunol* (2019) 10:2388. doi: 10.3389/fimmu.2019.02388

16. Pahlavanneshan S, Sayadmanesh A, Ebrahimiyan H, Basiri M. Toll-like receptor-based strategies for cancer immunotherapy. *J Immunol Res* (2021) 2021:9912188. doi: 10.1155/2021/9912188

frontiers in Immunology

ORIGINAL RESEARCH
published: 11 December 2020
doi: 10.3389/fimmu.2020.609456

Innovation in Nucleotide-Binding Oligomerization-Like Receptor and Toll-Like Receptor Sensing Drives the Major Histocompatibility Complex-II Free Atlantic Cod Immune System

Xingkun Jin[1,2,3], Bernat Morro[2], Ole K. Tørresen[1], Visila Moiche[2], Monica H. Solbakken[1], Kjetill S. Jakobsen[1], Sissel Jentoft[1] and Simon MacKenzie[2]**

[1] Centre for Ecological and Evolutionary Synthesis (CEES), Department of Biosciences, University of Oslo, Oslo, Norway, [2] Institute of Aquaculture, University of Stirling, Stirling, United Kingdom, [3] College of Oceanography, Hohai University, Nanjing, China

OPEN ACCESS

Edited by:
Jun-ichi Hikima,
University of Miyazaki, Japan

Reviewed by:
Jorge Galindo-Villegas,
Nord University, Norway
Sarah J. Poynter,
University of Waterloo, Canada

***Correspondence:**
Sissel Jentoft
sissel.jentoft@ibv.uio.no
Simon MacKenzie
simon.mackenzie@stir.ac.uk

Specialty section:
This article was submitted to Comparative Immunology, a section of the journal Frontiers in Immunology

Received: 23 September 2020
Accepted: 09 November 2020
Published: 11 December 2020

Citation:
Jin X, Morro B, Tørresen OK, Moiche V, Solbakken MH, Jakobsen KS, Jentoft S and MacKenzie S (2020) Innovation in Nucleotide-Binding Oligomerization-Like Receptor and Toll-Like Receptor Sensing Drives the Major Histocompatibility Complex-II Free Atlantic Cod Immune System. Front. Immunol. 11:609456. doi: 10.3389/fimmu.2020.609456

The absence of MHC class II antigen presentation and multiple pathogen recognition receptors in the Atlantic cod has not impaired its immune response however how underlying mechanisms have adapted remains largely unknown. In this study, *ex vivo* cod macrophages were challenged with various bacterial and viral microbe-associated molecular patterns (MAMP) to identify major response pathways. Cytosolic MAMP-PRR pathways based upon the NOD-like receptors (NLRs) and RIG-I-like receptors (RLRs) were identified as the critical response pathways. Our analyses suggest that internalization of exogenous ligands through scavenger receptors drives both pathways activating transcription factors like NF-kB (Nuclear factor-kappa B) and interferon regulatory factors (IRFs). Further, ligand-dependent differential expression of a unique TLR25 isoform and multiple NLR paralogues suggests (sub)neofunctionalization toward specific immune defensive strategies. Our results further demonstrate that the unique immune system of the Atlantic cod provides an unprecedented opportunity to explore the evolutionary history of PRR-based signaling in vertebrate immunity.

Keywords: cod, immune response, nucleotide-binding oligomerization-like receptor (NLR), macrophage, Toll-like receptor (TLR)

INTRODUCTION

In vertebrates, the genetic basis of immunity is considered highly conserved (1). With the increased use of high-throughput sequencing technologies, genomic resources from non-model species has become readily available and large efforts in comparative immunology has ensued (2–4). These studies have revealed several common denominators of vertebrate immunity, but also demonstrated considerable gene losses and expansions challenging our understanding of immune

system organization and functional compartmentalization in vertebrates. The genome sequencing of the Atlantic cod (5), and later a set of ~30 Gadiform genomes (2), demonstrated that this group of teleosts display a very distinct immune gene repertoire affecting both innate and adaptive immunity, with the lack major histocompatibility complex (MHC) class II, invariant chain (CD74) and CD4. All hallmarks of the perceived classical vertebrate adaptive immune system (2, 5). In parallel, teleosts display a wide range of gene expansions/contractions related to major histocompatibility complex class I as well as innate immune gene families such as pattern recognition receptors (PRRs) (6–8). PRRs are a strongly conserved feature of the immune system indispensable from insects to mammals and in plants (R protein) (1, 9). Classically, these receptors are associated with detecting microbe-associated or danger-associated molecular patterns (MAMPS and DAMPS) with subsequent initiation of inflammation. However, they have also been implicated in regulation of development, antigen presentation and autophagy (10, 11).

Genomic investigations have provided detailed characterizations of all known PRR families including Toll-like receptors (TLRs), C-type lectin receptors (CLRs), retinoic acid-inducible (RIG)-I-like receptors (RLRs), and nucleotide-binding oligomerization (NOD)-like receptors (NLRs) in an array of vertebrates (9). The PRR repertoire in teleost fish has proven to be very diverse compared to other vertebrate groups, and more so within the Gadiformes (12, 13). All homologs of mammalian surface-located TLRs have been lost, whereas there are large expansions of teleost-specific TLRs with unknown cellular location and ligand type. Furthermore, loss of RIG-I and NOD2 has been reported in parallel to the overall NLR repertoire being greatly expanded (5, 7, 12–14). These significant gene losses and expansions result in a peculiar genetic basis for innate immunity that suggests the existence of an alternative MAMP-PRR activation system. The functional implication of the PRR repertoire observed in Gadiformes is poorly understood. Furthermore, there is a lack of functional investigations targeting PRR interaction and signaling. So far, complete insight into these gene losses and expansions, and the expression pattern of the various paralogs, have been hampered by a fragmented genome assembly and the use of short-read technology in, e.g., RNA-Seq analyses.

Certain PRR-encoding gene family groups such as the NLRs appear to contain species-specific expansions that present multiple modified forms (neo/sub-functionalization) and different genomic organizational patterns (tandem/dispersed). Atlantic cod and other gadiform species contain a high number of tandem-repeated gene families that cause assembly collapse, as a consequence PRR genes are often fragmented or collapsed (7, 12, 15). Additionally, some of the Gadiformes PRRs demonstrate significant gene expansions and neofunctionalization (3, 16). In the Atlantic cod genome, genes from both the TLR and NLR families were found to be highly expanded, accompanied by a loss of several other crucial PRRs including certain cell membrane-bound TLRs (TLR1, TLR2, TLR4, and TLR5), RIG-I, and NOD2 (5, 7, 12–14). This significant gene loss suggests that the intracellular mechanisms in mediating MAMP-PRR activation are likely of extra necessity and importance (5, 13). However, the underlying mechanisms of this process are not fully understood. In this sense, short-read deep sequencing like Illumina RNA-Seq have produced extensive atlases of transcriptomes. In addition, long-read sequencing such as PacBio (yielding reads with average > 15 kb, up to 100 kb or even longer), have proven able to generate high contiguous long reads spanning repeats, and is progressively used in genome assembly and full-length transcriptomics (7, 14, 17, 18). Therefore, integrating both the short- and long-read sequencing approaches would ensure a more precise point-to-point interpretation of the response to immune challenges, especially in organisms with highly complex expanded gene families like Atlantic cod.

Here, we have used Atlantic cod macrophages to further elucidate the functional outcome of the Gadiformes PRR repertoire. Macrophages play a pivotal role in host defense, both phagocytizing non-self-agents and orchestrating subsequent innate and adaptive immune responses (19–21). As a consequence, tissue macrophages perform a critical immune surveillance role with their befitting diversity of PRRs (21). *Ex-vivo* Atlantic cod macrophage cultures were established and challenged with a set of MAMPs mimicking bacterial and viral infections. In addition, a set of well-known pharmacological signaling pathway blockers were used to further unravel cod PRR signaling pathways. Finally, using long-read sequencing technology, a comparison between the predicted transcriptome and the actual macrophage transcriptome was performed. We find that Atlantic cod macrophages efficiently engulf microbes, produce inflammatory mediators and generate a MAMP-specific immune response that agrees with the overall vertebrate models. Sensing of bacterial ultra-pure peptidoglycan uPGN (containing MDP, muramyl dipeptide, and iE-DAP, γ-D-Glu-mDAP), and of the viral mimic dsRNA is mediated by the NLR and RLR pathways respectively. Comparative analyses demonstrate a role for the internalization for exogenous ligand through scavenger receptors for MAMP-PRR interactions. Intracellular pathways identified through inhibition highlights a central role of TBK1 (TANK Binding Kinase 1) in signal coordination for NOD-based signaling. Our findings demonstrate that Atlantic cod appears to rely more on cytosolic MAMP sensing using NLR and RLR-based signaling supported by neo-functionalized PRRs.

MATERIAL AND METHODS

Samples

One-year old Atlantic cod, *Gadus morhua* L., reared in land-based tanks supplied with filtered sea water were obtained from Ardtoe Marine Facility (UK) during 2014-2015. They were kept at environmental temperature and fed on commercial dry pellets once a day. All procedures were in accordance with UK Home Office welfare guidelines. The fish were sacrificed with UK Home Office approved methods, using an overdose of the anesthetic benzocaine (Sigma-Aldrich) followed by brain concussion. The head kidney and spleen of each animal were dissected out and kept at 4°C in high glucose Dulbecco's Modified Eagle Medium (DMEM) (Sigma-Aldrich) and 0.2% Primocin™ (InvivoGen) until cell culture.

Macrophage Cell Culture

The sampled tissues were ground together through a 100 µm cell strainer (Fisher Scientific) in a proportion of 1:3 spleen to head kidney into a tube with fresh DMEM solution with 0.2% Primocin. Cells were precipitated by centrifugation at 1500 rpm for 5 min and resuspended in DMEM (0.2% Primocin and 10% chicken serum (Life Technologies)). The cell culture plates were coated with 0.5 ml of poly-D-lysine (Sigma-Aldrich) (0.1 mg/ml in no calcium, no magnesium Dulbecco's Phosphate-Buffered Saline (DPBS) (Life Technologies)) per well for 30 min, rinsed with 1.5 ml of DPBS per well, and left to be air-dried prior seeding. Twelve-welled plates (Thermo Scientific) were filled with 1 ml per well of the resuspended cells (which contained approximately 2 million cells per ml). The cell cultures were kept in an incubator at 15°C with 4% CO_2 supply. After one day and thereafter every two days (5 days in total), half of the medium per well was replaced with fresh DMEM (0.2% Primocin and 10% chicken serum from the same batch).

Phagocytosis Assay

Alexa fluor 488 labelled bacteria (*E. coli*, Sigma-Aldrich) and yeast (*S. cerevisiae*, Sigma-Aldrich) were used as phagocytosis targets. After 1 h and 3 h of incubation with bacteria and yeast respectively, macrophages from four individuals were analyzed using Guava® easyCyte™ 8HT Flow Cytometer (Merck Millipore) to measure phagocytosis. Flow cytometry assessment of the cell population demonstrated homogeneity (92%) and was gated for further functional assays (gate R1 in **Figures 1A, B**).

Microbe-Associated Molecular Patterns Immune Challenge

One hour prior to stimulation, the cell culture medium was replaced with serum-free DMEM, eliminating the possible interference of serum with the assay. Ten µl of 1mg/ml stock solutions of MAMPs (i.e., Lipopolysaccharide (LPS; LPS-EK; *E.coli*), Peptidoglycan (PGN; PGN-EK; *E.coli*), ultra-pure peptidoglycan (uPGN; PGN-*E.coli* ndss ultrapure), dsRNA (High Molecular Weight, HMW) and CpG [*E. coli* ssDNA/LyoVec)] per ml was used in all cases to challenge the cells for 3h and 12h (**Table S6**). All MAMPs were purchased from Invivogen.

Inhibition of the Immune Response to Ultra-Pure Peptidoglycan

MAPK Kinase Inhibitors PD (MEK1 and MEK2 Inhibitor, Sigma-Aldrich), SB (p38/ERK MAP Kinase Inhibitor, Sigma-Aldrich), and NOD1/2 inhibitor GEF (Gefitinib, Invivogen) were added to the cell cultures along with either solution buffer (control) or uPGN (10 µg/ml). The working concentrations of the inhibitors were, respectively, 2, 0.5, and 10 µM (**Table S6**). The cultures were incubated for 12 h. All possible combinations of inhibitors were tested.

Prostaglandin E_2 Measurement

Supernatants (serum-free DMEM with 0.2% primocin) of control and uPGN-challenged macrophages from 4 different individuals were preserved at −20°C prior testing. Prostaglandin E_2 (PGE_2) was quantified by a monoclonal EIA kit following the manufacturer instructions (Cayman, USA).

RNA Isolation and Quality Control

After the whole supernatant had been removed by pipetting, 250 µl of TriReagent® (Sigma-Aldrich, UK) was added to each well of a 12-welled plate. Total RNA of the macrophages was extracted by the phenol/1-bromo-3-chloropropane method (Sigma-Aldrich, UK) following the manufacturer's instructions, with 1 µl of glycogen (Roche) per 1 ml TriReagent® added to enhance the RNA precipitation during the isopropanol step. The total RNA samples were then subjected to NanoDrop (Thermo Scientific) to determine the RNA concentration, and Bioanalyzer (Agilent Technologies) to estimate the integrity and purity of the RNA samples. Only the samples with RIN values greater than 8 were kept. Qubit® (Life Technology) was used to quantify the concentrations of the samples that were going to be sent for sequencing. All samples were stored at -80°C.

cDNA Synthesis

Different cDNA synthesis protocols were used depending on the purpose of the samples, following the manufacturer's instructions of each kit. The Illumina RNA-seq cDNA library was prepared using 1 µg of RNA from each sample and TruSeq V2 kits (Illumina, CA, USA), with reduced RNA fragmentation time (3 min) to maximize obtention of longer reads. For PacBio IsoSeq, 1 µg of RNA per sample was used for first-strand synthesis by SMARTer PCR cDNA Synthesis Kit (Clontech). For quantitative RT-PCR (qPCR), 1 µg of total RNA per sample was used to synthesize cDNA with SuperScript III RNase Transcriptase (Invitrogen) and Oligo-dT primer (Invitrogen).

Library Preparation and Sequencing

Two rounds of Illumina RNA-seq were performed. For the first one, which consisted of a preliminary MAMP activation screening, RNA samples from macrophage cultures derived from 3 fish were pooled. In total, 9 pooled libraries were prepared: 3 control pooled samples (Ctl), 3 bacterial MAMP-activated pooled samples (Bac) and 3 dsRNA-activated pooled samples (Plc) (**Table S7**). They were loaded onto one lane of an eight-laned FlowCell Chip. The second round looked at the effects of exclusively uPGN on the cod macrophage transcriptome. For these, a total of 18 libraries were prepared, each individual fish had three aliquots of one control sample, one sample challenged with uPGN for 3 h and another one challenged with uPGN for 12 h. These were loaded onto two lanes of an eight-laned FlowCell Chip.

To prepare the libraries for IsoSeq, the Pacific Biosciences IsoSeq library preparation protocol was followed. Before library preparation, the cDNA was first size-selected using BluePippin (Sage Science) and then using AMPure® XP (Auto Q Biosciences) beads. Then they were sequenced on a Pacific Biosciences RS II instrument using P6v2/C4 chemistry (Pacific Biosciences of California Inc., Menlo Park, CA, USA). In total, 2 SMRT cells for 1–2kb, 3 SMRT cells for 2–3kb, and 4 SMRT cells for 3–6kb were used for sequencing.

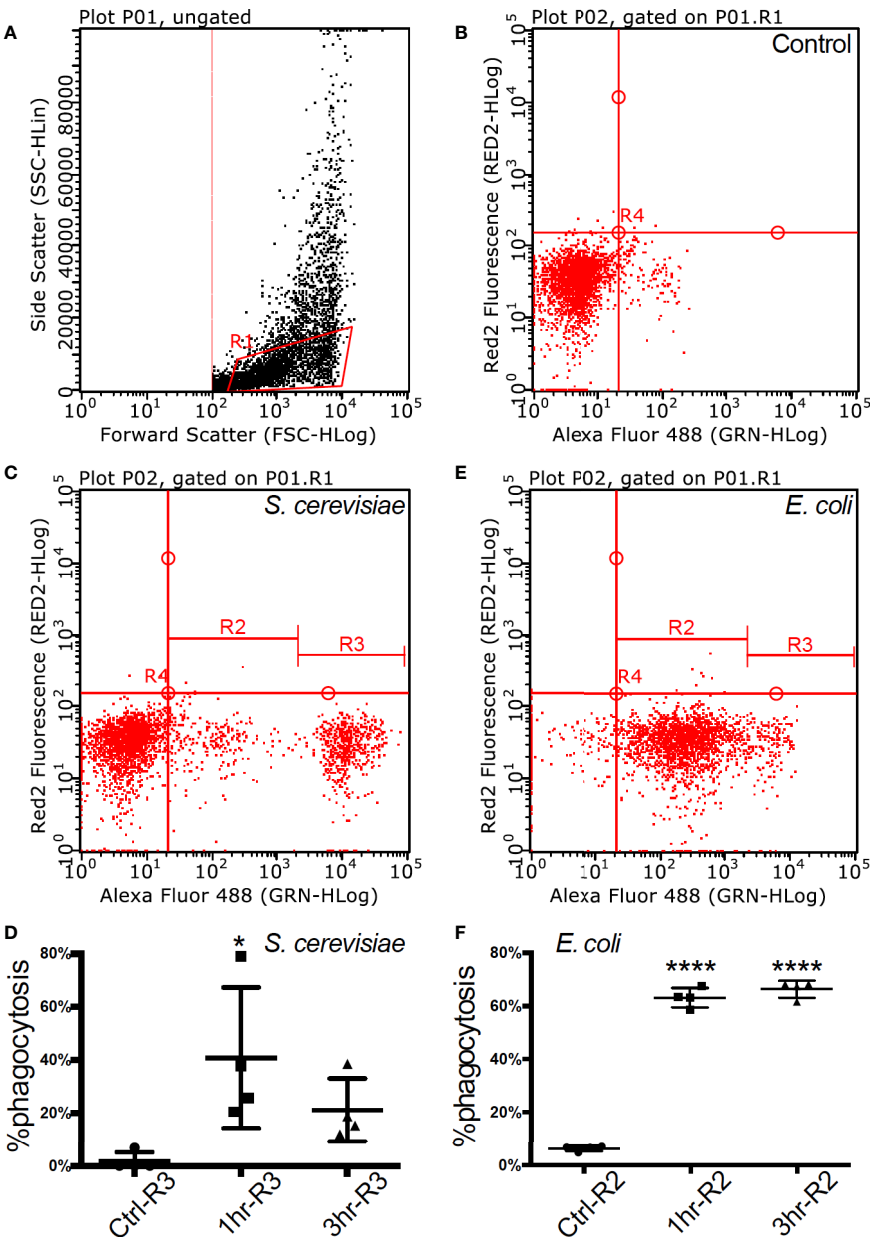

FIGURE 1 | Flow cytometry of fully functional Atlantic cod macrophages during phagocytosis (**A**). Scatter plot of cell complexity (y-axis) and size (x-axis) that shows the presence of two cell subpopulations: one of morphologically similar cells (R1) and another one of heterogeneous cells with regards to both parameters **(B–D)**. The first subpopulation was gated, and it is shown in an untreated resting state **(B)**, during phagocytosis of yeast **(C)**, and during phagocytosis of bacteria **(D)**, **(C, D)**. Macrophage abundance by size during an untreated resting state, after a 1-h and after a 3-h activation of yeast **(C)** and bacteria **(D)**. Asterisks represent statistical significance: * < 0.05, **** < 0.0001.

Absolute Quantitative RT-PCR

All primers for qPCR were designed using BatchPrimer3 v1.0 based on the target genes annotated in the latest cod genome assembly gadMor2 (**Table S8**) (14). Target genes were validated using thermal gradient RT-PCR and the products that met the quality criteria were cloned into bacterial plasmids. Two micrograms of cDNA were used as a template for PCR with gene-specific primers. Target mRNAs were amplified using MyTaq HS DNA Polymerases (Bioline, UK), and amplicons were run on 1% agarose gels, stained with ethidium bromide and purified with NucleoSpin® Gel and PCR Clean-up (Macherey-Nagel, Germany). Purified PCR products were ligated in pGEM-T easy vectors (Promega, USA) and transformed into *Escherichia coli* (DH5a strain). One selected transformant of each construct was grown to obtain plasmid DNA (Miniprep kit, Macherey-Nagel). All constructs were verified by Sanger DNA sequencing with T7 and SP6 primer sets (GATC Biotech, **Table S8**). Pro-inflammatory cytokines mRNAs for *il1b* and *il6* were selected on

account of their high inducibility during PAMP responses (**Figure S7**). See details for PCR program and reaction systems in **supplementary Information**. One-way ANOVA was used to test the statistical differences between indicated experimental contrast. Significance was reported if $P < 0.05$. Graphs were plotted using Prism6® (**Table S5**).

Transcriptome Assembly and Transcript Abundance Estimation

Raw Illumina reads from each sample were trimmed using Cutadapt (v1.4.2) with cutoff as Phred < 20. For the downstream differential gene and transcript expression analysis two pipelines were used (1): reference genome based using the Tuxedo pipeline (Tophat2, cufflinks and cummeRbund) (22): Trimmed reads from macrophage samples (3x Ctl, 3x Bac, 3x Plc) were mapped to the gadMor2 cod genome assembly (14) with the short read aligner Tophat2 (v2.0.9) (see Supporting Information for details). The reads from all samples were assembled by Cufflinks (v2.2.1) and the results were visualized and plotted by R package "CummeRbund" (2). The updated Tuxedo pipeline consisting of Hisat2-Stringtie-Ballgown (23). The new tuxedo pipeline was used to analyze the uPGN activated samples),. The trimmed reads from uPGN activation with different time-intervals were mapped to the same genome assembly by Hisat2 (v2.0.5), assembled, merged and their expression abundance was estimated by Stringtie (v1.3.2-Pre) with default settings (23). The results were visualized and plotted with the R package "Ballgown".

Transcriptomic Sequence Annotation

The nucleotide sequences of differentially expressed genes (DEGs) from the contrast between control and the various treatments were abstracted by Gffread from merged assemblies using Cufflinks and Stringtie (**Table S9**). The sequences were then annotated based on its similarities with human protein sequences and aligned to the human UniProt database (downloaded in Jan 2017) by Blastx (Blast + v2.2.29). The non-redundant DEGs were obtained by collapsing the assembled "gene identifier" from both gene and transcript clusters and the unique ones were kept. Subsequently, the overlapping analysis of those DEGs were conducted by Venn Diagram with its annotated human gene names. **Dammit** (v2.0.1) was used to predict open reading frames and annotate from polished IsoSeq transcripts.

Structure of Ultra-Pure Peptidoglycan-Responsive Pattern Recognition Receptors by Full-Length Transcriptome Sequencing

All the reads from three size-selected cDNA fractions were clustered and polished by IsoSeq_SA3nUP. After polishing by Quiver, 34,516 high-quality (hq) and 157,657 low-quality (lq) transcripts were obtained. All full-length transcript isoform sequences (with either high- or low-qualities) were merged, yielding 192,173 isoforms with average length of 2,351 bp. In total, 69.75% of the transcripts were uniquely mapped to the cod genome assembly (gadMor2) by aligner Star (2.5.3a) under instructions of IsoSeq_SA3nUP. The alignments of transcripts were sorted by Samtools (v0.1.19) and visualized with the R package "Gviz".

Synteny of *IFIH1* (Retinoic Acid-Inducible-II)

Full-length protein sequences of RIG-II for non-cod species were obtained from NCBI and used directly for phylogenetic analysis. Sequences were first aligned by ClustalW and a maximum likelihood tree was produced using Maximum Likelihood (ML) with 2,000 bootstraps by MEGA7. The evolutionary history was inferred by using the Maximum Likelihood method based on the JTT matrix-based model. Synteny analyses of IFIH1 among selected vertebrates are based on genome assemblies from NCBI (RefSeq Release 82), except cod, trout and grass carp whose genome resources are available elsewhere (**Table S4**).

Functional Gene Ontology Enrichment Analysis

Human gene identifiers were retrieved from UniProt-SwissProt for all DEGs. Gene clusters were further divided by different immune stimuli (dsRNA/uPGN) and expression patterns (up/down). Each of them was separately provided as input gene cluster and analyzed together. Cytoscape plugin ClueGO and CluePedia were to perform the GO enrichment analysis against KEGG (**Figure 5**) and comprehensive functional databases including KEGG, GO, WikiPathways, and REACTOME_Pathways (**Figure S5** and **Dataset S1**). The following ClueGO parameters were selected: Go Term Fusion; display pathways that with adjusted-p-values less than 0.05; GO tree interval levels from 3 to 8; GO term minimum numbers of genes (#) and percentage of genes (%): #4+6%, #2+3%, #3+4%, #2 +3% for dsRNA-Up, -Down, uPGN-Up, -Down respectively; kappa score 0.3; GO enrichment/depletion by two-sided hypergeometric test and corrected by Benjamini-Hocheberg; GO terms are presented as nodes and grouped together based on functional similarity. Node size is negatively proportional to the adjusted *p*-value for GO enrichment; interactome layout by Cytoscape plugin AllegroLayout with "Allegro Spring-Electric" option.

RESULTS

Ex Vivo Cod Macrophage Culture

Adherent cells derived from cod head-kidney and spleen differentiated into a homogeneous macrophage phenotype, with filiform pseudopodia, after three days in culture. Flow cytometry assessment of the cell population demonstrated homogeneity (92%) and was gated for further functional assays (gate R1 in **Figures 1A, B**, **Table S1**). Phagocytic capacity was tested with fluorescence-labelled microbes (FITC *Escherichia coli* and *Saccharomyces cerevisiae*) demonstrating 40.77 ± 26.54% (mean ± std. deviation) internalization of yeast within 1 h of incubation at 12 °C (**Figures 1C, D**, **Figure S1** and **Table S1**) and 66.42 ± 3.21% internalization of *E.coli* after 3 h of incubation (**Figures 1E, F**, **Figure S1** and **Table S1**).

The Antiviral Response Is Conserved in the Absence of Retinoic Acid-Inducible -I

To elucidate the bacterial and viral transcriptional response of the *ex vivo* macrophage culture, a collection of MAMPs were used to

mimic a bacterial ("Bac", LPS, PGN, CpG DNA) and viral ("dsRNA", HMW dsRNA) infection. In total, 101 up-regulated and 4 down-regulated genes were identified for group "Bac" (**Figure 2A**), and 688 up-regulated and 105 down-regulated genes for group "dsRNA" (**Figure 2B**). Analysis of annotated DEGs from both challenge groups revealed 46 up-regulated genes expressed in both treatments (**Figure 2C**, **Table S2**, **Data S1**). These were mostly related to membrane internalization and trafficking, activation of transcription and cellular signaling cascades including NF-KB and MAPKs pathways, inflammation-related cytokines, and feedback loop regulators (**Figure 2D**, **Table S2** and **Data S1**). DEGs (492 total) specific to dsRNA were classified into eight major gene clusters conservatively associated to the antiviral immune response including: i) JAK/STAT pathway; ii) RLRs pathway; iii) transcriptional factors; iv) NF-kB and MAPK signaling; v) CAMs (Cell adhesion molecules); vi) antigen presentation by MHC class I; vii) inflammasome and apoptosis; viii) Cytokines and effector proteins (**Figure 2D**, **Figure S2**, **Data S1**).

Interestingly, cod (*Gadus morhua*) (24), flounder (*Paralichthys olivaceus*) (25), chicken (*Gallus gallus*) (26) and the tree shrew (*Tupaia chinensis*) (27) lack RIG-I (*ddx58*), once considered to be indispensable in jawed vertebrates, and yet can initiate robust antiviral responses. As we observed RLR pathway activation, we looked at other RLR genes in the Atlantic cod genome including *ifih1* and *slc4a10*. Phylogenetic analysis placed the cod RIG-II (*ifih1*) into the teleost lineage as expected (**Figure 2E**). Further, synteny analysis revealed a conserved genomic gene array structure where *ifih1* is located, with flanking genes *kcnh7* and *slc4a10* being ubiquitously presented across all tested vertebrate genomes (**Figure 2F**, **Table S3**). Synteny in the teleost lineage was less conserved for *ifih1*-adjacent genes including *fap*, *gcg*, and *dpp4*, which displayed significant variation. Notably, these flanking genes were absent from the trout genome which might be due to the incompleteness of the genome assembly and/or genomic rearrangement. Moreover, a survey of functional studies in these 13 vertebrates using dsRNA (or in some cases viruses) as stimuli highlights a conserved antiviral signaling axis, where key components RLRs, TLR3, IRF3/7, type I IFN, and JAK/STAT are involved (**Figure 2G**, **Table S4**).

Ultra-Pure Peptidoglycan Drives Bacterial Microbe-Associated Molecular Patterns Recognition

In fish, the recognition of bacterial MAMPs and their respective roles in downstream signaling and activation remains under debate (28). In cod, the absence of homologs of the major cell surface mammalian TLRs allowed for further exploration of the downstream signaling pathway following LPS, PGN, and CpG DNA detection. Using *il1b* and *il6* mRNA expression as markers of MAMP recognition, a subsequent pro-inflammatory response, although non-significant, was shown in macrophages to LPS (**Figure 3A**) and CpG DNA (**Table S5**). Ultra-pure PGN (MDP, & iE-DAP) treatment induced a significant activation both 3- and 12-h post challenge with MAMPs, while peptidoglycan did not (**Figure 3A** and **Table S5**).

To further delineate the signaling pathways involved, we employed a suite of kinase inhibitors targeting p38 MAPK and MAPKK (MEK1 and MEK2), including a NOD1/2 inhibitor acting through RIPK2. None of the inhibitors significantly blocked uPGN-driven *il-1b* and *il-6* mRNA increases while used individually. However, when combined, a significant inhibition was observed (32.9% for *il-1b* and 29.5% for *il-6*) (**Figure 3B** and **Table S5**). Although sequence divergence may impact upon cod-specific MAPK inhibition, combinations of RIPK2 and MAPK inhibition produced a more pronounced effect in comparison to MAPKK and p38 inhibition.

uPGN-treated macrophage cultures that were positive for both *il1b* gene expression (**Figure 4A**) and extracellular secretion of the pro-inflammatory mediator prostaglandin E2 (PGE_2) (**Figure 4B**) were analyzed by RNA-Seq. uPGN-activated macrophages showed higher activation (414 DEGs) than in response to the previously used combination of bacterial MAMPs (LPS, PGN and CpG DNA) (105 DEGs). Interestingly, at 3 h post uPGN treatment only 5 up-regulated DEGs and no down-regulated DEGs were observed (**Figure 4C**), while 286 up-regulated and 123 down-regulated DEGs were identified after 12 h of treatment (**Figure 4D**, **Figure S3** and **Data S1**). The majority of DEGs (90%) were annotated, and functionally categorized based on six major pathways: i) G-protein-coupled receptors (GPCRs) and endocytosis; ii) PRRs sensing; iii) apoptosis; iv) NF-kB and MAPK; v) cytokines; and vi) transcription factors (**Figure 4E**, **Data S1**). Both *il1b* and *ripk2* were significantly regulated consistently with previous gene expression results.

Divergent Microbe-Associated Molecular Pattern-Pattern Recognition Receptor Recognition Systems Converge

The extensive repertoire of MAMP sensing in animals is underpinned by a diverse set of adaptors and signaling proteins that form pathways that ultimately activate the inflammatory response. In cod, dependence upon intracellular MAMP sensors may be expected to impact upon the activation of critical signaling pathways. Using GO enrichment analysis with cod DEGs annotated to human SwissProt identifiers, significantly enriched KEGG pathways for dsRNA- and uPGN up-regulated DEGs were shown to be partially shared (**Figure 5** and **Data S1**). Six major functional clusters with their associated DEGs highlighted extensive convergent signaling in cod macrophages upon distinct MAMP challenge (**Figure 5** and **Figure S5**), consistent with shared DEGs between dsRNA and uPGN (**Table S2**). It is also noteworthy that the MAMP sensing pathways, for both dsRNA and uPGN, in cod demonstrate stimuli-specific DEGs that converge upon common thematic regulators, thus providing diversity in MAMP-specific regulators of signaling. For dsRNA-specific pathways, RLR- and NLR-receptors, JAK-STAT signaling, IRF3/7 signaling, type-I IFN response and MHC class I antigen presentation pathways were shown to be conserved across vertebrates, from mammals (29) to teleosts (30–32) (**Data S1** and **Figure S5**). In contrast, the cod uPGN-specific pathway demonstrates a different MAMP sensing mechanism where NOD signaling, pro-inflammatory responses, type-II IFN responses and leukocyte differentiation mediated by *IFNG*, *IRF8* and *TGFB1*, are enriched.

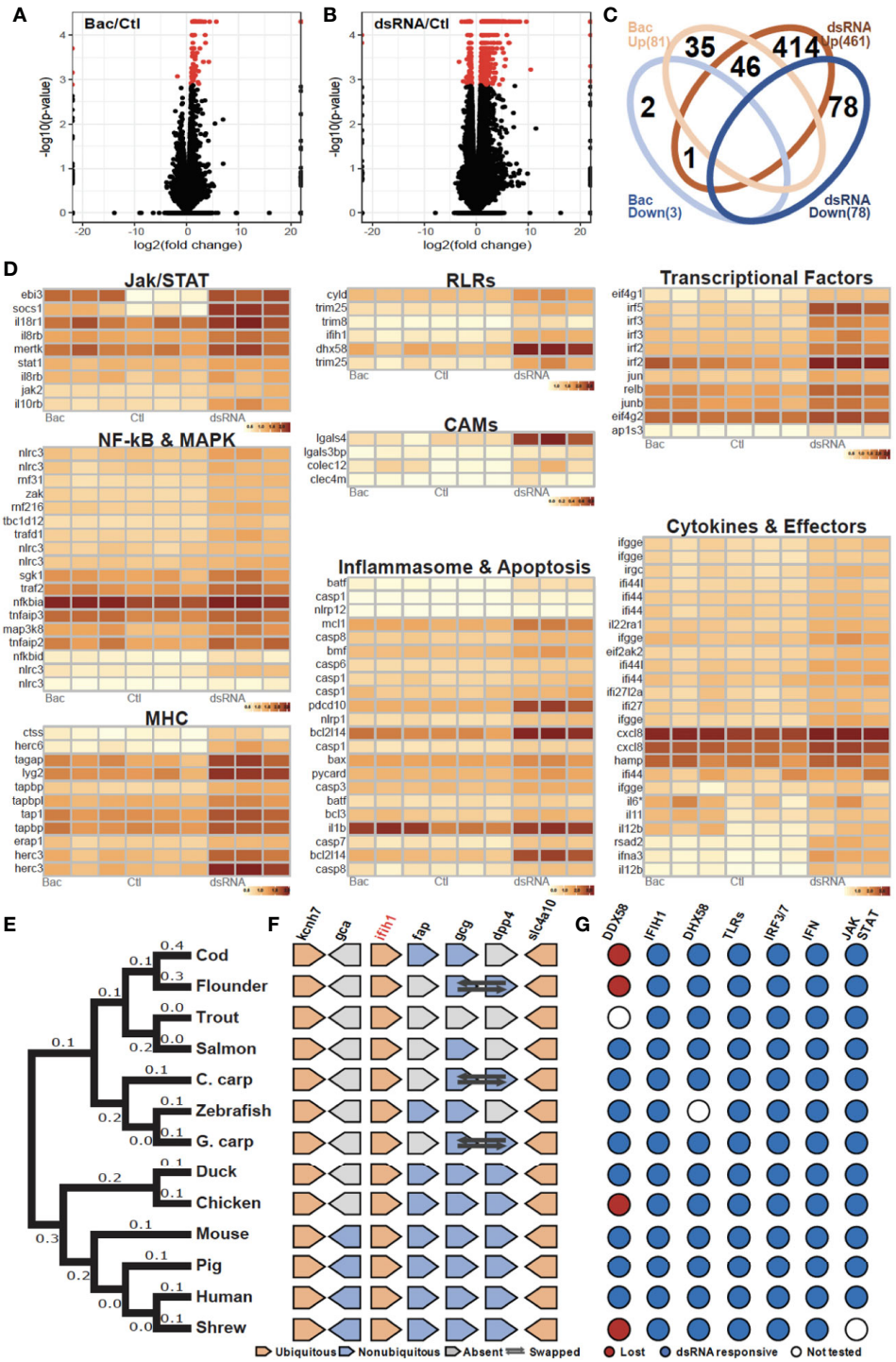

FIGURE 2 | Evolutionarily conserved antibacterial and antiviral response of cod macrophages **(A, B)**. Volcano plots of the expression patterns and statistical significance (shown in red, FDR < 0.05) of genes across three biological samples challenged with **(A)** bacteria-derived microbe-associated molecular patterns (MAMPs) (Bac) and **(B)** dsRNA contrasted with control samples (Ctl) **(C)**. Venn diagram showing number of overlapped up-regulated (UP) and down-regulated (DOWN) genes that had been annotated among Bac and Plc **(D)**. Transcript abundance (log_{10}FPKM+1) of selected DEGs, grouped based on shared signaling pathways **(E)**. Phylogenetic tree of *ifih1* from 13 vertebrates. Number of nucleotide substitutions per site are shown next to each branch **(F)**. Synteny analysis of *ifih1*. Pentagon shapes represent each gene, pointing in the direction of transcription. Ubiquitous genes are orange, absent genes are grey, and non-ubiquitous genes are blue. Dark arrows indicate swapped genes **(G)**. Antiviral responsiveness of the "RLRs-TLRs-IRF3/7-type1IFN-JAK/STAT" axis in 13 vertebrates, as shown by published studies. Red circles indicate lost genes, white circles untested genes, and blue circles responsive genes.

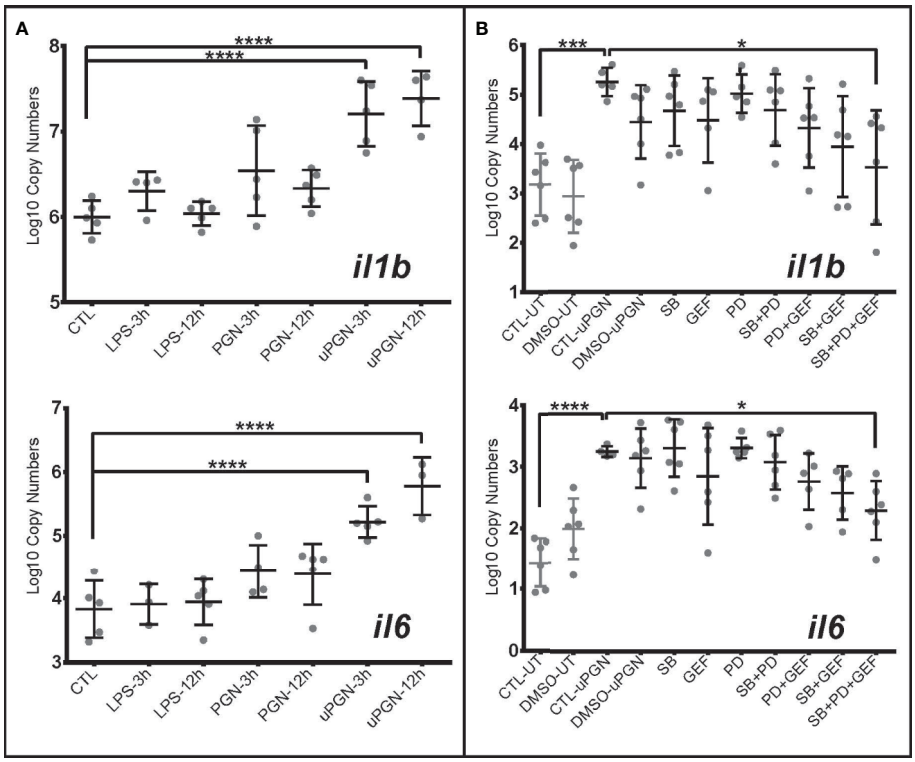

FIGURE 3 | Ultra-pure peptidoglycan (uPGN) triggers the strongest antibacterial response in Atlantic cod macrophages, mediated by NOD1 and MAPKs **(A, B)**. Copy number (log10) of interleukin *il6* and *il1b* in response to **(A)** an activation by various individual MAMPS during 3 and 12 h and **(B)** inhibition of nucleotide-binding oligomerization (NOD) pathway-relevant genes in uPGN-activated samples. PD, MEK1 and MEK2 Inhibitor; GEF, gefitinib; SB, p38 MAP Kinase Inhibitor. Whiskers show the standard deviation. Asterisks represent statistical significance: *<0.05, ***<0.001,**** <0.0001. Abbreviations: CTL, control; LPS, lipopolysaccharide; PGN, peptidoglycan; uPGN, Muramyl dipeptide peptidoglycan; UT, untreated; DMSO, dimethyl sulfoxide.

Evidence for (Sub) Neofunctionalization in Cod Pattern Recognition Receptor

To further capture the full-length mRNA isoforms, especially those of significance in MAMP sensing, long read PacBio transcriptome profiling (IsoSeq) was performed. After polishing by Quiver, 34,516 high-quality (hq) and 157,657 low-quality (lq) transcripts were obtained. Merging of the two, resulted in 192,173 isoforms with average length of 2,351 bp were obtained. In total, 69.75% of the transcripts were uniquely mapped to the cod genome assembly (gadMor2). For some of the low expressed genes detected using RNA-Seq (e.g., FPKM< 1), such as *colec12*, *nlrc3* and *ifih1* (RIG-II), long reads were not detected, probably due to low sequencing coverage. Most cod PRRs found in the Illumina sequencing data were captured at least once by IsoSeq. Inspection of the full-length transcripts of these PRRs obtained by IsoSeq validated the high sensitivity of short reads assembler Cufflinks and StringTie (**Figure S5**). For instance, three potential transcripts for RIG-III (*dhx58*) were assembled by Cufflinks, of which only one isoform "TCONS_00018715" was captured by IsoSeq (**Figure S6**). Accordingly, the most dominant (>75%) isoform "TCONS_00018715" had the highest abundance (FPKM=21.06) in untreated resting macrophages (Ctl). Additionally, two other isoforms "TCONS_00018716" (with an extra 5'-end exon), and "TCONS_00018717" (with exon skipping) were dsRNA-challenge specific. Multiple transcripts for *tlr25* were identified by StringTie (after filtering out transcripts with low variance (see **Supplementary Information** for details), of which only transcript "MSTRG.16445.4" were significantly activated by uPGN (Fold Change=2.831, FDR=0.016). Sequence alignment of all these transcripts towards *tlr25* isoforms (a~g) from Solbakken et al (12, 13)., showed that the isoform "MSTRG.16445.4" is identical to *TLR25d* (13) (**Figure S6**).

DISCUSSION

Experimental studies, prior to the discovery of the alternative arrangement of the Atlantic cod immune system (5, 33, 34), described the Atlantic cod immune response, including survival (35), fitness (36), pathogen elimination (37), and antibody-production (38), as being broadly similar to other teleost fish (39, 40). Furthermore, the loss of most membrane-bound TLRs, MHC II, CD74 invariant chain and the CD4 receptor does not appear to have imposed restrictions on the Gadiformes, a highly successful family (>400 reported species) (2). Therefore, a more prominent role, due to increased gene dosage, for intracellular PRRs and MHC I has been proposed (5, 13).

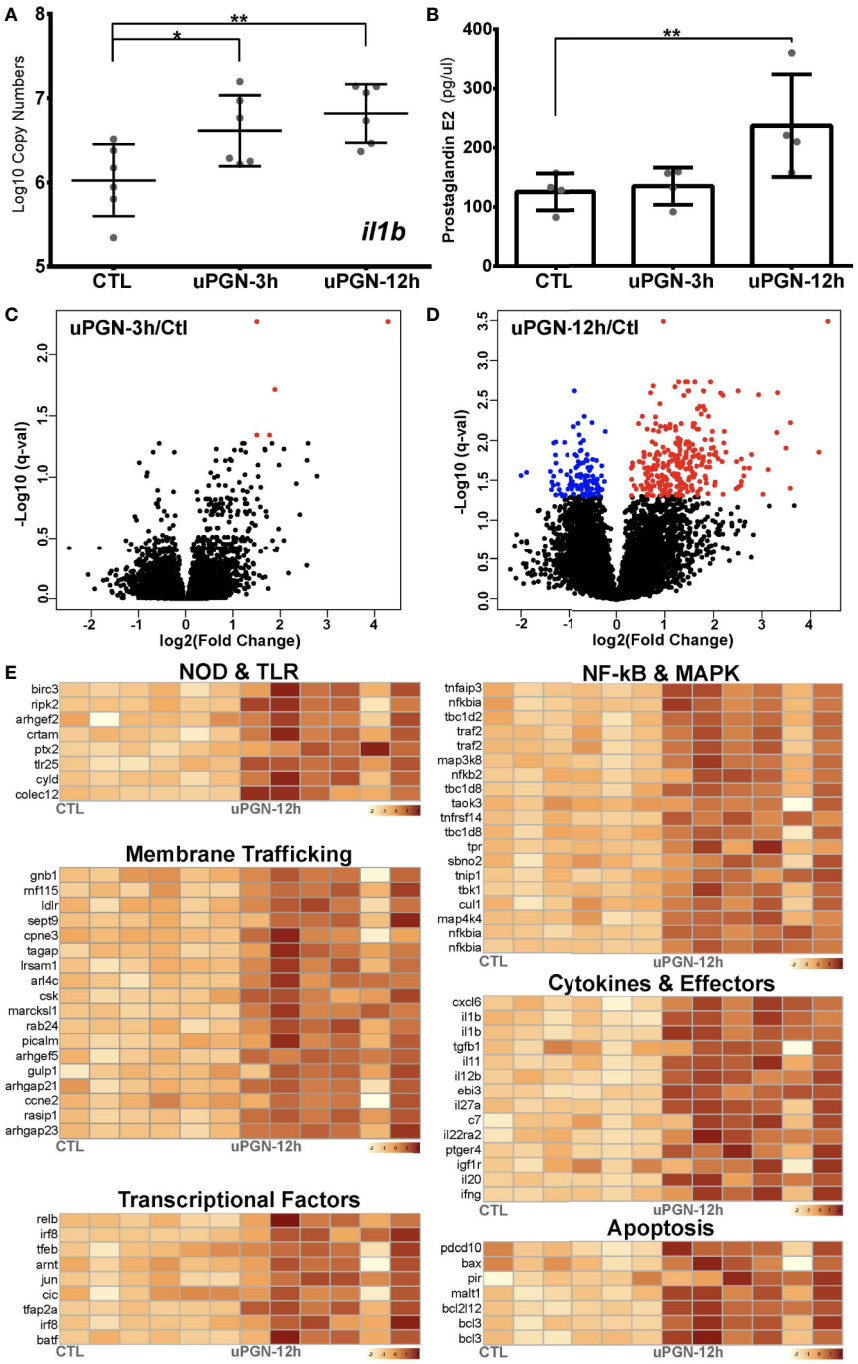

FIGURE 4 | Antibacterial response to uPGN challenge **(A, B)**. Immune response to uPGN measured by **(A)** copy number (log10) of *il1b* and **(B)** prostaglandin E_2 secretion in *ex-vivo* cultured cod macrophages **(C, D).** Volcano plots of the expression patterns and statistical significance (red if significantly up-regulated, blue if significantly down-regulated, FDR < 0.05) of genes across six biological samples challenged with uPGN for **(C)** 3 h and **(D)** 12 h contrasted with control samples **(E)**. Transcript abundance (log10FPKM+1) of selected DEGs challenged with uPGN for 12 h. Grouped based on shared signaling pathways.

In order to assess the MAMP-PRR response in cod, an *ex-vivo* macrophage cell culture model was developed. As one of the major professional antigen-presenting cells (APCs), highly phagocytic macrophages are responsible for innate-adaptive immunity cross-talk (21). Differentiated cod macrophages efficiently engulf microbes, produce several inflammatory mediators and generate a canonical time-dependent MAMP-specific immune response in agreement with vertebrate macrophage models (19, 20, 29) (multidimensional scaling; **Figures S2** and **S3**, functional clustering; **Figure 5**). The MAMP-activated cod macrophage

transcriptome is characterized by profound changes in the expression of cytokines, chemokines, antimicrobial peptides and transcriptional factors (**Data S1**), driven by a set of stimuli-specific gene-clusters tailored to cope with different MAMP-PRR signals. Consistently, functional interactomes for dsRNA and uPGN responsive DEGs are all convergent into functional pathways such as NF-kB and IRFs (**Figures 2** and **4**). Similar results were reported in *in-vivo* studies on cod using the facultative intracellular bacterium *Francisella noatunensis* (41). Our data demonstrates that in cod, macrophage immune response specificity is generated in a ligand-dependent manner in the absence of certain membrane-bound TLR interactions (**Figures 2** and **4**).

The co-evolution of both diversity and restriction across the different components of the immune system is an intriguing puzzle, but hampered by the challenge of developing suitable experimental models (42). Strong evolutionary constraints imposed upon metazoan regulatory molecular circuits ensure robust regulatory mechanisms whereas pressure to diversify recognition structures toward pathogens is critical (9). Interestingly, the deletions observed in the cod genome appear contradictory in that specific cell-surface TLR are absent thus reducing recognition capacity (5), although functionality in cod macrophages is not impaired. Studies in Atlantic cod suggest that endocytosis of lipoprotein and polyribonucleotides (dsRNA) is mediated by scavenger receptors (43). For exogenous dsRNA sensing, variations of membrane-trafficking delivery can trigger distinct immune responses (44, 45). Lipid-based dsRNA transfection induces a highly efficient and scavenger receptor Class-A (SR-As) independent endocytosis triggering TLR3-mediated apoptosis (44, 45). In contrast, directly adding dsRNA to the culture medium, as in this study, induces a SR-As-dependent endocytosis, mediated by the RLR family of cytosolic receptors as seen in mammalian cells (44, 45). In this study, cod macrophages increased the transcription of the Scavenger Receptor Class-A Member (SR-As) *colec12* (aka SCARA4) with both dsRNA and uPGN indicating activation of SR-As-dependent endocytosis. Moreover, many other vesicle-trafficking related pathways were significantly activated indicating a common response (**Figure 5** and **Data 1**). In accordance, elevated transcription of all cod RLRs, including *ifih1* and *dhx58*, post dsRNA challenge was observed. In contrast, no activation was observed for *tlr3* or its relevant adaptors including *myd88* and *trif*. PGN does not induce any inflammatory response *via* direct microinjection into cytosol in mammals, unless delivered by membrane encapsulated-vesicles (46). In fact, recent studies highlight the endosome as a crucial platform for NOD1/2-dependent ligand sensing and inflammatory signaling (47–49). Despite *nod1* not being significantly induced by uPGN (Fold-change: 1.7; *p*-val: 0.01; FDR: 0.13, **Figure S4**), transcription of its adaptor (*arhgef2*), enzymes (*ripk2, hk2*), and ubiquitination regulators (*birc3*, *cyld*, *tnfiap3*) were all consistently elevated in our study which is consistent with observations from studies in mammals (48, 50). Additionally, results from our blockade assays using a cocktail of

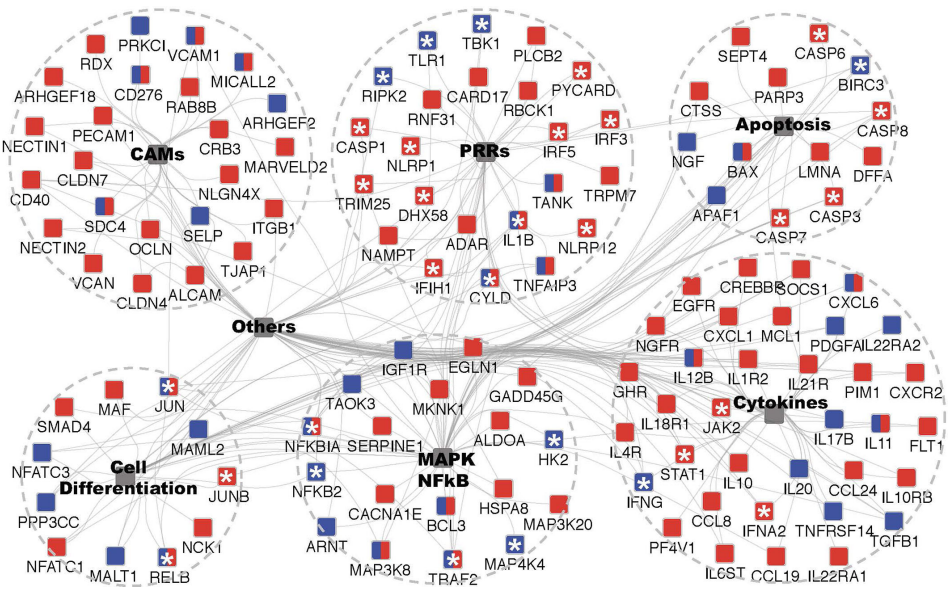

FIGURE 5 | GO enrichment analysis of microbe-associated molecular pattern (MAMP) up-regulated DEGs to identify underpinned functional pathways in activating the cod macrophage inflammatory response. GO enrichment and network visualization was conducted by Cytoscape plugin ClueGO and CluePedia. Cod up-regulated DEGs annotated to human SwissProt identifiers were mapped to KEGG (Kyoto Encyclopedia of Genes and Genomes) pathways database. Enriched KEGG terms that are shared the same cluster were collapsed into one integrative node (shaded grey) labelled with brief descriptions respectively (See **Figure S5** and **Dataset S1** for the full network). Six major inflammation-related functional pathways were shown, and the remaining ones were labelled with "Others". The associated DEGs with indicated KEGG pathways were color coded in a MAMP-dependent fashion, red and blue nodes denote dsRNA- and uPGN-responsive genes, respectively; whilst the dual-labelled nodes denote the common DEGs that are responsive to both MAMPs. Asterisks indicate genes that serve as key sensors, adaptors or regulators in mediating inflammatory response and had been intensively discussed in texts.

inhibitors against RIPK2 and MAPKs further validated the role of NOD-pathways in sensing uPGN in cod macrophages. Therefore, despite the absence of *nod2*, the NOD pathway in cod remains functional, in line with observations of NOD1-mediated antibacterial responses in birds lacking NOD2 including both duck (51) and chicken (52).

In addition to the loss of specific TLRs and the classical MHC II pathway, some intracellular PRRs including RIG-I and NOD2 were also found to be absent in the Atlantic cod (13). Similarly, RIG-I is lost in the coelacanth, spotted gar, cave fish, lamprey and tree shrew and NOD2 is absent in the spotted gar, frog, reptiles and birds (Ensembl Gene gain/loss tree). We found that the remaining MDA5/LGP2 and NOD1 initiate the RLR- and NOD-pathways specific to dsRNA and uPGN sensing, respectively, in Atlantic cod. In the tree shrew, MDA5 and LGP2 synergistically mediate dsRNA sensing regardless of molecular-weight differences in compensation for the loss of RIG-I (27). This is achieved by the RIG-I-specific adaptor, STING (Stimulator of interferon genes protein, encoded by *tmem173*), that acquired a novel MDA5 interacting function (27). In this study, the high-molecular-weight dsRNA was used as a general ligand for MDA5/LGP2. Further studies concerning the differences in ligand types (e.g., HMW v.s. LMW) and delivery routes (e.g., extracellularly or *via* liposome transfection) would provide additional information in partitioning the specificities of receptor profiles. In zebrafish, NOD1 knockout mediated by gene-editing dramatically affected many other NLRs members by inducing expression whilst conventional NF-κB and MAPK immune signaling pathways were unimpaired (53). Interestingly, in line with above mentioned PRRs, in dsRNA or uPGN challenged cod macrophages, other receptors such as *nlrc3s*, *nlrp1*, *nlrp12* and *tlr25* were also significantly up-regulated (**Figure 5** and **Data 1**). In contrast to mammals, the dramatically expanded NLR and TLR gene repertoire in the cod genome suggest a potential rapid functional shift (7, 14). TLR25, one of the teleost-specific TLRs, belongs to the TLR1 family and shares significant sequence similarity with mammalian TLR1 (12, 13). In this study, one of the TLR25 isoforms, *tlr25d*, was uniquely regulated by uPGN challenge, however no changes were observed in any Myddosome or Triffosome related factors leaving its downstream signaling in cod unclear. On the other hand, several NLR family members' associated adaptors including *pycard* and *casp1* were induced suggesting that these mediators of inflammasome formation are active in Atlantic cod as reported in mammals (54). Recent studies, in zebrafish, described a conserved functional role for the NLRP1 inflammasome in teleosts (55) and our observations further support a central role for NLRs in innate immunity in the Atlantic cod and across the Teleost fish.

The underlying molecular patterns of activation in cod macrophages point toward a conserved cytosolic MAMP-PRR recognition that link to supra molecular organizing centers which themselves appear to be conserved across vertebrate innate immune signaling (9, 31). RLRs, NLRs and TLRs engage in convergent signaling cascades to regulate the expression and degradation of pro-inflammatory mediators upon ligand sensing, that are highly conserved owing to strong functional and regulatory constraints (56, 57). Interestingly, in fish canonical LPS-TLR4 sensing is seemingly absent (58), with the exception of zebrafish, as a negative regulator of inflammation (28). In this study, no significant response to a standard LPS preparation was detected. However, a robust uPGN-NOD driven activation of inflammation coupled to an enrichment of the IRF8 pathway was observed (**Figure S5** and **Dataset S1**). In mice, IRF8-impairment led to reduced secretion of IL-12, an essential inducer of T helper (Th1) cell polarization, causing a dramatic increase in susceptibility to intracellular infections highlighting a critical defense function (59). Furthermore, a regulatory role for IRF8 has been suggested in MHC II antigen presentation (60, 61). Recently, MHC class I based cross-presentation through the acquisition of functional sorting motifs has been suggested as a mechanism in cod for MHC II loss (62). The cod macrophage model and further exploration of the IRF8 pathway provides a platform for further functional studies. Multiple genome-based studies across a wide range of fishes highlight an exceptional diversity at the level of cytosolic PRR families (63–65). It is tempting to speculate that the environment, both aquatic and internal, coupled to restricted adaptive immunity has driven innovation in cytosolic MAMP detection.

Available evidence, including this study, suggests that functionality including intracellular PRR systems are conserved throughout vertebrates, and thus, also provide an efficient host defense in the Gadiformes lineage contributing to their evolutionary success (31, 41, 66–68). In light of the loss of the majority of extracellular PRR capability and lack of MHC class II-based antigen presentation it suggests, at least in the Gadiformes, these functions may not be 'core' to the immune response and possibly bony fishes in general. Notably, evidence for sub- or neofunctionalization of PRR, in a ligand-dependent manner, is demonstrated *via* several NLRs paralogues and one of the TLR25 isoforms. Sub- or neofunctionalization following gene duplication of multigene gene families driven by selection is a recognized mechanism of genome innovation and adaptation (4). The dramatically diversified NLR and TLR paralogues, coupled with their complex protein-protein interactions *via* ligand-sensing and signal transduction domains, presumably allow the cod immune system to adapt to fast-evolving pathogens.

In summary, our results, based upon a novel *ex vivo* macrophage cell culture, demonstrate that intracellular PRR systems based upon RLR and NOD signaling, in the absence of RIG-I and NOD2, are critical drivers of the response to bacterial and viral pathogens in Atlantic cod. Our analysis highlighted the inflammatory response to be intimately linked to scavenger receptor-based internalization of MAMPs coupled to highly conserved intracellular signaling platforms. Cytosolic PRR capabilities in the Atlantic cod are functional, in line with most vertebrate studies, and are based upon canonical NF-kB and IRFs activation pathways. Additionally, we uncover that the multiple NLR paralogues and the unique TLR25 isoform identified in Atlantic cod display ligand-dependent differential expression suggesting (sub)neofunctionalisation toward specific immune defensive strategies. Our results further demonstrate that the extreme remodeling of the Atlantic cod immune system provides

an unprecedented opportunity to explore the evolutionary history of PRR-based signaling in vertebrate immunity.

AUTHOR'S NOTE

This manuscript has been released as a pre-print at bioRxiv 2020.08.07.241067; doi: https://doi.org/10.1101/2020.08.07.24106765.

DATA AVAILABILITY STATEMENT

The datasets presented in this study can be found in online repositories. The names of the repository/repositories and accession number(s) can be found in the article/**Supplementary Material**.

ETHICS STATEMENT

The animal study was reviewed and approved by Animal Welfare and Ethical Review Body (AWERB), University of Stirling. Application number: AWERB/1718/132/New Non ASPA.

AUTHOR CONTRIBUTIONS

SM, KJ, and SJ designed the study and obtained financial support. XJ, BM, VM, and SM participated in the experimental design, macrophage cell culture development, and sampling. XJ, BM, OT, and MS carried out bioinformatic analyses and posterior statistical analysis. All authors participated in drafting the final manuscript. All authors contributed to the article and approved the submitted version.

ACKNOWLEDGMENTS

The sequencing service was provided by the Norwegian Sequencing Centre (www.sequencing.uio.no), a national technology platform hosted by the University of Oslo and supported by the "Functional Genomics" and "Infrastructure" programs of the Research Council of Norway and the Southeastern Regional Health Authorities. All bioinformatics analysis was performed using Abel high performance computer cluster (under project Nos n9244kk), owned by the University of Oslo and the Norwegian metacenter for High Performance Computing (NOTUR), and operated by the Department for Research Computing at USIT, the University of Oslo IT-department. The project was supported by the Research Council of Norway (grant number 222378/F20 to KJ).

SUPPLEMENTARY MATERIAL

The Supplementary Material for this article can be found online at: https://www.frontiersin.org/articles/10.3389/fimmu.2020.609456/full#supplementary-material

SUPPLEMENTARY DATA SHEET 1 | Differential expression analysis and GOs/KEGGs enrichment output.

REFERENCES

1. Netea MG, Schlitzer A, Placek K, Joosten LAB, Schultze JL. Innate and Adaptive Immune Memory: an Evolutionary Continuum in the Host's Response to Pathogens. *Cell Host Microbe* (2019) 25(1):13–26. doi: 10.1016/j.chom.2018.12.006
2. Malmstrom M, Matschiner M, Torresen OK, Star B, Snipen LG, Hansen TF, et al. Evolution of the immune system influences speciation rates in teleost fishes. *Nat Genet* (2016) 48(10):1204–10. doi: 10.1038/ng.3645
3. Palti Y. Toll-like receptors in bony fish: From genomics to function. *Dev Comp Immunol* (2011) 35(12):1263–72. doi: 10.1016/j.dci.2011.03.006
4. Wang B, Wangkahart E, Secombes CJ, Wang T. Insights into the Evolution of the Suppressors of Cytokine Signaling (SOCS) Gene Family in Vertebrates. *Mol Biol Evol* (2019) 36(2):393–411. doi: 10.1093/molbev/msy230
5. Star B, Nederbragt AJ, Jentoft S, Grimholt U, Malmstrom M, Gregers TF, et al. The genome sequence of Atlantic cod reveals a unique immune system. *Nature* (2011) 477(7363):207–10. doi: 10.1038/nature10342
6. Roth O, Solbakken MH, Tørresen OK, Bayer T, Matschiner M, Baalsrud HT, et al. Evolution of male pregnancy associated with remodeling of canonical vertebrate immunity in seahorses and pipefishes. *Proc Natl Acad Sci* (2020) 117(17):9431. doi: 10.1073/pnas.1916251117
7. Tørresen OK, Brieuc MSO, Solbakken MH, Sørhus E, Nederbragt AJ, Jakobsen KS, et al. Genomic architecture of haddock (Melanogrammus aeglefinus) shows expansions of innate immune genes and short tandem repeats. *BMC Genomics* (2018) 19(1):240. doi: 10.1186/s12864-018-4616-y
8. Kang S, Kim J-H, Jo E, Lee SJ, Jung J, Kim B-M, et al. Chromosomal-level assembly of Takifugu obscurus (Abe, 1949) genome using third-generation DNA sequencing and Hi-C analysis. *Mol Ecol Resour* (2020) 20(2):520–30. doi: 10.1111/1755-0998.13132
9. Kieser KJ, Kagan JC. Multi-receptor detection of individual bacterial products by the innate immune system. *Nat Rev Immunol* (2017) 17(6):376–90. doi: 10.1038/nri.2017.25
10. Meunier E, Broz P. Evolutionary Convergence and Divergence in NLR Function and Structure. *Trends Immunol* (2017) 38(10):744–57. doi: 10.1016/j.it.2017.04.005
11. Stocks CJ, Schembri MA, Sweet MJ, Kapetanovic R. For when bacterial infections persist: Toll-like receptor-inducible direct antimicrobial pathways in macrophages. *J Leukoc Biol* (2018) 103(1):35–51. doi: 10.1002/JLB.4RI0917-358R
12. Solbakken MH, Voje KL, Jakobsen KS, Jentoft S. Linking species habitat and past palaeoclimatic events to evolution of the teleost innate immune system. *Proc Biol Sci* (2017) 284(1853):20162810. doi: 10.1098/rspb.2016.2810
13. Solbakken MH, Tørresen OK, Nederbragt AJ, Seppola M, Gregers TF, Jakobsen KS, et al. Evolutionary redesign of the Atlantic cod (Gadus morhua L.) Toll-like receptor repertoire by gene losses and expansions. *Sci Rep* (2016) 6:25211. doi: 10.1038/srep25211
14. Tørresen OK, Star B, Jentoft S, Reinar WB, Grove H, Miller JR, et al. An improved genome assembly uncovers prolific tandem repeats in Atlantic cod. *BMC Genomics* (2017) 18(1):95. doi: 10.1186/s12864-016-3448-x
15. Torresen OK, Star B, Mier P, Andrade-Navarro MA, Bateman A, Jarnot P, et al. Tandem repeats lead to sequence assembly errors and impose multi-level challenges for genome and protein databases. *Nucleic Acids Res* (2019) 47(21):10994–1006. doi: 10.1093/nar/gkz841
16. Franchi L, Warner N, Viani K, Nuñez G. Function of Nod-like receptors in microbial recognition and host defense. *Immunol Rev* (2009) 227(1):106–28. doi: 10.1111/j.1600-065X.2008.00734.x
17. Giolai M, Paajanen P, Verweij W, Witek K, Jones JDG, Clark MD. Comparative analysis of targeted long read sequencing approaches for characterization of a plant's immune receptor repertoire. *BMC Genomics* (2017) 18(1):564. doi: 10.1186/s12864-017-3936-7

18. Conesa A, Madrigal P, Tarazona S, Gomez-Cabrero D, Cervera A, McPherson A, et al. A survey of best practices for RNA-seq data analysis. *Genome Biol* (2016) 17:13. doi: 10.1186/s13059-016-0881-8
19. MacKenzie SA, Roher N, Boltaña S, Goetz FW. Peptidoglycan, not endotoxin, is the key mediator of cytokine gene expression induced in rainbow trout macrophages by crude LPS. *Mol Immunol* (2010) 47(7–8):1450–7. doi: 10.1016/j.molimm.2010.02.009
20. Callol A, Roher N, Amaro C, MacKenzie S. Characterization of PAMP/PRR interactions in European eel (Anguilla anguilla) macrophage-like primary cell cultures. *Fish Shellfish Immunol* (2013) 35(4):1216–23. doi: 10.1016/j.fsi.2013.07.037
21. Nakagaki BN, Vieira AT, Rezende RM, David BA, Menezes GB. Tissue macrophages as mediators of a healthy relationship with gut commensal microbiota. *Cell Immunol* (2018) 330:16–26. doi: 10.1016/j.cellimm.2018.01.017
22. Trapnell C, Roberts A, Goff L, Pertea G, Kim D, Kelley DR, et al. Differential gene and transcript expression analysis of RNA-seq experiments with TopHat and Cufflinks. *Nat Protoc* (2012) 7(3):562–78. doi: 10.1038/nprot.2012.016
23. Pertea M, Kim D, Pertea GM, Leek JT, Salzberg SL. Transcript-level expression analysis of RNA-seq experiments with HISAT, StringTie and Ballgown. *Nat Protoc* (2016) 11(9):1650–67. doi: 10.1038/nprot.2016.095
24. Eslamloo K, Xue X, Booman M, Smith NC, Rise ML. Transcriptome profiling of the antiviral immune response in Atlantic cod macrophages. *Dev Comp Immunol* (2016) 63:187–205. doi: 10.1016/j.dci.2016.05.021
25. Hikima J-I, Yi M-K, Ohtani M, Jung CY, Kim YK, Mun JY, et al. LGP2 Expression is Enhanced by Interferon Regulatory Factor 3 in Olive Flounder, Paralichthys olivaceus. *PloS One* (2012) 7(12):e51522. doi: 10.1371/journal.pone.0051522
26. Barber MRW, Aldridge JR, Webster RG, Magor KE. Association of RIG-I with innate immunity of ducks to influenza. *Proc Natl Acad Sci* (2010) 107 (13):5913. doi: 10.1073/pnas.1001755107
27. Xu L, Yu D, Fan Y, Peng L, Wu Y, Yao Y-G. Loss of RIG-I leads to a functional replacement with MDA5 in the Chinese tree shrew. *Proc Natl Acad Sci* (2016) 113(39):10950–5. doi: 10.1073/pnas.1604939113
28. Sepulcre MP, Alcaraz-Perez F, Lopez-Munoz A, Roca FJ, Meseguer J, Cayuela ML, et al. Evolution of lipopolysaccharide (LPS) recognition and signaling: fish TLR4 does not recognize LPS and negatively regulates NF-kappaB activation. *J Immunol (Baltimore Md 1950)* (2009) 182(4):1836–45. doi: 10.4049/jimmunol.0801755
29. Jia X, Yuan S, Wang Y, Fu Y, Ge Y, Ge Y, et al. The role of alternative polyadenylation in the antiviral innate immune response. *Nat Commun* (2017) 8:14605. doi: 10.1038/ncomms14605
30. Nie L, Zhang Y-S, Dong W-R, Xiang L-X, Shao J-Z. Involvement of zebrafish RIG-I in NF-κB and IFN signaling pathways: Insights into functional conservation of RIG-I in antiviral innate immunity. *Dev Comp Immunol* (2015) 48(1):95–101. doi: 10.1016/j.dci.2014.09.008
31. Inkpen SM, Solbakken MH, Jentoft S, Eslamloo K, Rise ML. Full characterization and transcript expression profiling of the interferon regulatory factor (IRF) gene family in Atlantic cod (Gadus morhua). *Dev Comp Immunol* (2019) 98:166–80. doi: 10.1016/j.dci.2019.03.015
32. Eslamloo K, Inkpen SM, Rise ML, Andreassen R. Discovery of microRNAs associated with the antiviral immune response of Atlantic cod macrophages. *Mol Immunol* (2018) 93:152–61. doi: 10.1016/j.molimm.2017.11.015
33. Magnadottir B, Jonsdottir H, Helgason S, Bjornsson B, Jorgensen TO, Pilstrom L. Humoral immune parameters in Atlantic cod (Gadus morhua L.): I. The effects of environmental temperature. *Comp Biochem Physiol B Biochem Mol Biol* (1999) 122:173–80 doi: 10.1016/s0305-0491(98)10157-8
34. Magnadóttir B. Innate immunity of fish (overview). *Fish Shellfish Immunol* (2006) 20(2):137–51. doi: 10.1016/j.fsi.2004.09.006
35. Jensen I, Seppola M, Steiro K, Sandaker E, Mennen S, Sommer A-I. Susceptibility of Atlantic cod Gadus morhua juveniles to different routes of experimental challenge with infectious pancreatic necrosis virus (IPNV). *Dis Aquat Organisms* (2009) 85(2):105–13. doi: 10.3354/dao02066
36. Lange S, Bambir S, Dodds AW, Magnadóttir B. The ontogeny of complement component C3 in Atlantic cod (Gadus morhua L.)—an immunohistochemical study. *Fish Shellfish Immunol* (2004) 16(3):359–67. doi: 10.1016/j.fsi.2003.06.001
37. Gudmundsdottir S, Magnadottir B, Bjornsdottir B, Arnadottir H, Gudmundsdottir BK. Specific and natural antibody response of cod juveniles vaccinated against Vibrio anguillarum. *Fish Shellfish Immunol* (2009) 26(4):619–24. doi: 10.1016/j.fsi.2008.09.017
38. Pilström L, Petersson A. Isolation and partial characterization of immunoglobulin from cod (Gadus morhua L.). *Dev Comp Immunol* (1991) 15(3):143–52. doi: 10.1016/0145-305X(91)90005-J
39. Grayfer L, Kerimoglu B, Yaparla A, Hodgkinson JW, Xie J, Belosevic M. Mechanisms of Fish Macrophage Antimicrobial Immunity. *Front Immunol* (2018) 9:(1105):173–80. doi: 10.3389/fimmu.2018.01105
40. Pereiro P, Figueras A, Novoa B. Insights into teleost interferon-gamma biology: An update. *Fish Shellfish Immunol* (2019) 90:150–64. doi: 10.1016/j.fsi.2019.04.002
41. Solbakken MH, Jentoft S, Reitan T, Mikkelsen H, Gregers TF, Bakke O, et al. Disentangling the immune response and host-pathogen interactions in Francisella noatunensis infected Atlantic cod. *Comp Biochem Physiol Part D: Genomics Proteomics* (2019) 30:333–46. doi: 10.1016/j.cbd.2019.04.004
42. Pasquier LD. Germline and somatic diversification of immune recognition elements in Metazoa. *Immunol Lett* (2006) 104(1):2–17. doi: 10.1016/j.imlet.2005.11.022
43. Sorensen KK, Melkko J, Smedsrod B. Scavenger-receptor-mediated endocytosis in endocardial endothelial cells of Atlantic cod Gadus morhua. *J Exp Biol* (1998) 201(Pt 11):1707–18.
44. Nellimarla S, Baid K, Loo Y-M, Gale M, Bowdish DM, Mossman KL. Class A scavenger receptor-mediated dsRNA internalization is independent of innate antiviral signaling and does not require PI3K activity(). *J Immunol (Baltimore Md 1950)* (2015) 195(8):3858–65. doi: 10.4049/jimmunol.1501028
45. Palchetti S, Starace D, De Cesaris P, Filippini A, Ziparo E, Riccioli A. Transfected Poly(I:C) Activates Different dsRNA Receptors, Leading to Apoptosis or Immunoadjuvant Response in Androgen-independent Prostate Cancer Cells. *J Biol Chem* (2015) 290(9):5470–83. doi: 10.1074/jbc.M114.601625
46. Kaparakis M, Turnbull L, Carneiro L, Firth S, Coleman HA, Parkington HC, et al. Bacterial membrane vesicles deliver peptidoglycan to NOD1 in epithelial cells. *Cell Microbiol* (2010) 12(3):372–85. doi: 10.1111/j.1462-5822.2009.01404.x
47. Nakamura N, Lill JR, Phung Q, Jiang Z, Bakalarski C, de Maziere A, et al. Endosomes are specialized platforms for bacterial sensing and NOD2 signalling. *Nature* (2014) 509(7499):240–4. doi: 10.1038/nature13133
48. Irving AT, Mimuro H, Kufer TA, Lo C, Wheeler R, Turner LJ, et al. The immune receptor NOD1 and kinase RIP2 interact with bacterial peptidoglycan on early endosomes to promote autophagy and inflammatory signaling. *Cell Host Microbe* (2014) 15(5):623–35. doi: 10.1016/j.chom.2014.04.001
49. Bonham KS, Kagan JC. Endosomes as Platforms for NOD-like Receptor Signaling. *Cell Host Microbe* (2014) 15(5):523–5. doi: 10.1016/j.chom.2014.05.001
50. Caruso R, Warner N, Inohara N, Nunez G. NOD1 and NOD2: signaling, host defense, and inflammatory disease. *Immunity* (2014) 41(6):898–908. doi: 10.1016/j.immuni.2014.12.010
51. Li H, Jin H, Li Y, Liu D, Foda MF, Jiang Y, et al. Molecular cloning and functional characterization of duck nucleotide-binding oligomerization domain 1 (NOD1). *Dev Comp Immunol* (2017) 74:82–9. doi: 10.1016/j.dci.2017.04.012
52. Tao Z, Zhu C, Song W, Xu W, Zhang S, Liu H, et al. Inductive expression of the NOD1 signalling pathway in chickens infected with Salmonella pullorum. *Br Poultry Sci* (2017) 58(3):242–50. doi: 10.1080/00071668.2017.1280771
53. Hu YW, Wu XM, Ren SS, Cao L, Nie P, Chang MX. NOD1 deficiency impairs CD44a/Lck as well as PI3K/Akt pathway. *Sci Rep* (2017) 7(1):2979. doi: 10.1038/s41598-017-03258-y
54. Lamkanfi M, Dixit VM. Inflammasomes: guardians of cytosolic sanctity. *Immunol Rev* (2009) 227(1):95–105. doi: 10.1111/j.1600-065X.2008.00730.x
55. Li J-Y, Gao K, Shao T, Fan D-D, Hu C-B, Sun C-C, et al. Characterization of an NLRP1 Inflammasome from Zebrafish Reveals a Unique Sequential Activation Mechanism Underlying Inflammatory Caspases in Ancient Vertebrates. *J Immunol* (2018) 201(7):1946. doi: 10.4049/jimmunol.1800498
56. Takeuchi O, Akira S. Pattern Recognition Receptors and Inflammation. *Cell* (2010) 140(6):805–20. doi: 10.1016/j.cell.2010.01.022
57. Newton K, Dixit VM. Signaling in innate immunity and inflammation. *Cold Spring Harbor Perspect Biol* (2012) 4(3):a006049. doi: 10.1101/cshperspect.a006049

58. Iliev DB RJ, Mackenzie S, Planas JV, Goetz FW. Endotoxin recognition: in fish or not in fish? *FEBS Lett* (2005) 579(29):6519–28. doi: 10.1016/j.febslet.2005.10.061
59. Turcotte K, Gauthier S, Malo D, Tam M, Stevenson MM, Gros P. Icsbp1/IRF-8 Is Required for Innate and Adaptive Immune Responses against Intracellular Pathogens. *J Immunol* (2007) 179(4):2467–76. doi: 10.4049/jimmunol.179.4.2467
60. Marquis J-F, Kapoustina O, Langlais D, Ruddy R, Dufour CR, Kim B-H, et al. Interferon Regulatory Factor 8 Regulates Pathways for Antigen Presentation in Myeloid Cells and during Tuberculosis. *PloS Genet* (2011) 7(6):e1002097. doi: 10.1371/journal.pgen.1002097
61. Berghout J, Langlais D, Radovanovic I, Tam M, MacMicking JD, Stevenson MM, et al. Irf8-Regulated Genomic Responses Drive Pathological Inflammation during Cerebral Malaria. *PloS Pathog* (2013) 9(7):e1003491. doi: 10.1371/journal.ppat.1003491
62. Malmstrøm M, Jentoft S, Gregers TF, Jakobsen KS. Unraveling the Evolution of the Atlantic Cod's (Gadus morhua L.) Alternative Immune Strategy. *PloS One* (2013) 8(9):e74004. doi: 10.1371/journal.pone.0074004
63. Howe K, Schiffer PH, Zielinski J, Wiehe T, Laird GK, Marioni JC, et al. Structure and evolutionary history of a large family of NLR proteins in the zebrafish. *Open Biol* (2016) 6(4):160009. doi: 10.1098/rsob.160009
64. Tørresen OK, Rise ML, Jin X, Star B, MacKenzie S, Jakobsen KS, et al. 3 - An improved version of the Atlantic cod genome and advancements in functional genomics: implications for the future of cod farming. In: S MacKenzie, S Jentoft, editors. *Genomics in Aquaculture*. San Diego: Academic Press (2016). p. 45–72. doi: 10.1016/B978-0-12-801418-9.00003-2
65. Motta V, Soares F, Sun T, Philpott DJ. NOD-like receptors: versatile cytosolic sentinels. *Physiol Rev* (2015) 95(1):149–78. doi: 10.1152/physrev.00009.2014
66. Eslamloo K, Ghorbani A, Xue X, Inkpen SM, Larijani M, Rise ML. Characterization and Transcript Expression Analyses of Atlantic Cod Viperin. *Front Immunol* (2019) 10(311):311. doi: 10.3389/fimmu.2019.00311
67. Solbakken MH, Jentoft S, Reitan T, Mikkelsen H, Jakobsen KS, Seppola M. Whole transcriptome analysis of the Atlantic cod vaccine response reveals subtle changes in adaptive immunity. *Comp Biochem Physiol Part D: Genomics Proteomics* (2019) 31:100597. doi: 10.1016/j.cbd.2019.100597
68. Soto-Dávila M, Hossain A, Chakraborty S, Rise ML, Santander J. Aeromonas salmonicida subsp. salmonicida Early Infection and Immune Response of Atlantic Cod (Gadus morhua L.) Primary Macrophages. *Front Immunol* (2019) 10(1237):1237. doi: 10.3389/fimmu.2019.01237

Conflict of Interest: The authors declare that the research was conducted in the absence of any commercial or financial relationships that could be construed as a potential conflict of interest.

frontiers in Immunology

ORIGINAL RESEARCH
published: 20 January 2022
doi: 10.3389/fimmu.2021.792901

Identification of the Association Between Toll-Like Receptors and T-Cell Activation in Takayasu's Arteritis

Yixiao Tian[1,2,3,4†‡], *Biqing Huang*[1,2,3,4†‡], *Jing Li*[1,2,3,4*†], *Xinping Tian*[1,2,3,4†] *and Xiaofeng Zeng*[1,2,3,4*†]

[1] Department of Rheumatology and Clinical Immunology, Chinese Academy of Medical Sciences & Peking Union Medical College, Peking Union Medical College Hospital (PUMCH), Beijing, China, [2] National Clinical Research Center for Dermatologic and Immunologic Diseases (NCRC-DID), Ministry of Science & Technology, Beijing, China, [3] State Key Laboratory of Complex Severe and Rare Diseases, Peking Union Medical College Hospital (PUMCH), Beijing, China, [4] Key Laboratory of Rheumatology and Clinical Immunology, Ministry of Education, Beijing, China

OPEN ACCESS

Edited by:
Subhasis Chattopadhyay, National Institute of Science Education and Research (NISER), India

Reviewed by:
Jin Hou, Second Military Medical University, China
Subhransu Sekhar Sahoo, Purdue University, United States

***Correspondence:**
Jing Li
lijing6515@pumch.cn
Xiaofeng Zeng
xiaofeng.zeng@cstar.org.cn

†ORCID:
Jing Li
orcid.org/0000-0003-2504-1629
Xiaofeng Zeng
orcid.org/0000-0002-3883-2318
Yixiao Tian
orcid.org/0000-0002-2710-848X
Biqing Huang
orcid.org/0000-0003-3962-1894
Xinping Tian
orcid.org/0000-0002-1511-7952

‡*These authors share first authorship*

Specialty section:
This article was submitted to T Cell Biology, a section of the journal Frontiers in Immunology

Received: *11 October 2021*
Accepted: *22 December 2021*
Published: *20 January 2022*

Citation:
Tian Y, Huang B, Li J, Tian X and Zeng X (2022) Identification of the Association Between Toll-Like Receptors and T-Cell Activation in Takayasu's Arteritis. Front. Immunol. 12:792901. doi: 10.3389/fimmu.2021.792901

To explore the relationships between Toll-like receptors (TLRs) and the activation and differentiation of T-cells in Takayasu's arteritis (TAK), using real-time fluorescence quantitative polymerase chain reaction, mRNA abundance of 29 target genes in peripheral blood mononuclear cells (PBMCs) were detected from 27 TAK patients and 10 healthy controls. Compared with the healthy control group, the untreated TAK group and the treated TAK group had an increased mRNA level of TLR2 and TLR4. A sample-to-sample matrix revealed that 80% of healthy controls could be separated from the TAK patients. Correlation analysis showed that the inactive-treated TAK group exhibited a unique pattern of inverse correlations between the TLRs gene clusters (including TLR1/2/4/6/8, BCL6, TIGIT, NR4A1, *etc*) and the gene cluster associated with T-cell activation and differentiation (including TCR, CD28, T-bet, GATA3, FOXP3, CCL5, *etc*). The dynamic gene co-expression network indicated the TAK groups had more active communication between TLRs and T-cell activation than healthy controls. BCL6, CCL5, FOXP3, GATA3, CD28, T-bet, TIGIT, IκBα, and NR4A1 were likely to have a close functional relation with TLRs at the inactive stage. The co-expression of TLR4 and TLR6 could serve as a biomarker of disease activity in treated TAK (the area under curve/sensitivity/specificity, 0.919/100%/90.9%). The largest gene co-expression cluster of the inactive-treated TAK group was associated with TLR signaling pathways, while the largest gene co-expression cluster of the active-treated TAK group was associated with the activation and differentiation of T-cells. The miRNA sequencing of the plasma exosomes combining miRDB, DIANA-TarBase, and miRTarBase databases suggested that the miR-548 family miR-584, miR-3613, and miR-335 might play an important role in the cross-talk between TLRs and T-cells at the inactive stage. This study found a novel relation between TLRs and T-cell in the pathogenesis of autoimmune diseases, proposed a new concept of TLR-co-expression signature which might distinguish different disease activity of TAK, and highlighted the miRNA of exosomes in TLR signaling pathway in TAK.

Keywords: T-cell activation, Toll-like receptor, Takayasu's arteritis, disease activity, co-stimulatory molecule, immune checkpoint, biomarker, miRNA - microRNA

INTRODUCTION

Toll-like receptors (TLRs) are a type of pattern recognition receptor that can initiate multiple immune responses by combining with pathogen-associated molecular patterns (PAMPs) and damage-associated molecular patterns (DAMPs). A growing number of studies have been demonstrated that TLRs take part in the pathogenesis of many kinds of autoimmune diseases (AIDs) through several mechanisms (1–3). Recently, NI-0101, an anti-toll-like receptor 4 monoclonal antibody was used in RA, which was the first clinical trial to target TLRs to treat autoimmune diseases (4). The dearth of knowledge on the role of TLRs in the pathogenesis of Takayasu's arteritis (TAK) is especially notable when compared to the relatively higher number of studies on their role in that of rheumatoid arthritis (RA), systemic lupus erythematosus (SLE), and multiple sclerosis (MS).

TAK is a primary large vessel vasculitis mainly affecting the aorta and its major branches. Patients with onset TAK are typically female, and more than 90% of them are under 30 years old. Annual TAK incidence rates are estimated to be 1.5 cases per million in Japan, and 0.2~2.6 cases per million in Europe and North America (5). The autoimmune inflammation of TAK appears to be dominantly driven by T-cells (6). Studies have shown that there are numerous associations between TLRs and the activation and differentiation of T-cells. For instance, TLRs expressed in innate immune cells, such as DCs and macrophages, can regulate the activation and differentiation of T-cells. On the other hand, TLRs expressed in T-cells can influence T-cells more directly. For instance, TLR1 and TLR9 are highly expressed in $CD4^+$ T cells, and $CD8^+$ T cells have abundant TLR3 and TLR4 expression (7). TLR7-mediated suppression of Th17 cells does not require dendritic cell involvement (8), TLR2 signaling alters the transcriptional program of differentiating and increases the proliferation of Th17 cells (9), TLR8 signaling suppresses glucose uptake and metabolism in Treg cells (10), and TLR2 signaling enhances the movement of Treg cells (11), which all act on T-cell directly. Thus, we hypothesized that TLRs regulate the activation and differentiation of T-cells in TAK. However, there have been only two studies in the literature on TLRs in the pathogenesis of TAK in PubMed database (12, 13). Kabeerdoss et al. found that the higher mRNA expression of TLR4 and its ligand S100s in peripheral blood mononuclear cells (PBMCs) of TAK patients compared to healthy controls and that after being stimulated with TLR4 ligand (12), PBMCs from TAK patients had a higher mRNA expression of IL-1β and IL-1R2 compared to that of HC (13). Taken together, it has been currently unknown whether TLRs are related to the disease activity or the activation and differentiation of T-cells in the pathogenesis of TAK.

In organisms, genes form molecular networks, these molecular networks tend to be modular, and similar modules combine to function (14–16). If a network has a high clustering coefficient, it suggests the presence of local cliques or clusters of connected molecules (17). Genes with high expression similarity or linked by the shortest path are often involved in the same biological pathway or are subjected to shared regulatory pathways (18–21). The identification of stable and reliable gene co-expression networks is essential to unravel the interactions and functional correlations between genes (22). Analysis of the gene co-expression network is one of basic approaches currently adopted by research on the relations between two clusters of genes (14, 15).

Additionally, in this study, we defined 'co-stimulatory molecules' as both negative and positive co-stimulatory molecules (23). After T cell receptor (TCR) activation, the fate of the T cells is controlled by signals from T cell co-stimulatory molecules and cytokines largely.

The aim of this study was to determine whether a relation exists between TLRs and the activation and differentiation of T-cells in TAK and to analyze the key molecules that play an important role in this regulation. This study may provide experimental evidence for targeting TLRs in the treatment of TAK.

METHODS

Figure 1 Summarized the basic workflow of this study.

Gene Function Annotation

Universal Protein Resource (UniProt) SwissProt database was used to annotate gene functions (24).

Functional Enrichment Analysis

Functional enrichment analysis was performed by the Metascape webserver (25) (https://metascape.org/), and the pathway databases consisted of Gene Ontology (GO) (26), KEGG (27), and WikiPathways (28). Enrichment analysis was performed by using a hypergeometric test with a *p*-value cutoff of 0.01. The enrichment results were visualized using the R Package ggplot2, the R Package Circlize, and Cytoscape V. 3.8.2.

Networks Based on Public Databases

The gene co-expression network was constructed using the COEXPEDIA database (29) (www.coexpedia.org), and the protein-protein interaction (PPI) networks were constructed using the STRING database (30) (https://www.string-db.org/).

Patients

Treated TAK patients fulfilling the 1990 ACR criteria (31) were enrolled. And we assessed the disease activity of TAK by the 1994 NIH criteria (32), which included the following.

1. Systemic features, such as fever, musculoskeletal (no other cause identified).
2. Elevated ESR.
3. New onset or aggravated features of vascular ischemia or inflammation, such as claudication, diminished or absent pulse, bruit, vascular pain (carotodynia), asymmetric blood pressure in either upper or lower limbs (or both).
4. Typical angiographic features.

If a TAK patient had two or more features, he was defined as "active TAK patient"; otherwise, we diagnosed the patient was

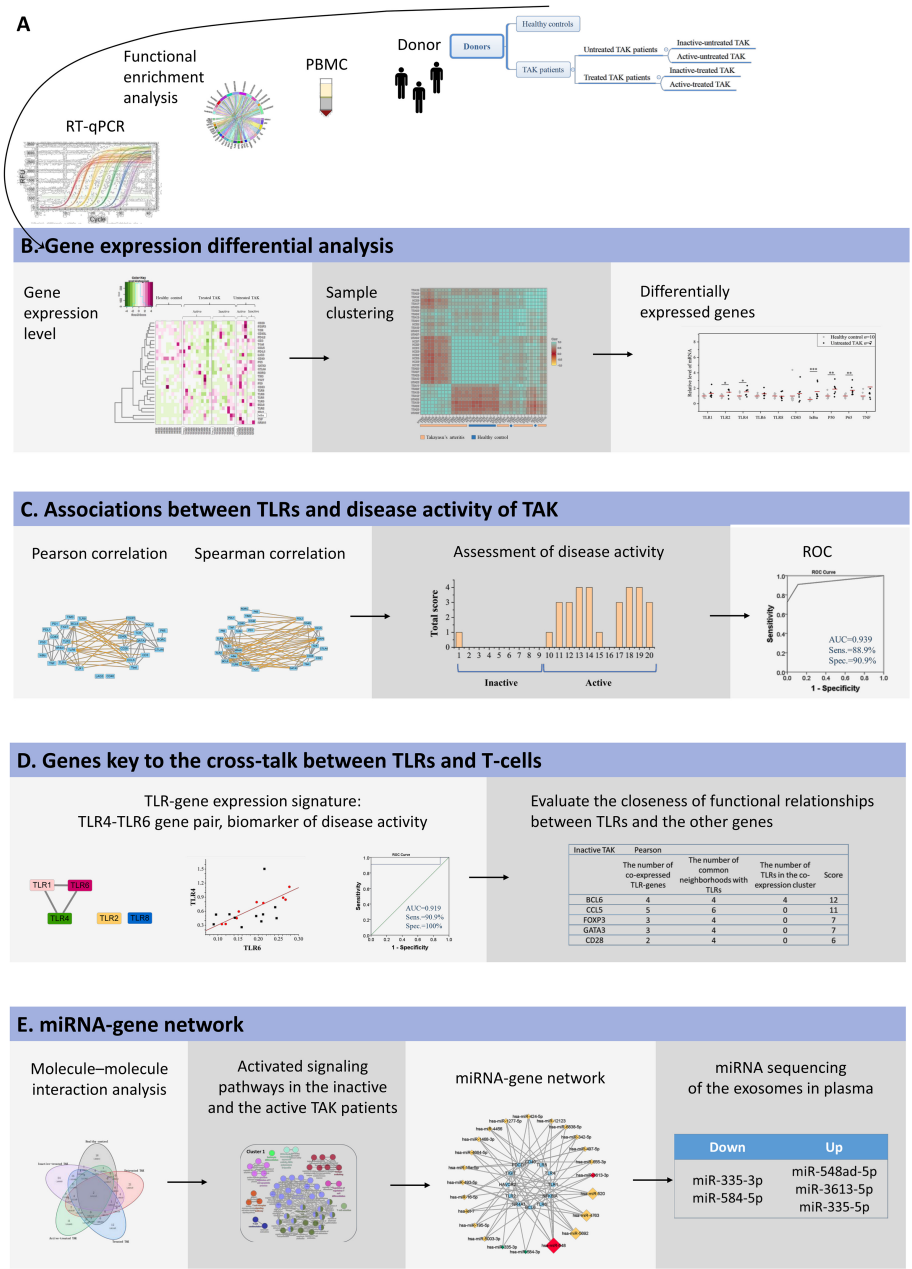

FIGURE 1 | The basic workflow of this study. **(A)** mRNA abundance of 29 target genes in PBMCs was measured using RT-qPCR, and these genes were highly enriched in TLR signaling pathways and the function of the activation and differentiation of T-cells by functional enrichment analysis. **(B)** Sample clustering analysis suggested that TAK patients had a different expression pattern of the selected genes from the healthy controls. Gene expression differential analysis demonstrated the upregulation of TLR signaling pathway in TAK, but no substantial difference in TLR signaling pathway was found between the inactive-treated TAK patients and the active-treated TAK patients. **(C)** Correlation analysis showed that the inactive-treated TAK group exhibited a unique pattern of inverse correlations between the TLRs gene cluster and the gene cluster associated with T-cell activation and differentiation, while the active-treated TAK group did not. And TLRs and their correlation cluster could distinguish active patients from inactive patients in TAK. **(D)** Dynamic gene co-expression network was constructed. TLR-co-expression signature of different stages was observed, and the degree of functional association between the other genes with TLRs was assessed. **(E)** To account for the co-expression in the greatest cluster of the inactive-treated TAK group, functional enrichment analysis, miRNA database prediction, and miRNA sequencing of plasma exosomes was performed, which indicated that miRNAs might play an important role in the cross-talk between TLR and T-cell in TAK patients.

at remission stage, and the patient was defined as "inactive TAK patient".

A patient that never received any TAK medication was defined as "untreated TAK patient", and a patient that was under treatment was defined as "treated TAK patient". Both the untreated and the treated patients were classified into the inactive group and the active group.

Written informed consent was obtained from all participants and the study was performed in accordance with the Declaration of Helsinki. And this study was approved by the Institutional Review Board of Peking Union Medical College Hospital, Beijing, China (S-478).

Collection and Processing of Human Blood Samples

PBMCs were isolated from patients by density-gradient centrifugation. Total RNA was prepared from the PBMCs using Trizol reagent (15596026, Thermo Fisher Scientific) (33). The RNA samples were diluted in RNase-free water, denatured at 65°C for 10 min. RNA concentration and purity were determined spectrophotometrically, and the RNA integrity was verified by denaturing RNA gel electrophoresis.

Real-Time Fluorescence Quantitative Polymerase Chain Reaction (RT-qPCR)

RNA was reverse transcribed using the PrimeScript™ RT reagent Kit with gDNA Eraser (RR047A, Takara). Genomic DNA (gDNA) was eliminated at 42°C for 2 min. Reverse transcription was performed using the following conditions: 37 °C for 15 min, 85 °C for 5 sec. RT-qPCR reactions were performed with the iTaqTM Universal SYBR® Green Supermix (725124, Bio-Rad) and primers were listed in **Supplementary Table 1**. The temperature cycle parameters in an Applied Biosystem 7900HT1 were: 95°C for 30 sec and 40 cycles of 95°C for 30 sec, 56°C for 30 sec and 72°C for 40 sec followed by a hold at 72°C for 40 sec. Gene expression was calculated using the $2^{-\Delta\Delta Cq}$ method. Melting curve analysis was performed from 65 to 95 °C.

The Targeted Genes

Total 29 genes were selected which were confirmed closely related to TLR signaling pathways and the function of the activation and differentiation of T-cells by GO and KEGG enrichment analysis, including BCL6, CCL5, CD28, CD3 (CD247), CD40, CD40L (CD40LG), CD83, CTLA4, FOXP3, GATA3, IκBα (NFKBIA), LAG3, NR4A1, P50 (NFKB1), P65 (RELA), PD-1 (PDCD1), PD-L1 (CD274), PD-L2 (PDCD1LG2), RORC, T-bet (TBX21), TCR (TRA), TIGIT, TIM3 (HAVCR2), TLR1, TLR2, TLR4, TLR6, TLR8, and TNF.

The Selection of Reference Genes

A list of 9 genes previously reported that were stably expressed in human PBMCs from the literature was compiled, including ACTB, β-glucuronidase, B2M, GAPDH, HPRT1, PGK1, RPL13A, SDHA, and YWHAZ. We Assessed the gene expression stability and selected the most appropriate housekeeping genes for each analysis using the geNorm (34), the NormFinder (35), and the BestKeeper software (36). As a result, B2M and YWHAZ were used as the internal reference genes for the comparison of healthy controls and untreated TAK patients, B2M and SDHA were used for the comparison of healthy controls and treated TAK patients and the comparison of the active-treated and the inactive-treated TAK patients, and HPRT1 and YWHAZ were used for the comparison of the untreated and the treated TAK patients and correlation analysis.

Dynamic Gene Co-Expression Network

We constructed the gene co-expression network of the healthy control group, the untreated TAK group, the treated TAK group, the inactive-treated TAK group, and the active-treated TAK group based on the qPCR dataset, respectively. The Pearson correlation has an advantage in predicting the interaction of molecules and is widely used as a measure of gene co-expression in many public databases (37, 38), so it was adopted the main approach in the network analysis and the results were available in the main text. However, Spearman correlation has an advantage in revealing the functional associations, so it was adopted as a complementary approach and the results are available in the **Supplementary Information** (39). Statistical analysis was performed using IBM SPSS statistic V.23 (Armonk, New York, USA). A p-value of less than 0.05 was considered significant. Cytoscape V. 3.8.2 was used to edit the networks.

Unsupervised Hierarchical Clustering Analysis and the Co-Expression Cluster

Samples were clustered based on the Pearson correlation coefficient for the profile of those 29 genes using the R package ggcorrplot. Hierarchical clustering of samples was carried out using Pearson correlation and Spearman correlation respectively (38). Data were partitioned into five clusters by cutting the clustering tree at the height of 1.0 and the co-expression clusters were defined which consist of similarly expressed genes. The clustered heatmap and hierarchical clustering trees were performed using the R package ggcorrplot and the R package ggplot2 by R V.4.1.0. A p-value of less than 0.05 was considered significant.

Scoring System for the Assessment of Disease Activity

The disease activity score was calculated using the algorithm as published before (40). To assess the disease activity of TAK, highly co-expressed gene pairs (defined as $|r| > 0.73$, $p < 0.01$) of the inactive-treated were selected. Regression equations were calculated by linear least squares. To qualify how well the data of an individual sample fit a regression line, we calculated the relative error (RE) as the ratio of the absolute error (AE) and the observed value of gene expression level. The AE is the absolute value of the difference between the predictive value and the observed value.

M-value was introduced which was equal to the RE:

$$M = \left| \left(y_{predictive\ \ value} - y_{observation}\right)/y_{observation} \right| . \quad (40)$$

Qualified the data of each sample to fit every regression line one by one. The M-value of each active or inactive patient was calculated. Then the patients were ranked by M-value. The threshold was set using the Youden index and was adjusted

when appropriate. A score of 1 was given if a patient had an *M*-value less than the threshold, 0 if a patient had an *M*-value greater than the threshold. The total score of a patient was the sum of each score of *M*-value. The threshold of the total score was set using the Youden index. Detailed protocols are available in ref.

Evaluate the Closeness of Gene-to-Gene Functional Relationships Between TLRs and the Other Genes

To predict the functional relationship between TLRs and the other genes through quantification, the following metrics were employed, and its rationale has been published (19–21, 41–43). Take BCL6 for an example.

1. The number of TLR-genes that were co-expressed with BCL6.
2. The number of common neighborhoods with TLRs. In the metric, all TLRs were processed as a whole-body corresponding to one gene.
3. The number of TLRs in the co-expression cluster that consisting of BCL6, which cluster was cut at the height of 1.0.

One gene of each metric was counted as one point. Calculated the total score of each gene assessed.

miRNA-Gene Network Prediction

The pipeline was composed of three major steps:

1. miRNAs targeting each gene were obtained from the miRDB database, which is a miRNA target prediction database (44, 45).
2. Counted the number of genes of each miRNA listed in (i), and the miRNA which targets more than one gene was selected.
3. Mapping according to the miRNA-gene pair list acquired in (ii). In this step, the miRNAs were pooled for miRNA families if there were more than one miRNA belonging to the same miRNA family.
4. Ranked the miRNAs or the miRNA family according to the number of genes targeted.

Plasma Preparation

Whole blood was collected from controls and TAK patients in ethylenediaminetetraacetic acid (EDTA) tubes and stored at 4°C. Plasma was isolated immediately from the whole blood by centrifugation (4°C, 800 × g for 10 min) in 4 hours. Then, the collected plasma was isolated by further centrifugation (4°C, 3,000 × g for 15 min) to remove cellular debris and large vesicles. Plasma samples were stored at −80°C until analysis.

Exosome Isolation and Quantification for miRNA Sequencing

Plasma samples were thawed at 37°C and filtered through a filtration membrane (0.8 μm). Next, the plasma was diluted 1:1.5 in filtered 0.01 M phosphate-buffered saline (PBS). Exosomes were purified by consecutive steps of size exclusion chromatography (SEC) on size exclusion columns and ultrafiltration tubes (100 kDa cutoff, Amicon). Successful exosome isolation was confirmed as follows.

1. Immunoblotting analysis revealed negative calnexin (Proteintech), positive CD63 (SanTAK-Cruz), positive CD9 (Proteintech), and positive TSG101(Absin).
2. Immuno-electron microscope analysis and nanoparticle tracking analysis (NTA) revealed that the isolated exosomes were 30~150 nM in diameter.

RNA was isolated using miRNeasy Mini Kit (Qiagen) from exosomes. All the RNA samples met the following RNA quality threshold.

1. The ratio of OD260/280 was between 1.8 and 2.0.
2. The RNA concentration was greater than 300 pg/μL.
3. The Cq value of miRNA-130b was less than or equal to 23.
4. 16S rRNA (-).

miRNA Sequencing

Small RNA libraries were prepared with the QIAseq miRNA Library Kit (QIAGEN). The quality of the libraries was validated on an Agilent Bioanalyzer 2100 and qPCR. Pair-end sequencing was performed on Illumina HiSeq2500.

Statistical Analysis

Normality was assessed with a Kolmogorov–Smirnov. Normally distributed continuous variables were provided as mean ± standard deviation and non-normally distributed continuous variables as median (interquartile). A Chi-square test was used for reporting associations between two categorical variables. Differences of continuous variables between groups were analyzed by the Mann–Whitney test. The correlation between gene expression levels was represented by the Pearson correlation coefficient. The models were otherwise validated by examining standardized residuals for normal distribution. Statistical analysis was performed using IBM SPSS statistic V.23 (Armonk, New York, USA). A *p*-value of less than 0.05 was considered significant.

RESULTS

Demographic Data, Clinical Features, and Laboratory Findings of Patients

Twenty-seven TAK patients were included. Based on the definition described above, 7 patients were classified into the untreated TAK group, and 20 patients were classified into the treated TAK group. Among them, 15 patients were assessed for remission, and 12 were assessed as being at the active stage following the NIH criteria described previously. Besides, 10 healthy subjects served as controls.

The demographic data and laboratory findings of patients were listed in **Supplementary Table 2**, and the individual patient data were seen in **Table 1**. There was no significant difference between the inactive-treated TAK group and the active-treated TAK group in age (p=0.82), sex (p=0.35), disease duration

TABLE 1 | Demographic data and clinical features of patients with Takayasu's arteritis.

	Age (years)	Gender	Disease duration (months)	ESR (mm/h) (ref. range, 0~20)	hs-CRP (mg/L) (ref. range, 0~8.00)	Interleukin 6 (pg/mL) (ref. range, <5.9)	TNF-α (pg/mL) (ref. range, <8.1)	Prednisone (mg/d)
Treated TAK patients (*n*=20)								
Inactive (n=11)								
# 1	32	F	3	5	1	4.4	8.8	24
# 2	51	F	12	21	2.86	3	7.5	10
# 3	39	F	88	11	2.92	2	6.4	0
# 4	34	F	51	12	0.84	2	4	5
# 5	49	F	34	9	0.17	2	6	7.5
# 6	28	F	40	7	0.91	2	6.1	7.5
# 7	26	F	5	17	0.31	2	11	45
# 8	59	F	43	12	0.44	2	4	35
# 9	37	F	44	13	0.21	2.4	5.6	10
Active (n=9)								
# 10	36	F	133	16	0.77	2	7.8	40
# 11	32	F	132	33	5.4	5.8	6.1	10
# 12	50	F	380	19	14.7	5.7	8	15
# 13	40	F	11	38	7.8	9.3	7.6	15
# 14	25	F	19	16	23.7	7.5	4	10
# 15	38	F	118	12	3.64	–	–	10
# 16	34	F	58	6	0.34	2	5.2	45
# 17	39	F	13	23	–	2.1	5.9	44
# 18	49	F	7	5	0.55	2.8	9.5	10
# 19	40	F	314	1	5.85	3.5	24.5	10
# 20	50	M	200	16	8.51	2	5.6	0
Untreated TAK patients (*n*=7)								
Inactive (n=3)								
# 21	34	F	176	7	0.34	2	4.3	0
# 22	27	F	5	14	0.16	25.7	4	0
# 23	38	F	48	5	0.32	3	4	0
Active (n=4)								
# 24	31	M	1	91	140.72	–	–	0
# 25	25	F	1	19	11.28	6.3	5.2	0
# 26	23	M	81	71	77.36	6.3	6.2	0
# 27	29	F	4	127	113.62	22.2	8.4	0

M, male; F, female; ESR, erythrocyte sedimentation rate; hs-CRP, hypersensitive- C reactive protein; TNF-α, Tumor Necrosis Factor-α; ref., reference.

(p=0.1), erythrocyte sedimentation rate (ESR) (p=0.33), IL-6 (p=0.1), tumor necrosis factor (TNF)-α (p=0.66), and the dose of corticosteroid (p=0.37). The active-treated TAK group had a higher hypersensitive-C reactive protein (hs-CRP) level than the inactive-treated TAK group (p=0.02).

Functional Enrichment Analysis and Interaction Analysis of Selected Genes

The function of the selected genes according to UniProt was summarized in **Supplementary Table 3**. To gain further insight into the function of the 29 selected genes, we performed a functional enrichment analysis based on GO, KEGG, and WikiPathways databases. The functional enrichment analysis results confirmed that the 29 selected genes were closely related to this research topic. **Figure 2A** showed these genes were highly enriched in TLR signaling pathways and the function of the activation and differentiation of T-cells. **Figure 2B** showed the one-to-one correspondence between the genes and some GO terms and KEGG pathways which were closely related to this research topic, including positive/negative regulation of T-cell activation, I-kappaB kinase/NF-kappaB signaling, and Toll-like receptor signaling pathway., and other functions or pathways that are crucial to the pathogenesis of AIDs, such as B-cell mediated immunity, regulation of interleukin production, external side of plasma membrane, NAD+ nucleosidase activity, DNA-binding transcription repressor activity, RNA polymerase II-specific, NOD-like receptor signaling pathway, RIG-I-like receptor signaling pathway, PI3K-Akt signaling pathway, and MAPK signaling pathway. The detailed enrichment results were seen in **Supplementary Table 4**.

Next, to characterize possible molecular interactions across these selected genes, we built a protein-protein interaction (PPI) map using the STRING database. **Figure 2C** showed the PPI network clustering-based K-means (k = 3). The 3 clusters were each labeled with a different color, in which the proteins were functionally related. The genes labeled as red coded the first signaling molecule of T-cell activation or co-stimulatory molecules except FOXP3, the genes labeled as blue coded key subset transcription factors, and most genes labeled as green belonged to TLR signaling pathway. Notably, NR4A1 was in the same cluster as RELA, NFKB1 and, NFKBIA. In addition to PPI networks, we also identified gene interaction using gene co-expression network (16). **Figure 2D** showed the gene co-expression network based on Coexpedia database, indicating

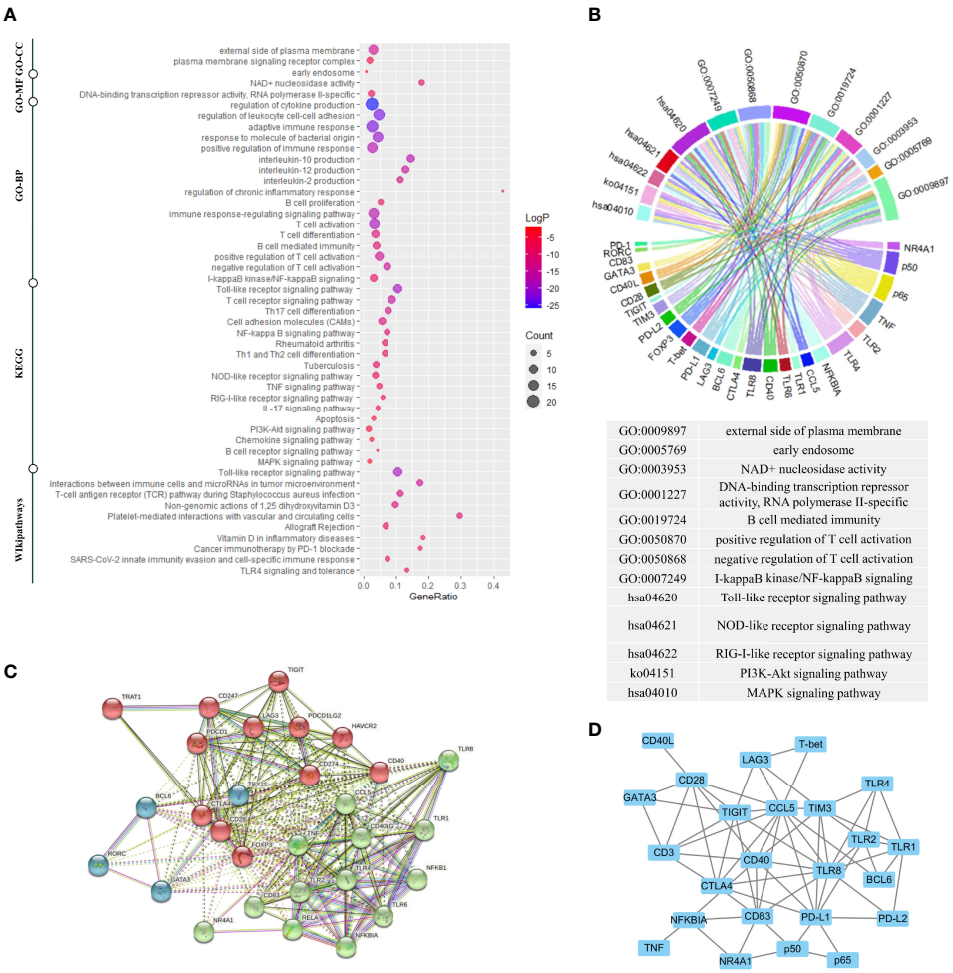

FIGURE 2 | Gene enrichment analysis, protein–protein interaction analysis, and gene co-expression analysis. **(A)** Gene enrichment analysis using multiple databases including the Kyoto Encyclopedia of Genes and Genomes (KEGG) database, the Gene Ontology (GO) database, and the WikiPathways database for targeted genes. **(B)** The genes corresponding to the enrichment results of GO analysis and KEGG analysis. **(C)** The protein–protein interaction (PPI) analysis based on the STRING database. **(D)** The gene co-expression analysis based on the COEXPEDIA database. Functional enrichment analysis indicated these genes were closely related to TLR signaling pathways and the function of the activation and differentiation of T-cells. PPI analysis and gene co-expression analysis indicated that there were strong associations among these genes, and experimental co-expression relationships would be compared with these database-interactions for newly discovered co-expression relationships.

the strong functional association among these genes. And these interactions would align with our experimental results later.

Sample Clustering Analysis and Gene Expression Differential Analysis in TLR Signaling Pathway

The heat map displayed the expression levels of the selected genes in individual samples, with red color indicating greater expression level, which showed a distinct pattern of gene expression in TAK patients compared with healthy controls, in untreated patients compared with treated patients, and in inactive patients compared with active patients (**Figure 3A**). Next, to identify the power of the selected genes to distinguish different sample groups, we performed the unsupervised hierarchical clustering of different samples based on the gene expression level calculated by Pearson correlation coefficients. A sample-to-sample matrix revealed that 80% (8/10) of healthy controls could be separated from the TAK patients by hierarchical cluster analysis, which suggested that TAK patients had a different expression pattern of the selected genes from the healthy controls (**Figure 3B**).

Among the selected genes, TLR1, TLR2, TLR4, TLR6, TLR8, CD83, IκBα, p50, p65, TNF, and CCL5 were key genes in TLR signaling pathway. As gene expression differential analysis showed, compared with the HC, the untreated TAK patients had higher mRNA levels of TLR2 (p=0.043), TLR4 (p=0.014), IκBα (p=0.00021), p50 (p=0.00046), and p65 (p=0.00031), and the treated TAK patients had higher mRNA levels of TLR2 (p=0.015), TLR4 (p=0.044), and IκBα (p=0.00016). Compared with the untreated TAK patients, the treated TAK patients had lower

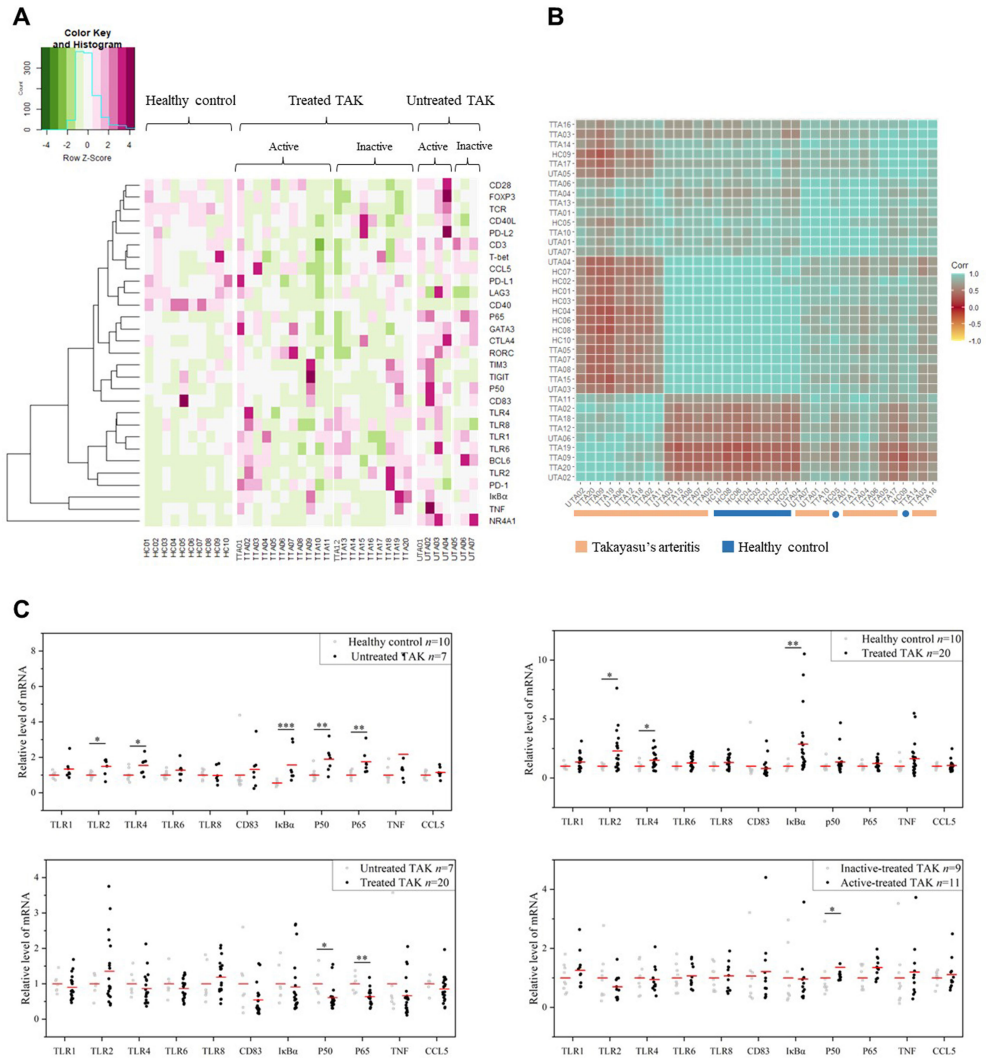

FIGURE 3 | The gene expression levels. **(A)** The heatmap showing gene expression levels with corresponding dendrograms using hierarchical clustering (Euclidean distance measure). **(B)** The heatmap of sample clustering using hierarchical clustering (Pearson correlation), suggesting that TAK patients had a different expression pattern of the selected genes from the healthy controls. **(C)** Gene expression differential analysis of TLR signaling pathway. Mann–Whitney test. *$p < 0.05$. **$p < 0.01$, ***$p < 0.001$. The red center line represented the mean value of the mRNA level. TAK, Takayasu's arteritis.

mRNA levels of p50 (p=0.013), and p65 (p=0.021). Compared the active-treated TAK patients with the inactive-treated TAK patients, p50 mRNA level (p=0.038) was higher and no increase in the mRNA level of TLRs was observed. (**Figure 3C**). Although there was evidence supporting the upregulation of TLR signaling pathway in TAK, no substantial differences in TLR signaling pathway were found between the inactive-treated TAK patients and the active-treated TAK patients.

TLRs and Their Correlation Cluster Distinguish Active Patients From Inactive Patients in TAK

To more rigorously evaluate the functional relations among these genes, we calculated the pairwise Pearson correlation and the pairwise Spearman correlation between each pair of genes. Although Pearson correlation is better suited for the establishment regression equations, we adopted Spearman correlation as a complementary analysis as Spearman correlation has some advantages in reflecting the functional associations between genes (39). Due to space limitations, most of the results based on Spearman correlation were provided in the supplementary materials, and Pearson correlation coefficient was presented in the text and adopted in the subsequent mathematical modeling. The most striking results to emerge from the data was that the inactive-treated TAK group exhibited a unique pattern of inverse correlations between the TLRs gene cluster (including TLR1/2/4/6/8, BCL6, TIGIT, NR4A1, IκBα, p50, TNF, CD83, PD-1, PD-L1, and TIM3), and the gene cluster associated with T-cell activation and differentiation (including TCR, CD28, T-bet, GATA3, FOXP3, CCL5, CD3, CD40L,

CTLA4, PD-L2), either performed by Pearson correlation (**Figure 4A**) or Spearman correlation analysis (**Supplementary Figure 1A**) analysis, while the active-treated TAK group did not (**Figure 4B** and **Supplementary Figure 1B**). To more clearly demonstrate this feature, **Supplementary Figures 1C–F** only showed the high correlations (defined as $|r| > 0.73$, $p < 0.01$).

CCL5 is a potent chemoattractant for blood monocytes, memory T-helper cells, and eosinophils, which is important in recruiting T-cells into inflammatory sites, and also activates the apoptotic cell death pathway in T cells (46). Among these inverse correlations, CCL5 was negatively co-expressed with TLR1 (Pearson's r= -0.675, p= 0.046), TLR2, TLR4 (Pearson's r= -0.878, p= 0.002), TLR6 (Pearson's r= -0.903, p= 0.001), and TLR8 (Pearson's r= -0.818, p= 0.007), and T-bet was negatively co-expressed with TLR4 (Pearson's r= -0.713, p= 0.031), TLR6 (Pearson's r= -0.755, p= 0.019), and TLR8 (Pearson's r= -0.837,

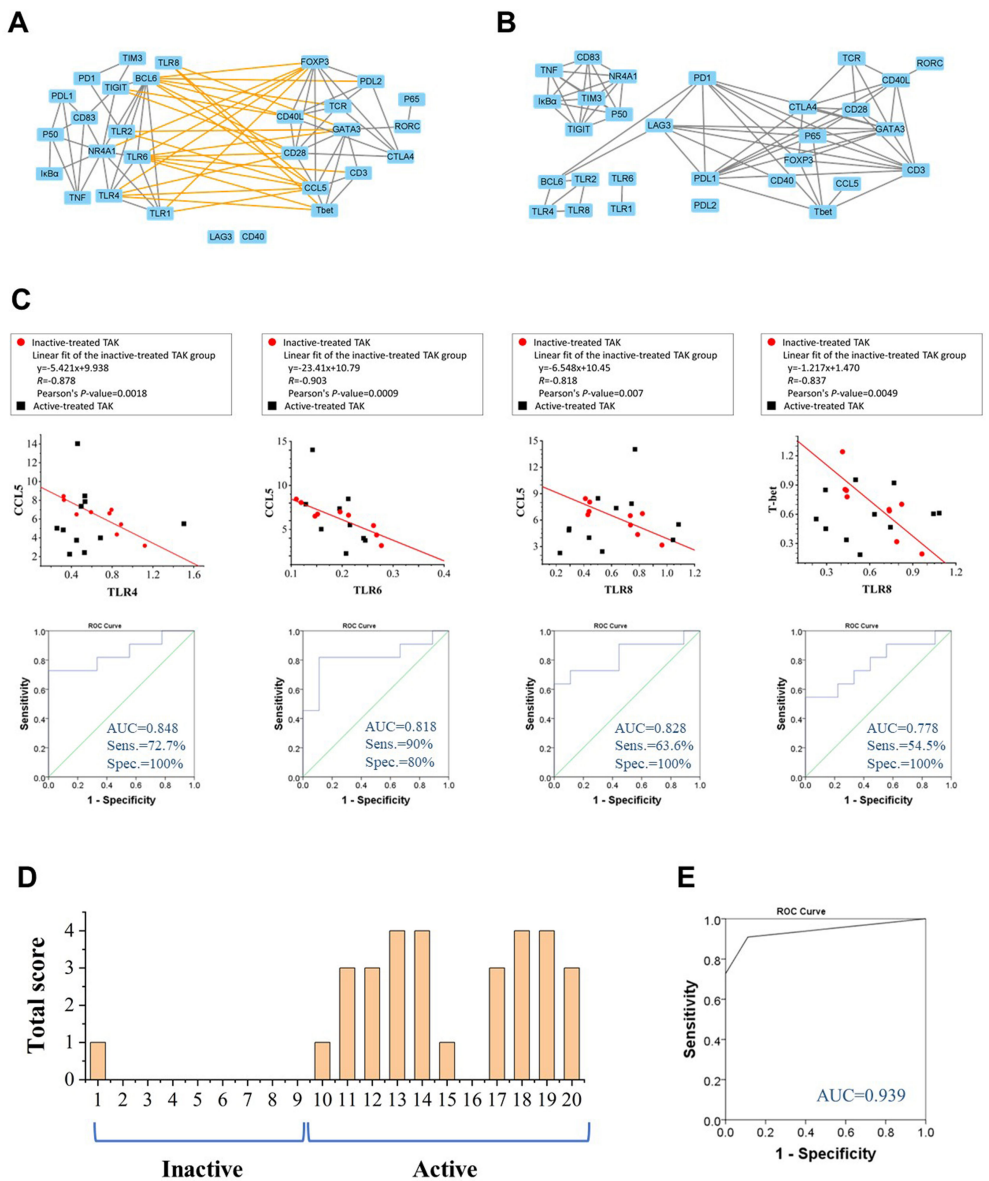

FIGURE 4 | Toll-like receptors (TLRs) and their correlation cluster distinguish active patients from inactive patients in TAK. **(A, B)** The Pearson correlation between the expression levels of each gene pair of the inactive-treated TAK group **(A)** and the active-treated TAK group **(B)** showed that the inactive-treated TAK group exhibited a unique pattern of inverse correlations between the TLRs gene cluster and the gene cluster associated with T-cell activation and differentiation, while the active-treated TAK group did not. **(C)** The scatter plots, the linear regression, and the receiver operating characteristic curve (ROC) of the TLR4-CCL5 pair, the TLR6-CCL5 pair, the TLR8-CCL5 pair, and the TLR8-Tbet pair. **(D, E)** The ROC analysis was used to evaluate the assessment accuracy for the disease activity of TAK. The total score of each treated-TAK patient **(D)** and the ROC **(E)** when assessing the disease activity using the summed scoring system consisting of the above 4 gene pairs. TAK, Takayasu's arteritis.

p= 0.005). We took the TLR4-CCL5 pair, the TLR6-CCL5 pair, the TLR8-CCL5 pair, and the TLR8-T-bet pair to establish linear regression models to assess the disease activity, and the values of AUC/sensitivity/specificity were 0.848/72.7%/100%, 0.818/63.6%/100%, 0.828/90%/80%, and 0.778/54.5%/100%, respectively (**Figure 4C**). We then calculated the total score from the above 4 gene-pair models for each patient to assess the disease activity as mentioned in *Method*, the AUC, the sensitivity, the specificity, the positive predictive value, and the negative predictive value were 0.939, 90.9%, 88.9%, 90.9%, and 88.9%, respectively, which had greater diagnostic accuracy than did the single models (**Figures 4D, E**). The assessment of individual patients was shown in **Supplementary Table 5**. The above results suggest that TLRs have a potential relationship with the disease activity of TAK, which requires further explanation.

Topological Analysis of Dynamic Gene Co-Expression Network Identifies the Functional Association Between TLRs and T-Cell Activation in TAK

The More Active Communication Between TLRs and T-Cell Activation in TAK Compared to Healthy Control

Gene co-expression network analysis is a useful method to link tightly co-expressed gene modules to phenotypic traits (47). To determine gene modules associated with distinct disease stages of TAK, we constructed a dynamic gene co-expression network for each group based on the pairwise Pearson correlations or Spearman correlations for all genes. (**Figure 5** and **Supplementary Figure 2**). Unsupervised hierarchical clustering was used to assess the function of genes. As a result, genes were organized into 5 clusters by cutting the clustering tree at the height of 1.0, which was indicated by red frames. Notably, genes belonging to the same cluster were like to have similar functions and were labeled with the same color. In active-treated TAK, the 5 clusters were as follows.

1. Cluster No. 1 (cutting the clustering tree at the height of 2.0)
    a. TLR1, TLR2, TLR4, TLR6, TLR8, and BCL6.
    b. CD83, TNF, NR4A1, IκBα, p50, NR4A1, TIM3, and TIGIT.
    c. CD40, PD-L1, PD-L2, LAG3, CD3, and p65.
2. Cluster No. 2 (cutting the clustering tree at the height of 2.0)
    a. TCR, CD28, CD40L, CTLA4, GATA3, and RORC.
    b. T-bet, CCL5, FOXP3, and PD-1

In inactive-treated TAK, the 5 clusters were as follows.

1. Cluster No. 1 (cutting the clustering tree at the height of 2.0)
    a. TLR1, TLR4, TLR6, BCL6, and CD40.
    b. TLR2, PD-1, TIM3, LAG3, TIGIT, and NR4A1.
2. Cluster No. 2 (cutting the clustering tree at the height of 2.0)
    a. TCR, CD28, CD40L, CTLA4, FOXP3, and PD-L2.
    b. CD3, CCL5, T-bet, GATA3, RORC, IκBα, and p65.
    c. PD-L1, p50, CD83, and TNF.

Comparing the two results, it could be seen that the 29 genes were divided into two broad categories: (i) TLR signaling pathway and (ii) the activation and differentiation of T-cells. But compared with the inactive group, CD83, TNF, IκBα, p50, p65 as well as the co-stimulatory molecules (including PD-L1, PD-L2, and LAG3) were more closely related to TLRs in the active group. Besides, to present the main framework of the network clearer, another dynamic network with the observed value of the Pearson correlation was 0.01 was shown in the right column of **Figure 5** and **Supplementary Figure 2**. This co-expression clustering revealed a functional association among the genes, providing insight into gene functions and networks.

To assess the functional communication among these genes at distinct stages, we calculated a number of topological network parameters commonly used to describe the network. Each of these networks had a short characteristic path length and a large clustering coefficient, suggesting that they participate in the biological processes that might be functionally related. Additionally, compared with the healthy controls, the active-treated TAK and the inactive-treated TAK showed shorter characteristic path length (healthy controls vs. active-treated TAK vs. inactive-treated TAK, Pearson correlation 3.265 vs. 2.362 vs. 2.333, Spearman correlation 4.410 vs. 2.439 vs. 3.392) and a larger clustering coefficient (Pearson correlation 0.317 vs. 0.581 vs. 0.549, Spearman correlation 0.432 vs.0.489 vs. 0.470), indicating the more active functional communication among these genes in TAK groups compared to healthy controls. The detailed parameters of these networks are shown in **Table 2**.

TLR-Co-Expression Signature: The Regression Equation Relating the TLR6 mRNA Level to the TLR4 mRNA Level Serves as a Biomarker of Active Disease in Treated TAK

There was a tight interplay among TLRs. **Figure 6A** was the PPI network based on the STRING database analysis. TLRs function as a homodimer or heterodimer, such as TLR1/TLR2, TLR2/TLR6, and TLR4/TLR6. Besides, there is some cross-talk between TLRs, for example, TLR7 and TLR9 (**Figure 6B**). Interestingly, the co-expressed-TLR-pairs in different groups were different (**Figure 6C**). The inactive-treated TAK group had high co-expression of TLR1 and TLR4 (r=0.804, p=0.009) which was absent in the active-treated TAK group, the untreated TAK group, or the HC group. The high co-expression of TLR4 and TLR6 (r=0.892, p=0.001) exist in the HC group (r=0.847, p=0.002) as well as the inactive-treated TAK group (r=0.892, p=0.001), while was absent in the active-treated TAK group. The different co-expressions might mean different functional relationships between TLRs at different stages.

Studies have found that a heterodimer of TLR4 and TLR6 promote a protracted sterile inflammatory response after being triggered by oxidized low-density lipoprotein (LDL) and β-amyloid, which involves the pathogenesis of atherosclerosis and Alzheimer's disease (48–50). We found that the regression equation relating the TLR6 mRNA level to the TLR4 mRNA level might be a biomarker of active disease in treated TAK. **Figure 6D** showed the scatter plots illustrating the difference in the co-expression of TLR4 and TLR6 between the inactive-treated TAK and the active-treated TAK. The points of the active-treated TAK group, except the point presented Patient No. 12, were scattered around the fitted line of the scatter points of the inactive-treated

TABLE 2 | Parameters of gene co-expression networks.

	Healthy control (n = 10)	Untreated patients with TAK (n = 7)	Treated patients with TAK (n = 20)	Treated patients with inactive TAK (n = 9)	Treated patients with active TAK (n = 11)
Pearson correlation					
Nodes	29	29	29	29	29
Edges	46	42	95	79	72
Average number of neighbors	3.286	3.154	6.552	5.852	5.263
Network diameter	7	11	4	6	6
Clustering coefficient	0.317	0.285	0.632	0.581	0.549
Characteristic path length	3.265	4.025	2.155	2.362	2.333
Spearman correlation					
Nodes	29	29	29	29	29
Edges	43	22	114	89	66
Average number of neighbors	3.071	2.222	8.143	6.357	4.714
Network diameter	11	9	4	6	9
Clustering coefficient	0.432	0.213	0.597	0.489	0.470
Characteristic path length	4.410	4.144	1.910	2.439	3.392

TAK, Takayasu's arteritis.

TAK group. The regression model was established and the threshold of *M*-value for assessing the disease activity was set to 0.173 according to the Youden index. Patients with an *M*-value of more than 0.173 got one score and were assessed as being in the active stage. And the AUC, the sensitivity, specificity, positive predictive value, and negative predictive value were 0.919, 100%, 90.9%, 100%, and 90%, respectively (**Figures 6E, F**). The details of the assessment were shown in **Supplementary Table 6**. The results indicated that the inactive stage of TAK could be characterized from the treated TAK by the co-expression of several TLR genes.

Genes Key to the Cross-Talk Between TLRs and the Activation and Differentiation of T-Cell in TAK

To identify genes closely related to TLRs in these genes key to the activation and differentiation of T-cells, we assessed the degree of functional association between the other genes were to TLRs, and the evaluation protocol is described in *Method*. Specific scores are shown in **Table 3** and the results are detailed below. In inactive-treated TAK, most of the genes exhibited functional association with TLRs. The 7 genes with the highest scores were BCL6 (12), CCL5 (11), FOXP3 (7), GATA3 (7), CD28 (6), T-bet (6), and NR4A1 (6) according to Pearson correlation analysis, and the 5 genes with the highest scores were BCL6 (16), TIGIT (14), IκBα (13), NR4A1 (12), and FOXP3 (11) according to Spearman correlation analysis. However, in the active-treated group, the functional association between these genes and TLRs did not seem to be as strong as the inactive-treated group **(Table 3**). The 3 genes with the highest scores were BCL6 (7), PD-1 (1), and LAG3 (1) according to Pearson correlation analysis, and the 5 genes with the highest scores were BCL6 (3), CD40 (3), and LAG3 (3) according to Spearman correlation analysis.

Due to space restrictions, we only showed the visualized results of BCL6 and FOXP3. BCL6 is the master transcriptional regulator of Tfh cell differentiation, which is required for germinal center formation and antibody affinity maturation (51). As gene expression differential analysis showed, compared to the healthy controls, both the untreated TAK group (p=0.007) and the treated TAK group (p=0.006) had an increased mRNA level of BCL6 (**Figure 7A**). In the inactive-treated TAK group, BCL6 was co-expressed with TLR1 (Pearson's r=0.700, p=0.036. Spearman's r=0.733, p=0.025), TLR2 (Pearson's r=0.783, p=0.013. Spearman's r=0.900, p=0.001), TLR4 (Pearson's r=0.890, p=0.0013. Spearman's r=0.817, p=0.007), and TLR6 (Pearson's r=0.870, p=0.0023. Spearman's r=0.900, p=0.001) (**Figure 7B**). In the inactive-treated TAK group, according to Pearson correlation analysis, BCL6 and TLR1/2/4/6/8 shared 4 co-expressed genes, including FOXP3, CCL5, NR4A1, and CD28, and according to Spearman correlation analysis, BCL6 and TLR1/2/4/6/8 shared 8 co-expressed genes, including FOXP3, IκBα, TIGIT, CCL5, NR4A1, CD28, GATA3, and TCR (**Figures 7C–F**).

FOXP3 is a transcriptional regulator which is crucial for the development and inhibitory function of regulatory T-cells (Treg) (52). As gene expression differential analysis showed, compared to the inactive-treated TAK group, the active-treated TAK group had an increased mRNA level of FOXP3 (p=0.004) (40) (**Figure 8A**). In the inactive-treated TAK group, FOXP3 was co-expressed with TLR1 (Pearson's r=0.774, p=0.014. Spearman's r=0.800, p=0.010), TLR4 (Pearson's r=0.883, p=0.0002. Spearman's r=0.883, p=0.002), and TLR6 (Pearson's r=0.840, p=0.005. Spearman's r=0.917, p=0.001) (**Figure 8B**). In the inactive-treated TAK group, according to Pearson correlation analysis, BCL6 and TLR1/2/4/6/8 shared 4 co-expressed genes, including BCL6, CCL5, NR4A1, and CD28, and according to Spearman correlation analysis, BCL6 and TLR1/2/4/6/8 shared 8 co-expressed genes, including BCL6, IκBα, TIGIT, CCL5, NR4A1, CD28, CD83, and TCR (**Figures 8C–F**).

NR4A1 is a key transcription factor that drives T cell dysfunction and plays an important role in the apoptosis of

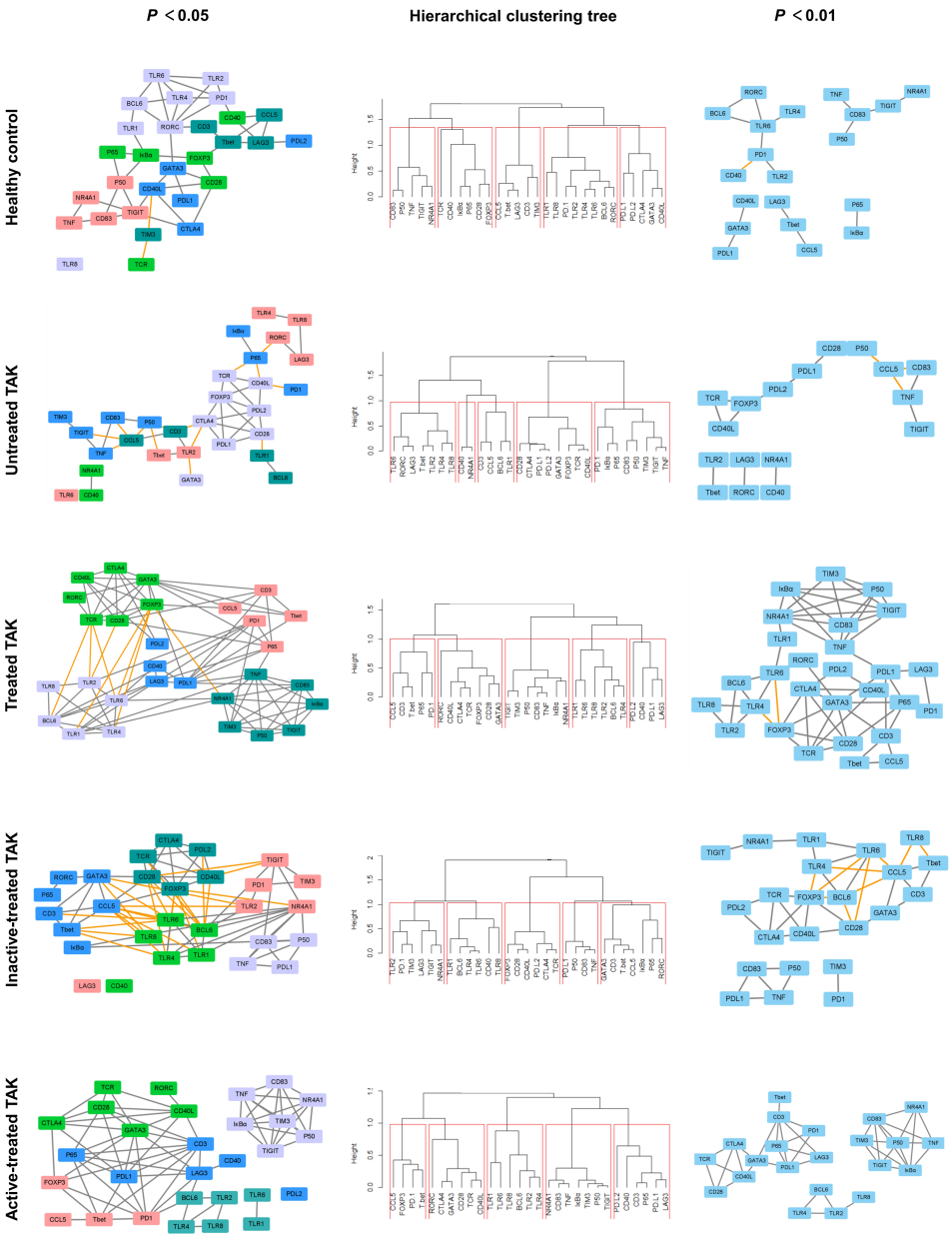

FIGURE 5 | Dynamic gene co-expression networks based on Pearson correlation. Left panel, the gene co-expression networks consisting of correlation with a *p*-value less than 0.05. Right panel, to more clearly demonstrate this feature, only the high correlations (defined as $|r| > 0.73$, $p < 0.01$) were shown. Middle panel, the hierarchical clustering trees using complete method. As a result, genes were organized into 5 clusters by cutting the clustering tree at the height of 1.0, which was indicated by red frames. Genes belonging to the same cluster were like to have similar functions and were labeled with the same color. The negative correlation was indicated by the yellow edge, while the positive correlation was gray in the networks.

self-reactive T cells (53, 54). The results suggested that NR4A1 is likely to be functionally related to TLRs in TAK. Compared to the healthy controls, the untreated TAK group (p=0.0001) had an increased mRNA level of NR4A1, and that compared to the untreated TAK group, the treated TAK group (p=0.000005) had a decreased mRNA level of NR4A1 (**Supplementary Figure 3**).

The details of the assessment were provided in **Supplementary Table 7**.

Different Signaling Pathways at Distinct Stages in TAK

To explore the possible mechanism and signaling pathways, we summarized the co-expression variations across different conditions, which reflected changes in the activated signaling pathways (**Figure 9A**). Compared with the HC group, the untreated TAK group had 35 gene co-expression relations uniquely and lost 39 gene co-expression relations. Compared with the untreated TAK group, the

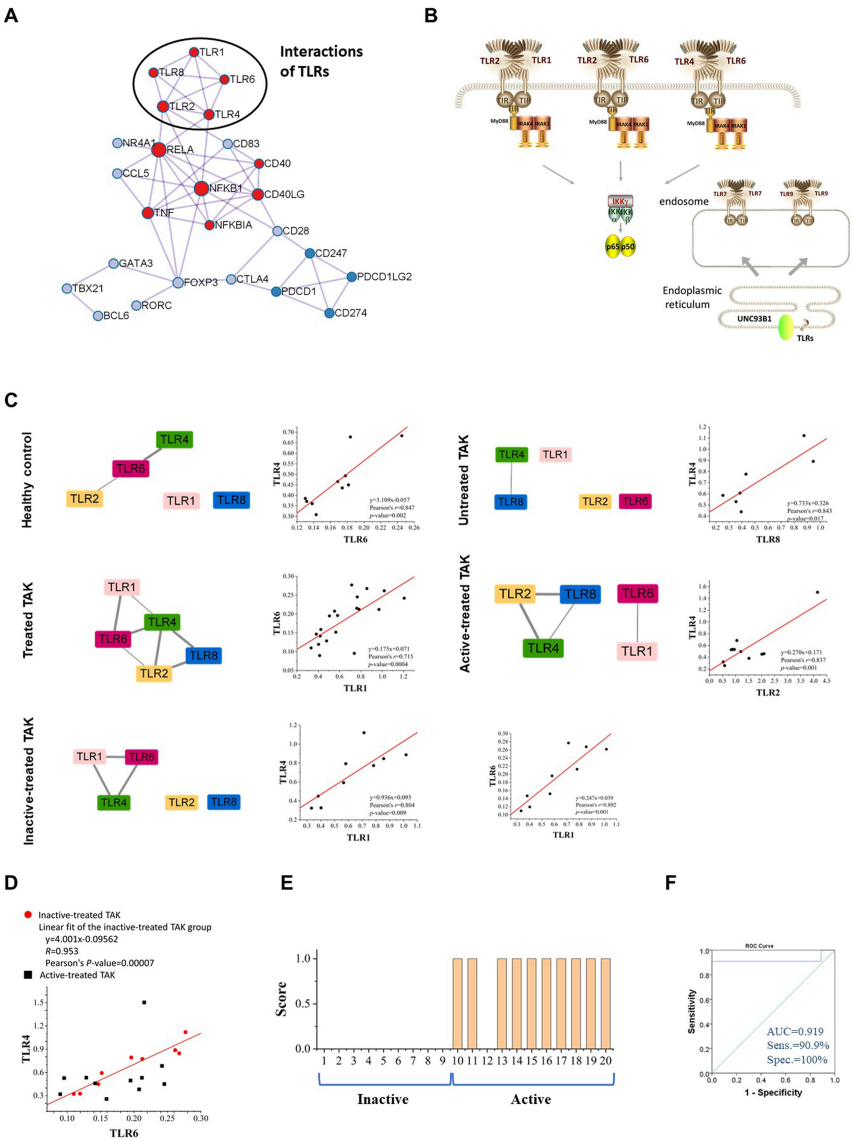

FIGURE 6 | TLR-expression signature serves as a biomarker of different disease and treatment stages in TAK. **(A)** The protein-protein interaction network using the molecular complex detection (MCODE) algorithm performed by Metascape database, indicating the tight relationship among TLRs. **(B)** The schematic drawing of the interaction or cross-talk between TLRs. **(C)** The TLR-expression signature of different disease and treatment stages of TAK and scatter plots, and the different co-expressions might mean different functional relationships between TLRs at different stages. **(D, E)** The regression equation relating the TLR6 mRNA level to the TLR4 mRNA level serves as a biomarker of active disease in treated TAK. The scatter plots **(D)**, the linear regression **(D)**, the score for the disease activity assessment of each treated TAK patient **(E)**, and the receiver operating characteristic curve (ROC) **(F)** of the TLR4-TLR6 pair. TAK, Takayasu's arteritis.

treated TAK group had 80 gene co-expression relations uniquely and lost 27 gene co-expression relations. Compared with the inactive-treated TAK group, the active-treated TAK group had 47 gene co-expression relations uniquely and lost 54 gene co-expression relations. As the treated TAK group, the inactive-treated TAK group, and the active-treated TAK group had so many gene co-expression relations that the relations with a *p*-value less than 0.01 were listed only, and the complete list was shown in **Supplementary Table 8**. We also built a Venn diagram to visualize overlapping co-expressions among the five conditions (**Figure 9B**). Besides, the newly discovered co-expression relationships which had never been reported in STRING or Coexpedia database were indicated red in **Figure 9A**. The results showed the differences in signaling pathways at distinct stages.

Next, to classify the genes based on function, the heatmaps of hierarchical clustering based on the Pearson correlation were conducted (**Figure 9C**). The heatmap of the treated TAK group was shown in **Supplementary Figure 4**. Notably, the five heatmaps of five groups had different clustering structures. The two largest clusters of each group for the subsequent analyses are detailed below.

TABLE 3 | Evaluation the closeness of gene-to-gene functional relationships between TLRs and the other genes.

Gene	Pearson correlation				Gene	Spearman correlation			
	The number of co-expressed TLR-genes	The number of common neighborhoods with TLRs	The number of TLRs in the co-expression cluster	Score		The number of co-expressed TLR-genes	The number of common neighborhoods with TLRs	The number of TLRs in the co-expression cluster	Score
Treated patients with inactive TAK									
BCL6	4	4	4	12	BCL6	4	8	4	16
CCL5	5	6	0	11	TIGIT	4	6	4	14
FOXP3	3	4	0	7	IκBα	4	5	4	13
GATA3	3	4	0	7	NR4A1	2	6	4	12
CD28	2	4	0	6	FOXP3	3	8	0	11
T-bet	3	3	0	6	CCL5	5	5	0	10
NR4A1	3	2	1	6	CD28	3	6	0	9
CD3	1	3	0	4	GATA3	3	4	0	7
CD40	0	0	4	4	T-bet	3	2	0	5
TIGIT	0	3	1	4	TCR	1	4	0	5
TCR	0	3	0	3	CD40L	0	5	0	5
CD40L	0	3	0	3	CD83	1	3	0	4
CTLA4	0	2	0	2	PD-L2	0	3	1	4
PD-1	1	0	1	2	LAG3	0	0	4	4
PD-L2	0	2	0	2	TNF	1	3	0	4
TIM3	0	1	1	2	CD3	0	2	0	2
CD83	0	1	0	1	P50	0	2	0	2
IκBα	0	1	0	1	CD40	0	1	0	1
P50	0	1	0	1	CTLA4	0	1	0	1
RORC	0	1	0	1	PD-L1	0	1	0	1
LAG3	0	0	1	1	P65	0	0	0	0
TNF	0	1	0	1	PD-1	0	0	0	0
P65	0	0	0	0	RORC	0	0	0	0
PD-L1	0	0	0	0	TIM3	0	0	0	0
Treated patients with active TAK									
BCL6	2	0	5	7	BCL6	0	1	2	3
PD-1	0	1	0	1	CD40	0	1	2	3
LAG3	0	1	0	1	LAG3	1	0	2	3
CD28	0	0	0	0	PD-L2	0	0	2	2
CD3	0	0	0	0	CD83	1	0	0	1
CD40	0	0	0	0	IκBα	1	0	0	1
CD83	0	0	0	0	P50	0	1	0	1
CTLA4	0	0	0	0	TIGIT	0	1	0	1
FOXP3	0	0	0	0	TIM3	0	1	0	1
GATA3	0	0	0	0	TNF	0	1	0	1
IκBα	0	0	0	0	NR4A1	0	1	0	1
P50	0	0	0	0	CD28	0	0	0	0
P65	0	0	0	0	CD3	0	0	0	0
PD-L1	0	0	0	0	CTLA4	0	0	0	0
PD-L2	0	0	0	0	FOXP3	0	0	0	0
RORC	0	0	0	0	GATA3	0	0	0	0
T-bet	0	0	0	0	P65	0	0	0	0
TCR	0	0	0	0	PD-1	0	0	0	0
TIGIT	0	0	0	0	PD-L1	0	0	0	0
TIM3	0	0	0	0	RORC	0	0	0	0
CCL5	0	0	0	0	T-bet	0	0	0	0
CD40L	0	0	0	0	TCR	0	0	0	0
TNF	0	0	0	0	CCL5	0	0	0	0
NR4A1	0	0	0	0	CD40L	0	0	0	0

BCL6, BCL6 transcription repressor; CD3, CD247; PD-1, programmed cell death 1, also known as PDCD1; PD-L1, CD274; PD-L2, PDCD1LG2; LAG3, lymphocyte activating 3; CTLA4, cytotoxic T-lymphocyte associated protein 4; FOXP3, forkhead box P3; GATA3, GATA binding protein 3; IκBα, NFκB inhibitor alpha; NFKB1 NFKB1, nuclear factor kappa B (NFκB) subunit 1, also known as p50; RELA, RELA proto-oncogene NFκB subunit, also known as p65; PD-L1, CD274; PD-L2, programmed cell death 1 ligand 2 also known as PDCD1LG2; RORC, RAR related orphan receptor C; T-bet, T-box transcription factor 21, also known as TBX21; TCR, T cell receptor; TIGIT, TNF superfamily member 14; HAVCR2, hepatitis A virus cellular receptor 2, also known as TIM3; CCL5, C-C motif chemokine ligand 5; CD40L, CD40LG; TNF, tumor necrosis factor;TAK, Takayasu's arteritis; TLRs, Toll-like receptors.

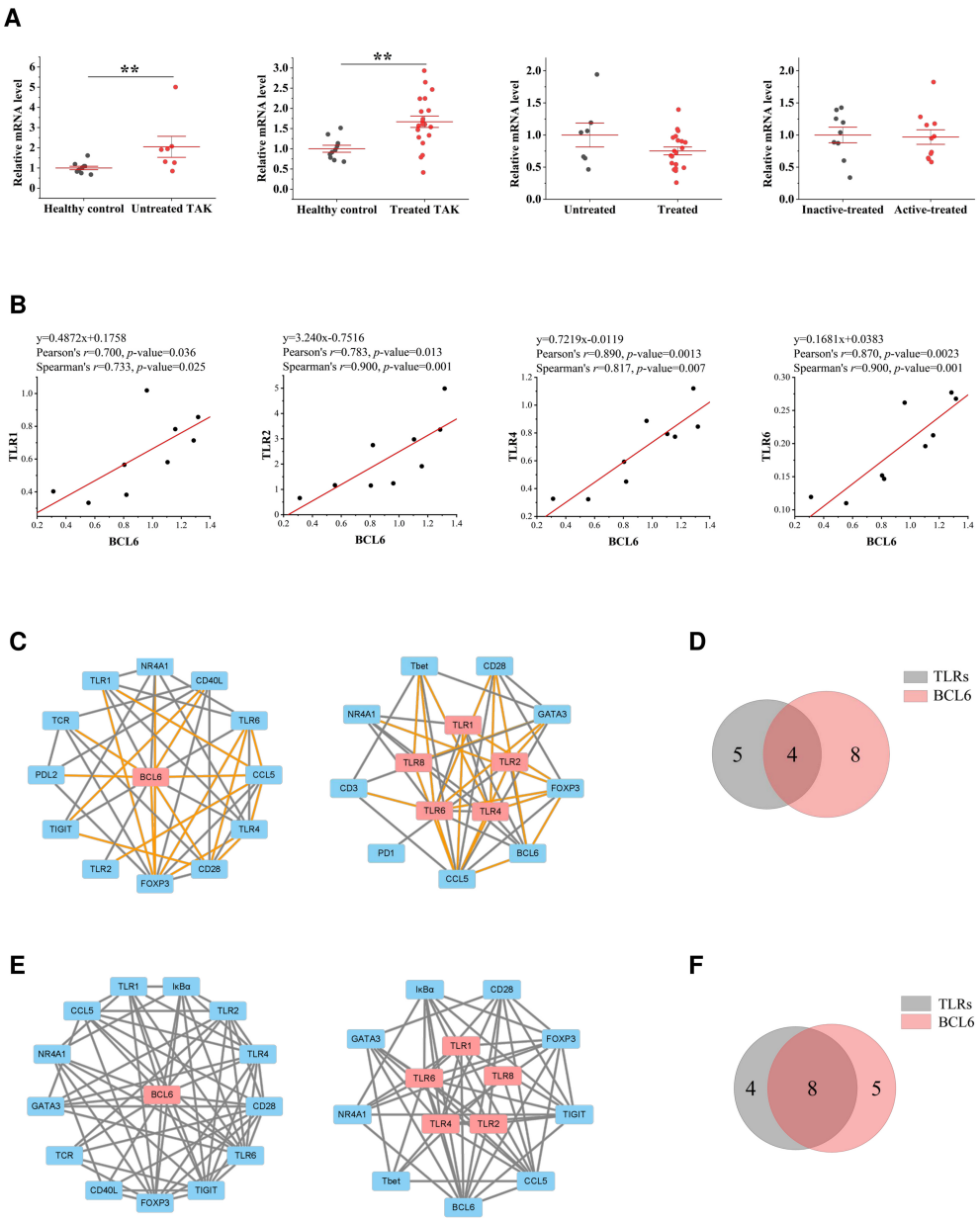

FIGURE 7 | The close functional relationship between BCL6 and Toll-like receptors (TLRs) in inactive-treated TAK. **(A)** Gene expression differential analysis. Mann–Whitney test. $^{**}p < 0.01$. The red center line represented the mean value of the mRNA level, and the error bar showed the standard deviation. **(B)** The scatter plots and the linear regression of the BCL6-TLR1 pair, the BCL6-TLR2 pair, the BCL6-TLR4 pair, and the BCL6-TLR6 pair in the inactive-treated TAK group, indicating that BCL6 was co-expressed with multiple TLRs. **(C)~(F)** BCL6 and TLRs shared multiple co-expressed genes. **(C)** The gene co-expression network consisting of BCL6 (left panel) or TLRs (right panel) and its/their neighborhoods based on Pearson correlation. **(D)** Intersections of the neighborhood-gene between BCL6 and TLRs based on Pearson correlation. **(E)** The gene co-expression network consisting of BCL6 (left panel) or TLRs (right panel) and its/their neighborhoods based on Spearman correlation. **(F)** Intersections of the neighborhood-gene between BCL6 and TLRs based on Spearman correlation. Healthy controls, n=10 people. Untreated TAK, n=7 people. Treated TAK, n=20 people. Active-treated TAK. n=11 people. Inactive-treated TAK, n=9 people. TAK, Takayasu's arteritis.

1. In the active-treated TAK (**Figure 10A**).
    a. Cluster 1 contained 14 genes, including CD274, LAG3, RELA, PDCD1, CD247, TRA, CD40LG, CD28, GATA3, CTLA4, FOXP3, TBX21, CCL5, and RORC.
    b. Cluster 2 contained 7 genes, including NFKB1, HAVCR2, TIGIT, NFKBIA, CD83, TNF, and NR4A1.
2. In the inactive-treated TAK (**Figure 10B**).
    a. Cluster 1 contained 13 genes, including TLR1, TLR2, TLR4, TLR6, TLR8, BCL6, NR4A1, NFKBIA, LAG3, HAVCR2, TIGIT, PDCD1, and CD40.
    b. Cluster 2 contained 6 genes, including TRA, CD40LG, CTLA4, PDCD1LG2, CD28, FOXP3.

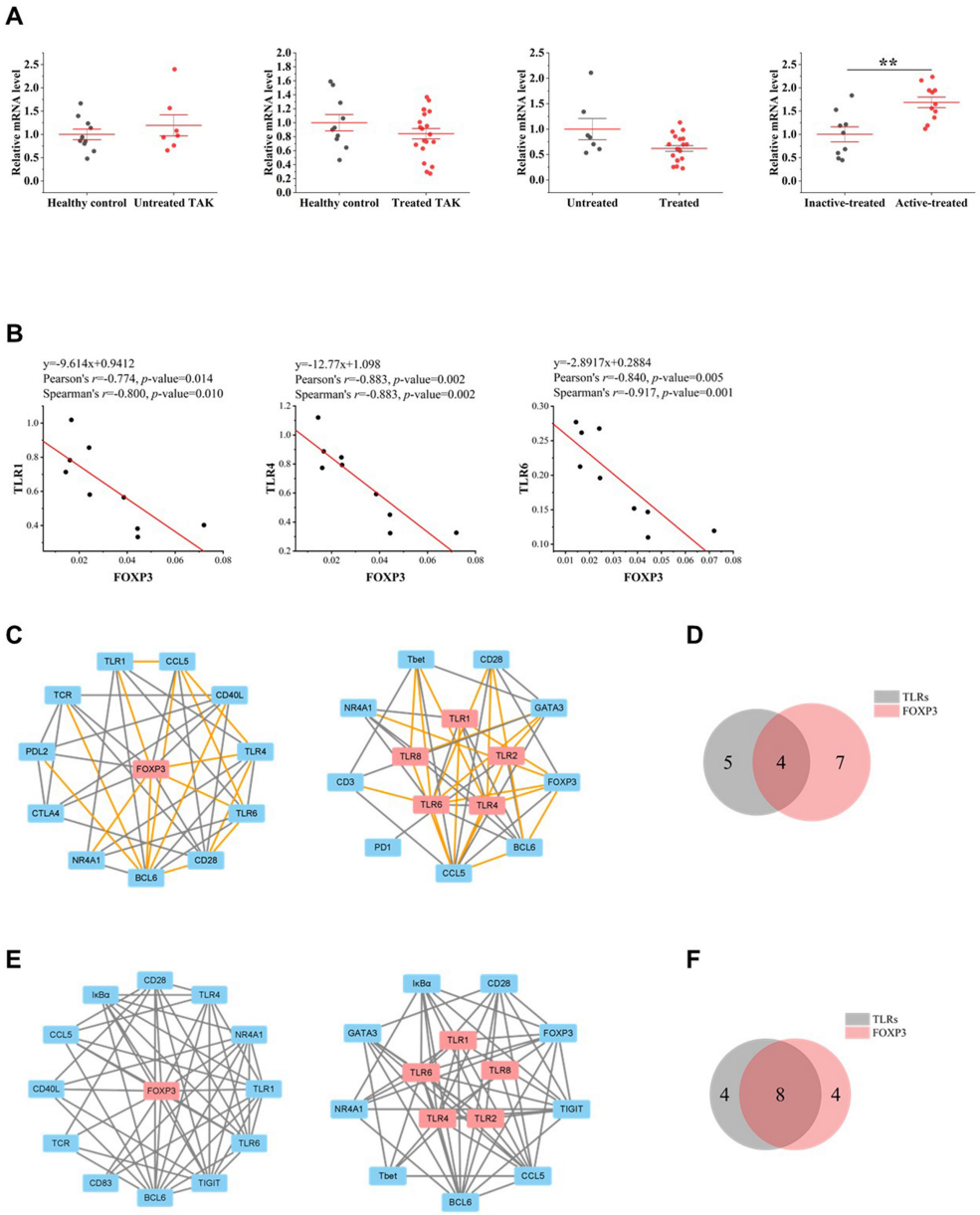

FIGURE 8 | The close functional relationship between FOXP3 and Toll-like receptors (TLRs) in inactive-treated TAK. **(A)** Gene expression differential analysis. Mann–Whitney test. $^{**}p < 0.01$. The red center line represented the mean value of the mRNA level, and the error bar showed the standard deviation. **(B)** The scatter plots and the linear regression of the FOXP3-TLR1 pair, the FOXP3-TLR4 pair, and the FOXP3-TLR6 pair in the inactive-treated TAK group, indicating that FOXP3 was co-expressed with multiple TLRs. **(C)~(F)** FOXP3 and TLRs shared multiple co-expressed genes. **(C)** The gene co-expression network consisting of FOXP3 (left panel) or TLRs (right panel) and its/their neighborhoods based on Pearson correlation. **(D)** Intersections of the neighborhood-gene between FOXP3 and TLRs based on Pearson correlation. **(E)** The gene co-expression network consisting of FOXP3 (left panel) or TLRs (right panel) and its/their neighborhoods based on Spearman correlation. **(F)** Intersections of the neighborhood-gene between FOXP3 and TLRs based on Spearman correlation. Healthy controls, n=10 people. Untreated TAK, n=7 people. Treated TAK, n=20 people. Active-treated TAK. n=11 people. Inactive-treated TAK, n=9 people. TAK, Takayasu's arteritis.

Additionally, we performed GO enrichment analysis to further explore the signaling pathways associated with the abovementioned clusters using Metascape database, and visualized the enrichment results using ClueGO to interrogate functionally grouped gene ontology. The enrichment results are detailed below. As the results showed, in the active-treated TAK group, genes in Cluster 1 were significantly enriched in the signaling pathways related to the activation and differentiation of T-cells, while genes in Cluster 2 were significantly enriched for the regulation of cytokine production and response to bacterium and lipopolysaccharide (**Figure 10C**). In the inactive-treated TAK group, genes in Cluster 1 were enriched for the regulation of cytokine production, the

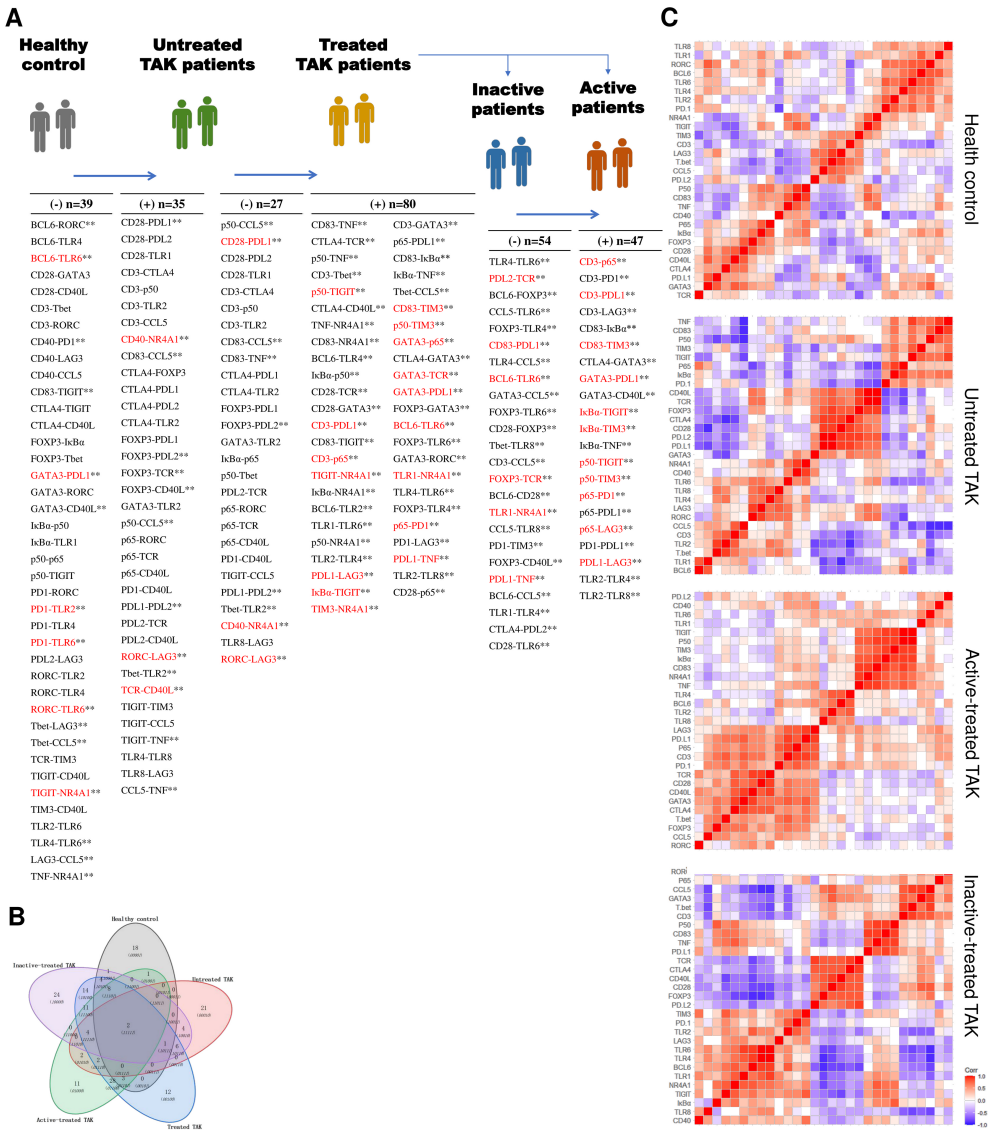

FIGURE 9 | Characteristic gene co-expressions across different conditions. **(A)** A list of characteristic co-expressed gene pairs comparing the two adjacent groups, which reflected changes in the activated signaling pathways. The newly discovered co-expression relationships which had never been reported in STRING or Coexpedia database were indicated red. Pearson correlation analysis. Untreated TAK Vs. healthy controls, $p < 0.05$. Treated TAK Vs. Untreated TAK, $p < 0.01$. Active-treated TAK Vs. inactive-treated TAK, $p < 0.01$. **p < 0.01. **(B)** Overlapping co-expressions among the five conditions. **(C)** Hierarchical clustering heatmaps of the target genes with the distance calculated using Pearson correlation. TAK, Takayasu's arteritis.

response to bacterium, peptide, and lipopolysaccharide, the TLR signaling pathway, the I-kappaB kinase/NF-kappaB signaling pathway, and the regulation of defense response, while genes in Cluster 2 were enriched for the regulation of T-cell activation and the regulation of IL-10 production (**Figure 10D**).

miRNAs Might Play an Important Role in the Cross-Talk Between TLR and T-Cell in TAK Patients

The co-expression in Cluster 1 of the inactive-treated TAK group was not presently understood, while Cluster 1 of the active-treated TAK group was led by the activation and differentiation of T-cells. We surmised that the miRNA network might take part in the expression of these genes, which could account for the co-expression of Cluster 1 of inactive-treated TAK group. We predicted the miRNA that targeted TLR1, TLR2, TLR4, TLR6, TLR8, BCL6, NR4A1, NFKBIA, LAG3, HAVCR2, TIGIT, PDCD1, and CD40 separately using the miRDB database (44, 45). Except for LAG3 among these genes, there were multiple miRNAs for each gene. We summarized the miRNA (rather than miRNA family) that might regulate two or more genes (**Supplementary Table 9**) and visualized the miRNA-gene regulatory network (**Supplementary**

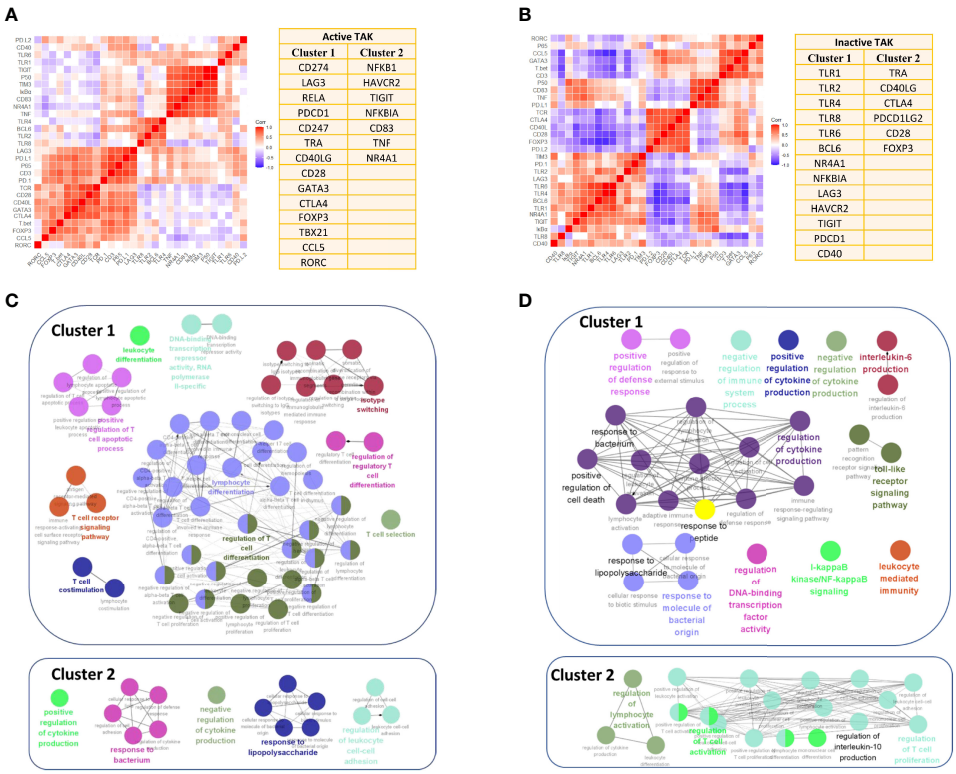

FIGURE 10 | Enrichment for activated signaling pathways of the inactive-treated and the active-treated TAK patients. **(A, B)** The two greatest gene clusters of the active-treated **(A)** and the inactive-treated TAK group **(B)**. **(C, D)** Functional enrichment analysis results of the active-treated **(C)** and the inactive-treated TAK group **(D)**, revealing the potentially activated signaling pathway at the active or the inactive stage of TAK. TAK, Takayasu's arteritis.

Figure 5), in which miRNAs belonging to the same family were merged and represented by one node.

Next, to test whether the miRNAs in the miRNA-gene network were differentially expressed, we sequenced miRNAs from the plasma exosomes from healthy control and TAK patients. We found that compared with the healthy controls, miR-548ad-5p showed a 25.6-fold upregulation (p=0.0012), miR-3613-5p showed a 2.35-fold upregulation (p=0.0012), and miR-335-5p showed a 2.07-fold upregulation (p=0.0039); while miR-335-3p showed a 3.23-fold downregulation (p=0.042) and miR-584-5p showed a 2.01-fold downregulation (p=0.0092). The network shown in **Figure 11** only consisted of the miRNA that might regulate three or more genes and two differentially expressed miRNAs (miR-335-2p and miR-584-3p). In the network, miR-548 was the node with the highest degree (7 genes), followed by miR-5692 (4 genes), miR-4763 (4 genes), and miR-520 (4 genes). **Figure 11** showed the results. The miR-548 family was associated with 7 genes (7/13) in Cluster 1 of the inactive-treated TAK group, including TLR1, TLR2, TLR4, TLR6, TLR8, BCL6, NFKBIA, NR4A1, and TIGIT, which suggested that the miR-548 family plays an important role in the co-expression of Cluster 1 of inactive-treated TAK group.

miRNA sequencing identified 29 differentially expressed miRNAs, 17 of which were increased and 12 were decreased. To validate whether the TLR signaling pathway might be regulated by these differentially expressed miRNAs, we performed miRNA sequencing analysis following the workflow in **Figure 12A**. First, to identify whether the differentially expressed miRNAs could be associated with specific functional categories, we performed an unsupervised hierarchical clustering of miRNA expression level based on Spearman correlation coefficient and conducted GO enrichment analysis for each cluster based on DIANA-TarBase, an experimentally validated database (55). **Figure 12B** showed miRNAs were partitioned into three clusters by cutting the clustering tree at the height of 1.1, and miRNAs belonging to the same cluster might have a close functional association. **Figure 12C** showed the hierarchical clustering heat map. The functional enrichment analysis was described as follows.

1. In Cluster 1, the most highly significant GO term was cellular nitrogen compound metabolic process (p-value= 9.44E-20), followed by small molecule metabolic process (p-value= 8.68E-15) and biosynthetic process (p-value= 9.03E-14). Notably, twelve 'TLR signaling pathway'-related GO terms were highly enriched in Cluster 1 (from 25th to 66th).
2. In Cluster 2, the most highly significant GO term was organelle (1.29E-185), followed by cellular nitrogen compound metabolic process (1.46E-92) and ion binding (1.07E-66). And twelve 'TLR signaling pathway'-related GO terms were highly enriched in Cluster 1 (from 83rd to 146th).

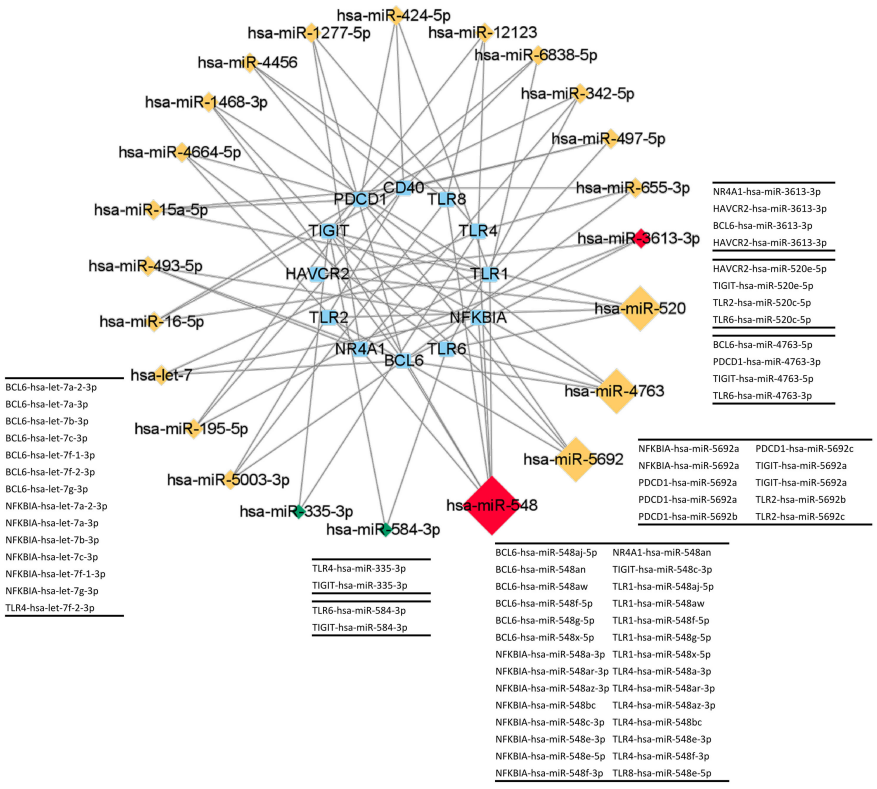

miRNA sequencing of the exosomes in plasma			
Down		**Up**	
miRNA	log_2Fc	miRNA	log_2Fc
hsa-miR-335-3p	-1.69*	hsa-miR-548ad-5p	4.68**
hsa-miR-584-5p	-1.01**	hsa-miR-3613-5p	1.23**
		hsa-miR-335-5p	1.05**

FIGURE 11 | The miRNAs might play an important role in the formation of TLRs-clustering at the inactive stage of TAK. The validation results of miRNA sequencing of plasma exosomes and the predicted miRNA-gene network (miRDB database) which only included the miRNA with a degree greater than or equal to 3 or the differentially expressed miRNA. Red and green colors of miRNA indicate upregulation and downregulation, respectively. Healthy controls, n=5 people. TAK patients, n=10 people. TAK, Takayasu's arteritis.

3. In Cluster 1, the most highly significant GO term was organelle (3.89E-189), followed by cellular nitrogen compound metabolic process (9.33E-102) and biosynthetic process (2.21E-67). And twelve 'TLR signaling pathway'-related GO terms were highly enriched in Cluster 1 (from 51st to 125th) (**Figure 12D**).

The experimentally validated database analysis indicated that TLR signaling pathway might be one of the major targets of the differentially expressed miRNA-mediated regulation, especially of the miRNAs belonging to Cluster 1.

Next, to validate whether one differentially expressed miRNA could target multiple selected genes, which might be involved in the gene co-expression of the inactive-treated TAK group, we constructed the miRNA-Gene-network based on the interactions of miRNAs and genes in the miRTarBase database, another experimentally validated database (56), and the screening condition of "support type" was set to "Functional MTI (miRNA target-interactions)". **Figure 12E** showed the result. Within the network, we identified 7 genes (including TLR1, TLR2, TLR4, BCL6, NFKBIA, NR4A1, and RORC) that had been validated to be regulated by the same miRNA, miR-335-5p, 4 genes (including TLR4, BCL6, FOXP3, and NFKB1) by miR-21-5p, and 4 genes (including CD40, CD40LG, NFKB1, and TNF) by miR-34a-5p. The results demonstrated that as follows:

1. In TAK, differentially expressed miRNAs that targeted multiple selected genes do exist.
2. TLRs, BCL6, and FOXP3 might be regulated by common miRNAs in TAK.

To sum up, these results suggested that miRNAs might play an important role in the cross-talk between TLR and T-cell in TAK patients.

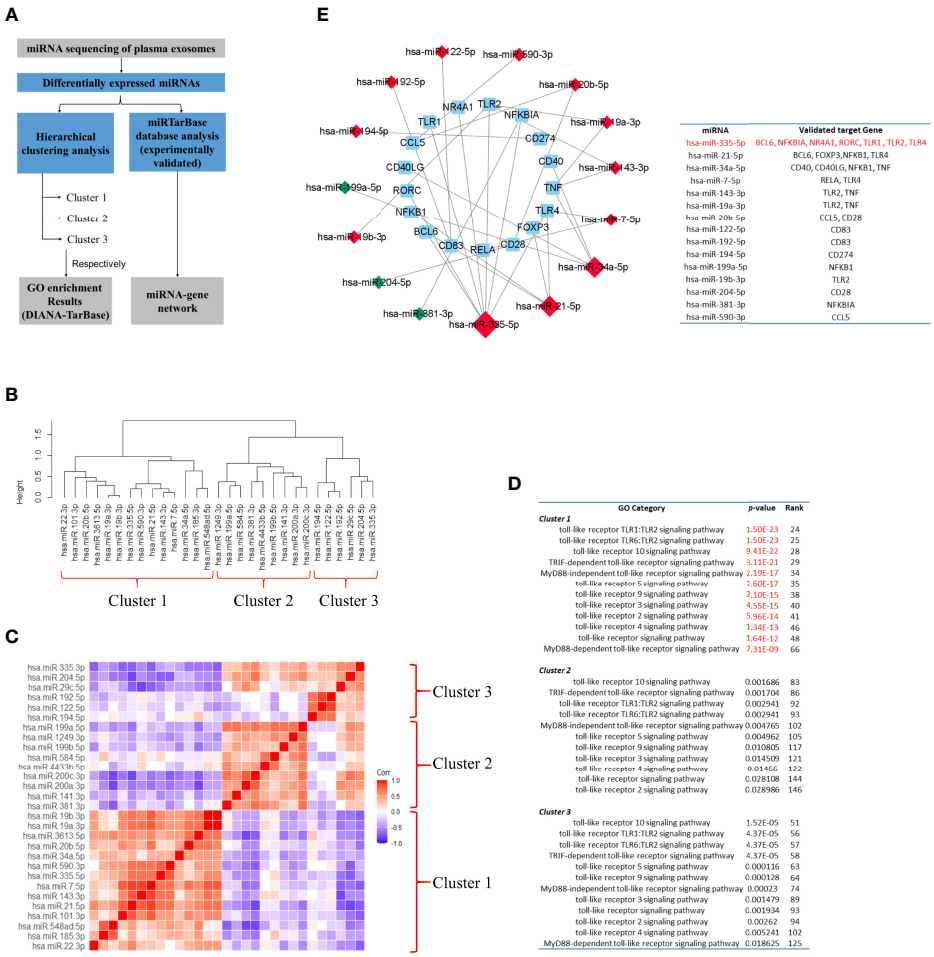

FIGURE 12 | Toll-like receptor signaling pathway might be one of the major targets of the differentially-expressed-miRNA-mediated regulation. **(A)** Workflow of miRNA sequencing analysis. miRNA was from plasma exosomes in Takayasu's arteritis (TAK) patients (n=10) and healthy controls (n=5). **(B)** The hierarchical clustering trees of miRNA expression level based on Spearman correlation coefficient using complete method. **(C)** The hierarchical clustering heatmaps of miRNA expression level based on Spearman correlation coefficient. **(D)** GO enrichment analysis for each cluster based on DIANA-TarBase, an experimentally validated database. The results indicated that TLR signaling pathway might be one of the major targets of the differentially expressed miRNA-mediated regulation, especially of the miRNAs belonging to Cluster 1. **(E)** Differentially expressed miRNAs. The miRNA-Gene-network based on miRTarBase database, an experimentally validated database, and the screening condition of "support type" was set to "Functional MTI (miRNA target-interactions). Red and green colors of miRNA indicated upregulation and downregulation, respectively. The results demonstrated that differentially expressed miRNAs that targeted multiple selected genes do exist in TAK, and TLRs, BCL6, and FOXP3 might be regulated by common miRNAs in TAK.

DISCUSSION

There have been a number of studies demonstrating that TLRs play an important role in the pathogenesis of many AIDs, such as RA, SLE, and MS, but in TAK, it is currently unclear whether TLRs are associated with the disease activity (1, 2). T-cell is one of the major driving forces for the inflammatory response in TAK progression (6). It has been currently unknown whether TLRs are related to the disease activity or the activation and differentiation of T-cells in TAK. In this work, we selected 29 genes that were functionally enriched for the TLR signaling pathway and the activation and differentiation of T-cells. Twenty-seven TAK patients were enrolled which were grouped into the untreated and the treated group (both were further separated into the inactive and the active group), and 10 adult healthy controls were included. The relative mRNA level data of PBMCs were acquired by RT-qPCR. First, differential gene expression analysis showed that the untreated TAK and the treated TAK had an increased mRNA level of TLR2 and TLR4 compared to healthy controls. A sample-to-sample matrix revealed that 80% of healthy controls could be separated from the TAK patients. These findings suggested that TAK patients had a different expression pattern of the selected genes from the healthy controls. Second, we identified the association between TLRs and the disease activity, as the linear regression models consisting of the TLR4-CCL5 pair, the TLR6-CCL5 pair, the TLR8-CCL5 pair, and the TLR8-T-bet pair could distinguish between active and inactive disease in TAK [the AUC/sensitivity/specificity, 0.939/90.9%/88.9%]. Third, we identified the

association between TLRs and the activation and differentiation of T-cells in TAK according to the following evidence: (1) As the dynamic gene co-expression network showed, compared with the healthy control group, the active-treated TAK group, and the inactive-treated TAK group had higher network connectivity, shorter characteristic path length, and a larger clustering coefficient, indicating the more active communication between TLRs and T-cell activation in TAK. (2) The inactive-treated TAK group exhibited a unique pattern of inverse correlations between the TLRs gene clusters (including TLR1/2/4/6/8, BCL6, TIGIT, NR4A1, and so on) and the gene cluster associated with T-cell activation and differentiation (including TCR, CD28, T-bet, GATA3, FOXP3, CCL5, and so on). Fourth, we explored the genes key to the cross-talk between TLRs and the activation and differentiation of T-cell in TAK. In inactive-treated TAK, BCL6, CCL5, FOXP3, GATA3, CD28, T-bet, TIGIT, IκBα, and NR4A1 were likely to have a close functional relation with TLRs. However, in the active-treated group, the association between these genes and TLRs did not seem to be as strong as the inactive-treated group, BCL6, PD-1, LAG3, and CD40 were likely to have a close functional relation with TLRs. Fifth, we analyzed the activated signaling pathways in the inactive-treated and the active-treated TAK group. Last, we predicted the miRNAs that involved the greatest cluster of the inactive-treated TAK group and validated that miRNA might play an important role in the cross-talk between TLR and T-cell in TAK by miRNA sequencing. Besides, we proposed a new concept of the TLR-co-expression signature which might distinguish different disease and treatment stages of TAK, such as the co-expression of TLR4 and TLR6, which serves as a biomarker of the active stage in treated TAK (AUC/sensitivity/specificity, 0.919/100%/90.9%). These findings were schematically summarized in **Figure 13**.

Elevated Levels of TLR2 and TLR4 in PBMCs From TAK Patients

An increased level of TLRs in PBMCs has been detected in some AIDs. For example, comparing SLE patients with healthy

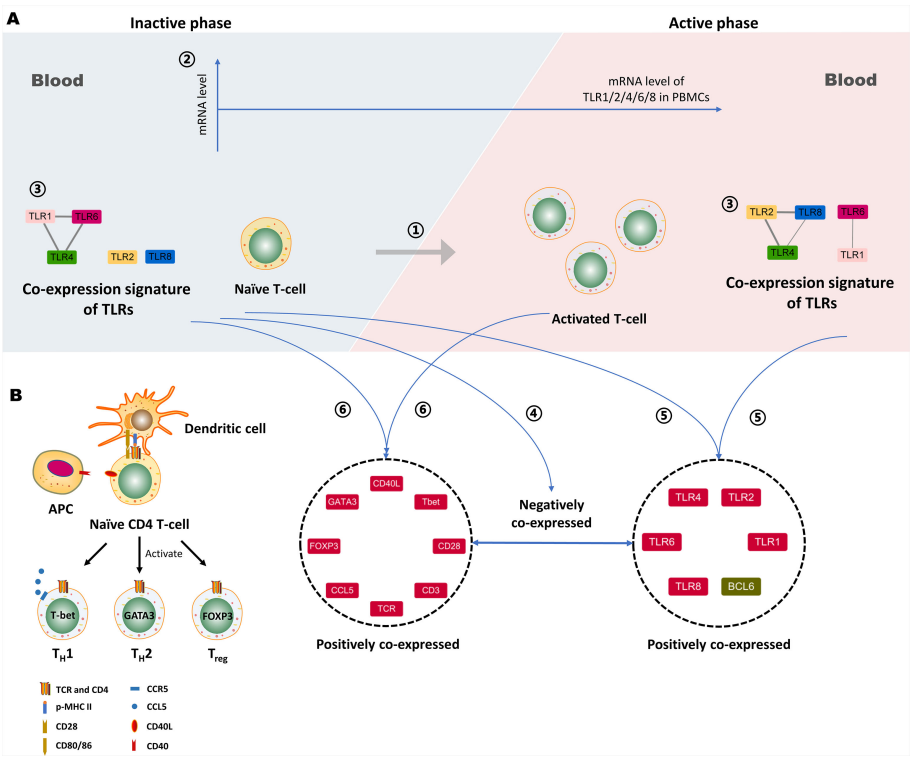

FIGURE 13 | Proposed working model depicting the association between Toll-like receptors (TLRs) and T-cell activation in Takayasu's arteritis (TAK). **(A)** ① The activation of autoreactive T cells contributes to the disease activity of TAK. ② The mRNA level of TLR1, -2, -4, -6 or, -8 in peripheral blood mononuclear cells (PBMCs) do not statistically change with alterations when patients with TAK enter the active phase, which was concluded from the comparison between the active patients and the inactive ones. ③ The gene co-expression of TLRs might serve as a biomarker that could distinguish active patients from inactive patients in TAK. ④ The negative gene co-expression between the TLRs cluster and the gene cluster associated with T-cell activation and differentiation is a characteristic of inactive-treated TAK patients that is absent in the active ones. ⑤ The inactive TAK patients and the active TAK patients share the characteristic of the positive co-expressed gene cluster comprising several key genes involved in the activation and differentiation of T-cells. ⑥ The inactive TAK patients and the active TAK patients have the common positive co-expressed gene cluster comprising TLRs and BCL6. Notably, BCL6 is tightly related to TLRs, and the underlying mechanisms deserve further exploration. Besides, miRNAs might play an important role in the above gene co-expression, and however, further investigation is needed to validate it. **(B)** The proteins coded by the genes in the left gene cluster play a key role in the activation and differentiation of T-cells. APC, Antigen-presenting cell.

controls, TLR2 expression on monocytes was reduced, and intracellular TLR9 expression of $CD19^+$ B-cells was elevated (57). Comparing Behcet's disease patients with healthy controls, TLR1 and TLR2 were elevated in B-cells, TLR1, 2, and 4 were more highly expressed in both $CD4^+$and $CD8^+$ T-cells, granulocytes displayed a higher expression of TLR1, 2, 4, and 6, and the expressions of TLR2, 4, and 5 were significantly increased on classical monocytes (58). However, few studies probed the effect of the treatment on the expressions of the TLRs in AIDs. For TAK, it has been unclear whether there are abnormal expressions of the TLRs in TAK, except TLR4. Besides, it also has been unclear whether the abnormal expressions of the TLRs are related to the medication and the disease activity, including TLR4. Our results complement and add to findings from previous TAK studies in that the mRNA expression of TLR4 and its ligand S100s in PBMCs from TAK patients were higher compared to healthy controls (12). We found that both the untreated and the treated TAK patients had increased mRNA levels of TLR2 and TLR4, and there was no statistically significant difference between the two groups, which demonstrated that the increased mRNA levels of TLR2 and TLR4 were independent from the medication. Besides, it was unanticipated that there was no statistically significant difference between the inactive and the active TAK patients in the mRNA expression of TLR2 and TLR4, which suggested that the elevated levels of TLR2 and TLR4 might be not resulted from the disease activity in TAK. However, the treated patients in this study had a relatively low serum level of TNF-α, which might imply relatively inactive TLR-signaling pathways in their peripheral blood.

Novel Association Between TLRs and Disease Activity in AIDs

Many studies have shown that TLRs play a dual role in the disease activity of AIDs. On the one hand, TLRs promote disease progression. TLRs can be activated by the DAMPs which are released from the injured tissue, such as high mobility group box-1 (HGMB1) (59) and self-nucleic acids (60, 61). On the other hand, TLRs although inhibit autoimmune inflammation. In SLE, TLRs can promote sterile inflammation activated by DAMPs released from damaged cells, which is closely related to the disease progression and autoantibody production (62). For example, TLR-7, -8, and -9, which are not only expressed in the innate immune cells, such as neutrophils, macrophages and dendritic cells (DCs), but also are expressed in the lymphocytes, such as T-cells, and B-cells (60, 63, 64), can be activated by the self-nucleic acids (DAMPs released from damaged cells) (60, 61), and in recent years, there has been an increasing interest in the mechanism of how TLRs directly regulate the adaptive immune response without the innate immune cells, which deepens our understanding of the role of TLRs in the pathogenesis of AIDs. On the other hand, TLRs have a dual role in the pathogenesis of SLE, and TLRs can protect the body against autoimmune inflammation. Low expression of TLR9 due to single nucleotide polymorphisms would increase SLE susceptibility in humans (65), and deletion of TLR8 and TLR9 would accelerate lupus development in mice (66–70). A variety of mechanisms for TLR9 to promote and limit AIDs have been discovered. The TLR9-dependent function of medullary thymic epithelial cells is required for the generation of regulatory T cells (Tregs) and the establishment of central tolerance (71). TLR9 can inhibit the production of autoantibodies mediated by TLR7, such as anti-RNA Ab, anti-Sm Ab, anti-RNA Ab, anti-IgG2a RF (68, 69, 72). The balance between TLR7 and TLR9 is important for the formation of autoreactive B cells (73). And UNC93B1 plays an important role in regulating the balance between TLR7 and TLR9 (74–77). In the endoplasmic reticulum, TLR7 competes with TLR9 to bind to UNC93B1, and the D34 position of UNC93B makes it biased to bind to TLR9 (78). In RA, TLRs also promote sterile inflammation. For example, TLR4 can be activated by high mobility group box-1 protein (HMGB1) in RA (59). Besides, the activation of TLRs caused by PAMPs also plays an important role in the pathogenesis of RA (79). In the clinic, some cytokines induced by TLRs are immunotherapeutic targets in AIDs, such as TNF-α, interleukin (IL)-6, interferon (IFN)-α, and IL-1β (7). Recently, NI-0101, an anti-toll-like receptor 4 monoclonal antibody was used in RA, which was the first clinical trial to target TLRs to treat autoimmune diseases (4). In this study, we observed a unique pattern of inverse correlations between the TLRs gene clusters and the gene cluster associated with T-cell activation and differentiation the inactive-treated TAK group, which suggests a novel relationship between TLRs and the disease activity in AIDs.

However, these potential mechanisms of these inverse correlations need to be elucidated in depth, and there are several fundamental questions to address. First, the inverse correlations between TLRs and the activation of T-cell should be described in more detailed, and some experimental data for the difference in the T-cell activation status are needed to be collected, including the expression of activation markers on T cells (such as CD69, CD25 and HLA-DR) and some cytokines (such as IFN-γ^+Th1, IL-4^+Th2, and IL-17^+Th17). Then, association studies cannot be used to infer causality. While there is a possible regulatory relationship between TLRs and T-cells in TAK, it is also possible that TLRs and T-cells are under the control of common upstream regulators. Furthermore, another question is why the inverse correlations exist in inactive TAK patients, but not in active TAK patients.

Activated Signaling Pathways in the Inactive and the Active TAK Patients

T-cell is one of the main forces for the autoimmune inflammation in TAK (6). It has been reported that multiple T-cell subtypes are related to the pathogenesis of TAK, including Th1, Th17, Th9, Tfh, and Th2-like Treg cells (80–83). In this study, the functional enrichment of the greatest cluster of the active-treated TAK group was centered on the activation and differentiation of T-cells, indicating the activation of T-cells at the active stage, which is consistent with previously reported studies. Notably, the functional enrichment of the greatest cluster of the inactive-treated TAK group was centered on the regulation of cytokine production, the response to bacterium, peptide, and

lipopolysaccharide, the TLR signaling pathway, the I-kappaB kinase/NF-kappaB signaling pathway, the regulation of defense response, and so on, which suggested the activated TLR-signaling pathways at the inactive stage.

The previous study has shown that BCL6 regulates nearly a third of the TLR4-regulated transcriptome, and that 90% of the BCL6 cistrome is collapsed following TLR4 activation in the macrophages (84). In B-cells, PELI1, which is activated by TLR3 and TLR4, directly interacted with BCL6, inducing lysine 63-mediated BCL6 polyubiquitination, and PELI1 expression levels positively correlated with BCL6 expression (85). Our results showed that BCL6 had a very similar expression pattern to that of TLRs, indicating that there is a stronger and closer association between multiple TLRs and BCL6, such as direct interactions and regulatory relationships, and this association warrants further study. The transcription factor BCL6 is required for driving Tfh cell differentiation and regulates their function. Recent studies have demonstrated the implications of Tfh cells with the disease activity of TAK (82), and our results suggested that TLRs might play a role in the regulation of Tfh cells.

miRNA-548 Family

miRNAs play an important role in regulating gene expression and the TLR-signaling pathways (86, 87). miRNAs with high sequence similarity form the miRNA family, co-regulating complex biological processes. Among them, the miR-548 family, with over 80 identified miRNAs, regulates the immune process in some diseases, such as cancer (88, 89). A large amount studies have shown that miRNA-548 suppresses tumor proliferate by binding WNT2 (90), murine double minute 2 (91), metastasis tumor-associated protein-2 (92), specificity protein 1 (93), cancerous inhibitor of protein phosphatase 2A (94), HMGB1 (95), and so on. Inhibiting or down-regulating miR-548 promotes the tumor proliferation (96). One study proposed to serve miRNA-548 as a prognosis predictor in primary central nervous system lymphoma (97). Our study showed that miR-548 played an important role in the pathogenesis of autoimmune disease, which might be related to the TLR signaling pathway.

It is worth noting that miRNA-548 family was increased in the serum exosomes from TAK patients than healthy controls, while the expression levels of its potential target genes were not decreased. While we have no clear explanation for this, we speculated that miRNAs might play an important role in the negative feedback regulation of TLR signaling pathways based on previous studies. Studies have shown that miRNAs play an important role as negative feedback to control inflammatory responses maintaining a level, avoiding excess inflammatory responses (98). For example, serum IL-6 levels increase with aging, whereas miR-192 in extracellular vesicles alleviated the prolonged inflammation associated with aging (99). Besides, the expression level of miRNA-541 [can attenuate pro-inflammatory cytokine expression (100)] in circulating extracellular vesicles was negatively correlated with the pro-inflammatory cytokine expression levels and the number of adverse local symptoms after vaccination (101). In these cases, although the expression levels of some targeted genes are still increased than normal, miRNAs in circulating extracellular vesicles have functioned as avoiding excessive inflammation. However, we have not been demonstrated the correlations between miR-548 as the RNA samples and serum exosomes were not from the same participants.

TLR-Co-Expression Signature

There are certain functional relationships among TLRs. First, TLRs function as a homodimer or heterodimer. TLR2 binds TLR1 or TLR6 to recognize distinct PAMPs (102, 103). The TLR4-TLR6-CD36 complex is activated by atherogenic lipids and amyloid-beta to stimulate sterile inflammation (48, 49). Second, there is some cross-talk between TLRs. In SLE, TLR9 can inhibit the production of autoantibodies mediated by TLR7, such as anti-RNA Ab, anti-Sm Ab, anti-RNA Ab, anti-IgG2a RF (68, 69, 72). The balance between TLR7 and TLR9 is important for the formation of autoreactive B cells (73). And UNC93B1 plays an important role in regulating the balance between TLR7 and TLR9 (74–77). In the endoplasmic reticulum, TLR7 competes with TLR9 to bind to UNC93B1, and the D34 position of UNC93B makes it biased to bind to TLR9 (78). In the endothelial cells transfected with TLR1in septic, the ability of TLR4 in these cells to respond to LPS was lost (104). TLR10 on peripheral blood monocytes reduces TLR2-induced cytokine production in Parkinson's disease (105), which is also a co-receptor of TLR2. Third, some TLR-genes locate the same gene cluster in the chromosome, and there are multiple associated SNPs of TLRs, such as TLR1, TLR6, and TLR10. For example, the observed multiple associated SNPs at the TLR6-TLR1-TLR10 gene cluster may play a role in prostate cancer risk (106). STRING database analysis showed strong PPIs among TLRs (**Figure 6A**). We observed the different co-expressed TLRs clusters of different disease and treatment stages in TAK, which might serve as a signature of transcriptome analysis for individualized treatment decision. For instance, the co-expression TLR4 and TLR6 could distinguish the active-treated TAK patients from the inactive ones.

Limitations

In the correlation analysis results, there were many non-strong correlations ($0.01<p<0.05$) between the expression levels, which might be related to the sample heterogeneity. For instance, some non-strong correlation in the treated TAK group became strong correlations ($p<or=0.01$) after further stratifying patients into subgroups according to disease activity. But the sample size is relatively small, so the active or inactive group could not be separated into subgroups.

Besides, there were limitations in the protocol for evaluating the closeness of functional relationships between TLRs and the other genes. Although the genes with a high score were likely to be closely connected in function with TLRs, the genes with a low score were not necessarily intimately linked with TLRs.

Notably, the reference genes had a large influence on the correlation analysis results. Stably expressed reference genes help find out the co-expression relations. Moreover, different reference genes may cause some differences in the results, and combining Pearson correlation and Spearman correlation help partially address the problem.

Last, larger clinical studies will be needed to validate our findings and to calibrate the diagnostic thresholds. In this cohort, the naïve TAK patients will be also classified into the active group and the inactive group as it might exhibit a different co-expression network from the TAK patients under treatment. Some experimental data for the difference in the T cell activation status (activation markers and cytokines) will be also collected to construct more accurate and more detailed models of the association between TLRs and T-cell activation in TAK.

CONCLUSIONS

This study identified the association between TLRs and T-cell activation in TAK, found a potentially novel role of TLRs in the pathogenesis of autoimmune diseases, and highlighted the function of miRNAs in the cross-talk between TLRs and T-cells in TAK, and more investigation is needed to further confirm the role of miRNAs in the cross-talk between TLR and T-cell in TAK patients and to elucidate the mechanisms.

DATA AVAILABILITY STATEMENT

We have deposited the miRNA data in the OMIX, China National Center for Bioinformation/Beijing Institute of Genomics, Chinese Academy of Sciences (https://ngdc.cncb.ac.cn/omix: accession no. OMIX807).

ETHICS STATEMENT

The studies involving human participants were reviewed and approved by the Institutional Review Board of Peking Union Medical College Hospital. The patients/participants provided their written informed consent to participate in this study.

AUTHOR CONTRIBUTIONS

YT performed the RT-qPCR experiments and analyzed the data. BH performed the experiment of miRNA sequencing and differential miRNA expression analysis. JL, YT, and XT designed the study. JL and YT wrote the paper mainly. XT and XZ made the critical revision. All authors have read and approved the paper.

FUNDING

This study was supported by National Science Foundation of China to JL with (grant numbers 81401333), and XZ with National Clinical Research Center for Dermatologic and Immunologic Diseases, the Chinese National Key Research and Development Program (grant number 2017YFC0907600, 2008BAI59B02) and the Chinese National High Technology Research and Development Program, Ministry of Science and Technology (grant number 2012AA02A513).

SUPPLEMENTARY MATERIAL

The Supplementary Material for this article can be found online at: https://www.frontiersin.org/articles/10.3389/fimmu.2021.792901/full#supplementary-material

REFERENCES

1. Chen JQ, Szodoray P, Zeher M. Toll-Like Receptor Pathways in Autoimmune Diseases. *Clin Rev Allergy Immunol* (2016) 50:1–17. doi: 10.1007/s12016-015-8473-z
2. Joosten LA, Abdollahi-Roodsaz S, Dinarello CA, O'Neill L, Netea MG. Toll-Like Receptors and Chronic Inflammation in Rheumatic Diseases: New Developments. *Nat Rev Rheumatol* (2016) 12:344–57. doi: 10.1038/nrrheum.2016.61
3. Deng J, Ma-Krupa W, Gewirtz AT, Younge BR, Goronzy JJ, Weyand CM. Toll-Like Receptors 4 and 5 Induce Distinct Types of Vasculitis. *Circ Res* (2009) 104:488–95. doi: 10.1161/circresaha.108.185777
4. Monnet E, Choy EH, McInnes I, Kobakhidze T, de Graaf K, Jacqmin P, et al. Efficacy and Safety of NI-0101, an Anti-Toll-Like Receptor 4 Monoclonal Antibody, in Patients With Rheumatoid Arthritis After Inadequate Response to Methotrexate: A Phase II Study. *Ann Rheum Dis* (2020) 79:316–23. doi: 10.1136/annrheumdis-2019-216487
5. Hellmann DB. 88 - Giant Cell Arteritis, Polymyalgia Rheumatica, and Takayasu's Arteritis. In: GS Firestein, RC Budd, SE Gabriel, IB McInnes and JR O'Dell, editors. *Kelley's of*, (*Ninth Edition*). Philadelphia: TextbookRheumatologyW.B. Saunders (2013). p. 1461–80.
6. Watanabe R, Berry GJ, Liang DH, Goronzy JJ, Weyand CM. Cellular Signaling Pathways in Medium and Large Vessel Vasculitis. *Front Immunol* (2020) 11:587089. doi: 10.3389/fimmu.2020.587089
7. Mansson A, Adner M, Cardell LO. Toll-Like Receptors in Cellular Subsets of Human Tonsil T Cells: Altered Expression During Recurrent Tonsillitis. *Respir Res* (2006) 7:36. doi: 10.1186/1465-9921-7-36
8. Ye J, Wang Y, Liu X, Li L, Opejin A, Hsueh EC, et al. TLR7 Signaling Regulates Th17 Cells and Autoimmunity: Novel Potential for Autoimmune Therapy. *J Immunol (Baltimore Md 1950)* (2017) 199:941–54. doi: 10.4049/jimmunol.1601890
9. Marks KE, Flaherty S, Patterson KM, Stratton M, Martinez GJ, Reynolds JM. Toll-Like Receptor 2 Induces Pathogenicity in Th17 Cells and Reveals a Role for IPCEF in Regulating Th17 Cell Migration. *Cell Rep* (2021) 35:109303. doi: 10.1016/j.celrep.2021.109303
10. Li L, Liu X, Sanders KL, Edwards JL, Ye J, Si F, et al. TLR8-Mediated Metabolic Control of Human Treg Function: A Mechanistic Target for Cancer Immunotherapy. *Cell Metab* (2019) 29:103–23.e5. doi: 10.1016/j.cmet.2018.09.020
11. Chodaczek G, Pagni PP, Christoffersson G, Ratliff SS, Toporkiewicz M, Wegrzyn AS, et al. The Effect of Toll-Like Receptor Stimulation on the Motility of Regulatory T Cells. *J Autoimmun* (2021) 116:102563. doi: 10.1016/j.jaut.2020.102563
12. Kabeerdoss J, Thomas M, Goel R, Mohan H, Danda S, Jeyaseelan L, et al. High Expression of S100 Calgranulin Genes in Peripheral Blood Mononuclear Cells From Patients With Takayasu Arteritis. *Cytokine* (2019) 114:61–6. doi: 10.1016/j.cyto.2018.11.033
13. Kabeerdoss J, Goel R, Mohan H, Danda D. High Expression of Pro-Inflammatory Cytokine Genes IL-1β and IL-1R2 Upon TLR4 Activation in Takayasu Arteritis. *Rheumatol Int* (2021). doi: 10.1007/s00296-020-04785-0
14. Barabási AL, Oltvai ZN. Network Biology: Understanding the Cell's Functional Organization. *Nat Rev Genet* (2004) 5:101–13. doi: 10.1038/nrg1272

15. Boccaletti S, Latora V, Moreno Y, Chavez M, Hwang DU. Complex Networks: Structure and Dynamics. *Phys Rep-Rev Section Phys Lett* (2006) 424:175–308. doi: 10.1016/j.physrep.2005.10.009
16. Vidal M, Cusick ME, Barabási AL. Interactome Networks and Human Disease. *Cell* (2011) 144:986–98. doi: 10.1016/j.cell.2011.02.016
17. Bray D. Molecular Networks: The Top-Down View. *Sci (New York NY)* (2003) 301:1864–5. doi: 10.1126/science.1089118
18. Zhou X, Kao MC, Wong WH. Transitive Functional Annotation by Shortest-Path Analysis of Gene Expression Data. *Proc Natl Acad Sci USA* (2002) 99:12783–8. doi: 10.1073/pnas.192159399
19. Butte AJ, Tamayo P, Slonim D, Golub TR, Kohane IS. Discovering Functional Relationships Between RNA Expression and Chemotherapeutic Susceptibility Using Relevance Networks. *Proc Natl Acad Sci USA* (2000) 97:12182–6. doi: 10.1073/pnas.220392197
20. Lee HK, Hsu AK, Sajdak J, Qin J, Pavlidis P. Coexpression Analysis of Human Genes Across Many Microarray Data Sets. *Genome Res* (2004) 14:1085–94. doi: 10.1101/gr.1910904
21. Eisen MB, Spellman PT, Brown PO, Botstein D. Cluster Analysis and Display of Genome-Wide Expression Patterns. *Proc Natl Acad Sci USA* (1998) 95:14863–8. doi: 10.1073/pnas.95.25.14863
22. Prieto C, Risueño A, Fontanillo C, De las Rivas J. Human Gene Coexpression Landscape: Confident Network Derived From Tissue Transcriptomic Profiles. *PloS One* (2008) 3:e3911. doi: 10.1371/journal.pone.0003911
23. Wei SC, Duffy CR, Allison JP. Fundamental Mechanisms of Immune Checkpoint Blockade Therapy. *Cancer Discov* (2018) 8:1069–86. doi: 10.1158/2159-8290.Cd-18-0367
24. Bateman A, Martin MJ, O'Donovan C, Magrane M, Apweiler R, Alpi E, et al. UniProt: A Hub for Protein Information. *Nucleic Acids Res* (2015) 43:D204–12. doi: 10.1093/nar/gku989
25. Zhou Y, Zhou B, Pache L, Chang M, Khodabakhshi AH, Tanaseichuk O, et al. Metascape Provides a Biologist-Oriented Resource for the Analysis of Systems-Level Datasets. *Nat Commun* (2019) 10:1523. doi: 10.1038/s41467-019-09234-6
26. Ashburner M, Ball CA, Blake JA, Botstein D, Butler H, Cherry JM, et al. Gene Ontology: Tool for the Unification of Biology. *Nat Genet* (2000) 25:25–9. doi: 10.1038/75556
27. Kanehisa M, Goto S. KEGG: Kyoto Encyclopedia of Genes and Genomes. *Nucleic Acids Res* (2000) 28:27–30. doi: 10.1093/nar/28.1.27
28. Slenter DN, Kutmon M, Hanspers K, Riutta A, Windsor J, Nunes N, et al. WikiPathways: A Multifaceted Pathway Database Bridging Metabolomics to Other Omics Research. *Nucleic Acids Res* (2018) 46:D661–7. doi: 10.1093/nar/gkx1064
29. Yang S, Kim CY, Hwang S, Kim E, Kim H, Shim H, et al. COEXPEDIA: Exploring Biomedical Hypotheses *via* Co-Expressions Associated With Medical Subject Headings (MeSH). *Nucleic Acids Res* (2017) 45:D389–d396. doi: 10.1093/nar/gkw868
30. Szklarczyk D, Gable AL, Lyon D, Junge A, Wyder S, Huerta-Cepas J, et al. STRING V11: Protein-Protein Association Networks With Increased Coverage, Supporting Functional Discovery in Genome-Wide Experimental Datasets. *Nucleic Acids Res* (2019) 47:D607–d613. doi: 10.1093/nar/gky1131
31. Bloch DA, Michel BA, Hunder GG, McShane DJ, Arend WP, Calabrese LH, et al. The American College of Rheumatology 1990 Criteria for the Classification of Vasculitis. Patients and Methods. *Arthritis Rheum* (1990) 33:1068–73. doi: 10.1002/art.1780330803
32. Kerr G. Takayasu's Arteritis. *Curr Opin Rheumatol* (1994) 6:32–8. doi: 10.1097/00002281-199401000-00006
33. Rio DC, Ares M Jr, Hannon GJ, Nilsen TW. Purification of RNA Using TRIzol (TRI Reagent). *Cold Spring Harbor Protoc* (2010) 2010:pdb.prot5439. doi: 10.1101/pdb.prot5439
34. Vandesompele J, De Preter K, Pattyn F, Poppe B, Van Roy N, De Paepe A, et al. Accurate Normalization of Real-Time Quantitative RT-PCR Data by Geometric Averaging of Multiple Internal Control Genes. *Genome Biol* (2002) 3:Research0034. doi: 10.1186/gb-2002-3-7-research0034
35. Andersen CL, Jensen JL, Orntoft TF. Normalization of Real-Time Quantitative Reverse Transcription-PCR Data: A Model-Based Variance Estimation Approach to Identify Genes Suited for Normalization, Applied to Bladder and Colon Cancer Data Sets. *Cancer Res* (2004) 64:5245–50. doi: 10.1158/0008-5472.Can-04-0496
36. Pfaffl MW, Tichopad A, Prgomet C, Neuvians TP. Determination of Stable Housekeeping Genes, Differentially Regulated Target Genes and Sample Integrity: BestKeeper - Excel-Based Tool Using Pair-Wise Correlations. *Biotechnol Lett* (2004) 26:509–15. doi: 10.1023/b:Bile.0000019559.84305.47
37. Obayashi T, Kinoshita K. Rank of Correlation Coefficient as a Comparable Measure for Biological Significance of Gene Coexpression. *DNA Res an Int J Rapid Publ Rep Genes Genomes* (2009) 16:249–60. doi: 10.1093/dnares/dsp016
38. Santos SD, Takahashi DY, Nakata A, Fujita A. A Comparative Study of Statistical Methods Used to Identify Dependencies Between Gene Expression Signals. *Briefings Bioinf* (2014) 15:906–18. doi: 10.1093/bib/bbt051
39. Kumari S, Nie J, Chen HS, Ma H, Stewart R, Li X, et al. Evaluation of Gene Association Methods for Coexpression Network Construction and Biological Knowledge Discovery. *PloS One* (2012) 7:e50411. doi: 10.1371/journal.pone.0050411
40. Tian Y, Li J, Tian X, Zeng X. Using the Co-Expression Network of T Cell-Activation-Related Genes to Assess the Disease Activity in Takayasu's Arteritis Patients. *Arthritis Res Ther* (2021) 23:303. doi: 10.1186/s13075-021-02636-2
41. D'Haeseleer P, Liang S, Somogyi R. Genetic Network Inference: From Co-Expression Clustering to Reverse Engineering. *Bioinf (Oxf Engl)* (2000) 16:707–26. doi: 10.1093/bioinformatics/16.8.707
42. Proctor RH, Brown DW, Plattner RD, Desjardins AE. Co-Expression of 15 Contiguous Genes Delineates a Fumonisin Biosynthetic Gene Cluster in Gibberella Moniliformis. *Fungal Genet Biol FG B* (2003) 38:237–49. doi: 10.1016/s1087-1845(02)00525-x
43. Kalhorzadeh P, Hu Z, Cools T, Amiard S, Willing EM, De Winne N, et al. Arabidopsis Thaliana RNase H2 Deficiency Counteracts the Needs for the WEE1 Checkpoint Kinase But Triggers Genome Instability. *Plant Cell* (2014) 26:3680–92. doi: 10.1105/tpc.114.128108
44. Wong N, Wang XW. miRDB: An Online Resource for microRNA Target Prediction and Functional Annotations. *Nucleic Acids Res* (2015) 43:D146–52. doi: 10.1093/nar/gku1104
45. Chen Y, Wang X. miRDB: An Online Database for Prediction of Functional microRNA Targets. *Nucleic Acids Res* (2020) 48:D127–d131. doi: 10.1093/nar/gkz757
46. Zeng Z, Lan T, Wei Y, Wei X. CCL5/CCR5 Axis in Human Diseases and Related Treatments. *Genes Dis* (2021) 9:12–27. doi: 10.1016/j.gendis.2021.08.004
47. Langfelder P, Horvath S. WGCNA: An R Package for Weighted Correlation Network Analysis. *BMC Bioinf* (2008) 9:559. doi: 10.1186/1471-2105-9-559
48. Stewart CR, Stuart LM, Wilkinson K, van Gils JM, Deng J, Halle A, et al. CD36 Ligands Promote Sterile Inflammation Through Assembly of a Toll-Like Receptor 4 and 6 Heterodimer. *Nat Immunol* (2010) 11:155–61. doi: 10.1038/ni.1836
49. Shmuel-Galia L, Klug Y, Porat Z, Charni M, Zarmi B, Shai Y. Intramembrane Attenuation of the TLR4-TLR6 Dimer Impairs Receptor Assembly and Reduces Microglia-Mediated Neurodegeneration. *J Biol Chem* (2017) 292:13415–27. doi: 10.1074/jbc.M117.784983
50. Truong R, Thankam FG, Agrawal DK. Immunological Mechanisms Underlying Sterile Inflammation in the Pathogenesis of Atherosclerosis: Potential Sites for Intervention. *Expert Rev Clin Immunol* (2021) 17:37–50. doi: 10.1080/1744666x.2020.1860757
51. Liu D, Yan J, Sun J, Liu B, Ma W, Li Y, et al. BCL6 Controls Contact-Dependent Help Delivery During Follicular T-B Cell Interactions. *Immunity* (2021) 54:2245–55.e4. doi: 10.1016/j.immuni.2021.08.003
52. Fontenot JD, Gavin MA, Rudensky AY. Foxp3 Programs the Development and Function of CD4+CD25+ Regulatory T Cells. *Nat Immunol* (2003) 4:330–6. doi: 10.1038/ni904
53. Chen J, López-Moyado IF, Seo H, Lio CJ, Hempleman LJ, Sekiya T, et al. NR4A Transcription Factors Limit CAR T Cell Function in Solid Tumours. *Nature* (2019) 567:530–4. doi: 10.1038/s41586-019-0985-x
54. Zhou T, Cheng J, Yang P, Wang Z, Liu C, Su X, et al. Inhibition of Nur77/Nurr1 Leads to Inefficient Clonal Deletion of Self-Reactive T Cells. *J Exp Med* (1996) 183:1879–92. doi: 10.1084/jem.183.4.1879
55. Vlachos IS, Paraskevopoulou MD, Karagkouni D, Georgakilas G, Vergoulis T, Kanellos I, et al. DIANA-TarBase V7.0: Indexing More Than Half a

Million Experimentally Supported miRNA:mRNA Interactions. *Nucleic Acids Res* (2015) 43:D153–9. doi: 10.1093/nar/gku1215
56. Chou CH, Chang NW, Shrestha S, Hsu SD, Lin YL, Lee WH, et al. Mirtarbase 2016: Updates to the Experimentally Validated miRNA-Target Interactions Database. *Nucleic Acids Res* (2016) 44:D239–47. doi: 10.1093/nar/gkv1258
57. Migita K, Miyashita T, Maeda Y, Nakamura M, Yatsuhashi H, Kimura H, et al. Toll-Like Receptor Expression in Lupus Peripheral Blood Mononuclear Cells. *J Rheumatol* (2007) 34:493–500.
58. van der Houwen TB, Dik WA, Goeijenbier M, Hayat M, Nagtzaam NMA, van Hagen M, et al. Leukocyte Toll-Like Receptor Expression in Pathergy Positive and Negative Behçet's Disease Patients. *Rheumatol (Oxf Engl)* (2020) 59:3971–9. doi: 10.1093/rheumatology/keaa251
59. Agalave NM, Larsson M, Abdelmoaty S, Su J, Baharpoor A, Lundback P, et al. Spinal HMGB1 Induces TLR4-Mediated Long-Lasting Hypersensitivity and Glial Activation and Regulates Pain-Like Behavior in Experimental Arthritis. *Pain* (2014) 155:1802–13. doi: 10.1016/j.pain.2014.06.007
60. Fillatreau S, Manfroi B, Dörner T. Toll-Like Receptor Signalling in B Cells During Systemic Lupus Erythematosus. *Nat Rev Rheumatol* (2021) 17:98–108. doi: 10.1038/s41584-020-00544-4
61. Vollmer J, Tluk S, Schmitz C, Hamm S, Jurk M, Forsbach A, et al. Immune Stimulation Mediated by Autoantigen Binding Sites Within Small Nuclear RNAs Involves Toll-Like Receptors 7 and 8. *J Exp Med* (2005) 202:1575–85. doi: 10.1084/jem.20051696
62. Gong T, Liu L, Jiang W, Zhou R. DAMP-Sensing Receptors in Sterile Inflammation and Inflammatory Diseases. *Nat Rev Immunol* (2020) 20:95–112. doi: 10.1038/s41577-019-0215-7
63. Soni C, Perez OA, Voss WN, Pucella JN, Serpas L, Mehl J, et al. Plasmacytoid Dendritic Cells and Type I Interferon Promote Extrafollicular B Cell Responses to Extracellular Self-DNA. *Immunity* (2020) 52:1022–1038.e7. doi: 10.1016/j.immuni.2020.04.015
64. Ye J, Wang YD, Liu X, Li LY, Opejin A, Hsueh EC, et al. TLR7 Signaling Regulates Th17 Cells and Autoimmunity: Novel Potential for Autoimmune Therapy. *J Immunol* (2017) 199:941–54. doi: 10.4049/jimmunol.1601890
65. Tao K, Fujii M, Tsukumo S, Maekawa Y, Kishihara K, Kimoto Y, et al. Genetic Variations of Toll-Like Receptor 9 Predispose to Systemic Lupus Erythematosus in Japanese Population. *Ann Rheum Dis* (2007) 66:905–9. doi: 10.1136/ard.2006.065961
66. Celhar T, Yasuga H, Lee HY, Zharkova O, Tripathi S, Thornhill SI, et al. Toll-Like Receptor 9 Deficiency Breaks Tolerance to RNA-Associated Antigens and Up-Regulates Toll-Like Receptor 7 Protein in Sle1 Mice. *Arthritis Rheumatol* (2018) 70:1597–609. doi: 10.1002/art.40535
67. Tran NL, Manzin-Lorenzi C, Santiago-Raber ML. Toll-Like Receptor 8 Deletion Accelerates Autoimmunity in a Mouse Model of Lupus Through a Toll-Like Receptor 7-Dependent Mechanism. *Immunology* (2015) 145:60–70. doi: 10.1111/imm.12426
68. Santiago-Raber ML, Dunand-Sauthier I, Wu T, Li QZ, Uematsu S, Akira S, et al. Critical Role of TLR7 in the Acceleration of Systemic Lupus Erythematosus in TLR9-Deficient Mice. *J Autoimmun* (2010) 34:339–48. doi: 10.1016/j.jaut.2009.11.001
69. Christensen SR, Shupe J, Nickerson K, Kashgarian M, Flavell RA, Shlomchik MJ. Toll-Like Receptor 7 and TLR9 Dictate Autoantibody Specificity and Have Opposing Inflammatory and Regulatory Roles in a Murine Model of Lupus. *Immunity* (2006) 25:417–28. doi: 10.1016/j.immuni.2006.07.013
70. Wu X, Peng SL. Toll-Like Receptor 9 Signaling Protects Against Murine Lupus. *Arthritis Rheum* (2006) 54:336–42. doi: 10.1002/art.21553
71. Vobořil M, Brabec T, Dobeš J, Šplichalová I, Březina J, Čepková A, et al. Toll-Like Receptor Signaling in Thymic Epithelium Controls Monocyte-Derived Dendritic Cell Recruitment and Treg Generation. *Nat Commun* (2020) 11:2361. doi: 10.1038/s41467-020-16081-3
72. Nickerson KM, Christensen SR, Shupe J, Kashgarian M, Kim D, Elkon K, et al. TLR9 Regulates TLR7- and MyD88-Dependent Autoantibody Production and Disease in a Murine Model of Lupus. *J Immunol (Baltimore Md 1950)* (2010) 184:1840–8. doi: 10.4049/jimmunol.0902592
73. Suthers AN, Sarantopoulos S. TLR7/TLR9- and B Cell Receptor-Signaling Crosstalk: Promotion of Potentially Dangerous B Cells. *Front Immunol* (2017) 8:775. doi: 10.3389/fimmu.2017.00775
74. Tabeta K, Hoebe K, Janssen EM, Du X, Georgel P, Crozat K, et al. The Unc93b1 Mutation 3d Disrupts Exogenous Antigen Presentation and Signaling *via* Toll-Like Receptors 3, 7 and 9. *Nat Immunol* (2006) 7:156–64. doi: 10.1038/ni1297
75. Majer O, Liu B, Woo BJ, Kreuk LSM, Van Dis E, Barton GM. Release From UNC93B1 Reinforces the Compartmentalized Activation of Select TLRs. *Nature* (2019) 575:371–4. doi: 10.1038/s41586-019-1611-7
76. Majer O, Liu B, Kreuk LSM, Krogan N, Barton GM. UNC93B1 Recruits Syntenin-1 to Dampen TLR7 Signalling and Prevent Autoimmunity. *Nature* (2019) 575:366–70. doi: 10.1038/s41586-019-1612-6
77. Sasai M, Iwasaki A. Love Triangle Between Unc93B1, TLR7, and TLR9 Prevents Fatal Attraction. *Immunity* (2011) 35:3–5. doi: 10.1016/j.immuni.2011.07.006
78. Fukui R, Saitoh S, Matsumoto F, Kozuka-Hata H, Oyama M, Tabeta K, et al. Unc93B1 Biases Toll-Like Receptor Responses to Nucleic Acid in Dendritic Cells Toward DNA- But Against RNA-Sensing. *J Exp Med* (2009) 206:1339–50. doi: 10.1084/jem.20082316
79. Arleevskaya MI, Larionova RV, Brooks WH, Bettacchioli E, Renaudineau Y. Toll-Like Receptors, Infections, and Rheumatoid Arthritis. *Clin Rev Allergy Immunol* (2020) 58:172–81. doi: 10.1007/s12016-019-08742-z
80. Saadoun D, Garrido M, Comarmond C, Desbois AC, Domont F, Savey L, et al. Th1 and Th17 Cytokines Drive Inflammation in Takayasu Arteritis. *Arthritis Rheumatol (Hoboken NJ)* (2015) 67:1353–60. doi: 10.1002/art.39037
81. Pan LL, Du J, Gao N, Liao H, Wan J, Ci WP, et al. IL-9-Producing Th9 Cells may Participate in Pathogenesis of Takayasu's Arteritis. *Clin Rheumatol* (2016) 35:3031–6. doi: 10.1007/s10067-016-3399-2
82. Desbois AC, Régnier P, Quiniou V, Lejoncour A, Maciejewski-Duval A, Comarmond C, et al. Specific Follicular Helper T Cell Signature in Takayasu Arteritis. *Arthritis Rheumatol (Hoboken NJ)* (2021) 73:1233–43. doi: 10.1002/art.41672
83. Gao N, Cui W, Zhao LM, Li TT, Zhang JH, Pan LL. Contribution of Th2-Like Treg Cells to the Pathogenesis of Takayasu's Arteritis. *Clin Exp Rheumatol* (2020) 38 Suppl:124 48–54.
84. Barish GD, Yu RT, Karunasiri M, Ocampo CB, Dixon J, Benner C, et al. Bcl-6 and NF-kappaB Cistromes Mediate Opposing Regulation of the Innate Immune Response. *Genes Dev* (2010) 24:2760–5. doi: 10.1101/gad.1998010
85. Park HY, Go H, Song HR, Kim S, Ha GH, Jeon YK, et al. Pellino 1 Promotes Lymphomagenesis by Deregulating BCL6 Polyubiquitination. *J Clin Invest* (2014) 124:4976–88. doi: 10.1172/jci75667
86. Figueroa-Hall LK, Paulus MP, Savitz J. Toll-Like Receptor Signaling in Depression. *Psychoneuroendocrinology* (2020) 121:104843. doi: 10.1016/j.psyneuen.2020.104843
87. He X, Jing Z, Cheng G. MicroRNAs: New Regulators of Toll-Like Receptor Signalling Pathways. *BioMed Res Int* (2014) 2014:945169. doi: 10.1155/2014/945169
88. Piriyapongsa J, Jordan IK. A Family of Human microRNA Genes From Miniature Inverted-Repeat Transposable Elements. *PloS One* (2007) 2:e203. doi: 10.1371/journal.pone.0000203
89. Liang T, Guo L, Liu C. Genome-Wide Analysis of Mir-548 Gene Family Reveals Evolutionary and Functional Implications. *J Biomed Biotechnol* (2012) 2012:679563. doi: 10.1155/2012/679563
90. Xu Y, Zhong YD, Zhao XX. MiR-548b Suppresses Proliferative Capacity of Colorectal Cancer by Binding WNT2. *Eur Rev Med Pharmacol Sci* (2020) 24:10535–41. doi: 10.26355/eurrev_202010_23406
91. Sha MX, Huang XW, Yin Q. MiR-548b-3p Inhibits Proliferation and Migration of Breast Cancer Cells by Targeting MDM2. *Eur Rev Med Pharmacol Sci* (2020) 24:3105–12. doi: 10.26355/eurrev_202003_20675
92. Pan Y, Liang W, Zhao X, Liu L, Qing Y, Li Y. miR-548b Inhibits the Proliferation and Invasion of Malignant Gliomas by Targeting Metastasis Tumor-Associated Protein-2. *Neuroreport* (2016) 27:1266–73. doi: 10.1097/wnr.0000000000000690
93. Qiu H, Zhang G, Song B, Jia J. MicroRNA-548b Inhibits Proliferation and Invasion of Hepatocellular Carcinoma Cells by Directly Targeting Specificity Protein 1. *Exp Ther Med* (2019) 18:2332–40. doi: 10.3892/etm.2019.7812
94. Lin L, Wang Y. miR-548b-3p Regulates Proliferation, Apoptosis, and Mitochondrial Function by Targeting CIP2A in Hepatocellular Carcinoma. *BioMed Res Int* (2018) 2018:7385426. doi: 10.1155/2018/7385426

95. Feng XE. miR-548b Suppresses Melanoma Cell Growth, Migration, and Invasion by Negatively Regulating Its Target Gene Hmgb1. *Cancer Biother Radiopharm* (2021) 36:189–201. doi: 10.1089/cbr.2019.3507
96. Jin M, Lu S, Wu Y, Yang C, Shi C, Wang Y, et al. Hsa_circ_0001944 Promotes the Growth and Metastasis in Bladder Cancer Cells by Acting as a Competitive Endogenous RNA for miR-548. *J Exp Clin Cancer Res CR* (2020) 39:186. doi: 10.1186/s13046-020-01697-6
97. Takashima Y, Kawaguchi A, Iwadate Y, Hondoh H, Fukai J, Kajiwara K, et al. miR-101, miR-548b, miR-554, and miR-1202 Are Reliable Prognosis Predictors of the miRNAs Associated With Cancer Immunity in Primary Central Nervous System Lymphoma. *PloS One* (2020) 15:e0229577. doi: 10.1371/journal.pone.0229577
98. Oshiumi H. Circulating Extracellular Vesicles Carry Immune Regulatory miRNAs and Regulate Vaccine Efficacy and Local Inflammatory Response After Vaccination. *Front Immunol* (2021) 12:685344. doi: 10.3389/fimmu.2021.685344
99. Tsukamoto H, Kouwaki T, Oshiumi H. Aging-Associated Extracellular Vesicles Contain Immune Regulatory microRNAs Alleviating Hyperinflammatory State and Immune Dysfunction in the Elderly. *iScience* (2020) 23:101520. doi: 10.1016/j.isci.2020.101520
100. Rosenberger CM, Podyminogin RL, Navarro G, Zhao GW, Askovich PS, Weiss MJ, et al. miR-451 Regulates Dendritic Cell Cytokine Responses to Influenza Infection. *J Immunol (Baltimore Md 1950)* (2012) 189:5965–75. doi: 10.4049/jimmunol.1201437
101. Miyashita Y, Ishikawa K, Fukushima Y, Kouwaki T, Nakamura K, Oshiumi H. Immune-Regulatory microRNA Expression Levels Within Circulating Extracellular Vesicles Correspond With the Appearance of Local Symptoms After Seasonal Flu Vaccination. *PloS One* (2019) 14:e0219510. doi: 10.1371/journal.pone.0219510
102. Jin MS, Kim SE, Heo JY, Lee ME, Kim HM, Paik S-G, et al. Crystal Structure of the TLR1-TLR2 Heterodimer Induced by Binding of a Tri-Acylated Lipopeptide. *Cell* (2007) 130:1071–82. doi: 10.1016/j.cell.2007.09.008
103. Mukherjee A, Roy S, Patidar A, Bodhale N, Dandapat J, Saha B, et al. TLR2 Dimer-Specific Ligands Selectively Activate Protein Kinase C Isoforms in Leishmania Infection. *Immunology* (2021) 164:318–31. doi: 10.1111/imm.13373
104. Spitzer JH, Visintin A, Mazzoni A, Kennedy MN, Segal DM. Toll-Like Receptor 1 Inhibits Toll-Like Receptor 4 Signaling in Endothelial Cells. *Eur J Immunol* (2002) 32:1182–7. doi: 10.1002/1521-4141(200204)32:4<1182::Aid-immu1182>3.0.Co;2-9
105. da Rocha Sobrinho HM, Saar Gomes R, da Silva DJ, Quixabeira VBL, Joosten LAB, Ribeiro de Barros Cardoso C, et al. Toll-Like Receptor 10 Controls TLR2-Induced Cytokine Production in Monocytes From Patients With Parkinson's Disease. *J Neurosci Res* (2021) 99:2511–24. doi: 10.1002/jnr.24916
106. Sun J, Wiklund F, Zheng SL, Chang B, Bälter K, Li L, et al. Sequence Variants in Toll-Like Receptor Gene Cluster (TLR6-TLR1-TLR10) and Prostate Cancer Risk. *J Natl Cancer Inst* (2005) 97:525–32. doi: 10.1093/jnci/dji070

Conflict of Interest: The authors declare that the research was conducted in the absence of any commercial or financial relationships that could be construed as a potential conflict of interest.

Publisher's Note: All claims expressed in this article are solely those of the authors and do not necessarily represent those of their affiliated organizations, or those of the publisher, the editors and the reviewers. Any product that may be evaluated in this article, or claim that may be made by its manufacturer, is not guaranteed or endorsed by the publisher.

frontiers in Immunology

ORIGINAL RESEARCH
published: 03 February 2022
doi: 10.3389/fimmu.2021.748996

Toll-Like Receptor-Induced Immune Responses During Early Childhood and Their Associations With Clinical Outcomes Following Acute Illness Among Infants in Sub-Saharan Africa

Luke S. Uebelhoer[1†], Agnes Gwela[2†], Bonnie Thiel[3], Sophie Nalukwago[4], John Mukisa[5], Christopher Lwanga[4], Justine Getonto[2], Emily Nyatichi[2], Grace Dena[2], Alexander Makazi[2], Shalton Mwaringa[2], Ezekiel Mupere[4,6], James A. Berkley[2,7], and Christina L. Lancioni[1] on behalf of the Childhood Acute Illness & Nutrition (CHAIN) Network*

[1] Department of Pediatrics, Oregon Health & Science University, Portland, OR, United States, [2] KEMRI-Wellcome Trust Research Programme, Kilifi, Kenya, [3] Tuberculosis Research Unit (TBRU), Case Western Reserve University, Cleveland, OH, United States, [4] Uganda-Case Western Reserve University Research Collaboration, Kampala, Uganda, [5] Department of Immunology and Molecular Biology, College of Health Sciences, Makerere University, Kampala, Uganda, [6] Department of Pediatrics and Child Health, College of Health Sciences, Makerere University, Kampala, Uganda, [7] Centre for Tropical Medicine & Global Health, University of Oxford, Oxford, United Kingdom

OPEN ACCESS

Edited by:
Simon Daniel Van Haren, Boston Children's Hospital and Harvard Medical School, United States

Reviewed by:
Steven O'Reilly, STipe Therapeutics, Denmark
Olubukola Temitope Idoko, University of London, United Kingdom

***Correspondence:**
Christina L. Lancioni
lancioni@ohsu.edu

[†]These authors have contributed equally to this work

Specialty section:
This article was submitted to Cytokines and Soluble Mediators in Immunity, a section of the journal Frontiers in Immunology

Received: 28 July 2021
Accepted: 28 December 2021
Published: 03 February 2022

Citation:
Uebelhoer LS, Gwela A, Thiel B, Nalukwago S, Mukisa J, Lwanga C, Getonto J, Nyatichi E, Dena G, Makazi A, Mwaringa S, Mupere E, Berkley JA and Lancioni CL (2022) Toll-Like Receptor-Induced Immune Responses During Early Childhood and Their Associations With Clinical Outcomes Following Acute Illness Among Infants in Sub-Saharan Africa. Front. Immunol. 12:748996. doi: 10.3389/fimmu.2021.748996

Severely ill children in low- and middle-income countries (LMICs) experience high rates of mortality from a broad range of infectious diseases, with the risk of infection-related death compounded by co-existing undernutrition. How undernutrition and acute illness impact immune responses in young children in LMICs remains understudied, and it is unclear what aspects of immunity are compromised in this highly vulnerable population. To address this knowledge gap, we profiled longitudinal whole blood cytokine responses to Toll-like receptor (TLR) ligands among severely ill children (n=63; 2-23 months old) with varied nutritional backgrounds, enrolled in the CHAIN Network cohort from Kampala, Uganda, and Kilifi, Kenya, and compared these responses to similar-aged well children in local communities (n=41). Cytokine responses to ligands for TLR-4 and TLR-7/8, as well as Staphylococcus enterotoxin B (SEB), demonstrated transient impairment in T cell function among acutely ill children, whereas innate cytokine responses were exaggerated during both acute illness and following clinical recovery. Nutritional status was associated with the magnitude of cytokine responses in all stimulated conditions. Among children who died following hospital discharge or required hospital re-admission, exaggerated production of interleukin-7 (IL-7) to all stimulation conditions, as well as leukopenia with reduced lymphocyte and monocyte counts, were observed. Overall, our findings demonstrate exaggerated innate immune responses to pathogen-associated molecules among acutely ill young children that persist during recovery. Heightened innate immune responses to TLR ligands may contribute to chronic systemic inflammation and dysregulated responses to subsequent infectious challenges. Further delineating

mechanisms of innate immune dysregulation in this population should be prioritized to identify novel interventions that promote immune homeostasis and improve outcomes.

Keywords: sepsis, toll-like receptor, lipopolysaccharide, malnutrition, pediatric, innate immunity, adaptive immunity

INTRODUCTION

Sepsis continues to be a significant cause of pediatric morbidity and mortality worldwide. Although pediatric mortality from sepsis has steadily decreased in well-resourced settings, in low- and middle- income countries (LMICs) the resources required to support patients with sepsis are scarce and outcomes remain exceptionally poor (1–7). Coupled with undernutrition, a highly prevalent condition among young children in LMICs, acute infection manifesting initially as diarrhea or pneumonia often progresses to sepsis, and these common infections continue to be primary drivers of death in children less than 5 years old worldwide (8–11).

Children in LMICs who present to hospital with acute illness are often severely stunted and/or wasted, with underlying environmental enteric dysfunction (EED) (12–15). EED is believed to be a major driver of recurrent infections, immune activation, and chronic inflammation during childhood. Changes in small bowel function accompanied by altered mucosal architecture results in malabsorption and an increase in pathogen translocation that predisposes young children to invasive infection and drives immune dysregulation (12–14, 16–21). Young children with EED often become trapped in a vicious cycle of malnutrition, infection, and inflammation that has been associated with compromised linear growth and neurodevelopment, impaired thymic development, intestinal dysbiosis, and nutritionally-acquired immunodeficiency syndrome (22–31).

The immune response to invasive infection is complex and highly variable due to the multitude of pathogens capable of inducing disease, and underlying host conditions such as age and presence of co-morbidities (32, 33). Studies of critically ill adults and children in resourced settings have suggested that specific immune phenotypes and responses are associated with poor outcomes (34). Both pro- and anti-inflammatory responses are involved: the former contributes to clearance of infection and recovery but can also lead to collateral tissue damage and organ failure; the latter limits local and systemic tissue injury by weakening the immune response, but can lead to secondary infections (33, 35, 36). Cells of the innate immune system, such as monocytes, dendritic cells, and natural killer cells, play a pivotal role in initiation of the immune response against pathogens, and in shaping subsequent adaptive immune responses. Pattern recognition receptors (PRR) on the innate cell surface [toll-like receptors (TLRs) and C-type lectin receptors [CLRs)], in the endosome (TLRs), and in the cytoplasm [retinoic acid-inducible gene-I-like receptors (RLRs) and nucleotide-binding oligomerization domain-like receptors [NLRs)] interact with pathogen-associated molecular patterns (PAMPs) to initiate pro-inflammatory immune responses against pathogens (37). However, the resultant tissue damage from this response releases alarmins and damage-associated molecular patterns (DAMPs) that perpetuate the pro-inflammatory response by autocrine action and can lead to organ dysfunction (38). Anti-inflammatory and tissue-repair immune responses are also elicited during both acute and convalescent phases of severe illness (39), and may contribute to secondary infections among patients who survive their initial infection. This post-sepsis response has been described as "immunoparalysis", or a state of cellular senescence, where immune cells remain locked in a functionally impaired state by either extrinsic (repeated pathogenic insult, global DAMP expression) or intrinsic (altered T cell repertoires, increased inhibitory receptor expression) factors (40). During sepsis-induced immunoparalysis, there is a massive attrition of lymphocytes that leads to the perpetuation of ongoing infectious foci, an increase in secondary infections, reactivation of latent viremias, and re-admission to hospital with poor outcomes (41–45).

For young children in LMICs, there remains a high mortality rate during hospitalization for severe infection, as well as an increased risk of death for several months following hospital discharge for those children who survived the acute phase of illness (46). The Childhood Acute Illness & Nutrition (CHAIN) Network (47–49) is a network of investigators and sites in LMICs dedicated to understanding biologic and social determinants of survival among highly vulnerable young children during and following severe illness. Working with young, undernourished children in LMICs admitted to hospital with severe illness as part of the CHAIN observational cohort study, and who survived through hospital discharge, we characterized TLR-induced whole blood cytokine responses during acute and convalescent phases of illness. Moreover, we sought to understand if underlying nutritional status was associated with altered host immune responses, and if immune profiles could be used to identify those acutely ill children who would go on to experience an event (death or re-admission) following hospital discharge. Interrogation of immune responses among highly vulnerable young children during severe illness is a critical first step to the identification of specific immunologic pathways associated with poor versus thriving outcomes, and in the development of novel interventions to improve pediatric post-hospitalization outcomes in LMICs.

MATERIALS AND METHODS

Participant Recruitment and Ethics Statement

Participants were enrolled in the Childhood Acute Illness & Nutrition (CHAIN) Network from January 2016-December 2019 (47–49). The CHAIN study protocol was reviewed and approved

by the Oxford Tropical Research Ethics Committee (OxTREC), the Scientific and Ethics Review Unit (SERU) of the Kenya Medical Research Institute (KEMRI), and the Makerere University College of Health Sciences, School of Biomedical Sciences Research and Ethics Committee, as well as the institutional review boards of all partner sites. Participating CHAIN sites were Kampala, Uganda, and Kilifi, Kenya. Written informed consent was obtained from a parent or guardian for all participating children prior to enrollment.

Study Design and Participant Demographics

Children requiring hospitalization at the Kampala and Kilifi CHAIN network sites, who survived their inpatient admission and had blood available for immunologic-based investigations, were eligible for inclusion in the present study. Children were admitted to hospital predominately for severe diarrhea, pneumonia, malaria, and/or anemia, and were commonly found to be malnourished. Children presenting with acute trauma or poisoning were ineligible; for a complete list of inclusion and exclusion criteria in the CHAIN Network study, please refer to Diallo et al. (49). Three subsets of children were included in this analysis: hospitalized children who experienced post-discharge events of re-admission or death (n=22); hospitalized children who did not experience a post-discharge event and survived to month 6 study end point (n=41); non-hospitalized age-matched, well children recruited from local neighborhoods (community participants/CP) serving as a reference group for comparison to hospitalized participants (n=41). Participant demographics are provided in **Table 1**. Nutritional status was stratified by mid-upper arm circumference (MUAC), defined by the CHAIN Network as: not wasted, MUAC ≥12.5cm (age ≥6 months) or MUAC ≥12cm (age <6 months); moderate wasting, MUAC 11.5 to <12.5cm (age ≥6months) or MUAC 11 to <12cm (age <6 months); severe wasting or kwashiorkor, MUAC <11.5cm (age ≥6 months) or MUAC <11cm (age <6 months) or bilateral pedal oedema not explained by other medical causes.

Whole Blood Cytokine Assay

Blood was collected for immunologic assays within 48 hours of hospital admission, the day of hospital discharge, and 6-months following index hospital admission (among survivors). For CP, blood was obtained at study enrollment only. Peripheral blood was drawn and collected in 2 ml sodium-heparin tubes (BD, catalog #367671) using a standardized SOP for venipuncture that included sterile technique and preparation of the skin with 70% alcohol. 200 µl of undiluted whole blood was aliquoted to individual 2 ml polypropylene tubes (Sarstedt, Germany) pre-prepared with the following stimulants diluted at 5x final concentration in 50 µl RPMI-1640: 1) none (resting condition); 2) ultrapure lipopolysaccharide (LPS, TLR-4 ligand, 0.2 µg/ml, *In vivo*gen, catalog #tlrl-smlps); 3) CL075 (thiazoquinoline derivative, TLR-7/8 ligand, 5 µg/ml, *In vivo*gen, catalog #tlrl-c75-5); 4) staphylococcal enterotoxin B (SEB, monovalent T cell mitogen, 1 µg/ml, Toxin Technology, catalog #BT202). Whole blood stimulation was performed in a water bath at 37°C for 12 hours. Stimulation conditions and incubation time were selected based on previous literature (50–57). To collect materials for cytokine analysis, tubes were spun at 2000 rpm (300 rcf) in a tabletop centrifuge, and the supernatant drawn off and stored at -80°C until batch analysis.

Multiplex Cytokine Analysis

A custom multiplex cytokine bead array was created using the existing EMD Millipore platform. The following panel of 25 cytokines/chemokines were included: G-CSF, GM-CSF, IFN-α2, IFN-γ, IL-10, MCP-3, IL-12p70, IL-15, sCD40L, IL-17A, IL-1RA, IL-1α, IL-9, IL-1β, IL-2, IL-4, IL-6, IL-7, IL-8, IP-10, MCP-1, Mip-1α, Mip-1β, RANTES, TNF-α. Frozen supernatants were gently thawed and diluted 1:5 using RPMI-1640 prior to performing the assay according to manufacturer's instructions. All conditions were plated in duplicate. The quality-control samples provided by the manufacturer were included on each plate. A minimum of 50 beads captured was set as the cutoff for each analyte; no analytes fell below this minimum during data acquisition. Plates were run on a Luminex 200™ machine and analyzed using xPONENT® software.

TABLE 1 | Participant demographics.

	Hospitalization cohorts		Community participants	P-value
	Post-discharge event (n=22)	No post-discharge event (n=41)	(n=41)	
Recruitment (Uganda)	9 (41%)	15 (37%)	15 (37%)	0.90[3]
Age (months; SD)	11.1 (5.3)	12 (4.7)	12.2 (5.1)	0.71[2]
Sex (female)	9 (41%)	19 (46%)	16 (39%)	0.80[3]
Nutritional status[1]				
Severe wasting	12 (55%)	17 (41%)	0	<0.0001[3]
Moderate wasting	3 (14%)	7 (17%)	2 (5%)	0.21[3]
Non-wasted	7 (32%)	17 (41%)	39 (95%)	<0.0001[3]
Mean MUAC[1] (cm)	11.19	12.52	13.82	<0.0001[2]
HIV-exposed	5 (23%)	5 (12%)	4 (10%)	0.34[3]
HIV-infected	4 (18%)	1 (2%)	0	0.05[4]

[1]*Nutritional status as determined by mid-upper arm circumference (MUAC) at hospital admission (hospitalized cohorts) or enrollment (community participants).*
[2]*Three-way comparisons performed using ANOVA.*
[3]*Three-way comparisons performed using Chi squared test.*
[4]*Two-way comparison between children with and without post-discharge events performed using Fisher's Exact test.*

Research Blood Analysis

All participants had complete blood counts with automated differential performed at all time points. Blood was analyzed using a Coulter Ac*T 5diff CP (Cap Pierce) Hematology Analyzer (Beckman Coulter).

Statistical Approach

Initial analysis compared resting and stimulated whole blood production of individual cytokines/chemokines between sick, hospitalized children versus children from the same communities (community participants/CP). For the stimulation conditions, background correction was performed prior to analysis and all cytokine/chemokine data underwent log2 transformation to achieve a normalized distribution. For the hospitalized cohort, quantitative cytokine/chemokine results from three time points corresponding to acute illness (hospital admission), early convalescence (hospital discharge), and late convalescence (6-months following initial admission), were compared to those obtained from CP at a single time point. To determine if an individual cytokine/chemokine response in the resting or a stimulation condition was predictive of belonging to the hospitalized versus community cohort, a multivariable logistic regression model incorporating age, sex, recruitment site, and MUAC (at relevant time point) as covariates was applied. Odds ratios and 95% confidence intervals are reported.

To determine the relationship between nutritional status and cytokine/chemokine responses among children in the hospitalized cohort, multivariable linear regression models including age, sex, and site as covariates were applied. Here, individual cytokine/chemokine responses from the resting and stimulation conditions were compared to MUAC at each relevant time point. Parameter estimates, referring to the slope of the relationship between MUAC and the individual cytokine/chemokine response, were calculated; negative and positive parameter estimates denote an indirect or direct relationship, respectively.

A composite cytokine signature that was predictive of belonging to the hospitalized versus community cohort for the resting and each stimulation condition was created, and used to assess the impact of nutritional status on each signature's predictive value for recent hospitalization. Using a stepwise logistic regression model with both forward and backward elimination for each stimulation condition, individual cytokines and chemokines showing an effect (threshold for selection was $p<0.2$) on the (log) odds of belonging to the hospitalized cohort were combined to find the best predictive immune signature, with age, sex and site included as covariates. The predictive (log) odds of each cytokine signature were then plotted against MUAC.

In addition, a logistic regression model including MUAC, age, sex, and site was developed to evaluate the relationship between stimulated cytokine/chemokine responses at hospital discharge and the odds ratio of a child experiencing a post-discharge event. Total white blood cell (WBC) and absolute lymphocyte, monocyte, and neutrophil counts were also compared between hospitalized children with and without post-discharge events in an unadjusted analysis, comparing medians to avoid the influence of outliers in data, using the Mann-Whitney test. To determine whether covariates had any effect on these differences, the data was winsorized at the lower 5^{th} and upper 95^{th} percentiles to exclude outliers, and a linear regression model including MUAC, age, sex and site as additional covariates was employed.

Due to the limited sample size of this pilot study, comparisons where unadjusted p-values were ≤0.05 are reported, as are p-values adjusted for multiple comparisons with false discovery rate (FDR) ≤0.1 using the Benjamini-Hochberg procedure.

RESULTS

Participants

A total of 63 hospitalized children (24 Kampala; 39 Kilifi) and 41 CPs (15 Kampala; 26 Kilifi) were included for analysis. The demographic breakdown of these participants, including age, sex, MUAC, nutritional status, and HIV status is listed in **Table 1**.

Children Hospitalized for Severe Illness Have a Reduced Innate Resting Cytokine Profile as Compared to Children in the Community During Both Acute and Convalescent Phases of Illness

We first examined the resting cytokine profiles in children who were hospitalized for severe illness (hospitalized cohort), as compared to CP. Whole blood cytokine/chemokine responses of hospitalized children at admission, discharge, and at 6-months post-discharge, were compared to CP at a single time point (enrollment). Hospitalized children had lower innate pro-inflammatory cytokine/chemokine levels compared to CP, that persisted throughout the acute and convalescent phases of illness. Lower resting values were predictive of recent hospitalization for numerous innate cytokines (**Figures 1A–C**). No evidence of increased baseline production of pro-inflammatory cytokines was observed in hospitalized children at any time point.

We next examined the relationship between nutritional status and resting immune profiles among hospitalized children during the early convalescent phase of illness when acute illness has resolved (hospital discharge), considering each cytokine individually. Comparing the relationship between MUAC and resting cytokine response, we observed a significant indirect relationship between MUAC and resting values for G-CSF, GM-CSF, IFN-α2, and IL-6 (**Figure 1D**).

To visualize how nutritional status interacts with the resting host cytokine signature during the early convalescent phase of illness, we created a model incorporating the resting whole blood cytokine responses that best discriminate between hospitalized and CP children (G-CSF, GM-CSF, MCP-3, IL-6, Mip-1β), and compared this to nutritional status as indicated by MUAC at time of hospital discharge in only hospitalized children. Here we observed that the identified resting cytokine signature was a poor predictor of recent hospitalization regardless of MUAC (**Figure 1E**).

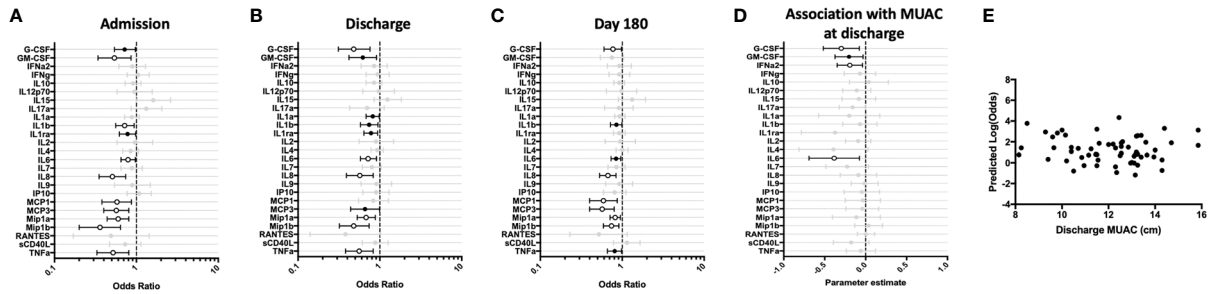

FIGURE 1 | Children hospitalized for severe illness show reduced levels of innate cytokines and chemokines compared to children in the community that persist into convalescence. Whole blood cytokine and chemokine responses were assessed in hospitalized participants at admission to hospital (n=43, **A**), hospital discharge (n=60, **B**), and 180 days-post-discharge (n=51, **C**), and compared to community participants (CP) at enrollment (n=41) using logistic regression taking into account age, sex, recruitment site, and MUAC (at relevant time point). Odds ratios denote higher or lower responses in hospitalized cohort compared to CP cohort. **(D)** Whole blood cytokine and chemokine responses were compared to nutritional status, as measured by MUAC, in hospitalized participants at discharge (n=60) using linear regression taking into account age, sex, and recruitment site. Parameter estimate refers to the slope of the relationship between MUAC and cytokine or chemokine responses; negative and positive parameter estimates denote an indirect or direct relationship, respectively. For **(A–D)**, filled circles indicate significance of $p \leq 0.05$; open circles indicate significance of $p \leq 0.1$ when adjusting for multiple comparisons. **(E)** To better understand the relationship between cytokine responses and nutritional status in hospitalized participants, a model was created using the cytokine signature (G-CSF, GM-CSF, MCP-3, IL-6, Mip-1-beta) that best discriminated between hospitalized (discharge time point) and CP cohorts. Here, the model adjusted for participant sex, age, and recruitment site, and the predictive strength of the model to reflect recent hospitalization (Y-axis) was plotted against participant MUJAC as measured at hospital discharge (X-axis).

Impaired Adaptive Th-1 Responses and Elevated Innate Responses to LPS Are Observed Among Hospitalized Children During the Acute and Convalescent Phases of Illness

To determine if cytokine responses to the TLR-4 agonist LPS were intact among young hospitalized children, we compared LPS-stimulated whole blood responses of the hospitalized cohort to those identified in the CP cohort. A cross-sectional comparison of these responses at hospital admission, discharge, and after 6-months of follow-up demonstrated that, as compared to children in the community, hospitalized children displayed a significantly enhanced innate pro-inflammatory cytokine response to TLR-4 stimulation during acute and early convalescent phases of illness. Increased cytokine values were predictive of recent hospitalization for several cytokines (**Figure 2**). IL-8 and Mip-1β remained elevated at the 6-month follow-up visit (**Figure 2C**). Conversely, hospitalized children showed an impaired Th-1 response to LPS during acute illness, as indicated by decreased IFN-γ and IP-10 responses compared to CP, that resolved during early convalescence. Here, reduced IFN-γ and IP-10 were predictive of recent hospitalization (**Figures 2A–C**).

We next examined the relationship between nutritional status and LPS-induced immune profile among hospitalized children during the early convalescent phase of illness when acute illness has resolved (hospital discharge), looking at each cytokine individually. Comparing the relationship between MUAC and LPS-induced cytokine response, we observed a direct relationship between LPS-induced G-CSF, GM-CSF, and sCD40L, whereas the relationship between MUAC and LPS-induced MCP-3 was indirect (**Figure 2D**).

To visualize how nutritional status interacts with the LPS-induced host cytokine signature during the early convalescent phase of illness, a model was created using the whole blood cytokine signature best discriminating between hospitalized and community children (G-CSF, IFN-γ, Mip-1β, IL-6, IL-8), and compared to nutritional status as indicated by MUAC at time of hospital discharge in only hospitalized children. Here we observed that the identified LPS-induced cytokine signature was highly variable in its ability to predict recent hospitalization regardless of MUAC (**Figure 2E**).

Innate and Th-1-Specific Adaptive Cytokine Responses to Thiazoquinoline, a TLR-7 and -8 Agonist, Are Impaired During the Acute and Convalescent Phases of Illness

Next, we assessed the immune responses of hospitalized children to thiazoquinoline (CL075), a compound that signals through the TLR-7 and -8 pathways. Whole blood cytokine responses in the hospitalized cohort demonstrated impaired innate and adaptive (Th-1) responses during both acute and convalescent phases of illness, as compared to CP cohort. GM-CSF, IFN-γ, IL-12p70, IL-1α, IL-1β, IP-10, and TNF-α were all lower at hospital admission compared to CP, with depressed IFN-γ and IL-12p70 persisting through 6-months of follow-up. These depressed cytokine values were associated with increased odds of recent hospitalization (**Figures 3A–C**).

We examined the relationship between nutritional status and CL075-induced immune profile among hospitalized children during the early convalescent phase of illness when acute illness has resolved (hospital discharge), looking at each cytokine individually. Comparing the relationship between MUAC and CL075-induced cytokine response, we observed a direct relationship between CL075-induced IL-12p70, IL-4, IL-7, and sCD40L, whereas the relationship between MUAC and CL075-induced MCP-3 was indirect (**Figure 3D**).

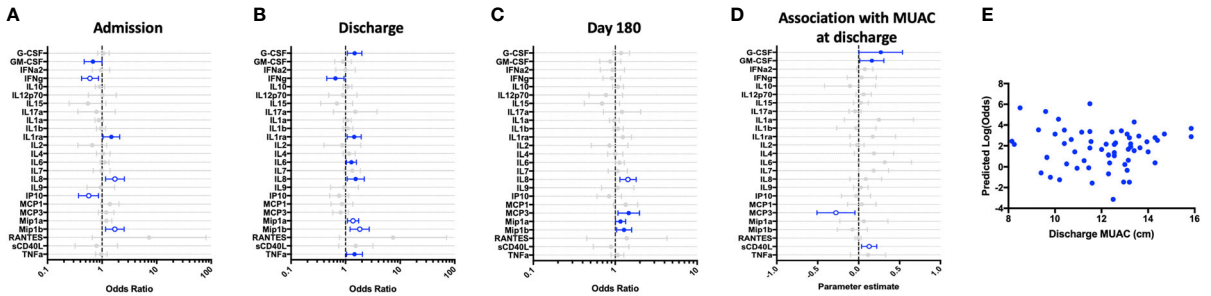

FIGURE 2 | Children hospitalized for severe illness show impaired Th-1 responses and increased innate responses to LPS when compared to children in the community that persist into convalescence. LPS-stimulated whole blood cytokine and chemokine responses were assessed in hospitalized participants at admission to hospital (n=43, **A**), hospital discharge (n=60, **B**), and 180 days-post-discharge (n=51, **C**), and compared to community participants (CP) at enrollment (n=41) using logistic regression taking into account age, sex, recruitment site, and MUAC (at relevant time point). Odds ratios denote higher or lower responses in hospitalized cohort compared to CP cohort. **(D)** Whole blood cytokine and chemokine responses were compared to nutritional status, as measured by MUAC, in hospitalized participants at discharge (n=60) using linear regression taking into account age, sex, and recruitment site. Parameter estimate refers to the slope of the relationship between MUAC and cytokine or chemokine responses; negative and positive parameter estimates denote an indirect or direct relationship, respectively. For **(A–D)**, filled circles indicate significance of p≤0.05; open circles indicate significance of p≤0.1 when adjusting for multiple comparisons. **(E)** To better understand the relationship between cytokine responses and nutritional status in hospitalized participants, a model was created using the cytokine signature (G-CSF, IFNg, Mip-1-beta, IL-6, IL-8) that best discriminated between hospitalized (discharge time point) and CP cohorts. Here, the model adjusted for participant sex, age, and recruitment site, and the predictive strength of the model to reflect recent hospitalization (Y-axis) was plotted against participant MUAC as measured at hospital discharge (X-axis).

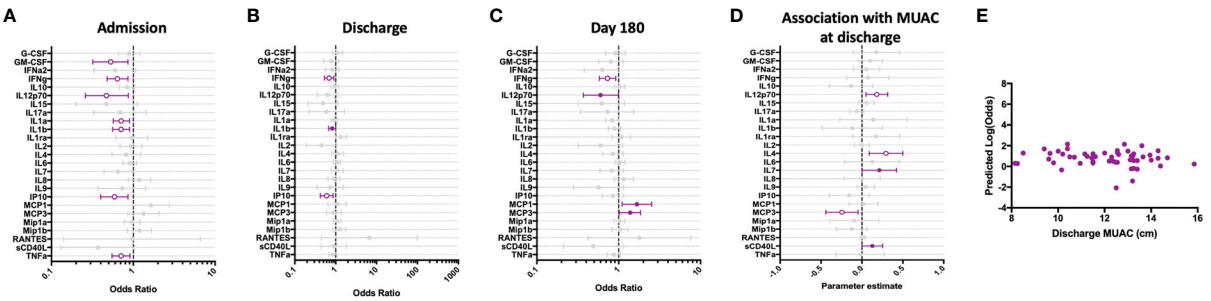

FIGURE 3 | Children hospitalized for severe illness show impaired Th-1 and innate responses to TLR-7/8 stimulation when compared to children in the community that persist into convalescence. CL075-stimulated whole blood cytokine and chemokine responses were assessed in hospitalized participants at admission to hospital (n=43, **A**), hospital discharge (n=60, **B**), and 180 days-post-discharge (n=51, **C**), and compared to community participants (CP) at enrollment (n=41) using logistic regression taking into account age, sex, recruitment site, and MUAC (at relevant time point). Odds ratios denote higher or lower responses in hospitalized cohort compared to CP cohort. **(D)** Whole blood cytokine and chemokine responses were compared to nutritional status, as measured by MUAC, in hospitalized participants at discharge (n=60) using linear regression taking into account age, sex, and recruitment site. Parameter estimate refers to the slope of the relationship between MUAC and cytokine or chemokine responses; negative and positive parameter estimates denote an indirect or direct relationship, respectively. For **(A–D)**, filled circles indicate significance of p≤0.05; open circles indicate significance of p≤0.1 when adjusting for multiple comparisons. **(E)** To better understand the relationship between cytokine responses and nutritional status in hospitalized participants, a model was created using IFNg, a cytokine that best discriminated between hospitalized (discharge time point) and CP cohorts. Here, the model adjusted for participant sex, age, and recruitment site, and the predictive strength of the model to reflect recent hospitalization (Y-axis) was plotted against participant MUAC as measured at hospital discharge (X-axis).

We next visualized how nutritional status interacts with CL075-induced host cytokine signature during the early convalescent phase of illness. A model was created using the whole blood cytokine signature best discriminating between hospitalized and community children (IFN-γ only), and compared to MUAC at hospital discharge among hospitalized children. We observed no clear relationship between the predictive value of CL075-induced IFN-γ responses for recent hospitalization and nutritional status as reflected by MUAC (**Figure 3E**).

Staphylococcus Enterotoxin B-Induced T Cell Responses in Whole Blood of Hospitalized Children Are Impaired During Acute Illness but Improve During Convalescence

To assess T cell responses to polyclonal activation, we stimulated whole blood with the superantigen staphylococcus enterotoxin B (SEB). As compared to children in the community, T cell responses to SEB were transiently impaired at hospital

admission, as indicated by decreased IFN-γ, IL-2, IL-9, and IL-17A (**Figure 4A**). However, all T cell responses, except for IFN-γ, had recovered to that seen in CP by hospital discharge (**Figure 4B**). Further, when assessed at 6-month follow-up, these responses were equivalent to those observed in CP (**Figure 4C**). Notably, innate cytokine responses (IL-6, IL-8, MCP-1 and Mip-1β) were elevated during the last convalescence phase of illness as compared to children in the community (**Figure 4C**).

We examined the relationship between nutritional status and SEB-induced immune profile among hospitalized children during the early convalescent phase of illness when acute illness has resolved (hospital discharge), looking at each cytokine individually. Comparing the relationship between MUAC and SEB-induced cytokine response, we observed a direct relationship between SEB-induced IL-4 and sCD40L; no other direct or indirect relationships were observed (**Figure 4D**).

We next visualized how nutritional status interacts with SEB-induced host cytokine signature during the early convalescent phase of illness. A model was created using the whole blood cytokine signature best discriminating between hospitalized and community children (IFN-γ only), and compared to MUAC at hospital discharge among hospitalized children. Here we observed no clear relationship between the predictive value of SEB-induced IFN-γ responses for recent hospitalization and nutritional status as reflected by MUAC (**Figure 4E**).

White Blood Cell Counts and IL-7 Production Are Altered Among Children With Post-Discharge Events

Children who experienced post-discharge events of hospital re-admission or death showed significantly lower total white blood cell counts, including absolute lymphocyte and monocyte counts, when compared to children who did not experience post-discharge events throughout 6-months of follow-up. This effect remained significant when the data was adjusted using a linear model taking into account MUAC, age, sex and site (**Figure 5**). No difference in absolute neutrophil count was noted in this analysis (**Figure 5D**). In addition, whole blood immune responses to TLRs and SEB were compared between children with and without post-discharge events (**Figure 6**). Increased IL-7 production to all tested stimuli among children with post-discharge events was observed. This increase in IL-7 responses was associated with increased odds of a post-discharge event (**Figures 6B–D**). No significant association between IL-7 levels and absolute lymphocyte counts were found in children with post-discharge events (data not shown). There was no significant impairment in cytokine production to any tested stimuli observed when comparing children with and without post-discharge events (**Figures 6A–D**).

DISCUSSION

In this study we examined resting and stimulated whole blood cytokine responses among young children living in LMICs, including children who required hospitalization for severe illness and well children recruited from local communities. The TLR agonists utilized in this study served as a method of interrogating functional host immune responses that may have been deranged as a result of severe acute illness and undernutrition, both common among children in LMICs. We specifically selected LPS, an agonist for TLR-4, to model innate responses to gram-negative pathogens that commonly cause severe illness in this population (58). CL075, a dual agonist for TLR-7 and TLR-8 that mimics single-stranded RNA, was selected for study given the high burden of viral infections in young children.

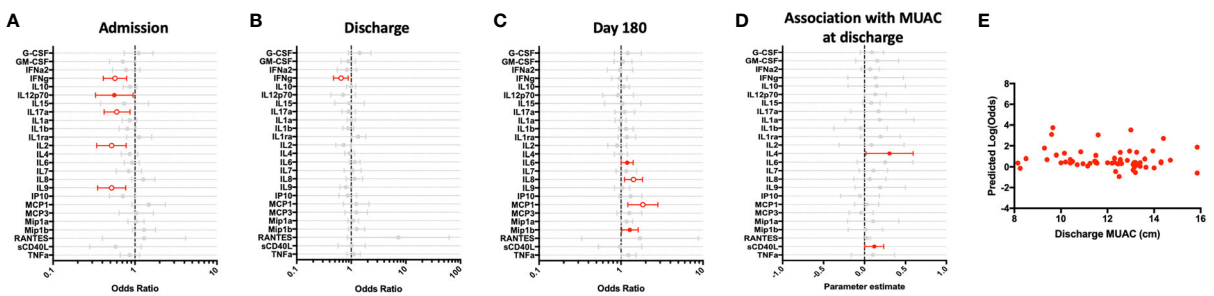

FIGURE 4 | Children hospitalized for severe illness exhibit an impaired T cell response to polyclonal stimulation when compared to children in the community that improves during convalescence. SEB-stimulated whole blood cytokine and chemokine responses were assessed in hospitalized participants at admission to hospital (n=43, **A**), hospital discharge (n=60, **B**), and 180 days-post-discharge (n=51, **C**), and compared to community participants (CP) at enrollment (n=41) using logistic regression taking into account age, sex, recruitment site, and MUAC. Odds ratios denote higher or lower responses in hospitalized cohort compared to CP cohort. **(D)** Whole blood cytokine and chemokine responses were compared to nutritional status, as measured by MUAC, in hospitalized participants at discharge (n=60) using linear regression taking into account age, sex, and recruitment site. Parameter estimate refers to the slope of the relationship between MUAC and cytokine or chemokine responses; negative and positive parameter estimates denote an indirect or direct relationship, respectively. For **(A–D)**, filled circles indicate significance of p≤0.05; open circles indicate significance of p≤0.1 when adjusting for multiple comparisons. **(E)** To better understand the relationship between cytokine responses and nutritional status in hospitalized participants, a model was created using IFNg, a cytokine that best discriminated between hospitalized (discharge time point) and CP cohorts. Here, the model adjusted for participant sex, age, and recruitment site, and the predictive strength of the model to reflect recent hospitalization (Y-axis) was plotted against participant MUAC as measured at hospital discharge (X-axis).

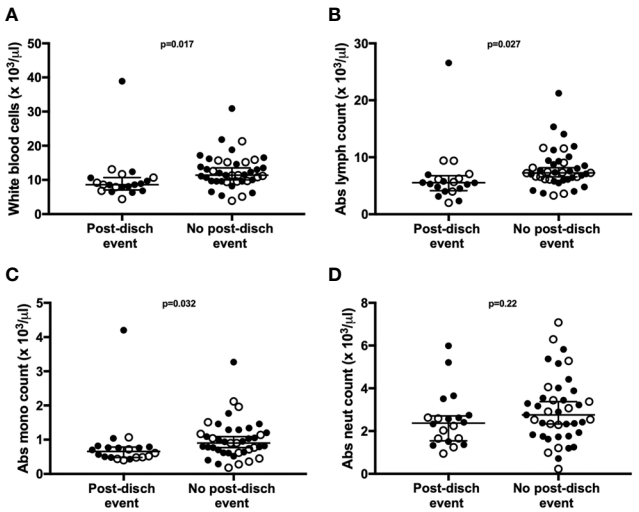

FIGURE 5 | Total lymphocyte, leukocyte, and monocyte counts are associated with post-discharge adverse events in children hospitalized for severe illness. Complete blood counts with differential were performed at hospital discharge and compared between participants with (n=20) and without (n=41) post-discharge events of death or re-admission to hospital. Shown are median values with interquartile range for white blood cell counts **(A)**, absolute lymphocyte counts **(B)**, absolute monocyte counts **(C)**, and absolute neutrophil counts **(D)**, displayed as cell number x10 ^{3}/μl of blood. P-values were calculated using Mann-Whitney test. Filled circles and open circles indicate participants from Kilifi, Kenya and Kampala, Uganda sites, respectively.

Based on prior studies of severely ill adults and children performed in well-resourced settings (40, 59–62), we anticipated that hospitalized children would exhibit limited pro-inflammatory cytokine/chemokine responses to the tested stimuli, with malnourished children and children who experience post-discharge events exhibiting the most muted responses. Our data revealed that the immune response to each stimulus was distinct, with heightened innate cytokine responses to LPS among hospitalized children that persisted through late convalescence, while cytokine responses to CL075 were compromised during both acute and early convalescent stages of illness. Responses to the T cell mitogen SEB demonstrated compromised production of several T-cell-associated cytokines (IFN-γ, IL-17A, IL-2, and IL-9) during acute illness, with exaggerated production of pro-inflammatory innate cytokines continuing through late convalescence. Our data suggest that the hospitalized cohort studied here may in fact not be suffering innate immune cell deficits; rather, the innate immune compartment in these children is primed for heightened responses to LPS. Children with post-discharge readmission or death were found to have significant depression in total white blood cell counts at the time of discharge, as well as lymphocyte and monocyte counts, a finding that mirrors similar observations made in adult sepsis cohorts from well-resourced settings (34, 40, 63). Surprisingly, there was no evidence of a compromised pro-inflammatory cytokine response at discharge among children with post-discharge events; rather, heightened production of IL-7 was observed against all tested stimuli. Although we did not identify a statistically significant correlation between IL-7 production and absolute lymphocyte counts in our limited sample size, our findings suggest a heightened drive to restore T cell homeostasis among children who would go on to have poor outcomes.

Our comparison of resting (unstimulated) and stimulated innate cytokine profiles among hospitalized children revealed unexpected findings. Specifically, unstimulated samples from hospitalized children exhibited lower levels of numerous innate cytokines during both acute and convalescent phases of illness as compared to children in the community. Interestingly, innate responses to LPS in this same cohort were elevated throughout the length of this study. This contrasts with a previously published study in a well-resourced setting suggesting that children with severe illness experience immunoparalysis and innate immune deficiencies (64). We also found no evidence for "LPS tolerance," a phenomenon where innate immune cells undergo metabolic and epigenetic alterations due to repeat immune challenge, resulting in cellular reprogramming and an overall reduction in the pro-inflammatory response (65–68).

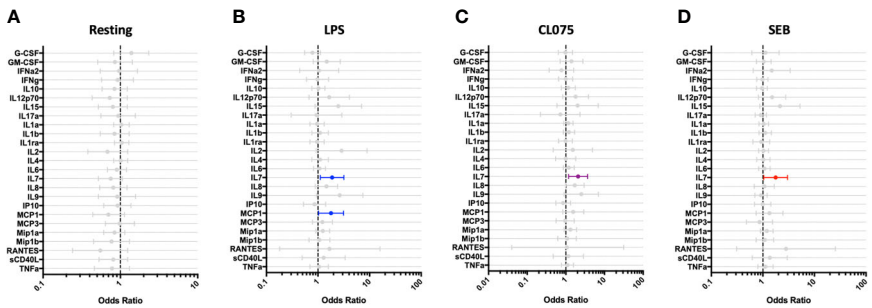

FIGURE 6 | IL-7 responses to multiple stimuli are altered among hospitalized children who experience post-discharge adverse events. Whole blood cytokine and chemokine responses at hospital discharge were compared between participants who experienced a post-hospital-discharge event of death or re-admission (n=22) and those who completed 6-months of follow-up with no event (n=41). Shown are odds ratios of experiencing post-discharge event in unstimulated **(A)** and PAMP-stimulated **(B–D)** whole blood, using logistic regression taking into account age, sex, recruitment site, and MUAC. Filled circles indicate significance of p≤0.05; open circles indicate significance of p≤0.1 when adjusting for multiple comparisons.

Rather, the sustained, altered innate cytokine responses to TLR-4 stimulation in our current young cohort is suggestive of the phenomenon of trained immunity. Trained immunity has been described following immunization with Bacillus Calmette-Guérin, as well as exposure to PAMPs including LPS (69) and β-glucan. Trained immunity refers to epigenetic reprogramming of innate cells that develops following an infectious insult or vaccination, leading to long term alterations in functional responses to subsequent stimuli (70, 71). We hypothesize that some hospitalized children in this cohort may have experienced an acute infection with a gram-negative pathogen that altered their long-term response to subsequent *in vitro* LPS-stimulations. In support of this, de Laval and colleagues recently demonstrated persistent immune alterations in mice after LPS stimulation that increased responsiveness of associated immune genes to secondary stimulation (69).

CL075 is a dual stimulant of endosomal TLR-7/8, targeting TLR-7-expressing plasmacytoid dendritic cells (pDCs) and B cells, and TLR-8-expressing monocytes and myeloid dendritic cells (mDCs) (72). TLR-7 activation in pDCs classically drives intracellular signaling *via* MyD88, induction of IRF-7, and endpoint secretion of IFN-α for anti-viral defense. Conversely, activation of TLR-8 in mDCs *via* the same signaling cascade results in secretion of IL-12p70, which polarizes activated naïve T cells towards IFN-γ-secreting Th-1 subsets. When compared to community counterparts, hospitalized children exhibited a sustained impairment in the secretion of all 3 cytokines (IFN-α, IL-12p70 & IFN-γ; **Figures 3A–C**), suggesting an upstream impact of illness and malnutrition on DC function. Furthermore, our data showed that IL-12p70 secretion was directly linked to MUAC (**Figure 3D**) even after adjusting for multiple comparisons, indicating that poor nutritional status may directly exacerbate poor DC function. A previous study assessing the impact of malnutrition on DC function in 81 Zambian children reported decreased total numbers and low activation during acute infection, which improved after recovery from illness. However, a subset of children (17%) with endotoxemia had 'anergic' type immature IL-10-secreting DCs which failed to drive T cell proliferation (73). DCs are pivotal regulators of immunity, performing individual innate functions and playing a key role in kick-starting adaptive immune responses. Failure of upstream DC responses thus have an obvious negative impact on downstream T cell responses, and we hypothesize that the altered response to LPS, low levels of IFN-γ in hospitalized children, and dysregulated IL-7 secretion could be a consequence of impaired DC responses to TLR-stimulation. Our evidence highlights the DC-T cell activation axis as a novel immune pathway for target therapies aiming to improve both innate and adaptive immunity among young children.

The hospitalized cohort presented here is potentially confounded by differences in nutritional status, with many children experiencing severe wasting in addition to severe, acute illness. Examining cytokine/chemokine responses in our whole blood assay among hospitalized children only (children in CP cohort were predominantly not wasted), we found that higher cytokines responses were directly related to improved nutritional status, as determined by MUAC. The notable exception to this was monocyte-chemotactic protein 3 (MCP-3), which showed an inverse relationship with MUAC. Both MCP-1 and MCP-3 are readily produced by adipocytes which are highly responsive to metabolic status and able to secrete bioactive molecules with downstream effects on immunity (74). Although MCP-1 is known to be increased in obese adults (75), as well as malnourished Ugandan children who have undergone re-feeding therapy (76), MCP-3 was not assessed in these prior studies. To our knowledge, this is the first report of MCP-3 expression in the context of infant nutritional status.

In addition to assessing the relationship between production of individual cytokines and nutritional status, we developed a cytokine signature to each tested stimulus and examined its relationship with MUAC. Here we observed that the resting and LPS-induced cytokine signatures were highly variable in their ability to predict recent acute illness among children, and this was not altered or improved by nutritional status. When only one dominant cytokine was utilized (IFN-γ), as when examining the relationship between CL075- and SEB-induced cytokine response and MUAC, the ability of the cytokine response to predict recent hospitalization was more consistent regardless of nutritional status. Our analysis indicates that composite cytokine and chemokine signature modeling in the context of nutritionally diverse severely ill pediatric cohorts may not be ideal for small sample sizes, as was available in this analysis.

Despite implementation of international guidelines, undernourished young children in LMICs with acute illness continue to have a markedly increased risk of death during hospital admission that persists following discharge. To further define risk factors that contribute to these post-discharge events, we analyzed the immune responses in our hospitalized cohort by separating children who died or were re-admitted to hospital from those who successfully completed 6-months of follow-up. Of all cytokines and chemokines analyzed, only increased IL-7 responses were associated with post-discharge events. IL-7 is a master regulator of both the naïve and memory T cell compartments; signaling through the IL-7 receptor is necessary for death, survival, and turnover of both CD4+ and CD8+ T cells (77). Low levels of IL-7 are detectable in human serum, and increased IL-7 production is thought to be a compensatory effect of lymphopenia in numerous disease states (78–82). Notably, IL-7 replacement therapy was recently studied in a Phase IIb trial among adults with sepsis (83). Although the study was not powered to observe difference in mortality, and baseline IL-7 levels were not reported, patients who received IL-7 therapy had significant increases in CD4+ and CD8+ T cell counts, and the treatment was well tolerated. We reviewed complete blood counts in our hospitalized cohort, and found significant decreases in total white blood cell, lymphocyte, and monocyte counts. It is likely that increased IL-7 production seen in children with post-discharge events reflects an increased drive for T cell proliferation and reduction in T cell apoptosis in an effort to restore adaptive immune homeostasis. Given these children had poor outcomes, this IL-7 compensatory response may have been

insufficient. Future studies in larger cohorts of young children are critical to identify specific targets for immune-based therapeutics that improve outcomes from severe infection.

Our study provides a longitudinal assessment of immune responses in an East African cohort of young children, with varied nutritional and illness status. It is important to note that this pilot study had a limited sample size, and children were hospitalized with a diversity of serious illnesses that limited our capacity to interrogate immune function in the context of specific presenting illness. Our study did not include cell phenotyping by flow cytometry, and thus we were unable to assess cellular phenotype and its association with disease state and outcome. However, the longitudinal nature of our study with defined clinical outcomes and access to a reference population of well children from the same community, combined with interrogation of two distinct TLR pathways and the mitogen SEB, has provided comprehensive insight into how serious acute illness in early childhood is associated with perturbations in both acute and long-term immune function and clinical outcomes. Importantly, our data suggest that the immune system of a child hospitalized for severe illness in LMICs is altered during the acute illness phase, as well as the early and convalescent phases of recovery. Notably, heightened innate responses to LPS and reduced Th-1 responses to CL075 persisted for up to 6 months following hospitalization, and may predispose children to a dysregulated immune response to subsequent infectious challenge. We have also shown that children who go on to have poor outcomes following hospitalization exhibit leukopenia at hospital discharge, as previously reported in well-resourced settings, and a trend towards heightened IL-7 response to all tested stimuli. These findings suggest that acute severe illness during early childhood may have a lasting impact on immune function, and emphasizes the importance of performing longitudinal studies to better understand how illness-associated immune dysregulation can be corrected to promote healthy outcomes.

DATA AVAILABILITY STATEMENT

The raw data supporting the conclusions of this article will be made available by the authors, without undue reservation.

ETHICS STATEMENT

The studies involving human participants were reviewed and approved by the Oxford Tropical Research Ethics Committee (OxTREC), the Scientific and Ethics Review Unit (SERU) of the Kenya Medical Research Institute (KEMRI), and the Makerere University College of Health Sciences, School of Biomedical Sciences Research and Ethics Committee. Written informed consent to participate in this study was provided by the participants' legal guardian/next of kin.

AUTHOR CONTRIBUTIONS

LU and AG contributed equally to the study. LU, AG, JB, and CLL contributed to conception and design of the study. LU, AG, SN, JG, EN, JM, CL, GD, AM, SM, and EM contributed to assay development and validation, performed and/or processed material for experiments, or were directly involved with participant enrollment and/or collection of essential materials or data. BT performed all statistical analyses. LU, CLL, AG, and JB contributed to writing the manuscript. All authors reviewed the manuscript and approved the submitted version.

FUNDING

This work was supported, in whole or in part, by the Bill & Melinda Gates Foundation [OPP 1131320]. Under the grant conditions of the Foundation, a Creative Commons Attribution 4.0 Generic License has already been assigned to the Author Accepted Manuscript version that might arise from this submission.

SUPPLEMENTARY MATERIAL

The Supplementary Material for this article can be found online at: https://www.frontiersin.org/articles/10.3389/fimmu.2021.748996/full#supplementary-material

REFERENCES

1. Angus DC, Linde-Zwirble WT, Lidicker J, Clermont G, Carcillo J, Pinsky MR. Epidemiology of Severe Sepsis in the United States: Analysis of Incidence, Outcome, and Associated Costs of Care. *Crit Care Med* (2001) 29(7):1303–10. doi: 10.1097/00003246-200107000-00002
2. Balamuth F, Weiss SL, Neuman MI, Scott H, Brady PW, Paul R, et al. Pediatric Severe Sepsis in U.S. Children's Hospitals. *Pediatr Crit Care Med* (2014) 15(9):798–805. doi: 10.1097/PCC.0000000000000225
3. Lagu T, Rothberg MB, Shieh MS, Pekow PS, Steingrub JS, Lindenauer PK. Hospitalizations, Costs, and Outcomes of Severe Sepsis in the United States 2003 to 2007. *Crit Care Med* (2012) 40(3):754–61. doi: 10.1097/CCM.0b013e318232db65
4. Lima LM, McCracken CE, Fortenberry JD, Hebbar KB. Use of Plasma Exchange in Pediatric Severe Sepsis in Children's Hospitals. *J Crit Care* (2018) 45:114–20. doi: 10.1016/j.jcrc.2018.01.028
5. Ranieri VM, Thompson BT, Barie PS, Dhainaut JF, Douglas IS, Finfer S, et al. Drotrecogin Alfa (Activated) in Adults With Septic Shock. *N Engl J Med* (2012) 366(22):2055–64. doi: 10.1056/NEJMoa1202290
6. Ruth A, McCracken CE, Fortenberry JD, Hall M, Simon HK, Hebbar KB. Pediatric Severe Sepsis: Current Trends and Outcomes From the Pediatric Health Information Systems Database. *Pediatr Crit Care Med* (2014) 15(9):828–38. doi: 10.1097/PCC.0000000000000254
7. Wooldridge G, Murthy S, Kissoon N. Core Outcome Set in Paediatric Sepsis in Low- and Middle-Income Countries: A Study Protocol. *BMJ Open* (2020) 10(4):e034960. doi: 10.1136/bmjopen-2019-034960
8. W.H.O. *Children: Improving Survival and Well-Being* (2020). Available at: https://www.who.int/news-room/fact-sheets/detail/children-reducing-mortality.
9. Page AL, de Rekeneire N, Sayadi S, Aberrane S, Janssens AC, Rieux C, et al. Infections in Children Admitted With Complicated Severe Acute Malnutrition in Niger. *PLoS One* (2013) 8(7):e68699. doi: 10.1371/journal.pone.0068699

10. Berkley JA, Ngari M, Thitiri J, Mwalekwa L, Timbwa M, Hamid F, et al. Daily Co-Trimoxazole Prophylaxis to Prevent Mortality in Children With Complicated Severe Acute Malnutrition: A Multicentre, Double-Blind, Randomised Placebo-Controlled Trial. *Lancet Glob Health* (2016) 4(7): e464–73. doi: 10.1016/S2214-109X(16)30096-1
11. Attia S, Versloot CJ, Voskuijl W, van Vliet SJ, Di Giovanni V, Zhang L, et al. Mortality in Children With Complicated Severe Acute Malnutrition Is Related to Intestinal and Systemic Inflammation: An Observational Cohort Study. *Am J Clin Nutr* (2016) 104(5):1441–9. doi: 10.3945/ajcn.116.130518
12. Keusch GT, Rosenberg IH, Denno DM, Duggan C, Guerrant RL, Lavery JV, et al. Implications of Acquired Environmental Enteric Dysfunction for Growth and Stunting in Infants and Children Living in Low- and Middle-Income Countries. *Food Nutr Bull* (2013) 34(3):357–64. doi: 10.1177/156482651303400308
13. Keusch GT, Plaut AG, Troncale FJ. Subclinical Malabsorption in Thailand. II. Intestinal Absorption in American Military and Peace Corps Personnel. *Am J Clin Nutr* (1972) 25(10):1067–79. doi: 10.1093/ajcn/25.10.1067
14. Keusch GT. Subclinical Malabsorption in Thailand. I. Intestinal Absorption in Thai Children. *Am J Clin Nutr* (1972) 25(10):1062–6. doi: 10.1093/ajcn/25.10.1062
15. Humphrey JH. Child Undernutrition, Tropical Enteropathy, Toilets, and Handwashing. *Lancet* (2009) 374(9694):1032–5. doi: 10.1016/S0140-6736(09)60950-8
16. Lindenbaum J, Gerson CD, Kent TH. Recovery of Small-Intestinal Structure and Function After Residence in the Tropics. I. Studies in Peace Corps Volunteers. *Ann Intern Med* (1971) 74(2):218–22. doi: 10.7326/0003-4819-74-2-218
17. Field CJ, Johnson IR, Schley PD. Nutrients and Their Role in Host Resistance to Infection. *J Leukoc Biol* (2002) 71(1):16–32.
18. Chacko CJ, Paulson KA, Mathan VI, Baker SJ. The Villus Architecture of the Small Intestine in the Tropics: A Necropsy Study. *J Pathol* (1969) 98(2):146–51. doi: 10.1002/path.1710980209
19. Syed S, Ali A, Duggan C. Environmental Enteric Dysfunction in Children. *J Pediatr Gastroenterol Nutr* (2016) 63(1):6–14. doi: 10.1097/MPG.0000000000001147
20. Keusch GT, Denno DM, Black RE, Duggan C, Guerrant RL, Lavery JV, et al. Environmental Enteric Dysfunction: Pathogenesis, Diagnosis, and Clinical Consequences. *Clin Infect Dis* (2014) 59(Suppl 4):S207–12. doi: 10.1093/cid/ciu485
21. Bourke CD, Jones KDJ, Prendergast AJ. Current Understanding of Innate Immune Cell Dysfunction in Childhood Undernutrition. *Front Immunol* (2019) 10:1728. doi: 10.3389/fimmu.2019.01728
22. Beisel WR. Nutrition in Pediatric HIV Infection: Setting the Research Agenda. Nutrition and Immune Function: Overview. *J Nutr* (1996) 126(10 Suppl):2611S–5S. doi: 10.1093/jn/126.suppl_10.2611S
23. Savino W. The Thymus Gland Is a Target in Malnutrition. *Eur J Clin Nutr* (2002) 56(Suppl 3):S46–9. doi: 10.1038/sj.ejcn.1601485
24. Campbell DI, Elia M, Lunn PG. Growth Faltering in Rural Gambian Infants Is Associated With Impaired Small Intestinal Barrier Function, Leading to Endotoxemia and Systemic Inflammation. *J Nutr* (2003) 133(5):1332–8. doi: 10.1093/jn/133.5.1332
25. Solomons NW. Environmental Contamination and Chronic Inflammation Influence Human Growth Potential. *J Nutr* (2003) 133(5):1237. doi: 10.1093/jn/133.5.1237
26. Campbell DI, Elia M, Lunn PG. Intestinal Inflammation Measured by Fecal Neopterin in Gambian Children With Enteropathy: Association With Growth Failure, Giardia Lamblia, and Intestinal Permeability. *J Pediatr Gastroenterol Nutr* (2004) 39(2):153–7. doi: 10.1097/00005176-200408000-00005
27. Schaible UE, Kaufmann SH. Malnutrition and Infection: Complex Mechanisms and Global Impacts. *PLoS Med* (2007) 4(5):e115. doi: 10.1371/journal.pmed.0040115
28. Black RE, Allen LH, Bhutta ZA, Caulfield LE, de Onis M, Ezzati M, et al. Maternal and Child Undernutrition: Global and Regional Exposures and Health Consequences. *Lancet* (2008) 371(9608):243–60. doi: 10.1016/S0140-6736(07)61690-0
29. Yatsunenko T, Rey FE, Manary MJ, Trehan I, Dominguez-Bello MG, Contreras M, et al. Human Gut Microbiome Viewed Across Age and Geography. *Nature* (2012) 486(7402):222–7. doi: 10.1038/nature11053
30. Subramanian S, Huq S, Yatsunenko T, Haque R, Mahfuz M, Alam MA, et al. Persistent Gut Microbiota Immaturity in Malnourished Bangladeshi Children. *Nature* (2014) 510(7505):417–21. doi: 10.1038/nature13421
31. John CC, Black MM, Nelson CA3rd. Neurodevelopment: The Impact of Nutrition and Inflammation During Early to Middle Childhood in Low-Resource Settings. *Pediatrics* (2017) 139(Suppl 1):S59–71. doi: 10.1542/peds.2016-2828H
32. Abraham E, Reinhart K, Opal S, Demeyer I, Doig C, Rodriguez AL, et al. Efficacy and Safety of Tifacogin (Recombinant Tissue Factor Pathway Inhibitor) in Severe Sepsis: A Randomized Controlled Trial. *JAMA* (2003) 290(2):238–47. doi: 10.1001/jama.290.2.238
33. Opal SM, Garber GE, LaRosa SP, Maki DG, Freebairn RC, Kinasewitz GT, et al. Systemic Host Responses in Severe Sepsis Analyzed by Causative Microorganism and Treatment Effects of Drotrecogin Alfa (Activated). *Clin Infect Dis* (2003) 37(1):50–8. doi: 10.1086/375593
34. Rimmele T, Payen D, Cantaluppi V, Marshall J, Gomez H, Gomez A, et al. Immune Cell Phenotype and Function in Sepsis. *Shock* (2016) 45(3):282–91. doi: 10.1097/SHK.0000000000000495
35. Angus DC, van der Poll T. Severe Sepsis and Septic Shock. *N Engl J Med* (2013) 369(9):840–51. doi: 10.1056/NEJMra1208623
36. van der Poll T, Opal SM. Host-Pathogen Interactions in Sepsis. *Lancet Infect Dis* (2008) 8(1):32–43. doi: 10.1016/S1473-3099(07)70265-7
37. Takeuchi O, Akira S. Pattern Recognition Receptors and Inflammation. *Cell* (2010) 140(6):805–20. doi: 10.1016/j.cell.2010.01.022
38. Chan JK, Roth J, Oppenheim JJ, Tracey KJ, Vogl T, Feldmann M, et al. Alarmins: Awaiting a Clinical Response. *J Clin Invest* (2012) 122(8):2711–9. doi: 10.1172/JCI62423
39. Njunge JM, Gwela A, Kibinge NK, Ngari M, Nyamako L, Nyatichi E, et al. Biomarkers of Post-Discharge Mortality Among Children With Complicated Severe Acute Malnutrition. *Sci Rep* (2019) 9(1):5981. doi: 10.1038/s41598-019-42436-y
40. Jensen IJ, Sjaastad FV, Griffith TS, Badovinac VP. Sepsis-Induced T Cell Immunoparalysis: The Ins and Outs of Impaired T Cell Immunity. *J Immunol* (2018) 200(5):1543–53. doi: 10.4049/jimmunol.1701618
41. Donnelly JP, Hohmann SF, Wang HE. Unplanned Readmissions After Hospitalization for Severe Sepsis at Academic Medical Center-Affiliated Hospitals. *Crit Care Med* (2015) 43(9):1916–27. doi: 10.1097/CCM.0000000000001147
42. Kutza AS, Muhl E, Hackstein H, Kirchner H, Bein G. High Incidence of Active Cytomegalovirus Infection Among Septic Patients. *Clin Infect Dis* (1998) 26(5):1076–82. doi: 10.1086/520307
43. Limaye AP, Kirby KA, Rubenfeld GD, Leisenring WM, Bulger EM, Neff MJ, et al. Cytomegalovirus Reactivation in Critically Ill Immunocompetent Patients. *JAMA* (2008) 300(4):413–22. doi: 10.1001/jama.300.4.413
44. Torgersen C, Moser P, Luckner G, Mayr V, Jochberger S, Hasibeder WR, et al. Macroscopic Postmortem Findings in 235 Surgical Intensive Care Patients With Sepsis. *Anesth Analg* (2009) 108(6):1841–7. doi: 10.1213/ane.0b013e318195e11d
45. Walton AH, Muenzer JT, Rasche D, Boomer JS, Sato B, Brownstein BH, et al. Reactivation of Multiple Viruses in Patients With Sepsis. *PLoS One* (2014) 9(2):e98819. doi: 10.1371/journal.pone.0098819
46. Wiens MO, Pawluk S, Kissoon N, Kumbakumba E, Ansermino JM, Singer J, et al. Pediatric Post-Discharge Mortality in Resource Poor Countries: A Systematic Review. *PLoS One* (2013) 8(6):e66698. doi: 10.1371/journal.pone.0066698
47. *The CHAIN Network* (2021). Available at: www.chainnetwork.org.
48. Childhood Acute Illness and Nutrition (CHAIN) Network: A Protocol for a Multi-Site Prospective Cohort Study to Identify Modifiable Risk Factors for Mortality Among Acutely Ill Children in Africa and Asia. *BMJ Open* (2019) 9(5):e028454. doi: 10.1136/bmjopen-2018-028454
49. Diallo AH, Sayeem Bin Shahid ASM, Khan AF, Saleem AF, Singa BO, Gnoumou BS, et al. Childhood Mortality During and After Acute Illness in Sub-Saharan Africa and South Asia - The CHAIN Cohort Study. *medRxiv* (2021), 2021.11.24.21266806. doi: 10.1101/2021.11.24.21266806
50. Bellete B, Coberly J, Barnes GL, Ko C, Chaisson RE, Comstock GW, et al. Evaluation of a Whole-Blood Interferon-Gamma Release Assay for the Detection of Mycobacterium Tuberculosis Infection in 2 Study Populations. *Clin Infect Dis* (2002) 34(11):1449–56. doi: 10.1086/340397

51. Dammermann W, Bentzien F, Komorowski L, Steinhagen K, Ullrich S, et al. CMV Specific Cytokine Release Assay in Whole Blood Is Optimized by Combining Synthetic CMV Peptides and Toll Like Receptor Agonists. *J Immunol Methods* (2014) 414:82–90. doi: 10.1016/j.jim.2014.10.011
52. Desch CE, Kovach NL, Present W, Broyles C, Harlan JM. Production of Human Tumor Necrosis Factor From Whole Blood *Ex Vivo*. *Lymphokine Res* (1989) 8(2):141–6.
53. Duffy D, Rouilly V, Libri V, Hasan M, Beitz B, David M, et al. Functional Analysis *via* Standardized Whole-Blood Stimulation Systems Defines the Boundaries of a Healthy Immune Response to Complex Stimuli. *Immunity* (2014) 40(3):436–50. doi: 10.1016/j.immuni.2014.03.002
54. Hanekom WA, Hughes J, Mavinkurve M, Mendillo M, Watkins M, Gamieldien H, et al. Novel Application of a Whole Blood Intracellular Cytokine Detection Assay to Quantitate Specific T-Cell Frequency in Field Studies. *J Immunol Methods* (2004) 291(1-2):185–95. doi: 10.1016/j.jim.2004.06.010
55. Ida JA, Shrestha N, Desai S, Pahwa S, Hanekom WA, Haslett PA. A Whole Blood Assay to Assess Peripheral Blood Dendritic Cell Function in Response to Toll-Like Receptor Stimulation. *J Immunol Methods* (2006) 310(1-2):86–99. doi: 10.1016/j.jim.2005.12.008
56. May L, van Bodegom D, Kuningas M, Meij JJ, de Craen AJ, Frolich M, et al. Performance of the Whole-Blood Stimulation Assay for Assessing Innate Immune Activation Under Field Conditions. *Cytokine* (2009) 45(3):184–9. doi: 10.1016/j.cyto.2008.12.010
57. Petrovsky N, Harrison LC. Cytokine-Based Human Whole Blood Assay for the Detection of Antigen-Reactive T Cells. *J Immunol Methods* (1995) 186 (1):37–46. doi: 10.1016/0022-1759(95)00127-V
58. Berkley JA, Lowe BS, Mwangi I, Williams T, Bauni E, Mwarumba S, et al. Bacteremia Among Children Admitted to a Rural Hospital in Kenya. *N Engl J Med* (2005) 352(1):39–47. doi: 10.1056/NEJMoa040275
59. Antonakos N, Tsaganos T, Oberle V, Tsangaris I, Lada M, Pistiki A, et al. Decreased Cytokine Production by Mononuclear Cells After Severe Gram-Negative Infections: Early Clinical Signs and Association With Final Outcome. *Crit Care* (2017) 21(1):48. doi: 10.1186/s13054-017-1625-1
60. Boomer JS, To K, Chang KC, Takasu O, Osborne DF, Walton AH, et al. Immunosuppression in Patients Who Die of Sepsis and Multiple Organ Failure. *JAMA* (2011) 306(23):2594–605. doi: 10.1001/jama.2011.1829
61. Hall MW, Greathouse KC, Thakkar RK, Sribnick EA, Muszynski JA. Immunoparalysis in Pediatric Critical Care. *Pediatr Clin North Am* (2017) 64(5):1089–102. doi: 10.1016/j.pcl.2017.06.008
62. Hibbert JE, Currie A, Strunk T. Sepsis-Induced Immunosuppression in Neonates. *Front Pediatr* (2018) 6:357. doi: 10.3389/fped.2018.00357
63. Drewry AM, Samra N, Skrupky LP, Fuller BM, Compton SM, Hotchkiss RS. Persistent Lymphopenia After Diagnosis of Sepsis Predicts Mortality. *Shock* (2014) 42(5):383–91. doi: 10.1097/SHK.0000000000000234
64. Hall MW, Knatz NL, Vetterly C, Tomarello S, Wewers MD, Volk HD, et al. Immunoparalysis and Nosocomial Infection in Children With Multiple Organ Dysfunction Syndrome. *Intensive Care Med* (2011) 37(3):525–32. doi: 10.1007/s00134-010-2088-x
65. Cavaillon JM, Adib-Conquy M. Bench-To-Bedside Review: Endotoxin Tolerance as a Model of Leukocyte Reprogramming in Sepsis. *Crit Care* (2006) 10(5):233. doi: 10.1186/cc5055
66. Novakovic B, Habibi E, Wang SY, Arts RJW, Davar R, Megchelenbrink W, et al. Beta-Glucan Reverses the Epigenetic State of LPS-Induced Immunological Tolerance. *Cell* (2016) 167(5):1354–68.e14. doi: 10.1016/j.cell.2016.09.034
67. Saeed S, Quintin J, Kerstens HH, Rao NA, Aghajanirefah A, Matarese F, et al. Epigenetic Programming of Monocyte-to-Macrophage Differentiation and Trained Innate Immunity. *Science* (2014) 345(6204):1251086. doi: 10.1126/science.1251086
68. van der Poll T, van de Veerdonk FL, Scicluna BP, Netea MG. The Immunopathology of Sepsis and Potential Therapeutic Targets. *Nat Rev Immunol* (2017) 17(7):407–20. doi: 10.1038/nri.2017.36
69. de Laval B, Maurizio J, Kandalla PK, Brisou G, Simonnet L, Huber C, et al. C/EBPbeta-Dependent Epigenetic Memory Induces Trained Immunity in Hematopoietic Stem Cells. *Cell Stem Cell* (2020) 26(5):793. doi: 10.1016/j.stem.2020.03.014
70. Foster SL, Hargreaves DC, Medzhitov R. Gene-Specific Control of Inflammation by TLR-Induced Chromatin Modifications. *Nature* (2007) 447(7147):972–8. doi: 10.1038/nature05836
71. Netea MG, Dominguez-Andres J, Barreiro LB, Chavakis T, Divangahi M, Fuchs E, et al. Defining Trained Immunity and Its Role in Health and Disease. *Nat Rev Immunol* (2020) 20(6):375–88. doi: 10.1038/s41577-020-0285-6
72. Kadowaki N, Ho S, Antonenko S, Malefyt RW, Kastelein RA, Bazan F, et al. Subsets of Human Dendritic Cell Precursors Express Different Toll-Like Receptors and Respond to Different Microbial Antigens. *J Exp Med* (2001) 194(6):863–9. doi: 10.1084/jem.194.6.863
73. Hughes SM, Amadi B, Mwiya M, Nkamba H, Tomkins A, Goldblatt D. Dendritic Cell Anergy Results From Endotoxemia in Severe Malnutrition. *J Immunol* (2009) 183(4):2818–26. doi: 10.4049/jimmunol.0803518
74. Alwarawrah Y, Kiernan K, MacIver NJ. Changes in Nutritional Status Impact Immune Cell Metabolism and Function. *Front Immunol* (2018) 9:1055. doi: 10.3389/fimmu.2018.01055
75. Kim CS, Park HS, Kawada T, Kim JH, Lim D, Hubbard NE, et al. Circulating Levels of MCP-1 and IL-8 Are Elevated in Human Obese Subjects and Associated With Obesity-Related Parameters. *Int J Obes (Lond)* (2006) 30 (9):1347–55. doi: 10.1038/sj.ijo.0803259
76. Bartz S, Mody A, Hornik C, Bain J, Muehlbauer M, Kiyimba T, et al. Severe Acute Malnutrition in Childhood: Hormonal and Metabolic Status at Presentation, Response to Treatment, and Predictors of Mortality. *J Clin Endocrinol Metab* (2014) 99(6):2128–37. doi: 10.1210/jc.2013-4018
77. Bradley LM, Haynes L, Swain SL. IL-7: Maintaining T-Cell Memory and Achieving Homeostasis. *Trends Immunol* (2005) 26(3):172–6. doi: 10.1016/j.it.2005.01.004
78. Fry TJ, Connick E, Falloon J, Lederman MM, Liewehr DJ, Spritzler J, et al. A Potential Role for Interleukin-7 in T-Cell Homeostasis. *Blood* (2001) 97 (10):2983–90. doi: 10.1182/blood.V97.10.2983
79. Kovacs JA, Lempicki RA, Sidorov IA, Adelsberger JW, Herpin B, Metcalf JA, et al. Identification of Dynamically Distinct Subpopulations of T Lymphocytes That Are Differentially Affected by HIV. *J Exp Med* (2001) 194(12):1731–41. doi: 10.1084/jem.194.12.1731
80. Lundstrom W, Fewkes NM, Mackall CL. IL-7 in Human Health and Disease. *Semin Immunol* (2012) 24(3):218–24. doi: 10.1016/j.smim.2012.02.005
81. Mavroukakis SA, Muehlbauer PM, White RLJr., Schwartzentruber DJ, et al. Clinical Pathways for Managing Patients Receiving Interleukin 2. *Clin J Oncol Nurs* (2001) 5(5):207–17.
82. Napolitano LA, Grant RM, Deeks SG, Schmidt D, De Rosa SC, Herzenberg LA, et al. Increased Production of IL-7 Accompanies HIV-1-Mediated T-Cell Depletion: Implications for T-Cell Homeostasis. *Nat Med* (2001) 7(1):73–9. doi: 10.1038/83381
83. Francois B, Jeannet R, Daix T, Walton AH, Shotwell MS, Unsinger J, et al. Interleukin-7 Restores Lymphocytes in Septic Shock: The IRIS-7 Randomized Clinical Trial. *JCI Insight* (2018) 3(5). doi: 10.1172/jci.insight.98960

Conflict of Interest: The authors declare that the research was conducted in the absence of any commercial or financial relationships that could be construed as a potential conflict of interest.

frontiers | Frontiers in Immunology

ORIGINAL RESEARCH
published: 03 June 2022
doi: 10.3389/fimmu.2022.879600

Estrogen May Enhance Toll-Like Receptor 4-Induced Inflammatory Pathways in People With HIV: Implications for Transgender Women on Hormone Therapy

Aaren Kettelhut[1], Emily Bowman[1], Janelle Gabriel[1], Brittany Hand[1], Namal P. M. Liyanage[2,3], Manjusha Kulkarni[1], Frances Avila-Soto[1], Jordan E. Lake[4†] and Nicholas T. Funderburg[1†]*

[1] Department of Health and Rehabilitation Sciences, The Ohio State University, Columbus, OH, United States, [2] Department of Microbial Infection and Immunity, The Ohio State University, Columbus, OH, United States, [3] Department of Veterinary Biosciences, The Ohio State University, Columbus, OH, United States, [4] Department of Internal Medicine, University of Texas Health Science Center at Houston, Houston, TX, United States

OPEN ACCESS

Edited by:
Anthony Jaworowski, RMIT University, Australia

Reviewed by:
Thomas A. Angelovich, RMIT University, Australia
Mabel Toribio, Massachusetts General Hospital and Harvard Medical School, United States

***Correspondence:**
Aaren Kettelhut
aaren.kettelhut@osumc.edu

†These authors share last authorship

Specialty section:
This article was submitted to Viral Immunology, a section of the journal Frontiers in Immunology

Received: *19 February 2022*
Accepted: *03 May 2022*
Published: *03 June 2022*

Citation:
Kettelhut A, Bowman E, Gabriel J, Hand B, Liyanage NPM, Kulkarni M, Avila-Soto F, Lake JE and Funderburg NT (2022) Estrogen May Enhance Toll-Like Receptor 4-Induced Inflammatory Pathways in People With HIV : Implications for Transgender Women on Hormone Therapy. Front. Immunol. 13:879600. doi: 10.3389/fimmu.2022.879600

Background: Transgender women (TW) are at increased risk for both human immunodeficiency virus (HIV) and cardiovascular disease (CVD). Antiretroviral therapy-treated HIV has been associated with a two-fold increased risk of CVD, potentially due to dysregulated Toll-like receptor (TLR)-induced immune activation. Use of estrogens in feminizing hormone therapy (FHT) may enhance inflammatory responses and the risk of cardiovascular mortality in TW. Despite this, the immunomodulatory effects of estrogen use in TW with HIV have been inadequately explored.

Methods: As an *in vitro* model for FHT, cryopreserved PBMCs (cryoPBMCs) from HIV negative (HIV-), HIV+ ART-suppressed (HIV+SP), and HIV+ ART-unsuppressed (HIV+USP) cisgender men were cultured overnight in the presence of 17-β estradiol or 17-α ethinylestradiol with and without the TLR4 agonist LPS or the TLR8 agonist ssPolyU. Monocyte activation (CD69, HLA-DR, CD38) was assessed by flow cytometry. Cytokine levels (IL-6, TNF-α, IL-1β, and IL-10) were measured in cell culture supernatants by Legendplex. Levels of phosphorylated TLR signaling molecules (JNK, MAPK p38) were assessed by Phosflow. Plasma levels of immune activation biomarkers (LPS-binding protein, monocyte activation markers sCD14 and sCD163, and inflammatory molecules IL-6 and TNF-α receptor I) were measured by ELISA.

Results: PBMCs from people with HIV (PWH) produced greater levels of inflammatory cytokines following exposure to LPS or ssPolyU compared to levels from cells of HIV- individuals. While estrogen exposure alone induced mild changes in immune activation, LPS-induced TLR4 activation was elevated with estrogen in cisgender men (CM) with HIV, increasing monocyte activation and inflammatory cytokine production (IL-6, TNF-α). Interestingly, testosterone inhibited LPS-induced cytokine production in CM regardless of HIV status. Plasma markers of immune activation and microbial translocation (e.g.,

sCD14, sCD163, LPS-binding protein) were generally higher in PWH compared to HIV- CM, and these markers were positively associated with *in vitro* responsiveness to estrogen and LPS in CM with HIV.

Conclusions: Our *in vitro* data suggest that estrogen exposure may enhance innate immune activation in PWH. Further examination is needed to fully understand the complex interactions of FHT, HIV, and CVD in TW, and determine optimal FHT regimens or supplementary treatments aimed at reducing excess immune activation.

Keywords: estrogen, inflammation, monocytes, toll-like receptor 4, human immunodeficiency virus, cardiovascular disease, transgender women

INTRODUCTION

Transgender women (TW) are an underserved population in medicine. Treatment with gender-affirming, feminizing hormone therapy (FHT) using estrogen-based supplementation can significantly improve quality of life (1, 2). Despite the success of FHT, long-term estrogen use may contribute to increased prevalence of chronic co-morbidities including metabolic, pulmonary, cardiovascular, and immunologic complications (3–5).

Prevalence of human immunodeficiency virus (HIV) and cardiovascular disease (CVD) is higher in TW compared to the general population (6–11). TW have an approximately 3-fold greater risk of myocardial infarction (MI) compared to their cisgender counterparts (11). Additionally, MI prevalence is greater in TW receiving FHT compared to TW not on FHT (9). Studies have identified a 3-fold increased risk of cardiovascular mortality with estrogen use in TW (4). Despite these findings, mechanisms underlying FHT-associated CVD risk have been incompletely explored.

Increased CVD risk as a consequence of FHT may be particularly concerning in TW with HIV as HIV is linked to heightened CV morbidity and mortality (12). Globally, the prevalence of HIV in TW is 19% compared to < 1% in the general population; the CDC reports TW are 49 times more likely to live with HIV than cisgender women (CW) (6, 7). Current antiretroviral therapy (ART) regimens successfully manage HIV progression, however, persistent immune activation is a strong predictor of CVD in people with HIV (PWH) (13–16). Chronic immune activation may be driven by multiple factors, including the activation of Toll-like receptors (TLRs) by microbial products that translocate through damaged gut lumen or by products of low-level HIV replication (14–30). Increased monocyte and macrophage activation has been implicated in the pathogenesis of HIV-associated CVD (31–33). Exposure to bacterial (e.g., lipopolysaccharide (LPS) or flagellin) or viral products (e.g., single-stranded polyuridine (ssPolyU), imiquimod, or HIV-1) triggers cellular activation and production of pro-inflammatory mediators. Compared to those without HIV, exposure of myeloid cells from PWH to TLR ligands can result in elevated inflammatory cytokines levels including IL-6, a molecule linked to increased morbidity and mortality in PWH (34–36).

Several studies demonstrate that estrogen may enhance inflammatory responses to TLR ligands (37–41). We have measured cardiometabolic profiles and associated inflammatory biomarkers in cisgender men (CM) and TW and reported increased immune activation in the latter, regardless of HIV status. We also observed slight elevations in the CVD-associated molecules TNF-α receptor I (TNFRI), oxidized low-density lipoprotein (oxLDL), and human extracellular newly-identified receptor for advanced glycation end products binding protein (EN-RAGE) in TW on FHT compared to those off FHT (42). Further work is needed to elucidate the mechanisms that contribute to cardiometabolic risk in TW with HIV. Here, we explored the *in vitro* consequences of estrogen (17-β estradiol or 17-α ethinylestradiol) exposure to TLR-stimulated peripheral blood mononuclear cells (cryoPBMCs) from CM who were HIV negative (HIV-), HIV-positive with ART suppression (HIV+SP), or HIV-positive and ART-naïve/unsuppressed (HIV+USP) to test our hypothesis that estrogen can enhance TLR responsiveness in monocytes from PWH compared to those without HIV. While this work will be limited in its generalizability to TW, as these individuals may experience greater health disparities associated with CVD due to minority stress and marginalization when compared to CM (43), this work serves as a model to elucidate the immune modulatory effects of exogenous estrogen in those assigned male at birth with HIV.

MATERIALS AND METHODS

Sample Collection and Cell Culture Methods

For HIV- donors, blood samples were collected by EDTA-containing Vacutainer tubes (BD Biosciences) from which PBMCs and plasma were isolated. PBMCs were freshly isolated by centrifugation over Ficoll-Hypaque and cryopreserved in freezing media made with 90% DMSO and 10% FBS at 1 ml per 1 x 10^7 cells. To isolate plasma, EDTA tubes were centrifuged for 10 minutes at 470 g.

CryoPBMCs and plasma from ART HIV+SP (viral load < 20 copies/mL) and HIV+USP (viral load > 10,000 copies/mL) PWH

Abbreviations: TW, Transgender women; CM, Cisgender men; CW, Cisgender women; FHT, Feminizing hormone therapy; 17B, 17-β estradiol; 17A, 17-α ethinylestradiol; HIV-, HIV negative; HIV+SP, HIV+ Suppressed; HIV+USP, HIV+ Unsuppressed.

were supplied by the Center for AIDS Research Network of Integrated Clinical Systems repository (CFAR CNICS). All cryopreserved cells were thawed with pre-warmed phenol red free RPMI 1640 (Gibco) that contained 10% Human Male AB OTC Serum, heat inactivated (ATCC Lot #A18049). Trypan Blue staining (1:1) was used to assess viability of thawed PBMCs. Cells were rested overnight (1 x 10^6/ml) in 12 well culture plates before stimulating with 0.001% of ethanol (vehicle control), 1 μM of 17-β estradiol (Sigma-Aldrich), 1 μM of 17-α ethinylestradiol (Sigma-Aldrich), or 1 μM of testosterone (Sigma-Aldrich) in the absence or presence of 100 ng/ml lipopolysaccharide (Sigma-Aldrich) or 1 μg/ml ssPolyU (*In vivo*gen) overnight in 37°C incubator with 5% CO_2. All hormones were obtained in powder form and solubilized in 100% ethanol before filtering. Concentrations of hormones were selected based on initial dose response assays. For phosphoflow experiments, cells were exposed to 0.001% of ethanol or 1 μM of 17-β estradiol in the presence or absence of 100 ng/ml lipopolysaccharide for 20 minutes in 37°C incubator before cell collection.

Flow Cytometry

Cells were collected and supernatants stored in -80°C for cytokine analysis. Cells were washed in 1X Dulbecco Phosphate Buffered Saline (PBS; Gibco) followed by flow wash buffer. Cells were stained for 15 minutes at room temperature in the dark, washed, and fixed in 1% paraformaldehyde (Thermoscientific). Monocytes were identified by size, granularity, and surface expression of CD14 (anti-CD14 Pacific Blue or Pacific Blue isotype; BD Biosciences Cat# 558121, RRID : AB_397041 or BD Biosciences Cat# 558118, RRID : AB_397039, respectively). Monocyte activation markers were measured using anti-CD38 (phycoerythrin [PE]; BD Biosciences Cat# 555460, RRID : AB_395853), anti-CD69 (PE-Cyanine7 [PeCy7]; BD Biosciences Cat# 335792, RRID : AB_1937286), anti-HLADR (APC-Cyanine7 [APCCy7]; BD Biosciences Cat# 335814, RRID : AB_399991) or their respective isotypes (BD Biosciences Cat# 555749, RRID : AB_396091; BD Biosciences Cat# 348798, RRID : AB_400386) by Miltenyi MACSQuant Analyzer 10 flow cytometer (Miltenyi Bioscience MACSQuant Analyzer 10, RRID : SCR_020268) and MACSQuant analysis software (MACSQuantify, RRID : SCR_020943).

Phosphoflow Cytometry

Cells were collected and washed in PBS and flow wash buffer, similar to above protocol, then stained for surface expression of CD14 (anti-CD14 V500 or isotype; BD Biosciences Cat# 561392, RRID : AB_10611862 or BD Biosciences Cat# 561221, RRID : AB_10566127 respectively) for 20 minutes in the dark at 37°C. Monocyte intracellular expression of phosphorylated proteins were measured using an intracellular staining protocol. Cells were lysed at 37°C for 10 minutes with lyse/fix buffer (BD Phosflow), washed with PBS, and permeabilized at 4°C for 30 minutes with Perm Buffer III (BD Phosflow). Cells were washed 3 times in stain buffer (BD Phosflow) before staining in the dark at room temperature for 1 hour with anti-JNK (pT183/pY185) (PE; BD Biosciences Cat# 562480, RRID : AB_11153134) and anti-p38 MAPK (pT180/pY182) (peridinium-chlorophyll-protein Complex-Cyanine 5.5 [PerCP-Cy5.5]; BD Biosciences Cat# 560406, RRID : AB_164529). Cells were analyzed by the MACSQuant Analyzer 10 and analysis software. Monocytes were again identified by size, granularity, and surface expression of CD14.

RNA Isolation, cDNA Conversion, and Quantitative Polymerase Chain Reaction

Cells were stimulated as described above with 0.001% of ethanol, 1 μM of 17-β estradiol, or 1 μM of 17-α ethinylestradiol in the absence or presence of 100 ng/ml lipopolysaccharide or 1 μg/ml ssPolyU for 24 hours in the 37°C incubator. Cells were collected, washed in PBS, and placed in 1% 2-Mercaptoethanol (Sigma Aldrich) supplemented lysing buffer (Qiagen) and stored at -80°C overnight for optimal cell lysing. Cell supernatants were collected for cytokine analysis and stored at -80°C. RNA was extracted using the RNeasy Mini Kit (Qiagen) and RNase-Free DNase set (Qiagen). Extracted RNA was converted to cDNA using the iScript cDNA Synthesis Kit (Bio-rad) and S1000 thermal cycler (Bio-rad). Resultant cDNA along with IQ Sybr Green Supermix (Bio-rad) and relevant forward and reverse primers were used for qPCR analysis. This analysis assessed expression of cytokines IL6 (F: 5'CCAGGAGCC CAGCTATGAAC 3', R: 5'CCCAGGGAGAAGGCAACTG 3') and TNF-α (F: 5'GAGGCCAAGCCCTGGTATG 3', R: 5'CGGGCCGATTGATCTCAGC 3') utilizing MicroAmp Optical 6-well reaction plates and Real-Time PCR System Quant Studio 3 (Applied Biosystems; QuantStudio 3 Real Time PCR System, RRID : SCR_018712). Results were analyzed using QuantStudio design and analysis software.

MAPK p38 Inhibition

Cryopreserved PBMCs were rested overnight (1 x 10^6/ml) in 12 well culture plates before stimulating with 0.001% of ethanol (vehicle control) or 1 μM of 17-β estradiol (Sigma-Aldrich) in the absence or presence of 100 ng/ml lipopolysaccharide (Sigma-Aldrich) with or without 10 μM of p38 inhibitor SB203580 (Sigma-Aldrich) overnight in 37°C incubator with 5% CO_2. Supernatants were collected for cytokine analysis and stored at -80°C.

Measurement of Cytokine Expression

Levels of inflammatory cytokines were measured in supernatants using the LEGENDplex HU Anti-virus response panel (13-plex) w/VbP (Biolegend). Supernatants collected from cells stimulated with ssPolyU or no stimulation were diluted 1:5 in provided assay buffer while those stimulated with LPS were diluted 1:100. LEGENDplex was run on MACSQuant 10 flow cytometer and analyzed by the LEGENDplex Data Analysis Software.

Plasma Biomarker Assessment

Plasma biomarker levels were measured by enzyme-linked immunosorbent assay (ELISA; R&D unless otherwise stated) using a SpectraMax 190 plate reader (SpectraMax 190 microplate reader, RRID : SCR_018932). These biomarkers include soluble CD14 (sCD14), soluble CD163 (sCD163), tumor necrosis factor receptor 1 (TNFR-1), high sensitivity interleukin 6 (HS IL6),

LPS-binding protein (LBP, Hycult Biotech), and β D-glucan (BDG, MyBioSource). Data was collected in SoftMax Pro 7.0.2 (SoftMax Pro Data Acquisition and Analysis Software, RRID : SCR_014240).

Statistical Analysis

Statistical analysis for flow, gene expression, and cytokine analyses were performed in GraphPad Prism 8 (GraphPad Prism, RRID : SCR_002798) utilizing nonparametric paired and unpaired *t* tests along with nonparametric 1- way ANOVA analysis to compare data between our 3 donor groups with our different stimulations. Statistical analysis for ELISA and demographic data were also performed in GraphPad Prism 8 utilizing nonparametric 1- way ANOVA analysis to compare clinical and plasma biomarker data between donor groups. Spearman correlations were utilized to assess relationships between measured plasma biomarkers, plasma biomarkers and clinical data, and plasma biomarkers and changes in cytokine production levels. Correlation heatmaps were created with R software to assess relationships between clinical information, baseline immunoinflammatory profiles, and cytokine responses.

RESULTS

Plasma Biomarkers of Immune Activation and Microbial Translocation are Elevated in PWH

Several studies, including our own, have reported increased levels of pro-inflammatory molecules in PWH and in TW on and off FHT compared to levels in CM, regardless of HIV status. Here, we explored the *in vitro* effects of estrogen on TLR-induced monocyte activation profiles in PWH. As a model for *in vivo* processes in TW initiating FHT, we utilized cryoPBMCs from 18 CM not known to have HIV and 29 CM with HIV, including individuals with HIV+SP (n=14) and HIV+USP (n=15) viral replication. Median viral loads (20 copies/mL and 98,138 copies/mL) and $CD4^+$ T-cell counts (708 and 334 cells/μL) were significantly different in HIV+SP and HIV+USP participants ($p<0.001$). While median age was not significantly different among groups (HIV- 45.0; HIV+SP 50.5; HIV+USP 49.0, $p>0.05$), racial identification was different between HIV- individuals and PWH, with more White and Asian participants among the former group ($p<0.01$) (**Table 1**). Participants were approved for enrollment under the IRB protocol ID 2019H0113.

Plasma biomarkers were measured to assess *in vivo* immune activation in participants with available samples (HIV- n=11, HIV +SP n=14, HIV HIV+USP n=15, **Table 1**), including potential drivers of inflammation in PWH (BDG and LBP), inflammatory molecules (IL-6, TNFRI), and monocyte activation markers (sCD14, sCD163). Of these, only CD14 and CD163 were significantly different between groups ($p<0.05$, $p<0.001$). *Post hoc* analysis revealed significant differences between HIV- and HIV+USP for both markers (CD14 $p<0.05$, CD163 $p<0.001$) and between HIV+SP and HIV+USP for CD163 ($p<0.05$). TNFRI was elevated in USP donors, while IL-6 and LBP increased in both groups with HIV compared to HN participants ($p>0.05$).

Antiretroviral Therapy Suppressed PWH Demonstrate Significant Positive Associations Between Markers of Immune Activation and LPS-Binding Protein

We assessed correlations among biomarkers and contributing mediators of immune activation in PWH to better understand activation profiles in participant groups. We found significant positive associations among LBP, IL-6, TNFRI, CD14, and CD163 in HIV+SP donors ($p<0.05$, **Figure 1B**). These associations, while not all statistically significant, remained in the HIV+USP group. Viral loads and $CD4^+$ T cell counts were negatively associated in HIV+USP donors ($p<0.05$); however, viral loads were not significantly associated with markers of

TABLE 1 | Baseline clinical characteristics and biomarkers of immune activation and inflammation in plasma of HIV- and HIV+ antiretroviral therapy-suppressed and -unsuppressed donors.

Clinical Data & Biomarkers	CM, HIV- (n=11)	CM, HIV+ ART-suppressed (n=14)	CM, HIV+ ART-unsuppressed (n=15)	P value
Age (years)	45.0 (25, 68)* (17)	50.5 (23, 60)	49.0 (23, 55)	p=0.8932
Race (%)±				**p=0.003**
White	61.1%* (18)	35.7%	40.0%	–
Black	11.1%* (18)	64.3%	60.0%	–
Asian	27.8%* (18)	0.0%	0.0%	–
Viral Load (copy/mL)	N/A	20	98138 (13464, 443509)	**p<0.0001**
CD4 T cell count (cells/μL)	N/A	708 (315, 1253)	334 (12, 866)	**p=0.0002**
BDG (pg/mL)	310.35 (236.33, 456.76)* (8)	273.94 (175.08, 904.11)* (12)	287.04 (191.17, 426.24)	p=0.5438
LBP (ng/mL)	12332.9 (5129.84, 15806.41)	15881.42 (4306.69, 28272.54)	16233.13 (4.4, 26356.45)	p=0.2816
IL-6 (pg/mL)	1.53 (0.43, 3.16)	1.96 (0.366, 22.18)	2.71 (0.818, 9.321)	p=0.2069
sCD14 (pg/mL)	1616.31 (1000.01, 1756.68)	1662.94 (1077.22, 2544.94)	1948.18 (974.50, 2573.15)	**p=0.0186**
sCD163 (ng/mL)	502.89 (265.19, 800.31)	620.35 (337.24, 1451.93)	1233.86 (473.86, 2668.30)	**p=0.0004**
TNFRI (pg/mL)	1145.50 (794.34, 1440.69)	1072.40 (686.92, 1966.95)	1298.50 (764.51, 2064.37)	p=0.1308

*Median values (and range) reported. Biomarker data was obtained from plasma samples of participants, if available, utilizing enyzme linked immunosorbent assay. CM, cisgender men; ART, antiretroviral therapy; BDG, β-d-Glucan; LBP, lipopolysaccharide binding protein; IL-6, interleukin-6; sCD14, soluble CD14; sCD163, soluble CD163; TNFRI, TNF-α Receptor I; N/A, not applicable; *# represents if the n is different than listed where *(#), with # representing any number, indicates n=# as a result of plasma or clinical data availability; significance by one-way ANOVA or ± chi-square test. Significant data bolded (p<0.05).*

inflammation (**Figure 1C**). Fewer associations were seen in HIV- donors, with only one association reaching significance ($p<0.05$, **Figure 1A**). Age and LBP were significantly and negatively associated in HIV- donors, otherwise age was not significantly associated with immune activation in any participant group.

PWH Enhance Responses to Toll-Like Receptor Agonism

Alterations in TLR expression and function have been reported in PWH (36, 44, 45). We examined the effects of TLR ligands on monocyte activation markers (CD69, HLA-DR, CD38, n=10 all groups) and cytokine production (IL-6, TNF-α, IL-1β, IL-10, HIV- n=15, HIV+SP n=12, HIV HIV+USP n=15) from cryoPBMCs. The proportion of monocytes that expressed CD69 and the mean fluorescence intensities (MFIs) of HLA-DR and CD38 were increased in all groups following exposure to LPS or ssPolyU. TLR-induced expression of activation markers tended to be higher in PWH compared to expression on cells from people without HIV (**Figures 2A–C**). Exposure of cells to LPS or ssPolyU also increased production of inflammatory cytokines from all participant groups. Despite higher baseline cytokine production in HIV- participants, LPS exposure resulted in greater production of cytokines from the cells of PWH compared to cells from HIV- individuals (**Figures 2D–G**).

17-β Estradiol Enhances LPS-Induced Activation Profiles in PWH

Estrogen may enhance TLR expression and function (37), therefore, we assessed alteration in cellular responses to LPS stimulation with estrogen treatment in our participants. Exposure of cells to either 17-β estradiol (17B) or 17-α ethinylestradiol (17A) alone inconsistently reduced expression of activation markers on monocytes from all participant groups (**Supplemental Figures 1A–C**). Exposure of cells from PWH to 17B, however, increased cytokine production, with significantly higher IL-6 production from HIV+SP versus HIV- cells ($p<0.05$, **Supplemental Figures 1D–G**).

Based on these results, and as 17B is the preferred estrogen for FHT (46), we focused on the effects of 17B in follow-up experiments. In combination with LPS, estrogen exposure typically enhanced monocyte activation marker expression in HIV+SP participants. HLA-DR expression levels were increased significantly in HIV+SP participants with the combination of estrogen and LPS compared to expression induced by LPS alone ($p<0.05$; **Figure 3A**). Cells from all groups increased cytokine production with combined treatment compared to LPS alone; IL-6 production was significantly increased with combined stimulation in HIV+SP PWH ($p<0.05$, **Figure 3B**). Greater production of IL-6 and TNF-α was seen in PWH compared to HIV- participants. Changes in mRNA expression of IL-6 and TNF-α reflected results

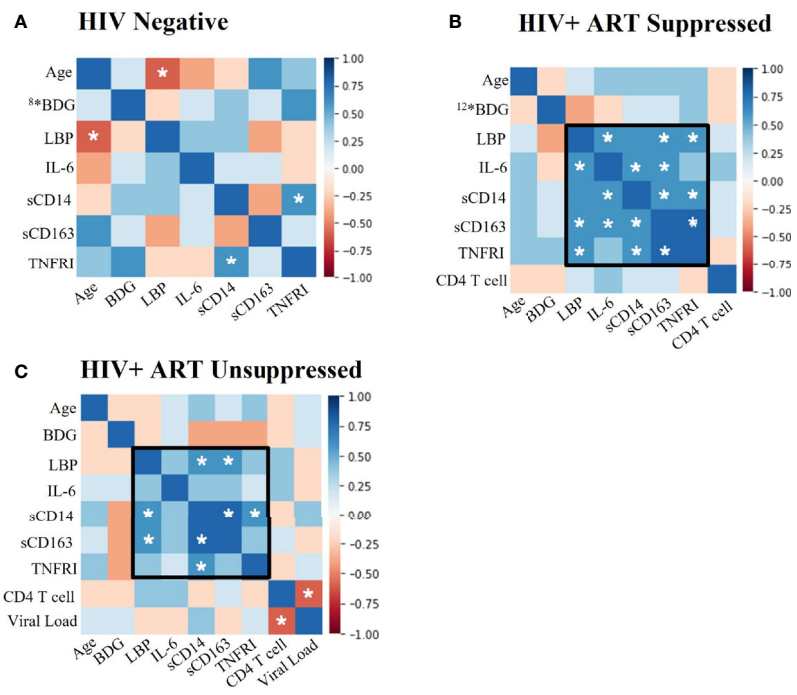

FIGURE 1 | Plasma biomarkers show significant positive associations between LBP and immunoinflammatory markers in PWH. Spearman Rank Correlation between clinical and plasma biomarker data in **(A)** HIV negative (n=11), **(B)** HIV+ ART-suppressed (n=14), and **(C)** HIV+ ART-unsuppressed (n=15) donor groups. PWH, people with HIV; ART, antiretroviral therapy; BDG, β-d-Glucan; LBP, lipopolysaccharide binding protein; IL-6, interleukin-6; sCD14, soluble CD14; sCD163, soluble CD163; TNFRI, TNF-α Receptor I; *#, where # represents any number, indicates a different n than listed where #* is equivalent to n=# due to issues in plasma availability; white stars represent significance of $p<0.05$.

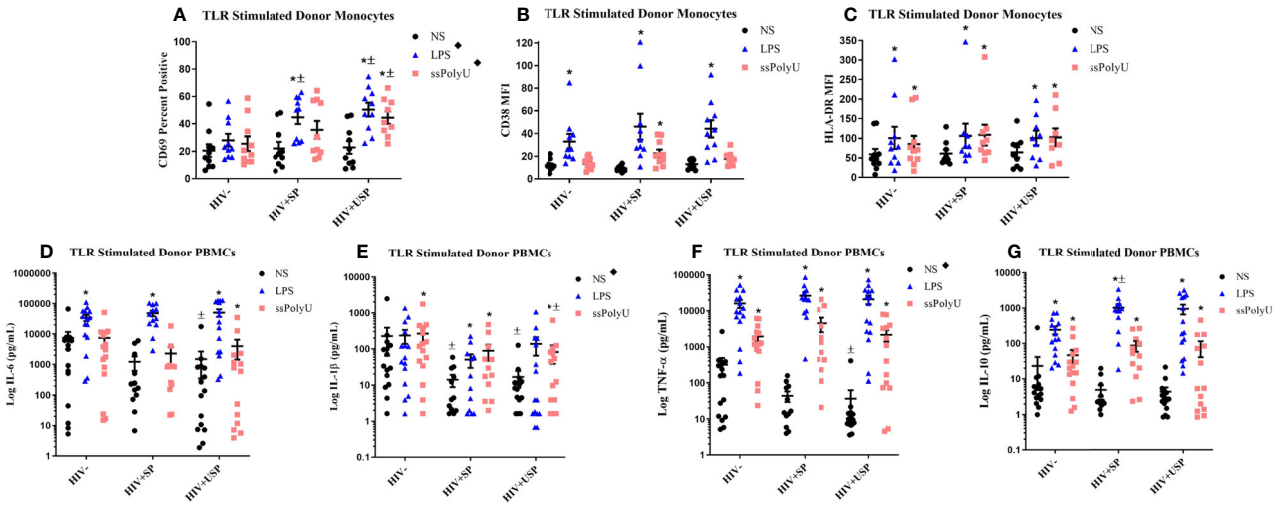

FIGURE 2 | Toll-like receptor stimulation increases monocyte activation markers and cytokine production with greater increases in PWH. HIV+ ART-suppressed (HIV+SP), HIV+ ART-unsuppressed (HIV+USP), and HIV negative (HIV-) cryopreserved peripheral blood mononuclear cells (PBMCs) from CM were thawed and rested overnight in phenol red free RPMI supplemented with 10% Human AB Serum. Cells were treated overnight with no stimulation (NS), 100 ng/mL of TLR4 agonist LPS, or 1 μg/mL of TLR8 agonist ssPolyU. **(A–C)** Cells were collected and stained for CD14+ monocytes and analyzed for levels of relevant activation markers (CD69, CD38, HLA-DR) expressed as percent positive cells or mean fluorescent intensity (MFI) (n=10 all groups). **(D–G)** Supernatants were collected for protein analysis of inflammatory cytokines (IL-1β, IL-6, TNF-α, IL-10) by multiplex bead assay (HIV- n=15, HIV+SP n=12, HIV+USP n=15). Data is represented as mean and standard error of measure in **(A–C)** raw or **(D–G)** log format and was analyzed by *Wilcoxon signed rank test, ± Mann Whitney U, or ◆one-way ANOVA ($^{*,\pm,\blacklozenge}p<0.05$). CM, cisgender men; ART, antiretroviral therapy; LPS, lipopolysaccharide; ssPolyU, single stranded polyuridine; TLR, Toll-like receptor; NS, no stimulation; PWH, people with HIV; IL, interleukin; TNF, tumor necrosis factor.

seen at the protein level (**Supplemental Figures 2–4**). For comparison, we tested cryoPBMC responses to testosterone in the absence or presence of LPS. Combined treatment with LPS showed increases in activation marker expression on monocytes from all groups (**Supplemental Figures 5A, B**). Cytokine production tended to increase with testosterone alone - albeit to a lesser degree than estrogen alone for IL-6 and TNF-α – but testosterone decreased cytokine production when combined with LPS in all groups compared to levels from cells exposed to LPS alone (**Supplemental Figures 5C, D**).

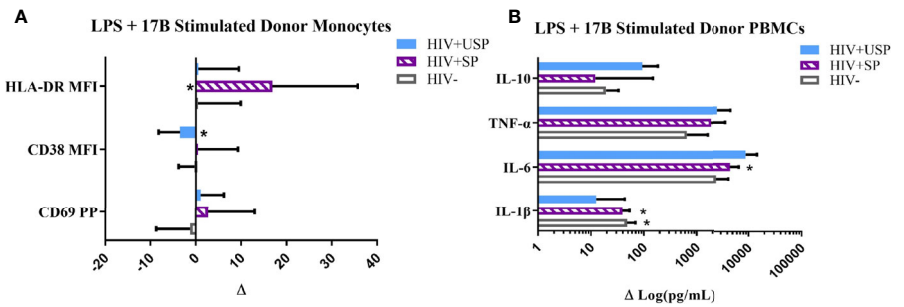

FIGURE 3 | Estrogen differentially modulates monocyte activation and cytokine production with LPS stimulation. HIV+ ART-suppressed (HIV+SP), HIV+ ART-unsuppressed (HIV+USP), and HIV negative (HIV-) cryopreserved peripheral blood mononuclear cells (PBMCs) from CM were thawed and rested overnight in phenol red free RPMI supplemented with 10% Human AB Serum. Cells were treated overnight with 0.001% ethanol (vehicle) or 1 μM of either 17β estradiol (17B) (17A) +/- 100 ng/mL of LPS. **(A)** Cells were collected and stained for CD14+ monocytes and analyzed for levels of relevant activation markers (CD69, CD38, HLA-DR) expressed as percent positive cells or mean fluorescent intensity (MFI) (n=10). **(B)** Supernatants were collected for protein analysis of inflammatory cytokines (IL-1β, IL-6, TNF-α, IL-10) by multiplex bead assay (HIV- n=15, HIV+SP n=12, HIV+USP n=15). Data is normalized to LPS + vehicle and is represented as delta change (Δ) of marker or cytokine expression with mean and standard error of measure shown. Data in **(B)** represented in log format. Data was analyzed by *Wilcoxon signed rank test which assessed for significant differences in activation marker expression or cytokine production between LPS + vehicle and LPS + 17B stimulation for each donor group ($^{*}p<0.05$). Mann Whitney U and one-way ANOVA analyses were also run, but no significant differences were found. CM, cisgender men; ART, antiretroviral therapy; LPS, lipopolysaccharide; IL, interleukin; TNF, tumor necrosis factor.

In Vivo Activation Profiles May Influence *Ex Vivo* Responsiveness to Estrogen and TLR Stimulation in PWH

We next examined relationships between *in vivo* profiles of inflammation and immune activation in our participant groups and the *ex vivo* responsiveness of PBMCs to TLR and estrogen stimulations. LPS-stimulated HIV- PBMCs showed negative associations between plasma IL-6 and LBP levels and *ex vivo* cytokine production (**Figure 4A**). Negative associations were also seen among several plasma biomarkers and LPS-induced cytokine production in our HIV+SP group (**Figure 4B**). In PWH, positive associations were observed between estrogen-induced cytokine production and participant activation profiles (**Figures 4B, C**). In those without HIV, however, estrogen-induced cytokine production had mixed associations with activation profiles. The relationships seen between estrogen-induced cytokine production and immune activation profiles remained consistent with the addition of LPS in both HIV- and HIV+SP participant groups. Combined LPS- and estrogen-induced cytokine production in HIV+USP participants no longer showed positive or significant associations with immune activation profiles.

Inhibition of MAPK p38 Abates 17β Enhanced LPS-Induced Inflammatory Responses

Estrogen may modulate activation of intracellular signaling including the phosphorylation of MAPK p38 and JNK, molecules that influence inflammatory responses to TLR stimulation (47–49). We analyzed phosphorylation of these signaling molecules in the monocytes of our participant groups in the presence or absence of TLR4 stimulation. Although not statistically significant, HIV- individuals on average showed upregulation of both the proportion of monocytes that had phosphorylated JNK and MAPK p38, as well as the MFI of these phosphorylated molecules, while variable responses were seen in the cells of HIV+SP and HIV+USP participants exposed to LPS (**Figure 5**). Treatment with 17B alone or in combination with LPS showed significant alterations in the percent positive (PP) monocytes for phosphorylated JNK (pJNK) in HIV- and HIV+USP individuals, while minor changes were induced in HIV+SP participants. Phosphorylated MAPK p38 (pMAPK p38) showed decreased or little change in the PP monocytes with 17B treatment alone, however, the addition of 17B to LPS stimulation significantly increased pMAPK p38 in HIV+SP participants when compared to HIV- individuals ($p<0.05$, **Figure 6**). As previously demonstrated, 17B stimulation enhances LPS-induced production of IL-6 and TNF-α to a greater degree in PWH (**Figure 3**). To further understand the mechanism by which estrogen may enhance inflammatory responses and the importance of MAPK p38 signaling in PWH, we inhibited MAPK p38 activation with SB203580. Inhibition of MAPK p38 decreased LPS-induced cytokine production in both HIV- and HIV+ SP groups (**Figure 7**). Inhibition appeared to also reduce estrogen's synergistic effects on IL-6 and TNF-α production with LPS stimulation, compared to production with LPS alone, in HIV+SP individuals (**Figures 7C, D**). The role of p38 activation in estrogen-induced cytokine production requires further study.

DISCUSSION

Transgender women are a clinically unique population who are especially vulnerable to both HIV and CVD. As HIV-induced

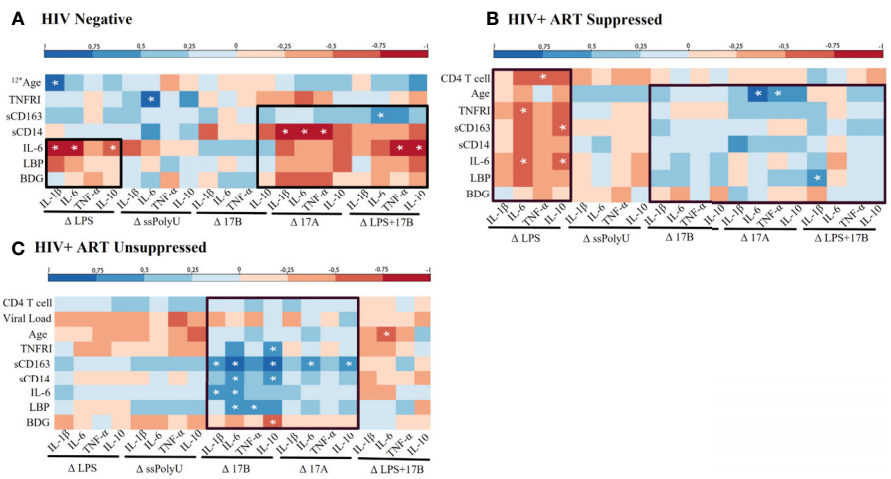

FIGURE 4 | Baseline *in vivo* inflammatory profiles may play a role in response to *in vitro* stimulations. Spearman Rank Correlation between clinical or plasma biomarker data and delta change (Δ) in cytokine production, determined by ELISA or bead assay respectively, by TLR and/or estrogen stimulation in **(A)** HIV negative (n=8), **(B)** HIV+ ART-suppressed (n=12), and **(C)** HIV+ ART-unsuppressed (n=15) donor groups. ART, antiretroviral therapy; LPS, lipopolysaccharide; ssPolyU, single stranded polyuridine; 17B, 17β estradiol; 17A, 17α ethinylestradiol; BDG, β-d-Glucan; LBP, lipopolysaccharide binding protein; IL-6, interleukin-6; sCD14, soluble CD14; sCD163, soluble CD163; TNFRI, TNF-α Receptor I; IL, interleukin; TNF, tumor necrosis factor; ELISA, enyzme linked immunosorbent assay. #* represents different n than listed where #* is equivalent to n=# due to issues in plasma availability *p<0.05.

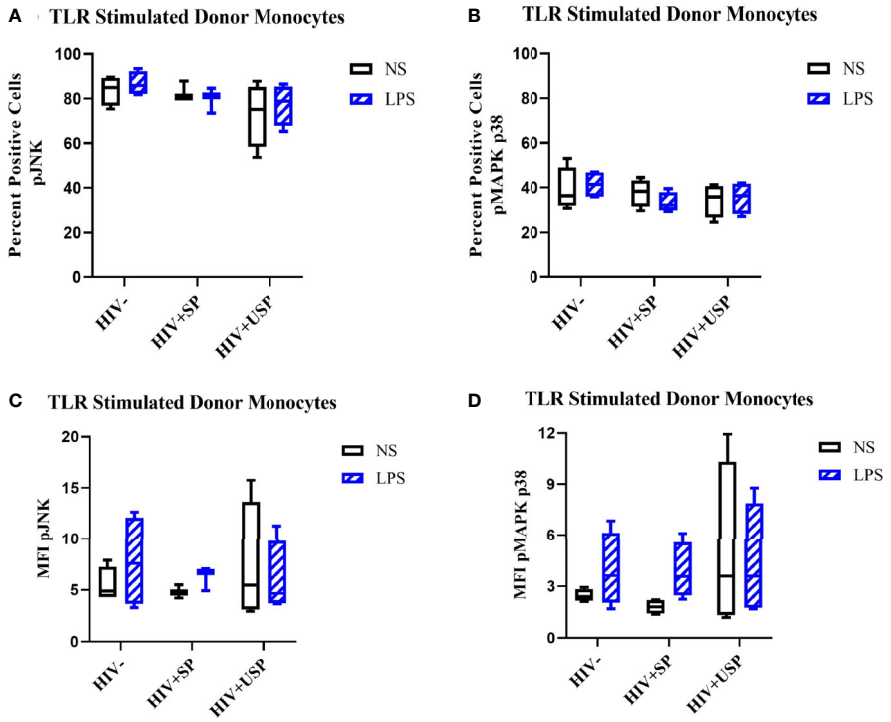

FIGURE 5 | LPS increases phosphorylation levels of JNK and p38 in HIV- and HIV+USP, but not HIV+SP, participants. HIV+ ART-suppressed (HIV+SP), HIV + ART-unsuppressed (HIV+USP), and HIV negative (HIV-) cryopreserved peripheral blood mononuclear cells (PBMCs) from CM were thawed and rested overnight in phenol red free RPMI supplemented with 10% Human AB Serum. Cells were treated for 20 minutes with no stimulation or 100 ng/mL of LPS. Cells were collected and stained for CD14+ monocytes and analyzed for intracellular levels of **(A, C)** phosphorylated c-Jun NH2-terminal kinase (n=4 all except HIV+SP n=3) or **(B, D)** mitogen activated protein kinase mammalian p38 (n=4 all) (pJNK or pMAPK p38 respectively) expressed as **(A, B)** percent positive cells or **(C, D)** MFI. Data is represented as mean and standard error of measure and was analyzed by Wilcoxon signed rank test, Mann Whitney U, or one-way ANOVA although no significant differences were found. CM, cisgender men; ART, antiretroviral therapy; LPS, lipopolysaccharide; TLR, Toll-like receptor; NS, no stimulation; MFI, mean fluorescent intensity.

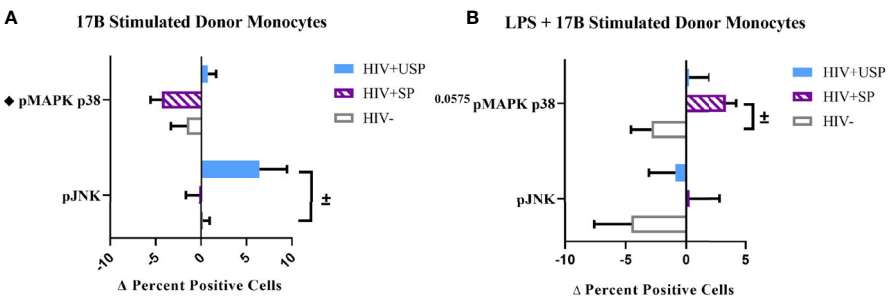

FIGURE 6 | Phosphorylation of MAPK p38 in HIV+SP participants is upregulated with 17B treatment in the presence of LPS, but not alone. HIV+ ART-suppressed (HIV+SP), HIV+ ART-unsuppressed (HIV+USP), and HIV negative (HIV-) cryopreserved peripheral blood mononuclear cells (PBMCs) from CM were thawed and rested overnight in phenol red free RPMI supplemented with 10% Human AB Serum. Cells were treated for 20 minutes with 0.001% ethanol (vehicle) or 1 μM of either 17β estradiol (17B) **(A)** alone (n=4 all except HIV+SP n=3) or **(B)** with 100 ng/mL of LPS (n=4 all). Cells were collected and stained for CD14+ monocytes and analyzed for intracellular levels of phosphorylated c-Jun NH2-terminal kinase or mitogen-activated protein kinase mammalian p38 (pJNK or pMAPK p38) expressed as delta change (Δ) in percent positive cells. Data is represented as mean and standard error of measure and normalized to vehicle control **(A)** alone or **(B)** with 100 ng/mL of LPS. Data was analyzed by $^{\pm}$Mann Whitney U or $^{\blacklozenge}$one-way ANOVA ($^{\pm,\blacklozenge}p<0.05$). CM, cisgender men; ART, antiretroviral therapy; LPS, lipopolysaccharide; TLR, Toll-like receptor.

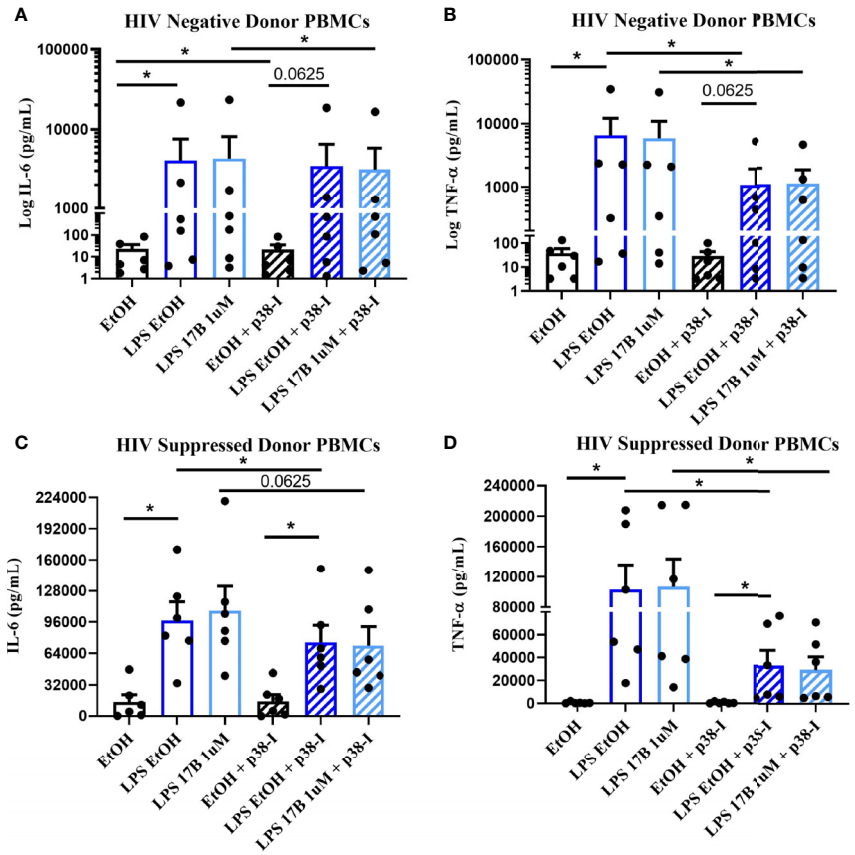

FIGURE 7 | Inhibition of MAPK p38 in the presence of LPS and 17B may downregulate IL-6 and TNF-α production in ART-suppressed participants. 6 HIV+ ART-suppressed and HIV negative cryopreserved peripheral blood mononuclear cells (PBMCs) from CM were thawed and rested overnight in phenol red free RPMI supplemented with 10% Human AB Serum. Cells were treated overnight with 0.001% ethanol (vehicle) or 1 μM of 17β estradiol (17B) +/- 100 ng/mL of LPS in the presence or absence of MAPK p38 inhibitor SB203580 10 μM (p38-I). Supernatants were collected for protein analysis of inflammatory cytokines **(A, C)** IL-6 or **(B, D)** TNF-α by multiplex bead assay. Data presented in **(A, B)** log or **(C, D)** raw format and was analyzed by *Wilcoxon signed rank test. CM, cisgender men; ART, antiretroviral therapy; LPS, lipopolysaccharide; IL, interleukin; EtOH, ethanol; TNF, tumor necrosis factor.

chronic immune activation and inflammation can contribute to CVD risk, and estrogen exposure may exacerbate inflammatory responses, research is needed to elucidate the effects of FHT in TW with HIV.

ART reduces AIDS morbidity and mortality in PWH. Despite its ability to suppress viral replication to undetectable levels and allow restoration of peripheral $CD4^+$ T cell counts in most individuals, gut permeability is often persistently altered in PWH due to incomplete restoration of $CD4^+$ T cells in the gut mucosa. LPS, a bacterial product which can translocate through the gut lining, may drive HIV-induced inflammatory states through activation of myeloid cells by TLR4 ligation (50). As expected, levels of LPS-binding protein, monocyte activation markers, and inflammatory molecules tended to be increased in PWH compared to levels in people without HIV (51–53). In this study, significant positive correlations among markers of monocyte activation, inflammation, and our marker of microbial translocation were identified within PWH, relationships that were not seen among the HIV- group, signaling that microbial translocation may play an influential role in altering immune activation in this cohort.

The expression and function of TLRs are thought to be altered in PWH due to chronic exposure to bacterial and viral products from microbial translocation, HIV replication, or co-infections. In this cohort, exposure of PBMCs to either TLR4 or TLR8 agonists, LPS and ssPolyU, increased inflammatory cytokine production and monocyte activation marker expression regardless of HIV serostatus. TLR-induced activation was notably higher in PWH despite reduced baseline levels. Altered immune responses to microbial products may have arisen in these individuals after long-term exposure to chronic inflammatory stimuli prompting epigenetic or metabolic reprogramming of innate immune cell responses, a phenomenon known as trained immunity. In PWH, trained immunity may optimize inflammatory responses to successive pathogens; in the setting of chronic TLR activation, however, a persistently elevated inflammatory response may promote pathways associated with cardiometabolic risk (54, 55).

Additional studies are needed to further assess the role of trained immunity in chronic HIV infection.

Several *in vivo* markers of monocyte activation and inflammation were inversely related to levels of cytokine production following *in vitro* LPS exposure among ART-suppressed PWH in our cohort. LPS desensitization, or reduced responsiveness to repeated exposure, in myeloid cells is an adaptive response to limit inflammation during chronic LPS exposure (56). Similar trends existed in HIV- individuals with elevated immune activation and LBP compared to those with reduced profiles of immune activation. While similar relationships were not consistently seen in HIV+USP individuals, there may be a unique interplay between high levels of HIV replication and products of microbial translocation that should be considered. Viral and bacterial products may trigger independent immune pathways and may differentially alter functional responses to TLR stimuli.

Chronic exposure to inflammatory stimuli *in vivo* may play a role in producing altered functional responses to TLR ligation. Studies of endogenous estrogen in human and animal models suggest estrogen modulates inflammation and TLR responsiveness (37). We hypothesized that estrogen exposure to HIV- cells would result in downregulation of immune activation, as estrogen may play an atheroprotective role, but these effects could be reversed in PWH due to functional reprogramming of cells after exposure to chronic inflammatory environments *in vivo*. While estrogen had mild effects on cellular activation in all donor groups, the directionality of the response to estrogen differed by HIV serostatus, with increases in inflammatory cytokines in PWH. Interestingly, estrogen's atheroprotective role in HIV- individuals may be reflected by the reduced cytokine production in those with greater *in vivo* activation profiles. In contrast, PWH tended to increase inflammatory cytokines in response to estrogen in individuals with greater *in vivo* immune activation, indicating a potential shift in the cellular response to estrogen with concurrent HIV infection.

Studies of HIV in CW have revealed faster progression to AIDS compared to men with HIV and similar viral loads, as well as altered levels of plasma markers of microbial and immune activation after treatment among CW versus CM with HIV (57, 58). These differences may be explained by estrogen's ability to modulate TLR-mediated pro-inflammatory pathways, which contribute to chronic immune activation associated with CV morbidity and mortality (57–61). The addition of 17-β estradiol tended to enhance LPS-induced expression of the activation marker HLA-DR on monocytes, and production of cytokines IL-6 and TNF-α from the PBMCs of PWH regardless of ART status; enhancement of these molecules by the addition of estrogen was reduced in those without HIV. Among HIV- individuals, increased immune activation was inversely associated with LPS-induced cytokine production following estrogen exposure, while cytokine production was directly related to *in vivo* immune activation in PWH. In the latter group, this effect differs from the indirect relationship seen with LPS alone indicating the presence of estrogen may alter functional desensitization to LPS in suppressed individuals with greater activation profiles. Previous cross-sectional biomarker data identified increased levels of inflammatory molecules associated with CVD risk, such as EN-RAGE, oxLDL, and TNFRI, in TW both on and off FHT compared to CM (42). In the presence of estrogen, elevated immune activation profiles in TW with HIV may indicate risk for enhanced inflammatory responses associated with CVD.

Estrogen can modulate the phosphorylation, and activation, of important intracellular signaling molecules in the TLR pathway including JNK and MAPK p38 (48, 49). Both of these kinases can induce upregulation of transcription factors associated with immune activation. While phosphorylation of JNK seemed to play a minor role in either HIV- or suppressed donors, phosphorylation of MAPK p38 in the presence of LPS stimulation was induced by 17-β estradiol in only ART-suppressed individuals. This may suggest that estrogen can upregulate activation of important TLR4 signaling molecules, and subsequent inflammation, during suppressive ART, but not among HIV- individuals. Inhibition of MAPK p38 normalized LPS and estrogen-induced cytokine production to levels seen with LPS alone in HIV+ SP, suggesting that MAPK p38 may play a partial role in additive effects of estrogen and LPS on cytokine production. While MAPK p38 phosphorylation in ART-suppressed individuals may be one mechanism by which estrogen alters HIV-induced inflammatory pathways, estrogen's effects are likely complex and multifactorial, as many factors are hypothesized to influence the effects of endogenous estrogen in humans. Multiple cellular receptors have been identified for estrogen, but their functions are incompletely understood. Further research is needed to unravel the intersections among estrogen, TLRs, and drivers of inflammation in PWH.

Limitations exist in this study, including the small number of participants. As an exploratory study, these numbers were satisfactory in revealing trends that require further elucidation. Another limitation of this study was the use of cryopreserved PBMCs, as baseline activation of cells may be elevated, although cell viability was not a concern. To mitigate this issue, cells were rested overnight with supplemented media and human serum. A dose-response study was utilized to select a concentration for estrogen. While the dose chosen was greater than physiological estrogen levels, higher levels of estrogen are associated with more anti-inflammatory responses (37) furthering our hypothesis that estrogen use in biological males may have altered effects on inflammation. Due to limitations in human subject enrollment from COVID-19 restrictions, we utilized cells from CM to best replicate the biological environment present in TW pre-FHT. While a convenient solution, studies would better represent this population with cells from TW, as these individuals have increased risk for co-morbidities such as obesity, diabetes, lipid dysregulation, and CVD regardless of HIV. Further study is also needed to understand the full effects of FHT, as FHT can utilize both estrogens and anti-androgens that block the effects of testosterone. We report here that testosterone may play a role in lowering LPS-induced inflammation in PWH. Despite these factors, our findings demonstrate the need for clinical studies

aimed at understanding the mechanistic role of estrogen to reduce CV mortality in TW with HIV.

Overall, this work suggests complex interactions may exist among HIV, CVD, and FHT in TW. As PWH are living longer, both increased frequency and severity of multiple end-organ diseases, such as CVDs, have been uncovered. While estrogen is a known modulator of TLR expression and function, the intensified responses to TLR activation with estrogen treatment in PWH cannot be fully explained by this phenomenon when compared to responses in HIV- individuals. This work demonstrates a unique synergistic effect of microbial-and-estrogen-induced immune activation in PWH independent of the increased activation seen with TLR ligation or estrogen treatment alone. Our findings may reflect alterations in cellular response due to chronic inflammatory stimuli that result in enhanced inflammatory pathways associated with CV morbidity.

To appropriately address clinical disparities in TW, current research assessing treatments aimed to reduce pivotal drivers of inflammation and downstream immune signaling underlying HIV-induced co-morbidities should be considered. As previously reviewed, studies range from altering the microbiota in the gut to reduce translocation of microbial products, to blocking the actions of important inflammatory molecules associated with HIV morbidity and mortality such as IL-6 (62). A multi-pronged approach with ART may be a beneficial route to provide equitable care. By understanding the mechanism behind estrogen-induced modulation of TLR pathways, we may identify important clinical indications for additional therapies in TW on FHT or identify alternative estrogen-like drugs designed to reduce deleterious immune effects in TW with HIV.

CONTRIBUTIONS

Estrogen has been recognized as an important modulator of immune activation including alterations in inflammation and Toll-like receptor function in innate immune cells. Mechanisms by which estrogen exerts these effects are incompletely understood and may depend on estrogen concentration, cell type, and cellular environments. While the use of estrogen in feminizing hormone therapy can improve quality of life in transgender women, research is needed to understand the side effects of long-term high dose usage. This is particularly concerning in the setting of HIV-associated chronic inflammation as Toll-like receptor 4 activation is linked to elevated systemic lipopolysaccharide and inflammation. Based on current literature, we propose that estrogen may upregulate immune activation of myeloid cells in people with HIV as a result of Toll-like receptor functional changes. The elevated immune activation seen here has been associated with increased risk for co-morbidities such as cardiovascular disease and higher mortality rates in people with HIV. As estrogen use in transgender women has been linked to three-fold increased risk of cardiovascular mortality, these results may provide a potential mechanism by which estrogen exerts deleterious effects and potential biomarkers that may indicate a need for additional immunotherapies or alternative estrogen-based therapies in people with HIV.

DATA AVAILABILITY STATEMENT

The original contributions presented in the study are included in the article/**Supplementary Material**. Further inquiries can be directed to the corresponding author.

ETHICS STATEMENT

The studies involving human participants were reviewed and approved by Institutional Review Board at Ohio State Wexner Medical Center. The patients/participants provided their written informed consent to participate in this study.

AUTHOR CONTRIBUTIONS

All authors contributed to experimental design, data analysis, and writing of the manuscript. AK and EB: performed experiments. BH: provided analytical expertise.

FUNDING

Research reported in our publication was supported by the National Institutes of Health supported by the National Institute of Allergic and Infectious Disease of the National Institutes of Health under grant numbers P30AI161943, 5R21AI143452 to JEL. This work was also supported, in part, by the National Center for Advancing Translational Sciences of the National Institutes of Health under Grant Numbers TL1TR002735 & UL1TR001450.

ACKNOWLEDGMENTS

We thank the Center for AIDS Research Network of Integrated Clinical Systems repository (CFAR CNICS) at Case Western Reserve University, Cleveland, OH, for supplying cryopreserved peripheral blood mononuclear cells from HIV-positive participants and relevant clinical and demographic information for our study. We also acknowledge the contributions provided by Jiao Yu at Case Western Reserve University for their design and creation of the correlation heatmaps seen here.

SUPPLEMENTARY MATERIAL

The Supplementary Material for this article can be found online at: https://www.frontiersin.org/articles/10.3389/fimmu.2022.879600/full#supplementary-material

REFERENCES

1. Nguyen HB, Chavez AM, Lipner E, Hantsoo L, Kornfield SL, Davies RD, et al. Gender-Affirming Hormone Use in Transgender Individuals: Impact on Behavioral Health and Cognition. *Curr Psychiatry Rep* (2018) 20(12):110. doi: 10.1007/s11920-018-0973-0
2. Tangpricha V, Safer JD. *Transgender Women: Evaluation and Management*. (2021). Available from: https://www.uptodate.com/contents/transgender-women-evaluation-and-management.
3. de Blok CJM, Wiepjes CM, van Velzen DM, Staphorsius AS, Nota NM, Gooren LJG, et al. Mortality Trends Over Five Decades in Adult Transgender People Receiving Hormone Treatment: A Report From the Amsterdam Cohort of Gender Dysphoria. *Lancet Diabetes Endocrinol* (2021) 9(10):663–70. doi: 10.1016/s2213-8587(21)00185-6
4. Asscheman H, Giltay EJ, Megens JA, de Ronde WP, van Trotsenburg MA, Gooren LJ. A Long-Term Follow-Up Study of Mortality in Transsexuals Receiving Treatment With Cross-Sex Hormones. *Eur J Endocrinol* (2011) 164 (4):635–42. doi: 10.1530/EJE-10-1038
5. Bretherton I, Spanos C, Leemaqz SY, Premaratne G, Grossmann M, Zajac JD, et al. Insulin Resistance in Transgender Individuals Correlates With Android Fat Mass. *Ther Adv Endocrinol Metab* (2021) 12:2042018820985681. doi: 10.1177/2042018820985681
6. Baral SD, Poteat T, Strömdahl S, Wirtz AL, Guadamuz TE, Beyrer C. Worldwide Burden of HIV in Transgender Women: A Systematic Review and Meta-Analysis. *Lancet Infect Dis* (2013) 13(3):214–22. doi: 10.1016/s1473-3099(12)70315-8
7. Silva-Santisteban A, Raymond HF, Salazar X, Villayzan J, Leon S, McFarland W, et al. Understanding the HIV/AIDS Epidemic in Transgender Women of Lima, Peru: Results From a Sero-Epidemiologic Study Using Respondent Driven Sampling. *AIDS Behav* (2012) 16(4):872–81. doi: 10.1007/s10461-011-0053-5
8. Wilson R, Spiers A, Ewan J, Johnson P, Jenkins C, Carr S. Effects of High Dose Oestrogen Therapy on Circulating Inflammatory Markers. *Maturitas* (2009) 62(3):281–6. doi: 10.1016/j.maturitas.2009.01.009
9. Wierckx K, Elaut E, Declercq E, Heylens G, De Cuypere G, Taes Y, et al. Prevalence of Cardiovascular Disease and Cancer During Cross-Sex Hormone Therapy in a Large Cohort of Trans Persons: A Case-Control Study. *Eur J Endocrinol* (2013) 169(4):471–8. doi: 10.1530/EJE-13-0493
10. Gooren LJ, Wierckx K, Giltay EJ. Cardiovascular Disease in Transsexual Persons Treated With Cross-Sex Hormones: Reversal of the Traditional Sex Difference in Cardiovascular Disease Pattern. *Eur J Endocrinol* (2014) 170 (6):809–19. doi: 10.1530/EJE-14-0011
11. Nokoff NJ, Scarbro S, Juarez-Colunga E, Moreau KL, Kempe A. Health and Cardiometabolic Disease in Transgender Adults in the United States: Behavioral Risk Factor Surveillance System 2015. *J Endocr Soc* (2018) 2 (4):349–60. doi: 10.1210/js.2017-00465
12. Shah ASV, Stelzle D, Lee KK, Beck EJ, Alam S, Clifford S, et al. Global Burden of Atherosclerotic Cardiovascular Disease in People Living With HIV: Systematic Review and Meta-Analysis. *Circulation* (2018) 138(11):1100–12. doi: 10.1161/CIRCULATIONAHA.117.033369
13. Hemkens LG, Bucher HC. HIV Infection and Cardiovascular Disease. *Eur Heart J* (2014) 35(21):1373–81. doi: 10.1093/eurheartj/eht528
14. Martinez-Picado J, Deeks SG. Persistent HIV-1 Replication During Antiretroviral Therapy. *Curr Opin HIV AIDS* (2016) 11(4):417–23. doi: 10.1097/COH.0000000000000287
15. Appay V, Sauce D. Immune Activation and Inflammation in HIV-1 Infection: Causes and Consequences. *J Pathol* (2008) 214(2):231–41. doi: 10.1002/path.2276
16. Kelesidis T, Kendall MA, Yang OO, Hodis HN, Currier JS. Biomarkers of Microbial Translocation and Macrophage Activation: Association With Progression of Subclinical Atherosclerosis in HIV-1 Infection. *J Infect Dis* (2012) 206(10):1558–67. doi: 10.1093/infdis/jis545
17. Ross AC, Rizk N, O'Riordan MA, Dogra V, El-Bejjani D, Storer N, et al. Relationship Between Inflammatory Markers, Endothelial Activation Markers, and Carotid Intima-Media Thickness in HIV-Infected Patients Receiving Antiretroviral Therapy. *Clin Infect Dis* (2009) 49(7):1119–27. doi: 10.1086/605578
18. Currier JS, Taylor A, Boyd F, Dezii CM, Kawabata H, Burtcel B, et al. Coronary Heart Disease in HIV-Infected Individuals. *J Acquir Immune Defic Syndr* (2003) 33(4):506–12. doi: 10.1097/00126334-200308010-00012
19. So-Armah KA, Tate JP, Chang CH, Butt AA, Gerschenson M, Gibert CL, et al. Do Biomarkers of Inflammation, Monocyte Activation, and Altered Coagulation Explain Excess Mortality Between HIV Infected and Uninfected People? *J Acquir Immune Defic Syndr* (2016) 72(2):206–13. doi: 10.1097/QAI.0000000000000954
20. McKibben RA, Margolick JB, Grinspoon S, Li X, Palella FJ Jr, Kingsley LA, et al. Elevated Levels of Monocyte Activation Markers Are Associated With Subclinical Atherosclerosis in Men With and Those Without HIV Infection. *J Infect Dis* (2015) 211(8):1219–28. doi: 10.1093/infdis/jiu594
21. Longenecker CT, Jiang Y, Orringer CE, Gilkeson RC, Debanne S, Funderburg NT, et al. Soluble CD14 Is Independently Associated With Coronary Calcification and Extent of Subclinical Vascular Disease in Treated HIV Infection. *AIDS* (2014) 28(7):969–77. doi: 10.1097/QAD.0000000000000158
22. Triant VA, Lee H, Hadigan C, Grinspoon SK. Increased Acute Myocardial Infarction Rates and Cardiovascular Risk Factors Among Patients With Human Immunodeficiency Virus Disease. *J Clin Endocrinol Metab* (2007) 92(7):2506–12. doi: 10.1210/jc.2006-2190
23. Zicari S, Sessa L, Cotugno N, Ruggiero A, Morrocchi E, Concato C, et al. Immune Activation, Inflammation, and Non-AIDS Co-Morbidities in HIV-Infected Patients Under Long-Term ART. *Viruses* (2019) 11(3):200. doi: 10.3390/v11030200
24. Dirajlal-Fargo S, El-Kamari V, Weiner L, Shan L, Sattar A, Kulkarni M, et al. Altered Intestinal Permeability and Fungal Translocation in Ugandan Children With Human Immunodeficiency Virus. *Clin Infect Dis* (2020) 70 (11):2413–22. doi: 10.1093/cid/ciz561
25. Dirajlal-Fargo S, Albar Z, Bowman E, Labbato D, Sattar A, Karungi C, et al. Increased Monocyte and T-Cell Activation in Treated HIV+ Ugandan Children: Associations With Gut Alteration and HIV Factors. *AIDS* (2020) 34(7):1009–18. doi: 10.1097/QAD.0000000000002505
26. Medzhitov R. Toll-Like Receptors and Innate Immunity. *Nat Rev Immunol* (2001) 1(2):135–45. doi: 10.1038/35100529
27. Kawasaki T, Kawai T. Toll-Like Receptor Signaling Pathways. *Front Immunol* (2014) 5:461. doi: 10.3389/fimmu.2014.00461
28. El-Zayat SR, Sibaii H, Mannaa FA. *Toll-Like Receptors Activation, Signaling, and Targeting: An Overview* Vol. 43. Bulletin of the National Research Centre (2019). doi: 10.1186/s42269-019-0227-2
29. Park BS, Lee JO. Recognition of Lipopolysaccharide Pattern by TLR4 Complexes. *Exp Mol Med* (2013) 45:e66. doi: 10.1038/emm.2013.97
30. Bernard MA, Han X, Inderbitzin S, Agbim I, Zhao H, Koziel H, et al. HIV-Derived ssRNA Binds to TLR8 to Induce Inflammation-Driven Macrophage Foam Cell Formation. *PloS One* (2014) 9(8):e104039. doi: 10.1371/journal.pone.0104039
31. Moore KJ, Sheedy FJ, Fisher EA. Macrophages in Atherosclerosis: A Dynamic Balance. *Nat Rev Immunol* (2013) 13(10):709–21. doi: 10.1038/nri3520
32. Woollard KJ, Geissmann F. Monocytes in Atherosclerosis: Subsets and Functions. *Nat Rev Cardiol* (2010) 7(2):77–86. doi: 10.1038/nrcardio.2009.228
33. Libby P. Inflammation in Atherosclerosis. *Nature* (2002) 420(6917):868–74. doi: 10.1038/nature01323
34. Borges AH, O'Connor JL, Phillips AN, Neaton JD, Grund B, Neuhaus J, et al. Interleukin 6 Is a Stronger Predictor of Clinical Events Than High-Sensitivity C-Reactive Protein or D-Dimer During HIV Infection. *J Infect Dis* (2016) 214 (3):408–16. doi: 10.1093/infdis/jiw173
35. Grund B, Baker JV, Deeks SG, Wolfson J, Wentworth D, Cozzi-Lepri A, et al. Relevance of Interleukin-6 and D-Dimer for Serious Non-AIDS Morbidity and Death Among HIV-Positive Adults on Suppressive Antiretroviral Therapy. *PloS One* (2016) 11(5):e0155100. doi: 10.1371/journal.pone.0155100
36. Jalbert E, Crawford TQ, D'Antoni ML, Keating SM, Norris PJ, Nakamoto BK, et al. IL-1Beta Enriched Monocytes Mount Massive IL-6 Responses to Common Inflammatory Triggers Among Chronically HIV-1 Infected Adults on Stable Anti-Retroviral Therapy at Risk for Cardiovascular Disease. *PloS One* (2013) 8(9):e75500. doi: 10.1371/journal.pone.0075500
37. Klein SL, Flanagan KL. Sex Differences in Immune Responses. *Nat Rev Immunol* (2016) 16(10):626–38. doi: 10.1038/nri.2016.90
38. Kovats S. Estrogen Receptors Regulate Innate Immune Cells and Signaling Pathways. *Cell Immunol* (2015) 294(2):63–9. doi: 10.1016/j.cellimm.2015.01.018

39. Young NA, Wu LC, Burd CJ, Friedman AK, Kaffenberger BH, Rajaram MV, et al. Estrogen Modulation of Endosome-Associated Toll-Like Receptor 8: An IFNalpha-Independent Mechanism of Sex-Bias in Systemic Lupus Erythematosus. *Clin Immunol* (2014) 151(1):66–77. doi: 10.1016/j.clim.2014.01.006
40. Filardo EJ, Quinn JA, Frackelton ARJr., Bland KI. Estrogen Action *via* the G Protein-Coupled Receptor, GPR30: Stimulation of Adenylyl Cyclase and cAMP-Mediated Attenuation of the Epidermal Growth Factor Receptor-to-MAPK Signaling Axis. *Mol Endocrinol* (2002) 16(1):70–84. doi: 10.1210/mend.16.1.0758
41. Kang L, Zhang X, Xie Y, Tu Y, Wang D, Liu Z, et al. Involvement of Estrogen Receptor Variant ER-Alpha36, Not GPR30, in Nongenomic Estrogen Signaling. *Mol Endocrinol* (2010) 24(4):709–21. doi: 10.1210/me.2009-0317
42. Lake JE, Wang R, Barrett B, Funderburg N, Bowman E, Debroy P, et al. Hormone Use and HIV Alter Cardiovascular Biomarker Profiles in Transgender Women [CROI Abstract 645]. In: *Special Issue: Abstracts From the 2020 Conference on Retroviruses and Opportunistic Infections*. Boston, Massachusetts: Top Antivir Med (2020). p. 483.
43. Streed CGJr., Beach LB, Caceres BA, Dowshen NL, Moreau KL, Mukherjee M, et al. Assessing and Addressing Cardiovascular Health in People Who Are Transgender and Gender Diverse: A Scientific Statement From the American Heart Association. *Circulation* (2021) 144(6):e136–e48. doi: 10.1161/CIR.0000000000001003
44. Funderburg N, Lederman MM, Feng Z, Drage MG, Jadlowsky J, Harding CV, et al. Human -Defensin-3 Activates Professional Antigen-Presenting Cells *via* Toll-Like Receptors 1 and 2. *Proc Natl Acad Sci USA* (2007) 104(47):18631–5. doi: 10.1073/pnas.0702130104
45. Hernandez JC, Stevenson M, Latz E, Urcuqui-Inchima S. HIV Type 1 Infection Up-Regulates TLR2 and TLR4 Expression and Function *In Vivo* and In Vitro. *AIDS Res Hum Retroviruses* (2012) 28(10):1313–28. doi: 10.1089/aid.2011.0297
46. Goldstein Z, Khan M, Reisman T, Safer JD. Managing the Risk of Venous Thromboembolism in Transgender Adults Undergoing Hormone Therapy. *J Blood Med* (2019) 10:209–16. doi: 10.2147/JBM.S166780
47. Prossnitz ER, Arterburn JB, Sklar LA. GPR30: A G Protein-Coupled Receptor for Estrogen. *Mol Cell Endocrinol* (2007) 265-266:138–42. doi: 10.1016/j.mce.2006.12.010
48. Fardoun MM, Issa K, Maaliki D, Nasser SA, Baydoun E, Eid AH. Estrogen Increases Expression of Vascular Alpha 2C Adrenoceptor Through the cAMP/Epac/JNK/AP-1 Pathway and Potentiates Cold-Induced Vasoconstriction. *Vascul Pharmacol* (2020) 131:106690. doi: 10.1016/j.vph.2020.106690
49. Seval Y, Cakmak H, Kayisli UA, Arici A. Estrogen-Mediated Regulation of P38 Mitogen-Activated Protein Kinase in Human Endometrium. *J Clin Endocrinol Metab* (2006) 91(6):2349–57. doi: 10.1210/jc.2005-2132
50. Ramendra R, Isnard S, Mehraj V, Chen J, Zhang Y, Finkelman M, et al. Circulating LPS and (1–>3)-Beta-D-Glucan: A Folie a Deux Contributing to HIV-Associated Immune Activation. *Front Immunol* (2019) 10:465. doi: 10.3389/fimmu.2019.00465
51. Nystrom J, Stenkvist J, Haggblom A, Weiland O, Nowak P. Low Levels of Microbial Translocation Marker LBP Are Associated With Sustained Viral Response After Anti-HCV Treatment in HIV-1/HCV Co-Infected Patients. *PloS One* (2015) 10(3):e0118643. doi: 10.1371/journal.pone.0118643
52. Neuhaus J, Jacobs DRJr., Baker JV, Calmy A, Duprez D, La Rosa A, et al. Markers of Inflammation, Coagulation, and Renal Function Are Elevated in Adults With HIV Infection. *J Infect Dis* (2010) 201(12):1788–95. doi: 10.1086/652749
53. Mendez-Lagares G, Romero-Sanchez MC, Ruiz-Mateos E, Genebat M, Ferrando-Martinez S, Munoz-Fernandez MA, et al. Long-Term Suppressive Combined Antiretroviral Treatment Does Not Normalize the Serum Level of Soluble CD14. *J Infect Dis* (2013) 207(8):1221–5. doi: 10.1093/infdis/jit025
54. Owen AM, Fults JB, Patil NK, Hernandez A, Bohannon JK. TLR Agonists as Mediators of Trained Immunity: Mechanistic Insight and Immunotherapeutic Potential to Combat Infection. *Front Immunol* (2020) 11:622614. doi: 10.3389/fimmu.2020.622614
55. van der Heijden WA, Van de Wijer L, Keramati F, Trypsteen W, Rutsaert S, Horst RT, et al. Chronic HIV Infection Induces Transcriptional and Functional Reprogramming of Innate Immune Cells. *JCI Insight* (2021) 6(7):e145928. doi: 10.1172/jci.insight.145928
56. Ruckdeschel K, Richter K. Lipopolysaccharide Desensitization of Macrophages Provides Protection Against Yersinia Enterocolitica-Induced Apoptosis. *Infect Immun* (2002) 70(9):5259–64. doi: 10.1128/IAI.70.9.5259-5264.2002
57. Krebs SJ, Slike BM, Sithinamsuwan P, Allen IE, Chalermchai T, Tipsuk S, et al. Sex Differences in Soluble Markers Vary Before and After the Initiation of Antiretroviral Therapy in Chronically HIV-Infected Individuals. *AIDS* (2016) 30(10):1533–42. doi: 10.1097/QAD.0000000000001096
58. Farzadegan H, Hoover DR, Astemborski J, Lyles CM, Margolick JB, Markham RB, et al. Sex Differences in HIV-1 Viral Load and Progression to AIDS. *Lancet* (1998) 352(9139):1510–4. doi: 10.1016/s0140-6736(98)02372-1
59. Hanna DB, Lin J, Post WS, Hodis HN, Xue X, Anastos K, et al. Association of Macrophage Inflammation Biomarkers With Progression of Subclinical Carotid Artery Atherosclerosis in HIV-Infected Women and Men. *J Infect Dis* (2017) 215(9):1352–61. doi: 10.1093/infdis/jix082
60. Meier A, Chang JJ, Chan ES, Pollard RB, Sidhu HK, Kulkarni S, et al. Sex Differences in the Toll-Like Receptor-Mediated Response of Plasmacytoid Dendritic Cells to HIV-1. *Nat Med* (2009) 15(8):955–9. doi: 10.1038/nm.2004
61. Fischer J, Jung N, Robinson N, Lehmann C. Sex Differences in Immune Responses to Infectious Diseases. *Infection* (2015) 43(4):399–403. doi: 10.1007/s15010-015-0791-9
62. Kettelhut A, Bowman E, Funderburg NT. Immunomodulatory and Anti-Inflammatory Strategies to Reduce Comorbidity Risk in People With HIV. *Curr HIV/AIDS Rep* (2020) 17(4):394–404. doi: 10.1007/s11904-020-00509-y

Author Disclaimer: The content is solely the responsibility of the authors and does not necessarily represent the official views of the National Institutes of Health.

Conflict of Interest: NF has served as a consultant for Gilead.

The remaining authors declare that the research was conducted in the absence of any commercial or financial relationships that could be construed as a potential conflict of interest.

Publisher's Note: All claims expressed in this article are solely those of the authors and do not necessarily represent those of their affiliated organizations, or those of the publisher, the editors and the reviewers. Any product that may be evaluated in this article, or claim that may be made by its manufacturer, is not guaranteed or endorsed by the publisher.

frontiers | Frontiers in Immunology

TYPE Case Report
PUBLISHED 02 February 2023
DOI 10.3389/fimmu.2023.1087502

OPEN ACCESS

EDITED BY
Oliver Planz,
University of Tübingen, Germany

REVIEWED BY
Jeffrey J. Pu,
University of Arizona, United States
Juan Jose Rodriguez Sevilla,
University of Texas MD Anderson Cancer Center, United States

*CORRESPONDENCE
Christoph T. Berger
christoph.berger@usb.ch

SPECIALTY SECTION
This article was submitted to Molecular Innate Immunity, a section of the journal Frontiers in Immunology

RECEIVED 02 November 2022
ACCEPTED 05 January 2023
PUBLISHED 02 February 2023

CITATION
Hirsiger JR, Tzankov A, Alborelli I, Recher M, Daikeler T, Parmentier S and Berger CT (2023) Case Report: mRNA vaccination-mediated STAT3 overactivation with agranulocytosis and clonal T-LGL expansion.
Front. Immunol. 14:1087502.
doi: 10.3389/fimmu.2023.1087502

Case Report: mRNA vaccination-mediated STAT3 overactivation with agranulocytosis and clonal T-LGL expansion

Julia R. Hirsiger[1], Alexandar Tzankov[2,3], Ilaria Alborelli[4], Mike Recher[5,6], Thomas Daikeler[6,7], Stefani Parmentier[8] and Christoph T. Berger[1,3,6*]

[1]Translational Immunology, Department of Biomedicine, University of Basel, Basel, Switzerland, [2]Institute for Pathology, University Hospital Basel, Basel, Switzerland, [3]University of Basel and ETH Zurich, Botnar Research Centre for Child Health, Basel, Switzerland, [4]Pathology, Institute of Medical Genetics and Pathology, University Hospital, Basel, Switzerland, [5]Primary Immunodeficiency, Department of Biomedicine, University of Basel, Basel, Switzerland, [6]University Center for Immunology, University Hospital Basel, Basel, Switzerland, [7]Rheumatology Clinic, University Hospital Basel, Basel, Switzerland, [8]Department of Hematology, Claraspital Basel, Basel, Switzerland

Vaccines against SARS-CoV-2 are the most effective measure against the COVID-19 pandemic. The safety profile of mRNA vaccines in patients with rare diseases has not been assessed systematically in the clinical trials, as these patients were typically excluded. This report describes the occurrence of agranulocytosis within days following the first dose of an mRNA-1273 vaccination against COVID-19 in a previously healthy older adult. The patient was diagnosed with a suspected STAT3 wild-type T-cell large granular lymphocytic leukaemia (T-LGL). Neutropenia was successfully treated with IVIG, glucocorticoids, and G-CSF. In vitro experiments aimed at elucidating the pathways potentially causing the mRNA vaccine-associated neutropenia indicated that the mRNA, but not the adenoviral Ad26.COV2.S vector vaccine, triggered strong IL-6/STAT3 activation in vitro, resulting in excessive T-cell activation and neutrophil degranulation in the patient but not in controls. mRNA-1273 activated TLR-3 suggesting TLR mediated IL-6/STAT3 pathway activation. To complete the primary series of COVID-19 immunization, we used a single dose of Ad26.COV2.S vector vaccine without reoccurrence of neutropenia. The T-LGL clone remained stable during the follow-up of more than 12 months without ongoing therapy. Our data suggest that switching the immunization platform may be a reasonable approach in subjects with rare associated hematologic side effects due to excess STAT3-mediated stimulation following mRNA vaccination. Using in vitro testing before re-administration of a (COVID) vaccine also has relevance for other rare immune events after (mRNA) vaccination.

KEYWORDS

T-LGL, STAT3, IL-6, neutropenia, COVID-19, mRNA vaccine, TLR (Toll like receptors), TLR3

Introduction

Large granular lymphocyte (LGL) leukaemia is a rare lymphoproliferative disease of the mature T cell or natural killer lineages (1). Patients can be asymptomatic, present with non-specific symptoms, or with neutropenia or neutropenic fever (2). Autoimmune diseases, most prominently rheumatoid arthritis (RA), have been associated with expansions of T-LGL clones or T-LGL leukaemia. In T-LGL cohorts, up to 26% of patients also have RA (2, 3), and in RA cohorts, T-LGL clones can be found in about 3.6% of the patients (4). T-LGL pathogenesis involves resistance to activation-induced cell death due to constitutive activation of the signal transducers and activators of transcription 3 (STAT3), providing survival signals to the T-cell clones (5). In many cases, STAT3 gain-of-function (GoF) mutations are found (6). In CD8 T-LGL, about 40% carry a STAT3 GoF mutation (7), but frequencies vary from 11-75% amongst cohorts (6). In contrast, CD4+ T-LGL is rarely associated with a STAT3 GoF mutation, but 15-55% of CD4+ T-LGL patients carry STAT5b mutations (6). Interleukin-6 (IL-6) signals *via* STAT3 and inhibits apoptosis in T-LGL (8). T-LGL populations may expand during infections (9–12) or after transplantation (13).

During the COVID-19 pandemic, novel mRNA vaccines were approved. The mRNA can cause activation of innate immune sensors, including toll-like receptor-3 (TLR-3) (14–16). TLR-3 activation induces IL-6/STAT3-activation. Subjects with immune diseases were excluded from the clinical mRNA vaccine trials. Hence, safety assessment in such patients depends on post-marketing vaccine safety surveillance and case reporting.

Methods

The local ethic commission approved the study (Ethikkommission Nordwest- und Zentralschweiz (EKNZ 2015-187)), and the patient provided written informed consent. Immunophenotyping was performed on peripheral blood mononuclear cells (PBMC) using: CD3 (AF®700, OKT3), CD4 (BV510™, SK3), CD8 (Pe-Cy7, SK1), TCRab (AF®488, IP26), CD57 (APC, HNK-1), CD95 (PE, DX2), and CD69 (BV785™, FN50). All samples were acquired on a BD LSRFortessa and analyzed using FlowJo v10.8.1.

For *in vitro* stimulations, we used mRNA-1273 [1:200] (Moderna®) or Ad26.COV2.S [1:200] (Janssen) on cells with or without 30 minutes pre-incubation with siltuximab [0.01-1.0 µg/ml] or tocilizumab [30µg/ml] for IL-6 blocking experiments, or IVIG [30µg/ml] as a control. For immuno-stainings assessing phosphorylation of STAT3 and TLR3, permeabilization was performed with Perm III buffer (BD Biosciences) and the following antibodies were used: anti-human pSTAT3 (Cell Signaling) or anti-human pTLR3 (Tyr759) (Invitrogen) (Cell Signaling) followed by anti-rabbit IgG detection antibody (AF®647 conjugate, Invitrogen). For intracellular cytokine stainings we used antibodies against IFNγ (APC, 4S.B3). The interferon-stimulated gene MX1 and IL-6 were quantified by qPCR. Reverse-transcription PCR was performed with GoTaq qPCR Master Mix in triplicates in a 7500 Fast Real-Time PCR System (Applied Biosystems). Genes were quantified by qPCR using the following primers: MX1 fwd: 5'-TTAACCTCCACAGAACCGCC-3', rev: 5'-GCGGAT CAGCTTCTCACCTT-3', IL-6 fwd: 5'- ACTCAC CTCTTCAGAACGAATTG-3', rev: 5'-AGCCATCTTTGGAAGGTT CAG-3'. qPCR data were normalized to two reference genes (GAPDH and PGK1) using previously described methods (17). Gene expression was normalized to the mean of n=5 healthy controls, and the fold change to the controls determined using the $2^{-\Delta\Delta Ct}$ method.

Gene sequencing for pathogenic STAT3 or STAT5b mutations was done on the Ion Torrent S5 platform using a validated customized Oncomine Lymphoma Panel (for details, see supplementary methods) (18).

Results

Clinical presentation of agranulocytosis following mRNA-1273 vaccination

In June 2021, a previously healthy woman in her 60s was referred with neutropenic fever. She had fatigue and malaise, starting 24 hours following the first dose of the COVID-19 vaccine mRNA-1273. On the sixth day post-vaccination, she developed fever (39°C), sore throat, coughing and vomiting. She denied taking non-steroidal anti-inflammatory drugs that could cause neutropenia (i.e. NSAIDs or metamizole). She is a non-obese, non-smoker and has no diabetes or hypertension. The only available blood count from four years earlier was normal. The physical examination was unremarkable. Specifically, it revealed no palpable lymph nodes or splenomegaly and no petechia, rash, or pharyngitis. The CT scans showed several marginally increased cervical lymph nodes without organomegaly, especially without splenomegaly. Systemic inflammation markers were very high with a C-reactive protein (CRP) of 285 mg/l (reference <5mg/l) and a ferritin peak level of 5276 ng/ml (reference <300ng/mL), compatible with macrophage activation (Figure 1). Tests for SARS-CoV2 and other infections (blood cultures, multiplexed PCR panels from stool and nasal swabs, serology for hepatitis viruses, CMV, and Parvovirus B19) were negative. PET-CT revealed pronounced diffuse hypermetabolism of the hematopoietic bone marrow and spleen. Bone marrow biopsy showed infiltration of $CD8^+$ T cells and hypercellularity with severely reduced granulopoiesis, consistent with pure white cell aplasia (Figure 2A). Interstitial T-cell lymphocytosis with some linearity and intravascular spread of the T cells was suggestive of T-LGL (19) (Figure 2B). Immunophenotyping of the lymphocytes in the peripheral blood and bone marrow identified a large CD8+ T cell population (~45% of all T cells) expressing $CD5^{dim}$, CD7, $CD16^{partial}$, TCRαβ, HLA-DR and that was negative for CD56, TCRγδ, CD30, CD10, CD25, and PD1 in the clinical routine lab, compatible with T-LGL. The T- and B-cell clonality and translocation analysis (20) showed a dominant TCRγ-rearrangement with a base pair length of 200 bp (type V-I) on a polyclonal background. There was no evidence of B-cell clonality or translocations (t(11;14), t(14;18)). Next-generation sequencing applying a custom lymphoma panel covering 68 genes commonly mutated in lymphomas (21, 22) identified no mutation, particularly not in *STAT3* or *STAT5b*. A diagnosis of possible T-LGL leukemia with pure white cell aplasia was made.

Treatment with a broad-spectrum antibiotic and recombinant human G-CSF was initiated, but peripheral agranulocytosis persisted. Only after treatment with intravenous immunoglobulins (IVIG 30g; given in four doses) and dexamethasone (16mg/day) was started

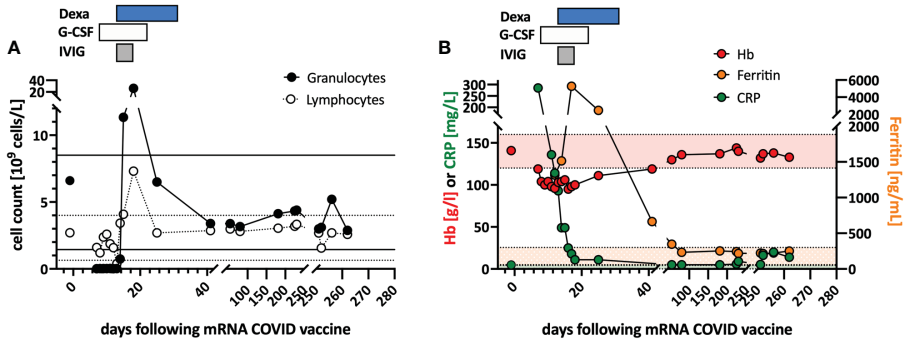

FIGURE 1
Clinical course and *in vitro* stimulation with mRNA-1273. **(A)** Longitudinal peripheral leucocyte and lymphocyte counts are shown. The black lines indicate the normal reference range of the granulocyte count, and the dotted lines the reference range for the lymphocyte count. **(B)** Longitudinal measurements of hemoglobin (red), c-reactive protein (CRP; green), and ferritin (orange) serum levels as markers of systemic inflammation are indicated. Shaded areas indicate the reference range for the markers (color coded). Treatments are indicated at the top of the graphs: DEXA, dexamethasone; G-CSF, granulocyte stimulating factor; IVIG, intravenous immunoglobulin.

agranulocytosis and systemic inflammation instantly resolved (Figure 1), and after two weeks, she recovered completely. During follow-up, the T-LGL population declined to about 34% of all T cells. No further treatment was initiated as she remained asymptomatic.

In January 2022, she was referred to our immunology clinic for counseling regarding completing the COVID-19 immunization series. She had a tonsillectomy for recurrent tonsillitis as a young adult. She never experienced an episode of cytopenia or

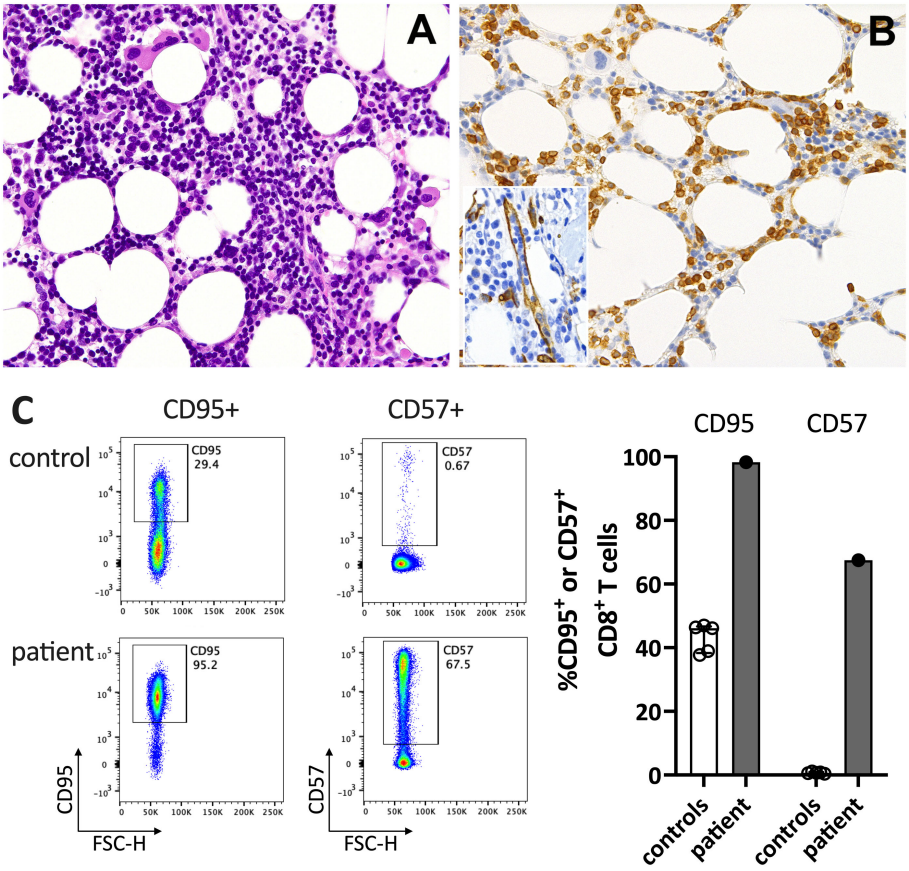

FIGURE 2
Immunohistochemistry of the bone marrow compatible with T-LGL. **(A)** H&E staining shows a hypercellular bone marrow with slightly increased and left-shifted megakaryopoiesis, substantially reduced and left-shifted myelopoiesis, and interstitial lymphocytosis. **(B)** Immunohistochemistry for anti-CD3 (T cells) confirmed significant interstitial T-cell lymphocytosis with some linearity and intravascular spread (shown as an insert in the figure; anti-CD34 was used to mark the vessels). Magnification 400x (CD3) and 630X (insert; CD34). **(C)** Flow cytometry plots (left) and data summary graph (right) show high CD95 and CD57 expression on T cells of the patient compared to healthy controls (ctrl; n=5). FSC-H= forward scatter height.

lymphocytosis prior to the here described event, and had no history of autoimmunity or opportunistic infections. Detailed patient history revealed mild oral sicca and recurrent arthralgias but no arthritis. Anti-nuclear antibodies (ANA), anti-neutrophilic cytoplasmatic antibodies (ANCA), rheumatoid factor and anti-citrullinated protein antibodies (ACPA) were negative. She had been vaccinated according to the Scottish immunization plan and never experienced relevant side-effects from a vaccine. Her sister has rheumatoid arthritis and her brother retroperitoneal fibrosis.

At his time, the clinical exam was unremarkable. She had no lymphadenopathy or splenomegaly. The white blood count (WBC) and CRP were normal. Anti-SARS-CoV-2-N(ucleoprotein)-IgG/IgM were negative and anti-S(pike)-IgG/IgM at low levels (61.8 U/mL (<0.7); Roche Elecsys® assay). The T-LGL clone was stable at about 800/ul. The $CD8^+$ T cells expressed high levels of CD95 and CD57, typical for T-LGL (Figure 2C).

mRNA-1273 mediated IL-6/STAT3 pathway activation *via* TLR stimulation

The patient's bone marrow T cells at diagnosis (Figure 3A), but not those of a control bone marrow (Supplementary Figure S1), and the patient's peripheral blood immune cells during follow-up (Figure 3B), showed high spontaneous STAT3 phosphorylation (pSTAT3). *In vitro* stimulation of peripheral blood mononuclear cells of the patient with the mRNA-1273 vaccine resulted in distinct STAT3 protein phosphorylation in monocytes and T cells of the patient (Figure 3C). This was associated with mRNA-vaccine-induced IL-6 production *in vitro* (Figure 3D). pSTAT3 activation could be blocked by the anti-IL-6 blocking antibody siltuximab and the anti-IL-6 receptor blocker tocilizumab (TCZ) (Figure 3E and Supplementary Figure S2), indicating IL-6 mediated pSTAT3 upregulation. The mRNA vaccine also activated T cells IL-6-dependently (Figure 3F).

The IL-6/STAT3 pathway can be activated by toll-like receptors, including TLR-3 (15). Virus-derived double-stranded RNA (dsRNA), but also endogenous mRNA, can act as activators of TLR3 (23). The novel mRNA vaccines were modified to dampen RNA-mediated TLR3 activation by reducing dsRNA formation and introducing nucleotides with less inflammatory properties (16). However, even modified mRNA vaccines activate innate immunity *via* TLR3 (16). We confirmed TLR3 activation by stimulating peripheral blood mononuclear cells with mRNA-1273 resulting in increased phosphorylation of TLR3 (Figure 3G). Combined, our data suggest that the mRNA-1273 activates (innate) immune cells *via* TLR to secrete IL-6, subsequently resulting in STAT3 phosphorylation.

Distinct immune activation following mRNA-1273 vs. AD26.COV2 stimulation

We next tested for differences in the *in vitro* immune activation between different COVID-19 vaccines, specifically mRNA-1273 and the adenoviral vector vaccine Ad26.COV2.S. We observed lower pSTAT3

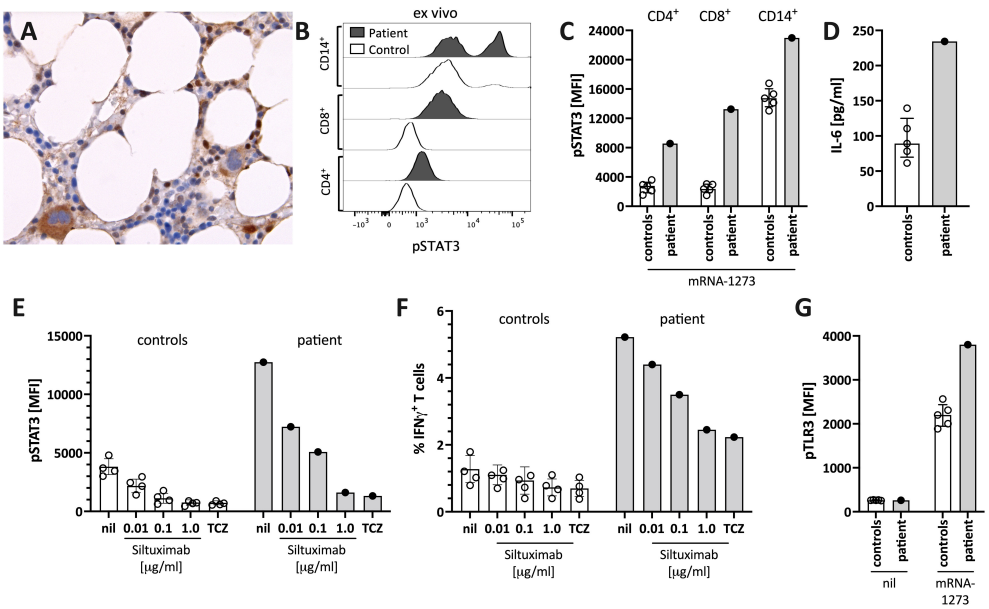

FIGURE 3
Enhanced STAT3/IL-6 pathway activation in the bone marrow and *in vitro* by mRNA-1273 stimulation. **(A)** Immunohistochemical staining for phosphorylated-STAT3 (pSTAT3) showing scattered positive interstitial cells, morphologically consistent with lymphocytes, suggestive of STAT3 activation at diagnosis; note the negatively staining erythropoiesis and the nuclear negativity of the megakaryocytes. Immunoperoxidase staining; original magnification 630x. **(B)** Histogram showing pSTAT3 in T cells ($CD4^+$ and $CD8^+$) and monocytes ($CD14^+$) directly *ex vivo*. **(C)** STAT3 phosphorylation (pSTAT3) following *in vitro* stimulation of peripheral blood immune cells with the mRNA-1273 vaccine. **(D)** Supernatants of PBMC stimulated with mRNA-1273 show higher IL-6 production (ELISA). **(E)** mRNA vaccine induced *in vitro* STAT3 phosphorylation was dose-dependently blocked by the anti-IL-6 antibody siltuximab and the IL-6 receptor blocker tocilizumab (TCZ; used at 30 µg/ml, which corresponds to the serum concentration of treated subjects (see also Supplementary Figure S2). **(F)** mRNA stimulation induced T cell activation, as indicated by IFNγ positive T cells, was inhibited by IL-6 blockade (siltuximab or TCZ). **(G)** mRNA-1273 stimulation resulted in TLR3 phosphorylation in monocytes of healthy controls, and even more pronounced of the patient. MFI= median fluorescence intensity in flow cytometry. nil= only mRNA-1273 without other blocking conditions; ctrl, healthy controls; px, patient.

10.3389/fimmu.2023.1087502

activation (Figure 4A), IFNγ production in CD8$^+$ T-cells (Figure 4B), as well as interferon-stimulated genes (ISG) (Figure 4C) and IL-6 (Figure 4D) induction when stimulating the patients' PBMC with Ad26.COV2.S compared to mRNA-1273. Additionally, direct *ex vivo* stimulation of whole blood with the mRNA vaccine resulted in strong neutrophil degranulation in the patient, which could not be recapitulated after polyclonal T-cell stimulation with agonistic anti-CD3/28 antibodies, suggesting a T cell-independent effect (Supplementary Figure S3). Whether this *in vitro* observed degranulation occurs *in vivo* will need to be tested.

Based on the *in vitro* data, we speculated that a strong mRNA vaccine-mediated IL-6/STAT3 activation contributed to the adverse reaction by TLR-mediated innate immune cell activation and indirectly by T-cell activation. Since the vector vaccine showed weaker stimulation of these pathways *in vitro*, we completed her COVID-19 immunization series with a single dose of Ad26.COV2.S, which was well tolerated and caused only mild T-cell-intrinsic STAT3 phosphorylation (Figure 4E). Her blood counts, including neutrophil count, remained stable.

Discussion

We provide evidence that the mRNA-1273 vaccine, and to a much lesser extent the Ad26.COV2.S vector vaccine induces STAT3 activation through TLR stimulation with the potential risk of exacerbating STAT3-dependent disease(s). We hypothesize that mRNA-vaccine-mediated STAT3 activation stimulated the T-LGL clone *via* IL-6 and activated innate cells in the reported case. Notably, clonal *STAT3* mutations have been directly linked to neutropenia in T-LGL (8). The increased IFNγ production in T cells following *in vitro* mRNA vaccine stimulation suggests that T cells may be activated either directly or *via* IL-6. Whether high IFNγ secretion contributed to the overactivation of innate immunity or neutropenia *in vivo* cannot be concluded based on the *in vitro* data and a single case. Interestingly, expansion of T cells causing progressive lymphadenopathy following mRNA vaccination has been reported in a patient with angioimmunoblastic T Cell lymphoma (24).

Based on the follow-up, the T-LGL clone persisted over months, but in the absence of symptoms and without the need for therapy, the T-LGL expansion may have been reactive and not reflect T-LGL leukemia.

The incidence of neutropenia following immunization with the mRNA vaccine BNT162b2 was reported as 2.6 per 100'000 vaccinated subjects. Notably, none of these cases was severe (defined as <500/ul neutrophils) and the incidence of neutropenia is about 40-times higher in patients with COVID-19 (88.4 per 100'000 cases) (25). In a cohort of 342 patients with inborn errors of immunity (IEI), one patient with common variable immunodeficiency developed severe neutropenia three days following BNT162b2 immunization. The patient required treatment with granulocyte stimulating factor and systemic corticosteroid therapy. Interestingly, the patient was subsequently diagnosed with T-LGL (26). To our knowledge, there are no other reports of severe neutropenia in T-LGL. Recently, good COVID-vaccine immunogenicity was demonstrated in a small cohort

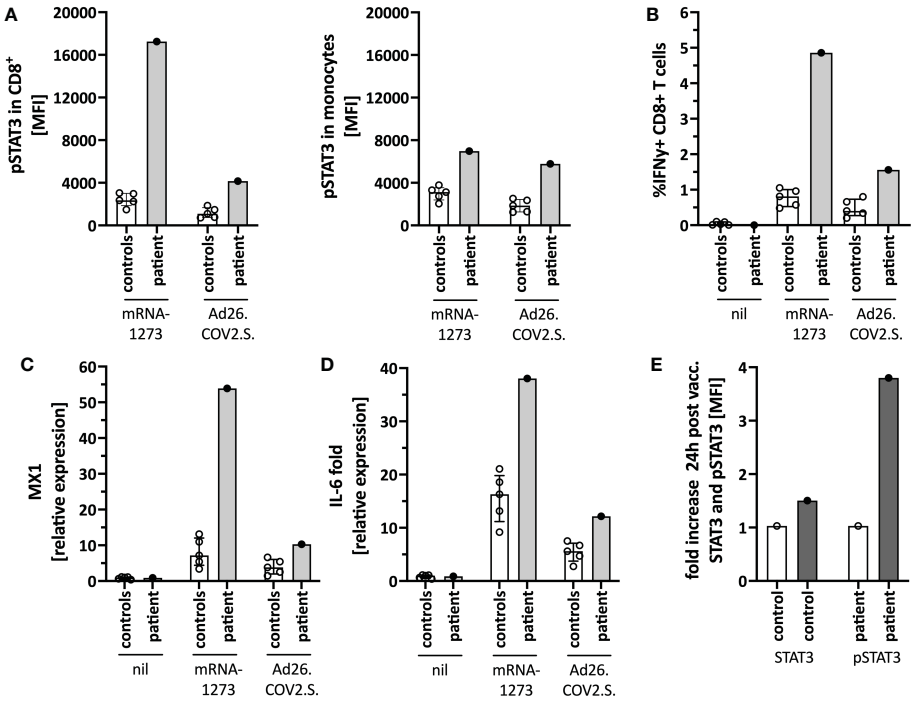

FIGURE 4
Immune activation by mRNA-1273 and Ad26.COV2.S vaccines. **(A)** STAT3 phosphorylation in CD8+T cells (left) and monocytes (right) following *in vitro* stimulation of peripheral blood immune cells with the mRNA-1273 vaccine or Ad26.COV2.S vector vaccine (pre-vaccine dose 2; i.e. different timepoint than in Figure 1D). **(B)** Vector vaccine stimulation induced lower T cell activation *in vitro* than the mRNA vaccine. **(C)** MX1 (=Interferon stimulated gene (ISG)) and **(D)** IL-6 induction upon *in vitro* stimulation with mRNA-1273 or Ad26.COV2.S is shown by qPCR. **(E)** Mild *in vivo* pSTAT3 activation 24 hours following vaccination with Ad26.COV2.S. Data is expressed as fold change of STAT3 or pSTAT3 activation 24h-post-vaccination normalized to an unvaccinated control. Nil= unstimulated condition= media only. ctrl= healthy controls; px= patient.

of mostly treated T-LGL patients (27). Safety data were not reported in this study.

Based on the *in vitro* findings, we completed immunization with the Ad26.COV2.S, which was well-tolerated. Thus, there was no rationale to re-expose her to an mRNA vaccine to test for causality. Our observation suggests that an alternative vaccination platform may be a personalized option for subjects experiencing STAT3-mediated adverse events following immunization with an mRNA vaccine.

Data availability statement

The original contributions presented in the study are included in the article/Supplementary Material. The NGS sequencing data presented in the study are deposited in the European Nucleotide Archive (ENA) repository, accession numbers PRJEB58739 and ERP143807. Further inquiries can be directed to the corresponding author.

Ethics statement

The studies involving human participants were reviewed and approved by ethics committee of Northwestern and Central Switzerland. The patients/participants provided their written informed consent to participate in this study. Written informed consent was obtained from the individual(s) for the publication of any potentially identifiable images or data included in this article.

Author contributions

JRH designed and performed experiments, analyzed data, and drafted the manuscript. AT, IA, MR, TD, and SP collected and analyzed data and edited the manuscript. CTB designed and funded the study, analyzed the data, and drafted the manuscript. All authors contributed to the article and approved the submitted version.

Funding

The study was funded by independent research funds to CTB. CTB and AT are supported by research grants from the Botnar Research Centre for Child Health, Basel, Switzerland.

Conflict of interest

The authors declare that the research was conducted in the absence of any commercial or financial relationships that could be construed as a potential conflict of interest.

Publisher's note

Supplementary material

The Supplementary Material for this article can be found online at: https://www.frontiersin.org/articles/10.3389/fimmu.2023.1087502/full#supplementary-material

References

1. Bigas A, Rodriguez-Sevilla JJ, Espinosa L, Gallardo F. Recent advances in T-cell lymphoid neoplasms. *Exp Hematol* (2022) 106:3–18. doi: 10.1016/j.exphem.2021.12.191

2. Lamy T, Loughran TPJr. Clinical features of large granular lymphocyte leukemia. *Semin Hematol* (2003) 40(3):185–95. doi: 10.1016/s0037-1963(03)00133-1

3. Dhodapkar MV, Li CY, Lust JA, Tefferi A, Phyliky RL. Clinical spectrum of clonal proliferations of T-large granular lymphocytes: a T-cell clonopathy of undetermined significance? *Blood* (1994) 84(5):1620–7. doi: 10.1182/blood.V84.5.1620.1620

4. Schwaneck EC, Renner R, Junker L, Einsele H, Gadeholt O, Geissinger E, et al. Prevalence and characteristics of persistent clonal T cell Large granular lymphocyte expansions in rheumatoid arthritis: A comprehensive analysis of 529 patients. *Arthritis Rheumatol* (2018) 70(12):1914–22. doi: 10.1002/art.40654

5. Lamy T, Moignet A, Loughran TPJr. LGL leukemia: from pathogenesis to treatment. *Blood* (2017) 129(9):1082–94. doi: 10.1182/blood-2016-08-692590

6. Teramo A, Barila G, Calabretto G, Vicenzetto C, Gasparini VR, Semenzato G, et al. Insights into genetic landscape of Large granular lymphocyte leukemia. *Front Oncol* (2020) 10:152. doi: 10.3389/fonc.2020.00152

7. Koskela HL, Eldfors S, Ellonen P, van Adrichem AJ, Kuusanmaki H, Andersson EI, et al. Somatic STAT3 mutations in large granular lymphocytic leukemia. *N Engl J Med* (2012) 366(20):1905–13. doi: 10.1056/NEJMoa1114885

8. Teramo A, Gattazzo C, Passeri F, Lico A, Tasca G, Cabrelle A, et al. Intrinsic and extrinsic mechanisms contribute to maintain the JAK/STAT pathway aberrantly activated in T-type large granular lymphocyte leukemia. *Blood* (2013) 121(19):3843–54, S1. doi: 10.1182/blood-2012-07-441378

9. Delobel P, Godel A, Thebault S, Alric L, Duffaut M. Transient clonal expansion of T-large granular lymphocytes during primary cytomegalovirus infection. *J Infect* (2006) 53 (2):e65–7. doi: 10.1016/j.jinf.2005.10.013

10. Rossi D, Franceschetti S, Capello D, De Paoli L, Lunghi M, Conconi A, et al. Transient monoclonal expansion of CD8+/CD57+ T-cell large granular lymphocytes after primary cytomegalovirus infection. *Am J Hematol* (2007) 82(12):1103–5. doi: 10.1002/ajh.20981

11. Smith P, Helbert M, Raftery M, Forster G, Cavenagh J. Paraproteins and monoclonal expansion of CD3+CD8+ CD56-CD57+ T lymphocytes in a patient with HIV infection. *Br J Haematol* (1999) 105(1):85–7. doi: 10.1111/j.1365-2141.1999.01293.x

12. Kondo H, Mori A, Watanabe J, Takada J, Takahashi Y, Iwasaki H. Pure red cell aplasia associated with parvovirus B19 infection in T-large granular lymphocyte leukemia. *Leuk Lymphoma* (2001) 42(6):1439–43. doi: 10.3109/10428190109097777

13. Nann-Rutti S, Tzankov A, Cantoni N, Halter J, Heim D, Tsakiris D, et al. Large Granular lymphocyte expansion after allogeneic hematopoietic stem cell transplant is associated with a cytomegalovirus reactivation and shows an indolent outcome. *Biol Blood Marrow Transplant* (2012) 18(11):1765–70. doi: 10.1016/j.bbmt.2012.07.007

14. Vlatkovic I. Non-immunotherapy application of LNP-mRNA: Maximizing efficacy and safety. *Biomedicines.* (2021) 9(5):530. doi: 10.3390/biomedicines9050530

15. Hu Y, Cong X, Chen L, Qi J, Wu X, Zhou M, et al. Synergy of TLR3 and 7 ligands significantly enhances function of DCs to present inactivated PRRSV antigen through TRIF/MyD88-NF-kappaB signaling pathway. *Sci Rep* (2016) 6:23977. doi: 10.1038/srep23977

16. Kariko K, Buckstein M, Ni H, Weissman D. Suppression of RNA recognition by toll-like receptors: the impact of nucleoside modification and the evolutionary origin of RNA. *Immunity.* (2005) 23(2):165–75. doi: 10.1016/j.immuni.2005.06.008

17. Hellemans J, Mortier G, De Paepe A, Speleman F, Vandesompele J. qBase relative quantification framework and software for management and automated analysis of real-time quantitative PCR data. *Genome Biol* (2007) 8(2):R19. doi: 10.1186/gb-2007-8-2-r19

18. Vela V, Juskevicius D, Prince SS, Cathomas G, Dertinger S, Diebold J, et al. Deciphering the genetic landscape of pulmonary lymphomas. *Mod Pathol* (2021) 34 (2):371–9. doi: 10.1038/s41379-020-00660-2

19. Morice WG, Kurtin PJ, Tefferi A, Hanson CA. Distinct bone marrow findings in T-cell granular lymphocytic leukemia revealed by paraffin section immunoperoxidase stains for CD8, TIA-1, and granzyme b. *Blood.* (2002) 99(1):268–74. doi: 10.1182/blood.v99.1.268

20. Meier VS, Rufle A, Gudat F. Simultaneous evaluation of T- and b-cell clonality, t (11;14) and t(14;18), in a single reaction by a four-color multiplex polymerase chain reaction assay and automated high-resolution fragment analysis: a method for the rapid molecular diagnosis of lymphoproliferative disorders applicable to fresh frozen and formalin-fixed, paraffin-embedded tissues, blood, and bone marrow aspirates. *Am J Pathol* (2001) 159(6):2031–43. doi: 10.1016/S0002-9440(10)63055-6

21. Juskevicius D, Lorber T, Gsponer J, Perrina V, Ruiz C, Stenner-Liewen F, et al. Distinct genetic evolution patterns of relapsing diffuse large b-cell lymphoma revealed by genome-wide copy number aberration and targeted sequencing analysis. *Leukemia* (2016) 30(12):2385–95. doi: 10.1038/leu.2016.135

22. Juskevicius D, Muller A, Hashwah H, Lundberg P, Tzankov A, Menter T. Characterization of the mutational profile of 11 diffuse large b-cell lymphoma cell lines. *Leuk Lymphoma* (2018) 59(7):1710–6. doi: 10.1080/10428194.2017.1387903

23. Kariko K, Ni H, Capodici J, Lamphier M, Weissman D. mRNA is an endogenous ligand for toll-like receptor 3. *J Biol Chem* (2004) 279(13):12542–50. doi: 10.1074/jbc.M310175200

24. Goldman S, Bron D, Tousseyn T, Vierasu I, Dewispelaere L, Heimann P, et al. Rapid progression of angioimmunoblastic T cell lymphoma following BNT162b2 mRNA vaccine booster shot: A case report. *Front Med (Lausanne)* (2021) 8:798095. doi: 10.3389/fmed.2021.798095

25. Sing CW, Tang CTL, Chui CSL, Fan M, Lai FTT, Li X, et al. COVID-19 vaccines and risks of hematological abnormalities: Nested case-control and self-controlled case series study. *Am J Hematol* (2022) 97(4):470–80. doi: 10.1002/ajh.26478

26. Milito C, Cinetto F, Garzi G, Palladino A, Puca M, Brambilla E, et al. Safety of mRNA COVID-19 vaccines in patients with inborn errors of immunity: an Italian multicentric study. *J Clin Immunol* (2022), 1–9. doi: 10.1007/s10875-022-01402-6

27. Cheon H, Elghawy O, Shemo BC, Feith DJ, Loughran TPJr. LGL leukemia patients exhibit substantial protective humoral responses following SARS-CoV-2 vaccination. *EJHaem.* (2022) 3(3):919–923. doi: 10.1002/jha2.472

frontiers | Frontiers in Immunology

TYPE Mini Review
PUBLISHED 20 April 2023
DOI 10.3389/fimmu.2023.1167972

OPEN ACCESS

EDITED BY
Oliver Planz,
University of Tübingen, Germany

REVIEWED BY
Sam Basta,
Queen's University, Canada
Karen Bohmwald,
Pontificia Universidad Católica de Chile, Chile

*CORRESPONDENCE
Byung S. Kim
bskim@northwestern.edu

SPECIALTY SECTION
This article was submitted to Molecular Innate Immunity, a section of the journal Frontiers in Immunology

RECEIVED 17 February 2023
ACCEPTED 11 April 2023
PUBLISHED 20 April 2023

CITATION
Kim BS (2023) Critical role of TLR activation in viral replication, persistence, and pathogenicity of Theiler's virus. *Front. Immunol.* 14:1167972. doi: 10.3389/fimmu.2023.1167972

Critical role of TLR activation in viral replication, persistence, and pathogenicity of Theiler's virus

Byung S. Kim*

Department of Microbiology-Immunology, Northwestern University Feinberg School of Medicine, Chicago, IL, United States

Theiler's murine encephalomyelitis virus (TMEV) establishes persistent viral infections in the central nervous system and induces chronic inflammatory demyelinating disease in susceptible mice. TMEV infects dendritic cells, macrophages, B cells, and glial cells. The state of TLR activation in the host plays a critical role in initial viral replication and persistence. The further activation of TLRs enhances viral replication and persistence, leading to the pathogenicity of TMEV-induced demyelinating disease. Various cytokines are produced via TLRs, and MDA-5 signals linked with NF-κB activation following TMEV infection. In turn, these signals further amplify TMEV replication and the persistence of virus-infected cells. The signals further elevate cytokine production, promoting the development of Th17 responses and preventing cellular apoptosis, which enables viral persistence. Excessive levels of cytokines, particularly IL-6 and IL-1β, facilitate the generation of pathogenic Th17 immune responses to viral antigens and autoantigens, leading to TMEV-induced demyelinating disease. These cytokines, together with TLR2 may prematurely generate functionally deficient CD25-FoxP3+ $CD4^+$ T cells, which are subsequently converted to Th17 cells. Furthermore, IL-6 and IL-17 synergistically inhibit the apoptosis of virus-infected cells and the cytolytic function of CD8+ T lymphocytes, prolonging the survival of virus-infected cells. The inhibition of apoptosis leads to the persistent activation of NF-κB and TLRs, which continuously provides an environment of excessive cytokines and consequently promotes autoimmune responses. Persistent or repeated infections of other viruses such as COVID-19 may result in similar continuous TLR activation and cytokine production, leading to autoimmune diseases.

KEYWORDS

TLRs, chronic viral infection, inflammation, apoptosis, autoimmunity

Abbreviations: MS, multiple sclerosis; CNS, central nervous system; TMEV, Theiler's murine encephalomyelitis virus; TMEV-IDD, TMEV-induced demyelinating disease; Tg, transgenic mice; TCR, T cell receptor; MHC, major histocompatibility complex.

1 Theiler's virus

Theiler's murine encephalomyelitis virus (TMEV) belongs to the family of picornavirus, possessing a single positive RNA genome (1, 2). The picornavirus family includes a wide range of human pathogens, including rhinoviruses, cardioviruses, enteroviruses, and aphthoviruses, and TMEV belongings to the cardioviral group (3, 4). Two major subgroups of TMEV have been identified. One subgroup including GDVII and FA viruses, causes rapid and fatal encephalitis. Another subgroup including the BeAn8386 and DA strains, is known as Theiler's original (TO) viruses. The inoculation of TO viruses intracerebrally into susceptible mice results in a biphasic neurological disease (2, 5–9). The early, acute phase displays flaccid limb paralysis and the degeneration of neurons (poliomyelitis). The late phase exhibits chronic, inflammatory demyelination (2). In contrast to the DA strain, the BeAn strain of the TO virus group is known to induce a clinically undetectable early-phase disease, although it results in a severe late-phase demyelinating disease (8, 9).

Viruses such as TMEV have been associated with CNS diseases including multiple sclerosis (10–14). Multiple sclerosis (MS) is a long-lasting autoimmune-mediated disease, resulting in demyelination in the white matter of the central nervous system (15). To understand the underlying pathogenic mechanisms of MS, several virus-induced models have been investigated (5, 7, 16, 17). Among virus-induced models, TMEV-induced demyelinating disease in mice has been extensively investigated because of the similarities in its histopathologic characteristics (2, 5, 18, 19). In addition, Saffold virus is an emerging human Theiler's virus group, infecting more than 90% of human populations, which implicates potential importance in public health (20–22). MS may therefore involve chronic viral infections associated with the development of pathogenic immune responses reactive to viral and/or self-antigens. To explain virus-induced demyelinating disease in mice, several hypotheses have been proposed. First, "bystander" damage to CNS tissues occurs because of the host immune response against viral determinants (23, 24). Second, autoimmune responses to myelin proteins from damages to the CNS by anti-viral immune responses cause the disease development (19, 25, 26). Third, CNS damage incurred by persistent antiviral and autoimmune responses are induced by chronic over-stimulation via TLRs and other pathogen pattern recognition receptors (19, 27). Defining the underlying pathogenic mechanisms associated with TLR engagement with well-defined disease system like TMEV-induced demyelination has paramount importance in understanding the role of TLRs on viral persistence, cytokine production, and development of pathogenic immune responses, including autoimmune responses.

Infection with TMEV causes demyelinating disease only in certain mouse strains. C57BL/6 (B6) mice represent a resistant strain and SJL/J (SJL) mice represent a susceptible strain (28, 29). The viral loads in the spinal cords of resistant C57BL/6 mice are significantly lower than those of susceptible SJL mice throughout the viral infection period (30). Various cell types are permissive to TMEV infection, and these include oligodendrocytes, microglia, and astrocytes in the CNS and the dendritic cells, macrophages, and B cells in the CNS and periphery (31–35). The major cell populations that support viral persistence during chronic TMEV infection are microglia and/or macrophages in the CNS (36–39). Viral replication in microglia from susceptible SJL mice is significantly higher than that in microglia from resistant C57BL/6 mice and the viral load is similarly greater in microglia from SJL mice infected with TMEV compared with microglia from C57BL/6 mice (39). Because TMEV persistence in the CNS is a critically important prerequisite in the pathogenesis of demyelination (30, 40, 41), viral persistence may lead to continuous inflammatory cytokine production and the consequent pathogenic immune responses in the development of TMEV-induced demyelinating disease (Figure 1).

2 TLR expression and activation status may determine the susceptibility to viral infection

Toll-like receptors (TLRs) include a family of members, which recognize microbial products. This family of receptors is known to closely associate with the induction of initial innate immune responses following bacterial and viral infections (42, 43). mRNAs for TLR1–9 are expressed in microglia and stimulation of TLRs on the cells upregulates the expression of MHC class II and costimulatory molecules, which enable the microglia to present antigens to $CD4^+$ T cells (38). Activated and/or differentiated cells are far more supportive of TMEV infection/replication (44–46). Consequently, the cytokine production levels in APCs, including microglia, in susceptible SJL mice are higher than those in resistant B6 mice (30, 39). For example, higher levels of TNFα, IL-6 and IL-1β are produced in microglia and macrophages from susceptible SJL mice after TMEV infection, compared with cells from resistant B6, B6.S, or B10.S mice (47–49). Similarly, viral loads in glia and

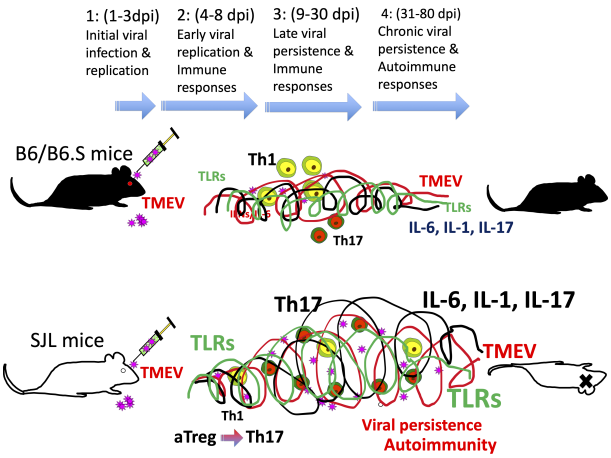

FIGURE 1
(1) 1-3 d post-infection: initial viral infection; (2) 4-8 d post-infection: early viral infection; (3) 9-30 d post-infection; (4) 31-80 d post-infection: chronic viral persistence. Resistant mice such as B6 and B6.S mice show rapid clearance of virus within 2-3 weeks, whereas susceptible SJL mice fail to clear viral persistence. Consequently, persistent TLR activation throughout infection leads to elevated levels of cytokines such as type I IFNs, IL-6, and IL-1beta, which favors stimulation of pathogenic Th17 response over protective Th1 response. Such pathogenic immune responses lead to the development of demyelinating disease in TMEV-infected SJL mice.

antigen-presenting cells (APCs) from susceptible SJL mice with TMEV-induced demyelinating disease are significantly greater than that in cells from resistant B6.S, B6, and F1(B6XSJL) mice (34, 39). However, the levels of costimulatory molecule expression on APCs from susceptible mice and their ability to stimulate T cells during chronic TMEV infection are significantly poorer, which steers the pathogenic T cell responses (34, 39). Elevated TLR2, 3, 4, and 7 signaling in APCs enhances viral infection and replication (39, 50). Thus, persistent viral infection accompanied by continuous excessive cytokine production leads to viral persistence and the development of pathogenic immune responses. The association of TLR signals with pathogenesis is further supported by the fact that the administration of bacterial lipopolysaccharide (LPS), a ligand for TLR4, or poly I:C, a ligand for TLR3, increases viral loads and elevates the level of inflammatory response (50, 51). Thus, the differences in the type and intensity of TLR signals on antigen-presenting cells may affect the levels of viral infection, replication, and production of IL-1β and IL-6, which are critical factors in the development of demyelinating disease (Figure 2A).

3 NF-κB activation via TLRs is necessary for TMEV replication and cytokine production

TMEV has a single RNA genome which is recognized by TLR7, and a dsRNA intermediate which is recognized by TLR3 (42, 43). Consequently, TMEV infection leads to activation of NF-κB, AP-1, and IRFs via the TLR signals, resulting in the production of various cytokines, including IL-1β and IL-6 (39, 52–54). The melanoma differentiation-associated gene 5 also recognizes viral messages and participates in the activation of NF-κB (55). The infection of primary glial cells results in the activation of a wide range of chemokine genes, including CXCL1, CXCL2, CXCL10, CCL2, CCL3, CCL4, CCL5, CCL7 and CCL12 (56–58). The production of chemokines and cytokines following various viral infections is dependent on the activation of NF-κB via pattern recognition receptors (32, 52, 59–62). These chemokines further activate CXCR3, CCR7 and CCR5 genes, which further promote the cellular recruitment and infiltration to the CNS (63, 64). In addition, IL-1β, IL-6, IFNα/β, and TNFα produced following TMEV infection further stimulate cells and upregulate the production of CCL2, CCL5, CXCL10 (65–67). These cytokines further promote the development of pathogenic Th17 cells and consequent demyelination (27, 34, 39, 68). Increases in the production of fibrin deposition, adhesion molecules (ICAM and VCAM), and endothelin-1 associated with blood–brain-barrier permeability, contributing to the pathogenesis of demyelinating disease have also been observed after TMEV infection (35, 69–72).

The treatment of resistant C57BL/6 mice with LPS, a ligand of TLR4, or IL-1β increases the viral load in the CNS and leads to the pathogenesis of demyelinating disease (51, 73). Similarly, administration of poly I:C, a ligand of TLR3 leads to the rapid progression of demyelinating disease in mice infected with TMEV (50). The activation of NF-κB via TLRs is associated with TMEV replication and the production of various inflammatory cytokines and chemokine (52, 66, 67). Furthermore, TNF-α, IL-6, and IL-1β produced after TMEV infection further activate NF-κB, promoting

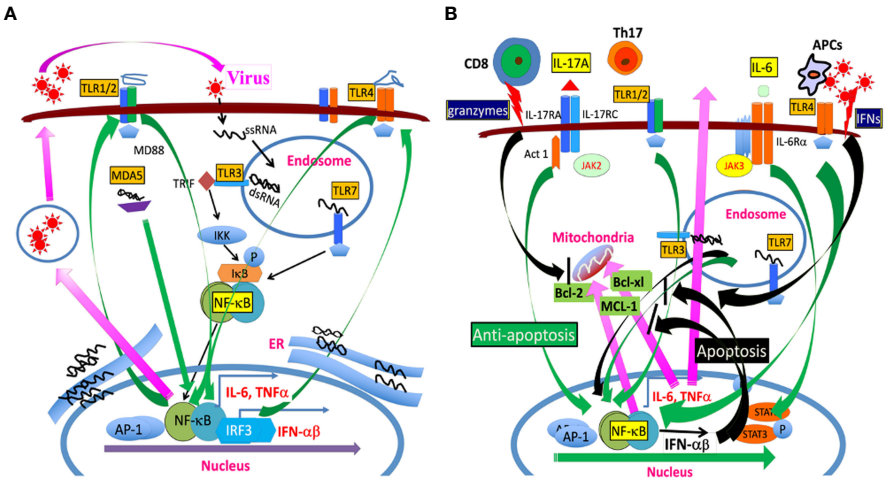

FIGURE 2
(A) TMEV infection releases a single-stranded RNA genome and double-stranded RNA replication intermediate in the endosome. The single-stranded RNA is recognized by TLR7 and the dsRNA intermediate is recognized by TLR3. The TLR signaling activates NF-κB, AP-1, and IRFs, which results in the production of various cytokines such as IL-6, IL-1beta, and type I IFNs. In addition, MDA5 also recognizes dsRNA replication intermediate, leading to NF-κB activation. These activations lead to the additional expression of TLR2/4 and other TLRs which further participates in activating NF-κB. The amplified NF-κB signaling further promotes TMEV replication because TMEV replication is dependent on the presence of activated NF-κB. **(B)** TLR signaling activates NF-κB, which results in the production of anti-apoptotic MCL-1, Bcl-2, Bcl-xL, and IL-6, inhibiting apoptosis induced by cytotoxic T cells and IFNs. IL-6 and IL-1beta further promote the generation of pathogenic Th17 cells. IL-17 produced by Th17 cells together with IL-6 synergistically inhibit the apoptosis of virus-infected cells by activating NF-κB and STAT3, leading to production of additional anti-apoptotic molecules in the mitochondria. The prolonged various TLR signals leading to NF-κB activation participate in the prolonged production of anti-apoptotic molecules and continuous TMEV replication.

increased TMEV replication. NF-κB activation further leads to stimulation of additional TLRs, amplifying pathogenic signals in the deployment of demyelinating disease (45, 52, 66, 74, 75). This is consistent with the fact that TMEV infection and replication are greater in the cells of susceptible mice and that excessive TLR signal and cytokine production, including IL-1β, IL-6, and TGFβ, further promotes the pathogenesis of demyelinating disease (47, 52, 66).

TMEV infection also activates NLRP3 via TLR signaling (74). Activation of NLRP3 inflammasome results in the production of IL-1β and PEG_2, promoting the pathogenesis (75, 76). TMEV-infected susceptible SJL mice produce much greater levels of IL-1β and other inflammatory cytokines compared with resistant mice. The presence of high levels of IL-1β and other inflammatory cytokines such as IL-6 promotes pathogenic Th17 responses (47, 68, 73). In addition, IL-17 from Th17 responses further promotes IL-6 production (77, 78), together inhibiting cellular apoptosis (68, 79). The excessive activation of PGE_2 signaling also contributes to pathogenesis (74, 80) by preventing the T cell killing of target cells (81). TMEV infection also results in the increased expression of PD-1 and PDL-1 via IL-6 signaling, inhibiting cytotoxic T cell function (81, 82). Moreover, the IL-1β signal induces IL-6 production and further promotes Th17 cell expansion (73, 83). Thus, elevated perpetual TLR signaling and consequent persistent cytokine overproduction lead to viral persistence by blocking apoptosis and consequently facilitate pathogenic immune responses in susceptible mice infected with TMEV.

4 Excessive cytokine production via TLR activation leads to pathogenic immune responses

TMEV-specific Th1 cells producing IFN-γ can lyse virus-infected cells in a Fas-dependent manner (84). The presence of capsid specific Th1 responses delays the development of demyelinating disease (85–87). In addition, mice deficient in IFN-γ or its receptor genes cannot efficiently clear TMEV infection, resulting in rapid development of demyelinating disease (88, 89). Similarly, deficiency in the IFN-γ receptor significantly accelerates the onset of disease in mice (90, 91). Thus, the level of Th1 responses may play a protective role in the development of TMEV-induced demyelinating disease.

Th17 cells, a subpopulation of Th cells which produce IL-17, are associated with the development of various autoimmune diseases (92–95). Th17 cells are developed in the presence of IL-6, and Th17 cell levels are significantly greater in susceptible mice infected with TMEV. The role of Th17 responses in the pathogenesis of TMEV-induced demyelinating disease has been verified by administrating anti-IL-17 antibodies (68) or using Th17-biased RORγt Tg mice (96). DCs infected with live TMEV producing various innate immune responses, but not epitope peptide-loaded DCs, are able to induce the development of Th17 responses (68). These results indicate that the virus-infected environment, including the presence of various cytokines, is required to induce pathogenic Th17 cells in the development of TMEV-induced demyelinating diseases.

High levels of FoxP3+CD4+ T cells, which constitute a subset of Th cells, appear first in the CNS of virus-infected mice (97, 98). The TLR2-mediated signal induced following TMEV infection may be involved in the early generation of $CD25^{-}FoxP3^{+}CD4^{+}$ T cells (54, 99, 100). $CD25^{lo}FoxP3^{+}CD4^{+}$ T cells are found in levels as much as two-fold higher in the CNS of virus-infected SJL mice compared with B6 mice (101). $CD25^{lo}FoxP3^{+}CD4^{+}$ T cells do not display a regulatory function (102), and the presence of a high level of $CD25^{lo}FoxP3^{+}CD4^{+}$ T cells may promote the development of TMEV-induced demyelinating disease (97). $CD25^{lo}FoxP3^{+}CD4^{+}$ T cells appear to undergo trans-differentiation into Th17 cells following the loss of FoxP3 expression (103, 104). Thus, these $CD25^{lo}FoxP3^{+}CD4^{+}$ T cells appearing early in the CNS of TMEV-infected mice may be converted into pathogenic Th17 cells in the presence of excessive cytokines (68, 101). Similarly elevated levels of $CD25^{-}FoxP3^{+}CD4^{+}$ T cells have been detected in patients with chronic hepatitis B virus infection (105) and systemic lupus (106).

Cytotoxic $CD8^{+}$ T cells producing IFN-γ and perforin play an important role in protection of mice from developing TMEV-induced demyelinating disease (107–109). Cytotoxic $CD8^{+}$ T cells recognizing viral determinants appear to participate in causing damages of virus-infected, myelin-producing oligodendrocytes and other cell types in the CNS (110–114). The presence of $CD8^{+}$ T cells is necessary to manifest clinical symptoms, but the protective role of these cells in the development of TMEV-induced demyelinating disease has also been demonstrated (111–114). Thus, certain $CD8^{+}$ T cell populations, depending on their specificity and or cytokine profile are likely to play different roles in the pathogenesis of TMEV-induced demyelination.

TMEV productively infects approximately 50% of primary $CD20^{+}$ B cells and 25% of $CD19^{+}CD20^{+}$ cells in susceptible SJL mice (27). TMEV-infected B cells express elevated levels of CD69 as well as MHC class II and costimulatory molecules and exhibit elevated levels of antibody production and enhanced antigen-presenting function to T cells. B cell activation after TMEV infection resembles B cells treated with TLR ligands for TLR2, TLR3, TLR4, TLR7, and TLR9 (27). These results strongly suggest that B cell activation following TMEV infection is associated with TLR signals, consistent with previous findings that various TLR-mediated signals activate B cells (115, 116). TMEV infection also triggers B cells of susceptible mice to produce the excessive production of IFN-α/β, IL-6, IL-1β, and PGE2 (27, 117). These innate immune responses further elevate the activation of B cells to produce antibodies to viral and self-antigens and vigorously promote pathogenic Th17 cell responses (27, 117–119).

B cells producing antibodies to TMEV capsid antigens are detected in the demyelinating lesions and spinal fluids of TMEV-infected mice (120–122). Plasma cells producing anti-TMEV antibodies are also detected in the meninges of CNS parenchyma (123). Antibodies to TMEV determinants play a protective role during the early stage of viral infection (124–126). In the absence of $CD8^{+}$ T cells, antibody response is critically important in protecting mice from Theiler's virus-induced encephalitis (125). In addition, the pathogenesis of TMEV-induced demyelinating disease is accelerated in mice treated with the monoclonal anti-CD20 antibody (127). However, the contribution of anti-TMEV antibodies to the protection of mice from demyelinating disease is relatively minor compared with the protection by $CD4^{+}$ Th1 and $CD8^{+}$ T cells (125, 128).

5 Role of NF-κB activated by TLRs in viral persistence

APCs from susceptible SJL mice are highly susceptible to TMEV infection and the viral infection leads to the activation of NF-κB via TLRs (27, 34, 52). The activation of NF-κB leads to the production of high levels of TNF-α, IL-1β, and IL-6, which are associated with activation of B cells and directional T cell responses (129–131). Type I IFNs produced in consequences of TLR activation contribute to the activation of NF-κB and cellular apoptosis (34, 52, 132, 133). In contrast, high levels of type I or II IFNs provide only transient protection against TMEV infection and thus high levels of these cytokines in susceptible SJL mice may not participate in controlling viral loads in TMEV-infected mice (34, 132, 134). The resistance of TMEV infection against type I IFNs is consistent with previous observations in other viruses (134–136).

Activation of NF-κB is necessary for TMEV replication (45) and consequently the state of host cell activation determines the level of viral replication (137). Following TMEV infection, TLR2, 3, 4, and 7 are associated with the production of various cytokines in different glial cells and professional antigen-presenting cells (27, 39, 52, 54, 138). TLR7 recognizes the single-stranded TMEV RNA genome and TLR3 interacts with the double-stranded RNA replication intermediate in the endosome (48, 52, 139). TMEV infection results in the engagement of various TLRs and other related signals to activate NF-κB, AP-1, and IRFs (54, 55, 140, 141). In turn, these signals result in the production of various cytokines, including TNFα, IL-1β and IL-6. NF-κB activation leads to the elevated expression and activation of TLRs including TLR2/4, which further activate NF-κB at a higher level (54). Such amplified NF-κB signaling further promotes the expression of anti-apoptotic Bcl-2 and Bcl-xL molecules, supporting vigorous TMEV replication (34, 142, 143). Such prevention of apoptosis following TMEV infection may result in further persistent viral replication and excessive cytokine production (Figure 2B).

6 Production of anti-apoptotic cytokines by virus-infected cells

IL-6 is a major cytokine produced following TMEV and other viral infections and displays an anti-apoptotic function (50, 144, 145). IL-6 inhibits the cytolytic function of $CD8^+$ T cells and drives Th17 responses. IL-17 produced by Th17 cells also inhibits cytolytic function of virus-reactive CD8+ T cells, further promoting TMEV persistence (68). Furthermore, IL-6 and IL-17 together synergistically inhibit cytotoxic function of virus-specific $CD8^+$ T cells (79). IL-17 is also known to enhance tumor growth in animals, supporting the inhibitory function of IL-17 on cytotoxic CD8+ T cells (146, 147). Cytotoxic CD8+ T cells and some CD4+ T cells induce the cytolysis of virus-infected cells through the granule exocytosis and or the activation of Fas–FasL pathway (86, 148–151). IL-17 upregulates the expression of Bcl-2 and Bcl-xl molecules via the NF-κB pathway and subsequently these prosurvival molecules protect the target cells from the apoptosis induced by cytotoxic CD4+ and CD8+ T cells (68). Nevertheless, the synergistic inhibition of apoptosis of virus-infected cells by IL-17 and IL-6 may serve as a powerful means for viral persistence. The inhibition of apoptosis extends the life of virus-infected cells, resulting in prolonged viral replication and persistence (Figure 2B). Thus, the interaction between virus and host cells via IL-17 and IL-6 and/or other cytokines results in persistent viral infection and prolonged harmful immune responses including various autoimmune responses, which ultimately lead to the development of TMEV-induced demyelinating disease (152). Similarly, persistent and or repeated infections of COVID-19 appear to stimulate TLRs, leading to cytokine storms and autoimmune responses in pathogenesis (153–156).

7 Viral persistence, continuous TLR signals, and cytokine storms lead to autoimmunity

Chronic infection with TMEV results in antibody responses to self-antigens including myelin basic protein (MBP) in the CNS of infected mice (25, 27, 157). Similarly, $CD4^+$ T cell responses to viral antigens and myelin-associated autoantigens, including MBP and proteolipid protein, have been detected during persistent infection with TMEV (19). In addition, a $CD8^+$ cytotoxic T cell population, recognizing both viral and self-antigens, has been identified in TMEV-infected SJL mice (158). Thus, various immune responses, including antibody, $CD4^+$ T cell, and $CD8^+$ T cell responses to viral and CNS autoantigens, are induced in mice with chronic TMEV infection. Sequestered autoantigens to the CNS may be released following TMEV-induced tissue damage, and these autoantigens subsequently induce autoimmune responses under constant elevated TLR stimulation and cytokine production (19, 27). The initial insults to the CNS by T cells reactive to viral antigens appear to be necessary to the pathogenesis of demyelinating disease (84, 113, 159). Such immune-mediated initial tissue damage in addition to virus-induced cellular apoptosis may be necessary to result in the development of TMEV-induced demyelinating disease.

Following intraperitoneal infection of systemic lupus erythematosus-prone NZBWF1 and BXSB male mice with TMEV or Coxsackie virus, the production of autoantibodies to several nuclear autoantigens has been rapidly accelerated (27). Since these mice have either duplicated or altered TLR genes (115, 160–162), the elevated expression of TLRs and their continuous stimulation is likely responsible for autoimmunity. These results strongly suggest that chronic TMEV infection continuously stimulates preexisting autoimmune cells via virus-induced TLR-mediated polyclonal activation. This notion is supported by the fact that the treatment of cells with the ligands of different TLRs activates B cells and T cells similarly to TMEV infection (27). Because virus-reactive T cell responses are required for the development of TMEV-induced demyelinating disease, immune-mediated tissue damage to the CNS may be necessary (68, 107, 111, 159). Therefore, these anti-viral and autoimmune responses appear to participate in protecting and/or damaging the related tissues (19, 68, 159, 163–165). However, the

presence of high levels of proinflammatory cytokines during chronic viral infection may lead to the development of harmful autoimmune responses (166–168). Taken together, persistent TMEV infection leads to continuous stimulation of various TLRs and consequently results in TLR-mediated polyclonal activation of B and T cells. Although the roles of autoimmune responses in the pathogenesis of TMEV-induced demyelinating disease are not certain, they are likely to contribute to the overall pathogenic outcome by participating in further tissue damage and/or cytokine production.

Author contributions

BK: writing—review and editing, funding acquisition.

Funding

This work was supported by the United States Public Health Service Grants (RO1 NS28752 and RO1 NS33008) and a grant from the National Multiple Sclerosis Society (RG 4001-A6).

Acknowledgments

I acknowledge all the colleagues who have participated in original contribution to this research in the past years.

Conflict of interest

The author declares that the research was conducted in the absence of any commercial or financial relationships that could be construed as a potential conflict of interest.

Publisher's note

References

1. Theiler M. Spontaneous encephalomyelitis of mice-a new virus disease. *J Exp Med* (1934) 80:122. doi: 10.1126/science.80.2066.122-b

2. Lipton HL. Theiler's virus infection in mice: an unusual biphasic disease process leading to demyelination infect. *Immun* (1975) 11:1147–55. doi: 10.1128/iai.11.5.1147-1155.1975

3. Nitayaphan S, Omilianowski D, Toth MM, Parks GD, Rueckert RR, Palmenberg AC, et al. Relationship of theiler's murine encephalomyelitis viruses to the cardiovirus genus of picornaviruses. *Intervirology* (1986) 26:140–8. doi: 10.1159/000149693

4. Acheson NH. *Fundamentals of molecular virology. 2nd ed*. John Wiley & Sons, Inc (2011).

5. Daniels JB, Pappenheimer AM, Richardson S. Observations on encephalomyelitis of mice (DA strain). *J Exp Med* (1952) 96:517. doi: 10.1084/jem.96.6.517

6. Lehrich JR, Arnason BG, Hochberg FH. Demyelinative myelopathy in mice induced by the DA virus. *J Neurol Sci* (1976) 29(2-4):149–60. doi: 10.1016/0022-510X(76)90167-2

7. Lipton HL, Friedmann A. Purification of theiler's murine encephalomyelitis virus and analysis of the structural virion polypeptides: correlation of the polypeptide profile with virulence. *J Virol* (1980) 33:1165–72. doi: 10.1128/jvi.33.3.1165-1172.1980

8. Dal Canto MC, Lipton HL. Primary demyelination in theiler's virus infection. an ultrastructural study. *Lab Invest* (1975) 33:626–37.

9. Lipton HL, Dal Canto MC. The TO strains of theiler's viruses cause "slow virus-like" infections in mice. *Ann Neurol* (1979) 6:25–8. doi: 10.1002/ana.410060106

10. Johnson RT. The possible viral etiology of multiple sclerosis. *Adv Neurol* (1975) 13:1–46.

11. McFarlin DE, McFarland HF. Multiple sclerosis (first of two parts). *N Engl J Med* (1982) 307(19):1183– 8. doi: 10.1056/NEJM198211043071905

12. Soldan SS, Berti R, Salem N, Secchiero P, Flamand L, Calabresi PA, et al. Association of human herpes virus 6 (HHV-6) with multiple sclerosis: increased IgM response to HHV-6 early antigen and detection of serum HHV-6 DNA. *Nat Med* (1997) 3(12):1394–7. doi: 10.1038/nm1297-1394

13. Akhyani N, Berti R, Brennan MB, Soldan SS, Eaton JM, McFarland HF, et al. Tissue distribution and variant characterization of human herpesvirus (HHV)-6: increased prevalence of HHV-6A in patients with multiple sclerosis. *J Infect Dis* (2000) 182(5):1321–5. doi: 10.1086/315893

14. Martinez A, Alvarez-Lafuente R, Mas A, Bartolome M, Garcia-Montojo M, de Las Heras V, et al. Environment-gene interaction in multiple sclerosis: human herpesvirus 6 and MHC2TA. *Hum Immunol* (2007) 68(8):685–9. doi: 10.1016/j.humimm.2007.05.005

15. Adams RaV M. *Principles of neurology*. New York: McGraw Hill (1977). p. 1041.

16. Buchmeier MJ, Lane TE. Viral-induced neurodegenerative disease. *Curr Opin Microbiol* (1999) 2(4):398–402. doi: 10.1016/S1369-5274(99)80070-8

17. Wege H, Siddell S, ter Meulen V. The biology and pathogenesis of coronaviruses. *Curr Top Microbiol Immunol* (1982) 99:165–200. doi: 10.1007/978-3-642-68528-6_5

18. Dal Canto MC, Kim BS, Miller SD, Melvold RW. Theiler's murine encephalomyelitis virus (TMEV)-induced demyelination: a model for human multiple clerosis. *Methods* (1996) 10(3):453–61. doi: 10.1006/meth.1996.0123

19. Miller SD, Vanderlugt CL, Begolka WS, Pao W, Yauch RL, Neville KL, et al. Persistent infection with theiler's virus leads to CNS autoimmunity via epitope spreading. *Nat Med* (1997) 3(10):1133–6. doi: 10.1038/nm1097-1133

20. Liang Z, Kumar AS, Jones MS, Knowles NJ, Lipton HL. Phylogenetic analysis of the species theilovirus: emerging murine and human pathogens. *J Virol* (2008) 82(23):11545–54. doi: 10.1128/JVI.01160-08

21. Chiu CY, Greninger AL, Kanada K, Kwok T, Fischer KF, Runckel C, et al. Identification of cardioviruses related to theiler's murine encephalomyelitis virus in human infections. *Proc Natl Acad Sci U.S.A.* (2008) 105(37):14124–9. doi: 10.1073/pnas.0805968105

22. Zoll J, Erkens Hulshof S, Lanke K, Verduyn Lunel F, Melchers WJ, Schoondermark-van de Ven E, et al. Saffold virus, a human theiler's-like cardiovirus, is ubiquitous and causes infection early in life. *PloS Pathog* (2009) 5(5):e1000416. doi: 10.1371/journal.ppat.1000416

23. Wisniewski HM, Bloom BR. Primary demyelination as a nonspecific consequence of a cell-mediated immune reaction. *J Exp Med* (1975) 141(2):346–59. doi: 10.1084/jem.141.2.346

24. Clatch RJ, Lipton HL, Miller SD. Characterization of theiler's murine encephalomyelitis virus (TMEV)-specific delayed-type hypersensitivity responses in TMEV-induced demyelinating disease: correlation with clinical signs. *J Immunol* (1986) 136:920–7. doi: 10.4049/jimmunol.136.3.920

25. Rauch HC, Montgomery IN, Hinman CL, Harb W, Benjamins JA. Chronic theiler's virus infection in mice: appearance of myelin basic protein in the cerebrospinal fluid and serum antibody directed against MBP. *J Neuroimmunol* (1987) 14:35–48. doi: 10.1016/0165-5728(87)90099-3

26. Yamada M, Zurbriggen A, Fujinami RS. Monoclonal antibody to theiler's murine encephalomyelitis virus defines a determinant on myelin and oligodendrocytes, and augments demyelination in experimental allergic encephalomyelitis. *J Exp Med* (1990) 171:1893–907. doi: 10.1084/jem.171.6.1893

27. Jin YH, Kim CX, Huang J, Kim BS. Infection and activation of b cells by theiler's murine encephalomyelitis virus (TMEV) leads to autoantibody production in an infectious model of multiple sclerosis. *Cells* (2020) 9(8):1787. doi: 10.3390/cells9081787

28. Lipton HL, Dal Canto MC. Susceptibility of inbred mice to chronic central nervous system infection by theiler's murine encephalomyelitis virus. *Infect Immun* (1979) 26:369–74. doi: 10.1128/iai.26.1.369-374.1979

29. Rodriguez M, David CS. Demyelination induced by theiler's virus: influence of the h-2 haplotype. *J Immunol* (1985) 135:2145–8. doi: 10.4049/jimmunol.135.3.2145

30. Jin YH, Mohindru M, Kang MH, Fuller AC, Kang B, Gallo D, et al. Differential virus replication, cytokine production, and antigen-presenting function by microglia from susceptible and resistant mice infected with theiler's virus. *J Virol* (2007) 81 (21):11690–702. doi: 10.1128/JVI.01034-07

31. Anderson R, Harting E, Frey MS, Leibowitz JL, Miranda RC. Theiler's murine encephalomyelitis virus induces rapid necrosis and delayed apoptosis in myelinated mouse cerebellar explant cultures. *Brain Res* (2000) 868(2):259–67. doi: 10.1016/S0006-8993(00)02338-6

32. Palma JP, Kim BS. Induction of selected chemokines in glial cells infected with theiler's virus. *J Neuroimmunol* (2001) 117(1-2):166–70. doi: 10.1016/S0165-5728(01)00326-5

33. Zheng L, Calenoff MA, Dal Canto MC. Astrocytes, not microglia, are the main cells responsible for viral persistence in theiler's murine encephalomyelitis virus infection leading to demyelination. *J Neuroimmunol* (2001) 118(2):256–67. doi: 10.1016/S0165-5728(01)00338-1

34. Hou W, So EY, Kim BS. Role of dendritic cells in differential susceptibility to viral demyelinating disease. *PloS Pathog* (2007) 3(8):e124. doi: 10.1371/journal.ppat.0030124

35. Jin YH, Kang B, Kang HS, Koh CS, Kim BS. Endothelin-1 contributes to the development of virus-induced demyelinating disease. *J Neuroinflamm* (2020) 17 (1):307. doi: 10.1186/s12974-020-01986-z

36. Clatch RJ, Miller SD, Metzner R, Dal Canto MC, Lipton HL. Monocytes/macrophages isolated from the mouse central nervous system contain infectious theiler's murine encephalomyelitis virus (TMEV). *Virology* (1990) 176:244–54. doi: 10.1016/0042-6822(90)90249-Q

37. Clatch RJ, Melvold RW, Miller SD, Lipton HL. Theiler's murine encephalomyelitis virus (TMEV)-induced demyelinating disease in mice is influenced by the h-2D region: correlation with TEMV-specific delayed-type hypersensitivity. *J Immunol* (1985) 135(2):1408–14. doi: 10.4049/jimmunol.135.2.1408

38. Olson JK, Miller SD. Microglia initiate central nervous system innate and adaptive immune responses through multiple TLRs. *J Immunol* (2004) 173(6):3916–24. doi: 10.4049/jimmunol.173.6.3916

39. Jin YH, Kang HS, Hou W, Meng L, Kim BS. The level of viral infection of antigen-presenting cells correlates with the level of development of theiler's murine encephalomyelitis virus-induced demyelinating disease. *J Virol* (2015) 89(3):1867–78. doi: 10.1128/JVI.02471-14

40. Lipton HL, Melvold R. Genetic analysis of susceptibility to theiler's virus-induced demyelinating disease in mice. *J Immunol* (1984) 132:1821–5. doi: 10.4049/jimmunol.132.4.1821

41. Lipton HL, Kumar AS, Trottier M. Theiler's virus persistence in the central nervous system of mice is associated with continuous viral replication and a difference in outcome of infection of infiltrating macrophages versus oligodendrocytes. *Virus Res* (2005) 111(2):214–23. doi: 10.1016/j.virusres.2005.04.010

42. Akira S. TLR signaling. *Curr Top Microbiol Immunol* (2006) 311:1–16. doi: 10.1007/3-540-32636-7_1

43. Diebold SS, Kaisho T, Hemmi H, Akira S. Innate antiviral responses by means of TLR7-mediated recognition of single-stranded RNA. *Science* (2004) 303:1529–31. doi: 10.1126/science.1093616

44. Son KN, Becker RP, Kallio P, Lipton HL. Theiler's virus-induced intrinsic apoptosis in M1-d macrophages is bax mediated and restricts virus infectivity: a mechanism for persistence of a cytolytic virus. *J Virol* (2008) 82(9):4502–10. doi: 10.1128/JVI.02349-07

45. Kang MH, So EY, Park H, Kim BS. Replication of theiler's virus requires NF-kappaB-activation: higher viral replication and spreading in astrocytes from susceptible mice. *Glia* (2008) 56(9):942–53. doi: 10.1002/glia.20668

46. Schneider KM, Watson NB, Minchenberg SB, Massa PT. The influence of macrophage growth factors on theiler's murine encephalomyelitis virus (TMEV) infection and activation of macrophages. *Cytokine* (2018) 102:83–93. doi: 10.1016/j.schres.2017.08.003

47. Chang JR, Zaczynska E, Katsetos CD, Platsoucas CD, Oleszak EL. Differential expression of TGF-beta, IL-2, and other cytokines in the CNS of theiler's murine encephalomyelitis virus-infected susceptible and resistant strains of mice. *Virology* (2000) 278(2):346–60. doi: 10.1006/viro.2000.0646

48. Petro TM. Disparate expression of IL-12 by SJL/J and B10.S macrophages during theiler's virus infection is associated with activity of TLR7 and mitogen-activated protein kinases. *Microbes Infect* (2005) 7:224–32. doi: 10.1016/j.micinf.2004.10.014

49. Moore TC, Bush KL, Cody L, Brown DM, Petro TM. Control of early theiler's murine encephalomyelitis virus replication in macrophages by interleukin-6 occurs in conjunction with STAT1 activation and nitric oxide production. *J Virol* (2012) 86 (19):10841–51. doi: 10.1128/JVI.01402-12

50. Jin YH, Kaneyama T, Kang MH, Kang HS, Koh CS, Kim BS. TLR3 signaling is either protective or pathogenic for the development of theiler's virus-induced demyelinating disease depending on the time of viral infection. *J Neuroinflamm* (2011) 8:178. doi: 10.1186/1742-2094-8-178

51. Pullen LC, Park SH, Miller SD, Dal Canto MC, Kim BS. Treatment with bacterial LPS renders genetically resistant C57BL/6 mice susceptible to theiler's virus-induced demyelinating disease. *J Immunol* (1995) 155(9):4497–503. doi: 10.4049/jimmunol.155.9.4497

52. So EY, Kang MH, Kim BS. Induction of chemokine and cytokine genes in astrocytes following infection with theiler's murine encephalomyelitis virus is mediated by the toll-like receptor 3. *Glia* (2006) 53:858–67. doi: 10.1002/glia.20346

53. Turrin NP. Central nervous system toll-like receptor expression in response to theiler's murine encephalomyelitis virus-induced demyelinating disese in resistnt and susceptible mouse strains. *Virol J* (2008) 5:154. doi: 10.1186/1743-422X-5-154

54. So EY, Kim BS. Theiler's virus infection induces TLR3-dependent upregulation of TLR2 critical for proinflammatory cytokine production. *Glia* (2009) 57:1216–26. doi: 10.1002/glia.20843

55. Jin YH, Kim SJ, So EY, Meng L, Colonna M, Kim BS. Melanoma differentiation-associated gene 5 is critical for protection against theiler's virus-induced demyelinating disease. *J Virol* (2012) 86:1531–43. doi: 10.1128/JVI.06457-11

56. Palma JP, Kim BS. The scope and activation mechanisms of chemokine gene expression in primary astrocytes following infection with theiler's virus. *J Neuroimmunol* (2004) 149:121–9. doi: 10.1016/j.jneuroim.2003.12.025

57. Rubio N, Sanz-Rodriguez F, Lipton HL. Theiler's virus induces the MIP-2 chemokine (CXCL2) in astrocytes from genetically susceptible but not from resistant mouse strains. *Cell Immunol* (2006) 239:31–40. doi: 10.1016/j.cellimm.2006.03.003

58. Rubio N, Sanz-Rodriguez F. Induction of the CXCL1 (KC) chemokine in mouse astrocytes by infection with the murine encephalomyelitis virus of theiler. *Virology* (2007) 358:98–108. doi: 10.1016/j.virol.2006.08.003

59. Asensio VC, Campbell IL. Chemokine gene expression in the brains of mice with lymphocytic choriomeningitis. *J Virol* (1997) 71:7832–40. doi: 10.1128/jvi.71.10.7832-7840.1997

60. Lane TE, Asensio VC, Yu N, Paoletti AD, Campbell IL, Buchmeier MJ. Dynamic regulation of alpha- and beta-chemokine expression in the central nervous system during mouse hepatitis virus-induced demyelinating disease. *J Immunol* (1998) 180:970–8. doi: 10.4049/jimmunol.160.2.970

61. Hoffman LM, Eife BT, Begolka WS, Miller SD, Karpus WJ. Central nervous system chemokine expression during theiler's virus-induced demyelinating disease. *J Neurovirol* (1999) 5:635–42. doi: 10.3109/13550289909021292

62. Noe KH, Cenciarelli C, Moyer SA, Rota PA, Shin ML. Requirements for measles virus induction of RANTES chemokine in human astrocytoma-derived U373 cells. *J Virol* (1999) 73:3117–24. doi: 10.1128/JVI.73.4.3117-3124.1999

63. Guidotti LG, Chisari FV. Noncytolytic control of viral infections by the innate and adaptive immune response. *Annu Rev Immunol* (2001) 19:65–91. doi: 10.1146/annurev.immunol.19.1.65

64. Ludewig B, Junt T, Hengartner B, Zinkernagel RM. Dendritic cells in autoimmune diseases. *Curr Opin Immunol* (2001) 13:657–62. doi: 10.1016/S0952-7915(01)00275-8

65. Veckman V, Österlund P, Fagerlund R, Melén K, Matikainen S, Julkunen I. TNF-α and IFN-α enhance influenza-a-virus-induced chemokine gene expression in human A549 lung epithelial cells. *Virology* (2006) 345:96–104. doi: 10.1016/j.virol.2005.09.043

66. Palma JP, Kwon D, Clipston NA, Kim BS. Infection with theiler's murine encephalomyelitis virus directly induces proinflammatory cytokines in primary astrocytes via NF-kappaB activation: potential role for the initiation of demyelinating disease. *J Virol* (2003) 77:6322–31. doi: 10.1128/JVI.77.11.6322-6331.2003

67. Olson JK. Effect of the innate immune response on development of theiler's murine encephalomyelitis virus-induced demyelinating disease. *J Neurovirol* (2014) 20:427–36. doi: 10.1007/s13365-014-0262-6

68. Hou W, Kang HS, Kim BS. Th17 cells enhance viral persistence and inhibit T cell cytotoxicity in a model of chronic virus infection. *J Exp Med* (2009) 206(2):313–28. doi: 10.1084/jem.20082030

69. Inoue A, Koh CS, Yamazaki M, Ichikawa M, Isobe M, Ishihara Y, et al. Anti-adhesion molecule therapy in theiler's murine encephalomyelitis virus-induced demyelinating disease. *Int Immunol* (1997) 9(12):1837–47. doi: 10.1093/intimm/9.12.1837

70. Olson JK, Girvin AM, Miller SD. Direct activation of innate and antigen-presenting functions of microglia following infection with theiler's virus. *J Virol* (2001) 75(20):9780–9. doi: 10.1128/JVI.75.20.9780-9789.2001

71. Pozner RG, Berria MI, Negrotto S, Schattner M, Gomez RM. Differential astrocyte response to theiler's murine encephalomyelitis virus infection. *Intervirology* (2005) 48(5):279–84. doi: 10.1159/000085095

72. Rubio N, Sanz-Rodriguez F, Arevalo MA. Up-regulation of the vascular cell adhesion molecule-1 (VCAM-1) induced by theiler's murine encephalomyelitis virus infection of murine brain astrocytes. *Cell Commun Adhes* (2010) 17(3):57–68. doi: 10.3109/15419061.2010.507827

73. Kim BS, Jin YH, Meng L, Hou W, Kang HS, Park HS, et al. IL-1 signal affects both protection and pathogenesis of virus-induced chronic CNS demyelinating disease. *J Neuroinflamm* (2012) 9:217. doi: 10.1186/1742-2094-9-217

74. Kim SJ, Jin YH, Kim BS. Prostaglandin E2 produced following infection with theiler's virus promotes the pathogenesis of demyelinating disease. *PloS One* (2017) 12 (4):e0176406. doi: 10.1371/journal.pone.0176406

75. Agostini L, Martinon F, Burns K, McDermott MF, Hawkins PN, Tschopp J. NALP3 forms an IL-1beta-processing inflammasome with increased activity in muckle-wells autoinflammatory disorder. *Immunity* (2004) 20:319–25. doi: 10.1016/S1074-7613(04)00046-9

76. Swanson KV, Deng M, Ting JP. The NLRP3 inflammasome: molecular activation and regulation to therapeutics. *Nat Rev Immunol* (2019) 19(8):477–89. doi: 10.1038/s41577-019-0165-0

77. Hwang SY, Kim JY, Kim KW, Park MK, Moon Y, Kim WU, et al. IL-17 induces production of IL-6 and IL-8 in rheumatoid arthritis synovial fibroblasts via NF-kappaB- and PI3-kinase/Akt-dependent pathways. *Arthritis Res Ther* (2004) 6:R120–8. doi: 10.1186/ar1038

78. Wang L, Yi T, Kortylewski M, Pardoll DW, Zeng D, Yu H. IL-17 can promote tumor growth through an IL-6-Stat3 signaling pathway. *J Exp Med* (2009) 206:1457–64. doi: 10.1084/jem.20090207

79. Hou W, Jin YH, Kang HS, Kim BS. Interleukin-6 (IL-6) and IL-17 synergistically promote viral persistence by inhibiting cellular apoptosis and cytotoxic T cell function. *J Virol* (2014) 88(15):8479–89. doi: 10.1128/JVI.00724-14

80. Weinlich R, Bortoluci KR, Chehab CF, Serezani CH, Ulbrich AG, Peters-Golden M, et al. TLR4/MYD88-dependent, LPS-induced synthesis of PGE2 by macrophages or dendritic cells prevents anti-CD3-mediated CD95L upregulation in T cells. *Cell Death Differ* (2008) 15:1901–9. doi: 10.1038/cdd.2008.128

81. Jin YH, Hou W, Kang HS, Koh CS, Kim BS. The role of interleukin-6 in the expression of PD-1 and PDL-1 on central nervous system cells following infection with theiler's murine encephalomyelitis virus. *J Virol* (2013) 87:11538–51. doi: 10.1128/JVI.01967-13

82. Chan LC, Li CW, Xia W, Hsu JM, Lee HH, Cha JH, et al. IL-6/JAK1 pathway drives PD-L1 Y112 phosphorylation to promote cancer immune evasion. *J Clin Invest* (2019) 129(8):3324–38. doi: 10.1172/JCI126022

83. Ben-Sasson SZ, Hu-Li J, Quiel J, Caucheltaux S, Ratner M, Shapira I, et al. IL-1 acts directly on CD4 T cells to enhance their antigen-driven expansion and differentiation. *Proc Natl Acad Sci USA* (2009) 106:7119–24. doi: 10.1073/pnas.0902745106

84. Palma JP, Yauch RL, Lang S, Kim BS. Potential role of CD4+ T cell-mediated apoptosis of activated astrocytes in theiler's virus-induced demyelination. *J Immunol* (1999) 162:6543–51. doi: 10.4049/jimmunol.162.11.6543

85. Crane MA, Yauch R, Dal Canto MC, Kim BS. Effect of immunization with theiler's virus on the course of demyelinating disease. *J Neuroimmunol* (1993) 45(1-2):67–73. doi: 10.1016/0165-5728(93)90165-U

86. Kang B, Kang HK, Kim BS. Identification of capsid epitopes of theiler's virus recognized by CNS-infiltrating CD4(+) T cells from virus-infected C57BL/6 mice. *Virus Res* (2005) 108(1-2):57–61. doi: 10.1016/j.virusres.2004.08.001

87. Rodriguez M, Roos RP, McGavern D, Zoecklein L, Pavelko K, Sang H, et al. The CD4-mediated immune response is critical in determining the outcome of infection using theiler's viruses with VP1 capsid protein point mutations. *Virology* (2000) 275 (1):9–19. doi: 10.1006/viro.2000.0493

88. Fiette L, Aubert C, Muller U, Huang S, Aguet M, Brahic M, et al. Theiler's virus infection of 129Sv mice that lack the interferon alpha/beta or interferon gamma receptors. *J Exp Med* (1995) 181(6):2069–76. doi: 10.1084/jem.181.6.2069

89. Rodriguez M, Zoecklein LJ, Howe CL, Pavelko KD, Gamez JD, Nakane S, et al. Gamma interferon is critical for neuronal viral clearance and protection in a susceptible mouse strain following early intracranial theiler's murine encephalomyelitis virus infection. *J Virol* (2003) 77(22):12252–65. doi: 10.1128/JVI.77.22.12252-12265.2003

90. Pullen LC, Miller SD, DalCanto MC, van der Meide PH, Kim BS. Alteration in the level of interferon-gamma results in acceleration of theiler's virus-induced demyelinating disease. *J Neuroimmunol* (1994) 55:143–52. doi: 10.1016/0165-5728(94)90004-3

91. Rodriguez M, Pavelko K, Coffman RL. Gamma interferon is critical for resistance to theiler's virus-induced demyelination. *J Virol* (1995) 69(11):7286–90. doi: 10.1128/jvi.69.11.7286-7290.1995

92. Harrington LE, Hatton RD, Mangan PR, Turner H, Murphy TL, Murphy KM, et al. Interleukin 17-producing CD4+ effector T cells develop via a lineage distinct from the T helper type 1 and 2 lineages. *Nat Immunol* (2005) 6(11):1123–32. doi: 10.1038/ni1254

93. Park H, Li Z, Yang XO, Chang SH, Nurieva R, Wang YH, et al. A distinct lineage of CD4 T cells regulates tissue inflammation by producing interleukin 17. *Nat Immunol* (2005) 6(11):1133–41. doi: 10.1038/ni1261

94. Steinman L. A brief history of T(H)17, the first major revision in the T(H)1/T (H)2 hypothesis of T cell-mediated tissue damage. *Nat Med* (2007) 13(2):139–45. doi: 10.1038/nm1551

95. Veldhoen M, Hocking RJ, Atkins CJ, Locksley RM, Stockinger B. TGFbeta in the context of an inflammatory cytokine milieu supports *de novo* differentiation of IL-17-producing T cells. *Immunity* (2006) 24(2):179–89. doi: 10.1016/j.immuni.2006.01.001

96. Martinez NE, Sato F, Kawai E, Omura S, Takahashi S, Yoh K, et al. Th17-biased RORgammat transgenic mice become susceptible to a viral model for multiple sclerosis. *Brain behavior immunit.* (2015) 43:86–97. doi: 10.1016/j.bbi.2014.07.008

97. Richards MH, Getts MT, Podojil JR, Jin YH, Kim BS, Miller SD. Virus expanded regulatory T cells control disease severity in the theiler's virus mouse model of MS. *J Autoimmun* (2011) 36(2):142–54. doi: 10.1016/j.jaut.2010.12.005

98. Zhao J, Zhao J, Perlman S. Virus-specific regulatory T cells ameliorate encephalitis by repressing effector T cell functions from priming to effector stages. *PloS Pathog* (2014) 10(8):e1004279. doi: 10.1371/journal.ppat.1004279

99. Nawijn MC, Motta AC, Gras R, Shirinbak S, Maazi H, van Oosterhout AJ. TLR-2 activation induces regulatory T cells and long-term suppression of asthma manifestations in mice. *PloS One* (2013) 8(2):e55307. doi: 10.1371/journal.pone.0055307

100. Yamazaki S, Okada K, Maruyama A, Matsumoto M, Yagita H, Seya T. TLR2-dependent induction of IL-10 and Foxp3+ CD25+ CD4+ regulatory T cells prevents effective anti-tumor immunity induced by Pam2 lipopeptides *in vivo*. *PloS One* (2011) 6 (4):e18833. doi: 10.1371/journal.pone.0018833

101. Kang HS, Hou W, Kim BS. Rapid expansion of virus-specific CD4+ T cell types in the CNS of susceptible mice infected with theiler's virus. *Int J Mol Sci* (2020) 21:7719. doi: 10.3390/ijms21207719

102. Zelenay S, Lopes-Carvalho T, Caramalho I, Moraes-Fontes MF, Rebelo M, Demengeot J. Foxp3+ CD25- CD4 T cells constitute a reservoir of committed regulatory cells that regain CD25 expression upon homeostatic expansion. *Proc Natl Acad Sci U.S.A.* (2005) 102(11):4091–6. doi: 10.1073/pnas.0408679102

103. Radhakrishnan S, Cabrera R, Schenk EL, Nava-Parada P, Bell MP, Van Keulen VP, et al. Reprogrammed FoxP3+ T regulatory cells become IL-17+ antigen-specific autoimmune effectors *in vitro* and *in vivo*. *J Immunol* (2008) 181(5):3137–47. doi: 10.4049/jimmunol.181.5.3137

104. Komatsu N, Okamoto K, Sawa S, Nakashima T, Oh-hora M, Kodama T, et al. Pathogenic conversion of Foxp3+ T cells into TH17 cells in autoimmune arthritis. *Nat Med* (2014) 20(1):62–8. doi: 10.1038/nm.3432

105. Stoop JN, Claassen MA, Woltman AM, Binda RS, Kuipers EJ, Janssen HL, et al. Intrahepatic regulatory T cells are phenotypically distinct from their peripheral counterparts in chronic HBV patients. *Clin Immunol* (2008) 129(3):419–27. doi: 10.1016/j.clim.2008.07.029

106. Bonelli M, Savitskaya A, Steiner CW, Rath E, Smolen JS, Scheinecker C. Phenotypic and functional analysis of CD4+ CD25- Foxp3+ T cells in patients with systemic lupus erythematosus. *J Immunol* (2009) 182(3):1689–95. doi: 10.4049/jimmunol.182.3.1689

107. Murray PD, McGavern DB, Lin X, Njenga MK, Leibowitz J, Pease LR, et al. Perforin-dependent neurologic injury in a viral model of multiple sclerosis. *J Neurosci* (1998) 18(18):7306–14. doi: 10.1523/JNEUROSCI.18-18-07306.1998

108. Palma JP, Lee HG, Mohindru M, Kang BS, DalCanto M, Miller SD, et al. Enhanced susceptibility to theiler's virus-induced demyelinating disease in perforin-deficient mice. *J Neuroimmunol* (2001) 116:125–35. doi: 10.1016/S0165-5728(01)00293-4

109. Pena Rossi C, McAllister A, Fiette L, Brahic M. Theiler's virus infection induces a specific cytotoxic T lymphocyte response. *Cell Immunol* (1991) 138:341–8. doi: 10.1016/0008-8749(91)90158-8

110. Lindsley MD, Thiemann R, Rodriguez M. Cytotoxic T cells isolated from the central nervous systems of mice infected with theiler's virus. *J Virol* (1991) 65:6612–20. doi: 10.1128/jvi.65.12.6612-6620.1991

111. Rivera-Quinones C, McGovern D, Schmeizer JD, Hunter SF, Low PA, Rodriguez M. Absence of neurological deficits following extensive demyelination in a class I-deficient murine model of multiple sclerosis. *Nat Med* (1998) 4:187–93. doi: 10.1038/nm0298-187

112. Borrow P, Tonks P, Welsh CJ, Nash AA. The role of CD8+T cells in the acute and chronic phases of theiler's murine encephalomyelitis virus-induced disease in mice. *J Gen Virol* (1992) 73:1861–5. doi: 10.1099/0022-1317-73-7-1861

113. Myoung J, Hou W, Kang B, Lyman MA, Kang JA, Kim BS. The immunodominant CD8+ T cell epitope region of theiler's virus in resistant C57BL/6 mice is critical for anti-viral immune responses, viral persistence, and binding to the host cells. *Virology* (2007) 360:159–71. doi: 10.1016/j.virol.2006.09.045

114. Begolka WS, Haynes LM, Olson JK, Padilla J, Neville KL, DalCanto M, et al. CD8-deficient SJL mice display enhanced susceptibility to theiler's virus infection and increased demyelinating pathology. *J Neurovirol* (2001) 7:409–20. doi: 10.1080/135502801753170264

115. Santiago-Raber ML, Baudino L, Izul S. Emerging roles of TLR7 and TLR9 in murine SLE. *J Autoimmun* (2009) 33:231–8. doi: 10.1016/j.jaut.2009.10.001

116. Mills KH. TLR-dependent T cell activation in autoimmunity. *Nat Rev Immunol* (2011) 11:807–22. doi: 10.1038/nri3095

117. Kiefer K, Oropallo MA, Cancro MP, Marshak-Rothstein A. Role of type I interferons in the activation of autoreactive b cells. *Immunol Cell Biol* (2012) 90:498–504. doi: 10.1038/icb.2012.10

118. Kishimoto T. Interleukin-6: from basic science to medicine–40 years in immunology. *Annu Rev Immunol* (2005) 23:1–21. doi: 10.1146/annurev.immunol.23.021704.115806

119. Kuno K, Matsushima K. The IL-1 receptor signaling pathway. *J Leukoc Biol* (1994) 56:542–7. doi: 10.1002/jlb.56.5.542

120. Cash E, Bandeira A, Chirinian S, Brahic M. Characterization of b lymphocytes present in the demyelinating lesions induced by theiler's virus. *J Immunol* (1989) 143 (3):984–8. doi: 10.4049/jimmunol.143.3.984

121. Roos RP, Nalefski EA, Nitayaphan S, Variakojis R, Singh KK. An isoelectric focusing overlay study of the humoral immune response in theiler's virus demyelinating disease. *JNeuroimmunol* (1987) 13:305–14. doi: 10.1016/0165-5728(87)90066-X

122. Zurbriggen A, Fujinami RS. A neutralization-resistant theiler's virus variant produces an altered disease pattern in the mouse central nervous system. *J Virol* (1989) 63:1505–13. doi: 10.1128/jvi.63.4.1505-1513.1989

123. Pachner AR, Li L, Lagunoff D. Plasma cells in the central nervous system in the theiler's virus model of multiple sclerosis. *J Neuroimmunol* (2011) 232(1-2):35–40. doi: 10.1016/j.jneuroim.2010.09.026

124. Cameron K, Zhang X, Seal B, Rodriguez M, Njenga MK. Antigens to viral capsid and non-capsid proteins are present in brain tissues and antibodies in sera of theiler's virus-infected mice. *J Virol Methods* (2001) 91(1):11–9. doi: 10.1016/S0166-0934(00)00246-9

125. Kang BS, Palma JP, Lyman MA, Dal Canto M, Kim BS. Antibody response is required for protection from theiler's virus-induced encephalitis in C57BL/6 mice in the absence of CD8(+) T cells. *Virology* (2005) 340(1):84–94. doi: 10.1016/j.virol.2005.06.028

126. Kim BS, Choe YK, Crane MA, Jue CR. Identification and localization of a limited number of predominant conformation-independent antibody epitopes of theiler's murine encephalomyelitus virus. *Immunol Lett* (1992) 31(2):199–205. doi: 10.1016/0165-2478(92)90146-F

127. Gilli F, Li L, Campbell SJ, Anthony DC, Pachner AR. The effect of b-cell depletion in the theiler's model of multiple sclerosis. *J Neurol Sci* (2015) 359(1-2):40–7. doi: 10.1016/j.jns.2015.10.012

128. Inoue A, Choe YK, Kim BS. Analysis of antibody responses to predominant linear epitopes of theiler's murine encephalomyelitis virus. *J Virol* (1994) 68:3324–33. doi: 10.1128/jvi.68.5.3324-3333.1994

129. Delhaye S, Paul S, Blakqori G, Minet M, Weber F, Staeheli P, et al. Neurons produce type I interferon during viral encephalitis. *Proc Natl Acad Sci U.S.A.* (2006) 103 (20):7835–40. doi: 10.1073/pnas.0602460103

130. Rubio N, Palomo M, Alcami A. Interferon-alpha/beta genes are up-regulated in murine brain astrocytes after infection with theiler's murine encephalomyelitis virus. *J Interferon Cytokine Res* (2010) 30(4):253–62. doi: 10.1089/jir.2009.0050

131. Jin YH, Hou W, Kim SJ, Fuller AC, Kang B, Goings G, et al. Type I interferon signals control theiler's virus infection site, cellular infiltration and T cell stimulation in the CNS. *J Neuroimmunol* (2010) 226:27–37. doi: 10.1016/j.jneuroim.2010.05.028

132. Jelachich ML, Lipyon HL. Restricted theiler's murine encephalomyelitis virus infection in murine macrophages induces apoptosis. *J Gen Virol* (1999) 80:1701–5. doi: 10.1099/0022-1317-80-7-1701

133. Yang CH, Murti A, Pfeffer SR, Basu L, Kim JG, Pfeffe LM. IFNα/β promotes cell survival by activating NF-κB. *Proc Nat Acad Sci USA* (2000) 97:13631–6. doi: 10.1073/pnas.250477397

134. Daher KA, Samuel CE. Mechanism of interferon action. differential effect of interferon on the synthesis of simian virus 40 and reovirus polypeptides in monkey kidney cells. *Virology* (1982) 117:379–90. doi: 10.1016/0042-6822(82)90477-9

135. Atreya PL, Kulkami S. Respiratory syncytial virus strain A2 is resistant to the antiviral effects of type I interferons and human MxA. *Virology* (1999) 261:227–41. doi: 10.1006/viro.1999.9835

136. Ho LJ, Hung LF, Weng CY, Wu WL, Chou P, Lin YL, et al. Dengue virus type 2 antagonizes IFN-alpha but not IFN-gamma antiviral effect via down-regulating Tyk2-STAT signaling in the human dendritic cell. *J Immunol* (2005) 174:8163–72. doi: 10.4049/jimmunol.174.12.8163

137. Jelachich ML, Bandyopadhyay P, Blum K, Lipton HL. Theiler's virus growth in murine macrophage cell lines depends on the state of differentiation. *Virology* (1995) 209:437–44. doi: 10.1006/viro.1995.1276

138. Turrin NP. Central nervous system toll-like receptor expression in response to theiler's murine encephalomyelitis virus-induced demyelination disease in resistant and susceptible mouse strains. *Virol J* (2008) 5:154. doi: 10.1186/1743-422X-5-154

139. Akira S, Hemmi H. Recognition of pathogen-associated molecular patterns by TLR family. *Immunol Lett* (2003) 85:85–95. doi: 10.1016/S0165-2478(02)00228-6

140. Diebold SS, Kaisho T, Hemmi H, Akira S, Sousa Re. Innate antiviral responses by means of TLR7-mediated recognition of single-stranded RNA. *Science* (2004) 303:1529–31. doi: 10.1126/science.1093616

141. Kawai T, Akira S. Toll-like receptors and their crosstalk with other innate receptors in infection and immunity. *Immunity* (2011) 34:637–50. doi: 10.1016/j.immuni.2011.05.006

142. Mattson MP, Meffert MK. Roles for NF-kappaB in nerve cell survival, plasticity, and disease. *Cell Deth Difer* (2006) 13(5):852–60. doi: 10.1038/sj.cdd.4401837

143. Sarnico I. NF-kappaB dimers in the regulation of neuronal survival. *Int Rev Neurobiol* (2009) 85:351–62. doi: 10.1016/S0074-7742(09)85024-1

144. Hsieh CY, Chen CA, Huang CY, Chang MC, Lee CN, Su YN, et al. IL-6-encoding tumor antigen generates potent cancer immunotherapy through antigen processing and anti-apoptotic pathways. *Mol Ther* (2007) 15(10):1890–7. doi: 10.1038/sj.mt.6300243

145. Jourdan M, Veyrune JL, De Vos J, Redal N, Couderc G, Klein B. A major role for mcl-1 antiapoptotic protein in the IL-6-induced survival of human myeloma cells. *Oncogene* (2003) 22(19):2950–9. doi: 10.1038/sj.onc.1206423

146. Asadzadeh Z, Mohammadi H, Safarzadeh E, Hemmatzadeh M, Mahdian-Shakib A, Jadidi-Niaragh F, et al. The paradox of Th17 cell functions in tumor immunity. *Cell Immunol* (2017) 322:15–25. doi: 10.1016/j.cellimm.2017.10.015

147. Varikuti S, Oghumu S, Elbaz M, Volpedo G, Ahirwar DK, Alarcon PC, et al. STAT1 gene deficient mice develop accelerated breast cancer growth and metastasis which is reduced by IL-17 blockade. *Oncoimmunol* (2017) 6:e1361088. doi: 10.1080/2162402X.2017.1361088

148. Kagi D, Vignaux F, Ledermann B, Burki K, Depraetere V, Nagata S, et al. Fas and perforin pathways as major mechanisms of T cell-mediated cytotoxicity. *Science* (1994) 265:528–30. doi: 10.1126/science.7518614

149. Lowin B, Hahne M, Mattmann C, Tschopp J. Cytolytic T-cell cytotoxicity is mediated through perforin and fas lytic pathways. *Proc Natl Acad Sci USA* (1994) 91:11571–5. doi: 10.1073/pnas.91.24.11571

150. Harty JT, Tvinnereim AR, White DW. CD8+ T cell effector mechanisms in resistance to infection. *Ann Rev Immunol* (2000) 18:275–308. doi: 10.1146/annurev.immunol.18.1.275

151. Jellison ER, Kim SK, Welsh RM. Cutting edge: MHC class II-restricted killing *in vivo* during viral infection. *J Immunol* (2005) 174:614–8. doi: 10.4049/jimmunol.174.2.614

152. Kim BS. Excessive innate immunity steers pathogenic adaptive immunity in the development of theiler's virus-induced demyelinating disease. (2021) 22(10):5254. doi: 10.3390/ijms22105254

153. Khanmohammadi S, Rezaei N. Role of toll-like receptors in the pathogenesis of COVID-19. *J Med Virol* (2021) 93:2735–9. doi: 10.1002/jmv.26826

154. Mabrey FL, Morrell ED, Wurfel MM. TLRs in COVID-19: how they drive immunopathology and the rationale for modulation. *Innate Immun* (2021) 27:503–13. doi: 10.1177/17534259211051364

155. Manik M, Singh RK. Role of toll-like receptors in modulation of cytokine storm signaling in SARS-CoV-2-induced COVID-19. *J Med Virol* (2022) 94:869–77. doi: 10.1002/jmv.27405

156. Chang SE, Feng A, Meng W, Apostolidis SA. New-onset IgG autoantibodies in hospitalized patients with COVID-19. *Nat Commun* (2021) 12(1):5417. doi: 10.1038/s41467-021-25509-3

157. Fujinami RS, Zurbriggen A, Powell HC. Monoclonal antibody defines determinant between theiler's virus and lipid-like structures. *J Neuroimmunol* (1988) 20:25–32. doi: 10.1016/0165-5728(88)90110-5

158. Tsunoda I, Kuang LQ, Kobayashi-Warren M, Fujinami RS. Central nervous system pathology caused by autoreactive CD8+ T-cell clones following virus infection. *J Virol* (2005) 79:14640–6. doi: 10.1128/JVI.79.23.14640-14646.2005

159. Myoung J, Kang HS, Hou W, Meng L, Dal Canto MC, Kim BS. Epitope-specific CD8+ T cells play a differential pathogenic role in the development of a viral disease model for multiple sclerosis. *J Virol* (2012) 86:13717–28. doi: 10.1128/JVI.01733-12

160. Patole PS, Grone HJ, Segerer S, Ciubar R, Belemezova E, Henger A, et al. Viral double-stranded RNA aggravates lupus nephritis through toll-like receptor 3 on glomerular mesangial cells and antigen-presenting cells. *J Am Soc Nephrol* (2005) 16:1326–38. doi: 10.1681/ASN.2004100820

161. Pisitkun P, Deane JA, Difilippantonio MJ, Tarasenko T, Satterthwaite AB, Bolland S. Autoreactive b cell responses to RNA-related antigens due to TLR7 gene duplication. *Science* (2006) 312:1669–72. doi: 10.1126/science.1124978

162. Green NM, Marshak-Rothstein A. Toll-like receptor driven b cell activation in the induction of systemic autoimmunity. *Semin Immunol* (2011) 23:106–12. doi: 10.1016/j.smim.2011.01.016

163. Myoung J, Bahk Yl, Kang HS, Dal Canto MC, Kim BS. Anti-capsid immunity level, not viral persistence level, correlates with the progression of theiler's virus-induced demyelinating disease in viral P1-transgenic mice. *J Virol* (2008) 82:5606–17. doi: 10.1128/JVI.02442-07

164. Drescher KM, Pease LR, Rodriguez M. Antiviral immune responses modulate the nature of central nervous system (CNS) disease in a murine model of multiple sclerosis. *Immunol Rev* (1997) 159:177–93. doi: 10.1111/j.1600-065X.1997.tb01015.x

165. Asakura K, Miller DJ, Pease LR, Rodriguez M. Targeting of IgMkappa antibodies to oligodendrocytes promotes CNS remyelination. *J Neurosci* (1998) 18:7700–8. doi: 10.1523/JNEUROSCI.18-19-07700.1998

166. Hirota K, Hashimoto M, Yoshitomi H, Tanaka S, Nomura T, Yamaguchi T, et al. T Cell self-reactivity forms a cytokine milieu for spontaneous development of IL-17+ Th cells that cause autoimmune arthritis. *J Exp Med* (2007) 204:41–7. doi: 10.1084/jem.20062259

167. Furuzawa-Carballeda J, Icaza-Chavez ME, Aguilar-Leon D, Uribe-Uribe N, Nunez-Pompa MC, Trigos-Diaz A, et al. Is the sars-CoV-2 virus a possible trigger agent for the development of achalasia? *Neurogastroenterol Motil* (2023) 35(3):e14502. doi: 10.1101/2022.09.19.22280068

168. Calzascia T, Pellegrini M, Lin A, Garza KM, Elford AR, Shahinian A, et al. CD4 T cells, lymphopenia, and IL-7 in a multistep pathway to autoimmunity. *Proc Natl Acad Sci USA* (2008) 105:2999–3004. doi: 10.1073/pnas.0712135105

frontiers | Frontiers in Immunology

TYPE Original Research
PUBLISHED 27 April 2023
DOI 10.3389/fimmu.2023.1158090

OPEN ACCESS

EDITED BY
Oliver Planz,
University of Tübingen, Germany

REVIEWED BY
Aruna Pal,
West Bengal University of Animal and Fishery Sciences, India
Zhangrui Cheng,
Royal Veterinary College (RVC), United Kingdom
Dhanashree Jagtap,
National Institute for Research in Reproductive Health (ICMR), India

*CORRESPONDENCE
Akio Miyamoto
akiomiya@obihiro.ac.jp

RECEIVED 03 February 2023
ACCEPTED 17 April 2023
PUBLISHED 27 April 2023

CITATION
Mansouri A, Yousef MS, Kowsar R, Usui N, Akthar I and Miyamoto A (2023) Sperm activate TLR2/TLR1 heterodimerization to induce a weak proinflammatory response in the bovine uterus.
Front. Immunol. 14:1158090.
doi: 10.3389/fimmu.2023.1158090

Sperm activate TLR2/TLR1 heterodimerization to induce a weak proinflammatory response in the bovine uterus

Alireza Mansouri[1], Mohamed Samy Yousef[1,2], Rasoul Kowsar[3], Nonoka Usui[1], Ihshan Akthar[1] and Akio Miyamoto[1]*

[1]Global AgroMedicine Research Center (GAMRC), Obihiro University of Agriculture and Veterinary Medicine, Obihiro, Japan, [2]Department of Theriogenology, Faculty of Veterinary Medicine, Assiut University, Assiut, Egypt, [3]Department of Animal Sciences, College of Agriculture, Isfahan University of Technology, Isfahan, Iran

Toll-like receptor 2 (TLR2) signaling pathway is involved in the sperm-triggered uterine inflammatory response at insemination, but its precise mechanism at molecular-level remains unknown. According to the ligand specificity, TLR2 forms a heterodimer with TLR1 or TLR6 as an initial step to mediate intracellular signaling, leading to a specific type of immune response. Hence, the present study aimed to identify the active TLR2 heterodimer (TLR2/1 or TLR2/6) that is involved in sperm-uterine immune crosstalk in bovine using various models. First, *in-vitro* (bovine endometrial epithelial cells, BEECs) and *ex-vivo* (bovine uterine explant) models were employed to test different TLR2 dimerization pathways in endometrial epithelia after exposure to sperm or TLR2 agonists; PAM3 (TLR2/1 agonist), and PAM2 (TLR2/6 agonist). Additionally, *in-silico* approaches were performed to confirm the dimer stability using *de novo* protein structure prediction model for bovine TLRs. The *in-vitro* approach revealed that sperm triggered the mRNA and protein expression of TLR1 and TLR2 but not TLR6 in BEECs. Moreover, this model disclosed that activation of TLR2/6 heterodimer, triggers a much stronger inflammatory response than TLR2/1 and sperm in bovine uterine epithelia. In the *ex-vivo* model that mimics the intact uterine tissue at insemination, sperm also induced the protein expression of both TLR1 and TLR2, but not TLR6, in bovine endometrium, particularly in uterine glands. Importantly, PAM3 and sperm induced similar and low mRNA expression of pro-inflammatory cytokines and TNFA protein to a lesser extent than PAM2 in endometrial epithelia. This implied that sperm might trigger a weak inflammatory response *via* TLR2/TLR1 activation which is similar to that of PAM3. Additionally, the *in-silico* analyses showed that the existence of bridging ligands is essential for heterodimer stability in bovine TLR2 with either TLR1 or TLR6. Altogether, the present findings revealed that sperm utilize TLR2/1, but not TLR2/6, heterodimerization to trigger a weak physiological inflammatory response in the bovine uterus. This might be the way to remove excess dead sperm remaining in the uterine lumen without tissue damage for providing an ideal uterine environment for early embryo reception and implantation.

KEYWORDS

sperm, endometrium, Toll-like receptor 2, dimerization, inflammation

Introduction

In bovine, during natural breeding or artificial insemination (AI), a massive number of sperm are introduced into the female reproductive tract (FRT) of the estrus animal to increase the probability of fertilization. In the course of the sperm's journey to the ova, sperm interact with the immune system of FRT.

Different Toll-like receptors (TLRs) have been found to be involved in the induction of inflammatory responses in the FRT (1–7). TLR2 play a key role in binding and immune-cross talk between sperm and FRT (1–3, 5–8). Active sperm cells bind to the bovine endometrium *via* the TLR2 and induce pro-inflammatory responses. However, sperm attachment to bovine oviduct epithelial cells is mediated also by TLR2 but leads to an anti-inflammatory response. The ovum releasing from the ovary lead to a tightly regulated sterile inflammatory response in bovine oviduct which is rapidly resolved during early corpus luteum formation (9). Meanwhile, TLR2 is also expressed in cumulus cells of cumulus-oocyte complexes (COCs) and plays immune protective functions critical for cell survival during ovulation and fertilization (10, 11).

Notably, sperm-induced weak inflammation in bovine endometrium has an essential role in uterine clearance prior to accept the embryo (3, 12). Despite numerous previous studies, the detailed molecular mechanism of sperm-uterine inflammatory signaling that regulated by TLR2 remains unclear.

TLRs are transmembrane proteins, consisting of three main domains: Extracellular domain or leucine-rich repeats (LRR), Transmembrane domain and Intracellular domain or Toll/IL-1R (TIR) domain. Ligand-induced dimerization plays a critical role in signaling through TLRs, in particular TLR2 and TLR4, due to the need for two TLR domains in the vicinity of each other to initiate TLR signaling cascade, consequently recruiting the main TLR domain-containing adaptors: MyD88, MAL/TIRAP, TRIF, TRAM, and SARM (13–15).

Ligand-induced dimerization has been proposed as a key event in the activation of TLR2 in human and mouse models (13, 14). Interestingly, TLR2/1 heterodimer has been more associated with a pro-inflammatory response compared with TLR2/6 complex, which has been shown to be related to both pro- and anti-inflammatory responses (13–16). Of note, TLR2 is involved in pro-inflammatory responses in the bovine uterus against sperm (1–3, 7).

Since dimerization is a prerequisite for any TLR2 activation, we hypothesized that the sperm-triggered physiological inflammatory response in bovine endometrium is regulated by different types of TLR2 dimerization (TLR2/1 or TLR2/6), though the structure of TLR2 dimers in bovine is unknown. *In-vitro* cell cultures using BEECs are considered as the starting point for studying any biological effect in bovine uterus (2, 7). However, this model cannot simulate the anatomical complexity of bovine uterus especially for sperm-uterine interaction (particularly uterine gland). Thus, the *ex-vivo* model using uterine explant has been performed to mimic the *in-vivo* conditions to identify different physiological interactions in bovine uterus (1).

In this study, we first employed *in-vitro* approach to evaluate the sperm-triggered TLR1, 2 and 6 expressions in endometrial epithelial cells to determine which TLR2 heterodimer is activated by sperm in bovine endometrium. Then using the same model, the degree of inflammatory response by different TLR2 agonists (i.e., PAM3 and PAM2) was evaluated and compared to sperm induced inflammation. Thereon, *ex-vivo* uterine explant culture model was used as a powerful and more physiological tool to verify the possible TLR2 dimerization mechanism in response to sperm in the uterine tissue in particular in the uterine glands.

Protein–protein interactions (PPI), including dimerization and protein complex, control all functions of the living cell during physiological and pathological conditions (17, 18). Recently, different *in-silico* approaches have been used to identify the biological pathways of PPI and highlight possible applications (19–21). TLRs molecular-level responses are extensively studied using computational biology approaches (19–21). Hence, *in-silico* model was employed for the first time to investigate dimerization process of TLR2 at molecular-level in bovine model. At first, the binding affinity of TLR2 with TLR1 and TLR6 was evaluated using known crystal structures of both mouse and human. Afterwards, the potential effect of PAM3 and PAM2 (TLR2/1 and TLR2/6 agonists, respectively) on TLR2 dimerization was investigated *via de novo* generated bovine TLRs.

Methodology

Study design

In-vitro, *ex-vivo* and *in-silico* investigations were conducted to define the signaling mechanism by which TLR2 is regulated during sperm-uterine immune interactions in non-pregnant cattle (Figure 1).

In-vitro approaches

Experimental design and *in-vitro* studies

In order to elucidate the heterodimeric form of TLR2 signaling in sperm- induced inflammation in bovine uterus at cellular level, BEECs were co-cultured with sperm (5 million/mL) for 3h. Furthermore, to investigate the contribution of TLR2 signaling (TLR2/1 and TLR2/6) cascade to uterine inflammation, the following experiments was conducted using different TLR2 agonists. Bovine endometrial epithelial cells (BEECs) were stimulated with PAM3 (TLR2/1 agonist, ab142085, Abcam) and PAM2 (TLR2/6 agonist, InvivoGen, USA) at 100 ng/mL concentration for 1h. The concentration of dose and time point were selected based on our previous reports in which those conditions were investigated in detail (2, 7). In brief, based on dose- and time-dependent investigations (10^4, 10^5 and 10^6 sperm/mL), 5 million/mL of sperm was used to induce the weak physiological inflammation after co-culture with BEECs for 3 h (8). As well, PAM3 (10, 100 and 1000 ng/mL) was applied, and 100 ng/ml was the first to induce the inflammatory response in BEECs at 1h of incubation in the similar level to that of sperm (2). Thus, 100 ng/mL of PAM3 and the same concentration of PAM2, were used in the present study to compare their inflammatory effects with sperm.

BEECs Culture

Initially, macroscopically healthy non-pregnant bovine uteri were carefully observed to be free of inflammation and abnormal color or any pathological lesions in slaughterhouse (Obihiro, Hokkaido, Japan), then collected and directly transferred to the laboratory under sterilized conditions and the uterine horn was used to isolate epithelial cells (2, 7). The isolated cells were cultured in Dulbecco's Modified Eagle Medium: Nutrient Mixture F-12

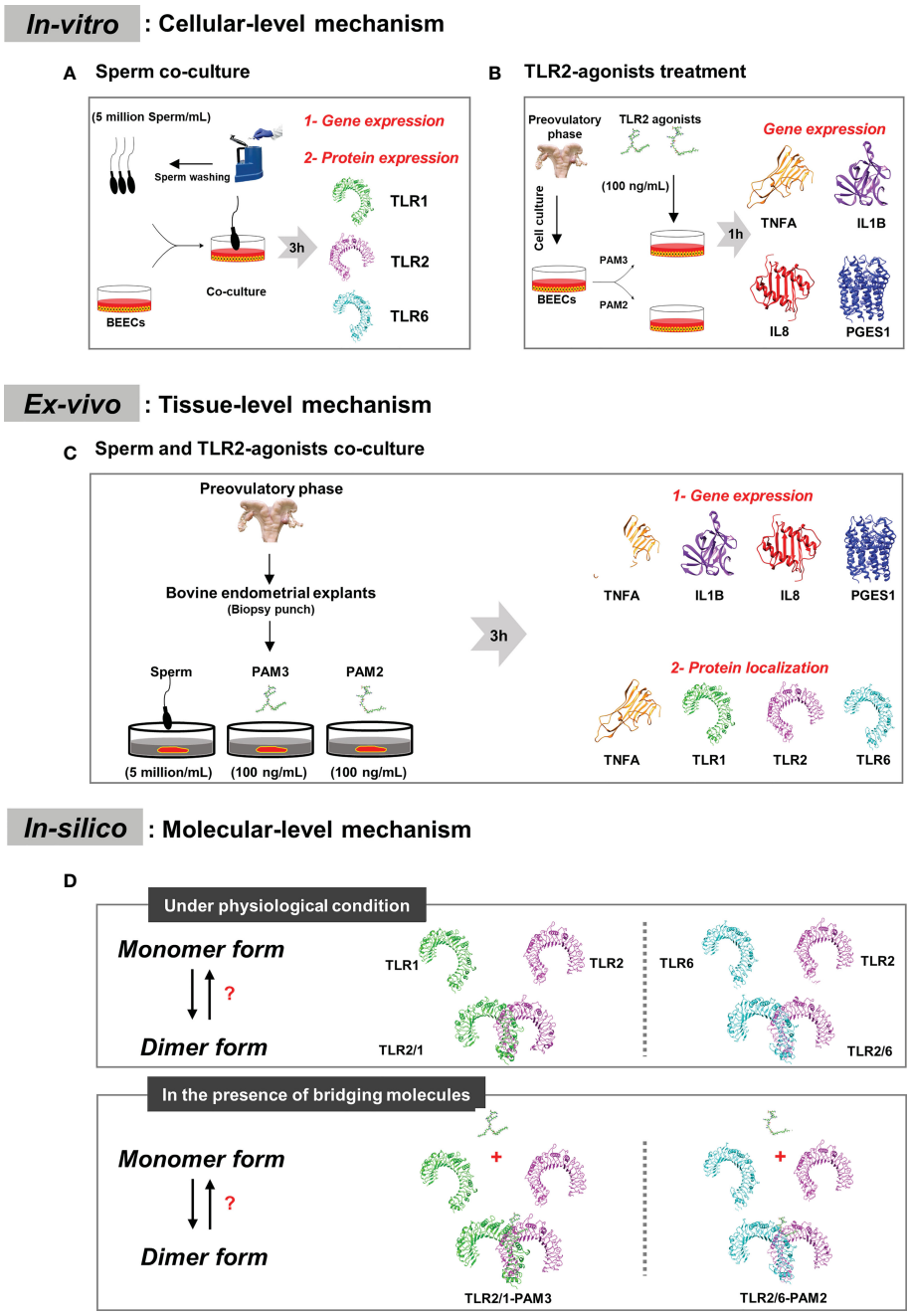

FIGURE 1
Plan representation of the research design. **(A)** *In-vitro* model: to detect which active TLR2 dimer can be employed by sperm in bovine endometrium at cellular level. BEECs monolayer were co-cultured with 5million sperm per mL for 3h. qRT-PCR and immunostaining analyses were done to investigate TLRs mRNA and protein expression. **(B)** *In-vitro* model: to study inflammation intensity through the two classical TLR2 signaling (TLR2/1 and TLR2/6 signaling cascades), BEECs monolayer were stimulated with 100 ng/mL of PAM3 (TLR2/1 agonist) and PAM2 (TLR2/6 agonist) for 1h. A time-dependent experiment (1, 6 and 12h) was done to confirm the difference between both TLR2 signaling pathway. Finally, qRT-PCR analysis was performed to consider the pro-inflammatory mRNA expression (*TNFA*, *IL1B*, *IL8* and *PGES1*). **(C)** *Ex-vivo* model: to compare sperm induced inflammation in endometrium with PAM3 and PAM2. Bovine endometrial explants were co-incubated with 5milion sperm/mL, and 100 ng/mL PAMs for 3h. First, qRT-PCR was employed to investigate the pro-inflammatory mRNA expression. Afterwards, immunostaining was used to evaluate and localize the strong inflammatory marker (TNFA) for all groups and signaling marker proteins (TLR1, TLR2 and TLR6) in endometrium for sperm group. **(D)** *In-silico* model: we investigated dimerization process for TLR2 in different condition, in absent and presence of TLR2 agonists. Additionally, we predict the effect of agonist on bovine TLR dimerization.

(DMEM/F12, Gibco, Grand Island, USA) supplemented with 1% amphotericin B, 0.1% gentamicin (Sigma-Aldrich, Steinheim, Germany), 10% heat-inactivated fetal calf serum (FCS) (Biowest USA) and 2.2% NaHCO3 using flask. The culture medium was replaced regularly with new media every 48 h. Upon reaching 70–80% confluence, the cells were collected with trypsinizing (0.05% trypsin EDTA; Amresco, Solon, OH, USA), transferred in 24-well and 12-well plates (Nalge Nunc International, Roskilde, Denmark) and cultured up to around 90% confluence (first passage). Estrogen (E2) and progesterone (P4) were added at preovulatory concentrations in the cell culture media (DMEM/F12, 1% amphotericin B, 0.1% gentamicin and 5% FCS) (2, 7).

BEECs co-cultured with sperm

The sub-confluent BEEC monolayers (after first passage) were washed twice with PBS and cultured in a medium supplemented by 0.1% FCS and gentamicin. The BEECs were co-cultured with 5 million/mL washed sperm, followed by washing cell twice with PBS, lysing with Trizol (Invitrogen, Carlsbad, USA), and storing at −80° C until RNA extraction. This experiment was repeated seven times using epithelial cells from seven different uteri (n=7). For preparing washed sperm, frozen semen straws (obtained from three Holstein bulls kept in the Genetics Hokkaido Association, Hokkaido, Japan) were thawed at 38.5°C for 30 sec, followed by washing three times at 200g for 10 min using sp-TALP (2, 7, 8). The sp-TALP consisted of 99 mM NaCl, 3.1 mM KCl, 25 mM $NaHCO_3$, 0.39 mM NaH_2PO_4, 10 mM HEPES free acid, 2 mM $CaCl_2$, 1.1 mM $MgCl_2$, 25.4 mM sodium lactate, 0.11 mg/ml sodium pyruvate, 50 µg/ml gentamycin and 6 mg/ml BSA (Sigma-Aldrich, USA) pH 7.4.

Stimulation of BEECs with agonists

The sub-confluent BEEC monolayers (after first passage) were washed twice with Phosphate Buffered Saline (PBS) and cultured in a medium supplemented by 0.1% FCS and gentamicin. The BEECs were either stimulated by 100 ng/mL PAM3 and PAM2 for 1, 6, 12 h. At the end of BEECs stimulation, cells were washed twice with PBS, lysed with Trizol (Invitrogen, Carlsbad, USA), and stored at −80°C until RNA extraction. This experiment was repeated seven times using epithelial cells from seven different uteri (n=7).

Ex-vivo approaches

Experimental design

In order to compare the endometrial response toward sperm and TLR2 agonists at the preovulatory phase, an *ex-vivo* model (bovine endometrial explants) was used, due to the advantage of investigating the protein localization in different compartments of the endometrium and the links between whole-animal condition and cellular function.

Sperm and agonist co-incubation with endometrial explants

Bovine endometrial explants were prepared as described previously (1). Briefly, pre-ovulatory bovine uteri were observed to be free of inflammation and abnormal color or any pathological lesions in slaughterhouse (Obihiro, Hokkaido, Japan), then collected and directly transferred to the laboratory for *ex-vivo* investigations under sterilized conditions. Afterwards, using an 8 mm biopsy punch, endometrial explant tissue disks were extracted from the glandular (intercaruncular) endometrial regions. Next, explants disks were placed into a plate with sp-TALP and put in the incubator (38.5°C and 5% CO_2) for 15 min (1).

To compare the sperm induced inflammation with agonists, explants were incubated with sperm (5 million sperm/mL) and TLR2 agonists (100 ng/mL) for 3h in the incubator (38.5 ^{0}C, 5% CO_2, 0.5mL sp-TALP per well in 24-well plate) and at the end of the incubation period the explants were processed for RNA extraction and immunofluorescence analysis. This experiment was repeated five times using explants from five different uteri (n=5).

PCR protocol

BEECs and uterine explants were subjected to RNA extraction, cDNA synthesis, and quantitative real-time PCR were done through following previous protocol (8). Trizol reagent (Thermo Fisher Scientific) were used to extract total RNA, followed by measuring RNA concentration using a spectrophotometer (Eppendorf, Munich, Germany), after that stored in RNA storage solution (Ambion, Austin, TX, USA) at −80°C until cDNA conversion step. The cDNA synthesis was performed as previously described (8), and the synthesized cDNA was stored at −30°C. Quantitative real-time PCR of target genes (*TNFA, IL1B, TLR2, TLR1, TLR6, IL8, PGES1* and *β-actin*, Supplementary Table 1) was carried out by QuantiTect SYBR Green PCR Master Mix (QIAGEN GmbH, Hilden, Germany) using an iCycler iQ (Bio-Rad Laboratories, Tokyo, Japan) (8). The calculated cycle threshold values were normalized using *β-actin* as an internal housekeeping gene by applying the Delta-Delta comparative threshold method to quantify the fold change between samples.

Immunofluorescence protocol

a) IF for monolayer cells

At first, monolayer cell was cultured on 24-well plates with 13mm diameter glass coverslips and grow to 90% confluence then co-cultured with 5 million sperm per mL for 3h. Cells were washed with PBS twice and fixed with 2 mL of 4% formaldehyde for 15 min at RT, followed by washing twice with PBS. After that, the cells were permeabilized with 2 mL of 0.1% Triton-X10 in PBS for 15 min on ice, followed by washing three times with PBS. Afterwards, the monolayer cells were blocked using 2mL blocking buffer (5% BSA in PBS) for 1h at RT. The cells were incubated with primary antibodies for TLR1, TLR2 and TLR6 (Supplementary Table 2) in humid chamber at 4°C overnight. After washing five times with PBS, the cells were incubated with Alexa Flour conjugated secondary antibody (Supplementary Table 2) for 1h at 4°C. After that, the cells were washed six times with PBS, followed by mounting in VECTASHIELD mounting medium containing DAPI (H-1200, Vector Laboratories, CA, USA).

b) IF for explant tissue

After the incubation, explants were rinsed in sp-TALP and fixed in 4% paraformaldehyde solution. Then, the fixed tissue samples were dehydrated using ethanol gradient (70, 80, 90, 95 and 100%), cleared

in absolute alcohol and xylene, followed by embedding in paraffin and sectioning in 5 µm thick slices. The endometrial sections were deparaffinized and rehydrated through placing on xylene, absolute alcohol and grades series of alcohol, in turn. After that, the tissue sections were blocked with normal goat serum (1:50, S-1000, Vector Laboratories, CA, USA) for 30 min at RT and followed by incubating overnight with primary antibodies for TLR1, TLR2, TLR6 and TNFA (Supplementary Table 2) at 4°C in a humidified chamber. Afterwards, the sections were incubated with Alexa Fluor conjugated secondary antibodies (Supplementary Table 2) for 30 min. Sections were washed, and coverslips were mounted using VECTASHIELD mounting medium containing DAPI. Finally, the sections were observed under fluorescence microscope (BZ-X800, Keyence).

In-silico approaches

Preparation of the molecules

In order to investigate TLR2 dimerization under both physiological state and agonist stimulation in a bovine model, an *in-silico* approach was conducted. To aim that, the TLR2/1-PAM3 (PDB ID: 2Z7X) and TLR2/6-PAM2 (PDB ID: 3A79) were selected for this research. The crystal structures of the TLRs extracellular domain of human (*Homo sapiens*) and mouse (*Mus musculus*) species are known (PDB ID of 2Z7X and 3A79, respectively) but have not yet been crystallized in bovine species (*Bos taurus*). Hence, we carried out Basic Local Alignment Search Tool (BLAST) to calculate the local similarity between bovine TLRs with human and mouse TLRs. It revealed an identity of 77.6% (Human - Bovine TLR2), 78.5% (Human - Bovine TLR1), 66.7% (Mouse - Bovine TLR2) and 72.1% (Mouse - Bovine TLR6).

Investigating the affinity between TLRs in heterodimer forms

The crystal structure of TLRs in the presence and absence of agonist, and the obtained initial structure from Haddock online server were used to investigate the affinity between TLRs (three repeats). For applying TLRs to the Haddock 2.4 web server (22), the residues involved in h-bond in TLRs interaction obtained through Ligplot analysis (23) were selected as active residues at the contacting site of TLRs. To obtain the initial structure for MD simulation, cluster 1 was selected as the best docked complex based on the highest HADDOCK score (according to the following formula: Score: 1.0 * Evdw + 0.2 * Eelec + 1.0 * Edesol + 0.1 * Eair). To calculate the binding free energies between TLRs in heterodimer forms, 150 ns MD simulation were applied to obtain trajectory MD simulation, followed by calculating binding free energy using molecular mechanics/Poisson–Boltzmann surface area (MM/PBSA) method (24–32) (Supplementary Data; Supplementary Figures 1–4).

The prediction of binding pockets of TLRs in human, mouse and bovine

The possible binding pockets on TLRs were identified through DoGSite Scorer web server, which is a strong tool for investigating potential binding pockets (33, 34). The DoGSite Scorer web server is used for mapping the possible binding pockets based on descriptors calculation (such as depth (A), surface (A^2), volume (A^3)). Furthermore, the druggability score is estimated through the support vector machine (SVM) method. The score of druggability classified from 0 to 1 while higher values are the potential pockets for the main binding sites. The pocket detection and analysis were performed for TLRs of three mammalian species (crystal structures of human, mouse, and *de novo* modeling of Bovine TLRs). Bovine TLR protein 3-D structure prediction was carried out after applying amino acid sequences of extracellular domain (Uniprot code: Q95LA9, B5TYW4 and Q704V6 for TLR2, TLR1 and TLR6, respectively) to I-TASSER server (27), followed by optimizing 3-D structures using 100 ns MD simulation.

Statistical analysis

The statistical analysis was conducted with SPSS® software version 22 (IBM, Armonk, Ny, USA). The data were first tested for normality using Kolmogorov–Smirnov test. A non-parametric Kruskal–Wallis test followed by a Mann–Whitney test were applied for non-normally distributed data of mRNA gene expressions. While One-way analysis of variance (ANOVA) and *post hoc* Tukey's test were used for normally distributed data obtained from TNFA immunofluorescence analysis. An unpaired two-tailed parametric Student's t-test was performed to evaluate the differences between two unpaired groups. The statistical significance was defined as $P< 0.05$.

Result

TLR2/1 heterodimer employed by sperm to induce inflammation in BEECs

In BEECs, sperm induced *TLR2* ($P <0.001$) and *TLR1* ($P <0.01$) mRNA expression, but not *TLR6* (Figure 2A). Moreover, the immunofluorescence analysis showed similar expression profiles for TLR2 ($P <0.01$) and TLR1 ($P <0.05$) after sperm co-culture with BEECs (Figure 2B).

The varying degrees of inflammatory reaction following endometrial activation of TLR2/1 and TLR2/6

The PAM3 increased the mRNA expression of *TNFA* and *IL8* ($P <0.05$) compared to the control. Meanwhile PAM2 significantly increased the mRNA expression of *TNFA* ($P <0.01$), *IL1B* ($P <0.01$), *IL8* ($P <0.001$), and *PGES1* ($P <0.001$) compared to the control. Compared to PAM3, PAM2 treatment significantly ($P <0.05$) increased the transcription levels of the pro-inflammatory genes (*TNFA*, *IL1B*, *IL8*, and *PGES1*). For instance, *TNFA*, *IL1B*, and *IL8* expressions were roughly 3-fold higher in the PAM2 group than in the PAM3 treatment (Figure 3). Additionally, a time-dependent exposure revealed that PAM2 over PAM3 increased *TNFA* mRNA

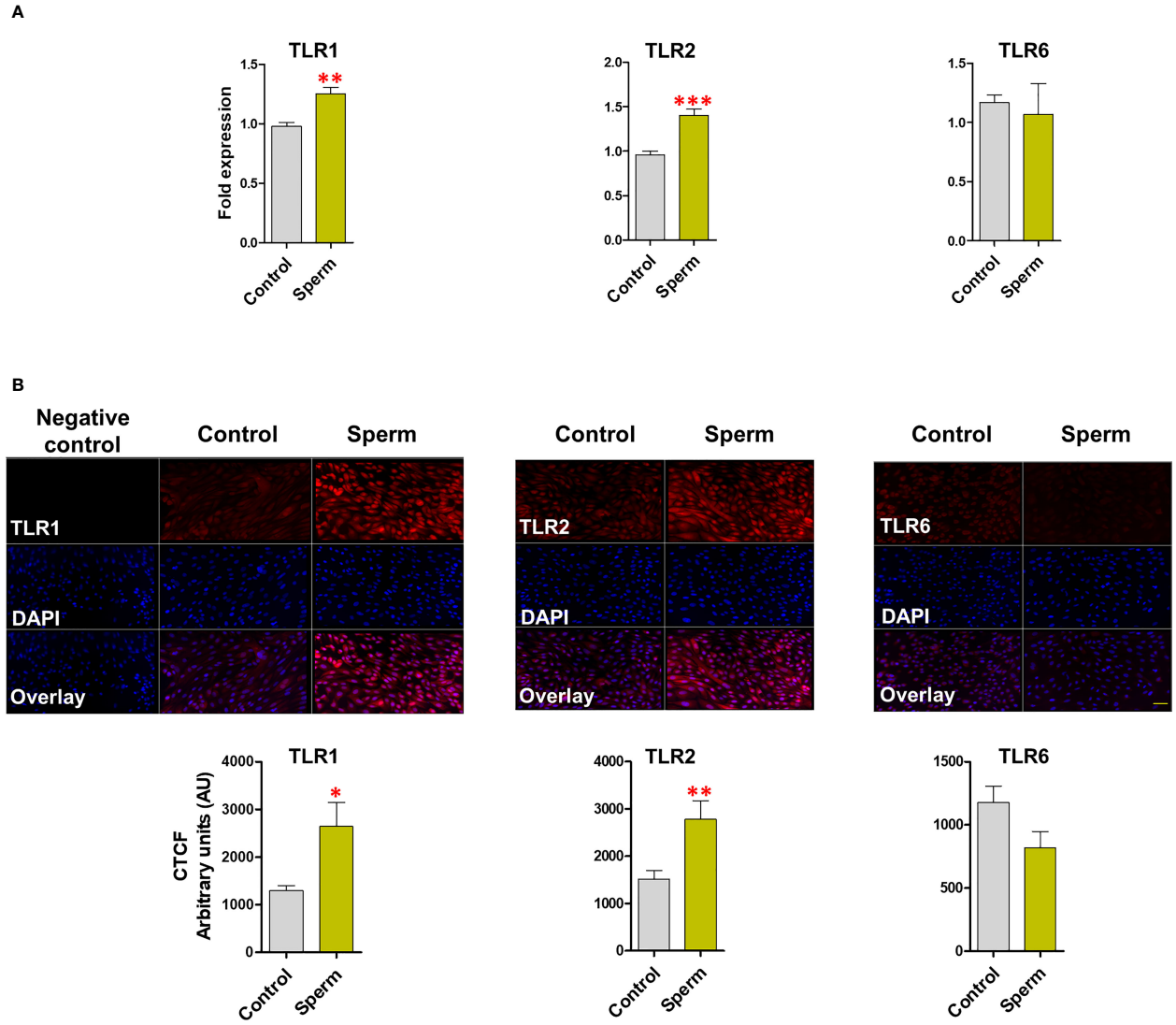

FIGURE 2
Sperm induce TLR2 and TLR1 (not TLR6) expression in BEECs. **(A)** Relative mRNA expression of *TLR1, 2* and *6* in BEECs after 3h co-culture with 5 million/mL sperm. **(B)** Immunofluorescence staining of TLR1, 2 and 6 in BEECs monolayer. This experiment was repeated seven times using epithelial cells from seven different uteri. Asterisks show a significance of difference (*P < 0.05, **P < 0.01, or ***P < 0.001) in the treatment group when compared to the control group. Bar = 50 µm.

expression in BEECs at various time points. (1, 6 and 12h) (Supplementary Figure 5).

Sperm induced the TLR2/1 protein expression in endometrial explants

The immunofluorescence analysis revealed that, TLR1, TLR2 and TLR6 is localized in the bovine endometrium, particularly in surface and glandular epithelium. It was obvious that sperm induce the protein expression of TLR2 (P <0.01) alongside TLR1 (P <0.05) in similar manner, in particular in the uterine gland and in the surface epithelium. On the other hand, for TLR6 expression, the intensity was not modulated compared to the control in the uterine gland and surface epithelium after sperm interaction with endometrial epithelia (Figure 4).

Sperm-induced inflammation in bovine endometrium is similar to that of PAM3 (TLR2/1 pathway)

PAM2 induced a higher (P < 0.05) mRNA expression of pro-inflammatory cytokines (*TNFA*, *IL1B and IL8*) in uterine explant compared to the control and sperm treatments. Of note, there was no significant difference (P > 0.05) between sperm and PAM3 groups for mRNA expression of the investigated cytokines (Figure 5A). However, *PGES1* gene expression did not show a significant change after stimulating the uterine explant with PAM3, PAM2 or sperm. In the same way, the intensity of TNFA protein expression was highly significant after PAM2 treatment in comparing to sperm and control (P < 0.05) particular in uterine gland of the endometrium compared to the control (Figure 5B).

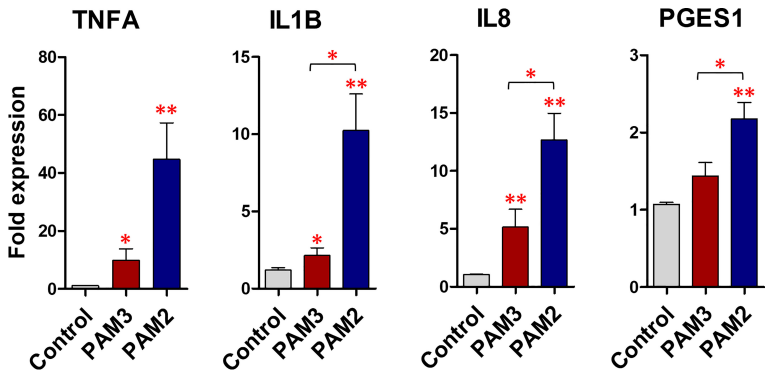

FIGURE 3
PAM3 and PAM2 induce a weak and strong inflammatory response, respectively, in BEECs. The relative mRNA expression of pro-inflammatory cytokines and *PGES1*, after stimulation with 100 ng/mL PAM2 and PAM3 for 1h. This experiment was repeated seven times using epithelial cells from seven different uteri. Asterisks show a significance of difference (*P < 0.05 or **P < 0.01, Mann–Whitney test).

Identical TLR2 dimerization process in human, mouse and bovine

In the present study, the *in-silico* analysis confirmed that TLR2 is not able to interact with TLR1 at cellular level in human and mouse models (Supplementary Results; Supplementary Table 3; Supplementary Figure 6). In contrast, TLR6 has a low affinity with TLR2. Our *in-silico* analyses clearly indicate that the affinity between TLRs is not considerable to stabilize dimer forms. Thus, the bridging molecules (ligands) are vastly required to stabilize TLR2 dimers (Supplementary Table 4).

The ectodomain of TLRs are split into three subdomains: N-terminal (LRRNT), central and C-terminal (LRRCT) (Figure 6A). The DoGSite Scorer predicted several binding pockets for all TLRs in humans, mouse and bovine (Figures 6B–D). The volume, surface and drugScore of the first predicted binding pockets (yellow pocket) of the all TLR proteins in the three species were indicated in Supplementary Table 5. The druggability score for this pocket in all TLRs is >0.7. Moreover, the physicochemical descriptors showed that TLRs of different species were almost identical (Figure 6). Based on phyciso–chemical properties, the volume (V) of internal pocket was 1803 Å^3 (LRR9-12), 1490 Å^3 (LRR7-12) and 1418 Å^3

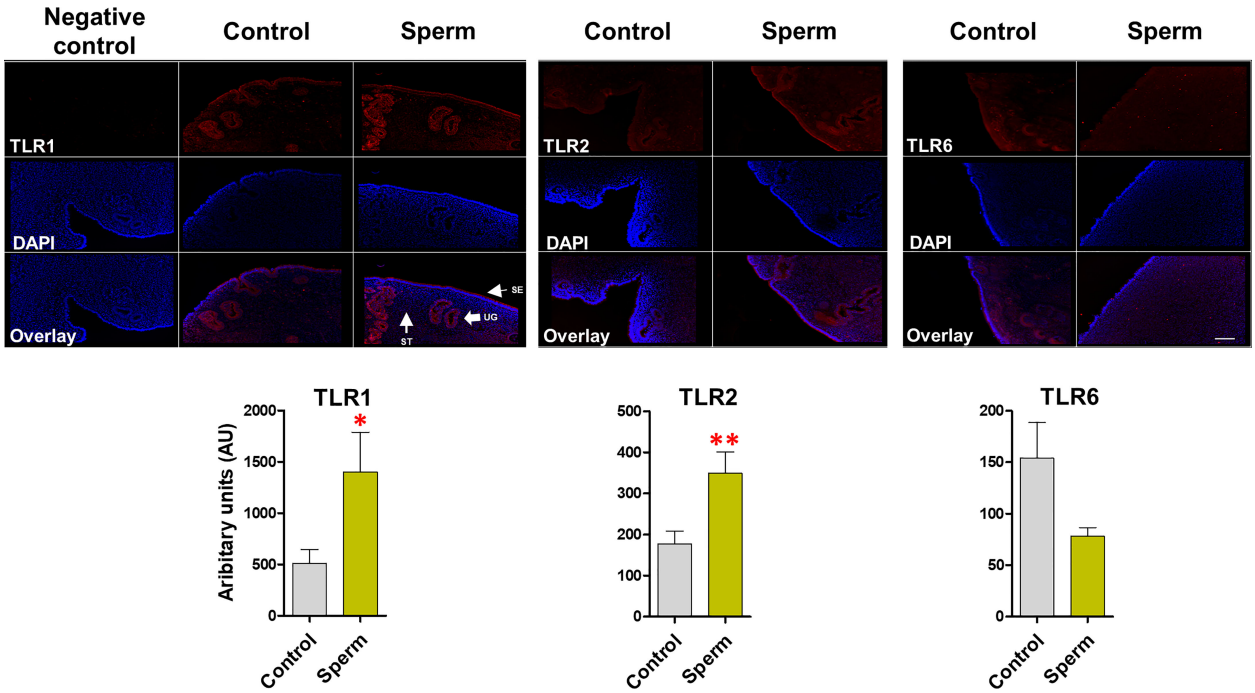

FIGURE 4
Sperm induce TLR2 and TLR1 (not TLR6) protein expression in bovine endometrial explants. The intense expression of TLR1 and TLR2 in uterine glands (UGs) and surface epithelium (SE) in sperm group. This experiment was repeated three times using explants from three different uteri. Asterisks show a significance of difference (*P < 0.05 or **P < 0.01) in the treatment group when compared to the control group. when compared to the control group. ST, stroma. Bar = 100 µm.

(LRR9-12) in human, mouse and bovine TLR2, respectively. Predicting the main binding pocket for TLR1 in the three species showed that the main binding pockets were located between LRR10-12 for human (V~533 Å^3) and LRR11-12 for both mouse (V~370 Å^3) and bovine (V~500 Å^3). The first predicted binding site of bovine TLR1 was almost identical to human and mouse. However, the volume and the surface were slightly different between species for TLR6 in bovine compared with TLR6 in human and mouse (Supplementary Table 5). Supplementary Figure 7 demonstrated that in the main binding site of TLR2 in three species, the type and sequence of amino acids were identical and conserved (in particular, the residue in the entrance of binding pocket).

Looking at the details of the present data, Phe 322 and Phe 349 in three species were selected as the entrance of binding pockets. Additionally, the data obtained from Ligplot analysis indicated that these Phe residues (349 and 322) play an important role in TLRs interaction with agonist and dimerization process (Supplementary Figures 6, 8). As for TLR1, the predicted main binding pocket for all three species was identical (approximately between Central LRR

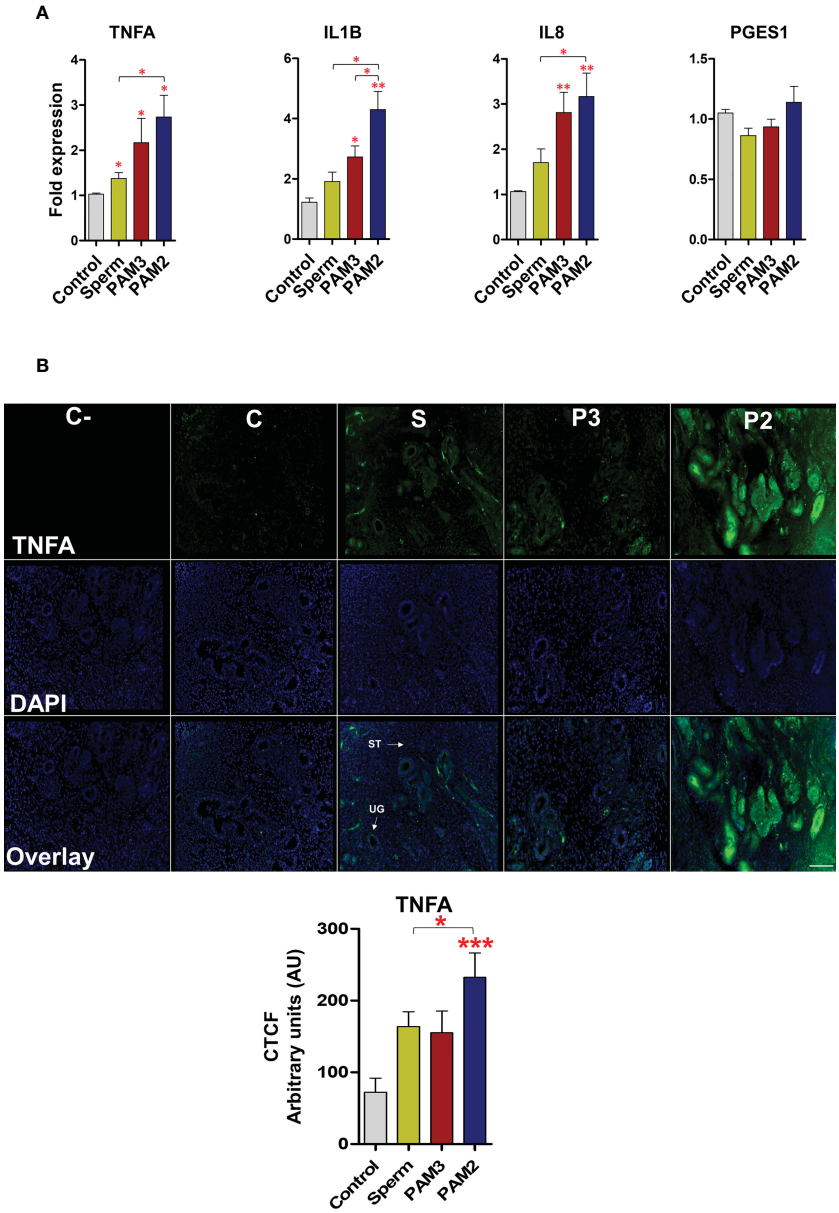

FIGURE 5
Sperm and PAM3 induce a weaker inflammation in bovine endometrial explants, compared with PAM2. **(A)** Relative mRNA expression of pro-inflammatory cytokines and *PGES1* after stimulation with 5 million/mL sperm, 100 ng/mL PAM3 and PAM2 for 3h. This experiment was repeated seven times using epithelial cells from seven different uteri. **(B)** Immunofluorescence staining for TNFA in endometrial explants **(C**: Negative control, C: Control, S: Sperm, P3: PAM3 and P2: PAM2). This experiment was repeated three times using explants from three different uteri. Asterisks show a significance of difference (*P < 0.05, **P < 0.01 or ***P < 0.001 , Mann–Whitney test) between the means of each two independent groups. Bar = 100 µm.

and c-terminal LRR). With regards to TLR6, in mouse experimentally crystal structure, the Phe 343 and Phe 365 block the internal channel of TLR6, compared with TLR1, consequently, this channel cannot be recognized as main binding site. This structural analysis supposed that the main binding sites of TLRs were similar and located in same place for the studied mammalian species (Figure 6).

Discussion

In this study, using a combination of experimental and *in-silico* modeling, we were able to demonstrate that the sperm-induced inflammatory response activates TLR2/1 heterodimer, but not TLR2/6 in bovine endometrium. Importantly, we revealed that sperm could induce a weak inflammatory response in bovine

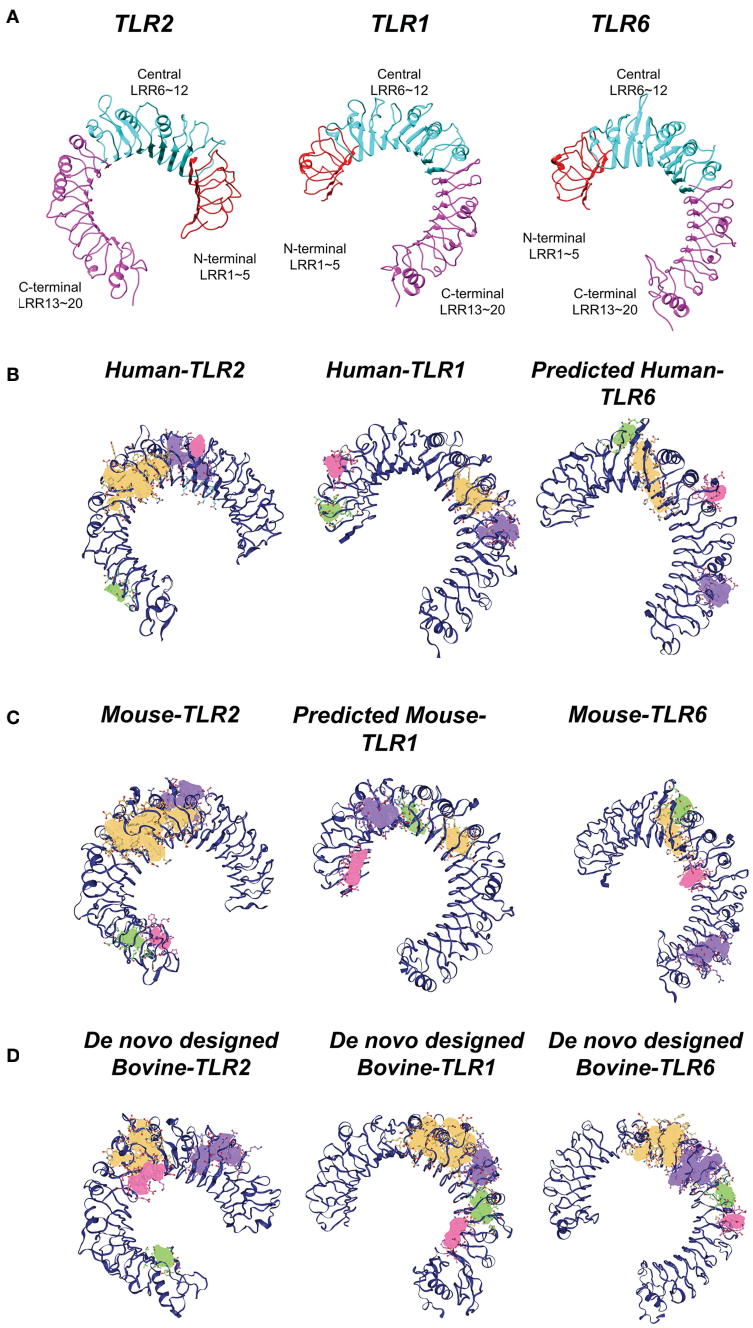

FIGURE 6
Structural analysis of TLRs in three mammalian classes (human, mouse, bovine). **(A)** Three subdomains of TLRs having 20 LRR units, namely N-terminal (LRRNT), central and C-terminal (LRRCT) in the ectodomain of TLRs. LRRNT (LRR 1~5), central (LRR 6~12) and LRRCT (LRR 13~20) colored by red, cyan and magenta, respectively. **(B)** Predicted potential binding pockets of human TLRs. **C)** Predicted potential binding pockets of mouse TLRs. **(D)** Predicted potential binding pockets of bovine TLRs. Different potential binding pockets of TLRs are shown by yellow (first pocket), violet (second pocket), green (third pocket), red (fourth pocket). The main binding site (yellow pocket) of TLR2 is similar (localized between LRR9-12, and the entrance is in LRR11-12) in the three species. Concerning TLR1, the main binding site (yellow pocket) is between central and LRRCT domains for all species. However, this internal channel is blocked by two phenalene in TLR6.

endometrium through "PAM3-like-weaker" TLR2/1 signalling rather than "PAM2-like-stronger" TLR2/6 pathway.

In fact, the TLR2 has an essential role in balancing pro- and anti-inflammatory immune responses in different cell types (2, 10, 16, 35–37). We previously reported that sperm induce transient and weak inflammatory response *via* the regulation of TLR2 signaling in bovine endometrium. On the other hand, heterodimerization of TLR2 with TLR1 or TLR6 has been extensively studied to develop a deep understanding of different immune responses resulted from TLR2 activation. With selective TLR2 heterodimerization, it was important to determine the active TLR2 heterodimer which is involved in sperm-induced inflammation in bovine uterus. Thus, in this study, at first, *in-vitro* BEECs co-culture was employed to assess the expression of TLR1, TLR2 and TLR6 by sperm. Notably, sperm upregulated the mRNA and protein expression of TLR1 and TLR2, but not TLR6 in BEECs, suggesting that sperm utilize TLR2/1 during sperm-uterine interactions. Moreover, the present data showed that the activation of TLR2/6 signaling pathway could lead to a stronger inflammation compared to TLR2/1 in uterine epithelial monolayer using specific agonists. Similarly, Murgueitio et al. (38) indicated that activating TLR2/6 signaling pathway resulted in 4-fold stronger inflammation than TLR2/1 in human embryonic kidney cells. To get the same level of inflammation in this kind of cells, they used 50 ng/mL of PAM2 versus 200 ng/mL PAM3 for 5h (38). In our *in-vitro* model, identical concentration from both PAMs (100 ng/mL) was applied to induce inflammation in bovine endometrial epithelia and interestingly, PAM2 induced a 3-fold higher inflammatory response compared to PAM3 and sperm. Altogether, *in-vitro* studies provided the initial evidence that sperm employ TLR2/1 signaling and activation of TLR2/1 signaling pathway led to a weak inflammatory response in BEECs.

Further, *ex-vivo* experimental model (i.e., preovulatory endometrial explants that physiologically mimic the intact uterine condition at insemination) was used to investigate the localization of TLR1, 2 and 6 in endometrium and to compare the inflammatory intensities of sperm and TLR2 agonists. We previously reported that sperm interact with the uterine glands to induce an acute and weak inflammatory response. This inflammatory response has been detected by the upregulation of key inflammatory markers TNFA, IL1B, IL8 and PGES as well as by the recruitment of inflammatory cells (i.e., neutrophils) (1–3, 7, 12). Notably, in cattle, sperm trigger the inflammatory cascade primarily *via* the TLR2 signaling of uterine glands (1). The present *ex-vivo* protein expression data showed similar upregulation profiles for TLR2 and TLR1, after sperm co-culture with uterine explants. Even though, TLR1, TLR2 and TLR6 localized in surface epithelium and uterine glands, sperm enhanced the expression of TLR1 and TLR2 but not TLR6 in these compartments, which strongly support a co-regulation of TLR2 and TLR1 receptors in particular in uterine glands during sperm-induced inflammatory response. Herein, TLR6 was not modulated after sperm exposure, possibly to prevent strong and long-term inflammatory reactions and tissue damage as high TLR6 that may

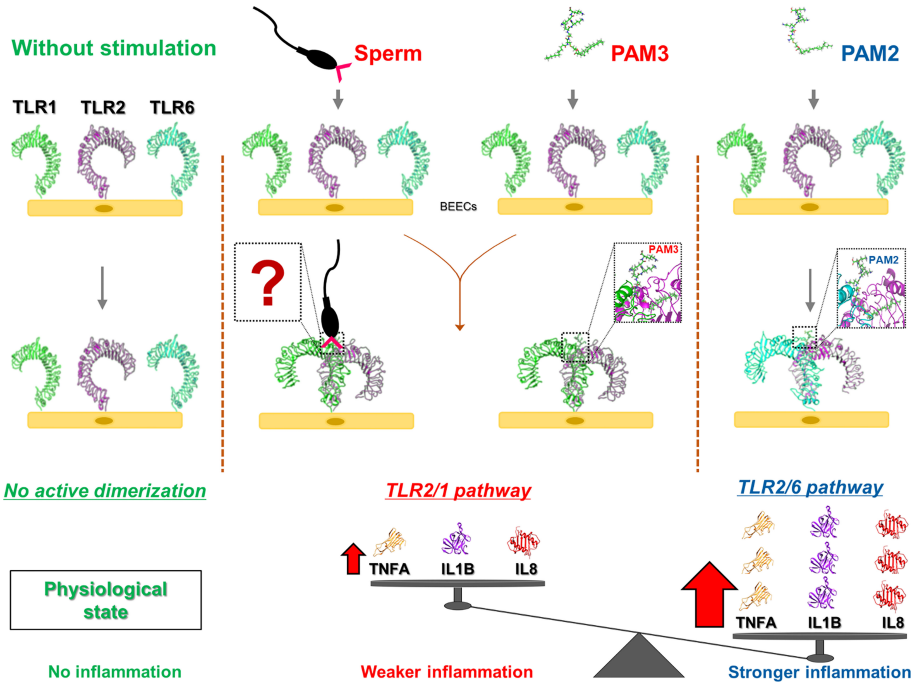

FIGURE 7
A graphic demo of our working hypothesis on the activation of possible TLR2 pathway signaling in sperm-induced inflammation in bovine endometrial epithelia. The model demonstrating that the stimulation of endometrial epithelia with different TLR2 agonist (PAM3: TLR2/1 and PAM2: TLR2/6) results in different intensity in inflammation response. In fact, initiating TLR2/1 signaling cascade could lead to weaker inflammation compared to TLR2/6. As for sperm-endometrial epithelial interaction, sperm induce TLR2/1 heterodimerization signaling, to trigger the weak and acute inflammation. We suppose that sperm may use small molecules from its surface (such as lipopeptides or glycans) to enhance TLR2/1 dimerization. However, further investigations are required to define the specific ligand(s) on the sperm cell membrane that regulate the initiation of TLR2/1 heterodimerization. "?" shows the unknown molecules form sperm surface side which may link TLR1 to TLR2.

correlate with higher-risk disease (39). Prominently, the mRNA and TNFA protein profiles of *ex-vivo* model clearly showed that sperm trigger a weak physiological inflammatory response in endometrial epithelia similar to that of the specific ligand of TLR2/1 heterodimer (PAM3). TNFA is one of the key inflammatory markers in the bovine uterus towards sperm in both physiological and pathological conditions (1, 7). Meanwhile, activation of TLR2/6 heterodimers led to a stronger inflammatory response in endometrial explants which assumed to be far from physiological sperm-triggered inflammation. Thus, these *ex-vivo* evidence reveal that, sperm employ TLR2/1 heterodimerization, in particular in uterine glands of the bovine uterus, to activate the specific inflammatory cascade. In fact, this kind of weak and transient inflammation is required to remove excess and dead sperm remaining in the uterine lumen and to complete this clearance within several hours without tissue damage for providing the ideal uterine environment for acceptance of early embryo and implantation.

Quite recently, Kar et al. (40) predicted the 3-D structure of bovine TLR2 as a reliable computational tool. However, the structures of bovine TLR1 and TLR6 are unavailable. Hence, in the present study, the binding affinity of TLR2 with TLR1 and TLR6 was evaluated using known crystal structures of both mouse and human. The *in-silico* models showed the evidence for the stabilized interactions between TLR2/1 and TLR2/6 heterodimers in presence of their agonists. Notably, the present study provided the first insight for bovine TLR2 heterodimerization at molecular level. Furthermore, the data revealed that the main binding sites of bovine TLRs were identical to human and mouse and occupied by their specific ligands. Therefore, in complementary with the experimental investigations, it could be concluded that TLR2/1 dimerization occurs in bovine uterus in the presence of sperm. However, the sperm surface molecule/(s) which could initiate and/or regulate this TLR2/1 dimerization process for the specific inflammatory cascade remained to be investigated.

Conclusion

Our results revealed that sperm utilize TLR2/1 pathway to induce a weak inflammatory response in bovine endometrium. Activation of TLR2/6 heterodimer could lead to an excessive inflammatory response compared to that of sperm or TLR2/1 (Figure 7). Further, *in-silico* findings revealed that the ectodomains of bovine TLR2 formed a hetero-dimer upon ligand binding to initiate cell signaling pathway. Altogether, our data strongly suggested that sperm utilize TLR2/1, but not TLR2/6, heterodimerization to induce the weak physiological inflammatory responses in the bovine uterus. However, further investigations are required to define the specific ligand(s) on the sperm cell membrane that is required to bridge and stabilize the TLR2/1 heterodimer.

Data availability statement

The original contributions presented in the study are included in the article/Supplementary Material. Further inquiries can be directed to the corresponding author.

Ethics statement

The animal study was reviewed and approved by Committee on the Ethics of Animal Experiments of the Obihiro University of Agriculture and Veterinary Medicine, Japan (Permit number 27-74).

Author contributions

AlM, MY, RK, IA and AM conceived and designed the experiments. AlM, MY, NU and IA performed the experiments. AlM, MY and IA analyzed the data. AlM, RK and, AM provided reagents/materials/analysis tools. AlM, MY, RK, IA and AM wrote the manuscript. All authors contributed to the article and approved the submitted version.

Funding

The present research work was funded by a Grant-in-Aid for Scientific Research (20H03122 and 23H02356) of Japan Society for the Promotion of Science (JSPS), and in part by Livestock Promotional Funds of Japan Racing Association (JRA).

Acknowledgments

The authors thank Genetics Hokkaido Association, Shimizu-Cho, Hokkaido, Japan, for providing cryopreserved semen straws used in this study.

Conflict of interest

The authors declare that the research was conducted in the absence of any commercial or financial relationships that could be construed as a potential conflict of interest.

Publisher's note

Supplementary material

The Supplementary Material for this article can be found online at: https://www.frontiersin.org/articles/10.3389/fimmu.2023.1158090/full#supplementary-material

References

1. Akthar I, Suarez SS, Morillo VA, Sasaki M, Ezz MA, Takahashi KI, et al. Sperm enter glands of preovulatory bovine endometrial explants and initiate inflammation. *Reproduction* (2020) 159:181–92. doi: 10.1530/REP-19-0414

2. Ezz MA, Marey MA, Elweza AE, Kawai T, Heppelmann M, Pfarrer C, et al. TLR2/4 signaling pathway mediates sperm-induced inflammation in bovine endometrial epithelial cells *in vitro*. *PloS One* (2019) 14:1–17. doi: 10.1371/journal.pone.0214516

3. Marey MA, Aboul Ezz M, Akthar I, Yousef MS, Imakawa K, Shimada M, et al. Sensing sperm *via* maternal immune system: a potential mechanism for controlling microenvironment for fertility in the cow. *J Anim Sci* (2020) 98:S88–95. doi: 10.1093/jas/skaa147

4. Kowsar R, Keshtegar B, Miyamoto A. Understanding the hidden relations between pro-and anti-inflammatory cytokine genes in bovine oviduct epithelium using a multilayer response surface method. *Sci Rep* (2019) 9:1–17. doi: 10.1038/s41598-019-39081-w

5. Morillo VA, Akthar I, Fiorenza MF, Takahashi K-I, Sasaki M, Marey MA, et al. Toll-like receptor 2 mediates the immune response of the bovine oviductal ampulla to sperm binding. *Mol Reprod Dev* (2020) 87:1059–69. doi: 10.1002/mrd.23422

6. Zinnah MA, Marey MA, Akhtar I, Elesh IF, Matsuno Y, Elweza AE, et al. Peptidoglycan disrupts early embryo-maternal crosstalk *via* suppression of ISGs expression induced by interferon-tau in the bovine endometrium. *Biochem Biophys Res Commun* (2020) 532:101–7. doi: 10.1016/j.bbrc.2020.08.006

7. Elesh IF, Marey MA, Zinnah MA, Akthar I, Kawai T, Naim F, et al. Peptidoglycan switches off the TLR2-mediated sperm recognition and triggers sperm localization in the bovine endometrium. *Front Immunol* (2021) 11:619408. doi: 10.3389/fimmu.2020.619408

8. Elweza AE, Ezz MA, Acosta TJ, Talukder AK, Shimizu T, Hayakawa H, et al. A proinflammatory response of bovine endometrial epithelial cells to active sperm *in vitro*. *Mol Reprod Dev* (2018) 85:215–26. doi: 10.1002/mrd.22955

9. Abdulrahman Alrabiah N, Simintiras CA, Evans ACO, Lonergan P, Fair T. Biochemical alterations in the follicular fluid of bovine peri-ovulatory follicles and their association with final oocyte maturation. *Reprod Fertil* (2022) 4:e220090. doi: 10.1530/raf-22-0090

10. Shimada M, Yanai Y, Okazaki T, Noma N, Kawashima I, Mori T, et al. Hyaluronan fragments generated by sperm-secreted hyaluronidase stimulate cytokine/chemokine production *via* the TLR 2 and TLR4 pathway in cumulus cells of ovulated COCs, which may enhance fertilization. *Development* (2008) 135:2001–11. doi: 10.1242/dev.020461

11. Shimada M, Hernandez-Gonzalez I, Gonzalez-Robanya I, Richards JAS. Induced expression of pattern recognition receptors in cumulus oocyte complexes: novel evidence for innate immune-like functions during ovulation. *Mol Endocrinol* (2006) 20:3228–39. doi: 10.1210/me.2006-0194

12. Akthar I, Marey MA, Kim Y, Shimada M, Suarez SS, Miyamoto A. Sperm interaction with the uterine innate immune system: toll-like receptor 2 (TLR2) is a main sensor in cattle. *Reprod Fertil Dev* (2021) 34:139–48. doi: 10.1071/RD21265

13. Kang JY, Nan X, Jin MS, Youn SJ, Ryu YH, Mah S, et al. Recognition of lipopeptide patterns by toll-like receptor 2-toll-like receptor 6 heterodimer. *Immunity* (2009) 31:873–84. doi: 10.1016/j.immuni.2009.09.018

14. Jin MS, Kim SE, Heo JY, Lee ME, Kim HM, Paik SG, et al. Crystal structure of the TLR1-TLR2 heterodimer induced by binding of a tri-acylated lipopeptide. *Cell* (2007) 130:1071–82. doi: 10.1016/j.cell.2007.09.008

15. Li JB, Lee DSW, Madrenas J. Evolving bacterial envelopes and plasticity of TLR2-dependent responses: basic research and translational opportunities. *Front Immunol* (2013) 4:347. doi: 10.3389/fimmu.2013.00347

16. DePaolo RW, Tang F, Kim IY, Han M, Levin N, Ciletti N, et al. Toll-like receptor 6 drives differentiation of tolerogenic dendritic cells and contributes to LcrV-mediated plague pathogenesis. *Cell Host Microbe* (2008) 4:350–61. doi: 10.1016/j.chom.2008.09.004

17. Jones S, Thornton JM. Principles of protein-protein interactions. *Proc Natl Acad Sci U.S.A.* (1996) 93:13–20. doi: 10.1073/pnas.93.1.13

18. Mansouri A, Kowsar R, Zakariazadeh M, Hakimi H, Miyamoto A. The impact of calcitriol and estradiol on the SARS-CoV-2 biological activity: a molecular modeling approach. *Sci Rep* (2022) 12:1–15. doi: 10.1038/s41598-022-04778-y

19. Su L, Wang Y, Wang J, Mifune Y, Morin MD, Jones BT, et al. Structural basis of TLR2/TLR1 activation by the synthetic agonist diprovocim. *J Med Chem* (2019) 62:2938–49. doi: 10.1021/acs.jmedchem.8b01583

20. Bouzari S, Savar N. In silico study of ligand binding site of toll-like receptor 5. *Adv BioMed Res* (2014) 3:41. doi: 10.4103/2277-9175.125730

21. Basith S, Manavalan B, Govindaraj RG, Choi S. In silico approach to inhibition of signaling pathways of toll-like receptors 2 and 4 by ST2L. *PloS One* (2011) 6:e23989. doi: 10.1371/journal.pone.0023989

22. van Zundert GCP, Rodrigues JPGLM, Trellet M, Schmitz C, Kastritis PL, Karaca E, et al. The HADDOCK2.2 web server: user-friendly integrative modeling of biomolecular complexes. *J Mol Biol* (2016) 428:720–5. doi: 10.1016/j.jmb.2015.09.014

23. Wallace AC, Laskowski RA, Thornton JM. LIGPLOT: a program to generate schematic diagrams of protein-ligand interactions. *Protein Eng* (1995) 8:127–34. doi: 10.1093/protein/8.2.127

24. Lee J, Cheng X, Swails JM, Yeom MS, Eastman PK, Lemkul JA, et al. CHARMM-GUI input generator for NAMD, GROMACS, AMBER, OpenMM, and CHARMM/OpenMM simulations using the CHARMM36 additive force field. *J Chem Theory Comput* (2016) 12:405–13. doi: 10.1021/acs.jctc.5b00935

25. Abraham MJ, Murtola T, Schulz R, Páll S, Smith JC, Hess B, et al. GROMACS: high performance molecular simulations through multi-level parallelism from laptops to supercomputers. *SoftwareX* (2015) 1–2:19–25. doi: 10.1016/j.softx.2015.06.001

26. Brooks BR, Brooks CL3rd, Mackerell ADJr, Nilsson L, Petrella RJ, Roux B, et al. CHARMM: the biomolecular simulation program. *J Comput Chem* (2009) 30:1545–614. doi: 10.1002/jcc.21287

27. Yang J, Yan R, Roy A, Xu D, Poisson J, Zhang Y. The I-TASSER suite: protein structure and function prediction. *Nat Methods* (2015) 12:7–8. doi: 10.1038/nmeth.3213

28. Kumari R, Kumar R, Lynn A. G_mmpbsa–a GROMACS tool for high-throughput MM-PBSA calculations. *J Chem Inf Model* (2014) 54:1951–62. doi: 10.1021/ci500020m

29. Farrokhpour H, Mansouri A, Najafi Chermahini A. Transport behavior of the enantiomers of lactic acid through the cyclic peptide nanotube: enantiomer discrimination. *J Phys Chem C* (2017) 121:8165–76. doi: 10.1021/acs.jpcc.7b00010

30. Farrokhpour H, Mansouri A, Rajabi AR, Najafi Chermahini A. The effect of the diameter of cyclic peptide nanotube on its chirality discrimination. *J Biomol Struct Dyn* (2019) 37:691–701. doi: 10.1080/07391102.2018.1436090

31. Mansouri A, Mahnam K. Designing new surfactant peptides for binding to carbon nanotubes *via* computational approaches. *J Mol Graph Model* (2017) 74:61–72. doi: 10.1016/j.jmgm.2017.02.016

32. Barzegar A, Mansouri A, Azamat J. Molecular dynamics simulation of non-covalent single-walled carbon nanotube functionalization with surfactant peptides. *J Mol Graph Model* (2016) 64:75–84. doi: 10.1016/j.jmgm.2016.01.003

33. Volkamer A, Kuhn D, Rippmann F, Rarey M. DoGSiteScorer: a web server for automatic binding site prediction, analysis and druggability assessment. *Bioinformatics* (2012) 28:2074–5. doi: 10.1093/bioinformatics/bts310

34. Fährrolfes R, Bietz S, Flachsenberg F, Meyder A, Nittinger E, Otto T, et al. ProteinsPlus: a web portal for structure analysis of macromolecules. *Nucleic Acids Res* (2017) 45:W337–43. doi: 10.1093/nar/gkx333

35. Sepehri Z, Kiani Z, Nasiri AA, Kohan F. Toll-like receptor 2 and type 2 diabetes. *Cell Mol Biol Lett* (2016) 21:2. doi: 10.1186/s11658-016-0002-4

36. Chau TA, McCully ML, Brintnell W, An G, Kasper KJ, Vinés ED, et al. Toll-like receptor 2 ligands on the staphylococcal cell wall downregulate superantigen-induced T cell activation and prevent toxic shock syndrome. *Nat Med* (2009) 15:641–8. doi: 10.1038/nm.1965

37. Schaefer TM, Desouza K, Fahey JV, Beagley KW, Wira CR. Toll-like receptor (TLR) expression and TLR-mediated cytokine/chemokine production by human uterine epithelial cells. *Immunology* (2004) 112:428–36. doi: 10.1111/j.1365-2567.2004.01898.x

38. Murgueitio MS, Henneke P, Glossmann H, Santos-Sierra S, Wolber G. Prospective virtual screening in a sparse data scenario: design of small-molecule TLR2 antagonists. *ChemMedChem* (2014) 9:813–22. doi: 10.1002/cmdc.201300445

39. Monlish DA, Greenberg ZJ, Bhatt ST, Leonard KM, Romine MP, Dong Q, et al. TLR2/6 signaling promotes the expansion of premalignant hematopoietic stem and progenitor cells in the NUP98–HOXD13 mouse model of MDS. *Exp Hematol* (2020) 88:42–55. doi: 10.1016/j.exphem.2020.07.001

40. Kar PP, Araveti PB, Kuriakose A, Srivastava A. Design of a multi-epitope protein as a subunit vaccine against lumpy skin disease using an immunoinformatics approach. *Sci Rep* (2022) 12:1–11. doi: 10.1038/s41598-022-23272-z

frontiers | Frontiers in Immunology

TYPE Original Research
PUBLISHED 20 June 2023
DOI 10.3389/fimmu.2023.1168252

OPEN ACCESS

EDITED BY
Ralf Kircheis,
Syntacoll GmbH, Germany

REVIEWED BY
Nancy Deng,
Ambagon Therapeutics Inc., United States
Alyson J. Smith,
Seattle Genetics, Inc., United States

*CORRESPONDENCE
Michael Burnet
michael.burnet@synovo.com

†These authors share first authorship

RECEIVED 17 February 2023
ACCEPTED 31 May 2023
PUBLISHED 20 June 2023

CITATION
Keppler M, Straß S, Geiger S, Fischer T, Späth N, Weinstein T, Schwamborn A, Guezguez J, Guse J-H, Laufer S and Burnet M (2023) Imidazoquinolines with improved pharmacokinetic properties induce a high IFNα to TNFα ratio *in vitro* and *in vivo*. *Front. Immunol.* 14:1168252. doi: 10.3389/fimmu.2023.1168252

Imidazoquinolines with improved pharmacokinetic properties induce a high IFNα to TNFα ratio *in vitro* and *in vivo*

Manuel Keppler[1†], Simon Straß[1,2†], Sophia Geiger[1], Tina Fischer[1], Nadja Späth[1], Thilo Weinstein[1], Anna Schwamborn[1], Jamil Guezguez[1], Jan-Hinrich Guse[1], Stefan Laufer[2] and Michael Burnet[1*]

[1]Synovo GmbH, Tübingen, Germany, [2]Pharmaceutical Chemistry, Institute for Pharmaceutical Sciences, Eberhard Karls University Tübingen, Tübingen, Germany

TLR Agonists have promising activity in preclinical models of viral infection and cancer. However, clinical use is only in topical application. Systemic uses of TLR-ligands such as Resiquimod, have failed due to adverse effects that limited dose and thus, efficacy. This issue could be related to pharmacokinetic properties that include fast elimination leading to low AUC with simultaneously high c_{max} at relevant doses. The high c_{max} is associated with a sharp, poorly tolerated cytokine pulse, suggesting that a compound with a higher AUC/c_{max}-ratio could provide a more sustained and tolerable immune activation. Our approach was to design TLR7/8-agonist Imidazoquinolines intended to partition to endosomes *via* acid trapping using a macrolide-carrier. This can potentially extend pharmacokinetics and simultaneously direct the compounds to the target compartment. The compounds have hTLR7/8-agonist activity (EC50 of the most active compound in cellular assays: 75-120 nM hTLR7, 2.8-3.1 μM hTLR8) and maximal hTLR7 activation between 40 and 80% of Resiquimod. The lead candidates induce secretion of IFNα from human Leukocytes in the same range as Resiquimod but induce at least 10-fold less TNFα in this system, consistent with a higher specificity for human TLR7. This pattern was reproduced *in vivo* in a murine system, where small molecules are thought not to activate TLR8. We found that Imidazoquinolines conjugated to a macrolide or, substances carrying an unlinked terminal secondary amine, had longer exposure compared with Resiquimod. The kinetics of pro-inflammatory cytokine release for these substances *in vivo* were slower and more extended (for comparable AUCs, approximately half-maximal plasma concentrations). Maximal IFNα plasma levels were reached 4 h post application. Resiquimod-treated groups had by then returned to baseline from a peak at 1 h. We propose that the characteristic cytokine profile is likely a consequence of altered pharmacokinetics and, potentially, enhanced endosomal tropism of the novel substances. In particular, our substances are designed to partition to cellular

compartments where the target receptor and a distinct combination of signaling molecules relevant to IFNα-release are located. These properties could address the tolerability issues of TLR7/8 ligands and provide insight into approaches to fine-tune the outcomes of TLR7/8 activation by small molecules.

KEYWORDS

TLR7, TLR8, resiquimod, imidazoquinoline, Interferon a (IFNa), macrolide, cytokine spectrum, pharmacokinetics

1 Introduction

The term immunotherapy is mostly associated with the treatment of cancer by checkpoint inhibitors, cell-based approaches or vaccinations (1). In a broader sense, immunotherapy describes therapeutic concepts aimed at modulating the host immune system to treat conditions related to neoplasia and infection as well as autoimmune conditions (2–4). The possibility of harnessing the diverse defense mechanisms of the immune system itself circumvents some of the limitations of pathogen- or neoplasm-directed pharmaceuticals, particularly the development of resistance to those drugs by mutations in their molecular targets. Correspondingly, immune activating therapies could be useful for infectious diseases for which a drug specifically targeting the pathogen itself is not yet available (4–6). One of the first treatments relying on immune activation to interfere with an ongoing infection or neoplasm was the use of recombinant Interferon alpha (IFNα) in the treatment of Hairy Cell Leukemia, Hepatitis B and Hepatitis C (before HBV/HCV were identified) (7–9). Indeed, recombinant IFNα was the first approved immunotherapeutic agent and the most thoroughly clinically characterized immune stimulant. It has been used for decades as a treatment of various viral diseases and cancers (8). While there has been a considerable focus on checkpoint blockade *via* antibodies targeting the PD1/PD-L1-axis (10), stimulation of the immune system through activation of pattern recognition receptors (PRRs) and particularly Toll-like-receptors (TLRs) is another promising concept that has been widely investigated, especially in dermatological cancers (11–13). In contrast to immunotherapies focused on blocking of inhibitory receptors and thus overcoming immunosuppression, agonists to PRRs activate immune response through increasing the expression of surface-bound and secreted mediators of inflammation making this stimulatory approach more similar to the direct use of recombinant cytokines such as IFNα as therapeutic agents (13–17).

Toll-like receptors are membrane-integral PRRs with varied representation in different species – 10 subtypes have been identified in humans and 12 in mice. Regardless of species, TLRs can generally be subdivided based on the orientation of their ectodomains either towards the extracellular space or the luminal space of endosomal vesicles. In humans, TLR1/2/4/5/6/10 are localized in the plasma membrane while TLR3/7/8/9 are restricted to vesicular membranes. TLR10 is not present in mice but TLR11/12/13 are and all localize to membranes of intracellular compartments (18). Ligand binding results in the formation of receptor dimers and recruitment of adapter proteins containing a TIR domain which vary with receptor type. The signaling cascade of all TLRs except for TLR3 uses the common adapter MyD88 to subsequently activate NFκB and IRF1/3/5/7/8 depending on receptor and cell type, with activation of NFκB and IRF5 being linked to the induction of pro-inflammatory cytokines and IRF1/3/5/7/8 having a role in regulating expression of type I interferons (19–21).

The endosomal nucleic acid-sensing TLRs 7/8/9 are similar in terms of their natural ligands, localization and direct engagement of MyD88. This is in contrast to plasma membrane-localized TLRs which employ additional adapters such as TIRAP and TRAM or TLR3 which uses TRIF as its downstream adapter. TLR7/8/9 can therefore be classified as a sub-family of TLRs (14, 19). TLR7 and 9 are highly expressed in plasmacytoid dendritic cells (pDCs), which play a central role at the interface between the innate and adaptive immune response to viral infections (22). However, their impact on cancer and immune evasion is ambiguous (23, 24). TLR8 is highly expressed in monocytes, macrophages and myeloid dendritic cells (mDCs) (25).

The outcome of intracellular TLR activation can vary considerably as a consequence of receptor expression being limited to specific cell types with characteristic signaling cascades and downstream mediators of inflammation (26). For example, TLR7 mediates release of large amounts of Type I IFN from pDCs. This is in contrast to its role in monocytes, where TLR7 activation by Imiquimod induces secretion of the classical inflammatory cytokines Interleukin-6 (IL6) and -1β (IL1β) but IFNα/β release is instead mediated by TLR8 (22, 27).

Ligand-dependent cytokine expression patterns in a single cell type have been demonstrated for TLR9, for which several classes of synthetic oligodeoxynucleotides (ODNs) with different signaling outcomes have been identified. A distinct induction of either IRF- or NFκB-relayed signaling was originally reported to be dependent on ODN sequence and has later been demonstrated to vary based on the subcellular location of receptor engagement (28–31). In this context TRAF3 and IKKα act as the central mediator of IRF7 phosphorylation and induction of type I IFNs following the activation of TLR9 and 7 (32–35).

Given the similarities in the respective signaling cascades, a similar spatial factor to the outcome of TLR7 activation is plausible, although not yet demonstrated (35). Clear differentiation of the signaling by TLR7 and 8 in native cells will, however, be

complicated because there is some overlap also in their ligand preferences. TLR9 signaling, however, can be distinguished because it recognizes unmethylated CpG motifs in DNA (36).

In addition to their ability to bind specific nucleic acid sequences, TLR7/8/9 possess dedicated binding sites for either guanosine (TLR7), uridine (TLR8) or cytosine (TLR9) and simultaneous engagement of both binding sites enhances receptor activation (11). While signaling through TLR9 appears to require a longer oligonucleotide ligand, several synthetic small molecules (mononucleotide analogs) sufficient to activate TLR7/8 are available. The most widely used class of small-molecule TLR7/8-activators are Imidazoquinolines, particularly the most prominent members of this class, Resiquimod (TLR7/8) and Imiquimod (TLR7). Imiquimod is the only FDA-approved agonist to an intracellular TLR to date. Its applications include the topical treatment of basal cell carcinoma or genital warts. Imiquimod probably interacts with other receptors in addition to TLR7 but its efficacy appears to depend on induction of IFNα, tumor necrosis factor α (TNFα), interleukin 12 (IL12) and other pro-inflammatory mediators (15).

The more potent Imidazoquinoline, Resiquimod, originally showed promise in various pre-clinical models of neoplastic or infectious disease (37–39), however, these results have not translated in wider clinical trials. Topical treatment of genital herpes with Resiquimod had encouraging effects in Phase II but not in Phase III (40). In the treatment of chronic Hepatitis C, oral Resiquimod could transiently reduce viral titers but effective doses caused systemic adverse effects consistent with an excess induction of inflammatory cytokines, particularly IFNα (41). Similar adverse events were observed for daily Imiquimod use (42). These adverse effects, often in the form of "flu like" symptoms, limit the systemic use of TLR7 and 8 activators and likewise IFNα. In the latter case, efforts have been made to increase the therapeutic window by PEGylation of recombinant IFNα to improve the pharmacokinetic profile (9), lengthen circulating half-life and allow longer intervals between treatments. Efficacy and adverse event benefits compared with the un-PEGylated cytokine were variable (43, 44).

Following a similar rationale, we hypothesized that the therapeutic index of small molecule TLR agonists like Resiquimod is limited by a range of factors: very steep dose response characteristics (all or nothing), the short half-life and poor tissue distribution necessitating the use of relatively high doses to achieve sufficient activation, the transient stimulation and, correspondingly, the high maximal concentrations relative to the AUC of pro-inflammatory cytokines that are induced.

The transient effects are due to the fact that Resiquimod is unstable and rapidly metabolized. After oral application major metabolites are 6-OH-Resiquimod and 7-OH-Resiquimod *via* CYP1A2; desethyl or N-oxide Resiquimod *via* CYP3A4; or 8-OH-Resiquimod *via* one of both enzymes. Unchanged Resiquimod is only detectable in minor amounts in either urine (< 5%) or feces (< 1%) (45, 46). Imiquimod metabolism is associated with the formation of at least five different monohydroxylated metabolites through CYP1A isoforms (47).

The binding sites of known small-molecule agonists of TLR7 and 8 are each located in the same motif. The aminoquinolyl moiety mediates agonistic receptor binding through stacking effects and through hydrogen bonds (48–51). The butyl side chain interacts hydrophobically with the binding pocket of the receptors. The length of 4 atoms appears optimal for interaction with hTLR7 while heteroatoms in this side group, such as an oxygen in Resiquimod, moderately increase the affinity (49, 50). A smaller contribution to the binding affinity is made by van der Waals interactions of the 2-methylpropan-2-ol side chain (49, 52).

Due to the slightly lower importance of that interaction, the 2-methylpropan-2-ol side chain was chosen as the starting point for modification and linking *via* side groups listed in reaction scheme 1 in Figure S1 (A1 to A4), which could be further extended by a macrolide (A1-mac and A2-mac; see Figure S2). The linking molecules functioned as a spacing between TLR agonistic imidazoquinolinone and macrolide but can also contribute hydrogen bonds as in the 2-methyl-propan-2-ol of Resiquimod. The macrolide site consists of Azithromycin coupled to the TLR binding site at the desosamine *via* an N-methyl iminodiacetyl. Azithromycin provides a high volume of distribution, concentration in immune cells and specifically endo/lysosomes, high exposure to liver, lung and spleen and sub-cellular separation from cytochrome p450 containing organelles (53–56). Compared with other common macrolides, it exhibits increased stability to acids, low hERG affinity, and a greater ability to concentrate in cells due to its dual amines (55, 57–59). Many of these effects are related to its properties as an amphiphilic di-basic compound for which the pk_as of the amines correspond well to those required to be neutral during membrane traverse but charged in acidic intracellular compartments. Accumulation of imidazoquinolines and 8-Oxoadenine in endosomal compartments of pDCs has been demonstrated by others and could be a necessary factor in the process of TLR-activation by those compounds (60).

Building on our previous experience with macrolide-derivatives (53, 61), we aimed to prepare TLR7/8 ligands with high exposure to the endo/lysosomal lumen by exploiting the properties of acid trapping in the assumption that amphiphiles would be ideal ligands for endosomal TLRs. Since endosomal tropism has been observed for both macrolides as well as imidazoquinolines, we propose that conjugation of imidazoquinoline TLR7/8 agonists to Azithromycin as a carrier molecule is likely to result in conjugates that accumulate intracellularly as well. We therefore designed imidazoquinoline-ligands in a way that would make them suitable for linkage to carrier molecules, such as Azithromycin, peptides or proteins, i.e. retain activity when conjugated. The ligands described here are intended to partition to their target organelles, either by manipulating the properties of the ligand substituents themselves, or *via* conjugation to Azithromycin, which would dominate the properties of the resulting compound. In parallel we optimized for high *in vivo* stability as well as favorable pharmacokinetic properties following parenteral application. Based on the expected pharmacokinetic properties of our ligands, we expected differences in release kinetics of inflammatory mediators, when compared to other Imidazoquinolines and, correspondingly, changes in maximal and cumulative plasma concentrations of those mediators. What we did not expect were changes in the cytokine spectrum induced by our ligands that may improve

tolerability. Here we report the initial characterization of the compounds as small molecules, that may be useful as immune stimulants in cancer and infection.

2 Methods

2.1 Synthesis and characterization

All chemicals were purchased from commercial sources and used as received. Reaction monitoring was performed *via* mass spectrometry (Finnigan LCQ Deca XP MAX, Software Xcalibur 2.0.7 SP1) and TLC (Merck TLC Silica gel 60 F254). TLC spots were detected with Hanessian's stain, based on a Cerium Molybdate solution and heat. NMR spectra were recorded with a Bruker Avance 400 (400 MHz) or Bruker Avance III (300 MHz). Substances were dissolved in $CDCl_3$ and chemical shifts (ppm) were referenced to $CHCl_3$/tetramethyl silane. Coupling constants (*J*) are given in Hz. After reaction steps solvents were evaporated with rotary evaporator (RV8 IKA, KNF SC 920) under vacuum. To purify substances, flash chromatography was performed (Interchim puriFlash 5.020 with Interchim PF-15SIHP-F0040 or PF-50SIHP-F0040 columns). Purity of reaction products was determined *via* HPLC (Varian ProStar) and ELS detection (Sedere Sedex 80). Mobile phases contained water (0.05% formic acid) and methanol (0.05% formic acid) as gradients. Stationary phase was ReproSil-Pur 120 C_{18}-AQ, 5 µm, 75x3 mm (Dr. Maisch). High resolution mass spectra were recorded with a Bruker maXis 4G ESI-TOF from Daltonik [JL1], using ESI^+ mode with following settings: Capillary voltage 4.5 kV, source temperature 200°C, gas flow 6 L/min, nebulizer gas pressure 1.2 bar, end plate offset – 0.5 kV and an m/z range of 100 to 1350. Detailed synthesis and reaction procedure can be found in SI.

2.2 Stability in whole blood, U937 and RPMI

Human blood products used in the *in vitro* assays (for cell stimulation and stability) were obtained from the center for transfusion medicine in Tübingen, Germany (Zentrum für Klinische Transfusionmedizin Tübingen GmbH, (ethical approval number ZKT-FoPro202106-2305-01). Test compounds (1 µM) in either culture medium (RPMI-1640 medium containing 10% fetal bovine serum, 60 mg/l Penicillin G sodium salt and 100 mg/l Streptomycin sulfate (all Biowest)), human blood (diluted 1:1 with culture medium) or a suspension of $5x10^6$ cells/ml U937 in culture medium were incubated at 37°C, 450 rpm on a shaking incubator. At the indicated time points 50 µL of blood, cell suspension or medium were collected and prepared for HPLC-MS/MS-Analysis as detailed below.

2.3 HPLC-MS/MS

All samples were extracted with 3 or 6 volumes acetonitrile containing terbuthylazine as an internal standard (ACN) relative to either sample weight or volume. Liquid samples (plasma, culture medium, cell suspensions in stability experiments) were diluted in either 3 (culture medium, cell suspensions) or 6 (plasma) volumes ACN, pellet and blood samples were extracted by addition of ACN followed by sonication for 5 min. Organ samples were digested with 0.5 µg/mg Proteinase K (Genaxxon) for 1 h at 50°C before being homogenized using a Fastprep FP-24 5G instrument (MP-Biomedicals). Homogenates were diluted with 6 volumes ACN and homogenized again. All extracts were cleared by centrifugation at ~20.000xg for 10 min at 4°C.

Quantification of analytes was performed on an Agilent 1260/1290 Infinity system fitted with an Agilent C18 Poroshell 120 column (4.6 x 50 mm, 2.7 µm) coupled to a triple quadrupole Sciex API 4000 MS/MS detector. The mobile phase was composed of water containing 0.1% formic acid (eluent A) and acetonitrile containing 0.1% formic acid (eluent B). Gradient used was: 5% B for 0.5 min, to 100% B in 4.5 min, 100% B for 2 min, to 5% B in 0.5 min, 5% for 2.5 min. MS detection parameters are listed in SI Table S1.

2.4 TLR7/8 SEAP reporter assay (HEK blue)

HEK blue hTLR7 or hTLR8 reporter cells (Invivogen) were cultivated in DMEM High Glucose (Biowest) according to the manufacturer's instructions. Cells were treated with test compounds and controls at various concentrations in serum-free DMEM and incubated at 37°C, 5% CO_2 for 24 h before supernatants were collected.

Relative secreted embryonic alkaline phosphatase (SEAP) activity in the supernatants was determined by quantification of para-Nitrophenyl Phosphate (pNPP)-turnover. Supernatants were diluted 10-fold in a solution containing 1 mM $MgCl_2$, 1 M diethanolamine and 1 mg/mL pNPP and incubated at RT for 15 min before the reaction was stopped by the addition of 0.25 volumes of 1 M NaOH. Absorbance was measured at 405 nm on a Versamax microplate reader (Molecular Devices) and normalized to the mean of >5 solvent controls.

2.5 Viability assay and live-dead staining (MTT and dye exclusion)

3-(4,5-dimethylthiazol-2-yl)-2,5-diphenyltetrazolium bromide (MTT) turnover was used to identify potential compound effects on cell metabolism and indirectly assay changes in cell number or viability. HEK Blue reporter cells were cultured and exposed to compounds as described above and 20 µl supernatant were collected for SEAP activity assays. U937 monocyte-like cells were cultured in RPMI-1640 containing 10% FBS, differentiated by addition of 100 nM PMA for 2 days and exposed to compounds at varying concentrations or solvent for 2 days. MTT dissolved in PBS was added to the cells to a final concentration of 1 mg/ml. Cells were then incubated at culture conditions for 1 h. Supernatants were removed after centrifugation at 400xg for 5 min and the formed formazan dye was dissolved in DMSO. Absorbance was measured at 570 nm and readings were normalized to solvent treated controls.

Exclusion of Helix NIR (BioLegend) was used to assay membrane integrity following compound treatment. Culture conditions for U937 were as described above, undifferentiated cells were incubated with varying concentrations of compound or with solvent. Helix NIR was added to the cells to a final concentration of 10 nM, cells were incubated at RT for 10 min and acquired on a ZE5 Cell Analyzer (Bio-Rad). The cutoff for positive staining was set to approximately the 99th percentile of unstained cells.

2.6 Full blood stimulation assay

Human peripheral blood of healthy donors was diluted in an equal volume of culture medium as described in 3.2, blood was treated with test compounds or controls at various concentrations and incubated at 37°C, 5% CO_2 for 6 h. Cells were pelleted by centrifugation at 400xg for 5 min and supernatants were collected.

2.7 Quantification of cytokines by ELISA or cytometric bead array

Cytokine concentrations in samples were quantified either by ELISA (hTNFα, R&D Systems; hIFNα, Mabtech) or cytometric bead arrays (CBA, LegendPlex mouse anti-virus response panel, BioLegend) according to the manufacturer's instructions. CBAs were acquired on a ZE5 Cell Analyzer (Bio-Rad) and analyzed using the LegendPlex Software Suite (Qognit/BioLegend). Absorbance of ELISA-samples was quantified using a Versamax microplate reader (Molecular Devices).

2.8 Experimental animals, sampling and compound formulation

Experimental Animals. All animal experiments were carried out in accordance with German law (35/9183.81-7/SYN 06/20). Mice, 8-18 weeks old, were purchased from Janvier Laboratories and maintained in a specific-pathogen-free animal facility with chow and water *ad libitum*. After arrival mice acclimated for a minimum of 7 days.

Formulation. Test compounds were prepared for application in either 1% Tween 80, 9% PEG400 in ultrapure water (Biowest) (i.v., i.p., p.o. application) or 5 mM citric acid in 0.9% saline (Braun) (subcutaneous application). If compounds were administered subcutaneously, injections were carried out into the neck crease.

Collection of Samples. Mice were bled from the tail vein at various timepoints. Heparin (Sigma) or K_2-EDTA (Sigma) was added to blood samples to a final coagulant concentration of 10-15 Unit or 5 mM. Plasma was generated by centrifugation at 6800xg for 8 min at 4°C and stored at -80°C until analyzed by ELISA or CBA. Animals were sacrificed after the indicated time points by CO_2 inhalation. Heart blood and organs for compound quantification by HPLC-MS/MS were collected post mortem and stored at –20°C until extracted as described above.

3 Results

Activity of the new compounds (Figure 1) on TLR7/8 was confirmed using the commercially available HEK-Blue reporter system. Corresponding to the dual specificity of structurally similar compounds described by others (1, 2), HEK-Blue hTLR7 and hTLR8 were used to assess relative potency on each receptor relative to Resiquimod (RSQ) as a reference compound. Results of the initial screening are in Table 1; Figure 2A. While all structural variants retained TLR7-agonism, activation of hTLR8 was reduced for compounds linked to a macrolide, carrying a protective group or a longer spacer between the aromatic polycycle and the piperidine as in A1. Maximal induction of SEAP varied between compounds and was generally highest for RSQ in repeated experiments, while other compounds either reached a lower maximum and subsequent decrease in signal at lower concentrations or became insoluble under the conditions used for the assay before reaching a plateau. Average maximal activity in HEK-Blue hTLR7 relative to RSQ was 58% for A1, 55% for A1-boc and 41% for A1-mac. The methyl-piperidine variants reached a higher maximal induction (A2-boc 86%, A2 81%, A2-mac 63%). SEAP secretion from HEK-Blue hTLR-8 was close to baseline for A1 as well as the protected or macrolide-bound variants A1-boc, A1-mac, A2-boc and A2-mac, with the former two showing low induction at very high concentrations without reaching a plateau at sub-toxic concentrations. A2 (57%), A3 (36%) and A4 (18%) retained activity, although at a lower maximal induction than that of RSQ.

The compound specific EC50 for the HEK-Blue system is listed in Table 1. To obtain reliable estimates, replicate measurements of a minimum of 2 experiments were normalized to the maximal SEAP activity of a compound in a given experiment and pooled before fitting a non-linear function to the data. For all compounds, we observed a reduction in SEAP activity in the supernatants above certain compound concentrations. Data points above those concentrations were excluded before curve fitting (Figures 2B; S3, S4).

The decrease in signal was assumed to be caused by toxic effects above certain concentrations, as indicated by a change in cell morphology and reduced attachment to the plate surface. Sensitivity of the reporter cells to toxic effects seemed to be closely related to serum concentrations during the assay and was less apparent if higher serum concentrations were used (Figure S5A). To confirm this, we performed an MTT assay on the HEK cells after collection of the supernatants for SEAP quantification (Figure 2C upper two panels). While there was some reduction in MTT conversion at concentrations similar to those for which we observed a decrease in SEAP secretion, obvious toxicity could only be observed at 20 µM and is likely to be related to poor solubility and crystalizing of the compounds at those concentrations. Further, a reduction in MTT conversion could be observed in U937 cells and was again most apparent for the poorly soluble A1-boc, with 50% dye formation relative to solvent controls at the highest concentration of 25 µM. Imiquimod and A1 reduced signal to <90% at concentrations ≥6.25 µM. In contrast, a dye exclusion assay in U937 cells could only confirm negative effects on membrane integrity for cells treated with 25 µM A1-boc, pointing to additional

10.3389/fimmu.2023.1168252

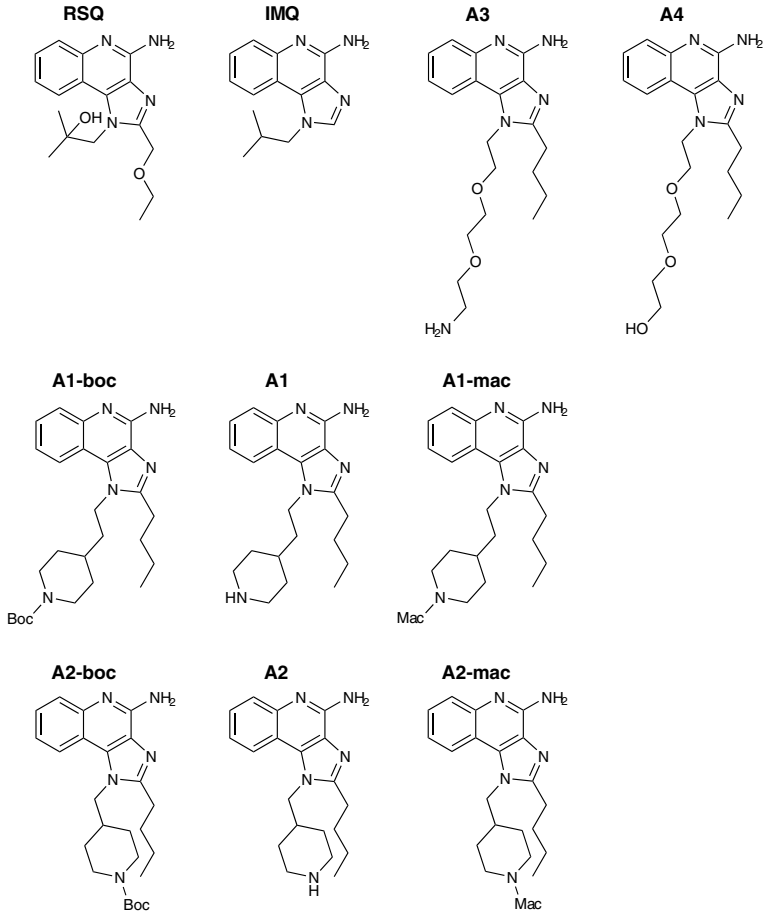

FIGURE 1
Compound structures.

compound effects on metabolism and proliferation of the cells as opposed to cell death.

A1 and A1-mac were selected for further studies based on their similar specificity and activity. Blood from 8 human donors was stimulated at varying concentrations of either test compounds or reference for 6 hours. Secretion of key cytokines was quantified by ELISA. IFNα and TNFα were selected as indicators for either NFκB- or IRF3/7-mediated signaling following stimulation.

TABLE 1 EC_{50} values for compounds in HEK-blue human TLR7 and human TLR8 receptor assay (expressed as 95% CI, ND noted for no calculation of curve fit possible (adj. $r^2 < 0.8$)) and average maximal SEAP secretion observed for a given compound relative to the maximum secretion observed in the assay.

Compound	TLR7 EC_{50} [μM]	TLR7 activity rel. to assay max	TLR8 EC_{50} [μM]	TLR8 activity rel. to assay max
RSQ	0.47 to 0.77	95% ± 5%	2.9 to 3.6	96% ± 4%
IMQ	5.2 to 8.3	35% ± 7%	ND	3% ± 1%
A1-boc	0.39 to 0.69	55% ± 7%	ND	4% ± 2%
A1	0.096 to 0.22	58% ± 16%	ND	11% ± 8%
A1-mac	0.40 to 0.74	41% ± 8%	ND	5% ± 3%
A2-boc	0.23 to 0.47	86% ± 9%	ND	4% ± 1%
A2	0.075 to 0.12	81% ± 13%	2.8 to 3.1	57% ± 9%
A2-mac	1.5 to 2.0	63% ± 9%	ND	4% ± 1%
A3	1.0 to 1.5	62% ± 9%	8.2 to 8.5	36% ± 4%
A4	1.5 to 2.1	84% ± 5%	11 to 13	18% ± 8%

10.3389/fimmu.2023.1168252

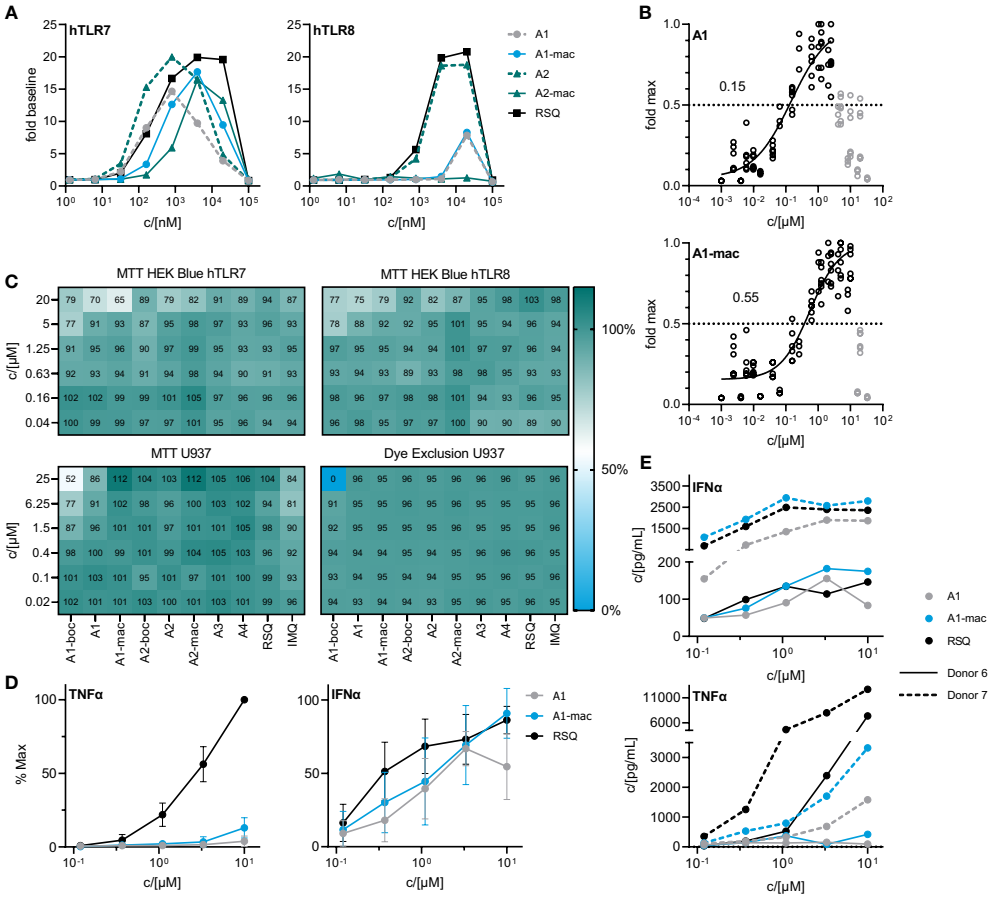

FIGURE 2
In vitro characterization of candidate molecules **(A)** SEAP activity in supernatants of HEK Blue reporter cells after 24 h stimulation with varying concentrations of test compounds relative to solvent controls. **(B)** Dose response of A1 and A1-mac in HEK Blue hTLR7. Circles represent normalized replicate measurements pooled from 3 experiments. Lines represent non-linear functions fit to the data to calculate compound-specific EC50; values in grey have been excluded before fitting. **(C)** Percent MTT conversion of compound-treated HEK-Blue reporter cells (top panels) or PMA-differentiated U937 relative to solvent controls OR percent of undifferentiated U937 excluding Helix NIR dye. **(D)** TNFα/IFNα in supernatants of human blood stimulated with A1, A1-mac or RSQ for 6 h, n=8, concentrations normalized to the maximum concentration of each cytokine for a given donor, data presented as mean ± 95% CI. **(E)** TNFα/IFNα in supernatant for two individual donors.

Maximal supernatant concentrations of both cytokines varied considerably between donors (Figure 2E; Figure S5B). When normalized to the maximal observed concentration for a given donor, relative IFNα induction was robust and similar for both A1 and A1-mac as well as the reference, while the highest TNFα concentrations were almost exclusively measured in supernatants of RSQ-treated samples (Figure 2D). This is consistent with the reduced affinity to TLR8 apparent in the reporter assay (Figure 2A). IFNα response for a given concentration was comparable for all compounds, in contrast to the lower activity of A1/A1-mac in the HEK-blue system. However, overexpression of a given TLR and signal transduction exclusively *via* NFκB instead of IRF3/7 make the HEK system useful to estimate affinity to a given receptor but might not reflect a more complex system with multiple adapter molecules involved in a primary immune cell.

One of the issues we addressed by coupling a TLR-activating structure to a macrolide was poor bioavailability of available TLR-agonists and the resulting limitations in possible routes for systemic treatment. We confirmed the stability of our macrolide conjugates in biological systems *in vitro*. In whole blood and cell based (U937) assays, compounds A1-mac and A2-mac were stable (Figure 3A) over 24 h. We next sought to investigate whether stable coupling to a carrier known for good tissue penetration and -distribution would translate to more favorable pharmacokinetics *in vivo*. To this end we compared bioavailability following intravenous (i.v.), oral (p.o.) or intraperitoneal (i.p.) application with cassettes containing A1-mac, A2-mac and RSQ. Blood samples taken from the tail vein at various times and organ samples collected terminally were then analyzed for compound concentrations by HPLC-MS/MS. Doses of compounds were selected based on known tolerance of TLR agonists per route and restricted by detection limits of analytical methods (i.v. 0.5 mg/kg; i.p. 2 mg/kg; p.o. 2 mg/kg). As expected, i.v. application (i.v. 0.5 mg/kg) showed highest blood concentrations for all substances (c_{max}: RSQ 854 nM; A1-mac 392 nM; A2-mac 352 nM 15 min after application) but also showed fast elimination (baseline level after 120 min) (Figure 3B) and low tissue distribution (Figure 3C). Surprisingly, the oral availability of macrolide-bound TLR agonists was lower than expected and on the same level as RSQ

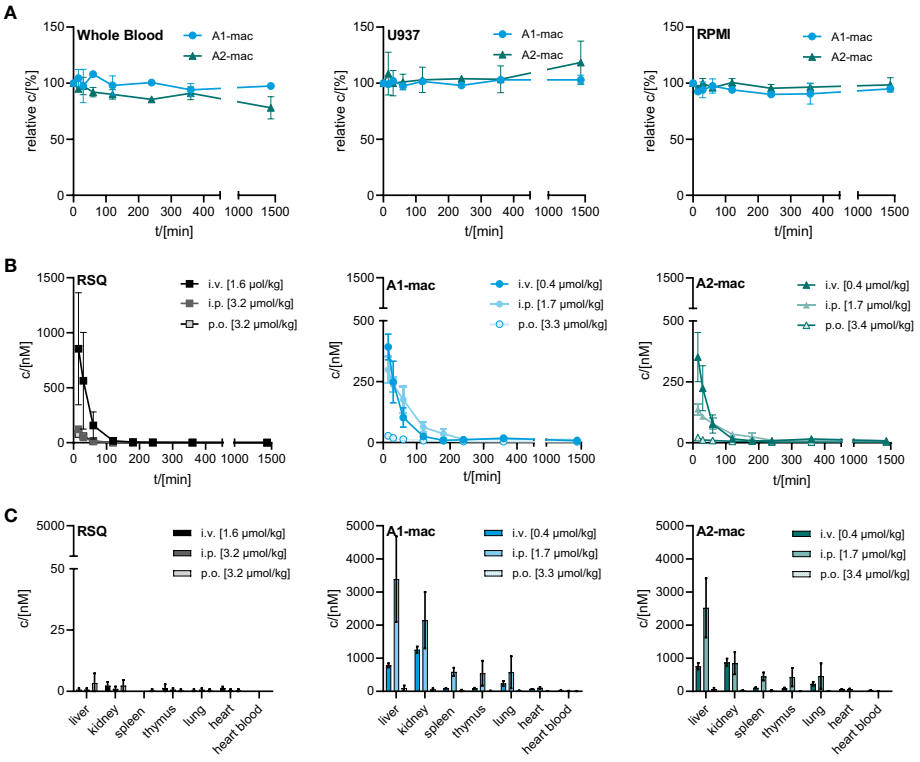

FIGURE 3
Stability and bioavailability of macrolide conjugates. **(A)** Stability of A1-mac and A2-mac was measured in human blood, U937 monocytes and RPMI medium over 24 h. **(B, C)** Concentration of RSQ, A1-mac and A2-mac in peripheral blood and organs was assessed *via* HLPC-MS after i.v., i.p. and p.o. compound administration in 10-week-old, female C57BL/6 mice (n=3 mice per group). Compounds were administered in cassettes (i.v. application: 1.6 µmol/kg RSQ, 0.4 µmol/kg A1-mac, 0.4 µmol/kg A2-mac; i.p. application: 3.2 µmol/kg RSQ, 1.7 µmol/kg A1-mac, 1.7 µmol/kg A2-mac, p.o. application: 3.2 µmol/kg RSQ, 3.3 µmol/kg A1-mac, 3.3 µmol/kg A2-mac). **(B)** Peripheral blood was collected 15, 30 60, 120, 180, 240, 360 and 1440 min after compound administration. **(C)** Organs were sampled 1440 min after compound administration. **(A–C)** Data are presented as mean ± SD.

(c_{max}: RSQ 41 nM; A1-mac 28 nM, A2-mac 22 nM 15 min after application). This observation was unexpected, as macrolide-based substances usually possess good oral availability. This is generally accompanied by good systemic distribution and accumulation in tissues (53, 54, 56) and the relatively low plasma concentrations in this case may also reflect retention in the gut epithelium, which has been observed for other similar conjugates (53). In contrast, i.p. administration showed a distribution more similar to other macrolide-conjugates described previously by us (53). Like i.v. treatment, i.p. (2 mg/kg), had rapid partition to blood (c_{max}: RSQ 123 nM; A1-mac 299 nM; A2-mac 138 nM 15 min after application) and high concentrations of compounds A1-mac and A2-mac in tissue with high levels in the liver (RSQ < LOD; A1-mac 3390 nM; A2-mac 2522 nM) and kidney (RSQ < LOD; A1-mac 586 nM; A2-mac 449 nM). Given the low levels following oral application and the risk that it may stimulate the gut excessively, the oral route was not used in subsequent *in vivo* studies.

We then compared the activity of A1 and A1-mac *in vivo*. Since receptor engagement and activities *in vitro* were very similar for A1 and A1-mac, we hoped to be able to identify changes in activity directly related to the macrolide carrier. Compounds were applied subcutaneously at 3, 6 or 12 µmol/kg. Plasma samples taken at various times before and after treatment were analyzed for cytokine concentrations. Organs, terminal heart blood and peripheral blood 1 h post-treatment were analyzed by HPLC-MS/MS. As in the last study (Figures 3B, C), high concentrations of A1-mac were found in liver (5099 nM for 12 µmol/kg) and kidney (5481 nM for 12 µmol/kg) 8 h after treatment (Figure 4A). This was not found for RSQ (33 nM in liver and 51 nM in kidney for 12 µmol/kg) and A1 (173 nM in liver and 636 nM in kidney for 12 µmol/kg). Levels of A1 were dose dependent for all organs, with lung (868 nM for 12 µmol/kg) and tail blood high after 1 h (1557 nM for 12 µmol/kg). Concentrations measured for RSQ were generally lower with spleen being (202 nM for 6 µmol/kg and 158 nM for 12 µmol/kg) the highest of the organs analyzed.

These pharmacokinetic data confirm the known effects of macrolides on half-life and volume of distribution, are in line with our previous study (Figure 3) and show that s.c. is a suitable application route. For A1, the higher concentrations across all tissues point to better overall penetration and stability when compared to RSQ, further supported by higher concentrations of A1 in peripheral blood 1 h post application (A1: 1557 nM, A1-mac: 696 nM, RSQ: 175 nM, for 12 µmol/kg). Whole blood was analyzed in these studies to take account of material portioned to cells.

Similar to the blood stimulation assays described earlier (Figure 2D), the induction of pro-inflammatory cytokines and

10.3389/fimmu.2023.1168252

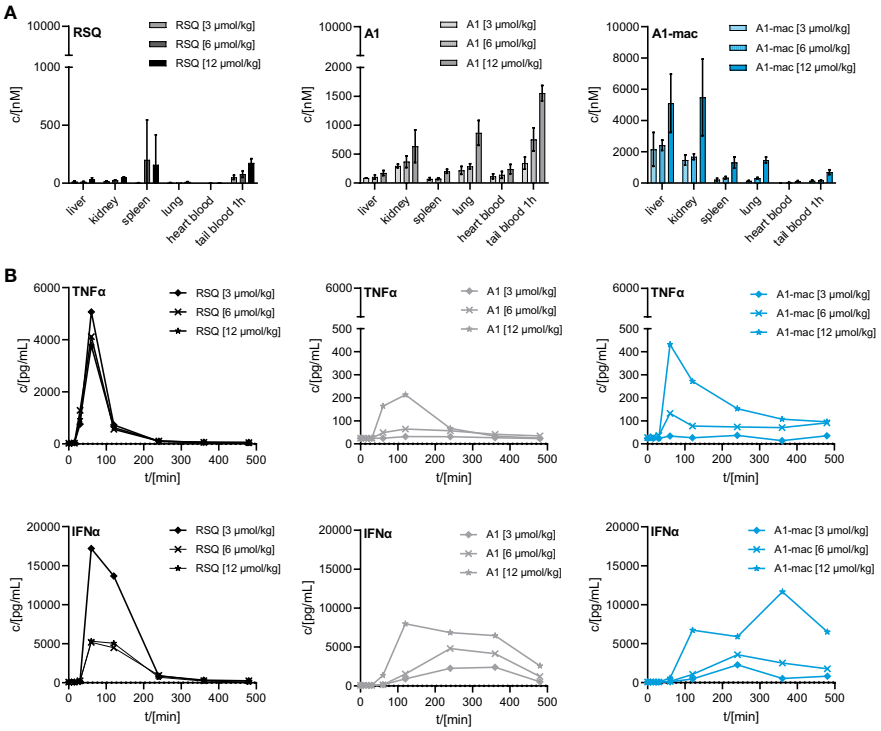

FIGURE 4
Concentration of RSQ, A1 and A1-mac in organs and cytokine profile in peripheral plasma over time after 3, 6 and 12 µmol/kg s.c. compound administration in 8-week-old, female C57BL/6 mice (n=3 mice per group). **(A)** Organs were sampled 8 h after treatment and compound concentration was determined *via* HPLC-MS/MS. Data are presented as mean ± SD. **(B)** Cytokine levels in tail plasma over time were determined *via* cytometric bead array. At each sampling timepoint the plasma of mice in one treatment group was pooled.

IFNα was clearly different between groups receiving RSQ and either A1 or A1-mac (Figure 4B). While RSQ treatment resulted in a sharp increase in TNFα and IFNα plasma levels, peaking 90 min post treatment and falling close to baseline after 240 min, release kinetics were generally slower in the groups receiving A1 or A1-mac. Mice treated with A1-mac had a lower TNFα peak at 90 min while in A1-treated mice it was at 120 min. IFNα levels stayed elevated over the 8 h period of the study in A1 and A1-mac treated groups.

Most striking was that in RSQ-treated groups, the peak TNFα concentrations were over 10 times higher than in A1 or A1-mac groups. The area under the curve calculated from the TNFα plasma values of mice receiving the lowest dose of 3 µmol/kg RSQ was about 4 times larger than the area calculated for any A1 or A1-mac treated group. In contrast to this, the AUCs for IFNα were similar between groups (Table 2 top section).

While we anticipated different release kinetics based on the differences in pharmacokinetics described earlier, the different cytokine release patterns were unexpected. Preference for TLR7 over TLR8 should not have an impact in murine systems (in which activity of RSQ is thought to be dependent on TLR7 under normal circumstances (62, 63)) and the release of TNFα as well as IFNα and other cytokines (Figure S6) were highest in the RSQ group receiving the lowest dose. We suspected this to be due to a saturation effect and possibly overshooting feedback mechanisms. The idea of negative feedback potentially decreasing the secretion of Type I IFN in RSQ treated animals after a short burst is supported by the higher IL10 levels observed only in those animals (Figure S6 bottom panels). In this case, differences in cytokine secretion could be explained simply by the higher potency of RSQ compared to A1/A1-mac. To rule out differences in potency as the reason for the varying cytokine profiles, we reduced RSQ doses to 0.1, 0.3, 1 and 3 µmol/kg and added 1 µmol/kg as an additional dose for A1 and A1-mac in a follow-up study. The doses were chosen so the lowest dose for a given compound would be at the threshold of detectable activity while reflecting the differences in maximal TLR7-activation we originally observed in the HEK reporter assay. When comparing the AUC in this study, we found a dose ratio of roughly 6-10 times the molar dose of RSQ leading to comparable amounts of IFNα in A1 and A1-mac treated groups, while 30-40 times the molar dose were necessary to induce similar levels of TNFα. More specifically, we could not find a dose for which RSQ would induce similarly high levels of type I Interferon without also leading to much higher release of TNFα than A1 and A1-mac (Figure 5C; Table 2 bottom section). This is not limited to a reduction of TNFα-secretion relative to Type I IFN but a similar pattern can be observed for other NFκB-induced cytokines (Figure 5D).

We conclude from this that the specific induction of high levels of Type I IFN is a characteristic feature of A1 and A1-mac and cannot be reproduced by any dose of RSQ. These characteristics might be related to the different stability and pharmacokinetic profile when compared to RSQ, to varying receptor specificity or to differences in subcellular partitioning of the compounds.

Distribution of compounds to different organs was similar in pattern but varied in concentration when compared to the previous study (Figures 5B, 4A). Taking the different dose ranges into

10.3389/fimmu.2023.1168252

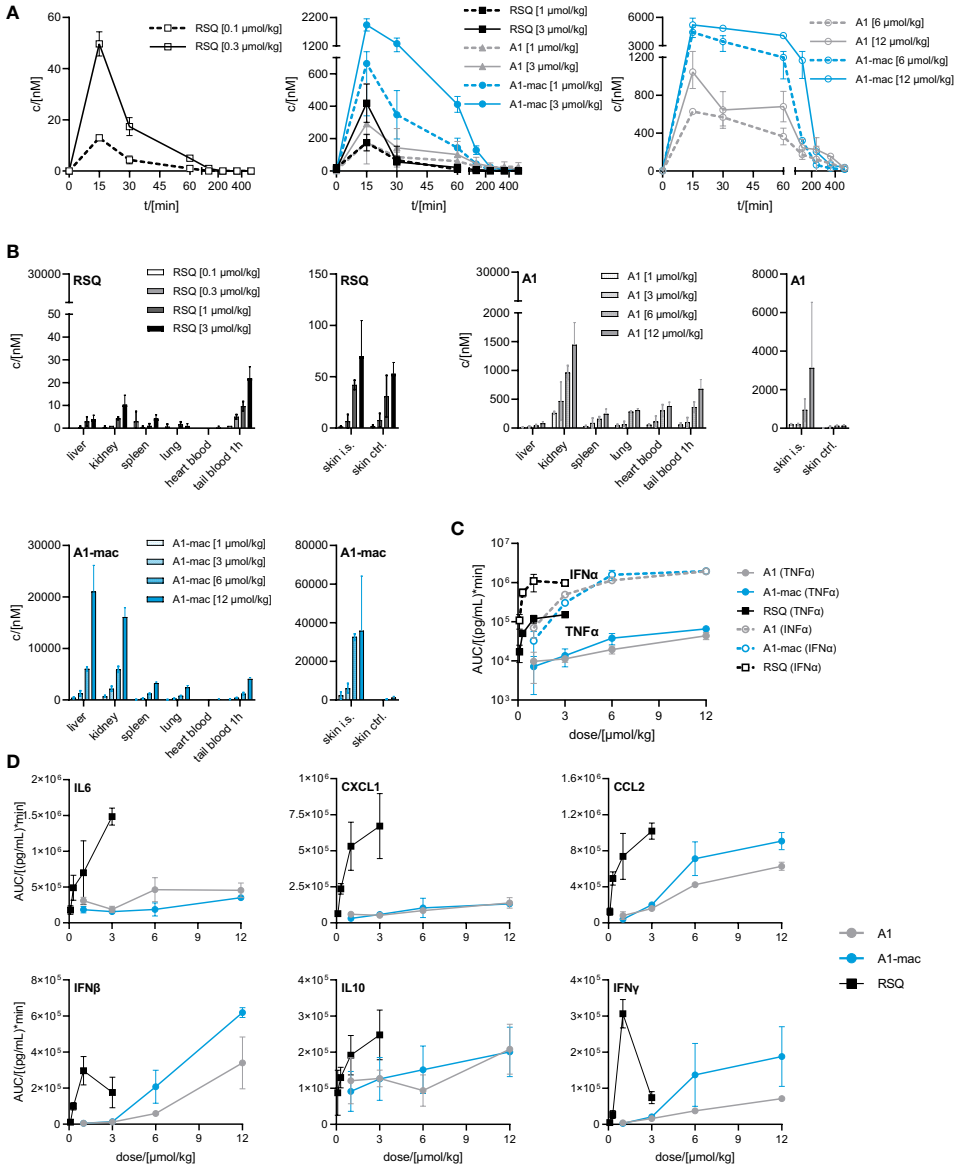

FIGURE 5
Pharmacokinetics and induction of TNFα, IFNα by A1 and A1-mac and RSQ. **(A–D)** Female, 18-week-old, C57BL/6 mice were treated s.c. with either 0.1, 0.3, 1, 3 µmol/kg RSQ, or 1, 3, 6 or 12 µmol/kg A1 or A1-mac (n=3 mice per group). Compound concentration in **(A)** peripheral blood collected *via* tail bleeding before, 15, 30 60, 120, 240, 360 and 480 min after s.c. compound application and **(B)** organs collected after 8 h was assessed *via* HPLC-MS/MS. **(A, B)** Data are presented as mean ± SD. **(C)** Levels of TNFα and IFNα as well as **(D)** IL6, CXCL1, CCL2, IFNβ, IFNγ and IL10 in tail plasma over time were determined *via* cytometric bead array. Area under the curve (AUC) of each cytokine was plotted against compound concentration. Data are represented as mean ± 95% confidence interval.

account, A1 and A1-mac reach higher concentrations in tissues than RSQ 8 h post compound application (in kidney at 3 µmol/kg RSQ: 10 nM A1: 469 nM A1-mac 2176 nM and in liver RSQ: <LLOQ A1: 45 nM A1-mac 6030 nM). Compound levels in peripheral plasma over time were analyzed in this study. We found that not only the macrolide conjugate but also the free agonist A1 was detectable in plasma over a longer period of time when compared to RSQ. This may, in part, be due to higher stability as well as retention at and slower release from the injection site for A1 and A1-mac (Figure 5B, narrow panels).

Since we could not attribute our observations to dose alone and there are specific cases in which murine TLR8 is reported to be activated (64), we added Imiquimod as the prototypical TLR7-agonist to act as an additional reference in our next study. Imiquimod itself is not solely reliant on TLR7 signaling to trigger its pro-inflammatory effects, being also an inhibitor of adenosine receptors (65). However, it is inactive on TLR8 and more similar to A1 and A1-mac in that regard. To account for the lower potency of Imiquimod when compared to the other compounds, we used a dose corresponding to the ~10-fold difference in potency relative to A1-mac indicated by the reporter assay detailed earlier. We further chose doses for A1, A1-mac and RSQ based on those which resulted in similar IFNα-AUC in the previous study and modified the protocol to include three consecutive daily treatments to assess

10.3389/fimmu.2023.1168252

TABLE 2 AUC of TNFα and IFNα measured in peripheral plasma over an 8 h period after application of equimolar doses (top section) or doses adjusted to the activity of the compounds (bottom section) in female C57BL/6.

	TNFα AUC [pg/ml·min]						IFNα AUC [pg/ml·min]						INFα AUC / TNFα AUC					
Dose [µmol/kg]	0.1	0.3	1	3	6	12	0.1	0.3	1	3	6	12	0.1	0.3	1	3	6	12
A1				6.5E +03	1.7E +04	3.5E +04				6.6E +05	1.3E +06	2.5E +06				77	72	102
A1-mac				6.9E +03	2.4E +04	7.6E +04				4.2E +05	9.2E +05	3.1E +06				39	41	60
RSQ				3.3E +05	2.8E +05	2.6E +05				2.2E +06	7.8E +05	8.0E +05				3	3	7
A1			9.7E +03	1.1E +04	2.0E +04	4.4E +04			7.0E +04	4.9E +05	1.1E +06	1.9E +06			7	44	58	44
A1-mac			7.2E +03	1.4E +04	3.8E +04	6.5E +04			3.3E +04	3.0E +05	1.6E +06	1.9E +06			5	22	42	30
RSQ	1.7E +04	5.0E +04	1.2E +05	1.5E +05			1.1E +05	5.6E +05	1.1E +06	9.7E +05			6	11	9	6		

Plasma of 3 individual animals per group was pooled and analyzed via CBA. Values in the right section show AUCs of IFNα normalized to the corresponding AUC of TNFα for a given compound and dose.

the effect of repeated applications on pharmacokinetics (induced metabolism, accumulation) and cytokine induction.

Organ concentrations (Figure S7; collected after 4, 28 and 52 h) were similar to previous studies, with highest concentrations in liver (RSQ: <LLOQ IMQ: 630 nM A1: 63 nM A1-mac: 2617 nM after 4 h; RSQ: <LLOQ IMQ: 824 nM A1: 82 nM A1-mac: 4461 nM after 28 h; RSQ: <LLOQ IMQ: 645 nM A1: 94 nM A1-mac: 6352 nM after 52 h). Interestingly, measured brain tissues showed baseline or close to baseline levels for RSQ (most likely at least partly due to the comparatively low dose), A1 and A1-mac, whilst IMQ was detected with increasing concentrations over the course of the study (32 nM after 4 h; 135 nM after 28 h, 177 nM after 52 h), in line with earlier publications and our observations connecting IMQ brain concentrations with systemic inflammatory responses (66, 67). While there were some minor deviations in compound plasma levels between the first and consecutive treatments (all peaked 60 min after each application; day 1: RSQ <LLOQ IMQ 796 nM, A1 171 nM, A1-mac 755 nM; day 2: RSQ <LLOQ, IMQ 606 nM, A1 85 nM, A1-mac 585 nM; day 3: RSQ <LLOQ, IMQ 608 nM, A1 66 nM, A1-mac 639 nM; Figure 6B), the most prominent effect of repeated doses is a decline in Interferon-secretion after the first treatment. Secretion of TNFα was fairly similar after each of the repeated treatments and remained low for all treatments with A1 and A1-mac in comparison with IMQ and RSQ (Figure 6C shows days 1 and 2). IFNα induction was reduced after the second treatment for all compounds and plasma levels on the third day generally remained below the limit of detection. The decrease in INFα levels on the second day was more pronounced for A1 and A1-mac, both being at the limit of detection for type I Interferon concentrations in plasma after the second treatment (Figure 6A).

The induction of IFNα and TNFα after treatment with RSQ or IMQ were very similar in their kinetics as well as the ratio of both cytokines. A1- and A1-mac-treated animals showed a delayed and more sustained induction of IFNα and little TNFα in peripheral plasma after the first treatment, as in previous studies.

4 Conclusion

The similarities between IMQ and RSQ in cytokine induction make differences in receptor specificity an unlikely explanation for the divergent cytokine profile induced by A1/A1-mac. We hypothesize that these observations are due to either PK and specifically release kinetics from the injection site or possibly partitioning to specific cellular compartments. The differences in PK are clear from the data reported here.

Additionally, we consider the option that subcellular location may be relevant in "polarizing" TLR7-mediated signaling based on: firstly, the observations made by others demonstrating the outcome of TLR9 activation is dependent on the cellular compartment in which activation occurs (28–31); and, secondly, the considerable overlap between adapter molecules employed by TLR7 and 9 to either activate NFκB or cause phosphorylation of IRF7, particularly TRAF6 or TRAF3. Thirdly, our own observations that a structurally similar fluorescent tool compound consisting of a macrolide core conjugated to a coumarin dye accumulated in endosomal compartments (Laux et al., in review) which could be organelles relevant to IRF7 activation as well as the research of others demonstrating endosomal uptake of both macrolides and imidazoquinolines (55, 60). In conclusion, we consider the possibility that preferential uptake of our compounds in those organelles causes their characteristic cytokine induction, although preferential partitioning to specific endosomes needs to be explicitly demonstrated.

Irrespective of the exact mechanism causing them, these data suggest that the compounds have profound and distinct properties and biological activities relative to well-known compounds like RSQ and IMQ. The new class differs from previous compounds in stability, distribution, spectrum and duration of action. The conserved activity of the macrolide conjugate A1-mac indicates that the compounds tolerate large bulky substituents at the linkage

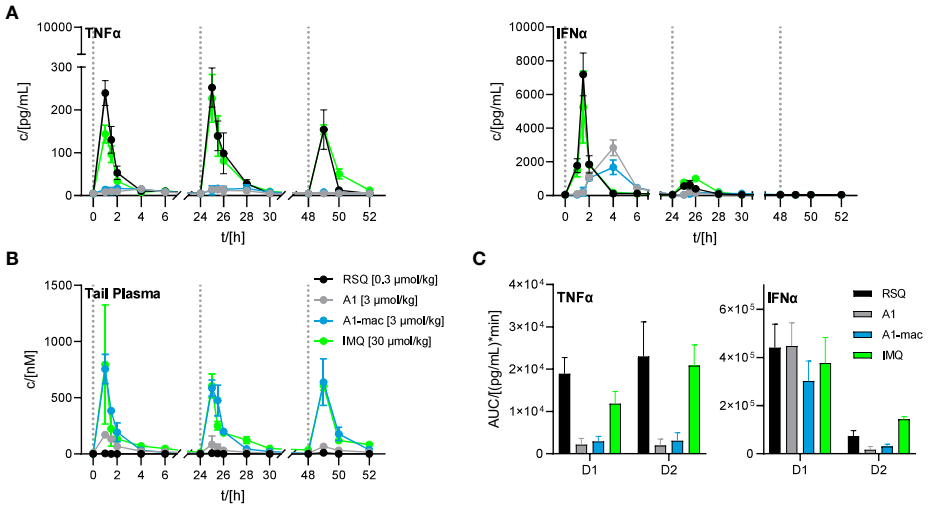

FIGURE 6
Effect of repeated applications of A1, A1-mac, RSQ and IMQ. Dotted lines indicate the time of repeated compound applications. **(A)** Cytokine levels in pooled tail plasma of mice from individual treatment groups (n=3 per pool and time point), error bars represent range of two replicate measurements. **(B)** Peripheral blood was collected from the tail vein before, 15, 30 60, 120, 240, 360 and 480 min after s.c. treatment. Compound concentration in peripheral plasma was analyzed by HPLC-MS/MS, data presented as mean ± SD. **(C)** AUC of TNFα/IFNα in peripheral plasma calculated from the data in **(A)** for days 1 and 2 of treatment, data represent calculated AUC ± 95% CI.

position and are also suitable for linkage to other macromolecules This makes them potentially useful reagents for addition of immune stimulatory properties to other compounds and agents such as polymers, proteins and antibodies.

The absence of a strong TNFα signal could increase the tolerability of the compounds in clinical use. It remains to be seen whether this is advantageous for applications in oncology. However, a variety of tumors appear to benefit from high TNFα levels and this aspect may require more nuanced investigation.

This cytokine profile with its emphasis on IFNα may potentially suit applications in treatment of viral infections. The potency and specificity of the compounds as well as their induction of patient-specific quantities of type I IFN could make them suitable as an alternative to treatment with a fixed dose of recombinant IFNα. Nevertheless, the loss of the IFNα response on successive application may indicate a risk of receptor saturation and immune exhaustion. The impact of time between treatments on this effect has been demonstrated for RSQ in the past (68) and careful attention is required to define a suitable dosing interval before application in a clinical setting.

Data availability statement

The original contributions presented in the study are included in the article/Supplementary Materials. Further inquiries can be directed to the corresponding author.

Ethics statement

The studies involving human participants were reviewed and approved by the Ethik-Kommission, Medizinische Fakultät, Universitätsklinikum Tübingen. Written informed consent for participation was not required for this study in accordance with the national legislation and the institutional requirements. The animal studies were reviewed and approved by the Regierungspräsidium Tübingen under application no. 35/9183.81-7/SYN 06/20.

Author contributions

SS and JHG were involved in compound synthesis and characterization. SG, NS, TF, SS, and MK designed and carried out *in vitro* experiments and processed samples from *in vivo* studies. SG, TW, MB, and MK designed and carried out *in vivo* experiments. AS, JG, SS, and MK processed samples for and data from HPLC-MS/MS measurements. MK, SS, SG, and MB wrote the manuscript. MB and SL supervised the project and provided funding. All authors proof-read the manuscript. All authors contributed to the article and approved the submitted version.

Acknowledgments

We would like to thank colleagues from Synovo GmbH and the University of Tübingen who assisted in this research. Special thanks to the members of the *in vivo* facility and the team of the analytics/bioanalytics department at both institutions.

Conflict of interest

Authors MK, SS, SG, TF, NS, TW, AS, JG, JHG, and MB were employed by the company Synovo GmbH. MK, SS, JHG, and MB are named as inventors in the corresponding patent.

The remaining author declares that the research was conducted in the absence of any commercial or financial relationships that could be construed as a potential conflict of interest.

Publisher's note

All claims expressed in this article are solely those of the authors and do not necessarily represent those of their affiliated organizations, or those of the publisher, the editors and the reviewers. Any product that may be evaluated in this article, or claim that may be made by its manufacturer, is not guaranteed or endorsed by the publisher.

Supplementary material

The Supplementary Material for this article can be found online at: https://www.frontiersin.org/articles/10.3389/fimmu.2023.1168252/full#supplementary-material

References

1. Waldman AD, Fritz JM, Lenardo MJ. A guide to cancer immunotherapy: from T cell basic science to clinical practice. *Nat Rev Immunol* (2020) 20(11):651–68. doi: 10.1038/s41577-020-0306-5

2. Boardman DA, Levings MK. Cancer immunotherapies repurposed for use in autoimmunity. *Nat BioMed Eng* (2019) 3(4):247–7. doi: 10.1038/s41551-019-0359-6

3. Kaufmann SHE, Dorhoi A, Hotchkiss RS, Bartenschlager R. Host-directed therapies for bacterial and viral infections. *Nat Rev Drug Discovery* (2017) 17(1):35–56. doi: 10.1038/nrd.2017.162

4. Wallis RS, O'Garra A, Sher A, Wack A. Host-directed immunotherapy of viral and bacterial infections: past, present and future. *Nat Rev Immunol* (2023) 23(2):121–33. doi: 10.1038/s41577-022-00734-z

5. Wykes MN, Lewin SR. Immune checkpoint blockade in infectious diseases. *Nat Rev Immunol* (2017) 18(2):91–104. doi: 10.1038/nri.2017.112

6. McCulloch TR, Wells TJ, Souza-Fonseca-Guimaraes F. Towards efficient immunotherapy for bacterial infection. *Trends Microbiol* (2022) 30(2):158–69. doi: 10.1016/j.tim.2021.05.005

7. Aricò E, Castiello L, Capone I, Gabriele L, Belardelli F. Type I interferons and cancer: an evolving story demanding novel clinical applications. *Cancers (Basel)* (2019) 11(12):1943. doi: 10.3390/cancers11121943

8. Borden EC. Interferons α and β in cancer: therapeutic opportunities from new insights. *Nat Rev Drug Discovery* (2019) 18(3):219–34. doi: 10.1038/s41573-018-0011-2

9. Heim MH. 25 years of interferon-based treatment of chronic hepatitis c: an epoch coming to an end. *Nat Rev Immunol* (2013) 13(7):535–42. doi: 10.1038/nri3463

10. Twomey JD, Zhang B. Cancer immunotherapy update: FDA-approved checkpoint inhibitors and companion diagnostics. *AAPS J* (2021) 23(2):1–11. doi: 10.1208/s12248-021-00574-0

11. Fitzgerald KA, Kagan JC. Toll-like receptors and the control of immunity. *Cell.* (2020) 180(6):1044–66. doi: 10.1016/j.cell.2020.02.041

12. Chi H, Li C, Zhao FS, Zhang L, Ng TB, Jin G, et al. Anti-tumor activity of toll-like receptor 7 agonists. *Frontiers in Pharmacology* (2017) 8:304. doi: 10.3389/fphar.2017.00304

13. Pradere JP, Dapito DH, Schwabe RF. *The yin and yang of toll-like receptors in cancer. vol. 33, oncogene.* Nature Publishing Group (2014) 33(27):3485–95. doi: 10.1038/onc.2013.302

14. Kawai T, Akira S. TLR signaling. *Semin Immunol* (2007) 19(1):24–32. doi: 10.1016/j.smim.2006.12.004

15. Stanley MA. Imiquimod and the imidazoquinolones: mechanism of action and therapeutic potential. *Clin Exp Dermatol* (2002) 27(7):571–7. doi: 10.1046/j.1365-2230.2002.01151.x

16. Chen X, Zhang Y, Fu Y. The critical role of toll-like receptor-mediated signaling in cancer immunotherapy. *Med Drug Discovery* (2022) 14:100122. doi: 10.1016/j.medidd.2022.100122

17. Kaczanowska S, Joseph AM, Davila E. TLR agonists: our best frenemy in cancer immunotherapy. *J Leukoc Biol* (2013) 93(6):847–63. doi: 10.1189/jlb.1012501

18. Botos I, Segal DM, Davies DR. The structural biology of toll-like receptors. *Structure.* (2011) 19(4):447–59. doi: 10.1016/j.str.2011.02.004

19. Kawasaki T, Kawai T. Toll-like receptor signaling pathways. *Front Immunol* (2014) 5(SEP):461. doi: 10.3389/fimmu.2014.00461

20. Schoenemeyer A, Barnes BJ, Mancl ME, Latz E, Goutagny N, Pitha PM, et al. The interferon regulatory factor, IRF5, is a central mediator of toll-like receptor 7 signaling. *J Biol Chem* (2005) 280(17):17005–12. doi: 10.1074/jbc.M412584200

21. Jefferies CA. Regulating IRFs in IFN driven disease. *Front Immunol* (2019) 10 (MAR):325. doi: 10.3389/fimmu.2019.00325

22. Gilliet M, Cao W, Liu YJ. Plasmacytoid dendritic cells: sensing nucleic acids in viral infection and autoimmune diseases. *Nat Rev Immunol* (2008) 8(8):594–606. doi: 10.1038/nri2358

23. Poropatich K, Dominguez D, Chan WC, Andrade J, Zha Y, Wray B, et al. OX40 + plasmacytoid dendritic cells in the tumor microenvironment promote antitumor immunity. *J Clin Invest* (2020) 130(7):3528–42. doi: 10.1172/JCI131992DS1

24. Zhou B, Lawrence T, Liang Y. The role of plasmacytoid dendritic cells in cancers. *Front Immunol* (2021) 12:4414. doi: 10.3389/fimmu.2021.749190

25. Cervantes JL, Weinerman B, Basole C, Salazar JC. TLR8: the forgotten relative revindicated. *Cell Mol Immunol* (2012) 9(6):434–8. doi: 10.1038/cmi.2012.38

26. Gorden KB, Gorski KS, Gibson SJ, Kedl RM, Kieper WC, Qiu X, et al. Synthetic TLR agonists reveal functional differences between human TLR7 and TLR8. *J Immunol* (2005) 174(3):1259–68. doi: 10.4049/jimmunol.174.3.1259

27. de Marcken M, Dhaliwal K, Danielsen AC, Gautron AS, Dominguez-Villar M. TLR7 and TLR8 activate distinct pathways in monocytes during RNA virus infection. *Sci Signal* (2019) 12(605):1–19. doi: 10.1126/scisignal.aaw1347

28. Guiducci C, Ott G, Chan JH, Damon E, Calacsan C, Matray T, et al. Properties regulating the nature of the plasmacytoid dendritic cell response to toll-like receptor 9 activation. *J Exp Med* (2006) 203(8):1999–2008. doi: 10.1084/jem.20060401

29. Haas T, Schmitz F, Heit A, Wagner H. Sequence independent interferon-α induction by multimerized phosphodiester DNA depends on spatial regulation of toll-like receptor-9 activation in plasmacytoid dendritic cells. *Immunology* (2009) 126 (2):290. doi: 10.1111/j.1365-2567.2008.02897.x

30. Honda K, Ohba Y, Yanai H, Hegishi H, Mizutani T, Takaoka A, et al. Spatiotemporal regulation of MyD88-IRF-7 signalling for robust type-I interferon induction. *Nature.* (2005) 434(7036):1035–40. doi: 10.1038/nature03547

31. Sasai M, Linehan MM, Iwasaki A. Bifurcation of toll-like receptor 9 signaling by adaptor protein 3. *Science* (2010) 329(5998):1530–4. doi: 10.1126/science.1187029

32. Oganesyan G, Saha SK, Guo B, He JQ, Shahangian A, Zarnegar B, et al. Critical role of TRAF3 in the toll-like receptor-dependent and -independent antiviral response. *Nat* (2005) 439(7073):208–11. doi: 10.1038/nature04374

33. Häcker H, Redecke V, Blagoev B, Kratchmarova I, Hsu LC, Wang GG, et al. Specificity in toll-like receptor signalling through distinct effector functions of TRAF3 and TRAF6. *Nat* (2005) 439(7073):204–7. doi: 10.1038/nature04369

34. Hoshino K, Sugiyama T, Matsumoto M, Tanaka T, Saito M, Hemmi H, et al. IκB kinase-α is critical for interferon-α production induced by toll-like receptors 7 and 9. *Nat* (2006) 440(7086):949–53. doi: 10.1038/nature04641

35. Coroadinha S, Brown RJP, Weber L, Vieyres G. The railmap of type I interferon induction: subcellular network plan and how viruses can change tracks. *Cells* (2022) 11 (19):3149. doi: 10.3390/cells11193149

36. Blasius AL, Beutler B. Intracellular toll-like receptors. *Immunity* (2010) 32 (3):305–15. doi: 10.1016/j.immuni.2010.03.012

37. Jurk M, Heil F, Vollmer J, Schetter C, Krieg AM, Wagner H, et al. Human TLR7 or TLR8 independently confer responsiveness to the antiviral compound r-848. *Nat Immunol* (2002) 3(6):499–9. doi: 10.1038/ni0602-499

38. Michaelis KA, Norgard MA, Zhu X, Levasseur PR, Sivagnanam S, Liudahl SM, et al. The TLR7/8 agonist R848 remodels tumor and host responses to promote survival in pancreatic cancer. *Nat Commun* (2019) 10(1):1–15. doi: 10.1038/s41467-019-12657-w

39. Meyer T, Surber C, French LE, Stockfleth E. Resiquimod, a topical drug for viral skin lesions and skin cancer. *Expert Opin Investig Drugs* (2013) 22(1):149–59. doi: 10.1517/13543784.2013.749236

40. Fife KH, Meng TC, Ferris DG, Liu P. Effect of resiquimod 0.01% gel on lesion healing and viral shedding when applied to genital herpes lesions. *Antimicrob Agents Chemother* (2008) 52(2):477. doi: 10.1128/aac.01173-07

41. Pockros PJ, Guyader D, Patton H, Tong MJ, Wright T, McHutchison JG, et al. Oral resiquimod in chronic HCV infection: safety and efficacy in 2 placebo-controlled, double-blind phase IIa studies. *J Hepatol* (2007) 47(2):174–82. doi: 10.1016/j.jhep.2007.02.025

42. Savage P, Horton V, Moore J, Owens M, Witt P, Gore ME. A phase I clinical trial of imiquimod, an oral interferon inducer, administered daily. *Br J Cancer* (1996) 74 (9):1482. doi: 10.1038/bjc.1996.569

43. Eigentler TK, Gutzmer R, Hauschild A, Heinzerling L, Schadendorf D, Nashan D, et al. Adjuvant treatment with pegylated interferon α-2a versus low-dose interferon α-2a in patients with high-risk melanoma: a randomized phase III DeCOG trial. *Ann Oncol* (2016) 27(8):1625–32. doi: 10.1093/annonc/mdw225

44. Ichael M, Ried WF, Hiffman ILS, Ajender KR, Eddy R, Oleman C, et al. Peginterferon Alfa-2a plus ribavirin for chronic hepatitis c virus infection. *N Engl J Med* (2002) 347(13):975–82. doi: 10.1056/NEJMoa020047

45. A Safety, Efficacy and Pharmacokinetics Study of CD11301 for the Treatment of Cutaneous T-Cell Lymphoma (CTCL) - Full Text View - ClinicalTrials.gov [Internet]. Identifier NCT03292406 [cited 2023 Jun 5]. Available from: https://clinicaltrials.gov/ct2/show/NCT03292406

46. Liu X, Vlasak SL, McQuinn RL. Resiquimod Metabolism in Human Liver Microsomes: Enzyme Characterization and the Influence of Nadph Regenerating Systems. *Abstracts from the 10th North American ISSX Meeting, Drug Metabolism Reviews* (2000) 32(Supplement 2):258. doi: 10.1080/03602532.2000.11864616

47. Mescher M, Tigges J, Rolfes KM, Shen AL, Yee JS, Vogeley C, et al. The toll-like receptor agonist imiquimod is metabolized by aryl hydrocarbon receptor-regulated cytochrome P450 enzymes in human keratinocytes and mouse liver. *Arch Toxicol* (2019) 93(7):1917–26. doi: 10.1007/s00204-019-02488-5

48. Tanji H, Ohto U, Shibata T, Miyake K, Shimizu T. Structural reorganization of the toll-like receptor 8 dimer induced by agonistic ligands. *Science* (2013) 339 (6126):1426–9. doi: 10.1126/science.1229159

49. Zhang Z, Ohto U, Shibata T, Krayukhina E, Taoka M, Yamauchi Y, et al. Structural analysis reveals that toll-like receptor 7 is a dual receptor for guanosine and single-stranded RNA. *Immunity* (2016) 45(4):737–48. doi: 10.1016/j.immuni.2016.09.011

50. Zhang Z, Ohto U, Shibata T, Taoka M, Yamauchi Y, Sato R, et al. Structural analyses of toll-like receptor 7 reveal detailed RNA sequence specificity and recognition mechanism of agonistic ligands. *Cell Rep* (2018) 25(12):3371–3381.e5. doi: 10.1016/j.celrep.2018.11.081

51. Yang Y, Csakai A, Jiang S, Smith C, Tanji H, Huang J, et al. Tetrasubstituted imidazoles as incognito toll-like receptor 8 a(nta)gonists. *Nat Commun* (2021) 12(1):1–9. doi: 10.1038/s41467-021-24536-4

52. Shukla NM, Malladi SS, Mutz CA, Balakrishna R, David SA. Structure-activity relationships in human toll-like receptor 7-active imidazoquinoline analogues. *J Med Chem* (2010) 53(11):4450–65. doi: 10.1021/jm100358c

53. Straß S, Schwamborn A, Keppler M, Cloos N, Guezguez J, Guse JH, et al. Synthesis, characterization, and *in vivo* distribution of intracellular delivered macrolide short-chain fatty acid derivatives. *ChemMedChem.* (2021) 16(14):2254–69. doi: 10.1002/cmdc.202100139

54. Garver E, Hugger ED, Shearn SP, Rao A, Dawson PA, Davis CB, et al. Involvement of intestinal uptake transporters in the absorption of azithromycin and clarithromycin in the rat. *Drug Metab Dispos* (2008) 36(12):2492–8. doi: 10.1124/dmd.108.022285

55. Togami K, Chono S, Morimoto K. Subcellular distribution of azithromycin and clarithromycin in rat alveolar macrophages (NR8383) in vitro. *Biol Pharm Bull* (2013) 36(9):1494–1499. doi: 10.1248/bpb.b13-00423

56. Togami K, Chono S, Morimoto K. Distribution characteristics of clarithromycin and azithromycin, macrolide antimicrobial agents used for treatment of respiratory infections, in lung epithelial lining fluid and alveolar macrophages. *Biopharm Drug Dispos* (2011) 32(7):389–97. doi: 10.1002/bdd.767

57. Bosnar M, Kelnerić Ž, Munić V, Eraković V, Parnham MJ. Cellular uptake and efflux of azithromycin, erythromycin, clarithromycin, telithromycin, and cethromycin. *Antimicrob Agents Chemother* (2005) 49(6):2372–7. doi: 10.1128/AAC.49.6.2372-2377.2005

58. Wilms EB, Touw DJ, Heijerman HGM. Pharmacokinetics of azithromycin in plasma, blood, polymorphonuclear neutrophils and sputum during long-term therapy in patients with cystic fibrosis. *Ther Drug Monit* (2006) 28(2):219–25. doi: 10.1097/01.ftd.0000195617.69721.a5

59. Gladue RP, Bright GM, Isaacson RE, Newborg MF. *In vitro* and *in vivo* uptake of azithromycin (CP-62,993) by phagocytic cells: possible mechanism of delivery and release at sites of infection. *Antimicrob Agents Chemother* (1989) 33(3):277–82. doi: 10.1128/AAC.33.3.277

60. Russo C, Cornella-Taracido I, Galli-Stampino L, Jain R, Harrington E, Isome Y, et al. Small molecule toll-like receptor 7 agonists localize to the MHC class II loading compartment of human plasmacytoid dendritic cells. *Blood.* (2011) 117(21):5683–91. doi: 10.1182/blood-2010-12-328138

61. Strass S, Heinzel C, Cloos N, Keppler M, Guse J, Burnet M, et al. P139 effect of lysosomal short chain fatty acid delivery on immune response. *Gastroenterology.* (2020) 158(3):S20. doi: 10.1093/ibd/zaa010.029

62. Hemmi H, Kaisho T, Takeuchi O, Sato S, Sanjo H, Hoshino K, et al. Small-antiviral compounds activate immune cells *via* the TLR7 MyD88-dependent signaling pathway. *Nat Immunol* (2002) 3(2):196–200. doi: 10.1038/ni758

63. Forsbach A, Nemorin J-G, Montino C, Müller C, Samulowitz U, Vicari AP, et al. Identification of RNA sequence motifs stimulating sequence-specific TLR8-dependent immune responses. *J Immunol* (2008) 180(6):3729–38. doi: 10.4049/jimmunol.180.6.3729

64. Gorden KKB, Qiu XX, Binsfeld CCA, Vasilakos JP, Alkan SS. Cutting edge: activation of murine TLR8 by a combination of imidazoquinoline immune response modifiers and PolyT oligodeoxynucleotides. *J Immunol* (2006) 177(10):6584–7. doi: 10.4049/jimmunol.177.10.6584

65. Schön MP, Schön M, Klotz KN. The small antitumoral immune response modifier imiquimod interacts with adenosine receptor signaling in a TLR7- and TLR8-independent fashion. *J Invest Dermatol* (2006) 126(6):1338–47. doi: 10.1038/sj.jid.5700286

66. McColl A, Thomson CA, Nerurkar L, Graham GJ, Cavanagh J. TLR7-mediated skin inflammation remotely triggers chemokine expression and leukocyte accumulation in the brain. *J Neuroinflamm* (2016) 13(1):1–16. doi: 10.1186/s12974-016-0562-2

67. Nerurkar L, Mccoll A, Graham G, Cavanagh J. The systemic response to topical aldara treatment is mediated through direct TLR7 stimulation as imiquimod enters the circulation. *Sci Rep* (2017) 7(1):16570. doi: 10.1038/s41598-017-16707-5

68. Bourquin C, Hotz C, Noerenberg D, Voelkl A, Heidegger S, Roetzer LC, et al. Systemic cancer therapy with a small molecule agonist of toll-like receptor 7 can be improved by circumventing TLR tolerance. *Cancer Res* (2011) 71(15):5123–33. doi: 10.1158/0008-5472.CAN-10-3903

frontiers | Frontiers in Immunology

TYPE Original Research
PUBLISHED 20 July 2023
DOI 10.3389/fimmu.2023.1197650

OPEN ACCESS

EDITED BY
Oliver Planz,
University of Tübingen, Germany

REVIEWED BY
Christophe Pellefigues,
CNRS EMR8252 Centre de Recherche sur l'Inflammation, France
Elaine Tritto,
Novartis Institutes for BioMedical Research, Switzerland

*CORRESPONDENCE
Matthijs Moerland
mmoerland@chdr.nl

RECEIVED 31 March 2023
ACCEPTED 20 June 2023
PUBLISHED 20 July 2023

CITATION
Assil S, Buters TP, Hameeteman PW, Hallard C, Treijtel N, Niemeyer – Van der Kolk T, de Kam ML, Florencia EFIII, Prens EP, van Doorn MBA, Rissmann R, Klarenbeek NB, Jansen MAA and Moerland M (2023) Oral prednisolone suppresses skin inflammation in a healthy volunteer imiquimod challenge model. *Front. Immunol.* 14:1197650. doi: 10.3389/fimmu.2023.1197650

Oral prednisolone suppresses skin inflammation in a healthy volunteer imiquimod challenge model

Salma Assil[1,2], Thomas P. Buters[1,3,4], Pieter W. Hameeteman[1], Charlie Hallard[1], Nicoline Treijtel[1], Tessa Niemeyer – Van der Kolk[1], Marieke L. de Kam[1], Edwin F. I. I. I. Florencia[4], Errol P. Prens[4], Martijn B. A. van Doorn[4], Robert Rissmann[1,2,3], Naomi B. Klarenbeek[1,3], Manon A. A. Jansen[1] and Matthijs Moerland[1,3]*

[1]Centre for Human Drug Research, Leiden, Netherlands, [2]Division of Biotherapeutics, Leiden Academic Centre for Drug Research, Leiden University, Leiden, Netherlands, [3]Leiden University Medical Centre, Leiden, Netherlands, [4]Department of Dermatology Erasmus Medical Centre, Rotterdam, Netherlands

Imiquimod (IMQ) is a topical agent that induces local inflammation *via* the Toll-like receptor 7 pathway. Recently, an IMQ-driven skin inflammation model was developed in healthy volunteers for proof-of-pharmacology trials. The aim of this study was to profile the cellular, biochemical, and clinical effects of the marketed anti-inflammatory compound prednisolone in an IMQ model. This randomized, double-blind, placebo-controlled study was conducted in 24 healthy volunteers. Oral prednisolone (0.25 mg/kg/dose) or placebo (1:1) was administered twice daily for 6 consecutive days. Two days after treatment initiation with prednisolone or placebo, 5 mg imiquimod (IMQ) once daily for two following days was applied under occlusion on the tape-stripped skin of the back for 48 h in healthy volunteers. Non-invasive (imaging and biophysical) and invasive (skin punch biopsies and blister induction) assessments were performed, as well as IMQ *ex vivo* stimulation of whole blood. Prednisolone reduced blood perfusion and skin erythema following 48 h of IMQ application (95% CI [–26.4%, –4.3%], p = 0.0111 and 95% CI [–7.96, –2.13], p = 0.0016). Oral prednisolone suppressed the IMQ-elevated total cell count (95% CI [–79.7%, –16.3%], p = 0.0165), NK and dendritic cells (95% CI [–68.7%, –5.2%], p = 0.0333, 95% CI [–76.9%, –13.9%], p = 0.0184), and classical monocytes (95% CI [–76.7%, –26.6%], p = 0.0043) in blister fluid. Notably, TNF, IL-6, IL-8, and Mx-A responses in blister exudate were also reduced by prednisolone compared to placebo. Oral prednisolone suppresses IMQ-induced skin inflammation, which underlines the value of this cutaneous challenge model in clinical pharmacology studies of novel anti-inflammatory compounds. In these studies, prednisolone can be used as a benchmark.

KEYWORDS

TLR7, imiquimod, corticosteroids, inflammatory model, healthy volunteer

Introduction

Early phase clinical research commonly evaluates the safety, tolerability, and pharmacological activity of novel compounds (1–3). For anti-inflammatory and immunomodulatory compounds, immune challenge models are becoming increasingly popular to demonstrate 'proof of pharmacology' at an early clinical stage, thereby providing insight into the mechanism of action and providing target engagement (4). These pharmacological challenge models are often translated from animal work and can guide drug developers on dose selection and dosing regimens for subsequent phase II studies in the target population.

A widely used preclinical model to study (modulation of) inflammation, also applied in healthy volunteers (HV), is the topical imiquimod (IMQ) challenge, which drives a toll-like receptor (TLR) 7-mediated response. The TLR-dependent pathway activates nuclear factor kappa B (NF-κB) signaling and IRF *via* My-D88, which is important for an early immune response, such as secretion of pro-inflammatory cytokines, including interferon (IFN) -α, interleukin (IL)-1, IL-1RA, IL-6, and IL-8 (5). IMQ applied under occlusion for 48 h drives a transient local reversible inflammatory response indicated by an increase in blood perfusion, erythema, and cytokine production (6). The IMQ model is valuable for the evaluation of the potential combined effect of IMQ and omiganan (a synthetic indolicidin) in HV (7). The IMQ challenge can be valuable for proof-of-mechanism studies of compounds that target TLR7-mediated responses. However, formal benchmarking of the topical IMQ challenge model in humans, using a registered anti-inflammatory drug has not yet been performed.

An alternative human innate immune challenge model is intradermal LPS challenge, which drives TLR4-mediated responses. Corticosteroid treatment (oral prednisolone and topical clobetasol propionate) suppressed the characteristics of the dermal inflammatory reaction, which was also reflected by a reduction in inflammatory cell attraction in the blister fluid (8, 9). Moreover, for the topical IMQ model, profiling of effects of a known strong anti-inflammatory compound that is widely used in dermatology, such as oral prednisolone, would be valuable to benchmark the model for future evaluations of novel anti-inflammatory or immunomodulatory compounds.

Therefore, in this study, we aimed to profile the cellular, biochemical and clinical effects of oral prednisolone on the IMQ skin inflammation model in healthy volunteers with the goal of i) benchmarking the IMQ model for future novel anti-inflammatory compounds, ii) expanding the mechanistic insights into the IMQ-driven skin response by a more thorough molecular and cellular evaluation, and iii) gaining insight into the immunomodulatory mechanism of prednisolone in TLR7-mediated tissue inflammation.

Materials and methods

This randomized, double-blind, placebo-controlled, investigator-initiated study was conducted according to the Dutch Act on Medical Research involving Human Subjects (WMO), and the study protocol was approved by the Medical Ethics Committee (Stichting Beoordeling Ethiek Biomedisch Onderzoek, Assen, The Netherlands) prior to the start of the clinical phase. The subjects provided written informed consent before any study-related procedures were undertaken.

Study design and subjects

A total of 24 healthy male and female Caucasian (Fitzpatrick skin type I–III) volunteers, aged between 18 and 45 years, were enrolled in this study. Health status was confirmed by medical history, physical examination, laboratory tests, and 12-lead electrocardiography (ECG). None of the participants had a family history of psoriasis, no pathological skin conditions at the treatment area, no history of hypertrophic scarring or keloids, no prior use of imiquimod, and no known hypersensitivity to prednisolone.

Treatment and IMQ challenge

Participants were equally randomized into two groups to receive oral prednisolone (0.25 mg/kg/dose) or placebo, twice daily with a 10–12-hour interval between doses, over a period of six consecutive days. On the sixth day, the volunteers received only one dose of prednisolone or placebo in the morning. The treatments were administered under supervision at the clinical research unit to ensure treatment compliance. After two days of pre-treatment with oral prednisolone or placebo, challenge with IMQ commenced (6). For this purpose, the upper back was divided into seven rectangles measuring 4 × 3 cm. Each treatment area was tape-stripped 20 times (D-Squame, CuDerm, Dallas, TX) to induce mild barrier skin disruption, whereas the trans-epidermal water loss (TEWL) (AquaFlux, Biox Systems) was used to quantify skin permeability (6, 7). A TEWL between 15 and 20 g/m^2/h was considered as mild barrier skin disruption. No IMQ was applied to the first two areas since they represented the non-treated areas, while in the other three to five areas, 5 mg IMQ (100 mg Aldara®) was applied for either 24 h or 48 h (depending on the assigned cohort) under occlusion by a 12 mm Finn chamber (Bipharma, Almere, The Netherlands) to initiate an inflammatory skin reaction. Subjects were randomized on (pre-)treatment (prednisolone or placebo) and the time point of invasive measurements (blister and biopsy), as illustrated in Figure 1.

Imaging-based endpoints

The subjects underwent multiple assessments to evaluate the inflammatory skin response before the IMQ challenge and 24, 48, 72, 168, and 216 h after IMQ application. A single treatment site was selected to evaluate non-invasive endpoints throughout the study period (Figure 1), resulting in N = 12 per time point. An overview of the number of samples per time-point is presented in Table S1. Erythema was graded in two ways: by a physician using a 4-point scale ranging from 0 (absent) to 3 (severe) and by

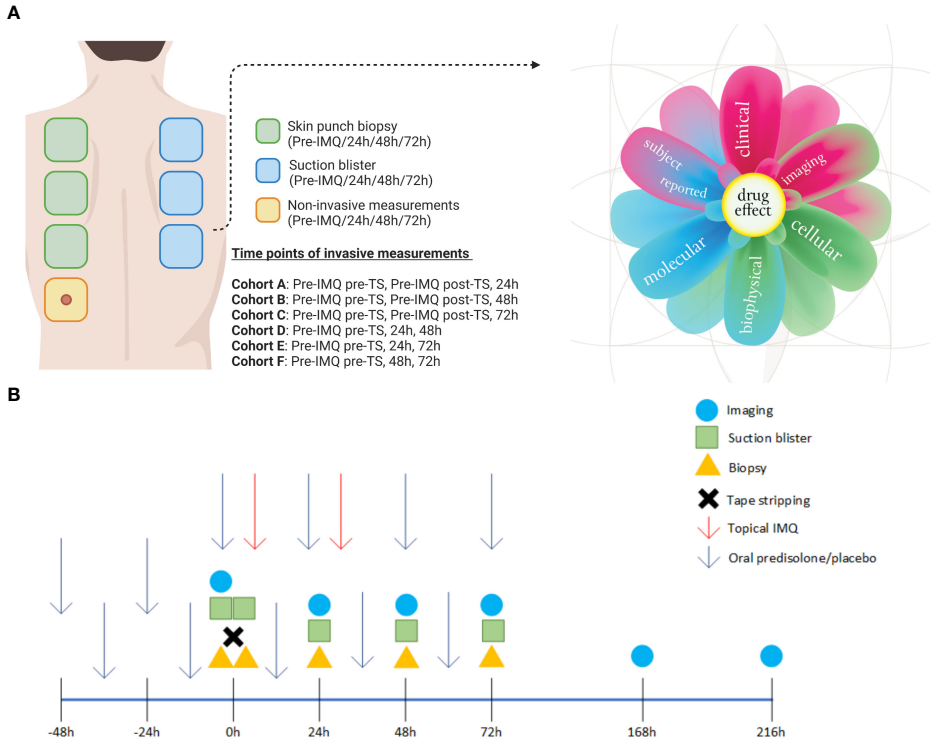

FIGURE 1
Overview of the treated sites on the back and study schedule. **(A)** A total of three biopsies and three blisters were obtained from each subject, with the timing and location of each procedure determined by their assigned cohort. One site on the back was used solely for non-invasive measurements throughout the study period. The skin responses were evaluated using a multi-modal approach and are represented in the "derma flower." **(B)** A schematic overview of all assessments performed relative to dosing. Created with BioRender.com. Derma flower created by F. van Meurs, adapted for this manuscript.

multispectral photoanalysis (Antera 3D, Miravex, Ireland). Perfusion was quantified using laser speckle contrast imaging (LSCI; PeriCam PSI System, Perimed Jäfälla, Sweden) and Optical Coherence Tomography (OCT; VivoSight, Michelson Diagnostics Maidstone, UK). The latter was also used to measure epidermal thickness. All skin assessments were performed under standardized conditions at room temperature (20–24°C).

Biopsy and blister exudate assessments

Suction blisters and 3 mm biopsy samples were taken from the IMQ-treated areas and control areas at the indicated time points, depending on the cohort and randomization (Figure 1). Three biopsies and three blisters were collected from each healthy volunteer. Suction blisters were induced according to the method described by Buters et al. (8). Biopsies were placed in RNAlater medium directly after harvest and stored at 4°C until analysis at the Immunology Laboratory of Erasmus Medical Center, Rotterdam, Netherlands. Immunohistochemical staining was performed to obtain scoring of markers CD11c (Clone 5D11; Cell Marque), CD14 (Clone EPR3653; Cell Marque), CD1a (Clone EP3622; Cell Marque), CD4 (Clone SP35; Ventana), CD8 (Clone SP57; Ventana), and HLA-DR (CR3/43; Dako) using a 6-point rating scale; 0 = negative, 1 = minimal, 2 = few, 3 = moderate, 4 = many, and 5 =excessive.

Blister fluid was collected in a V-bottom plate containing 50 µl 3% sodium citrate (Sigma) in PBS (Gibco) and kept on ice. The plate was centrifuged, and the supernatant was weighed to estimate the volume and then frozen at −80°C for cytokine analysis (Meso Scale Discovery, Rockville, Maryland, USA). The following cytokines were analyzed: TNF, ASC, IL-1β, IL-6, IL-10, IL-8, IFN-γ, and downstream marker for type 1 interferon Mx-A (V-plex proinflammatory panel of MSD and Mx-A protein ELISA kit from BioVendor). The cell pellet was resuspended in RoboSep buffer (StemCell). A cocktail of fluorescent antibodies against cell surface markers was added to the cells and incubated for 30 min on ice. The stained samples were washed with PBS and measured using MACSQuant 16 (Miltenyi Biotec GmbH). Flow cytometry data were analyzed with Flowlogic 7.2 (Inivai). Parallel to the blister fluid, peripheral blood was collected by venipuncture using a sodium heparin vacutainer (BD). Approximately 100 µl of whole blood was treated with red blood cell lysis buffer (eBioscience), washed with PBS, and resuspended in RoboSep buffer. Staining was similar to that of the previously mentioned blister cells and served as a template for the gating strategy. The following antibodies were used: CD56-PE (cat# 130-113-312, Miltenyi Biotec), CD14-PE-Vio615 (cat# 130-110-526, Miltenyi Biotec), CD16-VioBrighT FITC (cat# 130-119-616, Miltenyi Biotec), CD66b-AF700 (cat# 305114, Biolegend), CD19-BV650 (cat# 302238, Biolegend), CD20-BV650 (cat# 302336, Biolegend), HLA DR-APC (cat# 130-

111-790, Miltenyi Biotec), CD4-VioBlue (cat# 130-114-534, Miltenyi Biotec), CD8-BV570 (cat# 301038, Biolegend), CD45-VioGreen (cat# 130-110-638, Miltenyi Biotec), CD1c-PE-Vio770 (cat# 130-110-538, Miltenyi Biotec), CD3-APC-Vio770 (cat# 130-113-136, Miltenyi Biotec), 7AAD (cat# 130-111-568, Miltenyi Biotec). An overview of the gating strategy is shown in Figure S2. Cell populations (Single live cells) were classified according to the following profile: $CD45^+$ $HLA\text{-}DR^-$ $CD66b^+$ $CD16^+$ neutrophils, $CD45^+$ $HLA\text{-}DR^+$ $CD14^+$ $CD16^-$ classical monocytes, $CD45^+$ $HLA\text{-}DR^+$ $CD14^+$ $CD16^+$ intermediate monocytes, $CD45^+$ $HLA\text{-}DR^+$ $CD14^-$ $CD16^+$ non-classical monocytes, $CD45^+$ $HLA\text{-}DR^+$ $CD19^-$ $CD20^-$ $CD14^-$ $CD16^-$ $CD1c^+$ dendritic cells, $CD45^+$ $HLA\text{-}DR^-$ $CD56^+$ NK Cells, $CD45^+$ $HLA\text{-}DR^-$ $CD3^+$ $CD4^+$ $CD8^-$ T helper cells, $CD45^+$ $HLA\text{-}DR^-$ $CD3^+$ $CD4^-$ $CD8^+$ cytotoxic T cells, and $CD45^+$ $HLA\text{-}DR^+$ $CD19^+$ $CD20^+$ B cells.

Ex vivo whole blood stimulation

To investigate the extent of systemic immune suppression with prednisolone (*ex vivo* drug activity), IMQ whole-blood stimulation was used with cytokine release as a readout. Blood was drawn from healthy volunteers at four time points: pre-dose, 48, 52, and 96 h after the initial prednisolone/placebo dose. Blood samples were drawn 48 h and 96 h after initial dose but before the morning prednisolone/placebo dose. The sample taken 52 h after the first administration was taken 4 h after the previous prednisolone/placebo dose. At these time points, sodium heparinized whole blood was stimulated with 20 µg/ml IMQ (cat# tlrl-imq, InvivoGen) for 24 h. After incubation, the cultures were spun down, and the supernatant was collected and frozen at −80°C for cytokine analysis. The samples were shipped to Ardena (Assen, Netherlands) for analysis. The following cytokines were analyzed: IL-1β, IL-6, IFN-γ (V-plex proinflammatory panel of MSD), IP-10 (V-plex chemokine panel of MSD), and Mx-A (human Mx-A protein ELISA kit from BioVendor).

Statistics

All repeatedly measured PD endpoints were summarized (n, mean, SD, min, and max values) according to treatment and time. Repeatedly measured continuous PD endpoints were analyzed using a mixed model analysis of covariance with fixed factor treatment, time, and treatment by time, with a random factor subject as a covariate. The baseline for whole blood stimulation was the pre-prednisolone/placebo treatment measurement. A summary table of the analysis results per variable was generated with estimates of the difference of the different contrasts and a back-transformed estimate of the difference in percentage for log-transformed parameters, 95% confidence intervals (in percentage for log-transformed parameters), Least Square Means (geometric means for log transformed parameters), and the p-value of the contrasts. Statistical analyses were performed using SAS for Windows V9.4 M6 (SAS Institute Inc., Cary, NC, USA).

Results

Twenty-one female (87.5%) and three male (12.5%) Caucasian subjects participated in the study and completed the study without withdrawal. The mean age was 26.3 ± 4.6 years. Headache was the most frequent adverse event; however, it was mild in nature and probably related to the administration of prednisolone. No serious adverse events were reported during the study.

Oral corticosteroids suppress the clinical response induced by topical IMQ application

Oral prednisolone or placebo was administered at 0.25 mg/kg per dose b.i.d. for a period of six consecutive days, and the effects on IMQ-driven clinical responses were evaluated. IMQ was applied for a maximum of 48 h under occlusion, after the skin was tape-stripped 20 times. Maximal responses were observed 48 h after IMQ application in the placebo group (Figures 2A, B). Treatment with prednisolone resulted in a reduction in the IMQ-driven response from 24 h to 72 h, quantified by imaging of blood perfusion (estimated difference: −16.1%, 95% confidence interval (CI) [−26.4%, −4.3%], p = 0.0111), erythema (estimated difference: −5.04, 95% CI [−7.96, −2.13], p = 0.0016), and epidermal thickness (estimated difference: −0.018, 95% CI [−0.029, −0.006], p = 0.0044), compared to placebo (Figures 2A-C). A visual overview of the blood perfusion and erythema is shown in Figure 2D. Application of IMQ (for 24 and 48 h) on the skin resulted in a thickened epidermis, disappearance of the rete ridges and dilatation of the blood vessels (Figure 2E). Furthermore, prednisolone treatment shifted the clinically scored erythema response from moderate to mild (at 48 h) and reduced the proportion of clinically scored erythema (Figure S1). All quantified responses (perfusion, erythema, and epidermal thickness) were reversible and returned to baseline during the follow-up phase (168 and 216 h).

Oral corticosteroids reduce the IMQ-driven cell infiltration in blister exudate and biopsy

In earlier skin challenge research, cellular responses were studied using invasive techniques including suction blisters and skin punch biopsies (6–9). In this study, we implemented the same approach by inducing suction blisters and taking skin punch biopsies at the indicated time points, resulting in a total of three blisters and three biopsies per subject (Figure 1). Biopsy samples were stained for dermal immune cell infiltration and scored by an independent investigator blinded to the treatment.

In addition, immune cells in the blister exudate were evaluated using flow cytometry. A full overview of the analyzed immune cell subsets is shown in Figure 3. The average time for blister induction was (estimated mean, 95% CI) 86.7 min, 95% CI [71.9, 101.4] in the placebo

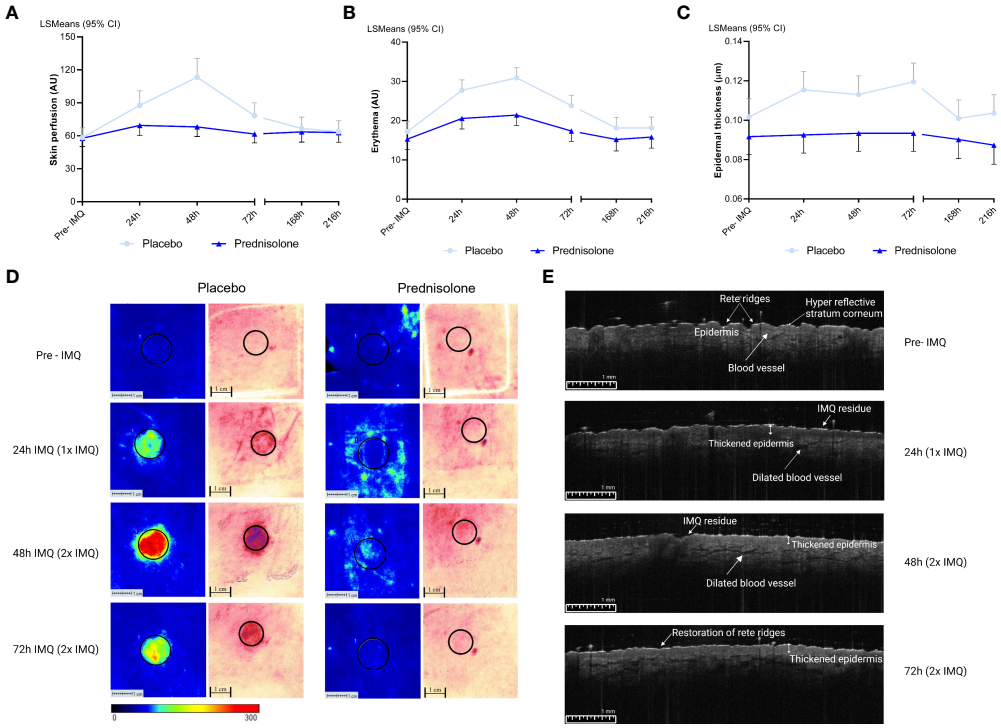

FIGURE 2
Imaging and biophysical based assessments. Pre-IMQ timepoint refers to assessment prior to IMQ application, whereas 24h refers to 1x IMQ application and 48h to 2x IMQ application. 72h refers to 2x IMQ application however measured 24 hours post last IMQ application. For the following measurements prednisolone is compared to placebo. **(A)** Skin perfusion by LSCI, estimated difference: -16.1%, 95% CI [-26.4%, -4.3%], p= 0.0111. **(B)** Erythema measured by multispectral camera, estimated difference: -5.04, 95% CI [-7.96, -2.13], p= 0.0016. **(C)** Epidermal thickness by OCT, estimated difference: -0.018, 95% CI [-0.029, -0.006], p= 0.0044. **(D)** A visual overview of LSCI and multispectral imaging in the prednisolone and placebo group. A ROI of 12 mm was selected for quantification. **(E)** OCT image of one subject of the placebo group after application of IMQ over time. CI, confidence interval; IMQ, Imiquimod; LSCI, Laser speckle contrast imaging; LSMeans, Least Squares Mean; OCT, Optical coherence tomography.

group and 84.1 min, 95% CI [69.4, 98.8] in the prednisolone group (data not shown). No significant difference in the time required for blister formation was observed between the groups (estimated difference: −2.5, 95% CI [−23.4, 18.3], p = 0.8034). The total number of cells ($CD45^+$) increased mildly following IMQ application, with a peak of 624.6 ± 469.5 cells in blister exudate at 48 h (after 2× IMQ application) (Figure 3A). IMQ increased the number of $CD45^+$ HLA-DR^- $CD56^+$ (NK cells), reaching a maximum of 84.2 ± 89.76 cells also at 48 h (after 2× IMQ application) (Figure 3B). The infiltration was followed by other innate immune cells, such as $CD45^+$ HLA-DR^+ $CD19^-$ $CD20^-$ $CD14^-$ $CD16^-$ $CD1c^+$ (dendritic cells) and $CD45^+$ HLA-DR^+ $CD14^+$ $CD16^-$ ("classical monocytes") peaking at 72 h (24 h after the second IMQ application) with mean ± SD of 26.0 ± 21.06 cells and 25.3 ± 27.7 cells, respectively; however, this resulted in a weaker response compared to the influx of NK cells (Figures 3C, D). Although neutrophils are strongly involved in innate immune responses, no infiltration of $CD45^+$ HLA-DR^- $CD66b^+$ $CD16^+$ (neutrophils) was observed after IMQ application, resulting in cell counts of <5 cells (data not shown). Similar low cell counts were observed for $CD45^+$ HLA-DR^+ $CD14^+$ $CD16^+$ ("intermediate monocytes"), $CD45^+$ HLA-DR^+ $CD14^-$ $CD16^+$ ("non-classical monocytes"), and $CD45^+$ HLA-DR^+ $CD19^+$ $CD20^+$ (B cells) (data not shown). IMQ treatment did not result in a significant increase in B cells in the blister fluid (data not shown), nor did it substantially attract $CD45^+$ HLA-DR^- $CD3^+$ $CD4^+$ $CD8^-$ (T helper cells) and $CD45^+$ HLA-DR^- $CD3^+$ $CD4^-$ $CD8^+$ (cytotoxic T cells) (Figures 3E, F). Prednisolone reduced the number of immune cells in blister fluid. This reduction, compared to placebo, was observed for total cells, NK cells, dendritic cells, and classical monocytes (−58.8%, 95% CI [−79.7%, −16.3%], p = 0.0165; −45.5%, 95% CI [−68.7%, −5.2%], p = 0.0333; −55.4%, 95% CI [−76.9%, −13.9%], p = 0.0184; and −58.6%, 95% CI [−76.7%, −26.6%], p = 0.0043, respectively). Although no substantial changes were observed following IMQ challenge, prednisolone significantly reduced the number of T cell subsets (estimated difference: −76.0%, 95% CI [−92.4%, −4.7%], p = 0.0168 for T helper cells and estimated difference: −70.5%, 95% CI [−89.6%, −16.0%], p = 0.0242) for cytotoxic T cells.

Immune cell subsets in biopsies, quantified by IHC, showed a comparable picture to the cells analyzed by flow cytometry in blister fluid. Administration of prednisolone reduced HLA-DR and infiltrating CD11c (dendritic cells), $CD4^+$ (T helper cells), CD1a (Langerhans cells), and $CD8^+$ cells (cytotoxic T cells) (Figure 4). Time courses of IMQ and prednisolone effects were comparable between biopsy and blister-derived immune cells.

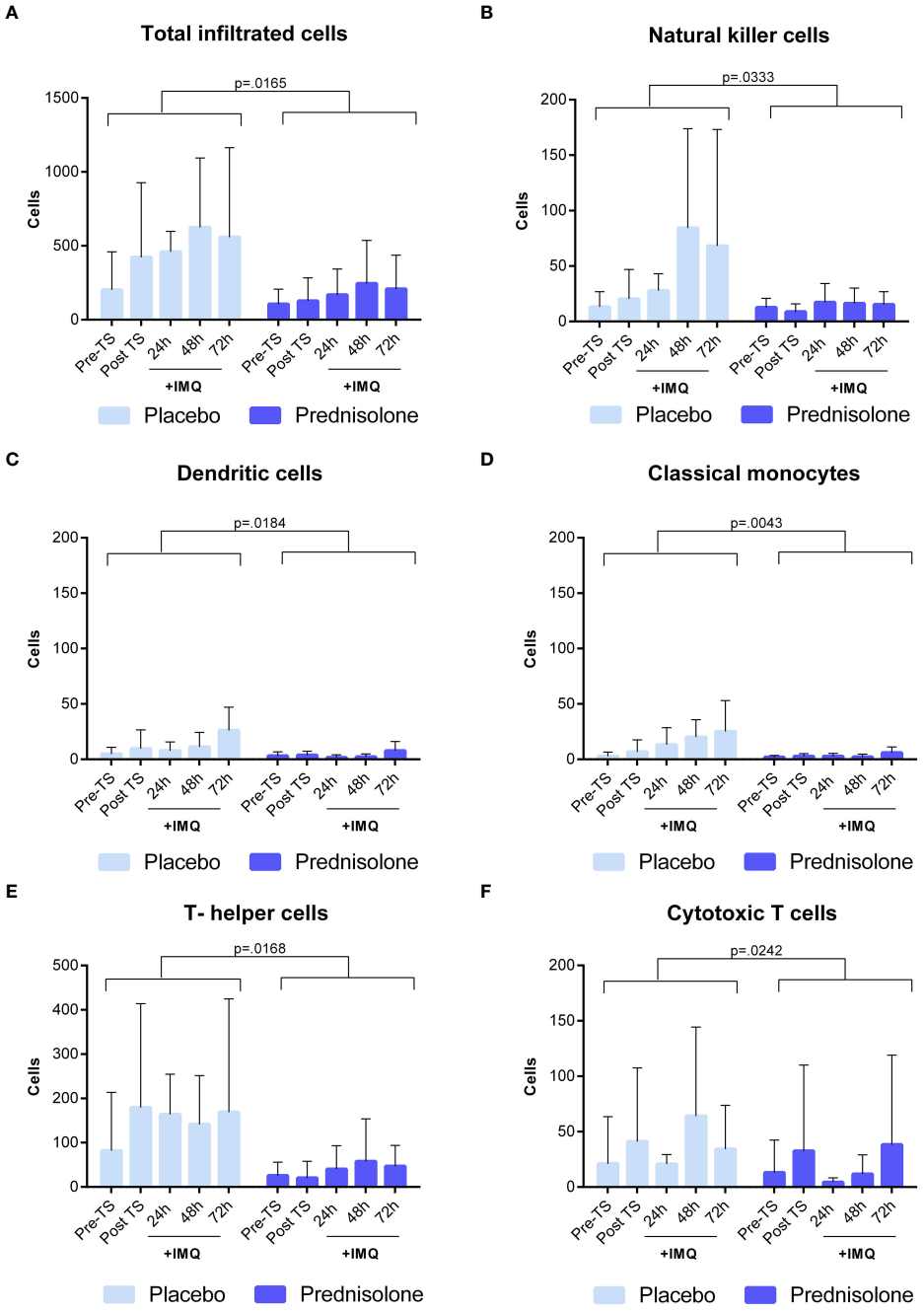

FIGURE 3
Oral prednisolone reduces IMQ- driven immune cell infiltration. **(A)** Total cells **(B)** Natural killer cells **(C)** Dendritic cells **(D)** Classical monocytes **(E)** T helper cells **(F)** Cytotoxic T cells. Immune cells in blister exudate were quantified by flow cytometry at different time points, pre and post IMQ application. Data are presented as mean ± SD. SD, standard deviation; TS, tape stripped.

Oral corticosteroids suppress IMQ-driven cytokine responses in blister exudate and whole blood cultures

In addition to the dermal cellular response, cytokine levels were analyzed in the blister exudate to evaluate of NF- κB- and IRF7-driven responses. IMQ application induced a mild IL-6 response at 24 and 48 h (Figures 5A, B) but had no clear effect on the levels of NF- κB-driven cytokines IL-1β IL-8 and IL-10 (Figures 5C–E). IMQ increased the Mx-A concentration in the blister fluid, with a peak at 48 and 72 h (Figure 5F), indicating activation of the IRF7 pathway. Prednisolone treatment reduced the levels of NF-κB-driven cytokines (IL-6, IL-8, and TNF), IL-1β, and Mx-A (Figures 5A–C, F). No formal statistical analysis for cytokines IL-6, IL-1β, and Mx-A was conducted for the contrast placebo versus prednisolone, because the immune suppression by prednisolone was so strong that most cytokine levels were below the LLOQ. ASC and IFN-γ concentrations in blister fluid are very low, and therefore, have not been reported.

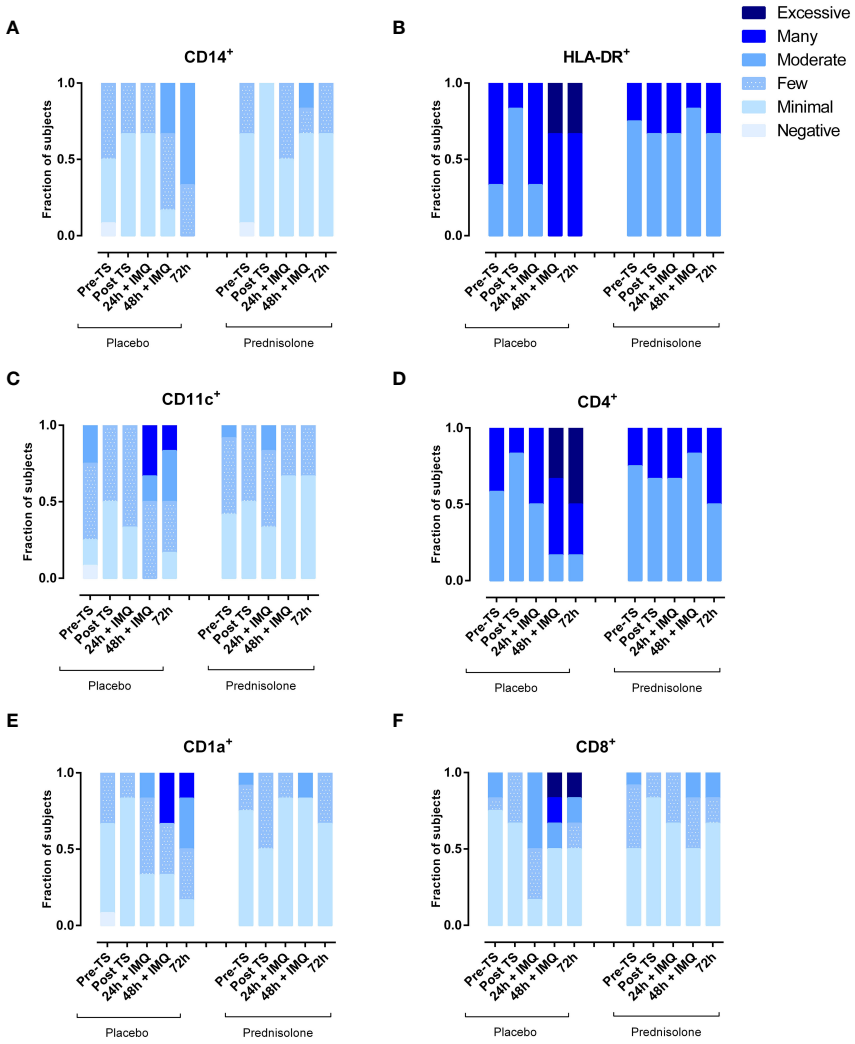

FIGURE 4
Prednisolone reduces infiltration of IMQ-driven immune cells as measured by IHC in skin punch biopsies. **(A)** Macrophages **(B)** HLA-DR **(C)** myeloid dendritic cells **(D)** T helper cells **(E)** Langerhans cells **(F)** Cytotoxic T cells. TS, tape stripped.

Whole blood samples, drawn from study participants at predefined time points, were stimulated with IMQ for the evaluation of *ex vivo* prednisolone activity. Stimulation with IMQ led to an increase in IL-1β, IFN-γ, and IL-6 levels (Figures 6A-C), but not in a detectable Mx-A response (data not shown). An overview of the *ex vivo* results, including those of the unstimulated control conditions, is provided in Table S2. Overall, prednisolone compared to placebo had a significant effect on IFN-γ and IL-1β concentrations (estimated difference: −86.8%, 95% CI [−94.1%, −70.3%, p <0.0001), −55.8%, 95% CI [−78.8%, −8.3%], p = 0.0301, respectively), but not IL-6 (estimated difference: −44.1%, 95% CI [−69.1%, 1.0%], p = 0.0537). However, prednisolone treatment resulted in a statistically significant reduction in IMQ-driven cytokines (IL-1β, IL-6, and IFN-γ), with a maximum inhibitory effect at 52 h post-administration, with an estimated difference of −92.9%, 95% CI [−96.8%, −84.3%], p <0.0001, estimated difference: −87.1%, 95% CI [−93.2%, −75.7%], p <0.0001; estimated difference: −99.0%, 95% CI [−99.6%, 97.4%], p <0.0001, respectively. Interestingly, prednisolone had no effect on IMQ-induced response at time points 48 and 96 h. No statistical analysis was performed on the IP-10 concentration, given that more than 60% of the samples were above the ULOQ.

Discussion

This study aimed to characterize the effects of orally administered prednisolone on TLR7-driven immune responses using *in vivo skin* and *ex vivo* whole-blood IMQ challenges. Prednisolone significantly suppressed the objectified transient clinical response to IMQ (imaging-based perfusion and erythema) as well as clinically graded erythema. An interesting finding was the inhibitory effect of prednisolone on epidermal thickness measured by optical coherence tomography, a noninvasive technique that generates 2D images of tissue microstructure. In a psoriasiform murine model, an abundance of infiltrating cells resulted in a significant increase in epidermal thickness (10). This is in line with our study, which showed

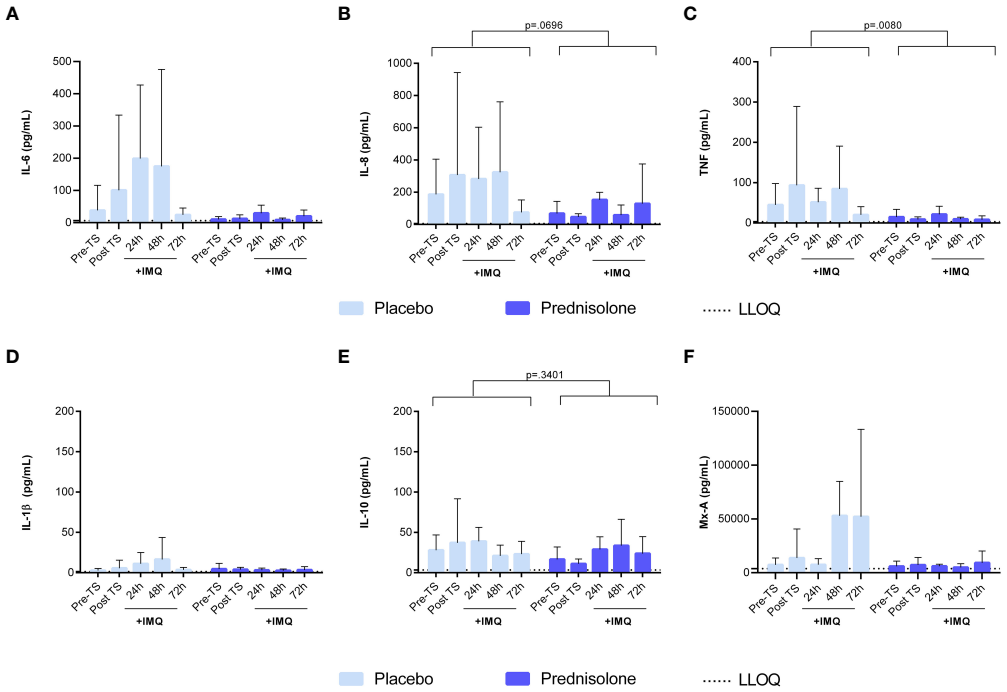

FIGURE 5
Prednisolone suppresses the NF-κB driven cytokines and IRF7 driven response in blister fluid. **(A)** IL-6 **(B)** IL-8 **(C)** TNF **(D)** IL-1b **(E)** IL-10 **(F)** Mx-A. Cytokine concentrations in blister fluid were analysed by MSD and Mx-A by ELISA. Data are presented as mean ± SD. For IL-6, IL-1b and Mx-A no statistical model was applied as the majority of the values were <LLOQ in the prednisolone group. ELISA, enzyme- linked immunosorbent assay; IL, interleukin; LLOQ, lower limit of quantification; MSD, meso scale discovery; TNF, tumor necrosis factor; TS, tape stripped.

an IMQ-driven increase in epidermal thickness at 48 h, suggesting the initiation of an inflammatory response.

To our knowledge, this is the first clinical study to examine the effect of prednisolone on TLR7-driven cellular and cytokine responses *in vivo*. Previous studies have evaluated the local immune response following topical IMQ application. In these studies, dermal cellular and cytokine responses to IMQ were characterized using immunohistochemistry and qPCR. IMQ treatment upregulated chemokines (IP-10), pro-inflammatory cytokines (IL-6), and interferons (Mx-A and IFN-γ). Elevated CD14, CD1a, CD11c, CD4+, and CD8+ cell numbers were observed following IMQ application on tape-stripped skin, peaking at 48- and 72-hour post-dose, comparable to the IHC results in this study (6, 7). However, the current study also evaluated IMQ-driven cellular responses in the skin by flow cytometric analysis of suction blister exudate, providing a more quantitative impression of the inflammatory response. Upon IMQ treatment, a mild influx of NK cells, dendritic cells, and classical monocytes was observed. Oral administration of prednisolone fully suppressed this cell infiltration, confirming the strong anti-inflammatory activity of the compound. Notably, no traces of neutrophils were found in blister fluid, indicating that the applied IMQ regimen did not drive neutrophil attraction, which contradicts earlier preclinical findings, following topical IMQ treatment for 5–6 consecutive days in mice (11). This results in an influx of neutrophils that accumulate beneath the stratum corneum. The absence of neutrophil infiltration in our study may be explained by the duration of IMQ application. The current duration of 48 h IMQ application might not be sufficient to initiate neutrophil influx; therefore, a prolonged application is suggested to align more with the duration in preclinical studies. In contrast to IMQ, LPS drives an acute and strong innate immune response characterized by an influx of neutrophils (peaking at 10 h), monocytes, and NK cells (peaking at 24 h post injection) (8).

TLR7 activation generally drives IRF and NF-κB signaling, playing an important role in the recruitment of immune cells to the dermis (12). Topical application of IMQ resulted in a clear increase in Mx-A concentrations in the blister exudate at 48 and 72 h, indicative of IRF-mediated production of type 1 interferons. Although it is expected to initiate NF- κB signaling and cytokine production (12–14), only a mild IL-6 response was observed, whereas other NF- κB-driven cytokine responses (IL-8, IL-1β, and IL-10) were limited or absent. The relatively mild inflammatory response at the molecular level may be explained by a potentially limited IMQ exposure, related to the partial delivery of applied IMQ to the dermal tissue. Alternatively, the low NF- κB responses may be explained by the timing of the sampling: the innate immune system is activated in phases, with the initial phase resulting in the secretion of proinflammatory cytokines generally occurring within 24 h (5, 15, 16). It is possible that our first post-IMQ blister time point was too late to detect the early innate immune response driven by IMQ. Lastly, it is possible that IMQ in this formulation and in the current regimen, for these types of innate immune challenges, is simply a weak immune agonist compared to LPS. This is also supported by the relatively mild cellular responses observed. Despite the small cytokine responses, a

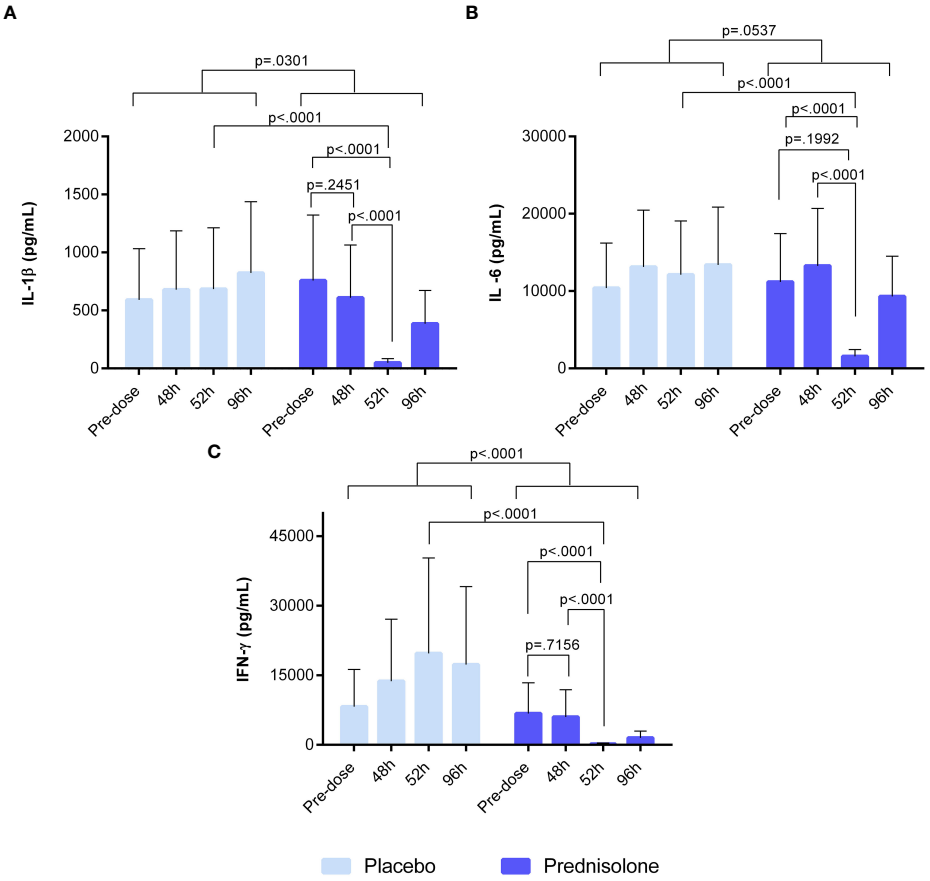

FIGURE 6
Ex-vivo whole blood stimulated with 20 µg/ml IMQ. **(A)** IL-1b **(B)** IL-6 **(C)** IFN-g. Cytokine concentrations in blood were analysed by V-plex and MSD. Pre-dose time point refers to sample taken prior to prednisolone/placebo dosing. The time point 48h refers to sample taken at 48h after initial dose but before the 5th dose of prednisolone/placebo. Sample taken at 52h refers to time point 4 hours after 5th dose. At 96h after prednisolone/placebo, the sample was taken before the 8th dose. IFN, interferon; IL, interleukin; MSD, meso scale discovery.

clear effect of prednisolone treatment was observed: Mx-A, IL-6, TNF, and IL-1β responses to IMQ were significantly lower in prednisolone-treated volunteers (although for Mx-A, IL-6, and IL-1β, no formal p-value could be calculated given the substantial number of samples with cytokine levels below the limit of quantification in the prednisolone-treated group). For future studies, the abovementioned readouts can be used to evaluate the effect of IMQ.

Interestingly, oral prednisolone and topical clobetasol treatment did not significantly suppress dermal cytokine responses in an earlier human challenge study that applied intradermal LPS injections, driving TLR4-mediated responses (8). This contrasts with the effects of prednisolone on the IMQ-driven cytokine responses observed in the current study. The difference in treatment response might be explained by the more pronounced dermal cytokine response driven by LPS (~5- to 100-fold) compared to IMQ. This difference in challenge response size, also reflected at the cellular level, may be explained by the different routes of administration—intradermal for LPS versus topical for IMQ—leading to differences in intradermal concentrations. Furthermore, LPS may act as a potent immune agonist. The argument that a stronger immune response is more difficult to counteract by corticosteroids is contradicted by the efficient suppression of LPS-driven skin perfusion, erythema, and local cell attraction by prednisolone and clobetasol. Therefore, the successful suppression of IMQ-driven cytokine responses by prednisolone, versus the poor suppression of LPS-driven responses of the same cytokines, should be investigated at the physiological level: the difference between TLR4 and TLR7 signaling.

Finally, the *ex vivo* pharmacological activity of prednisolone was monitored using whole-blood IMQ. Prednisolone treatment resulted in a significant reduction of IFN-γ, IL-1β, and IL-6 release, but only when measured at 52 h after initiation of prednisolone treatment, which was 4 h after the previous prednisolone intake. Cytokine release was not suppressed 48 and 96 h after the first prednisolone administration. This may be explained by the pharmacokinetic profile of prednisolone which is complex in humans (17). Prednisolone is rapidly absorbed and available between 80% and 100% after oral intake. The plasma concentration peaks 1 to 2 h after administration and the corresponding half-lives vary between 2.5 and 6.6 h and are dose-dependent (18, 19). At 48 and 96 h, shortly before the next prednisolone dose, the suppressive effect of prednisolone was negligible because the systemic concentration of the drug was

considered low. Of interest, the reductions in cytokine levels in blister fluid are less dependent on the pharmacokinetic profile of prednisolone, which is concordant with the literature describing that no relationship has been demonstrated between prednisolone concentration in blood and therapeutic effect (20, 21). This discrepancy between the systemic drug activity measured in whole blood cultures *ex vivo* and the peripheral drug effect evaluated in skin *in vivo* underlines the value of *in vivo* human immune challenges such as the topical IMQ challenge for evaluation of drug effects.

In this clinical study, we successfully demonstrated that orally administered prednisolone at a conventional clinical dose suppresses IMQ-induced skin inflammation in healthy volunteers, which underlines the potential value of this cutaneous challenge model for future clinical pharmacology studies with novel anti-inflammatory compounds targeting the TLR7 pathway. In these studies, prednisolone can be used as a benchmark.

Data availability statement

The original contributions presented in the study are included in the article/Supplementary Material. Further inquiries can be directed to the corresponding author.

Ethics statement

The studies involving human participants were reviewed and approved by Stichting Beoordeling Ethiek Biomedisch Onderzoek. The patients/participants provided their written informed consent to participate in this study.

Author contributions

MM devised the project and main conceptual ideas together with SA, TB, NT, and MJ. SA, TB, MJ, and MM worked out technical details and study design. SA and TB coordinated the clinical trial. PH coordinated and performed bioanalysis. NK carried the medical responsibility. SA, TB, MM, MJ, CH, and PH analyzed and interpreted data. MK carried out statistical analysis. SA, TB, MJ, and MM wrote the manuscript. All authors listed have made a substantial, direct, and intellectual contribution to the work and approved it for publication.

Funding

This research was funded by the Centre for Human Drug Research, Leiden, The Netherlands.

Acknowledgments

The authors thank all the healthy volunteers who participated in this clinical research. In addition, the authors thank the operational staff members who were involved in the setup, clinical conduct, and data analysis of this study.

Conflict of interest

The authors declare that the research was conducted in the absence of any commercial or financial relationships that could be construed as a potential conflict of interest.

Publisher's note

Supplementary material

The Supplementary Material for this article can be found online at: https://www.frontiersin.org/articles/10.3389/fimmu.2023.1197650/full#supplementary-material

SUPPLEMENTARY FIGURE 1
Clinical erythema assessment by physician.

SUPPLEMENTARY FIGURE 2
Gating strategy used for flow cytometry analysis of the blister exudate.

SUPPLEMENTARY TABLE 1
Overview of number of samples per assessment.

SUPPLEMENTARY TABLE 2
Overview of whole blood *ex vivo* results stimulated and unstimulated with IMQ 20µg/ml.

References

1. Borcherding SM. Drugs: from discovery to approval. *J Pharm Technol* (2004) 20:364–4. doi: 10.1177/875512250402000621

2. Pocock SJ. *Clinical trials: a practical approach*. Chichester: Wiley & Sons (2013) p. 1–263.

3. Sedgwick P. What are the four phases of clinical research trials? *BMJ* (2014) 348:1–2. doi: 10.1136/bmj.g3727

4. Cohen AF, Burggraaf J, van Gerven JMA, Moerland M, Groeneveld GJ. The use of biomarkers in human pharmacology (Phase I) studies. *Annu Rev Pharmacol Toxicol* (2015) 55(1):55–74. doi: 10.1146/annurev-pharmtox-011613-135918

5. Flutter B, Nestle FO. TLRs to cytokines: mechanistic insights from the imiquimod mouse model of psoriasis. *Eur J Immunol* (2013) 43(12):3138–46. doi: 10.1002/eji.201343801

6. van der Kolk T, Assil S, Rijneveld R, Klaassen ES, Feiss G, Florencia E, et al. Comprehensive, multimodal characterization of an imiquimod-induced human skin inflammation model for drug development. *Cts-Clinical Transl Sci* (2018) 11(6):607–15. doi: 10.1111/cts.12563

7. Niemeyer-van der Kolk T, Assil S, Buters TP, Rijsbergen M, Klaassen ES, Feiss G, et al. Omiganan enhances imiquimod-induced inflammatory responses in skin of healthy volunteers. *Clin Transl Sci* (2020) 13(3):573–9. doi: 10.1111/cts.12741

8. Buters TP, Hameeteman PW, Jansen IME, van Hindevoort FC, Ten Voorde W, Florencia E, et al. Intradermal lipopolysaccharide challenge as an acute *in vivo* inflammatory model in healthy volunteers. *Br J Clin Pharmacol* (2022) 88(2):680–90. doi: 10.1111/bcp.14999

9. Buters TP, Hameeteman PW, Jansen IME, van Hindevoort FC, ten Voorde W, Grievink HW, et al. Clinical, cellular, and molecular effects of corticosteroids on the response to intradermal lipopolysaccharide administration in healthy volunteers. *Clin Pharmacol \& Ther* (2022) 111(4):964–71. doi: 10.1002/cpt.2516

10. Silver R, Helms A, Fu W, Wang H, Diaconu D, Loyd CM, et al. Using optical coherence tomography for the longitudinal non-invasive evaluation of epidermal thickness in a murine model of chronic skin inflammation. *Ski Res Technol Off J Int Soc Bioeng Ski [and] Int Soc Digit Imaging Ski [and] Int Soc Ski Imaging* (2012) 18 (2):225–31. doi: 10.1111/j.1600-0846.2011.00558.x

11. van der Fits L, Mourits S, Voerman JSA, Kant M, Boon L, Laman JD, et al. Imiquimod-induced psoriasis-like skin inflammation in mice is mediated *via* the IL-23/IL-17 axis. *J Immunol* (2009) 182(9):5836–45. doi: 10.4049/jimmunol.0802999

12. Schön MP, Schön M. Imiquimod: mode of action. *Br J Dermatol* (2007) 157 (SUPPL. 2):8–13. doi: 10.1111/j.1365-2133.2007.08265.x

13. Megyeri K, Au WC, Rosztoczy I, Raj NB, Miller RL, Tomai MA, et al. Stimulation of interferon and cytokine gene expression by imiquimod and stimulation by Sendai virus utilize similar signal transduction pathways. *Mol Cell Biol* (1995) 15(4):2207–18. doi: 10.1128/MCB.15.4.2207

14. Gibson SJ, Imbertson LM, Wagner TL, Testerman TL, Reiter MJ, Miller RL, et al. Cellular requirements for cytokine production in response to the immunomodulators imiquimod and s-27609. *J Interf Cytokine Res Off J Int Soc Interf Cytokine Res* (1995) 15 (6):537–45. doi: 10.1089/jir.1995.15.537

15. Olesen CM, Fuchs CSK, Philipsen PA, Hædersdal M, Agner T, Clausen M-L. Advancement through epidermis using tape stripping technique and reflectance confocal microscopy. *Sci Rep* (2019) 9(1):12217. doi: 10.1038/s41598-019-48698-w

16. Heib V, Becker M, Warger T, Rechtsteiner G, Tertilt C, Klein M, et al. Mast cells are crucial for early inflammation, migration of langerhans cells, and CTL responses following topical application of TLR7 ligand in mice. *Blood [Internet]* (2007) 110 (3):946–53. doi: 10.1182/blood-2006-07-036889

17. Bashar T, Apu MNH, Mostaid MS, Islam MS, Hasnat A. Pharmacokinetics and bioavailability study of a prednisolone tablet as a single oral dose in bangladeshi healthy volunteers. *Dose-Response* (2018) 16(3):1–6. doi: 10.1177/1559325818783932

18. Tanner A, Bochner F, Caffin J, Halliday J, Powell L. Dose-dependent prednisolone kinetics. *Clin Pharmacol Ther* (1979) 25(5 Pt 1):571–8. doi: 10.1002/cpt1979255part1571

19. Al-Habet S, Rogers HJ. Pharmacokinetics of intravenous and oral prednisolone. *Br J Clin Pharmacol* (1980) 10(5):503–8. doi: 10.1111/j.1365-2125.1980.tb01796.x

20. Pickup ME. Clinical pharmacokinetics of prednisone and prednisolone. *Clin Pharmacokinet* (1979) 4(2):111–28. doi: 10.2165/00003088-197904020-00004

21. Kauh E, Mixson L, Malice MP, Mesens S, Ramael S, Burke J, et al. Prednisone affects inflammation, glucose tolerance, and bone, turnover within hours of treatment in healthy individuals. *Eur J Endocrinol* (2012) 166(3):459–67. doi: 10.1530/EJE-11-0751

frontiers | Frontiers in Immunology

TYPE Original Research
PUBLISHED 24 August 2023
DOI 10.3389/fimmu.2023.1232586

OPEN ACCESS

EDITED BY
Oliver Planz,
University of Tübingen, Germany

REVIEWED BY
Samuel Lara-Reyna,
University of Birmingham, United Kingdom
Leah Marie Wuescher,
University of Toledo, United States
Sonali Singh,
University of Nottingham, United Kingdom
Anne Rokstad,
Norwegian University of Science and Technology, Norway

*CORRESPONDENCE
Lindsay E. Fitzpatrick
lindsay.fitzpatrick@queensu.ca

RECEIVED 31 May 2023
ACCEPTED 02 August 2023
PUBLISHED 24 August 2023

CITATION
McKiel LA, Ballantyne LL, Negri GL, Woodhouse KA and Fitzpatrick LE (2023) MyD88-dependent Toll-like receptor 2 signaling modulates macrophage activation on lysate-adsorbed Teflon™ AF surfaces in an *in vitro* biomaterial host response model.
Front. Immunol. 14:1232586.
doi: 10.3389/fimmu.2023.1232586

MyD88-dependent Toll-like receptor 2 signaling modulates macrophage activation on lysate-adsorbed Teflon™ AF surfaces in an *in vitro* biomaterial host response model

Laura A. McKiel[1], Laurel L. Ballantyne[1,2], Gian Luca Negri[3], Kimberly A. Woodhouse[1] and Lindsay E. Fitzpatrick[1,2,4]*

[1]Department of Chemical Engineering, Faculty of Engineering and Applied Sciences, Queen's University, Kingston, ON, Canada, [2]Centre for Health Innovation, Queen's University and Kingston Health Sciences, Kingston, ON, Canada, [3]Independent Researcher, Kingston, ON, Canada, [4]Department of Biomedical and Molecular Sciences, Faculty of Health Sciences, Queen's University, Kingston, ON, Canada

The adsorbed protein layer on an implanted biomaterial surface is known to mediate downstream cell-material interactions that drive the host response. While the adsorption of plasma-derived proteins has been studied extensively, the adsorption of damage-associated molecular patterns (DAMPs) derived from damaged cells and matrix surrounding the implant remains poorly understood. Previously, our group developed a DAMP-adsorption model in which 3T3 fibroblast lysates were used as a complex source of cell-derived DAMPs and we demonstrated that biomaterials with adsorbed lysate potently activated RAW-Blue macrophages via Toll-like receptor 2 (TLR2). In the present study, we characterized the response of mouse bone marrow derived macrophages (BMDM) from wildtype (WT), TLR2$^{-/-}$ and MyD88$^{-/-}$ mice on Teflon™ AF surfaces pre-adsorbed with 10% plasma or lysate-spiked plasma (10% w/w total protein from 3T3 fibroblast lysate) for 24 hours. WT BMDM cultured on adsorbates derived from 10% lysate in plasma had significantly higher gene and protein expression of IL-1β, IL-6, TNF-α, IL-10, RANTES/CCL5 and CXCL1/KC, compared to 10% plasma-adsorbed surfaces. Furthermore, the upregulation of pro-inflammatory cytokine and chemokine expression in the 10% lysate in plasma condition was attenuated in TLR2$^{-/-}$ and MyD88$^{-/-}$ BMDM. Proteomic analysis of the adsorbed protein layers showed that even this relatively small addition of lysate-derived proteins within plasma (10% w/w) caused a significant change to the adsorbed protein profile. The 10% plasma condition had fibrinogen, albumin, apolipoproteins, complement, and fibronectin among the top 25 most abundant proteins. While proteins layers generated from 10% lysate in plasma retained fibrinogen and fibronectin among the top 25 proteins, there was a disproportionate increase in intracellular proteins, including histones, tubulins, actins, and vimentin. Furthermore, we identified 7 DAMPs or DAMP-related proteins enriched in the 10% plasma condition (fibrinogen, apolipoproteins), compared to 39 DAMPs enriched in the 10% lysate in plasma

condition, including high mobility group box 1 and histones. Together, these findings indicate that DAMPs and other intracellular proteins readily adsorb to biomaterial surfaces in competition with plasma proteins, and that adsorbed DAMPs induce an inflammatory response in adherent macrophages that is mediated by the MyD88-dependent TLR2 signaling pathway.

KEYWORDS

biomaterials, macrophage, toll-like receptors, damage-associated molecular patterns, protein adsorption, foreign body reaction, insulin infusion cannulas, polytetrafluoroethylene

1 Introduction

The immune response to biomaterial implants, known as the foreign body reaction (FBR), is a significant challenge in the biomedical engineering field (1). The FBR describes a chronic inflammatory response to an implanted material or device, which culminates in the fibrous encapsulation of the implant (1). For certain applications, including some drug delivery devices, the fibrotic capsule prevents the implant from performing its intended function, resulting in implant failure (1). The FBR is initiated upon material implantation and the associated tissue damage. The implant surface rapidly adsorbs proteins from the surrounding fluid phase that contains both blood released from damaged blood vessels and contents released from damaged cells in the implant microenvironment, which includes damage-associated molecular patterns (DAMPs) (1). Neutrophils and then macrophages are recruited to the implant site, and interact with the implant via this adsorbed protein layer (1). Macrophages are known to be key players in the progression of the FBR; they are present at the implant site as early as 24 hours and remain for the lifetime of the implant, they fuse to form foreign body giant cells (FBGC) that are hallmarks of the FBR, and they orchestrate further leukocyte recruitment and downstream tissue remodeling events through paracrine signaling (2).

Due to its impact on the performance and longevity of long-term implants, fibrous capsule formation is frequently the target of research that aims to understand molecular mechanisms that drive the FBR and develop strategies for reducing or eliminating this adverse host response. However, short-term implants, such as glucose sensors and insulin infusion sets (IIS) used in insulin pump therapy, are also adversely impacted by the host response long before fibrosis occurs. In 2019, the Centers for Disease Control and Prevention (CDC) estimated that there were 1.6 million people in the United States of America living with type 1 diabetes (T1D) (3) and, of these, approximately 30 to 40% use insulin pump technology (e.g. continuous subcutaneous insulin infusion (CSII) systems) to deliver insulin and manage blood glucose levels (4). However, there are many challenges with CSII, including complications related to the IIS (5). The IIS consists of a polytetrafluorethylene (PTFE; tradename Teflon^{TM}) or stainless-steel cannula that is inserted into the subcutaneous fat and delivers an insulin analogue solution from the pump to the subcutaneous tissue. Most IIS are approved to be worn for 2 - 3 days, while a newly approved extended infusion set (EIS) can be worn up to 7 days (5). Beyond the recommended wear time, and sometimes even within this period, insulin delivery can become inconsistent, rapidly leading to potentially dangerous side effects of unexplained hyperglycemia and diabetic ketoacidosis (5–7). Emerging evidence suggests that the challenges with variable insulin adsorption in CSII are due, in part, to the acute inflammatory response at the insulin infusion site (8–10).

The acute inflammatory response to biomaterials, including IIS, is characterized by the early events of protein adsorption and macrophage adhesion, activation, and fusion on the material surface. Adsorption of blood-derived proteins on biomaterials surfaces and the response of macrophages to blood-derived adsorbed protein layers has been extensively investigated since the early 1970's, and have focused primarily on adsorption of a handful of plasma proteins, such as albumin, immunoglobulin-γ, fibrinogen, high molecular weight kininogen, complement C3, lipoproteins, fibronectin and vitronectin (11–21). The introduction of proteomic analysis of adsorbed protein layers on biomaterial surfaces has clearly demonstrated that adsorbed protein profiles are significantly more diverse than originally reported but continue to focus predominantly on *in vitro* protein adsorption models using plasma or serum (22–26). However, one proteomic study of proteins adsorbed to the polyethylene glycol (PEG)-based hydrogels *in vivo* demonstrated proteins from the intracellular compartment and extracellular matrix also adsorb within the protein layer (27). In this study, we focus instead on the *in vitro* adsorption of tissue damage products, collectively referred to as DAMPs, and the response of primary mouse bone marrow derived macrophages. This study builds upon previous work from our group demonstrating that DAMP-containing fibroblast lysates adsorb to polymeric surfaces in the presence of blood proteins and induce a pro-inflammatory and pro-fibrotic response in the RAW264.7 and RAW-Blue mouse macrophage cell lines over 120 hours, which mimics the cytokine secretion profile and macrophage fusion of *in vivo* macrophage-material interactions (28, 29). Furthermore, this pro-inflammatory response was shown to occur primarily through Toll-like receptor 2 (TLR2) signaling (28–30). TLR2 is a cell surface TLR that, upon ligation, forms a heterodimer with either TLR1 or TLR6 and induces the myeloid differentiation

primary-response gene 88 (MyD88)-dependent activation of nuclear factor-κB (NF-κB) transcription factors, and the production of pro-inflammatory cytokines, such as tumour necrosis factor α (TNF-α), interleukin 1 beta (IL-1β), and interleukin 6 (IL-6) (31). Other research has also implicated the TLR adaptor protein MyD88 as a critical factor mediating fibrous capsule formation surrounding subcutaneous implants in mice (32). Therefore, we sought to investigate TLR2 and MyD88 as potential targets for reducing the severity of FBR and its impact on biomedical devices and implants.

While role of DAMPs and TLRs in the induction of sterile inflammatory responses is well established (33), the relative importance of TLR signaling in biomaterial host responses remains unclear. Therefore, in this work we evaluated macrophage cultured on model PTFE surfaces using an *in vitro* protein adsorption model that incorporates DAMPs within a plasma-derived protein layer (28) and investigated the role of TLR2- and MyD88-dependent signaling pathways. We first characterized the responses of primary bone marrow derived macrophages (BMDMs) from wildtype (WT), TLR2 knockout ($TLR2^{-/-}$), and MyD88 knockout ($MyD88^{-/-}$) mice to Teflon™ AF surfaces with adsorbed DAMPs and plasma proteins. We then characterized the profile of adsorbed proteins derived from plasma or lysate-spiked plasma using mass spectrometry (MS)-based proteomics to explore what lysate-derived proteins adsorbed within the plasma protein layer and identify potential DAMPs that may contribute to the activation of surface adherent macrophage via TLR2/MyD88 signaling. Plasma anticoagulated with calcium chelators (e.g. K2 EDTA, citrate) were used in this study to inactivate both the complement and coagulation cascades, thus enabling the effect of DAMPs within the adsorbed protein layer to be elucidated. These *in vitro* results provide evidence that TLR-dependent signaling contributes to the acute inflammatory response to model Teflon™ AF surfaces, and merits further investigation into its ability to modulate FBR.

2 Materials and methods

2.1 Teflon™ AF surface preparation

Amorphous fluoropolymer Teflon™ AF 1600 (Sigma-Aldrich, St. Louis, MO), hereafter referred to simply as Teflon™ AF, was used as a cell culture substrate to model the commercial PTFE IIS cannulas. Teflon™ AF is a copolymer of 65 mol% 2-bistrifluoromethyl-4,5-difluoro-1,3-dioxole (PDD) and 35 mol% tetrafluoroethylene (TFE), and has previously been used to model PTFE surfaces by our group (29, 30) and others (34, 35) due to its similar characteristics to PTFE, including wettability (36). However, while both Teflon™ AF and PTFE are fluoropolymers, they have different surface chemistries due to the oxygen content of the PDD comonomer in Teflon™ AF. Teflon™ AF can be easily incorporated into cell culture systems, as it is soluble in perfluorinated solvents and can be cast from solution (29, 30). Furthermore, the amorphous structure of Teflon™ AF imparts excellent optical clarity, which is beneficial when visualizing adherent cells.

Teflon™ AF was dissolved in a fluorinated solvent (FC-40, Sigma-Aldrich) at 1 mg/mL and coated onto 6 well polystyrene plates, using the protocol originally developed by the Grainger group (35). Plates were dried in a vacuum oven (50 cmHg, 40 °C) for 48 hours to remove solvent. The wells were then cleaned with 70% (by volume) ethanol for one hour, followed by 30 minutes of ultraviolet (UV) sterilization (30, 35). Endotoxin-free water washes were performed on the wells for 1 hour (three times), 12 hours, and 24 hours prior to use to remove any remaining solvent. All batches of Teflon™ AF-coated wells were tested indirectly for endotoxin (n = 3 per batch, plated in duplicate) with a LAL Pyrochrome kit (CapeCod and Associates, East Falmouth, MA), and endotoxin levels were consistently below 0.05 EU/mL. Details on the indirect endotoxin assay methods have been previously described (30).

2.2 Plasma and lysate preparations

Innovative Grade US Origin Mouse C57BL6 Plasma (InnovativeResearch, Novi, MI) was used to generated adsorbed protein layers (10% plasma and 10% lysate in plasma) for macrophage experiments. For the proteomic analysis, citrated mouse plasma from C57BL/6J mice, generously provided by Prof. David Lillicrap (Queen's University, Kingston, ON, Canada), was used. Mouse fibroblast lysate was generated by freeze-thaw cycling mouse NIH3T3 fibroblasts (ATCC, Manassas, VA), as described previously (28, 30). Briefly, NIH3T3 murine fibroblasts were maintained in Dulbecco's modified Eagle's medium (DMEM; Sigma-Aldrich, St. Louis, MO) containing 10% fetal bovine serum (FBS; Wisent, St. Bruno, QC) and 1% penicillin/streptomycin. To generate lysate, fibroblasts were washed in phosphate buffered saline (PBS; Gibco, Waltham, MA), resuspended at 5 $x10^6$ cells/mL in PBS, and freeze–thaw cycled three times in a −80°C freezer and 37°C water bath. The total protein concentration of plasma and lysate was quantified using a microBCA assay (Thermo Scientific, Waltham, MA) according to manufacturer instructions, and protein solutions were aliquoted and stored at −80°C for future use.

2.3 Protein adsorption on Teflon™ AF surfaces

Mouse plasma was diluted to 10 vol% in PBS and was referred to hereafter as "10% plasma" or abbreviated as "Pla". Lysate was spiked into the 10% plasma solution, such that lysate made up 10% of the total protein concentration and was referred to hereafter as "10% lysate in plasma" or abbreviated as "LysPla". Teflon™ AF-coated 6 well plates were pre-conditioned with 10% plasma (420 μg/cm^2), 10% lysate in plasma (420 μg total protein/cm^2 = 42 μg lysate protein/cm^2 + 378 μg plasma protein/cm^2), or assay media (RPMI 1640 with 10% FBS; for Pam3SCK4 positive controls) for 60 minutes. The FBS used in this study was not heat inactivated. Following protein adsorption, surfaces were gently washed with

PBS (three times, 5 minutes) then used immediately for cell culture or proteomic experiments.

2.4 Primary macrophage isolation and treatment

All animal work was approved by the Queen's University (Kingston, ON, Canada) UACC (AUP 2018-1849). Bone marrow isolations were performed on wildtype (C57BL/6J, WT, stock# 000664), TLR2 knockout (TLR2$^{-/-}$, stock# 004650) (37), and MyD88 knockout (MyD88$^{-/-}$, stock# 009088) (38) mice (Jackson Laboratories, Bar Harbour, ME) that were bred and raised under sterile conditions in the Queen's University Animal Care Facility. Prior to bone marrow isolations, mouse genotype was confirmed by PCR using a 1% agarose gel, based on manufacturer's recommended protocols. The hind legs were removed and cleaned of tissue, then the bone marrow was flushed from the femur and tibia with sterile PBS, and red blood cells were with lysed with ammonium chloride. The remaining bone marrow cells were incubated in RPMI media (RPMI 1640, Sigma-Aldrich) containing 20% L929 supernatant, 10% FBS, and 50 µg/mL gentamicin and allowed to differentiate for at least 7 days (39). Differentiated bone marrow derived macrophages (BMDM) were used on day 7 to 10 for all experiments. Each isolation pooled bone marrow from multiple mice (WT: 8 mice, TLR2$^{-/-}$ & MyD88$^{-/-}$: 6 mice) and equal numbers of male and female mice were used for each bone marrow isolation to account for differences in TLR expression of murine macrophages between sexes (40). Four separate bone marrow isolations (from different litters of mice) were performed for each mouse genotype, giving a total of 32 WT mice, 24 TLR2$^{-/-}$ mice and 24 MyD88$^{-/-}$ mice used for this study.

BMDMs were washed with PBS (Gibco, Waltham, MA) and detached by incubation in TrypLE™ (Gibco) at 37 °C for 10 minutes. Cells were counted, resuspended in assay media, and plated in triplicate at 2.6 x 10^5 cells/cm^2 in the prepared Teflon™ AF coated wells with adsorbed protein layers. Pam3CSK4 (150 ng/mL, Cat. No. tlrl-pms, purity ≥ 95% (UHPLC), Invivogen) was included as a positive control for TLR2 signaling. Cells were cultured under the above conditions for 24 hours, followed by supernatant collection and RNA isolation for downstream analysis.

2.5 Flow cytometry

After the differentiation period, BMDM viability and differentiation was confirmed using flow cytometry (41). Cells were washed with PBS and detached by incubation in TrypLE™ (Gibco) at 37 °C for 10 minutes. Cells were resuspended at approximately 2 x 10^6 cells/100 µL in PBS and incubated in 10 µg/mL anti-mouse CD16/32 (TruStain fcX™; Biolegend) on ice for 10 minutes, followed by incubation with Zombie NIR® (cat. No. 423105, Biolegend, San Diego, CA), 500 ng/ml of anti-mouse F4/80 (cat. No. 123115, Biolegend) and 1.25 µg/mL anti-mouse CD11b (cat no. 101235, Biolegend) on ice protected from light for 20 minutes. Cells were washed three times with staining buffer (5% FBS), and then resuspended in PBS. Flow cytometry was performed using a Beckman Coulter Cytoflex machine. Dead cells and cellular debris were gated out using a cell viability dye (Zombie NIR®, Biolegend), and an unstained control was used to confirm successful cell staining.

2.6 Quantitative PCR

RNA was collected from BMDMs after being cultured for 24 hours on Teflon™ AF surfaces using the RNeasy® mini kit (Qiagen, Hilden, Germany) according to manufacturer's instructions. RNA was eluted in 30 µL of TE buffer and stored at -80 °C for future use. RNA concentrations and purity were measured using a NanoDrop One Spectrophotometer (Thermo Fisher Scientific, Waltham, MA) and all RNA samples had A260/A280 ≥ 1.8, A260/A230 ≥ 2.0. RNA quality was confirmed via non-denaturing agarose gel electrophoresis, by ensuring a 28S/18S intensity ratio of 2 or higher and no visible smear below the 18S band.

Isolated RNA was transcribed into cDNA using the iScript™ Reverse Transcription Supermix (BioRad) with 1 µg of RNA in each 20 µL reaction, according to manufacturer instructions. No reverse transcriptase (NRT) controls were made with RNA from WT BMDMs from each experimental condition (10% plasma, 10% lysate in plasma, Pam3CSK4) and run in a qPCR experiment to confirm there was no genomic DNA contamination after the RNA isolation procedure.

Specific murine primers for *Il10*, *Nos2*, and *Tnfα* were purchased from BioRad (*Il10*: qMmuCED0044967, *Nos2*: qMmuCID0023087, *Tnfα*: qMmuCEP0028054).The remaining primers were designed using PrimerBlast (42) and are listed in Table 1. qPCR was performed using SsoAdvanced Universal SYBR Green Supermix (BioRad), according to manufacturer instructions. The qPCR assay was run in a BioRad CFX384 system using 10 µL reactions in a 384 well plate, with 300 nM primers and 10 ng cDNA at 60 °C, with three biological replicates and conditions plated in quadruplicate. The relative gene expression ratio (R) was calculated using 2 reference genes (*Rplp0*, *Rpl13*), as described below (43). A plate of NRT controls was run to confirm there was no genomic DNA contamination in the RNA samples, and no amplification occurred in any NRT wells. No template controls (NTCs) were included in all assays (n = 3), and melt curves were performed at the end of every experiment to ensure no primer-dimers were formed.

Data analysis of qPCR experiments was performed using a method described by Vandesompele et al. (43–45), which calculates the relative gene expression of each sample using the Ct values, and accounts for the use of two reference genes. Each biological replicate (n = 3, per experiment) was treated separately (46), and the geometric mean of the relative gene expression (R) was reported for each experiment (N = 4). Results were normalized to the 10% plasma condition (negative control) for each genotype. A two-way ANOVA of the log transformed normalized relative expression (NRE) was performed in GraphPad Prism 8.4.2 (GraphPad Software, San Diego, CA) to determine statistical difference in relative gene expression among treatment groups within a given genotype using an $\alpha = 0.05$, as described by Taylor et al. (47).

TABLE 1 Primer sequences used in qPCR.

Gene	Accession Number	Forward Sequence (5′-3′)	Reverse Sequence (5′-3′)
Arg1	NM_007482.3	GTACATTGGCTTGCGAGACG	ATCGGCCTTTTCTTCCTTCCC
IL-1β	NM_008361.4	TGCCACCTTTTGACAGTGATG	ATGTGCTGCTGCGAGATTTG
IL-6	NM_031168	TAGTCCTTCCTACCCCAATTTCC	TTGGTCCTTAGCCACTCCTTC
MyD88	NM_010851.3	GAGGATATACTGAAGGAGCTGAAGTC	CCTGGTTCTGCTGCTTACCT
*Rpl13a	NM_009438.5	ATCCCTCCACCCTATGACAA	GCCCCAGGTAAGCAAACTT
*Rplp0	NM_007475.5	GGGCATCACCACGAAAATCTC	CTGCCGTTGTCAAACACCT
TGF-β1	NM_011577.2	AGCTGCGCTTGCAGAGATTA	AGCCCTGTATTCCGTCTCCT
TLR2	NM_011905.3	GGTGCGGACTGTTTCCTTCT	GAGATTTGACGCTTTGTCTGAGG
TLR4	NM_021297.3	TCCACTGGTTGCAGAAAATGC	TTAGGAACTACCTCTATGCAGGG

Arg1, Arginase 1; IL-1b, Interleukin 1 beta; IL-6, Interleukin 6; MyD88, Myeloid differentiation primary-response gene 88; Rpl13a, Ribosomal protein L13a; Rplp0, Ribosomal protein lateral stalk subunit P; TGF-β1, Transforming growth factor beta 1; TLR2, Toll-like receptor 2; TLR4, Toll-like receptor 4.
*Reference gene.

Changes in gene expression were only considered significant if median relative expression ratio (R) was less than 0.5 or greater than 2 ($0.5 > R > 2$) and the associated $\log_2$NRE p-value was less than 0.05.

2.7 Multiplexed bead-based cytokine assay

The supernatants of BMDMs cultured on Teflon™ AF-coated 6 well plates for 24 hours under the conditions of interest were collected, centrifuged at 1000 x g for 10 minutes to remove cellular debris, and stored at -80 °C for future analysis. The BMDM secretion of a variety of chemokines and cytokines was assessed using a Luminex assay (MilliPlex Magnetic 9-plex custom kit; MilliporeSigma, Burlington, MA), according to manufacturer directions. Samples were run undiluted in duplicate to measure the concentration of IL-1β, IL-6, IL-10, TNF-α, CXCL1 (keratinocyte chemoattractant, KC), CCL2 (monocyte chemotactic protein 1, MCP-1), CCL3 (macrophage inflammatory protein-1α, MIP-1 α), CCL5 (regulated upon activation, normal T cell expressed and secreted; RANTES), and vascular endothelial growth factor-A (VEGF-A) in the BMDM supernatant. Samples were plated across three 96 well plates, ensuring that samples from all conditions were present on each plate. On one plate the RANTES and VEGF-A samples did not pass the internal quality control, therefore, those points were excluded in the data analysis. Data was processed to obtain standard curves and cytokine concentrations using the BioPlex system (Ellis lab, Queen's University; BioRad). Cytokine concentrations that were detectable but below the lowest standard were extrapolated and included in the data analysis. Non-detectable cytokine concentrations below the lower limit of detection excluded. Data points that were outside the lower and upper bounds of 1.5 times the interquartile range were considered outliers and excluded. Statistical analysis was performed in GraphPad Prism 8.4.3 (GraphPad Software, San Diego, CA) using a Brown-Forsythe and Welch ANOVA and Dunnett T3 *post-hoc* tests to determine significant differences among conditions. According to a power analysis, $p < 0.05$ was considered a statistically significant difference. Conditions that had less than 3 data points were not statistically analyzed. Results are displayed as mean ± SD, unless otherwise stated.

2.8 Proteomic analysis of adsorbed protein layers

2.8.1 Liquid chromatography-tandem mass spectroscopy

Teflon™ AF coated well plates pre-conditioned with 10% plasma (with citrate) or 10% lysate in plasma were stored at 4 °C with 2 ml PBS/well overnight and then shipped on ice to the SPARC BioCentre (Molecular Analysis) at the Hospital for Sick Children (Toronto, Canada). The adsorbed protein from media containing 10% FBS was not analyzed. Proteomic samples were prepared using suspension trapping or S-trap high recovery method by the Sparc BioCenter. Briefly, adsorbed proteins from duplicate wells were scrapped into 8M urea, 5% sodium dodecyl sulfate (SDS) in 50 mM triethylamonium bicarbonate (TEAB) at pH 7.55 (50 µL). Samples were reduced using 4.6 mM tris carboxy ethyl phosphene (TCEP) at 37 °C for 15 minutes, then alkylated using 18.5 mM iodoacetamide in the dark for 30 minutes. Samples were loaded on to the S-Trap column (Protifi, Farmingdale, NY, USA) and digested on-column using 2.5 µg trypsin (Pierce) at 47 °C for 2 hours. Peptides were then eluted from the S-Trap column using four stepwise buffers: (1) 50mM TEAB (pH 8.0); (2) 0.1% formic acid; (3) 50% acetonitrile, 0.2% formic acid; and (4) 80% acetonitrile, 0.2% formic acid. The peptide solutions were lyophilized using a Speedvac, and resuspended in 2% acetonitrile, 0.1% formic acid.

Liquid chromatography–tandem mass spectrometry (LC–MS/MS) analysis was performed using an EASY-nLC 1200 nano-LC system coupled to a Orbitrap Fusion Lumos (Thermo Scientific). Peptides (1 µg peptide per sample) were loaded onto a PepMax RSLC EASY-Spray column (Thermo, 75 µm x 50 cm filled with 2 µM C18 beads; 900 Bar, 60°C) and separated over a 60-minute gradient of 3-35% organic phase (0.1% formic acid in acetonitrile) at 250 nl/min. Peptides were then analyzed using the Orbitrap Fusion Lumos mass spectrometer

operating at 120 000 resolution over a mass range of m/z 375-1500. The raw data was searched against the mouse protein sequence database (Uniprot_UP000000589_Mouse_15092020.fasta) using Thermo Scientific Proteome Discoverer software (version 2.5.0.400).

2.8.2 Proteomics analysis and protein classification

The database search results were imported to Scaffold (Scaffold_5.1.2) and the protein intensities, normalized on total precursor intensities, were retrieved. Proteins with FDR < 0.01 and covered by at least 2 peptides (FDR< 0.01) were retained for downstream analysis. Missing values were imputed by random sampling from the 1st percentile of all data distribution.

Differential protein expression analysis was calculated by moderate t-test using limma r package (48) on the log2 transformed protein intensities. A multiple testing adjusted p-value < 0.05 was considered significant (49). Gene set enrichment analysis (GSEA) was performed with the r package fgsea (50) (minsize = 2, maxsize = 500) on the ranked t-statistic, using the mouse gene ontology (GO) terms from the Molecular Signature Database (MSigDB) (51). GO enrichment was calculated for proteins significantly upregulated in Pla versus LysPla by a fold-change greater than 2; and proteins significantly upregulated in LysPla versus Pla by a fold-change greater than 2, by the gprofiler r package (52, 53) (organism = "mmusculus", ordered_query = FALSE, exclude_iea = TRUE, user_threshold = 0.05, correction method = "g_SCS", domain_scope = "annotated").

A list of protein DAMPs was compiled from literature (Supplemental Table 1) and the list of proteins with differential expression (adjusted p-value < 0.05) was manually searched for known DAMP species in Excel (Microsoft) using the search terms listed. Identified DAMPs were highlighted in a volcano plot of the log2 foldchange (Pla vs LysPla) vs log(adjusted p-value) generated in GraphPad Prism. The mass spectrometry proteomics data have been deposited to the ProteomeXchange Consortium via the PRIDE (54) partner repository with the dataset identifier PXD042730.

3 Results

Prior to bone marrow isolation, mice were genotyped using TLR2 and MyD88 primers to confirm knockout genotype (Supplemental Figure 1). BMDM from WT, TLR2$^{-/-}$ and MyD88$^{-/-}$ bone marrow isolates were successfully differentiated into macrophages, with more than 93.5% of the populations staining positive for F4/80 and CD11b (Supplemental Figure 2). Representative light microscopy images showing BMDM morphology for each mouse strain and three culture conditions are provided in Supplemental Figure 3.

3.1 Gene expression of macrophages on Teflon™ AF

We first quantified the gene expression profile of cytokines and growth factors with well-documented roles in the progression of biomaterial host responses to study the effect of the adsorbed protein layer derived from 10% lysate in plasma on WT, TLR2$^{-/-}$ and MyD88$^{-/-}$ BMDM, compared to adsorbed protein layers derived only from plasma and soluble TLR2 agonist, Pam3CSK4. The mRNA expression of pro-inflammatory cytokines (IL-1β, IL-6 and TNF-α), anti-inflammatory cytokine IL-10 and pro-fibrotic growth factor TGF-β1 was quantified after 24 hours.

The expression of genes encoding cytokines IL-1β, IL-6 and IL-10 was significantly upregulated in WT BMDMs exposed to adsorbed 10% lysate in plasma (LysPla) and Pam3CSK4 (Pam), compared to adsorbed 10% plasma (Pla) after 24 hours (Figures 1A, B, D). The effect of lysate and Pam3CSK4 was lost in TLR2$^{-/-}$ and MyD88$^{-/-}$ BMDMs, where gene expression appeared to be similar or slightly downregulated compared to 10% plasma, though these differences failed to show a statistically significant effect. Conversely, TNF-α mRNA expression was downregulated approximately 3-fold in WT BMDMs on adsorbed lysate at 24 hours ($R = 0.32$, $p < 0.01$ for LysPla vs Pla), while adsorbed lysate had no effect in the TLR2$^{-/-}$ or MyD88$^{-/-}$ BMDM (Figure 1C). Treatment with Pam3CSK4 caused a two-fold downregulation in TNF-α expression at 24 hours for the TLR2$^{-/-}$ BMDM ($R = 0.48$, $p < 0.001$ for Pam vs Pla), but had no effect at the mRNA level for the WT or MyD88$^{-/-}$ BMDM. The expression of TGF-β was also slightly downregulated at 24 hours in the WT BMDM for the lysate and Pam3CSK4 conditions ($R = 0.53$ and 0.57 respectively, $p < 0.001$ vs Pla), but was not considered to be biologically relevant as $R > 0.05$. No modulation of TGF-β expression was observed for any conditions in the TLR2$^{-/-}$ or MyD88$^{-/-}$ BMDM (Figure 1E).

We next looked at the expression of genes encoding enzymes nitric oxide synthase 2 (Nos2) and Arginase 1 (Arg1) to gain insight into macrophage arginine metabolism (Figure 2) (55). Relative to BMDM cultured on adsorbates derived from 10% plasma, WT BMDM cultured on lysate-containing adsorbates had increased expression of both Nos2 and Arg1 ($R = 18.9$ and 37.9, $p < 0.001$, respectively). Treatment with Pam3CSK4 yielded a 50.5-fold increase in Nos2 expression and 27.9-fold increase in Arg1 expression, compared to 10% plasma ($p < 0.001$). BMDM derived from TLR2-deficient and MyD88-deficient mice did not have a significant response in Nos2 or Arg1 at the gene expression level following 24 hours of culture ($0.5 < R < 2$ and/or p-value of $\log_2$NRE > 0.05 compared to 10% plasma).

The expression of genes encoding TLR2, TLR4, and Myd88 were also analyzed to study the influence of the TLR2 and MyD88 knockouts, which were created using targeted mutations at the genomic level, meaning the genes are still encoded in the mRNA but not made into functional proteins (Figure 3) (37, 38). No significant changes in the normalized gene expression of TLR2 or MyD88 were observed for any conditions or mouse strains (i.e., $0.5 < R < 2$ and/or p-value of $\log_2$NRE > 0.05).

3.2 Cytokine production of macrophages on Teflon™ AF

The production of pro-inflammatory (IL-1β, IL-6, MCP-1, MIP-1α, RANTES/CCL5, TNF-α, KC/CXCL1), anti-

10.3389/fimmu.2023.1232586

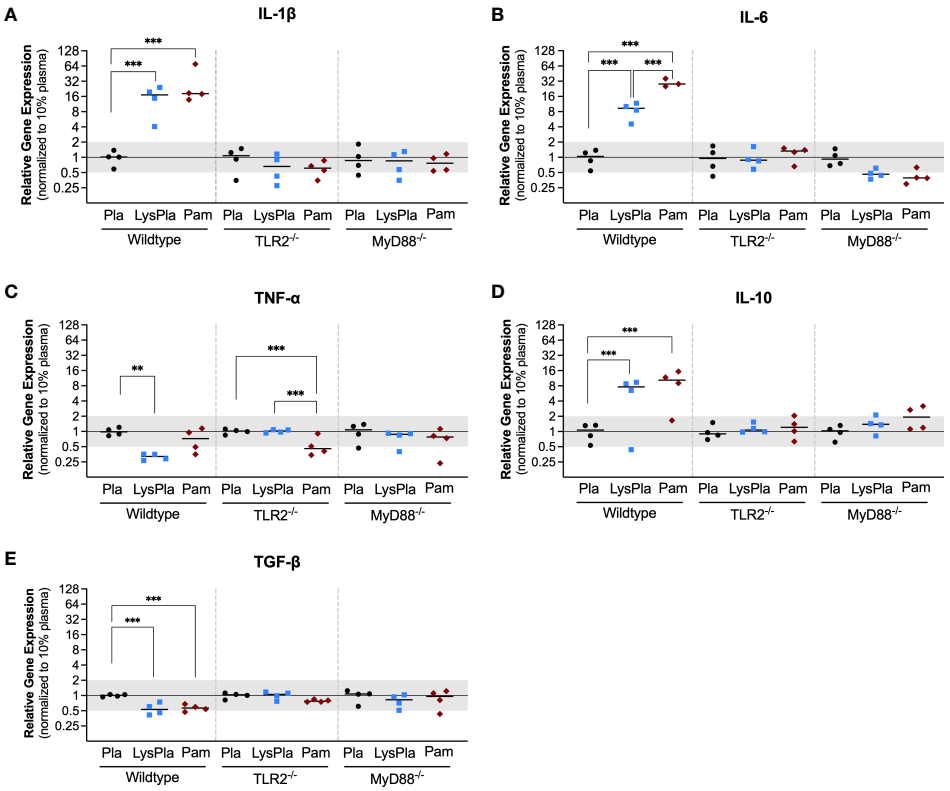

FIGURE 1
Relative gene expression of cytokines IL-1β **(A)**, IL-6 **(B)**, TNF-α **(C)**, IL-10 **(D)** and TGF-β **(E)** in WT, TLR2-/-, and MyD88-/- BMDMs cultured on Teflon™ AF for 24 hours. Each point represents the mean result of one experiment, where each condition had three biological replicates and was plated in triplicate for the qPCR assay. Results are displayed as median (bar) and individual (points) mean relative gene expression for each experiment. Pla, adsorbed 10% plasma (negative control); LysPla, adsorbed 10% lysate in plasma; Pam, Pam3CSK4 (TLR2 positive control). A two-way ANOVA of the log transformed NRE was used to determine statistical difference in relative gene expression among treatment groups within a given genotype, using an $\alpha = 0.05$. Changes in gene expression were considered significant if the median relative expression ratio was less than 0.5 or greater than 2 ($0.5 > R > 2$) and the associated log2NRE p-value was less than 0.05, compared to 10% plasma within the same genotype. **$p < 0.01$ or ***$p < 0.001$ for associated log2NRE values.

inflammatory (IL-10), and angiogenic (VEGF-A) factors by BMDMs cultured on Teflon™ AF for 24 hours was assessed using a multiplexed bead-based cytokine assay (MilliPlex®, MilliporeSigma). In WT BMDM, exposure to adsorbed lysate significantly increased the secretion of pro-inflammatory cytokines and chemokines (IL-1β: 10.1-fold, IL-6: 128.8-fold, RANTES/CCL5: 28.9-fold, TNF-α: 23.2-fold, KC: 30.0-fold; $p < 0.01$) and anti-inflammatory cytokine IL-10 (33.63-fold, $p < 0.01$), when compared to adsorbed plasma (Figure 4; please refer to Supplemental Figure 4 to view only WT data). Similarly, treatment with soluble Pam3CSK4 also increased cytokine secretion (IL-6: 837.4-fold, RANTES/CCL5: 66.4-fold, TNF-α: 18.4-fold, IL-10: 130.5-fold, KC/CXCL1: 49.7-fold, $p < 0.001$), although the increased expression of IL-1β (24.36-fold) was not statistically significant ($p > 0.05$) due to high variability in IL-1β expression in the Pam3CSK4 group. VEGF-A was detected in the WT BMDM supernatants, however no differences in concentration were observed among the three treatments ($p > 0.05$, Supplemental Figure 4H). Exposure to the adsorbed lysate condition appeared to have a similar effect on WT BMDM cytokine secretion when compared to the soluble TLR2 agonist, although Pam3CSK4 treatment did yield higher concentrations of IL-6, KC, and IL-10 ($p < 0.01$ for WT LysPla vs WT Pam). No significant differences were observed for MIP-1α, MCP-1 or VEGF for WT BMDM cultured on 10% plasma, 10% lysate in plasma or with Pam3CSK4 (Supplemental Figures 4E, F, H).

Next, we focused on the effect of TLR2 and MyD88 on the concentration of cytokines that were increased in WT BMDM in response to lysate or Pam3CSK4 conditions. When cultured on Teflon™ AF pre-conditioned with 10% plasma, BMDM mouse strain (WT, TLR2-/-, MyD88-/-) had no effect on the concentration of cytokines ($p > 0.05$), except for IL-6 and KC (Figure 4). While no difference in IL-6 concentration was observed between WT and TLR2$^{-/-}$ BMDM on plasma-adsorbed surfaces, IL-6 was reduced in the MyD88$^{-/-}$ BMDM compared to TLR2$^{-/-}$ BMDM ($p < 0.05$, Figure 4B). The supernatant concentration of KC was lower for TLR2$^{-/-}$ and MyD88$^{-/-}$ BMDM on adsorbed plasma, compared to the WT BMDM on plasma ($p < 0.05$) (Figure 4F).

In contrast to WT macrophage, exposure to the adsorbed lysate did not elicit an increase in cytokine production in TLR2-deficient and MyD88-deficient macrophages ($p > 0.05$ for compared to the 10% plasma), supporting our earlier findings in RAW264.7 and RAW-Blue macrophages that TLR2 was the main mediator of macrophage activation in response to adsorbed lysate (28, 29).

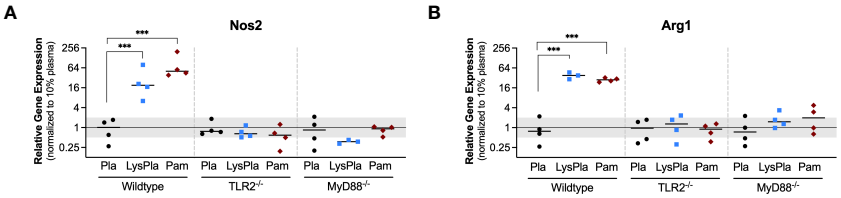

FIGURE 2
Relative gene expression of metabolic enzymes Nos1 **(A)** and Arg1 **(B)** in WT, TLR2-/-, and MyD88-/- BMDMs cultured on Teflon™ AF for 24 hours. Each point represents the mean result of one experiment, where each condition had three biological replicates and was plated in triplicate for the qPCR assay. Results are displayed as mean ± SD, with individual points showing the mean relative gene expression for each experiment. Pla, adsorbed 10% plasma (negative control); LyPla, adsorbed 10% lysate in plasma; Pam, Pam3CSK4 (TLR2 positive control). A two-way ANOVA of the log transformed NRE was used to determine statistical difference in relative gene expression among treatment groups within a given genotype, using an $\alpha = 0.05$. Changes in gene expression were considered significant if the median relative expression ratio was less than 0.5 or greater than 2 ($0.5 > R > 2$) and the associated log2NRE p-value was less than 0.05, compared to 10% plasma within the same genotype. *** $p < 0.001$ for associated log2NRE values.

Furthermore, WT BMDM had significantly higher concentrations of cytokines (IL-1β, IL-6, TNF-α, RANTES, IL-10 and KC) on lysate-containing adsorbates, compared to TLR2$^{-/-}$ and MyD88$^{-/-}$ BMDM. As expected, the TLR2$^{-/-}$ and MyD88$^{-/-}$ BMDM also failed to respond to Pam3CSK4 stimulation ($p > 0.05$, compared to 10% plasma; comparisons not shown in Figure 4), with the exception that TLR2$^{-/-}$ BMDM had decreased TNF-α (5.4-fold decrease, $p < 0.05$) and KC (2.4-fold decrease, $p < 0.001$) expression compared to 10% plasma. No differences in cytokine concentrations were found between TLR2 and MyD88 knockout macrophages for any conditions; except for IL-6 and KC. IL-6 was lower in MyD88$^{-/-}$ supernatants, compared to TLR2$^{-/-}$ for Pam3CSK4 ($p < 0.05$, Figure 4B), while KC concentrations were lower in MyD88$^{-/-}$ supernatants compared to TLR2$^{-/-}$ for 10% plasma and 10% lysate in plasma ($p < 0.05$, Figure 4F).

3.3 Proteomic analysis of adsorbed protein layers on Teflon™ AF surfaces

Next, we analyzed the composition of the adsorbed protein layers generated from 10% plasma and 10% lysate in plasma using LC-MS/MS to determine whether the potent TLR2-dependent macrophage activation on the lysate-adsorbed surfaces was associated with the presence of known DAMPs within the adsorbed protein layer. The proteomic analysis identified 321 proteins in the adsorbed layers derived from 10% plasma, while 2556 were identified in the adsorbed layers derived from the 10% lysate in plasma mixtures (Figure 5A). To better understand how a 10% w/w spike of lysate affected the adsorption of plasma proteins, we then compared the 25 proteins with the highest log2 transformed protein intensities in each condition (Figure 5B). The 10% plasma condition yielded a list of proteins that included many of the well-studied proteins in adsorption literature, including fibrinogen (Fgb, Fga, Fgg), albumin (Alb), apolipoproteins (Apoa1, Apoe, Apoa4, Apob, Apom), complement (C3, C4), fibronectin (Fn1), and kininogen 1 (Kng1). Proteins layers generated from plasma that contained a 10% w/w spike of lysate proteins retained fibrinogen (Fgb, Fgg, Fga) and fibronectin (Fn1) remained among the top 25 proteins. However, these lysate-containing adsorbed protein layers had a disproportionate increase in intracellular proteins, including histones (H2bu1, H3c13, H4f16, Hist1h2af, Hist2h2bb), tubulins (Tuba1a, Tuba1b, Tuba1c, Tubb2a, Tubb2b, Tubb4b, Tubb5), actins (Acta2, Actb, Actg1), vimentin (Vim) and myosin 9 (Myh9). The full list of identified proteins in both adsorbed proteins layers and their relative intensities is provided in Supplemental Data File 1.

We then identified proteins that were enriched in either condition using a moderate T-test on the log2 transformed protein intensities, where a multiple testing adjusted (Benjamini) p-value < 0.05 and fold-change > 2 in absolute value were considered significant. A complete list of significantly enriched proteins with their fold-change and adjusted p-value are provided in Supplemental Data File 2. Functional enrichment analysis was calculated for all proteins differentially expressed in either the 10% plasma or 10% lysate in plasma conditions (Supplemental Data File 3) and the top ten enriched pathways for each adsorbed protein layer are shown in Figure 5C.

Finally, we sought to determine if the 10% lysate in plasma protein layer was enriched for DAMPs, which may account for the increased TLR2-/MyD88-dependent macrophage activation observed on these surfaces. However, DAMPs, to our knowledge, currently do not have a specific annotation with the gene ontology databases we consulted. Therefore, a manual approach was required. We first compiled a list of putative protein DAMPs from published literature (Supplementary Table 1) and then manually searched the protein lists for protein or protein classes reported as DAMPs within literature. Using this approach, we identified 39 DAMPs or DAMP-related proteins enriched in the 10% lysate in plasma condition, compared to seven in the 10% plasma condition (Figure 6). A caveat to this manual approach is that the list does not represent an exhaustive list of all putative DAMPs within the literature, and therefore, we view these results as hypothesis, rather than conclusion, generating.

4 Discussion

Within the field of biomaterials, it is well-established that the adsorbed protein layer on an implanted biomaterial surface mediates cell-material interactions and the progression of the host

10.3389/fimmu.2023.1232586

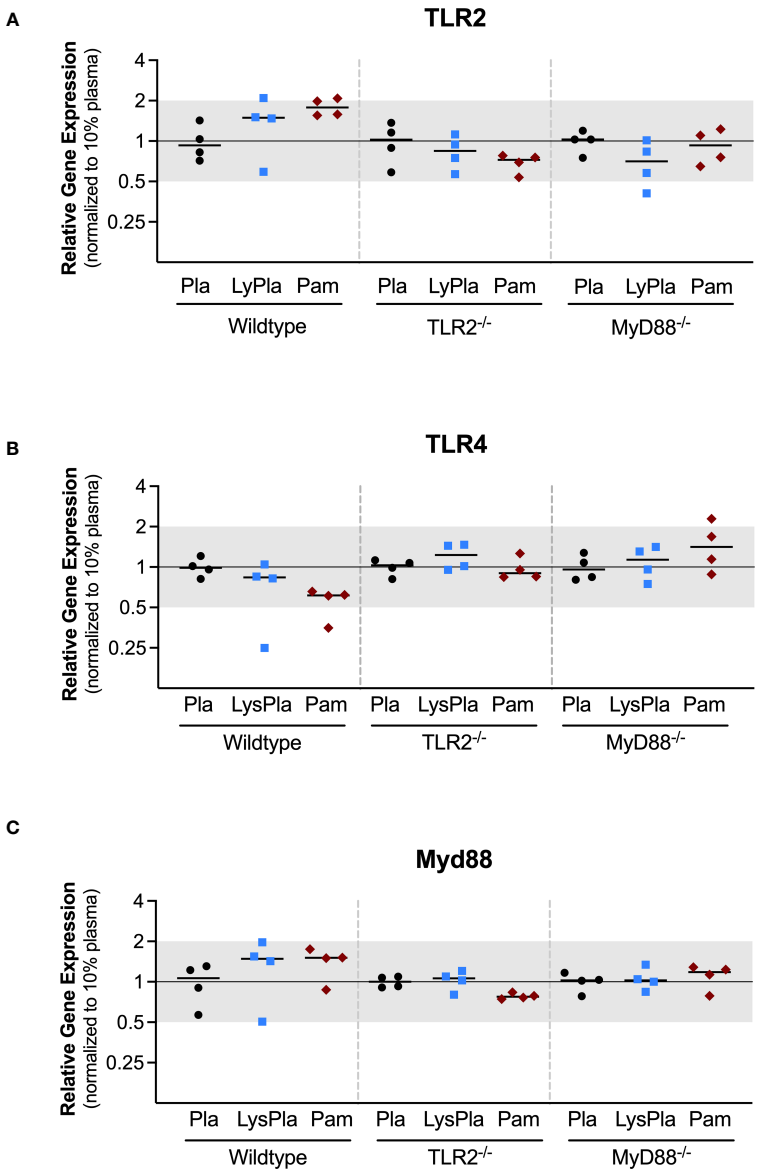

FIGURE 3
Relative expression of genes encoding TLR proteins TLR2 **(A)**, TLR4 **(B)**, and Myd88 **(C)** in WT, TLR2-/-, and MyD88-/- BMDMs cultured on Teflon™ AF for 24 hours. Each point represents the mean result of one experiment, where each condition had three biological replicates and was plated in triplicate for the qPCR assay. Results are displayed as mean ± SD, with individual points showing the mean relative gene expression for each experiment. Pla, adsorbed 10% plasma (negative control); LyPla, adsorbed 10% lysate in plasma; Pam, Pam3CSK4 (TLR2 positive control). * $p < 0.05$ compared to 10% plasma within the same genotype. A two-way ANOVA of the log transformed NRE was used to determine statistical difference in relative gene expression among treatment groups within a given genotype, using an $\alpha = 0.05$. Changes in gene expression were considered significant if median relative expression ratio was less than 0.5 or greater than 2 ($0.5 > R > 2$) and the associated log2NRE p-value was less than 0.05, compared to 10% plasma within the same genotype.

response. The adsorption of blood proteins has been studied extensively for more than fifty years (11, 13, 20) and provides a strong foundation for understanding cell-material interactions. During biomaterial implantation, damage to the local tissue would lead not only to blood leakage from damaged vasculature, but also the release of DAMPs from damage extracellular matrix and cells within the implant site (27). However, little is understood regarding the adsorption of non-blood derived proteins or other types of molecules. In 2018, our group first demonstrated that molecules within 3T3 fibroblast lysates adsorb to biomaterial surfaces and potently activate macrophages in a TLR2-dependent manner (28), even in the presence of serum proteins. We went on to demonstrate that the cytokine profile of RAW264.7 macrophages, a mouse macrophage cell line, over 5 days recapitulated the cytokine profile reported during *in vivo* macrophage-material interactions, induced low rates of macrophage fusion and promoted the late expression of pro-fibrotic TGF-β1 (29). However, these studies were limited by the use cell lines and protein layers derived from 100% fibroblast lysate. Furthermore, no characterization of the adsorbed protein layers was conducted to understand what types of molecules

10.3389/fimmu.2023.1232586

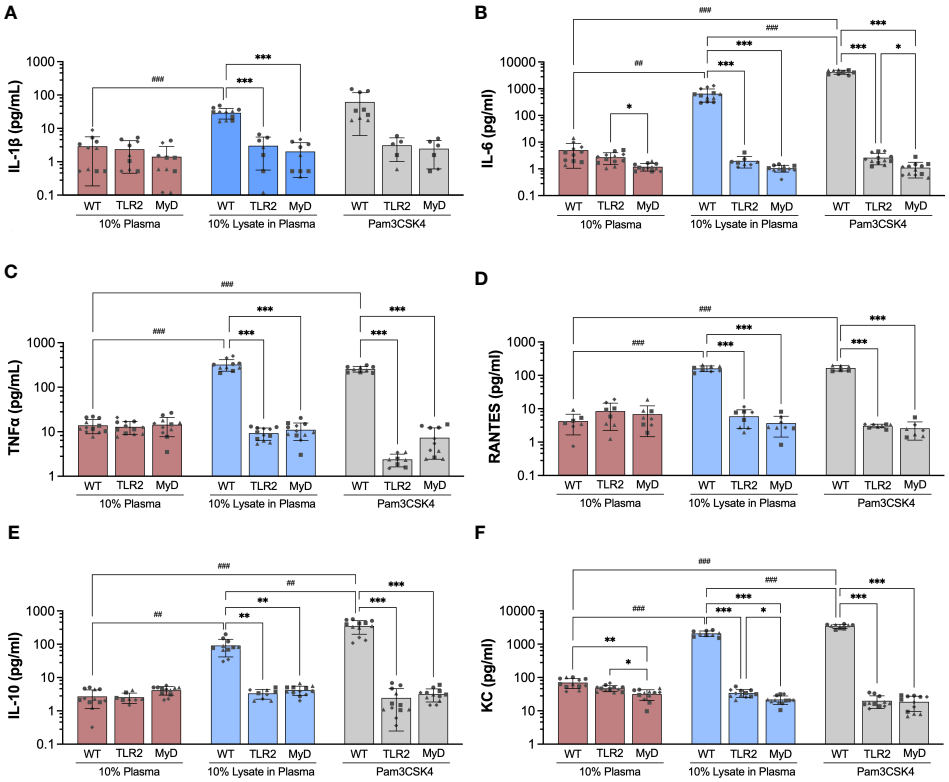

FIGURE 4
Concentration of IL-1β **(A)**, IL-6 **(B)**, TNF-α **(C)**, RANTES **(D)**, IL-10 **(E)** and KC **(F)** in supernatant of wildtype (WT), TLR2-/- (TLR2), and MyD88-/- (MyD) BMDMs cultured for 24 hours on Teflon™ AF with adsorbed 10% plasma (red bar), 10% lysate in plasma (blue bar) or with Pam3CSK4 (grey bar). Results are displayed as mean ± SD for four independent experiments (symbols ●, ■,◆, ▲ indicating experiment 1, 2, 3 and 4, respectively), each containing 3 replicates (n = 12). A Brown-Forsythe and Welch ANOVA and Dunnett T3 post-hoc tests were used to determine significant differences among conditions, with $\alpha = 0.05$. $^{\#\#}p < 0.01$ and $^{\#\#\#}p < 0.001$ compared among WT groups. *p < 0.05, **p < 0.01 and ***p < 0.001 compared to WT within a treatment group.

were adsorbing to the biomaterial surfaces. In the present study, we address these limitations by using primary mouse macrophages and adsorbed protein layers derived from either mouse plasma or plasma spiked with lysate (10 w/w%) to better model *in vivo* protein adsorption, and lysate adsorption in competition with plasma proteins. Furthermore, we further characterized the relative importance of TLR2 and TLR adapter protein, MyD88, in the response to adsorbates containing lysate-derived molecules using macrophage-derived from knockout mice. The study aimed to elucidate the ability of lysate-derived molecules to adsorb onto Teflon™ AF surfaces in the presence of blood proteins and activate primary mouse macrophages. To this end, K2 EDTA and citrated plasma preparations were used to eliminate the effect of the complement cascade (56–59), which is recognized as an important factor in biomaterial host responses (56, 58, 60, 61). As 10% FBS was used, some degree of complement activation was possible in all samples. However, our previous work found that adsorbed protein layers derived from 10% FBS, 10% plasma and 10% heat-inactivated FBS yielded similar, minimal NF-κB/AP-1 activity in mouse reporter macrophages, supporting our assumption that complement activation was negligible in this model, compared to the effect of the adsorbed lysate (30).

In the present study, we demonstrated that adsorbed protein layers derived from mouse plasma spiked with small amounts of mouse lysate (10% w/w total protein) induced a potent pro-inflammatory response in primary mouse macrophages at 24 hours. This response was characterized by increased gene expression and cytokine concentration of acute phase cytokines (IL-1β, IL-6, TNF-α, IL-10) and chemokines (RANTES/CCL5, KC/CXCL1), and was dependent on TLR2/MyD88 signaling. This increased cytokine and chemokine expression was consistent with reported cytokine expression within *in vivo* implant sites during the early phase (e.g. day 4 and 7) of the FBR to synthetic biomaterial implants (62).

While the gene and protein expression data showed consistent trends for most factors, a notable exception was TNF-α. While the secreted protein concentration was significantly elevated (~ 60-fold increase compared to 10% plasma), the relative gene expression at 24 hours was similar or slightly downregulated in the lysate condition, compared to plasma. Baer and colleagues have shown a similar trend in TNF-α gene expression of BMDMs exposed to LPS over time, where up to 3 hours post-exposure the mRNA expression of TNF-α increased, and then over time decreased to baseline levels (63). Their work, as well as the work here, demonstrates that TNF-α is an early response cytokine, and over time it can become downregulated as other pro-inflammatory and anti-inflammatory cytokines are produced (63). Baer et al. and others have shown that the NF-κB p50 subunit is responsible for the

10.3389/fimmu.2023.1232586

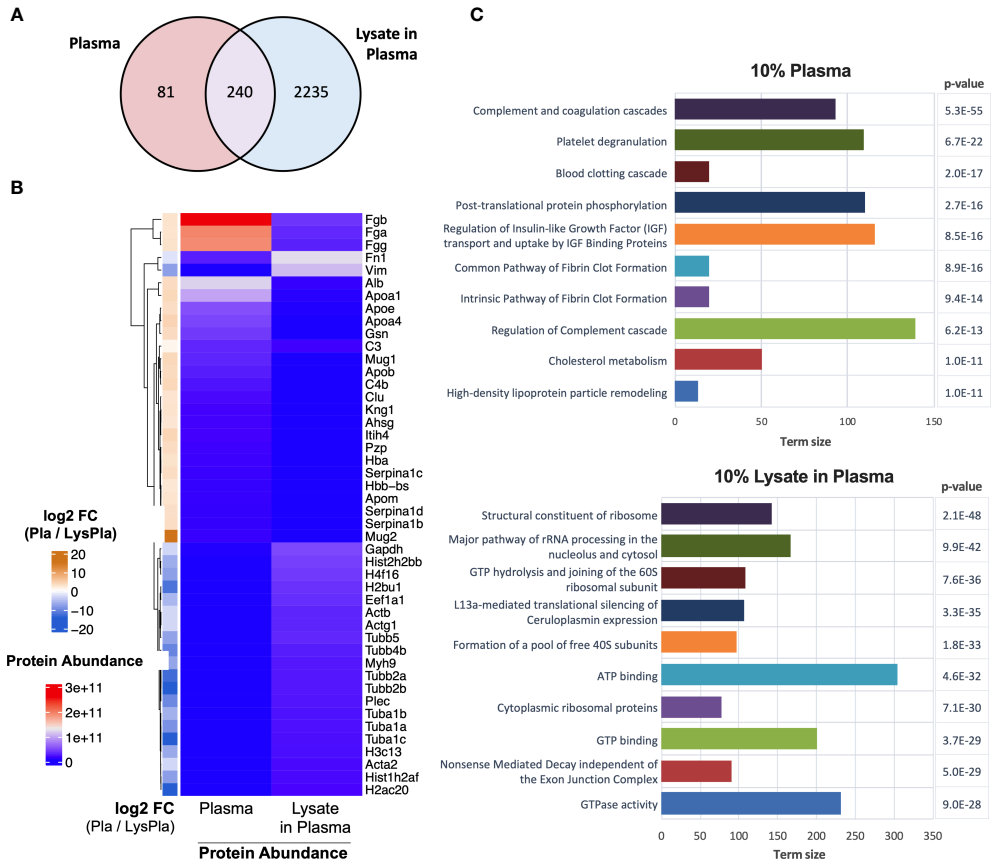

FIGURE 5
Proteomic analysis of adsorbed proteins layers by LC-MS/MS. **(A)** Venn diagram of identified proteins in adsorbates derived from 10% plasma and 10% lysate in plasma on Teflon™ AF surfaces. **(B)** Heat map of top 25 abundant proteins identified in adsorbed protein layers derived from 10% plasma and 10% lysate in Plasma adsorbed proteins with corresponding log2 fold-change for plasma vs lysate in plasma. **(C)** The top ten GO terms enriched in differentially expressed (fold-change > 2) in either the 10% plasma (upper) or 10% lysate in plasma (lower) conditions. Differential protein expression analysis was calculated by moderate t-test using limma r package (48) on the log2 transformed protein intensities. A multiple testing adjusted p-value < 0.05 was considered significant (49).

downregulation of TNF-α in murine and human primary macrophages (63, 64). Alexander et al. have also demonstrated that in mouse macrophages TNF-α is regulated by IL-10 (65). Therefore, the upregulation of IL-10 secretion in WT BMDMs exposed to lysate is a likely contributing factor to the downregulation of TNF-α gene expression in these macrophages.

The gene expression of metabolic enzymes Nos2 and Arg1 was compared to gain insight into the metabolic state and polarization of lysate-stimulated macrophages (55). Lysate-stimulated WT macrophages upregulated the gene expression of both enzymes, with Arg1 having a slightly higher fold-increase compared to Nos2, relative to the macrophages on plasma-adsorbed Teflon™ AF. Although Nos2 and Arg1 are typically regarded as distinct metabolic markers of M1 and M2 macrophage phenotypes, there are several reports of macrophages expressing both enzymes under specific conditions, including a TLR-dependent response to mycobacterium that induced Arg1 expression (66). Considering the two extremes of macrophage polarization, the WT macrophage population stimulated by adsorbed lysate or Pam3CSK4 appear to lie on the spectrum between a classical M1 macrophage phenotype characterized by high IL-6, TNF-α, Nos2 and an alternative M2 macrophage phenotype with high IL-10 and Arg1 expression. This cytokine profile is consistent with previous reports that Pam3CSK4 induced an immunosuppressive M2-like macrophages from human monocytes that express both IL-10 and IL-6, which makes Pam3CSK4 unique among TLR agonists that generally induce an M1 phenotype (67–69). Similarly, others have shown that Pam3CSK4 induced human monocytes to produce IL-1β and IL-6 via canonical (p65/RelA) NF-κB signaling pathway and IL-10 via the non-canonical (p100/p52) pathway (70). However, the cytokine and gene expression data reflect the global population and lack the robust selection of immunophenotyping markers required for macrophage polarization analysis. Therefore, we cannot determine whether the lysate-containing adsorbates promote a similar immunosuppressive M2-like phenotype as with Pam3CSK4 (although the profile are highly similar), a mixture of M1 and M2 macrophage populations, or a hybrid M1/M2 macrophage phenotype that has been observed *in vivo* at implant sites (71–73). Regardless, the induction of both pro-inflammatory and anti-inflammatory mediators may reflect the fact that the adsorbates derived from lysate and plasma contained a multitude of potential stimuli or activate macrophages via a similar signaling mechanism as

10.3389/fimmu.2023.1232586

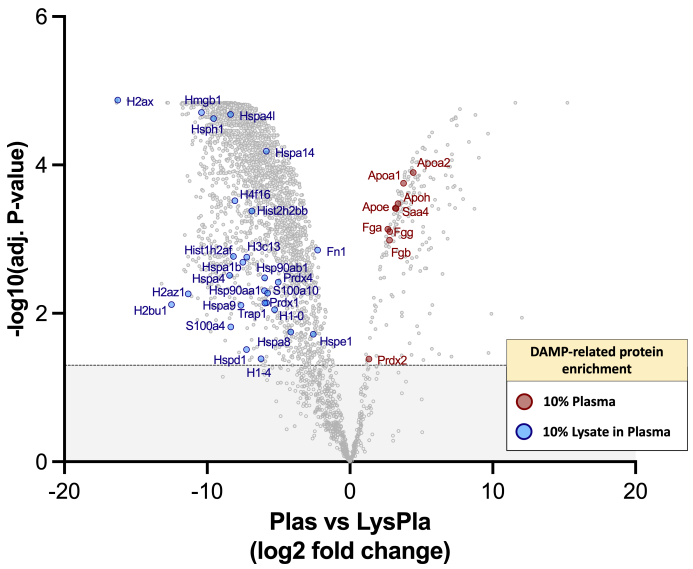

FIGURE 6
DAMPs identified with adsorbed protein layers on Teflon™ AF surfaces following 1 hr incubation at 37 oC in 10% plasma or 10% (w/w) lysate in plasma. Volcano plot representing the statistical analysis of the normalized proteins intensities in plasma samples versus lysate in plasma samples, with DAMPs labeled. The x-axis shows the log2 foldchange of each identified protein and the y-axis the corresponding –log10 P value. Proteins with adjusted p-values greater than 0.05 (shown as dotted line) were considered significant.

Pam3CSK4. Conversely, Teflon AF™ surfaces with adsorbates derived solely from mouse plasma yielded low (~ 10 pg/ml or lower) expression of many of the cytokines associated with polarization and/or FBR (e.g., IL-1β, IL-6, TNF-α, IL-10), suggesting adsorbed molecules derived from K2 EDTA plasma did not significantly activate the WT macrophages. This negligible activation on the plasma adsorbates was expected, as the calcium chelation by the plasma anticoagulant (K2 EDTA) inhibits activation of the complement cascade, which otherwise would also induce an inflammatory response (26). Chemokines MCP-1 and MIP-1α and angiogenic growth factor VEGF were expressed at higher concentrations ranging (~ 100 to 800 pg/ml) on all surfaces, indicating their expression was induced by the 10% plasma condition or a basal expression for BMDM on Teflon™ AF surfaces.

MyD88 is a critical adaptor protein for TLR2/1 and TLR2/6 heterodimers, but also all other TLR (except TLR3) as well as IL-1β signaling (74). Therefore, it was expected that the loss of the MyD88 protein may have a more robust effect on the macrophage response than the more selective loss of TLR2. However, TLR2 and MyD88 knockout macrophages yielded highly similar cytokine expression profiles at the protein and mRNA level in this model. This supports our original hypothesis that TLR2 is the primary TLR2 mediator of macrophage activation in response to Teflon™ AF surfaces pre-adsorbed with 10% lysate in plasma. These results are significant as they open the door for potential therapeutic strategies that target DAMP-induced macrophage activation in a broader (MyD88) or more selective (TLR2) manner.

Proteomic analysis of the adsorbed protein layers generated from 10% plasma or 10% lysate in plasma on the Teflon™ AF surfaces clearly demonstrated that even small amounts of cell-derived molecules in the presence of blood-derived molecules can significantly alter the adsorbed protein profile on Teflon™ AF surfaces. Teflon™ AF is a hydrophobic fluoropolymer that was used to model Teflon™ cannulas of IIS. Hydrophobic fluoropolymers are known to bind serum protein almost instantaneously and have high protein retention (75, 76). Here, Teflon™ AF surfaces pre-adsorbed with 10% plasma yielded proteomic profile abundant (in terms of protein intensities) in fibrinogen, albumin, apolipoproteins, complement proteins and fibronectin. This profile is consistent with previous proteomic studies of protein adsorption from heparinized plasma for other hydrophobic materials (61), as well as earlier work with Teflon™ (PTFE) using more traditional protein adsorption methodologies (75, 76). Protein adsorption from blood and blood products has been an active area of research in the biomaterials field for more than fifty years, and was recently summarized in a comprehensive series of reviews on blood-material interactions and its subsequent effects on biocompatibility (24, 60, 77–79).

Proteomic analysis of adsorbed protein layers generated *in vivo* is less well characterized. Swartzlander et al. used LC-MS/MS proteomic to characterize the protein layers adsorbed on hydrophilic polyethylene glycol (PEG) hydrogels following a 30-minute subcutaneous implantation in mice. In this study, albumin was the most abundant protein, while apolipoproteins, complement C3, murinoglobulin 1 (Mug1) were also among the "top 20" adsorbed proteins, similar to the 10% Plasma Teflon™ AF condition in the current study. Many of the other abundant proteins in the PEG hydrogels were associated with the acute inflammatory and wound healing processes, and located within the extracellular compartment (27). However, approximately 10% of the identified proteins came from the intracellular compartment, in particular the cytoskeleton and cytosol (27), suggesting that *in vivo* protein adsorption layers do acquire proteins released damaged cells in the surroundings.

We demonstrated that by adding 10% (w/w of total protein) lysate proteins to the plasma significantly altered the adsorbed protein profile on Teflon™ AF surfaces. Although fibrinogen and fibronectin remained in the top 25 proteins, many other blood proteins, including albumin (ranked 36th) and complement C3 (ranked 30th) were replaced primarily by the cytoskeletal proteins (actins, tubulins, vimentin, myosin) and histones. Significantly, the 10% lysate in plasma adsorbates were enriched for well characterized DAMPs high mobility group box 1 (HMGB1) and core histones (80), as well as putative DAMPs heat shock proteins (HSP70, HSP60) and S100 proteins (33). As the 10% lysate in plasma surfaces activated primary mouse macrophages in a TLR2/MyD88-dependent manner, we were particularly interested in DAMPs that are known to act via this pathway. HMGB1 is a nuclear chromatin-binding protein, but when released from cells via either active secretion or passive release in response to tissue damage, it mediates inflammation via its interaction with TLR4 and receptor for advanced glycation end-products (RAGE) (81). There are conflicting reports on the ability of HMGB1 to induce a cytokine response via TLR2. However, a recent study revealed that HMGB1 interacts with TLR2, but function in complex with other known TLR2 agonists to enhance TLR2 signaling (82). When released to the extracellular fluid in response to trauma or severe cellular stress, histones (H1, H2A, H2B, H3, and H4) signal through TLR2, TLR4 and TLR9 to induce the production of cytokines (e.g., IL-6, IL-10 TNF-α), activate the NALP3 inflammasome and complex with other DAMPs (e.g., DNA, HMGB1) to act as a co-activator (80, 83–85). With the adsorbed protein layer derived from 10% lysate in plasma, 16 proteins from the H1, H2A, H2B, H3 and H4 families were identified and enriched, compared to 10% plasma only. Extracellular peroxiredoxin-1 (Prdx-1) has been found to induce chemokine production via TLR2/4/MyD88 (KC/CXCL1, MIP-2α/CXCL2, MCP-1/CCL2) and TLR4/TRIFF (RANTES/CCL5) (86), and trigger sterile inflammation in models of acute injury, including ischemic brain injuries, acute liver injury and acute lung injury (87–90). We also noted the presence of putative DAMPs, such as HSP, which have conflicting evidence of true DAMP activity. While HSP are frequently cited as DAMPs, there is controversy within the literature regarding the role of extracellular HSP in immunity (91). While earlier work showed HSP acted as DAMPs via TLR, later studies suggest that this response was due, at least in part, to contaminants within the recombinant protein preparations (92).

4.1 Study limitations

The concentration of cytokines was reported per well and was not normalized to the number of cells in each condition. Therefore, it is possible that differences in reported cytokine concentrations among the experimental conditions may reflect differences in the number of BMDM. However, visual observations of the wells at 24 hours (representative images shown in Supplemental Figure 1) did not reveal a notable difference in cell density. As most cytokine concentrations differed by an order of magnitude or more between the wildtype condition and knockout strains, we do not anticipate that variations in cell density among samples (if present) would change the study conclusion that lysate-containing adsorbates stimulated macrophages in a TLR2/MyD88 dependent manner.

Collectively, the proteomic profile of the adsorbed protein layer on Teflon™ AF substrates pre-conditioned with 10% lysate in plasma provides multiple potential ligands that may elicit, either alone or in combination, a TLR2/MyD88-dependent macrophage response observed on lysate-derived adsorbates within this study, as well as our previous work with RAW-264.7 and RAW-Blue reporter macrophages. However, there are multiple limitations and caveats that must be acknowledged before drawing any definitive conclusions regarding the mechanisms of action of the adsorbed lysate model and its relevance to biomaterial host responses and the FBR. First, the proteomic method used to analyze the adsorbed protein layer generates a relative abundance of proteins present in each condition that does not linearly correlate with the actual protein copy numbers in each sample. Furthermore, these results will be influenced by multiple factors, including the number of tryptic peptides each protein generates after trypsin digestion, the ionizability of the peptides and other factors (24, 93). Therefore, the presence of proteins of interest require validation using other methods, such as immunological assays (ELISA, Western Blot) or targeted MS assays (93). Furthermore, immunodepletion or blocking of proteins of interest would be required to demonstrate the relative importance of that protein's contribution to macrophage activation. Moving beyond validating the presence and function of different proteins within the adsorbed protein layers generated in the present model, there is the critical question of whether this model is useful and predictive of macrophage-material interactions *in vivo*. Our work supports previous studies by Stephanie Bryant and colleagues, who have demonstrated that MyD88-dependent signaling is a key regulator of inflammatory cell recruitment and fibrous capsule formation in PEG-hydrogel implant models *in vivo* (32). Compared to the proteomic analysis of *in vivo* generated protein layers on PEG hydrogels, the 10% lysate in plasma was more enriched for intracellular proteins, suggesting that reducing the amount of lysate may result in a more accurate model of *in vivo* protein layers. However, PEG is a hydrophilic hydrogel and Teflon™ AF is a hydrophobic amorphous polymer, and the two materials differ in many properties that are known to influence protein adsorption. Another approach to improve the physiological relevance of this present model is to use an anticoagulant that preserves the complement and elements of the coagulation cascade. For example, the thrombin inhibitor lepirudin preserves the complement cascade and the coagulation cascade upstream of thrombin, making a more representative plasma model of the *in vivo* environment (94). Recent proteomic analysis of adsorbed protein layers from human lepirudin-plasma demonstrated distinct differences in the levels of complement and coagulation activators and inhibitors present on the surface of three types of alginate microsphere (26). As adsorbed complement components and activation of the alternative amplification loop on material surfaces are important factors in biomaterial host responses, the use of lepiruinated plasma with a lysate spike should be considered for the further development of *in vitro* protein adsorbption models

related to biomaterial inflammatory responses (56–61, 95). Ultimately, a proteomic analysis of *in vivo*-generated adsorbed protein layers on Teflon™ AF surfaces would provide a more useful comparison to determine how well this *in vitro* model or future iterations recapitulate the *in vivo* scenario. Furthermore, *in vivo* studies exploring the response of TLR2- and MyD88-deficient mice to Teflon™ or Teflon™ AF implants are required to demonstrate the important of TLR2-signaling within the host response to the fluoropolymers, and other biomaterials. Finally, as the present and preceding studies of the effect of adsorbed lysate-derived molecules have focused on mouse macrophages, it is necessary to validate these findings using human macrophage models in future research.

5 Conclusion

In summary, our study provides evidence that adsorbed protein layers containing plasma and cell lysate activate primary bone-derived macrophages in a TLR2-dependent manner to express pro-inflammatory (IL-1β, IL-6, TNF-α, RANTES, Nos2) and anti-inflammatory or tolerizing factors (IL-10, Arg1). Proteomic profiling of the adsorbed layers from lysate-containing plasma solutions suggests that known intracellular DAMPs, such as HMGB1 and histones, are enriched on the surface of the Teflon™ AF, and that subsets of these proteins are known to induce sterile inflammatory responses through TLR2. Further studies will be required to validate the presence of these TLR2-binding DAMPs and their contribution to macrophage activation in the present *in vitro* model of macrophage-material interactions, as well as assess TLR2/MyD88-dependent signaling within *in vivo* biomaterial implant models. Overall, our study contributes to the growing body of evidence supporting TLRs as modulators of macrophage-material interactions and biomaterial host responses.

Data availability statement

The proteomic datasets presented in this study can be found in online repositories. The names of the repository/repositories and accession number(s) can be found in the article/Supplementary Material. All other raw data supporting the conclusions of this article will be made available by the authors, without undue reservation.

Ethics statement

The animal study was approved by University Animal Care Committee (UACC; AUP 2018-1849) at Queen's University (Kingston, ON, Canada). The study was conducted in accordance with the local legislation and institutional requirements.

Author contributions

LM and LF contributed to the conception, design of the study, formal analysis of the data. LM wrote the first draft of the manuscript. LM and LB performed the investigation, validation and contributed to the methodology. GN performed the proteomic data analysis and visualization, and writing (review and editing). KW and LF contributed resources, writing (review and editing), supervision and funding acquisition. All authors contributed to manuscript revision, read, and approved the submitted version.

Funding

The authors gratefully acknowledge operational funding from Canadian Institutes of Health Research Project (PTJ 162251) and Queen's University Senate Advisory Research Committee, and infrastructure funding from the Canadian Foundation for Innovation John Evan's Leadership Fund (Project 34137) and the Ministry of Research and Innovation Ontario Research Fund (Project 34137). LM was supported by a Natural Sciences and Engineering Research Council of Canada (NSERC) Canadian Graduate Scholarship Master's Award and an Ontario Graduate Scholarship.

Acknowledgments

The authors would like to thank Jenny Thiele for performing the Milliplex assay of BMDM supernatants and giving advice on data analysis. The authors also wish to thank Leanne Wybenga-Groot and Craig Simpson of SPARC BioCentre (Molecular Analysis), The Hospital for Sick Children, Toronto, Canada for assistance with the proteomic sample preparation and processing, as well as advice on experimental planning and data analysis. This manuscript contains content which first appeared in the thesis of Laura A. McKiel (96).

Conflict of interest

The authors declare that the research was conducted in the absence of any commercial or financial relationships that could be construed as a potential conflict of interest.

Publisher's note

Supplementary material

The Supplementary Material for this article can be found online at: https://www.frontiersin.org/articles/10.3389/fimmu.2023.1232586/full#supplementary-material

References

1. Anderson JM, Rodriguez A, Chang DT. Foreign body reaction to biomaterials. *Semin Immunol* (2008) 20(2):86–100. doi: 10.1016/j.smim.2007.11.004

2. Doloff JC, Veiseh O, Vegas AJ, Tam HH, Farah S, Ma M, et al. Colony stimulating factor-1 receptor is a central component of the foreign body response to biomaterial implants in rodents and non-human primates. *Nat Mater* (2017) 16(6):671–80. doi: 10.1038/nmat4866

3. National Diabetes Statistics Report. *Centers for Disease Control and Prevention*. Atlanta, GA: US Department of Health and Human Services (2020).

4. Umpierrez GE, Klonoff DC. Diabetes technology update: use of insulin pumps and continuous glucose monitoring in the hospital. *Diabetes Care* (2018) 41(8):1579–89. doi: 10.2337/dci18-0002

5. Schmid V, Hohberg C, Borchert M, Forst T, Pfützner A. Pilot study for assessment of optimal frequency for changing catheters in insulin pump therapy - trouble starts on day 3. *J Diabetes Sci Technol* (2010) 4:976–82. doi: 10.1177/193229681000400429

6. Pfützner A, Sachsenheimer D, Grenningloh M, Heschel M, Walther-Johannesen L, Gharabli R, et al. Using insulin infusion sets in CSII for longer than the recommended usage time leads to a high risk for adverse events. *J Diabetes Sci Technol* (2015) 9:1292–8. doi: 10.1177/1932296815604438

7. Gibney M, Xue Z, Swinney M, Bialonczyk D, Hirsch L. Reduced silent occlusions with a novel catheter infusion set (BD flowSmart): results from two open-label comparative studies. *Diabetes Technol Ther* (2016) 18(3):136–43. doi: 10.1089/dia.2015.0342

8. Hauzenberger JR, Hipszer BR, Loeum C, McCue PA, DeStefano M, Torjman MC, et al. Detailed analysis of insulin absorption variability and the tissue response to continuous subcutaneous insulin infusion catheter implantation in swine. *Diabetes Technol Ther* (2017) 19:641–50. doi: 10.1089/dia.2017.0175

9. Hauzenberger JR, Münzker J, Kotzbeck P, Asslaber M, Bubalo V, Joseph JI, et al. Systematic in *vivo* evaluation of the time-dependent inflammatory response to steel and Teflon insulin infusion catheters. *Sci Rep* (2018) 8:1132. doi: 10.1038/s41598-017-18790-0

10. Heinemann L. Variability of insulin absorption and insulin action. *Diabetes Technol Ther* (2002) 4:673–82. doi: 10.1089/152091502320798312

11. Brash JL, ten Hove P. Effect of plasma dilution on adsorption of fibrinogen to solid surfaces. *Thromb Haemost* (1984) 51(3):326–30. doi: 10.1055/s-0038-1661093

12. Ellingsen JE. A study on the mechanism of protein adsorption to TiO2. *Biomaterials* (1991) 12(6):593–6. doi: 10.1016/0142-9612(91)90057-H

13. Horbett TA. Mass action effects on competitive adsorption of fibrinogen from hemoglobin solutions and from plasma. *Thromb Haemost* (1984) 51(2):174–81. doi: 10.1055/s-0038-1661052

14. Horbett TA, Weathersby PK, Hoffman AS. The preferential adsorption of hemoglobin to polyethylene. *J Bioeng* (1977) 1(2):61–77.

15. Roach P, Farrar D, Perry CC. Interpretation of protein adsorption: surface-induced conformational changes. *J Am Chem Soc* (2005) 127(22):8168–73. doi: 10.1021/ja042898o

16. Undin T, Lind SB, Dahlin AP. MS for investigation of time-dependent protein adsorption on surfaces in complex biological samples. *Future Sci OA* (2015) 1(4): FSO32. doi: 10.4155/fso.15.32

17. Wojciechowski P, Ten Hove P, Brash JL. Phenomenology and mechanism of the transient adsorption of fibrinogen from plasma (VrOman effect). *J Colloid Interface Sci* (1986) 111:455–65. doi: 10.1016/0021-9797(86)90048-2

18. Cornelius RM, Archambault J, Brash JL. Identification of apolipoprotein A-I as a major adsorbate on biomaterial surfaces after blood or plasma contact. *Biomaterials* (2002) 23(17):3583–7. doi: 10.1016/S0142-9612(02)00083-2

19. Brash JL, Lyman DJ. Adsorption of plasma proteins in solution to uncharged, hydrophobic polymer surfaces. *J BioMed Mater Res* (1969) 3(1):175–89. doi: 10.1002/jbm.820030114

20. VrOman L, Adams AL, Fischer GC, Munoz PC. Interaction of high molecular weight kininogen, factor XII, and fibrinogen in plasma at interfaces. *Blood* (1980) 55 (1):156–9. doi: 10.1182/blood.V55.1.156.156

21. Slack SM, Posso SE, Horbett TA. Measurement of fibrinogen adsorption from blood plasma using 125I-fibrinogen and a direct ELISA technique. *J Biomater Sci Polym Ed* (1991) 3(1):49–67. doi: 10.1163/156856292x00079

22. Vyner MC, Amsden BG. Polymer chain flexibility-induced differences in fetuin A adsorption and its implications on cell attachment and proliferation. *Acta Biomater* (2016) 31:89–98. doi: 10.1016/j.actbio.2015.11.039

23. Buck E, Lee S, Stone LS, Cerruti M. Protein adsorption on surfaces functionalized with COOH groups promotes anti-inflammatory macrophage responses. *ACS Appl Mater Interfaces* (2021) 13(6):7021–36. doi: 10.1021/acsami.0c16509

24. Kim J. Systematic approach to characterize the dynamics of protein adsorption on the surface of biomaterials using proteomics. *Colloids Surf B Biointerfaces* (2020) 188:110756. doi: 10.1016/j.colsurfb.2019.110756

25. Romero-Gavilan F, Cerqueira A, Anitua E, Tejero R, Garcia-Arnaez I, Martinez-Ramos C, et al. Protein adsorption/desorption dynamics on Ca-enriched titanium surfaces: biological implications. *J Biol Inorg Chem* (2021) 26(6):715–26. doi: 10.1007/s00775-021-01886-4

26. Coron AE, Fonseca DM, Sharma A, Slupphaug G, Strand BL, Rokstad AMA. MS-proteomics provides insight into the host responses towards alginate microspheres. *Mater Today Bio* (2022) 17:100490. doi: 10.1016/j.mtbio.2022.100490

27. Swartzlander MD, Barnes CA, Blakney AK, Kaar JL, Kyriakides TR, Bryant SJ. Linking the foreign body response and protein adsorption to PEG-based hydrogels using proteomics. *Biomaterials* (2015) 41:26–36. doi: 10.1016/j.biomaterials.2014.11.026

28. McKiel LA, Fitzpatrick LE. Toll-like receptor 2-dependent NF-kappaB/AP-1 activation by damage-associated molecular patterns adsorbed on polymeric surfaces. *ACS Biomater Sci Eng* (2018) 4(11):3792–801. doi: 10.1021/acsbiomaterials.8b00613

29. Kaushal A, Zhang Y, Ballantyne LL, Fitzpatrick LE. The extended effect of adsorbed damage-associated molecular patterns and Toll-like receptor 2 signaling on macrophage-material interactions. *Front Bioeng Biotechnol* (2022) 10:959512. doi: 10.3389/fbioe.2022.959512

30. McKiel LA, Woodhouse KA, Fitzpatrick LE. A macrophage reporter cell assay to examine toll-like receptor-mediated NF-kB/AP-1 signaling on adsorbed protein layers on polymeric surfaces. *J Vis Exp* (2020) 155):e60317. doi: 10.3791/60317

31. Kawai T, Akira S. The role of pattern-recognition receptors in innate immunity: update on Toll-like receptors. *Nat Immunol* (2010) 11(5):373–84. doi: 10.1038/ni.1863

32. Amer LD, Saleh LS, Walker C, Thomas S, Janssen WJ, Alper S, et al. Inflammation via myeloid differentiation primary response gene 88 signaling mediates the fibrotic response to implantable synthetic poly(ethylene glycol) hydrogels. *Acta Biomater* (2019) 100:105–17. doi: 10.1016/j.actbio.2019.09.043

33. Gong T, Liu L, Jiang W, Zhou R. DAMP-sensing receptors in sterile inflammation and inflammatory diseases. *Nat Rev Immunol* (2020) 20(2):95–112. doi: 10.1038/s41577-019-0215-7

34. Godek ML, Michel R, Chamberlain LM, Castner DG, Grainger DW. Adsorbed serum albumin is permissive to macrophage attachment to perfluorocarbon polymer surfaces in culture. *J BioMed Mater Res A* (2009) 88(2):503–19. doi: 10.1002/jbm.a.31886

35. Godek ML, Sampson JA, Duchsherer NL, McElwee Q, Grainger DW. Rho GTPase protein expression and activation in murine monocytes/macrophages is not modulated by model biomaterial surfaces in serum-containing in *vitro* cultures. *J Biomater Sci Polym Ed* (2006) 17(10):1141–58. doi: 10.1163/156856206778530731

36. Anamelechi CC, Truskey GA, Reichert WM. Mylar and Teflon-AF as cell culture substrates for studying endothelial cell adhesion. *Biomaterials* (2005) 26 (34):6887–96. doi: 10.1016/j.biomaterials.2005.04.027

37. Wooten RM, Ma Y, Yoder RA, Brown JP, Weis JH, Zachary JF, et al. Toll-like receptor 2 is required for innate, but not acquired, host defense to Borrelia burgdorferi. *J Immunol* (2002) 168(1):348–55. doi: 10.4049/jimmunol.168.1.348

38. Hou B, Reizis B, DeFranco AL. Toll-like receptors activate innate and adaptive immunity by using dendritic cell-intrinsic and -extrinsic mechanisms. *Immunity* (2008) 29(2):272–82. doi: 10.1016/j.immuni.2008.05.016

39. Mulder R, Banete A, Basta S. Spleen-derived macrophages are readily polarized into classically activated (M1) or alternatively activated (M2) states. *Immunobiology* (2014) 219(10):737–45. doi: 10.1016/j.imbio.2014.05.005

40. Marriott I, Bost KL, Huet-Hudson YM. Sexual dimorphism in expression of receptors for bacterial lipopolysaccharides in murine macrophages: A possible mechanism for gender-based differences in endotoxic shock susceptibility. *J Reprod Immunol* (2006) 71(1):12–27. doi: 10.1016/j.jri.2006.01.004

41. Misharin AV, Morales-Nebreda L, Mutlu GM, Budinger GR, Perlman H. Flow cytometric analysis of macrophages and dendritic cell subsets in the mouse lung. *Am J Respir Cell Mol Biol* (2013) 49(4):503–10. doi: 10.1165/rcmb.2013-0086MA

42. Ye J, Coulouris G, Zaretskaya I, Cutcutache I, Rozen S, Madden TL. Primer-BLAST: a tool to design target-specific primers for polymerase chain reaction. *BMC Bioinf* (2012) 13:134. doi: 10.1186/1471-2105-13-134

43. Hellemans J, Vandesompele J. Selection of reliable reference genes for RT-qPCR analysis. *Methods Mol Biol* (2014) 1160:19–26. doi: 10.1007/978-1-4939-0733-5_3

44. Vandesompele J, De Preter K, Pattyn F, Poppe B, Van Roy N, De Paepe A, et al. Accurate norMalization of real-time quantitative RT-PCR data by geometric averaging of multiple internal control genes. *Genome Biol* (2002) 3(7):RESEARCH0034. doi: 10.1186/gb-2002-3-7-research0034

45. Hellemans J, Mortier G, De Paepe A, Speleman F, Vandesompele J. qBase relative quantification framework and software for management and automated analysis of real-time quantitative PCR data. *Genome Biol* (2007) 8(2):R19. doi: 10.1186/gb-2007-8-2-r19

46. Livak KJ, Schmittgen TD. Analysis of relative gene expression data using real-time quantitative PCR and the 2(-Delta Delta C(T)) Method. *Methods* (2001) 25 (4):402–8. doi: 10.1006/meth.2001.1262

47. Taylor SC, Nadeau K, Abbasi M, Lachance C, Nguyen M, Fenrich J. The ultimate qPCR experiment: producing publication quality, reproducible data the first time. *Trends Biotechnol* (2019) 37(7):761–74. doi: 10.1016/j.tibtech.2018.12.002

48. Ritchie ME, Phipson B, Wu D, Hu Y, Law CW, Shi W, et al. limma powers differential expression analyses for RNA-sequencing and microarray studies. *Nucleic Acids Res* (2015) 43(7):e47. doi: 10.1093/nar/gkv007

49. Benjamini Y, Hochberg Y. Controlling the false discovery rate: A practical and powerful approach to multiple testing, journal of the royal statistical society. *Ser B (Methodological)* (1995) 57(1):289–300. doi: 10.1111/j.2517-6161.1995.tb02031.x

50. Korotkevich G, Sukhov V, Budin N, Shpak B, Artyomov MN, Sergushichev A. Fast gene set enrichment analysis. *bioRxiv* (2021) 060012. doi: 10.1101/060012

51. Subramanian A, Tamayo P, Mootha VK, Mukherjee S, Ebert BL, Gillette MA, et al. Gene set enrichment analysis: a knowledge-based approach for interpreting genome-wide expression profiles. *Proc Natl Acad Sci U.S.A.* (2005) 102(43):15545–50. doi: 10.1073/pnas.0506580102

52. Kolberg L, Raudvere U, Kuzmin I, Vilo J, Peterson H. gprofiler2 – an R package for gene list functional enrichment analysis and namespace conversion toolset g: Profiler [version 2; peer review: 2 approved]. *F1000Research* (2020) 9(ELIXIR):709. doi: 10.12688/f1000research.24956.2

53. Raudvere U, Kolberg L, Kuzmin I, Arak T, Adler P, Peterson H, et al. g:Profiler: a web server for functional enrichment analysis and conversions of gene lists (2019 update). *Nucleic Acids Res* (2019) 47(W1):W191–8. doi: 10.1093/nar/gkz369

54. Perez-Riverol Y, Bai J, Bandla C, Garcia-Seisdedos D, HewapathIrana S, KamatChinathan S, et al. The PRIDE database resources in 2022: a hub for mass spectrometry-based proteomics evidences. *Nucleic Acids Res* (2022) 50(D1):D543–52. doi: 10.1093/nar/gkab1038

55. Kieler M, Hofmann M, Schabbauer G. More than just protein building blocks: how amino acids and related metabolic pathways fuel macrophage polarization. *FEBS J* (2021) 288(12):3694–714. doi: 10.1111/febs.15715

56. Gorbet MB, Sefton MV. Complement inhibition reduces material-induced leukocyte activation with PEG modified polystyrene beads (Tentagel) but not polystyrene beads. *J BioMed Mater Res A* (2005) 74(4):511–22. doi: 10.1002/jbm.a.30354

57. Gorbet MB, Sefton MV. Biomaterial-associated thrombosis: roles of coagulation factors, complement, platelets and leukocytes. *Biomaterials* (2004) 25(26):5681–703. doi: 10.1016/j.biomaterials.2004.01.023

58. Ekdahl KN, Fromell K, Mannes M, Grinnemo KH, Huber-Lang M, Teramura Y, et al. Therapeutic regulation of complement activation in extracorporeal circuits and intravascular treatments with special reference to the alternative pathway amplification loop. *Immunol Rev* (2023) 313(1):91–103. doi: 10.1111/imr.13148

59. Liu W, Xiong S, Du J, Song Y, Wang T, Zhang Y, et al. Deciphering key foreign body reaction-related transcription factors and genes through transcriptome analysis. *Front Mol Biosci* (2022) 9:843391. doi: 10.3389/fmolb.2022.843391

60. Gorbet M, Sperling C, Maitz MF, Siedlecki CA, Werner C, Sefton MV. The blood compatibility challenge. Part 3: Material associated activation of blood cascades and cells. *Acta Biomater* (2019) 94:25–32. doi: 10.1016/j.actbio.2019.06.020

61. Wells LA, Guo H, Emili A, Sefton MV. The profile of adsorbed plasma and serum proteins on methacrylic acid copolymer beads: Effect on complement activation. *Biomaterials* (2017) 118:74–83. doi: 10.1016/j.biomaterials.2016.11.036

62. Rodriguez A, Meyerson H, Anderson JM. Quantitative in *vivo* cytokine analysis at synthetic biomaterial implant sites. *J BioMed Mater Res A* (2009) 89(1):152–9. doi: 10.1002/jbm.a.31939

63. Baer M, Dillner A, Schwartz RC, Sedon C, Nedospasov S, Johnson PF. Tumor necrosis factor alpha transcription in macrophages is attenuated by an autocrine factor that preferentially induces NF-kappaB p50. *Mol Cell Biol* (1998) 18(10):5678–89. doi: 10.1128/MCB.18.10.5678

64. Liu H, Sidiropoulos P, Song G, Pagliari LJ, Birrer MJ, Stein B, et al. TNF-alpha gene expression in macrophages: regulation by NF-kappa B is independent of c-Jun or C/EBP beta. *J Immunol* (2000) 164(8):4277–85. doi: 10.4049/jimmunol.164.8.4277

65. Alexander AF, Kelsey I, Forbes H, Miller-Jensen K. Single-cell secretion analysis reveals a dual role for IL-10 in restraining and resolving the TLR4-induced inflammatory response. *Cell Rep* (2021) 36(12):109728. doi: 10.1016/j.celrep.2021.109728

66. El Kasmi KC, Qualls JE, Pesce JT, Smith AM, Thompson RW, Henao-Tamayo M, et al. Toll-like receptor-induced arginase 1 in macrophages thwarts effective immunity against intracellular pathogens. *Nat Immunol* (2008) 9(12):1399–406. doi: 10.1038/ni.1671

67. Bayik D, Tross D, Haile LA, Verthelyi D, Klinman DM. Regulation of the maturation of human monocytes into immunosuppressive macrophages. *Blood Adv* (2017) 1(26):2510–9. doi: 10.1182/bloodadvances.2017011221

68. Wang J, Shirota Y, Bayik D, Shirota H, Tross D, Gulley JL, et al. Effect of TLR agonists on the differentiation and function of human monocytic myeloid-derived suppressor cells. *J Immunol* (2015) 194(9):4215–21. doi: 10.4049/jimmunol.1402004

69. Liu Y, Luo S, Zhan Y, Wang J, Zhao R, Li Y, et al. Increased expression of PPAR-gamma modulates monocytes into a M2-like phenotype in SLE patients: an implicative protective mechanism and potential therapeutic strategy of systemic lupus erythematosus. *Front Immunol* (2020) 11:579372. doi: 10.3389/fimmu.2020.579372

70. Funderburg NT, Jadlowsky JK, Lederman MM, Feng Z, Weinberg A, Sieg SF. The Toll-like receptor 1/2 agonists Pam(3) CSK(4) and human beta-defensin-3 differentially induce interleukin-10 and nuclear factor-kappaB signalling patterns in human monocytes. *Immunology* (2011) 134(2):151–60. doi: 10.1111/j.1365-2567.2011.03475.x

71. Witherel CE, Abebayehu D, Barker TH, Spiller KL. Macrophage and fibroblast interactions in biomaterial-mediated fibrosis. *Adv Healthc Mater* (2019) 8(4):e1801451. doi: 10.1002/adhm.201801451

72. Palmer JA, Abberton KM, Mitchell GM, Morrison WA. Macrophage phenotype in response to implanted synthetic scaffolds: an immunohistochemical study in the rat. *Cells Tissues Organs* (2014) 199(2-3):169–83. doi: 10.1159/000363693

73. Badylak SF, Valentin JE, Ravindra AK, McCabe GP, Stewart-Akers AM. Macrophage phenotype as a determinant of biologic scaffold remodeling. *Tissue Eng Part A* (2008) 14(11):1835–42. doi: 10.1089/ten.tea.2007.0264

74. Adachi O, Kawai T, Takeda K, Matsumoto M, Tsutsui H, Sakagami M, et al. Targeted disruption of the MyD88 gene results in loss of IL-1- and IL-18-mediated function. *Immunity* (1998) 9(1):143–50. doi: 10.1016/S1074-7613(00)80596-8

75. Zardeneta G, Mukai H, Marker V, Milam SB. Protein interactions with particulate Teflon: implications for the foreign body response. *J Oral Maxillofac Surg* (1996) 54(7):873–8. doi: 10.1016/S0278-2391(96)90540-6

76. Bohnert JL, Fowler BC, Horbett TA, Hoffman AS. Plasma gas discharge deposited fluorocarbon polymers exhibit reduced elutability of adsorbed albumin and fibrinogen. *J Biomater Sci Polym Ed* (1990) 1(4):279–97. doi: 10.1163/156856289x00154

77. Maitz MF, Martins MCL, Grabow N, Matschegewski C, Huang N, Chaikof EL, et al. The blood compatibility challenge. Part 4: Surface modification for hemocompatible materials: Passive and active approaches to guide blood-material interactions. *Acta Biomater* (2019) 94:33–43. doi: 10.1016/j.actbio.2019.06.019

78. Brash JL, Horbett TA, Latour RA, Tengvall P. The blood compatibility challenge. Part 2: Protein adsorption phenomena governing blood reactivity. *Acta Biomater* (2019) 94:11–24. doi: 10.1016/j.actbio.2019.06.022

79. Jaffer IH, Weitz JI. The blood compatibility challenge. Part 1: Blood-contacting medical devices: The scope of the problem. *Acta Biomater* (2019) 94:2–10. doi: 10.1016/j.actbio.2019.06.021

80. Richards CM, McRae SA, Ranger AL, Klegeris A. Extracellular histones as damage-associated molecular patterns in neuroinflammatory responses. *Rev Neurosci* (2022) 34(5):533–58. doi: 10.1515/revneuro-2022-0091

81. Yang H, Wang H, Andersson U. Targeting inflammation driven by HMGB1. *Front Immunol* (2020) 11:484. doi: 10.3389/fimmu.2020.00484

82. Aucott H, Sowinska A, Harris HE, Lundback P. Ligation of free HMGB1 to TLR2 in the absence of ligand is negatively regulated by the C-terminal tail domain. *Mol Med* (2018) 24(1):19. doi: 10.1186/s10020-018-0021-x

83. Chen R, Kang R, Fan XG, Tang D. Release and activity of histone in diseases. *Cell Death Dis* (2014) 5(8):e1370. doi: 10.1038/cddis.2014.337

84. Ekaney ML, Otto GP, Sossdorf M, Sponholz C, Boehringer M, Loesche W, et al. Impact of plasma histones in human sepsis and their contribution to cellular injury and inflammation. *Crit Care* (2014) 18(5):543. doi: 10.1186/s13054-014-0543-8

85. Huang H, Evankovich J, Yan W, Nace G, Zhang L, Ross M, et al. Endogenous histones function as alarmins in sterile inflammatory liver injury through Toll-like receptor 9 in mice. *Hepatology* (2011) 54(3):999–1008. doi: 10.1002/hep.24501

86. Zeng-Brouwers J, Beckmann J, Nastase MV, Iozzo RV, Schaefer L. *De novo* expression of circulating biglycan evokes an innate inflammatory tissue response via MyD88/TRIF pathways. *Matrix Biol* (2014) 35:132–42. doi: 10.1016/j.matbio.2013.12.003

87. He Y, Li S, Tang D, Peng Y, Meng J, Peng S, et al. Circulating Peroxiredoxin-1 is a novel damage-associated molecular pattern and aggravates acute liver injury via promoting inflammation. *Free Radic Biol Med* (2019) 137:24–36. doi: 10.1016/j.freeradbiomed.2019.04.012

88. Shichita T, Hasegawa E, Kimura A, Morita R, Sakaguchi R, Takada I, et al. Peroxiredoxin family proteins are key initiators of post-ischemic inflammation in the brain. *Nat Med* (2012) 18(6):911–7. doi: 10.1038/nm.2749

89. Riddell JR, Bshara W, Moser MT, Spernyak JA, Foster BA, Gollnick SO. Peroxiredoxin 1 controls prostate cancer growth through Toll-like receptor 4-dependent regulation of tumor vasculature. *Cancer Res* (2011) 71(5):1637–46. doi: 10.1158/0008-5472.CAN-10-3674

90. Riddell JR, Wang XY, Minderman H, Gollnick SO. Peroxiredoxin 1 stimulates secretion of proinflammatory cytokines by binding to TLR4. *J Immunol* (2010) 184(2):1022–30. doi: 10.4049/jimmunol.0901945

91. van Eden W, Spiering R, Broere F, van der Zee R. A case of mistaken identity: HSPs are no DAMPs but DAMPERs. *Cell Stress Chaperones* (2012) 17(3):281–92. doi: 10.1007/s12192-011-0311-5

92. Bausinger H, Lipsker D, Ziylan U, Manie S, Briand JP, Cazenave JP, et al. Endotoxin-free heat-shock protein 70 fails to induce APC activation. *Eur J Immunol* (2002) 32(12):3708–13. doi: 10.1002/1521-4141(200212)32:12<3708::AID-IMMU3708>3.0.CO;2-C

93. Nakayasu ES, Gritsenko M, Piehowski PD, Gao Y, Orton DJ, Schepmoes AA, et al. Tutorial: best practices and considerations for mass-spectrometry-based protein

biomarker discovery and validation. *Nat Protoc* (2021) 16(8):3737–60. doi: 10.1038/s41596-021-00566-6

94. Mollnes TE, Brekke OL, Fung M, Fure H, Christiansen D, Bergseth G, et al. Essential role of the C5a receptor in E coli-induced oxidative burst and phagocytosis revealed by a novel lepirudin-based human whole blood model of inflammation. *Blood* (2002) 100(5):1869–77. doi: 10.1182/blood.V100.5.1869.h81702001869_1869_1877

95. Andersson J, Ekdahl KN, Lambris JD, Nilsson B. Binding of C3 fragments on top of adsorbed plasma proteins during complement activation on a model biomaterial surface. *Biomaterials* (2005) 26(13):1477–85. doi: 10.1016/j.biomaterials.2004.05.011

96. McKiel LA, Woodhouse KA, Fitzpatrick LE. The role of Toll-like receptor signaling in the macrophage response to implanted materials. *MRS Commun* (2020) 10:55–68. doi: 10.1557/mrc.2019.154

frontiers | Frontiers in Immunology

TYPE Original Research
PUBLISHED 14 September 2023
DOI 10.3389/fimmu.2023.1240552

OPEN ACCESS

EDITED BY
Oliver Planz,
University of Tübingen, Germany

REVIEWED BY
Lydia Marie Roberts,
National Institute of Allergy and Infectious Diseases (NIH), United States
Michihito Kyo,
Harvard Medical School, United States

*CORRESPONDENCE
Stavros Selemidis
stavros.selemidis@rmit.edu.au

RECEIVED 15 June 2023
ACCEPTED 28 August 2023
PUBLISHED 14 September 2023

CITATION
Miles MA, Liong S, Liong F, Coward-Smith M, Trollope GS, Oseghale O, Erlich JR, Brooks RD, Logan JM, Hickey S, Wang H, Bozinovski S, O'Leary JJ, Brooks DA and Selemidis S (2023) TLR7 promotes chronic airway disease in RSV-infected mice. *Front. Immunol.* 14:1240552. doi: 10.3389/fimmu.2023.1240552

TLR7 promotes chronic airway disease in RSV-infected mice

Mark A. Miles[1], Stella Liong[1], Felicia Liong[1], Madison Coward-Smith[1], Gemma S. Trollope[1], Osezua Oseghale[1], Jonathan R. Erlich[1], Robert D. Brooks[2], Jessica M. Logan[2], Shane Hickey[2], Hao Wang[1], Steven Bozinovski[1], John J. O'Leary[3,4], Doug A. Brooks[2,3] and Stavros Selemidis[1]*

[1]Centre for Respiratory Science and Health, School of Health and Biomedical Sciences, RMIT University, Bundoora, VIC, Australia, [2]Clinical and Health Sciences, University of South Australia, Adelaide, SA, Australia, [3]Discipline of Histopathology, School of Medicine, Trinity Translational Medicine Institute (TTMI), Trinity College Dublin, Dublin, Ireland, [4]Sir Patrick Dun's Laboratory, Central Pathology Laboratory, St James's Hospital, Dublin, Ireland

Respiratory syncytial virus (RSV) commonly infects the upper respiratory tract (URT) of humans, manifesting with mild cold or flu-like symptoms. However, in infants and the elderly, severe disease of the lower respiratory tract (LRT) often occurs and can develop into chronic airway disease. A better understanding of how an acute RSV infection transitions to a LRT chronic inflammatory disease is critically important to improve patient care and long-term health outcomes. To model acute and chronic phases of the disease, we infected wild-type C57BL/6 and toll-like receptor 7 knockout (TLR7 KO) mice with RSV and temporally assessed nasal, airway and lung inflammation for up to 42 days post-infection. We show that TLR7 reduced viral titers in the URT during acute infection but promoted pronounced pathogenic and chronic airway inflammation and hyperreactivity in the LRT. This study defines a hitherto unappreciated molecular mechanism of lower respiratory pathogenesis to RSV, highlighting the potential of TLR7 modulation to constrain RSV pathology to the URT.

KEYWORDS

toll-like receptor 7, respiratory syncytial virus, inflammation, airway hyperreactivity, viral infection

1 Introduction

Respiratory syncytial virus (RSV) causes widespread global infection, with most children under the age of two being infected. While infection typically manifests in the upper respiratory tract (URT) and presents as a mild cold, it is estimated that a tenth of the 34 million global cases annually progress to a lower respiratory tract (LRT) infection (LRTI) leading to bronchiolitis and even hospitalization, particularly in the young children and elderly (1). Indeed, nearly a quarter of LRTI-related deaths in young children are associated with RSV, and this disease is the leading cause of hospitalization in infants (2). Although high-risk groups such as pre-term infants or those with existing respiratory or

congenital heart disease are more likely to be hospitalized, most children experiencing severe RSV infection have been previously healthy; highlighting the indiscriminate nature of the disease progression (3). Frequent reinfection is also common in older children and adults, highlighting a susceptibility issue and lack of established long-term immunity after infection (4). Encouragingly, two RSV vaccines were recently FDA approved for use in older adults (5, 6), although effective therapeutic interventions for all patients with an RSV infection is still limited (7).

Infants who develop severe bronchiolitis due to RSV infection are at risk of developing recurrent wheezing, asthma and/or allergic sensitization (8, 9), emphasizing the potential long-term disease burden caused by this virus. The increased susceptibility of infected individuals to other respiratory disease (e.g. asthma), could be due to heightened RSV-driven airway reactivity and/or tissue injury, which has resulted from RSV infection during infant lung development (10). Pulmonary and mucosal immunoregulatory responses of immune and epithelial cells to RSV infection are also important determinants of disease severity and exacerbation in both children and adults (11). This is likely due to the developing immune landscape in infants, which is temporally shaped by its response to environmental and pathological challenges in early life (12). RSV infection also tends to create an age-dependent type-2 skewed immunological environment in infants that often results in a suboptimal antiviral response and chronic inflammation (13). Furthermore, adults (stronger Th1 immune bias) are more likely to succumb to RSV infection when neutrophil numbers in the mucosa are high at the time of inoculation (14). Mouse studies using C57BL/6 mice (representing a Th1 skewed animal model) recapitulating the human challenge trials described above revealed neutrophilic inflammation promoted an exacerbated cytotoxic CD8+ T cell response that underpins the long-term respiratory disease, including airway hyperactivity (14). An important balance of host Th1, Th2 and Th17 antiviral and proinflammatory immune responses is therefore required to ensure efficient viral clearance and to avoid uncontrolled excessive inflammation (11), which can have damaging effects on the airways and can also enhance viral pathogenicity.

RSV is a single-stranded RNA (ssRNA) virus that enters host cells via a pH-independent fusion mechanism, although proteolytic cleavage of the Fusion protein by host furin was reported in a low pH-dependent manner in early endosomes, implicating the involvement of the endocytic pathway in RSV biology (15, 16). However, RSV infection of certain cell types occurs directly into the cytosol and is independent of endosomal compartments (17). Pattern recognition receptors (PRRs) such as toll-like receptors (TLRs), some of which reside within the endosome, initiate important innate responses to infection upon sensing of pathogen-associated molecular patterns (18), but as RSV can enter directly into the cytosol this may limit detection by these TLRs until later in the infection process. TLR7 senses endosomally localized ssRNA and its activation triggers downstream induction of transcription factor genes, such as interferon regulatory factors (IRFs) or nuclear factor-κB (NFκB), to mediate host antiviral responses that are critical for establishing an appropriate immune response. The sensing of ssRNA viruses, such as influenza A (IAV), SARS-CoV2 and RSV, is dependent on a high level of TLR7 being expressed in plasmacytoid dendritic cells (pDCs), patrolling monocytes, macrophages and B cells, and is necessary to modulate various arms of the innate and adaptive immune system (19). Retinoic acid-inducible gene I (RIG-I)-like receptors (RLRs) are another family of PRRs that also potently induce type I IFN responses upon cytosolic sensing of ssRNA (20), and these are important for early antiviral responses to RSV infection (21). Due to the potential of RSV to be sensed in either the cytosol by RLRs and/or the endosome by TLR7/8, both systems may contribute to hyperinflammation in response to RSV infection either individually, sequentially or simultaneously.

TLR7 has a potential protective role during the acute phases of viral infection (22–25) by driving an early Th1 response in the lungs to evoke an antiviral response. However, a hyperinflammatory "cytokine storm" setting within the airways and lungs could arise if TLR7-mediated inflammatory responses are not appropriately resolved following viral clearance. This has been recently shown for SARS-CoV2 infection where pDC-dependent TLR7 activation by the virus drives type I IFN signaling and mediates both transcriptional and epigenetic alterations in macrophages to favor their hyperactivation in patients with severe COVID-19 (26). Similarly, during severe IAV infection, the pharmacological suppression of TLR7 reduced monocyte- and neutrophil-driven lung inflammation, which restricted the resultant downstream pathology (27). The establishment of an immunopathological niche following improper immune regulation and excess inflammation can potentiate viral pathogenicity and exacerbate chronic airway inflammatory disease (28). Fewer studies have investigated the role of TLR7 in RSV infection, which is the focus herein. While these studies have identified enhanced mucus production in the airways (29) or delayed innate pDC immune responses that impact viral clearance (30) in TLR7-deficient mice, the ability of TLR7 to potentiate RSV-induced chronic respiratory disease has not been previously investigated. Interestingly, RSV transcripts were detected in the lungs of mice several months following infection and reportedly correlated with chronic airway hyperreactivity (31). As viral RNA can engage TLR7, RSV persistence may stimulate concurrent inflammation by TLR7, possibly driving a chronic inflammatory phenotype.

Here, we have interrogated the role of TLR7 in both acute and chronic RSV-induced pathogenesis with a focus on URT (nasal) and LRT (upper airways and lung) responses.

2 Results

2.1 TLR7 modestly regulates viral clearance in the URT to suppress localized inflammation

To assess the impact of TLR7 during acute and chronic RSV infection, WT and TLR7 KO mice were infected with RSV and airway and lung inflammation subsequently measured at early (4 or 7 dpi) or late (42 dpi) timepoints to model different phases of the disease. We first investigated nasal tissue to understand the contribution of TLR7 to antiviral responses in the URT. Gene expression analysis of the nasal tissue revealed that early infection (4 dpi) did not alter TLR expression, including that of TLR7 despite virus being present and

evoking elevated IRF-7 and IFN-β expression (Figures 1A, B). Indeed, the expression of RIG-I/DDX58 and its positive regulator LGP2/DHX58 were higher at this timepoint. Deletion of TLR7 did not change the levels of virus, IFN-β or DHX58, although the expression of TLR8 and TLR9 was significantly higher than in WT mice, suggesting the presence of active TLR7 may suppress other TLR activation/function. TLR7 expression rose significantly at 7 dpi in WT mice, although this was not associated with any changes in type I IFN (Figure 1A). Interestingly, significant levels of virus were detected in the nasal tissue of TLR7 KO mice at 7 dpi (Figure 1C) and this coincided with significantly elevated expression of PRRs in these mice. Furthermore, we were able to detect viral RNA in the nasal tissue of some mice of either genotype at 42 dpi (Figure 1C, Supplementary Table S1), although PRR expression had returned to near uninfected levels by this time.

The expression of TLR7 in the lungs of WT mice increased significantly after RSV infection, at 4 and 7 dpi, but did not appear to persist chronically, despite the detection of residual viral mRNA at 42 dpi (Figure 1D). Upregulation of various TLRs and RLRs similarly occurred in the presence or absence of TLR7 at 4 dpi and were retained at 7 dpi, but only in WT mice (Figure 1D). PRR regulation was significantly suppressed in the lungs of TLR7 KO mice at 7 dpi. Unlike in the nasal tissue, this difference did not impact acute clearance of RSV in the lungs as viral titres remained the same in both genotypes (Figure 1F), implying that antiviral responses were not compromised in the LRT of TLR7 KO mice. Indeed, IFN-β and IRF-7 expression in the lung were elevated upon RSV infection at 4 dpi in both genotypes, with significantly higher IFN-β levels in TLR7 KO mice (Figure 1E). Resolution of type I IFN expression was evident at day 7 and occurred more dramatically in TLR7 KO mice. The low level mRNA viral transcripts detected at 42 dpi were consistent with previous observations of chronic RSV persistence in the lungs (32) and a statistically significant higher viral titre in the lung was observed in TLR7 KO mice at 42 dpi (Figure 1F, Supplementary Table S1).

These data indicate that RSV infection engages various IFN-stimulating sensors in the URT where TLR7 modestly contributes to viral clearance. Interestingly, we failed to detect upregulation of inflammatory response genes in the nasal tissue of WT mice in response to acute RSV infection. In contrast, a significant elevation of various Th1 inflammatory markers IFNγ, IL-1β and TNFα was evident in the nasal tissue of TLR7 KO mice at 7 dpi (Figure 2A). This correlated with the increased expression of the DC marker CD11c/ITGAX as well as the T cell markers CD4, CD8 and CD69 (Figure 2B). Expression of the monocyte/macrophage/granulocyte marker CD11b/ITGAM was unaltered in both mouse genotypes and was accompanied by insignificant increases in CCL3. Additionally, upregulation of PDCA-1/BST2 expression (commonly expressed by pDCs and B cells) was consistent in both mouse genotypes during acute infection (Figure 2B). Strikingly, both WT and TLR7 KO mice displayed elevated nasal expression of CD8 at 42 dpi but this was significantly dampened in TLR7 KO mice (Figure 2B). Furthermore, increased IFNγ expression was additionally detected in the nasal tissue of WT mice at 42 dpi but not in TLR7 KO mice.

These analyses imply that RSV infection induces a dominant antiviral response in the URT of WT mice, and suggests a potential suppression mechanism of acute Th1 cytokine responses by TLR7 in the URT (up to 7 dpi), which likely contributes to the observed chronic persistence of a functional CD8+ cytotoxic T cell and IFNγ response in the URT at day 42.

2.2 TLR7 potentiates enhanced acute and chronic airway inflammation following RSV infection

Our data thus far indicated that TLR7 assists with viral clearance in the URT but its antiviral effects in the LRT are dispensable. Rather, better resolution of type I IFN in the LRT was achieved in the absence of TLR7 without compromising viral clearance. TLR7 also initiates important proinflammatory signals, which we found were suppressed in the URT, and given the apparent TLR7-dependent antiviral persistence in the LRT, sustained TLR7 activation (as observed by elevated lung TLR7 expression at 7 dpi) may contribute to hyperinflammatory responses that can potentially exacerbate LRT pathology. Infiltration of immune cells as a measure of inflammation into the large airways was assessed by bronchoalveolar lavage (BAL) across acute and chronic infection. Airway inflammation peaked at 7 dpi and was significantly lower in TLR7 KO mice across acute timepoints (Figure 3A). This result was in concordance with type I IFN suppression in the nasal tissue at 7 dpi and is consistent with a sequence of antiviral resolution in the URT preceding the dissemination of a robust inflammatory response in the LRT. Interestingly, a significant population of immune cells were retained in the airways of infected WT mice at 42 dpi, but not in TLR7 KO mice. Considering the equivalent level of virus detected acutely in the lungs, this observation indicates that TLR7 enhances airway inflammation without improving viral clearance.

Flow cytometric labelling of immune cell markers revealed that RSV infection induced an early airway influx of innate immune responder cells, comprised of macrophages, monocytes, neutrophils, natural killer (NK) and DCs at 4 dpi (Figure 3B). Eosinophilia also accompanied infection. There were significantly less pDCs and myeloid dendritic cells (mDCs), macrophages and monocytes in RSV-infected TLR7 KO mice at this timepoint. The frequency of patrolling and inflammatory monocytes in the airways was also significantly reduced in infected TLR7 KO mice (Supplementary Figure S1A). By 7 dpi, the numbers of Ly6C^{hi} inflammatory monocytes and mDCs increased in WT mice while other innate immune cells had decreased. Similar to the inflammation at 4 dpi, the airways of TLR7 KO mice contained less innate immune cell numbers at 7 dpi with significantly lower NK cells and monocytes. There was no difference in the composition of cells in the airways of infected mice between genotypes at 7 dpi (Supplementary Figure S1A). Interestingly, a significant number of pDCs, Ly6C^{lo} patrolling monocytes and eosinophils persisted in the airways of infected WT mice at 42 dpi, with non-significant trends of macrophage and NK cell populations also present (Figure 3B). These lingering cells were absent in infected TLR7 KO mice at 42 dpi.

10.3389/fimmu.2023.1240552

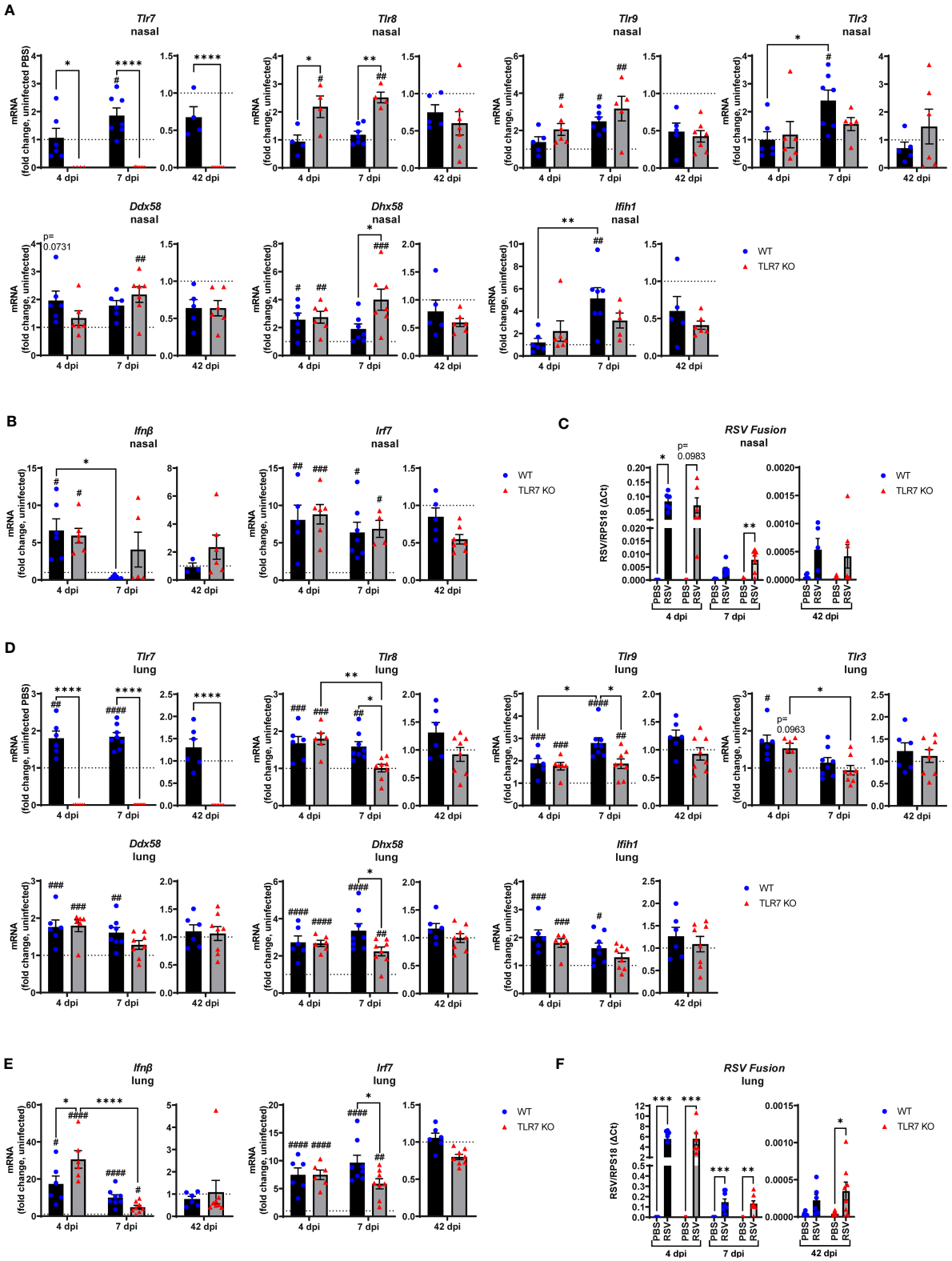

FIGURE 1
Gene expression analysis of pattern recognition receptors, type I IFN and viral titers in the nasal and lung tissue of RSV infected mice. WT C57BL/6 or TLR7 KO mice were infected with RSV (0.5-2x10^7 PFUs) or PBS via intranasal administration. mRNA expression of **(A, D)** pattern recognition receptors, **(B, E)** type I IFN or **(C, F)** RSV Fusion gene was quantified in nasal or lung tissue after 4, 7 or 42 dpi. Responses are relative to RPS18 and expressed as a fold-change above uninfected controls of each mouse genotype. Data are expressed as mean ± SEM, n = 4-8 mice per experimental group from a single experiment. Statistical analysis was conducted using two-way ANOVA test followed by Tukey's *post hoc* test for multiple comparison to compare differences between genotype or infection timepoints (*p < 0.05, **p < 0.01, ****p<0.0001). A Sidak's *post hoc* test was performed to compare differences between uninfected controls (fold change of 1) and respective infected groups for each genotype (***p<0.001, $^{\#}$p < 0.05, $^{\#\#}$p < 0.01, $^{\#\#\#}$p < 0.001, $^{\#\#\#\#}$p < 0.0001).

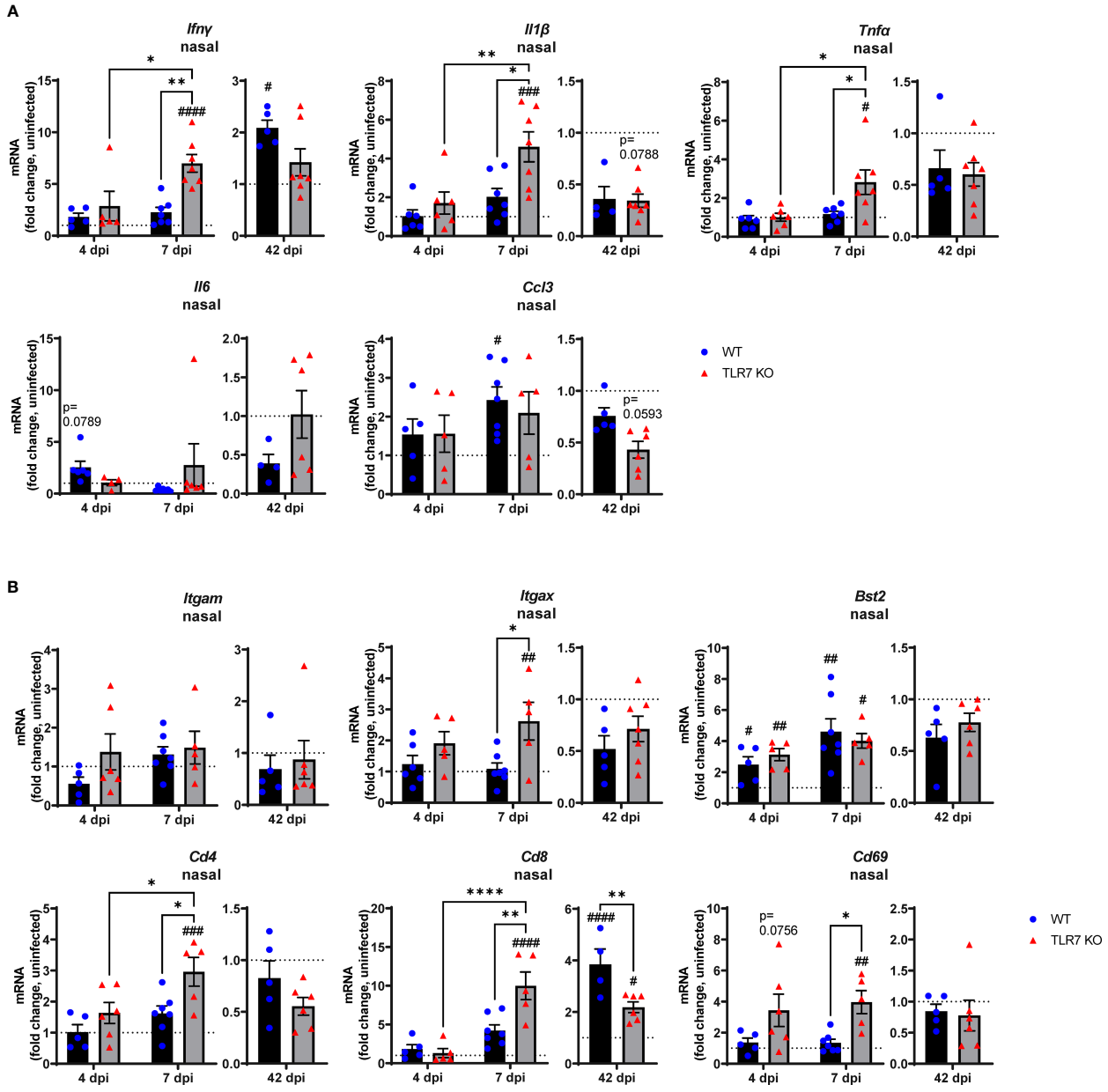

FIGURE 2
TLR7 suppresses acute inflammatory signaling in the nasal tissue following RSV infection. WT C57BL/6 or TLR7 KO mice were infected with RSV (0.5-2x10^7 PFUs) or PBS via intranasal administration. Nasal tissue mRNA expression of various **(A)** proinflammatory cytokines and **(B)** immune specific markers was quantified after 4, 7 or 42 dpi. Responses are relative to RPS18 and expressed as a fold-change above uninfected controls of each mouse genotype. Data are expressed as mean ± SEM, n = 4-8 mice per experimental group from a single experiment. Statistical analysis was conducted using two-way ANOVA test followed by Tukey's *post hoc* test for multiple comparison to compare differences between genotype or infection timepoints (*p < 0.05, **p < 0.01, ****p<0.0001). A Sidak's *post hoc* test was performed to compare differences between uninfected controls (fold change of 1) and respective infected groups for each genotype ($^{\#}$p < 0.05, $^{\#\#}$p < 0.01, $^{\#\#\#}$p < 0.001, $^{\#\#\#\#}$p < 0.0001).

Analysis of the adaptive T cell response revealed the migration of a dominant population of CD4+ helper T cells to the airways of infected mice of both genotypes at 4 dpi, but the T cell response eventually shifted towards a CD8+ cytotoxic phenotype by 7 dpi (Figure 3C, Supplementary Figure S1B). Despite RSV infection increasing CD8+ cytotoxic T cells to similar frequencies in both genotypes, approximately half as many CD8+ cytotoxic T cells were detected in TLR7 KO mice at 7 dpi, although this did not affect overall viral clearance. Interestingly, CD8+ cytotoxic T cells persisted in the airways of infected mice at 42 dpi at similar frequencies in both genotypes, but total cell numbers were lower in TLR7 KO mice. Furthermore, we noted that WT mice exhibited a greater CD8+:CD4+ T cell ratio at 42 dpi compared to TLR7 KO mice. These data reveal an acute TLR7-dependent enhanced total cellular immune response in the airways of RSV-infected mice and a chronic persistence of a subset of immune cells namely CD8+

10.3389/fimmu.2023.1240552

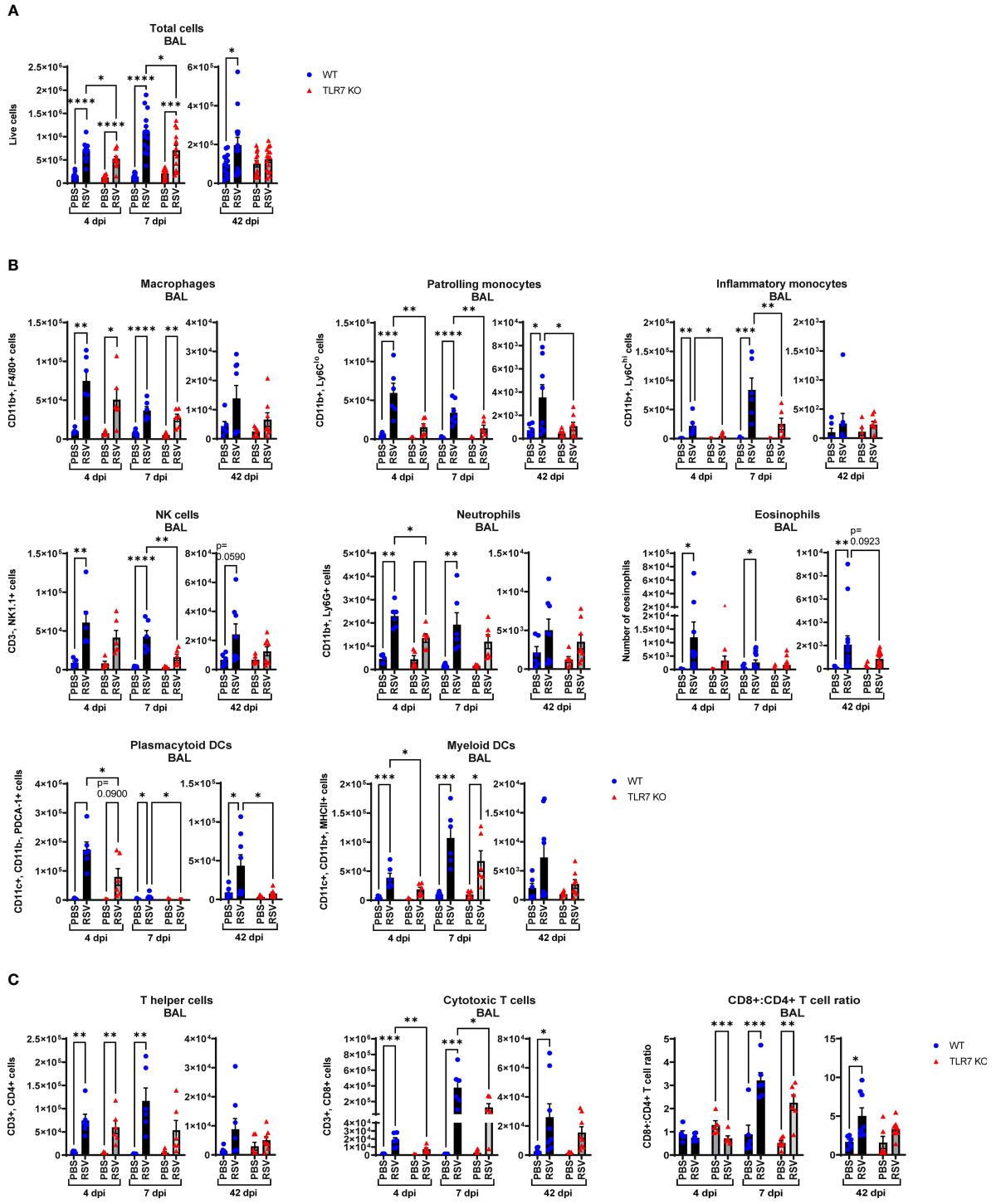

FIGURE 3
RSV-induced airway immune infiltration is reduced in TLR7 KO mice. WT C57BL/6 or TLR7 KO mice were infected with RSV (0.5-2x10^7 PFUs) or PBS via intranasal administration and analysis performed after 4, 7 or 42 dpi. **(A)** Airway inflammation was assessed by counting the total number of live cells isolated from the bronchoalveolar lavage (BAL) fluid. Data are expressed as mean ± SEM, n = 12-16 mice per experimental group from three independent experiments. Immune cell populations in the airways collected in the BAL fluid were determined by flow cytometry. **(B)** Innate immune cell types: interstitial macrophages (CD11b$^+$ F4/80$^+$), patrolling monocytes (CD11b$^+$ Ly6C^{lo}), inflammatory monocytes (CD11b$^+$ Ly6C^{hi}), NK cells (CD3$^-$ NK1.1$^+$), neutrophils (CD11b$^+$ Ly6G$^+$), plasmacytoid DCs (CD11c$^+$ CD11b$^-$ PDCA-1$^+$) and myeloid DCs (CD11c$^+$ CD11b$^+$ MHCII$^+$). Numbers of differentially stained eosinophils was determined by counting 500 cells from random fields by standard morphological criteria relative to the total number of isolated cells. **(C)** Adaptive T cell subtypes: T helper (CD3$^+$ CD4$^+$) and cytotoxic T cells (CD3$^+$ CD8$^+$). Cell populations were measured as absolute number of CD45$^+$ population per total live cells. Data are expressed as mean ± SEM, n = 5-8 mice per experimental group from two independent experiments. Statistical analysis was conducted using two-way ANOVA test followed by Tukey's *post hoc* test for multiple comparison test (*p < 0.05, **p < 0.01, ***p<0.001, ****p<0.0001).

cytotoxic T cells, NK cells, patrolling monocytes, eosinophils and pDCs.

2.3 RSV infection provokes TLR7-dependent lung pathology

Our analysis of persistent immune cell infiltration detected in the BAL fluid indicated that this model of RSV infection induces chronic inflammation of the larger airways in the LRT that is driven by TLR7. As mentioned earlier, severe RSV infection of the LRT can manifest in some individuals leading to bronchiolitis and pneumonia. RSV infection induced lung oedema in WT mice at 7 dpi, as evidenced by significantly heavier lung weights compared to uninfected lungs, but this oedema was absent in TLR7 KO mice infected with RSV (Figure 4A). This may be an indication of the greater infiltration of inflammatory cells to the lungs of TLR7 expressing mice following infection, consistent with enhanced airway infiltration.

Haematoxylin and eosin (H&E) staining of lung sections was conducted to assess the level of inflammation within the lung tissue. Acute alveolitis was evident in RSV-infected WT mice while TLR7 KO mice showed no difference in alveolar inflammation with infection (Figures 4B, C). Inflammation into the alveolar wall near the bronchioles peaked at 7 dpi in WT mice whereas in TLR7 KO mice there was significantly less infiltration of inflammatory cells around the bronchioles. Additionally, RSV infection resulted in an insignificant trend towards chronic alveolitis at 42 dpi in WT mice but this was not evident in TLR7 KO mice. There were overall fewer inflammatory cells infiltrating the lung tissue of TLR7 KO mice compared to WT mice during acute infection. No significant differences in the degree of immune infiltration of infected lungs were detected at 42 dpi in either mouse genotype, suggesting a resolution of immune lung infiltration, at least by H&E observation. This histological analysis indicates that RSV infection induces an infiltration of cells into the deep airway spaces of the lung, which is likely to be TLR7-dependent, leading to chronic alveolitis and enhanced bronchiolar inflammation.

We further analyzed the infiltrating immune cell types in the lungs following RSV infection at both acute and chronic stages. Significant changes in immune cell numbers (monocytes, DCs and NK cells) in the lungs of WT mice following infection were evident at 7 dpi (Figure 5A). The lungs of infected TLR7 KO mice consisted of significantly less pDCs, and a trend towards less NK cells, mDCs monocytes at 7 dpi (Figure 5A). Populations of CD4+ and CD8+ T cell subtypes were similar in the infected lungs of either mouse genotype. While infection at day 7 increased the CD8+:CD4+ T cell ratio in the lungs of both genotypes, this was significantly lower in TLR7 KO mice (Figure 5B). This, in conjunction with the immune analysis of the airways, implied an overall reduced T cell effector response in the absence of TLR7, without compromising viral clearance. However, unlike in the upper airways of the LRT, infection did not result in any chronic increases of immune cells in the lungs at 42 dpi.

These data show that RSV infection causes a TLR7-dependent infiltration of inflammatory cells to the deeper lung tissue and that the chronic inflammatory phenotype, in addition to the acute phase of infection, is mainly localized to the upper airways of the LRT.

2.4 TLR7 drives an exacerbated Th1/Th2 proinflammatory profile in the lungs following RSV infection

To further dissect the immunopathological mechanism driven by TLR7-mediated hyperinflammatory responses in the LRT during RSV infection, we analyzed the expression of key Th1 and Th2 cytokine mediators as alterations in these responses can influence the severity of RSV infection and risk of subsequent respiratory illness, particularly in early life (33, 34). Early inflammasome activation was induced 4 dpi, as evidenced by increased expression of NLRP3 and IL-18, as well as IL-6 and TNFα upregulation in the lungs of both mouse genotypes (Figure 6A). Lung IL-1β gene and protein expression were higher at 7 dpi in WT mice, as were NLRP3, IL-6 and TNFα gene levels, however these proinflammatory markers were suppressed in the absence of TLR7. This also correlated with a TLR7-dependent alteration in chemotactic factors: where infection raised the levels of CXCL2, CCL3 and CCL11 chemokines at 4 and 7 dpi in WT mice, but these responses were blunted in TLR7 KO mice (Figure 6B), most likely accounting for the reduced airway infiltration of neutrophils, macrophages and eosinophils in TLR7 KO mice.

Inflammasome activation has direct effects on shaping the Th1, Th2 and Th17 immune responses (35). Infection promoted early expression of the Th1 cytokine IFNγ in the lungs at day 4 that dramatically rose by more than 10-fold at 7 dpi (Figure 6C). Gene expression of another Th1 cytokine IL-12 in the lung did not change with infection. The levels of IFNγ were similar between genotypes at 4 dpi, but TLR7 KO mice expressed significantly less IFNγ at 7 dpi. This observation in the lungs of TLR7 KO mice at 7 dpi contrasts with the nasal tissue analysis in which these mice displayed higher IFNγ expression at the same timepoint (Figure 2A). However, secreted protein levels of IFNγ in the BALF at 7 dpi (Figure 6C) mirrored the nasal tissue data demonstrating higher IFNγ levels in the airways of TLR7 KO mice, consistent with delayed viral clearance in the URT. This suggests that the loss of TLR7 enhances Th1 responses in the URT, but limits hyperactivation in the LRT. In regard to Th2 cytokines, higher IL-13 expression was detected at 4 dpi in WT lungs and was retained at 7 dpi (Figure 6D). This early IL-13 response at 4 dpi was blunted in TLR7 KO mice, but rose to similar levels to WT mice at 7 dpi. In contrast, the IL-4 response was not evident until 7 dpi and was only detected in the WT lung.

The expression profile of the panel of inflammatory cytokines and chemokines analyzed was unaltered in the infected lung tissue of both genotypes of mice at 42 dpi. This is in contrast to the URT, where only infected WT mice showed significantly higher IFNγ expression in the nasal tissue (Figure 2A) or BALF (Figure 6C) at the day 42 timepoint. Analysis of the IFNγ:IL-13 ratio as an indicator of Th1 versus Th2 response supported the notion of a dominant Th1 response in the lungs of infected WT mice at day 7, which was retained at day 42 (Figure 6E). This analysis also

10.3389/fimmu.2023.1240552

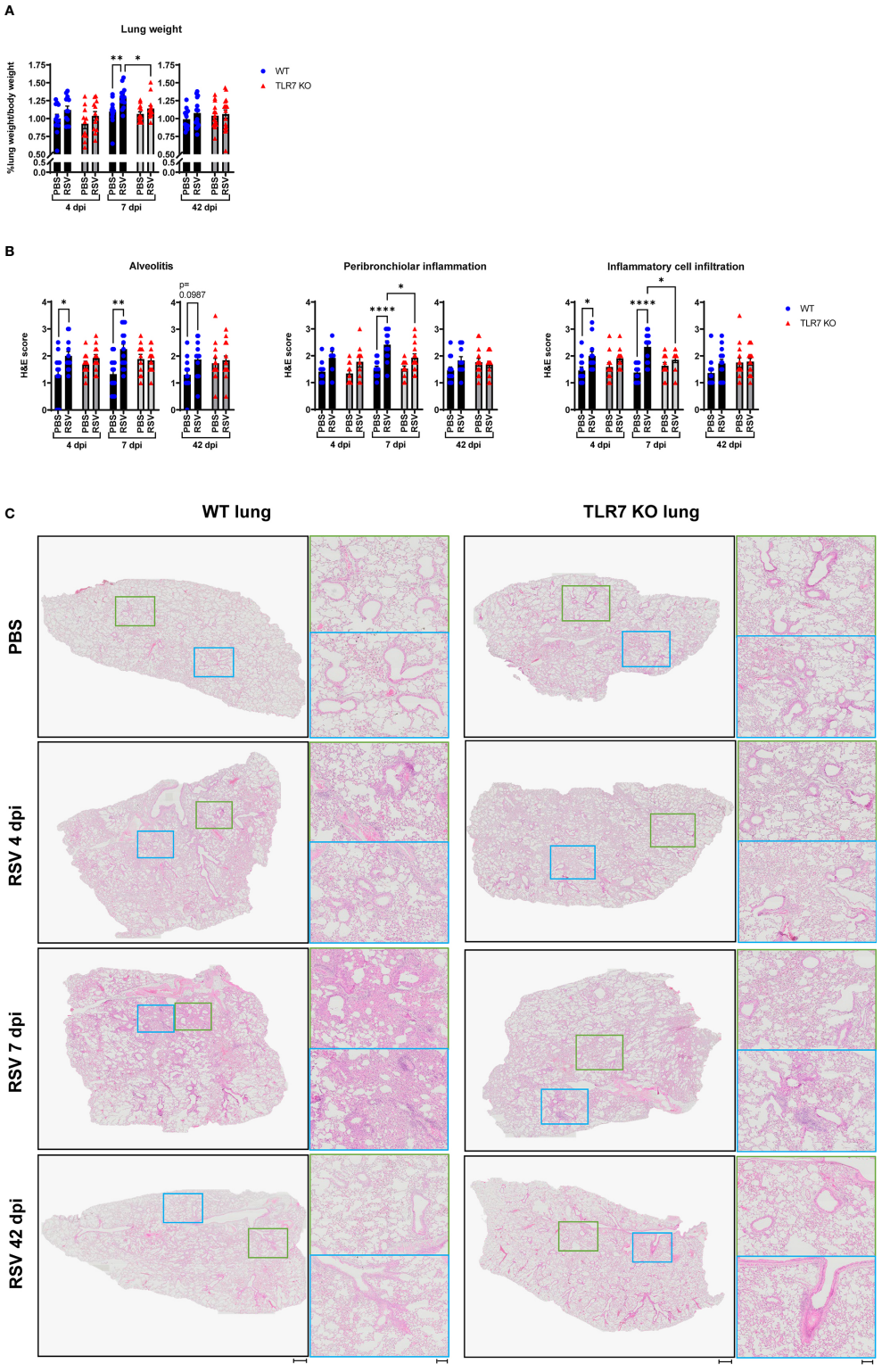

FIGURE 4
TLR7 KO mice have reduced lung pathology following RSV infection. WT C57BL/6 or TLR7 KO mice were infected with RSV (0.5-2x10^7 PFUs) or PBS via intranasal administration, then lung pathology was assessed after 4, 7 or 42 dpi. **(A)** Pulmonary oedema was assessed by measuring the wet lung weight to bodyweight ratio. **(B)** Lung histopathological analysis was assessed for alveolitis (alveolar inflammation of parenchyma), total inflammatory cell infiltrate and peribronchiolar inflammation (inflammation around bronchiolar airway wall) using a scoring system of 0–5 for each individual mouse, where higher numbers indicate increased severity. Each section was scored blindly by two independent assessors. **(C)** Representative images displaying lung inflammation from paraffin embedded lung sectioned (4 µm) longitudinally and stained with H&E. Scale bars represent 1 mm in the overview and 100 µm for the zoomed images. Data are expressed as mean ± SEM, n = 12-16 mice per experimental group from three independent experiments. Statistical analysis was conducted using two-way ANOVA test followed by Tukey's *post hoc* test for multiple comparison test (*p < 0.05, **p < 0.01, ****p<0.0001).

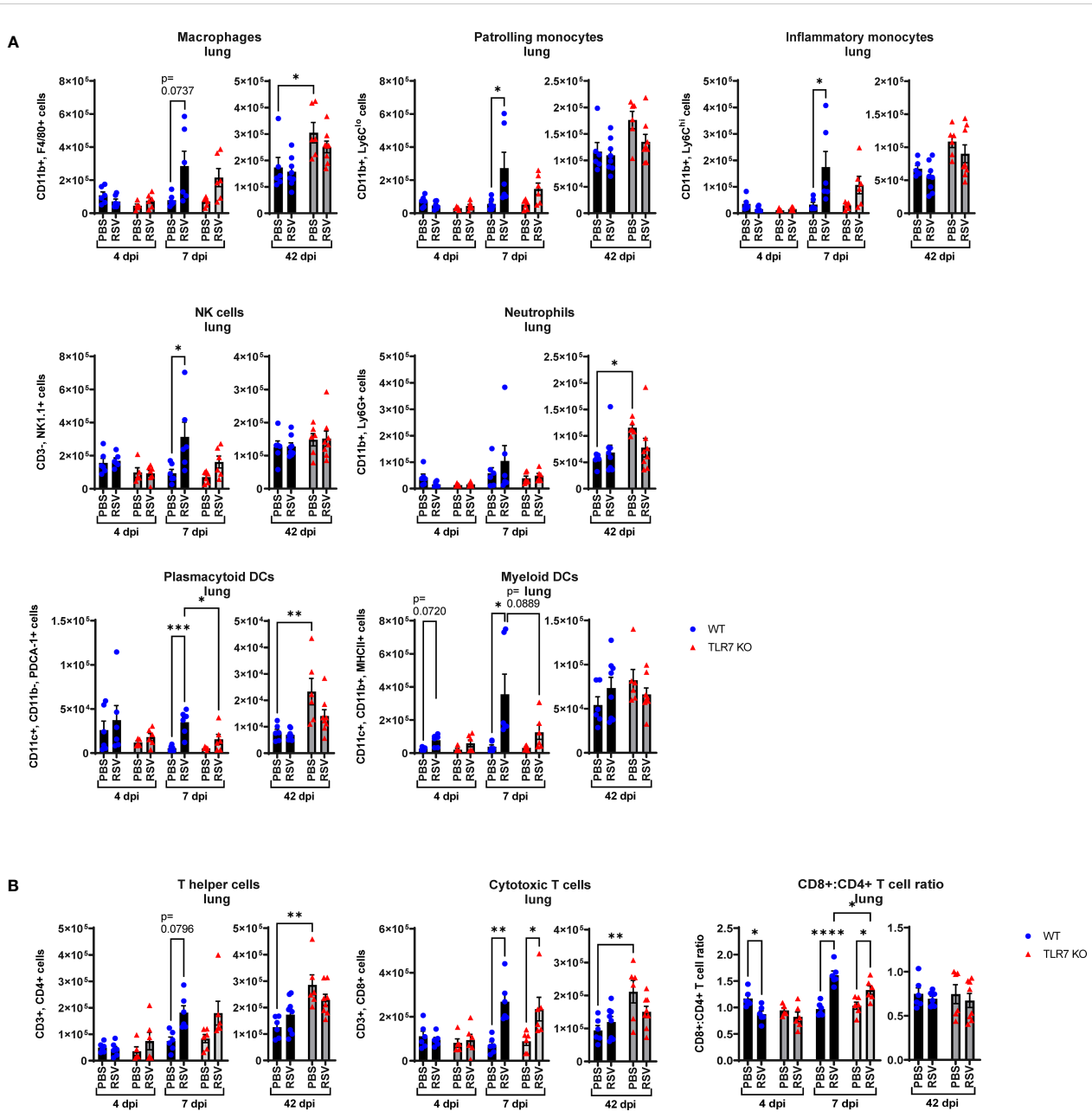

FIGURE 5
RSV-induced lung infiltration of innate immune cells is reduced in TLR7 KO mice. WT C57BL/6 or TLR7 KO mice were infected with RSV (0.5-2x10^7 PFUs) or PBS via intranasal administration. Immune cell populations in lung tissue were determined by flow cytometry after 4, 7 or 42 dpi. **(A)** Innate immune cell types: interstitial macrophages (CD11b$^+$ F4/80$^+$), patrolling monocytes (CD11b$^+$ Ly6C^{lo}), inflammatory monocytes (CD11b$^+$ Ly6C^{hi}), NK cells (CD3$^-$ NK1.1$^+$), neutrophils (CD11b$^+$ Ly6G$^+$), plasmacytoid DCs (CD11c$^+$ CD11b$^-$ PDCA-1$^+$) and myeloid DCs (CD11c$^+$ CD11b$^+$ MCHCII$^+$). **(B)** Adaptive T cell types: T helper (CD3$^+$ CD4$^+$) and cytotoxic T cells (CD3$^+$ CD8$^+$). Cell populations are measured as absolute number of CD45$^+$ population per 10,000 counting beads. Data are expressed as mean ± SEM, n = 5-8 mice per experimental group from two independent experiments. Statistical analysis was conducted using two-way ANOVA test followed by Tukey's *post hoc* test for multiple comparison test (*p < 0.05, **p < 0.01, ***p<0.001, ****p<0.0001).

suggested that the lungs of infected TLR7 KO mice did not exhibit a dominant Th1 or Th2 phenotype at either acute or chronic timepoints. Conversely, the IFNγ:IL-4 ratio, as an alternative measure of Th1 versus Th2, was higher in infected TLR7 KO mice at 4 dpi, although eventually rose to the same degree in both genotypes at 7 dpi, supporting an overall Th1 dominant response at early timepoints. Despite a significant influx of Th2-dominant eosinophils to the airways of WT mice (Figure 3B), IL-5 expression did not change during infection (Figure 6D). Furthermore, acute RSV infection increased expression of mucin genes Muc5b and Muc5ac in the lung, suggesting enhanced mucus production and goblet cell hyperplasia with infection (Figure 6F). Consistent with the suppressed inflammatory profile, Muc5ac expression was significantly reduced in TLR7 KO mice at 7 dpi.

IL-17A levels were also high at 4 dpi although expression was significantly higher in TLR7 KO mice (Figure 6G), suggesting these

10.3389/fimmu.2023.1240552

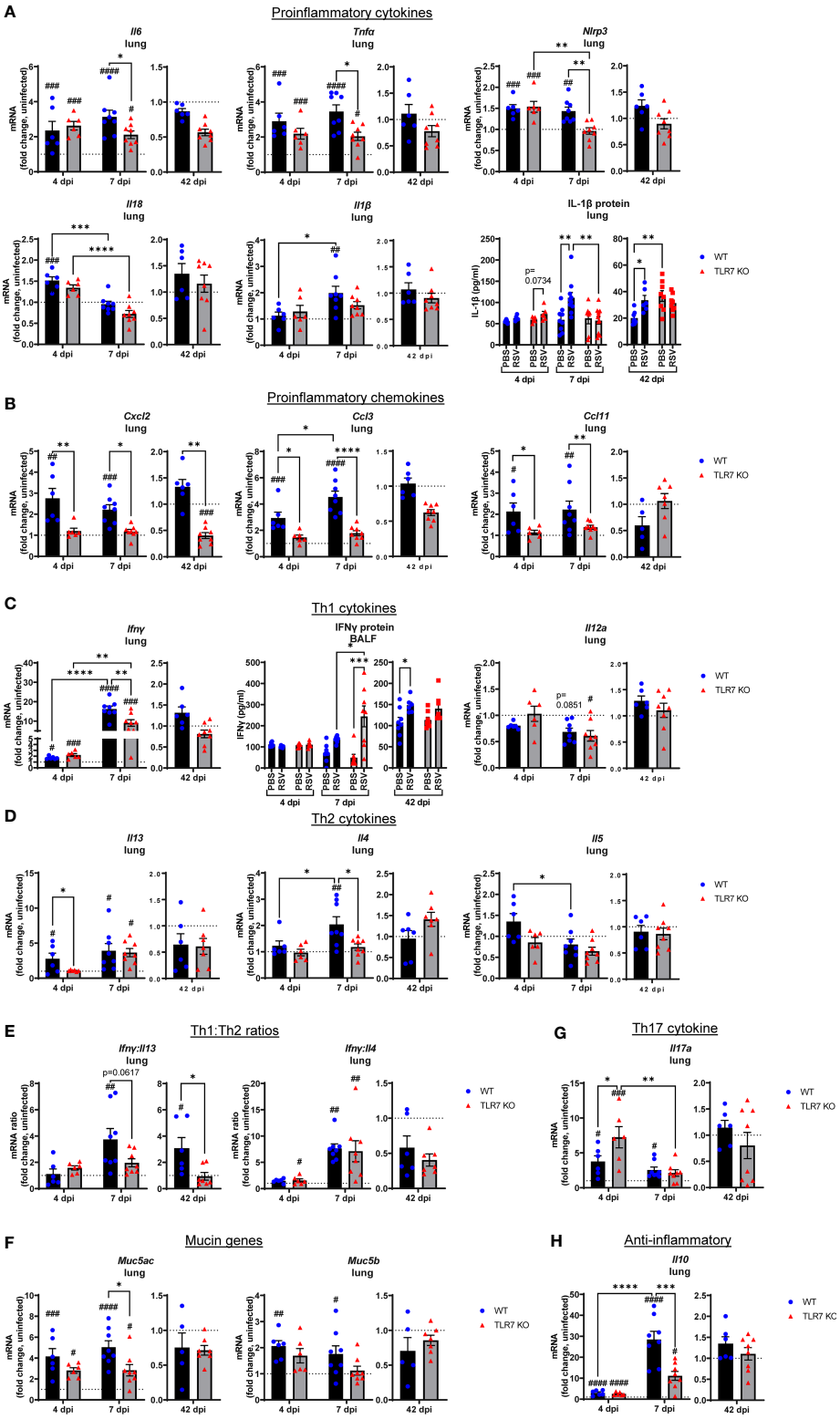

FIGURE 6
Reduced pro-inflammatory mediators in the lungs of TLR7 KO mice. Lung mRNA expression from WT C57BL/6 or TLR7 KO mice infected with RSV (0.5-2x10^7 PFUs) or PBS was analyzed after 4, 7 or 42 dpi. **(A)** Proinflammatory cytokines, **(B)** proinflammatory chemokines, **(C)** Th1 cytokines, **(D)** Th2 cytokines, **(E)** Th1:Th2 cytokine ratios, **(F)** mucin genes, **(G)** Th17 and **(H)** anti-inflammatory cytokines were measured. Proteins levels of **(A)** IL-1β from the lung or **(C)** IFNγ from the BALF were also quantitated by ELISA. Responses are relative to RPS18 and expressed as a fold-change above uninfected controls of each mouse genotype. Data are expressed as mean ± SEM, n = 5-8 mice per experimental group from a single experiment. Statistical analysis was conducted using two-way ANOVA test followed by Tukey's *post hoc* test for multiple comparison to compare differences between genotype or infection timepoints (*p < 0.05, **p < 0.01, ****p<0.0001). A Sidak's *post hoc* test was performed to compare differences between uninfected controls (fold change of 1) and respective infected groups for each genotype (***p<0.001, $^{\#}$p < 0.05, $^{\#\#}$p < 0.01, $^{\#\#\#}$p < 0.001, $^{\#\#\#\#}$p < 0.0001).

mice had an enhanced Th17 profile during early infection, but this response was resolved in both genotypes by day 7. The lung profile of IL-10, which is considered to exert suppressive effects on inflammation, mirrored the IFNγ response. Infection induced equivalent levels of IL-10 at 4 dpi in both genotypes, which then rose dramatically in WT mice at 7 dpi, but this increase was significantly less in TLR7 KO mice (Figure 6H). This suggests that the overall reduction of the Th1/Th2 response in the lungs of TLR7 KO mice is paralleled by the reduced need for inflammatory suppression signaling.

These data demonstrate that TLR7 promotes a profound hyperinflammatory response to RSV infection in the LRT following effective early antiviral responses by driving a strong Th1 dominant phenotype in the lung, which persists chronically. Loss of TLR7 improves the resolution of this inflammatory response (at 7 dpi) in the LRT by balancing the Th1/Th2 landscape that ultimately reduces the acute and chronic immunopathology caused by excess immune infiltration of the airways present in TLR7 proficient mice.

2.5 RSV infection induces a TLR7-dependent inflammatory response in alveolar macrophages

The above experiments revealed that the RSV-induced inflammatory signal is predominantly derived from the LRT rather than the URT (nasal compartment), suggesting that immune infiltration to the upper airways is heavily influenced by the Th1/Th2 cytokine signals in the lung. As RSV disseminates to the LRT it commonly infects and stimulates pulmonary macrophages, although these cells do not efficiently support RSV replication but are important initiators of inflammation in the lung (36). Studies have also reported an indirect activation mechanism of alveolar macrophages (AMΦ) by upstream pDCs via TLR7, which may drive a "cytokine storm" in the LRT (26, 27). Thus, Th1/Th2 signaling in the lung can likely influence the polarization of macrophage subtypes and vice versa. RSV infection induced an early Th2-skewed M2 "anti-inflammatory" macrophage response at 4 dpi in the airways that shifted to a Th1 dominant M1 "inflammatory" macrophage response at day 7 (Figure 7A). Both M1 and M2 macrophage responses were blunted in TLR7 KO mice across acute infection timepoints, consistent with the cytokine gene expression in the lung. Moreover, populations of M2 macrophages from lung tissue increased significantly in infected WT mice at 7 dpi while no significant increases in M2 populations were observed in TLR7 KO mice (Figure 7B). The M1 macrophage population and overall M1:M2 ratios did not change significantly in the lung following infection in either genotype. However, M1:M2 ratios in the upper airways suggested RSV infection induced an early Th2 dominant inflammatory response disseminating from the URT in a TLR7 dependent manner.

Additional experiments on naive AMΦ isolated from WT or TLR7 KO mice and subsequently infected *ex vivo* with RSV were performed to assess the intrinsic effects of RSV on these cells. RSV induced a cell-intrinsic increase in TLR7, TLR8 and TLR9 expression in WT-derived AMΦ, and this was accompanied by enhanced IFN-β expression, which was curiously higher in macrophages lacking TLR7, although the viral load remained equivalent (Figure 7C). Therefore, these results may account for the elevated IFN-β levels observed in the lungs of infected TLR7 KO mice at early timepoints (Figure 1B). Measurement of secreted IFN-β protein into the culture supernatant also revealed increased production of IFN-β protein by TLR7-deficient AMΦ upon exposure to RSV compared to WT macrophages (Figure 7D). In addition, there was no significant increase in TLR8 or TLR9 expression observed in TLR7 KO macrophages. Infection boosted IL-1β, IL6 and NLRP3 levels in TLR7 expressing AMΦ but these proinflammatory markers were suppressed upon TLR7 deficiency. Additionally, anti-inflammatory IL-10 was only significantly elevated in TLR7-deficient AMΦs. We were unable to detect either basal or stimulated gene expression of IL-4, IL-5, IL-13 and IFNγ in AMΦ. These experiments reveal that direct RSV infection of AMΦ preferentially activates a TLR7-dependent proinflammatory response that is ineffectively regulated and somewhat suppresses type I IFN.

2.6 RSV infection provokes TLR7-dependent chronic airway hyperreactivity that correlates with CD8+:CD4+ T cell ratios in the airways

We next determined if the chronic persistence of airway inflammation offered by TLR7 contributed to airway hyperreactivity as a functional consequence of poorly resolved acute hyperinflammatory responses in the LRT. Mice were subjected to methacholine (MCh) challenge after 4, 7 or 42 dpi then Newtonian resistance (Rn, central airways resistance), tissue dampening (G, small airway and alveolar resistance) and total lung resistance (Rrs, total airway resistance) were measured. WT mice infected with RSV displayed overall higher resistance parameters than uninfected mice at 4 and 7 dpi (Figures 8A, B). Importantly, central airway and total lung resistance were significantly higher in infected WT mice at 42 dpi, illustrating the presence of chronic airway and lung hyperreactivity (Figures 8C, D). There was also a non-significant trend for enhanced alveolar (G) resistance in infected WT mice at 42 dpi. In contrast, uninfected and RSV-infected TLR7 KO mice displayed similar responses to MCh for all resistance parameters at 42 dpi, indicating these mice did not experience airway hyperreactivity. We then stratified the number of immune cells retained in the airways at 42 dpi with the extent of central airway hyperreactivity at maximal MCh (100 mg/mL). A positive correlation was identified between the CD8+:CD4+ T cell ratios in the airways and maximum airway hyperreactivity (Figure 9).

These experiments demonstrate that TLR7 drives chronic airway hyperreactivity following RSV infection and this correlates with the CD8+:CD4+ T cell ratio in the airways.

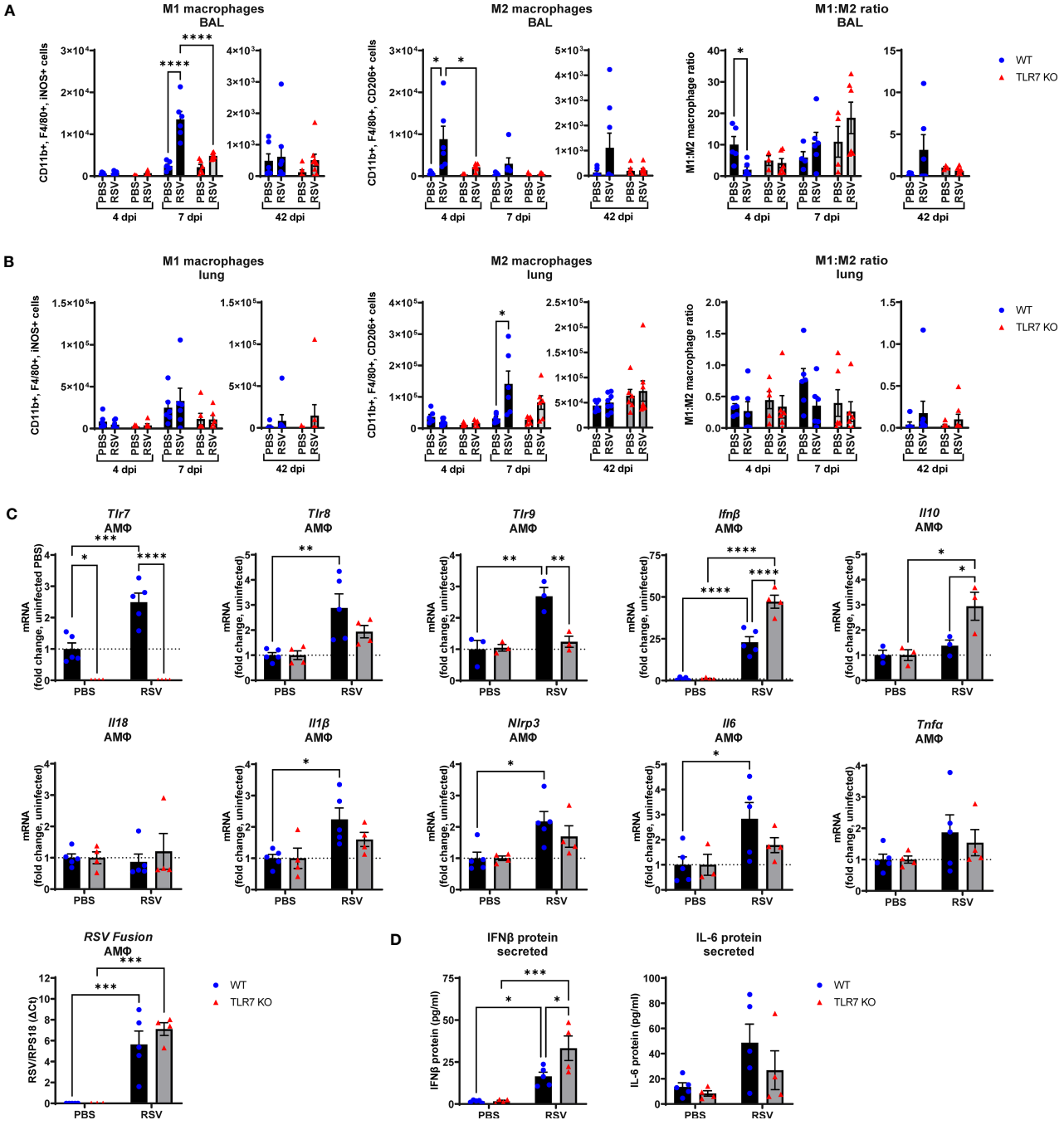

FIGURE 7
RSV infection stimulates proinflammatory responses in alveolar macrophages. WT C57BL/6 or TLR7 KO mice were infected with RSV (0.5-2x10^7 PFUs) or PBS. After 4, 7 or 42 dpi, macrophage subtypes M1 "inflammatory" (CD11b$^+$ F4/80$^+$ iNOS$^+$) and M2 "anti-inflammatory" (CD11b$^+$ F4/80$^+$ CD206$^+$) were isolated from the **(A)** airways (BAL) or **(B)** lung tissue and assessed by flow cytometry. Cell populations were measured as absolute number of CD45$^+$ population per 10,000 counting beads (lung) or total live cells (BAL). Data are expressed as mean ± SEM, n = 5-8 mice per experimental group from two independent experiments. **(C)** Alveolar macrophages (AMΦ) were isolated and infected *ex vivo* with RSV (MOI 1) for 24 h. Expression of indicated genes was then performed, and is presented relative to RPS18 as a fold-change above uninfected controls of each genotype. **(D)** Secreted protein was also measured in the cell culture supernatant by ELISA. Data are expressed as mean ± SEM, n = 3-5 per treatment group from three independent experiments. Statistical analysis was conducted using two-way ANOVA test followed by Tukey's *post hoc* test for multiple comparison test (*p < 0.05, **p < 0.01, ***p<0.001, ****p<0.0001).

3 Discussion

Inflammation is critical for regulating viral clearance and establishing immunological memory, however uncontrolled, widespread inflammation may prolong disease pathology resulting in tissue damage, disease progression, and even autoimmunity. TLR7 is an important immune sensor and key driver of inflammation following viral infection that has been

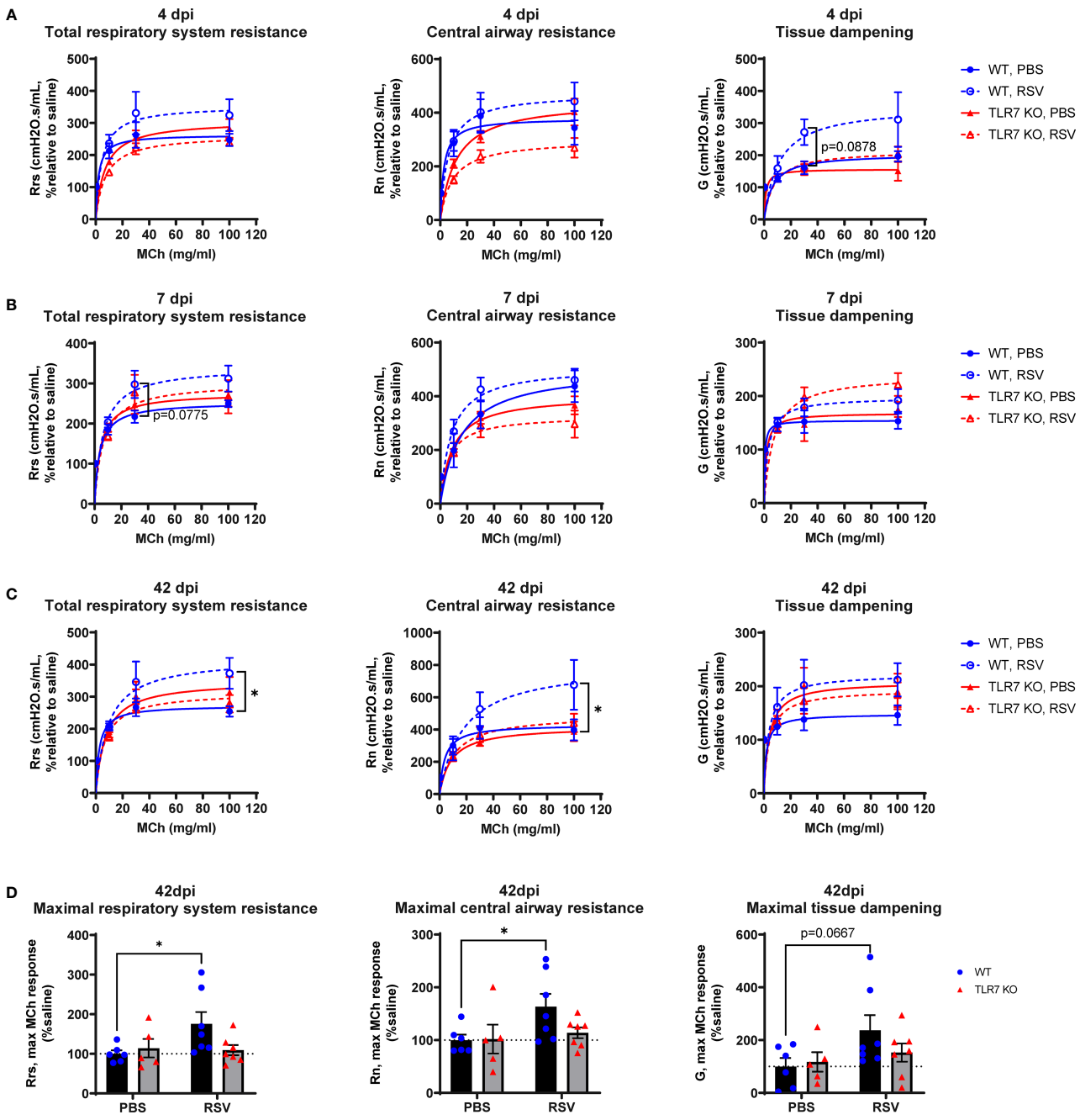

FIGURE 8
TLR7 KO mice are spared from RSV-induced chronic airway hyperreactivity. WT C57BL/6 or TLR7 KO mice were infected with RSV (0.5-2x10^7 PFUs) or PBS. Mice were anaesthetized after 4, 7 or 42 dpi, connected to the Flexivent FX1 system and mechanically ventilated at 300 breaths per minute. Lung function was performed in response to increasing doses of nebulized methacholine (MCh; 0, 3, 10, 30 and 100 mg/ml). Dose response curves of central airways resistance (Rn, Newtonian resistance), total respiratory system resistance (Rrs) and tissue dampening (G) is presented relative to 0 mg/ml MCh (saline) after **(A)** 4, **(B)** 7 or **(C)** 42 dpi. **(D)** Maximal resistance (100 mg/ml MCh) parameters at 42 dpi relative to 0 mg/ml MCh (saline) are shown. Data are expressed as mean ± SEM, n = 5-8 mice per experimental group from two independent experiments. Statistical analysis was conducted using two-way ANOVA test followed by Tukey's *post hoc* test for multiple comparison test (*p < 0.05).

implicated in hyperinflammatory responses in autoimmunity, influenza and SARS-CoV2 infection (26, 27, 37, 38). We reasoned that TLR7 plays a significant role in controlling the URT infection and the immunopathology provoked by RSV in the LRT, where chronic respiratory disease manifests.

Mice infected with RSV developed airway hyperreactivity several weeks after infection, consistent with previous neonatal and adult mouse models of RSV (39, 40). Strikingly, the absence of TLR7 prevented RSV-infected mice from developing chronic airway hyperreactivity. Our study showed that the acute phase of RSV infection established a TLR7-dependent inflammatory niche within the LRT that facilitated the development of chronic respiratory disease. While TLR7 suppressed inflammatory markers in the nasal tissue, this enhanced the progression of

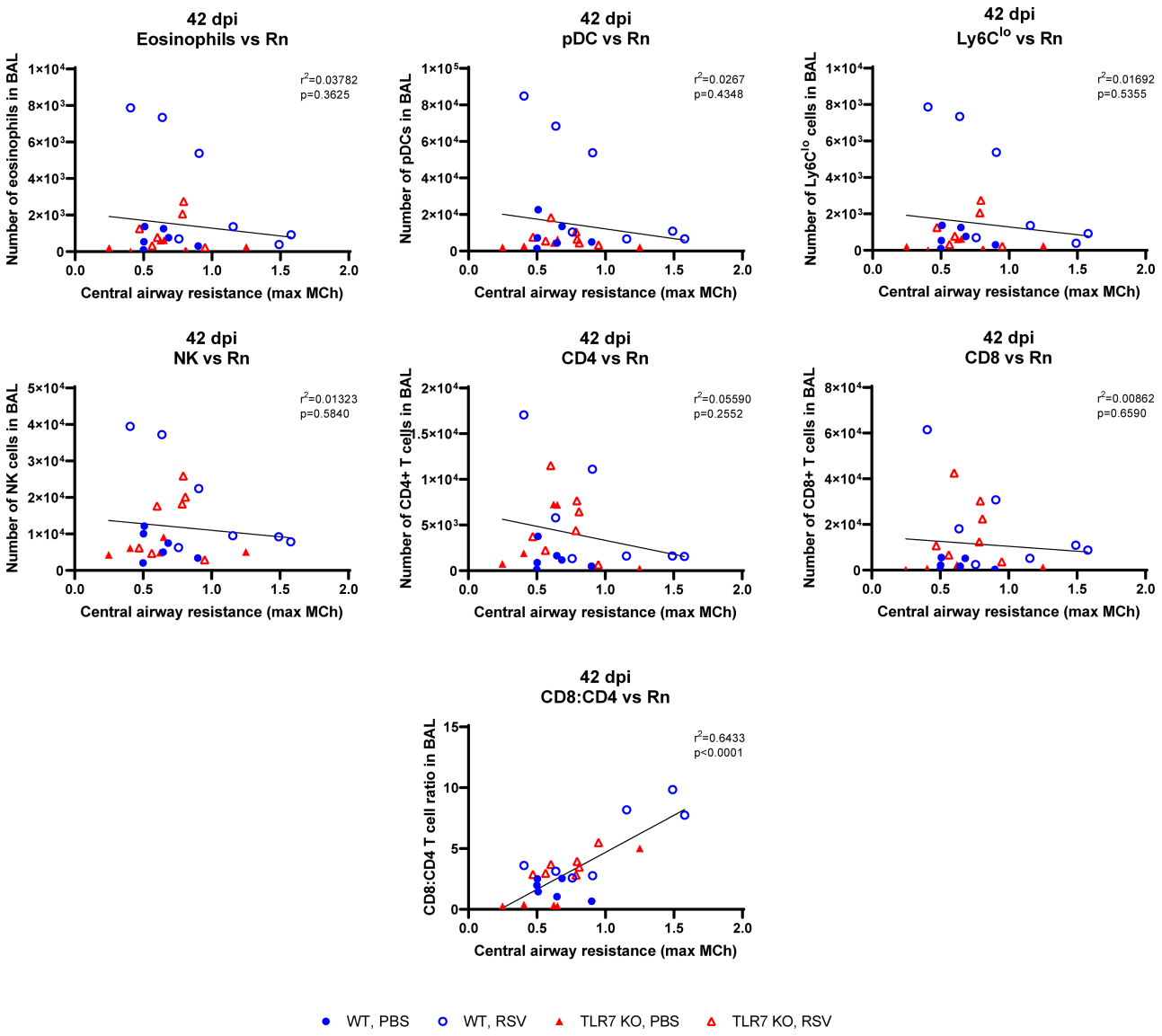

FIGURE 9
CD8+:CD4+ T cell ratios in the airways correlate with airway hyperresponsiveness. Correlations at 42 dpi were made of the maximal central airways resistance (100 mg/ml MCh) with the number of immune cells present in the airways (BAL) of each mouse. Data are expressed as mean ± SEM, n = 5-8 mice per experimental group from two independent experiments. Statistical analysis was conducted using a simple linear regression test.

inflammation and immune infiltration in the LRT, which added little benefit to the host response to infection, but rather expedited long-term immunopathological consequences. In contrast, the absence of TLR7 in the URT provoked a localized inflammatory response in the nasal tissue that modestly impacted viral clearance, but prevented the dissemination and establishment of a hyperinflammatory environment in the LRT. Overall, these observations illustrated a sub-optimal resolution of the host immune response in the LRT that is driven by TLR7, which contributes to hyperinflammatory signaling, lung pathology and persistent immune infiltration of the airways, leading to chronic airway hyperreactivity (Figure 10). It is unclear whether this effect can occur upon direct engagement of TLR7 in the absence of a productive infection, although we reason that this sustained immune response, rather than persistent viral mRNA, induced chronic airway hyperreactivity as mice lacking TLR7 effectively resolved inflammation of the LRT and did not experience airway hyperreactivity.

TLR7 paradoxically contributed different immune responses in the URT and LRT in response to RSV infection. We did not detect a strong proinflammatory signal in the nasal tissue during acute infection implying that the immune response in the URT was predominantly antiviral, which was likely propagated early by cytosolic RLRs. Loss of TLR7 modestly impeded clearance of the virus in the nasal tissue as viral titres were higher in TLR7 KO mice at 7 dpi, and this coincided with the upregulation of IFNγ, IL-1β and TNFα, as well as CD8+ T cells. In contrast, early (day 4) antiviral responses in the LRT of TLR7 KO mice were not impaired. This was accompanied by intact levels of proinflammatory mediators and concomitant airway infiltration of NK cells,

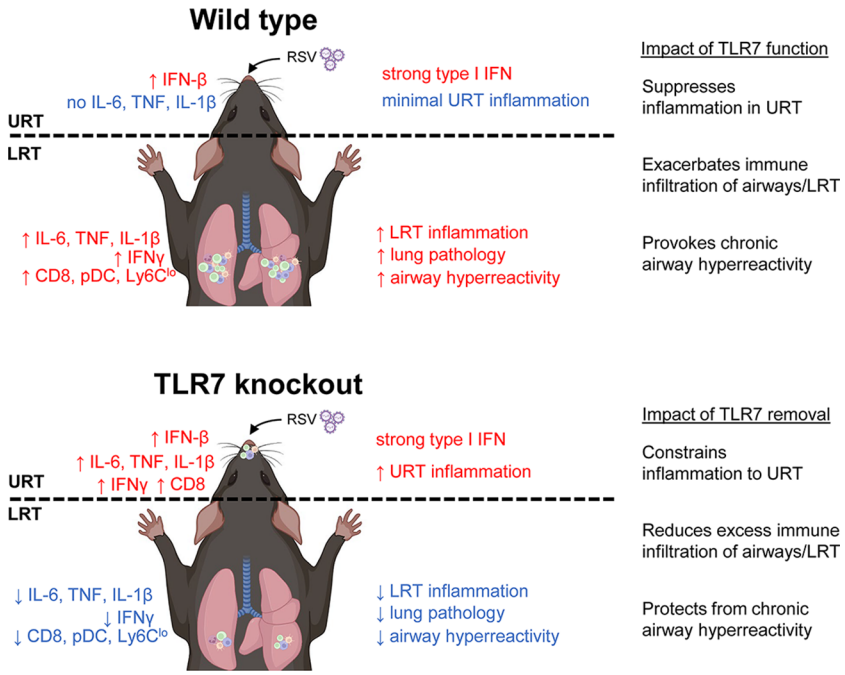

FIGURE 10
Proposed mechanism of TLR7-dependent LRT disease caused by RSV infection. In wild type (TLR7-proficient mice), RSV infection induces a strong type I IFN response in the URT (most likely modulated by RLRs) with minimal inflammation. However, inflammation of the LRT ensues involving infiltration of various innate and T cell immune subtypes that is potentiated by TLR7 and resolution of this is lacking resulting in persistent LRT inflammation, lung pathology and chronic airway hyperreactivity. In contrast, infection of TLR7 knockout mice induces type I IFN and persistent inflammatory signaling in the URT, implying that TLR7 has anti-inflammatory properties in the nasal tissue. The resulting inflammation of the LRT is thereby subdued and this reduces lung pathology and spares mice from chronic airway hyperreactivity.

macrophages and CD4+ T cells, with no observed impact on viral titres in the lung. This is consistent with the engagement of various PRRs driving the antiviral responses to RSV infection (41–43) and illustrates that, unlike in the URT, TLR7 is dispensable for antiviral effects in the LRT in this model. Only TLR7 expressing mice displayed heightened inflammatory responses, lung pathology and immune infiltration of the airways in the LRT at 7 dpi; suggesting that the initial PRR response to infection combined with the secondary TLR7 response to effect a dual immune activation scenario, which might explain the heightened inflammation. Moreover, sustained levels of some inflammatory markers implicated in driving immunopathology, for instance elevated NLRP3 inflammasome activity, or NK cell or M1 macrophage populations (44–46), were lessened in the LRT of TLR7 KO mice. This effect was probably facilitated by the lack of CXCL2 and CCL3 upregulation in these mice although the observed lack of effect on viral titres highlights LRT viral clearance was not compromised.

Our data also imply that the RSV-induced inflammatory response is compartmentalized to the URT in TLR7 KO mice, thereby sparing the LRT from exacerbated immune infiltration and the development of critical lung pathology. Markers of inflammation were significantly elevated in the nasal tissue of TLR7 KO mice at 7 dpi but there was reduced immune infiltration to the rest of the airways, suggesting that the inflammatory response was localized to the URT. Importantly, less pDCs were present in the upper airways of the LRT early during infection, which likely influenced the airway responses of AMΦ and CD8+ T cells, as has been reported for SARS-CoV2 (26) and RSV (47) respectively. As such, we found the TLR7-mediated response to RSV in AMΦ primarily promoted inflammatory signaling. Thus, reduced AMΦ activation in TLR7 KO mice (a result of lower pDC stimulation or viral dissemination), is likely to limit inflammation in the LRT. CCL3-mediated chemotaxis has also been noted to influence the migration and function of CD8+ T cells to sites of infection following RSV exposure (48). Nasal aspirates obtained from infants hospitalized with severe RSV-induced bronchiolitis contained higher levels of CCL3, neutrophils, monocytes and Th2-CD8+ T cell subtypes, suggesting that these markers in the nasal tissue correlate with the severity of pathology in the LRT (49, 50). Interestingly, the expression of CCL3 in the nasal tissue of TLR7 KO mice was indifferent from WT mice at 7 dpi. This, combined with the severely blunted levels of CCL3 in the lungs of TLR7 KO mice at the same timepoint, supports an overall reduced LRT pathology in TLR7-deficient mice, further suggesting the partial localization of the inflammatory response to the URT in those mice.

A deeper analysis of the Th1/Th2 immune landscape in our model shed further light on the potential mechanisms underlying the manifestation of chronic RSV disease, particularly given the known contribution of Th2 dominant immune activation observed in infant cases of severe RSV infection, potentiating asthma and allergy sensitization (9, 51, 52). Notably, infection of neonatal mice with RSV enhanced the airway hyperreactivity response to subsequent allergen challenge, with higher eosinophil,

macrophage and CD4+ T cell accumulation and elevated IL-4, IL-5 and IL-13 cytokines (53). In our study, the relative proportions of M2 compared to M1 macrophages in the upper airways of WT mice was highest during early infection and, in concordance with eosinophilia and expression of IL-13 in the lung, suggested a Th2 dominant phenotype that was absent in TLR7 KO mice. In WT mice at day 7, we observed a dominant population of M1 macrophages, which coincided with a Th1-skewed phenotype in the lung accompanied by high IFNγ:IL-13 ratios that persisted to day 42. The IFNγ:IL-4 ratios in the lung show that the loss of TLR7 appeared to initiate a stronger Th1 response during early infection, although there was no difference at 7 dpi. Neither mouse genotype exhibited significantly altered IL-5 levels, which is often associated with severe eosinophilic asthma, particularly following RSV infection (54). This suggests that the airway eosinophilia we observed in WT mice was probably driven by IL-13 and IL-4 resulting in a less overall severe eosinophilic pathology to infection, and suggesting other cell types contributed to the immunopathology observed (55). Interestingly, RSV-induced airway hyperreactivity has been reported to occur independently of increases in IL-13 (56). This suggests that the mechanism behind chronic manifestations of RSV disease, at least in older cohorts, might stem from hyperinflammatory reactions of prolonged Th1 responses, and not an exacerbated Th2 inflammatory response. Overall, this analysis implies that RSV infection induces a TLR7-mediated imbalance of Th1/Th2 responses, likely driving an early Th2 skew in the URT followed by a Th1 skew in the LRT later in the infection and pathogenesis process. Loss of TLR7 appeared to stabilize this Th1/Th2 balance, which improved acute lung pathology and had lasting effects on chronic disease.

We observed a population of pDCs retained in the airways up to 42 dpi, implying antigen presentation was occurring several weeks following acute responses to infection. Consistent with other studies (31, 32, 57, 58), low levels of RSV mRNA persisted in the lungs (and nasal tissue) at 42 dpi, but there were equivalent, if not higher amounts in TLR7 KO mice; which correlated with significantly less pDCs, patrolling monocytes and cytotoxic T cells. Thus, while TLR7 modestly influenced viral load in the URT, our data imply TLR7 is an unlikely contributor to RSV viral persistence. It remains unclear whether the mRNA transcripts detected at day 42 and thereafter represent the presence of virus capable of replication and potential reactivation. The use of standard plaque assays employed to detect replicating RSV from lung tissue is limited to acute infection protocols as the sensitivity falls below the detection limit of the assay after 7 dpi RSV (39). However, Schwarze et al. (32) were able to amplify the G, F, NS1, NS2 and M2 genes by RT-PCR from lungs of RSV infected mice up to 60 dpi, suggesting that the RSV genome can persist and contains the intact regions required for cell fusion and replication rather than being random viral fragments. Persisting viral RNA and presentation could indeed stimulate chronic activation of lingering CD8+ T cells, leading to T cell exhaustion and even airway immunopathology (59), although pre-existing RSV-specific "memory" CD8+ T cells within the airways of healthy individuals, correlated with reduced disease severity following RSV challenge (60). Importantly, we identified that mice experiencing the greatest airway and lung resistance upon MCh challenge (RSV-infected WT mice after 42 dpi) had the highest CD8+:CD4+ T cells ratios in the airways. This correlation existed in both mouse genotypes although TLR7 KO mice displayed a lower CD8+:CD4+ T cell ratio and minimal airway hyperreactivity. This is consistent with a study that reported infants who developed respiratory distress or were infected with RSV or human metapneumovirus had a skewed CD8+:CD4+ T cell ratio and increased IL-6 levels in their airways (61). The degree of the CD8+ T cell response also correlated with disease severity. Our results imply a potential relationship between RSV-induced airway hyperreactivity and CD8+ T cell persistence in the airways, and that the magnitude of this persistence is likely exacerbated by the TLR7-mediated hyperinflammatory responses during acute infection. Future experiments suppressing pulmonary T cell recruitment will provide important insight into the chronic consequences of T cell-mediated immunopathology during RSV infection.

Using TLR7 KO mice, Lukacs et al. (29) reported IL-17A-dependent mucus production during early RSV infection (3 dpi) that was increased in TLR7-deficient mice. IL-17A levels were similarly higher in TLR7 KO mice in our study, although we observed an overall reduction of immune infiltration in the BALF across 4 and 7 dpi. Conversely, we found that expression of mucin genes was lower in TLR7 KO mice implying excess mucus secretion in response to infection occurred in the presence of TLR7. This complemented our observations of LRT pathology. Consistent with Lukacs et al. (29), there was no difference in T cell numbers in the lungs, although we did observe slightly less DC subsets, NK cells and monocytes, overall emphasizing that the alteration in the immune response to RSV infection in TLR7 KO mice primarily impacted airway pathology in both models. IL-17A levels have been implicated in autoimmune disease pathogenesis and contribute to impaired lung function caused by respiratory viruses like RSV (62, 63). It is possible that the modulation of the IL-17A signal following its early Th17 response was better regulated in TLR7 KO mice as IL-6, an IL-17A-stimulating factor (64), was more effectively resolved and type I IFN, which is an IL-17A suppressing factor (65), was initially higher. Furthermore, Th17 cells reportedly influenced CD8+ cytotoxic T cell function in the airways in a model of chronic obstructive pulmonary disease (COPD) (66, 67) and impacted their virus-specific functions (68). Different strains of RSV A elicit slightly different immune responses and pulmonary pathophysiology in mice (69) and may account for the differences between our study and Lukacs et al. (29). We used RSV A Long strain, which induces a stronger type I IFN response in both epithelial and immune cells than RSV A2 strain (70). A greater type I IFN response, as observed in our RSV-infected TLR7 KO mice at 4 dpi, improves the rate of viral clearance and reduces pathology (71), thus infection with RSV A Long may represent a less severe, acute model in comparison to some other viral subtypes. Host responses to this strain also appear to favor Th1 immunity as Th1 but not Th2 cytokines were preferentially upregulated following RSV A Long infection compared to the line 19 strain, and this reduced the mucus-related pathology (72, 73). There is also evidence to suggest that the A2 strain can evade TLR recognition (70). Lukacs et al. (29) did not report IFN levels in the lungs, but observed no difference in IFN expression when DCs were infected with RSV *ex vivo*.

Host inflammatory responses to infection need to appropriately complement the acute antiviral mechanisms that clear the virus and cause minimal tissue damage and immunopathology. Our study demonstrates that TLR7 promotes a modest antiviral effect in the URT, but potentiates prolonged airway inflammation in the LRT, establishing a persistent inflammatory phenotype that drives chronic airway hyperreactivity. Therefore, the specific modulation of TLR7 during acute RSV infection may prevent individuals from developing severe RSV-induced pathology. For the first time, we can consider the novel approach of confining viral infections to the URT in order to prevent the serious inflammatory and pathophysiological ramifications of viral penetration into the LRT.

4 Materials and methods

4.1 Mice

Female C57BL/6J mice were obtained from the Animal Resources Centre (Western Australia, Australia). Homozygous TLR7 knockout mice (B6.129S1-Tlr7^{tm1Flv}/J) were obtained from The Jackson Laboratory (Maine, USA) and bred in-house at the RMIT University animal research facility (Bundoora, Australia). Mice were housed in a 12 h light/12 h dark cycle with food and water.

4.2 Preparation of RSV stocks

Human respiratory syncytial virus (RSV A Long strain) was kindly provided by Prof. Patrick Reading (Department of Immunology and Microbiology, The Peter Doherty Institute for Infection and Immunity, University of Melbourne). RSV stocks were propagated on HEp-2 cells by incubating infected cells at 37°C, 5% CO2 for 3–4 days until at least an 80% cytopathic effect was observed. Culture medium was then removed, cell debris pelleted, and supernatant filter sterilized with a 0.22 µm Filter-Stericup. Virus was precipitated using poly-ethylene glycol (PEG) 6000 (Merck) and NaCl to a final concentration of 10% by incubating on ice for 2 h with gentle shaking. Virus was then pelleted and resuspended in phosphate buffered saline (PBS, Sigma, USA) + 1% fetal bovine serum (FBS; Sigma, USA). Viral titres were determined by plaque assay using HEp-2 cells.

4.3 RSV infection

For *in vivo* infection, 8–14-week-old female mice were anaesthetized by isoflurane inhalation and inoculated intranasally with 5×10^6 (acute infection) or 2×10^7 (long-term infection) plaque forming units (PFU) of RSV-A or PBS for controls in a 35 µL volume. Data were compared against PBS mice to control for any baseline anti-inflammatory effects from the anesthetic procedure. The greater viral inoculum administered for the long-term infection experiments was based on previous studies assessing RSV-induced chronic defects in lung function (31, 58). Mice were weighed and monitored daily. Mice were euthanized by injection (i.p) of a mixture of ketamine (180 mg/kg) and xylazine (32 mg/kg) at experimental endpoints. All animal experiments were conducted according to approval obtained from the RMIT University Animal Ethics Committee (Ethics number 23328) and in compliance with the guidelines of the National Health and Medical Research Council of Australia on animal experimentation.

For *ex vivo* infection, primary alveolar macrophages were extracted from bronchoalveolar lavage (BAL) and grown in Dulbecco's Modified Eagle's Medium (DMEM; Thermofisher, USA) containing 4.5 g/L of glucose, 110 mg of sodium pyruvate and 10% FBS in flat 96-well plates (10^5 cells per well) and allowed to adhere for 3–4 h prior to infection. Media was then replaced, and cells infected with RSV at a multiplicity of infection (MOI) of 1 and incubated at 37°C, 5% CO2 for 24 h before direct cell lysis for RNA extraction.

4.4 Airways inflammation

To assess airway inflammation, bronchoalveolar lavage fluid (BALF) was isolated by an incision of the lower jaw to the top of the rib cage to expose the salivary glands, which were separated to expose the top of the trachea. A small incision on the trachea was made and a sheathed 21-Gauge needle was inserted into the lumen. The lung was then lavaged with 300–400 µL aliquots of PBS repeatedly with gentle massaging of the chest with each aspirate collected until a volume of 1 mL was collected. The total number of live cells in the BALF was determined via Acridine Orange staining (Thermofisher) and counted using a hemocytometer. Differential staining of BAL was performed as previously described (74) and scored using standard morphological criteria counting at least 500 cells/slide from random fields.

4.5 Histology analysis of lungs

The left lung was dissected from mice and immersed in neutral buffered formalin (10%). After fixation, the lung tissue was processed, embedded in paraffin wax, and longitudinal 4 µm sections cut and stained with hematoxylin and eosin (H&E). Slides were scanned by light microscopy using the Olympus VS-120 Slide Scanner (Olympus Life Sciences, VIC, Australia). Histology was analyzed blindly by two independent assessors using Olympus OlyVIA imaging software. Each sample was scored from 0–5 for each individual mouse (higher numbers indicate increased severity). At least five random fields from each lung section were assessed for alveolar inflammation of the parenchyma (alveolitis), inflammation around the bronchiolar airway wall (peribronchiolar inflammation), and total inflammatory cell infiltration. Alveolitis was defined based on the regularity and branching of the alveoli as well as the density of cells within the alveolar spaces (interstitium). Peribronchiolar inflammation was characterized by immune cell infiltration into the alveolar wall around the bronchioles. Analysis of bronchioles were limited to airways of 100- to 350-µm luminal diameter. The

degree of inflammatory cellular infiltrate was taken by observing the density of cells throughout the entire lung section.

4.6 Gene expression analysis by reverse-transcriptase quantitative PCR

Lungs and nasal tissue were harvested for RNA extraction using the RNeasy Mini kit (Qiagen, USA), as per manufacturer's instructions. RNA sample concentration and quality were measured using the Nanodrop one Spectrophotometer (Thermofisher). The cDNA synthesis was performed on 1–2 µg of total RNA using the High-Capacity cDNA Reverse Transcription Kit (Applied Biosystems, CA, USA) according to the following settings: 25°C for 10 min, 37°C for 120 min, 85°C for 5 min. Quantitative polymerase chain reaction was carried out using the TaqMan Fast Advanced Master Mix (Thermofisher) and analyzed on the QuantStudio 7 Flex Real-Time PCR system (Thermofisher). PCR primers used in this study were included in the Assay on-Demand Gene Expression Assay Mix (Thermofisher). Additionally, RSV titres were measured using custom designed forward and reverse oligonucleotides for the F gene: 5′-TTGGATCTGCAATCGCCA-3′, 5′-CTTTTGATCTTGTTCACT TCTCCTTCT-3′ using Fast SYBR Green PCR Master Mix (Thermofisher). The following program settings were used for amplification: 50°C for 2 min, 95°C for 2 min, then 40 cycles of 95° C for 1 s and 60°C for 20 s. The quantitative values were obtained from the average threshold cycle (Ct) number of each sample run in triplicate and gene expression analysis performed using the comparative Ct method. Target gene expression was normalized against RPS18 mRNA expression for each sample and expressed relative to the indicated control. Mean Ct numbers for RPS18 for each experimental group are shown in Supplementary Table S1.

4.7 Cytokine protein levels by enzyme-linked immunosorbent assay

Enzyme-linked immunosorbent assays (ELISA) were performed to quantitate cytokine protein levels from whole lung tissue (IL-1β), BALF (secreted IFNγ) or cell culture supernatants (secreted IFNβ or IL-6). Individual mouse IL-1 beta/IL-1F2, IFN-gamma, IFN-beta or IL-6 DuoSet ELISA kits were used (R&D System, MN, USA). Lung lysates were generated by resuspending tissue in RIPA buffer containing protease inhibitor and passing tissue through a 25-Gauge needle multiple times. Protein concentrations were determined from cleared lysates using the Pierce BCA Protein Assay kit (ThermoFisher) according to manufacturer's instructions. One hundred micrograms of protein was added in duplicate to pre-coated 96-well plate and incubations performed according to manufacturer's instructions. To measure secreted proteins, 100 µl of BALF or cell culture supernatant was added in duplicate and processed in the same manner. The 96-well plate was read on the CLARIOstar (BMG) at a wavelength of 450 nm. Cytokine titres in the samples were determined by plotting the optical densities, using a four-parameter fit for the standard curve and expressed in pg/mL.

4.8 Immunophenotyping by flow cytometry

Whole lung was finely minced using scissors and then enzymatically digested using 1% Liberase (Sigma) for 45 min at 37°C shaking at 700 rpm. Tissues were homogenized then single cell suspensions prepared by straining through a 40 µm strainer. After lysing the red blood cells with ACK lysis buffer, cells were stained with cocktail mixtures of fluorescent-labelled anti-mouse antibodies diluted in FACS buffer (PBS + 2.5% FBS) for 30 min on ice. The following Biolegend antibodies were used (unless stated otherwise): CD45-PerCP (30-F11), CD3e-APC (145-2C11; BD Pharmingen), CD4-BV605 (RM4-5), CD8a-PE-Cy7 (53-6.7), NK1.1-FITC (PK136), CD11b-BV421 (M1/70), CD11c-PE-Cy7 (N418; eBioscience), PDCA-1-PE (JF05-1C2.4.1; Miltenyi Biotec), MHC-II-APC (M5/114.15.2), Ly6C-FITC (HK1.4), Ly6G-APC-Cy7 (1A8), F4/80-PE (BM8; eBiocience), iNOS-FITC (6; BD Transductions Laboratories) and CD206-PE-Cy7 (MMR; eBioscience). CD16/32 (2.4G2) and LIVE/DEAD Fixable Aqua Dead Cell Stain Kit (Invitrogen) were contained within each antibody cocktail mixture to block of Fc-mediated adherence of the antibodies and to exclude dead cells, respectively. Samples were processed on a BD LSRFortessaTM X-20 flow cytometry analyzer with DIVA software (Becton Dickinson Bioscience, USA) and data analyzed using FlowJo software (Tree Star, Inc.). Cells were analyzed as a percentage of the CD45-positive (live cells) and lung cells expressed in absolute numbers per 10,000 counting beads and amount of tissue (g) processed. BAL cells were expressed in absolute numbers relative to live cell counts. A representative gating strategy is shown in Supplementary Figure S2.

4.9 Airway hyperresponsiveness and lung function

Mice were anesthetized by ketamine (80 mg/kg) and xylazine (16 mg/kg) after which tracheotomy was performed by inserting an 18-Gauge canular into the trachea. Airway reactivity in response to increasing doses of nebulized methacholine (MCh; Sigma) or PBS was measured *in vivo* using the Flexivent FX1 (SCIREQ®, QC, Canada). Forced oscillation technique was used to measure the pressure, flow and volume responses to measure total airway resistance (Rrs), Newtonian resistance (Rn; representing resistance of the central/conducting airways) and tissue dampening (G; representing resistance of the small airways and alveolar space).

4.10 Statistical analysis

All data are expressed as the mean ± SEM. All comparisons were performed using GraphPad Prism (GraphPad Software Version 8.2, USA) and performed by two-way ANOVA followed by Tukey's or Sidak's *post-hoc* tests for multiple comparison (stated in figure legends). Statistical significance was considered at $p<0.05$.

Data availability statement

The original contributions presented in the study are included in the article/Supplementary Material. Further inquiries can be directed to the corresponding author.

Ethics statement

The animal study was approved by RMIT University Animal Ethics Committee. The study was conducted in accordance with the local legislation and institutional requirements.

Author contributions

MM, SL, FL, MC-S, GT, JE, OO performed the experiments. MM and SS drafted the manuscript. All authors provided intellectual input and edited the manuscript. MM, JO'L, DB and SS conceptualized and designed the study. RB, SH, JL, HW, SB, DB, JO'L and SS contributed to the experimental design of this research project. DB, JO'L and SS obtained the funding for the research. SS supervised and managed the overall study. All authors contributed to the article and approved the submitted version.

Funding

This work was supported by The National Health and Medical Research Council of Australia (Project I.D. 1122506, 1128276).

Acknowledgments

The authors wish to thank Professor Patrick Reading from the Peter Doherty Institute, The University of Melbourne, Australia for providing the RSV stocks.

Conflict of interest

The authors declare that the research was conducted in the absence of any commercial or financial relationships that could be construed as a potential conflict of interest.

Publisher's note

All claims expressed in this article are solely those of the authors and do not necessarily represent those of their affiliated organizations, or those of the publisher, the editors and the reviewers. Any product that may be evaluated in this article, or claim that may be made by its manufacturer, is not guaranteed or endorsed by the publisher.

Supplementary material

The Supplementary Material for this article can be found online at: https://www.frontiersin.org/articles/10.3389/fimmu.2023.1240552/full#supplementary-material

References

1. Nair H, Nokes DJ, Gessner BD, Dherani M, Madhi SA, Singleton RJ, et al. Global burden of acute lower respiratory infections due to respiratory syncytial virus in young children: a systematic review and meta-analysis. *Lancet* (2010) 375:1545–55. doi: 10.1016/S0140-6736(10)60206-1

2. Shi T, Mcallister DA, O'brien KL, Simoes EAF, Madhi SA, Gessner BD, et al. Global, regional, and national disease burden estimates of acute lower respiratory infections due to respiratory syncytial virus in young children in 2015: a systematic review and modelling study. *Lancet* (2017) 390:946–58. doi: 10.1016/S0140-6736(17)30938-8

3. Hall CB, Weinberg GA, Iwane MK, Blumkin AK, Edwards KM, Staat MA, et al. The burden of respiratory syncytial virus infection in young children. *N Engl J Med* (2009) 360:588–98. doi: 10.1056/NEJMoa0804877

4. Glezen WP, Taber LH, Frank AL, Kasel JA. Risk of primary infection and reinfection with respiratory syncytial virus. *Am J Dis Child* (1986) 140:543–6. doi: 10.1001/archpedi.1986.02140200053026

5. Papi A, Ison MG, Langley JM, Lee DG, Leroux-Roels I, Martinon-Torres F, et al. Respiratory syncytial virus prefusion F protein vaccine in older adults. *N Engl J Med* (2023) 388:595–608. doi: 10.1056/NEJMoa2209604

6. Walsh EE, Pérez Marc G, Zareba AM, Falsey AR, Jiang Q, Patton M, et al. Efficacy and safety of a bivalent RSV prefusion F vaccine in older adults. *N Engl J Med* (2023) 388:1465–77. doi: 10.1056/NEJMoa2213836

7. Behzadi MA, Leyva-Grado VH. Overview of current therapeutics and novel candidates against influenza, respiratory syncytial virus, and Middle East respiratory syndrome coronavirus infections. *Front Microbiol* (2019) 10:1327. doi: 10.3389/fmicb.2019.01327

8. Sigurs N, Bjarnason R, Sigurbergsson F, Kjellman B. Respiratory syncytial virus bronchiolitis in infancy is an important risk factor for asthma and allergy at age 7. *Am J Respir Crit Care Med* (2000) 161:1501–7. doi: 10.1164/ajrccm.161.5.9906076

9. Sigurs N, Aljassim F, Kjellman B, Robinson PD, Sigurbergsson F, Bjarnason R, et al. Asthma and allergy patterns over 18 years after severe RSV bronchiolitis in the first year of life. *Thorax* (2010) 65:1045–52. doi: 10.1136/thx.2009.121582

10. Wu P, Hartert TV. Evidence for a causal relationship between respiratory syncytial virus infection and asthma. *Expert Rev Anti Infect Ther* (2011) 9:731–45. doi: 10.1586/eri.11.92

11. Barnes MVC, Openshaw PJM, Thwaites RS. Mucosal immune responses to respiratory syncytial virus. *Cells* (2022) 11. doi: 10.3390/cells11071153

12. Torow N, Marsland BJ, Hornef MW, Gollwitzer ES. Neonatal mucosal immunology. *Mucosal Immunol* (2017) 10:5–17. doi: 10.1038/mi.2016.81

13. Vu LD, Siefker D, Jones TL, You D, Taylor R, Devincenzo J, et al. Elevated levels of type 2 respiratory innate lymphoid cells in human infants with severe respiratory syncytial virus bronchiolitis. *Am J Respir Crit Care Med* (2019) 200:1414–23. doi: 10.1164/rccm.201812-2366OC

14. Habibi MS, Thwaites RS, Chang M, Jozwik A, Paras A, Kirsebom F, et al. Neutrophilic inflammation in the respiratory mucosa predisposes to RSV infection. *Science* (2020) 370. doi: 10.1126/science.aba9301

15. Krzyzaniak MA, Zumstein MT, Gerez JA, Picotti P, Helenius A. Host cell entry of respiratory syncytial virus involves macropinocytosis followed by proteolytic activation of the F protein. *PloS Pathog* (2013) 9:e1003309. doi: 10.1371/journal.ppat.1003309

16. White JM, Whittaker GR. Fusion of enveloped viruses in endosomes. *Traffic* (2016) 17:593–614. doi: 10.1111/tra.12389

17. Hornung V, Schlender J, Guenthner-Biller M, Rothenfusser S, Endres S, Conzelmann KK, et al. Replication-dependent potent IFN-alpha induction in human plasmacytoid dendritic cells by a single-stranded RNA virus. *J Immunol* (2004) 173:5935–43. doi: 10.4049/jimmunol.173.10.5935

18. Lee BL, Barton GM. Trafficking of endosomal Toll-like receptors. *Trends Cell Biol* (2014) 24:360–9. doi: 10.1016/j.tcb.2013.12.002

19. Petes C, Odoardi N, Gee K. The toll for trafficking: toll-like receptor 7 delivery to the endosome. *Front Immunol* (2017) 8:1075. doi: 10.3389/fimmu.2017.01075

20. Rehwinkel J, Gack MU. RIG-I-like receptors: their regulation and roles in RNA sensing. *Nat Rev Immunol* (2020) 20:537–51. doi: 10.1038/s41577-020-0288-3

21. Liu P, Jamaluddin M, Li K, Garofalo RP, Casola A, Brasier AR. Retinoic acid-inducible gene I mediates early antiviral response and Toll-like receptor 3 expression in respiratory syncytial virus-infected airway epithelial cells. *J Virol* (2007) 81:1401–11. doi: 10.1128/JVI.01740-06

22. Lund JM, Alexopoulou L, Sato A, Karow M, Adams NC, Gale NW, et al. Recognition of single-stranded RNA viruses by Toll-like receptor 7. *Proc Natl Acad Sci USA* (2004) 101:5598–603. doi: 10.1073/pnas.0400937101

23. Goff PH, Hayashi T, He W, Yao S, Cottam HB, Tan GS, et al. Synthetic toll-like receptor 4 (TLR4) and TLR7 ligands work additively via myD88 to induce protective antiviral immunity in mice. *J Virol* (2017) 91. doi: 10.1128/JVI.01050-17

24. Li C, To KKW, Zhang AJX, Lee ACY, Zhu H, Mak WWN, et al. Co-stimulation with TLR7 agonist imiquimod and inactivated influenza virus particles promotes mouse B cell activation, differentiation, and accelerated antigen specific antibody production. *Front Immunol* (2018) 9:2370. doi: 10.3389/fimmu.2018.02370

25. To EE, Erlich J, Liong F, Luong R, Liong S, Bozinovski S, et al. Intranasal and epicutaneous administration of Toll-like receptor 7 (TLR7) agonists provides protection against influenza A virus-induced morbidity in mice. *Sci Rep* (2019) 9:2366. doi: 10.1038/s41598-019-38864-5

26. Laurent P, Yang C, Rendeiro AF, Nilsson-Payant BE, Carrau L, Chandar V, et al. Sensing of SARS-CoV-2 by pDCs and their subsequent production of IFN-I contribute to macrophage-induced cytokine storm during COVID-19. *Sci Immunol* (2022) 7: eadd4906. doi: 10.1126/sciimmunol.add4906

27. Rappe JCF, Finsterbusch K, Crotta S, Mack M, Priestnall SL, Wack A. A TLR7 antagonist restricts interferon-dependent and -independent immunopathology in a mouse model of severe influenza. *J Exp Med* (2021) 218. doi: 10.1084/jem.20201631

28. Tan KS, Lim RL, Liu J, Ong HH, Tan VJ, Lim HF, et al. Respiratory viral infections in exacerbation of chronic airway inflammatory diseases: novel mechanisms and insights from the upper airway epithelium. *Front Cell Dev Biol* (2020) 8:99. doi: 10.3389/fcell.2020.00099

29. Lukacs NW, Smit JJ, Mukherjee S, Morris SB, Nunez G, Lindell DM. Respiratory virus-induced TLR7 activation controls IL-17-associated increased mucus via IL-23 regulation. *J Immunol* (2010) 185:2231–9. doi: 10.4049/jimmunol.1000733

30. Davidson S, Kaiko G, Loh Z, Lalwani A, Zhang V, Spann K, et al. Plasmacytoid dendritic cells promote host defense against acute pneumovirus infection via the TLR7-MyD88-dependent signaling pathway. *J Immunol (Baltimore Md.: 1950)* (2011) 186:5938–48. doi: 10.4049/jimmunol.1002635

31. Estripeaut D, Torres JP, Somers CS, Tagliabue C, Khokhar S, Bhoj VG, et al. Respiratory syncytial virus persistence in the lungs correlates with airway hyperreactivity in the mouse model. *J Infect Dis* (2008) 198:1435–43. doi: 10.1086/592714

32. Schwarze J, O'donnell DR, Rohwedder A, Openshaw PJ. Latency and persistence of respiratory syncytial virus despite T cell immunity. *Am J Respir Crit Care Med* (2004) 169:801–5. doi: 10.1164/rccm.200308-1203OC

33. Puthothu B, Krueger M, Forster J, Heinzmann A. Association between severe respiratory syncytial virus infection and IL13/IL4 haplotypes. *J Infect Dis* (2006) 193:438–41. doi: 10.1086/499316

34. Saluzzo S, Gorki AD, Rana BMJ, Martins R, Scanlon S, Starkl P, et al. First-breath-induced type 2 pathways shape the lung immune environment. *Cell Rep* (2017) 18:1893–905. doi: 10.1016/j.celrep.2017.01.071

35. Martynova E, Rizvanov A, Urbanowicz RA, Khaiboullina S. Inflammasome contribution to the activation of th1, th2, and th17 immune responses. *Front Microbiol* (2022) 13:851835. doi: 10.3389/fmicb.2022.851835

36. Makris S, Bajorek M, Culley FJ, Goritzka M, Johansson C. Alveolar macrophages can control respiratory syncytial virus infection in the absence of type I interferons. *J Innate Immun* (2016) 8:452–63. doi: 10.1159/000446824

37. Berland R, Fernandez L, Kari E, Han JH, Lomakin I, Akira S, et al. Toll-like receptor 7-dependent loss of B cell tolerance in pathogenic autoantibody knockin mice. *Immunity* (2006) 25:429–40. doi: 10.1016/j.immuni.2006.07.014

38. Santiago-Raber ML, Dunand-Sauthier I, Wu T, Li QZ, Uematsu S, Akira S, et al. Critical role of TLR7 in the acceleration of systemic lupus erythematosus in TLR9-deficient mice. *J Autoimmun* (2010) 34:339–48. doi: 10.1016/j.jaut.2009.11.001

39. Chávez-Bueno S, Mejías A, Gómez AM, Olsen KD, Ríos AM, Fonseca-Aten M, et al. Respiratory syncytial virus-induced acute and chronic airway disease is independent of genetic background: an experimental murine model. *Virol J* (2005) 2:46. doi: 10.1186/1743-422X-2-46

40. You D, Becnel D, Wang K, Ripple M, Daly M, Cormier SA. Exposure of neonates to respiratory syncytial virus is critical in determining subsequent airway response in adults. *Respir Res* (2006) 7:107. doi: 10.1186/1465-9921-7-107

41. Rudd BD, Smit JJ, Flavell RA, Alexopoulou L, Schaller MA, Gruber A, et al. Deletion of TLR3 alters the pulmonary immune environment and mucus production during respiratory syncytial virus infection. *J Immunol* (2006) 176:1937–42. doi: 10.4049/jimmunol.176.3.1937

42. Bhoj VG, Sun Q, Bhoj EJ, Somers C, Chen X, Torres JP, et al. MAVS and MyD88 are essential for innate immunity but not cytotoxic T lymphocyte response against respiratory syncytial virus. *Proc Natl Acad Sci USA* (2008) 105:14046–51. doi: 10.1073/pnas.0804717105

43. Marr N, Wang T-I, Kam SHY, Hu YS, Sharma AA, Lam A, et al. Attenuation of respiratory syncytial virus–induced and RIG-I–dependent type I IFN responses in human neonates and very young children. *J Immunol* (2014) 192:948–57. doi: 10.4049/jimmunol.1302007

44. Tate MD, Ong JDH, Dowling JK, Mcauley JL, Robertson AB, Latz E, et al. Reassessing the role of the NLRP3 inflammasome during pathogenic influenza A virus infection via temporal inhibition. *Sci Rep* (2016) 6:27912. doi: 10.1038/srep27912

45. Wynn TA, Vannella KM. Macrophages in tissue repair, regeneration, and fibrosis. *Immunity* (2016) 44:450–62. doi: 10.1016/j.immuni.2016.02.015

46. Scharenberg M, Vangeti S, Kekäläinen E, Bergman P, Al-Ameri M, Johansson N, et al. Influenza A virus infection induces hyperresponsiveness in human lung tissue-resident and peripheral blood NK cells. *Front Immunol* (2019) 10:1116. doi: 10.3389/fimmu.2019.01116

47. Kim TH, Oh DS, Jung HE, Chang J, Lee HK. Plasmacytoid Dendritic Cells Contribute to the Production of IFN-β via TLR7-MyD88-Dependent Pathway and CTL Priming during Respiratory Syncytial Virus Infection. *Viruses* (2019) 11:730. doi: 10.3390/v11080730

48. Trifilo MJ, Bergmann CC, Kuziel WA, Lane TE. CC chemokine ligand 3 (CCL3) regulates CD8(+)-T-cell effector function and migration following viral infection. *J Virol* (2003) 77:4004–14. doi: 10.1128/JVI.77.7.4004-4014.2003

49. Heinonen S, Velazquez VM, Ye F, Mertz S, Acero-Bedoya S, Smith B, et al. Immune profiles provide insights into respiratory syncytial virus disease severity in young children. *Sci Transl Med* (2020) 12. doi: 10.1126/scitranslmed.aaw0268

50. Siefker DT, Vu L, You D, Mcbride A, Taylor R, Jones TL, et al. Respiratory syncytial virus disease severity is associated with distinct CD8(+) T-cell profiles. *Am J Respir Crit Care Med* (2020) 201:325–34. doi: 10.1164/rccm.201903-0588OC

51. Becker Y. Respiratory syncytial virus (RSV) evades the human adaptive immune system by skewing the Th1/Th2 cytokine balance toward increased levels of Th2 cytokines and IgE, markers of allergy–a review. *Virus Genes* (2006) 33:235–52. doi: 10.1007/s11262-006-0064-x

52. Carroll KN, Wu P, Gebretsadik T, Griffin MR, Dupont WD, Mitchel EF, et al. The severity-dependent relationship of infant bronchiolitis on the risk and morbidity of early childhood asthma. *J Allergy Clin Immunol* (2009) 123:1055–61, 1061.e1. doi: 10.1016/j.jaci.2009.02.021

53. Zhang D, Yang J, Zhao Y, Shan J, Wang L, Yang G, et al. RSV infection in neonatal mice induces pulmonary eosinophilia responsible for asthmatic reaction. *Front Immunol* (2022) 13:817113. doi: 10.3389/fimmu.2022.817113

54. Pelaia C, Paoletti G, Puggioni F, Racca F, Pelaia G, Canonica GW, et al. Interleukin-5 in the pathophysiology of severe asthma. *Front Physiol* (2019) 10:1514. doi: 10.3389/fphys.2019.01514

55. Russell RJ, Chachi L, Fitzgerald JM, Backer V, Olivenstein R, Titlestad IL, et al. Effect of tralokinumab, an interleukin-13 neutralising monoclonal antibody, on eosinophilic airway inflammation in uncontrolled moderate-to-severe asthma (MESOS): a multicentre, double-blind, randomised, placebo-controlled phase 2 trial. *Lancet Respir Med* (2018) 6:499–510. doi: 10.1016/S2213-2600(18)30201-7

56. Park JW, Taube C, Yang ES, Joetham A, Balhorn A, Takeda K, et al. Respiratory syncytial virus-induced airway hyperresponsiveness is independent of IL-13 compared with that induced by allergen. *J Allergy Clin Immunol* (2003) 112:1078–87. doi: 10.1016/j.jaci.2003.08.046

57. Mejías A, Chávez-Bueno S, Gómez AM, Somers C, Estripeaut D, Torres JP, et al. Respiratory syncytial virus persistence: evidence in the mouse model. *Pediatr Infect Dis J* (2008) 27:S60–2. doi: 10.1097/INF.0b013e3181684d52

58. Torres JP, Gomez AM, Khokhar S, Bhoj VG, Tagliabue C, Chang ML, et al. Respiratory Syncytial Virus (RSV) RNA loads in peripheral blood correlates with disease severity in mice. *Respir Res* (2010) 11:125. doi: 10.1186/1465-9921-11-125

59. Schmidt ME, Knudson CJ, Hartwig SM, Pewe LL, Meyerholz DK, Langlois RA, et al. Memory CD8 T cells mediate severe immunopathology following respiratory syncytial virus infection. *PloS Pathog* (2018) 14:e1006810. doi: 10.1371/journal.ppat.1006810

60. Jozwik A, Habibi MS, Paras A, Zhu J, Guvenel A, Dhariwal J, et al. RSV-specific airway resident memory CD8+ T cells and differential disease severity after experimental human infection. *Nat Commun* (2015) 6:10224. doi: 10.1038/ncomms10224

61. Connors TJ, Ravindranath TM, Bickham KL, Gordon CL, Zhang F, Levin B, et al. Airway CD8(+) T cells are associated with lung injury during infant viral respiratory tract infection. *Am J Respir Cell Mol Biol* (2016) 54:822–30. doi: 10.1165/rcmb.2015-0297OC

62. Kuwabara T, Ishikawa F, Kondo M, Kakiuchi T. The role of IL-17 and related cytokines in inflammatory autoimmune diseases. *Mediators Inflammation* (2017) 2017:3908061. doi: 10.1155/2017/3908061

63. Liu X, Nguyen TH, Sokulsky L, Li X, Garcia Netto K, Hsu AC, et al. IL-17A is a common and critical driver of impaired lung function and immunopathology induced by influenza virus, rhinovirus and respiratory syncytial virus. *Respirology* (2021) 26:1049–59. doi: 10.1111/resp.14141

64. Zhou L, Ivanov Ii, Spolski R, Min R, Shenderov K, Egawa T, et al. IL-6 programs T(H)-17 cell differentiation by promoting sequential engagement of the IL-21 and IL-23 pathways. *Nat Immunol* (2007) 8:967–74. doi: 10.1038/ni1488

65. Zhang X, Jin J, Tang Y, Speer D, Sujkowska D, Markovic-Plese S. IFN-beta1a inhibits the secretion of Th17-polarizing cytokines in human dendritic cells via TLR7 up-regulation. *J Immunol* (2009) 182:3928–36. doi: 10.4049/jimmunol.0802226

66. Chang Y, Nadigel J, Boulais N, Bourbeau J, Maltais F, Eidelman DH, et al. CD8 positive T cells express IL-17 in patients with chronic obstructive pulmonary disease. *Respir Res* (2011) 12:43. doi: 10.1186/1465-9921-12-43

67. Duan MC, Huang Y, Zhong XN, Tang HJ. Th17 cell enhances CD8 T-cell cytotoxicity via IL-21 production in emphysema mice. *Mediators Inflammation* (2012) 2012:898053. doi: 10.1155/2012/898053

68. Hou W, Jin YH, Kang HS, Kim BS. Interleukin-6 (IL-6) and IL-17 synergistically promote viral persistence by inhibiting cellular apoptosis and cytotoxic T cell function. *J Virol* (2014) 88:8479–89. doi: 10.1128/JVI.00724-14

69. Lukacs NW, Moore ML, Rudd BD, Berlin AA, Collins RD, Olson SJ, et al. Differential immune responses and pulmonary pathophysiology are induced by two different strains of respiratory syncytial virus. *Am J Pathol* (2006) 169:977–86. doi: 10.2353/ajpath.2006.051055

70. Schlender J, Hornung V, Finke S, Günthner-Biller M, Marozin S, Brzózka K, et al. Inhibition of toll-like receptor 7- and 9-mediated alpha/beta interferon production in human plasmacytoid dendritic cells by respiratory syncytial virus and measles virus. *J Virol* (2005) 79:5507–15. doi: 10.1128/JVI.79.9.5507-5515.2005

71. Hijano DR, Vu LD, Kauvar LM, Tripp RA, Polack FP, Cormier SA. Role of type I interferon (IFN) in the respiratory syncytial virus (RSV) immune response and disease severity. *Front Immunol* (2019) 10:566. doi: 10.3389/fimmu.2019.00566

72. Huang Y, Anderson R. Modulation of protective immunity, eosinophilia, and cytokine responses by selective mutagenesis of a recombinant G protein vaccine against respiratory syncytial virus. *J Virol* (2005) 79:4527–32. doi: 10.1128/JVI.79.7.4527-4532.2005

73. Moore ML, Chi MH, Luongo C, Lukacs NW, Polosukhin VV, Huckabee MM, et al. A chimeric A2 strain of respiratory syncytial virus (RSV) with the fusion protein of RSV strain line 19 exhibits enhanced viral load, mucus, and airway dysfunction. *J Virol* (2009) 83:4185–94. doi: 10.1128/JVI.01853-08

74. Vlahos R, Stambas J, Bozinovski S, Broughton BR, Drummond GR, Selemidis S. Inhibition of Nox2 oxidase activity ameliorates influenza A virus-induced lung inflammation. *PloS Pathog* (2011) 7:e1001271. doi: 10.1371/journal.ppat.1001271

frontiers | Frontiers in Immunology

TYPE Review
PUBLISHED 23 October 2023
DOI 10.3389/fimmu.2023.1227833

OPEN ACCESS

EDITED BY
Ralf Kircheis,
Syntacoll GmbH, Germany

REVIEWED BY
Hiroaki Shime,
Nagoya City University, Japan
Angela Pizzolla,
Peter MacCallum Cancer Centre, Australia

*CORRESPONDENCE
Zhengping Zhuang
zhengping.zhuang@nih.gov

†These authors share senior authorship

RECEIVED 23 May 2023
ACCEPTED 10 October 2023
PUBLISHED 23 October 2023

CITATION
Chakraborty S, Ye J, Wang H, Sun M, Zhang Y, Sang X and Zhuang Z (2023) Application of toll-like receptors (TLRs) and their agonists in cancer vaccines and immunotherapy. *Front. Immunol.* 14:1227833. doi: 10.3389/fimmu.2023.1227833

Application of toll-like receptors (TLRs) and their agonists in cancer vaccines and immunotherapy

Samik Chakraborty[1,2†], Juan Ye[1], Herui Wang[1], Mitchell Sun[1], Yaping Zhang[1], Xueyu Sang[1] and Zhengping Zhuang[1*†]

[1]Neuro-Oncology Branch, National Cancer Institute, National Institutes of Health, Bethesda, MD, United States, [2]NE1 Inc., New York, NY, United States

Toll-like receptors (TLRs) are pattern recognition receptors (PRRs) expressed in various immune cell types and perform multiple purposes and duties involved in the induction of innate and adaptive immunity. Their capability to propagate immunity makes them attractive targets for the expansion of numerous immunotherapeutic approaches targeting cancer. These immunotherapeutic strategies include using TLR ligands/agonists as monotherapy or combined therapeutic strategies. Several TLR agonists have demonstrated significant efficacy in advanced clinical trials. In recent years, multiple reports established the applicability of TLR agonists as adjuvants to chemotherapeutic drugs, radiation, and immunotherapies, including cancer vaccines. Cancer vaccines are a relatively novel approach in the field of cancer immunotherapy and are currently under extensive evaluation for treating different cancers. In the present review, we tried to deliver an inclusive discussion of the significant TLR agonists and discussed their application and challenges to their incorporation into cancer immunotherapy approaches, particularly highlighting the usage of TLR agonists as functional adjuvants to cancer vaccines. Finally, we present the translational potential of rWTC-MBTA vaccination [irradiated whole tumor cells (rWTC) pulsed with phagocytic agonists Mannan-BAM, TLR ligands, and anti-CD40 agonisticAntibody], an autologous cancer vaccine leveraging membrane-bound Mannan-BAM, and the immune-inducing prowess of TLR agonists as a probable immunotherapy in multiple cancer types.

KEYWORDS

TLR - toll-like receptor, TLR agonists, cancer vaccine, immunotherapy, adjuvant, cancer immuno therapy

Introduction

Emerging strategies in cancer immunotherapy, including immune checkpoint inhibitors (ICIs), cancer vaccines, and chimeric antigen receptor-T cells (CAR-T), have shown exceptional promise in clinical trials, giving rise to a plethora of ongoing research and development in this field (1). ICIs, including antibodies targeting anti-CTLA4 and anti-PD-1/PDL-1, have significantly progressed in various clinical trials to treat diverse cancer types (1). Meanwhile, adoptive cell therapies like CAR-T have shown promising results in treating multiple hematopoietic malignancies (2). Additionally, regulatory agencies have approved several preventive and therapeutic cancer vaccines for treating different cancers with numerous other vaccines in various development stages (3–7). These immunotherapies have underscored the importance of stimulating a robust anti-tumor immune response in cancer patients as a potential avenue for combating cancer. Exploring and harnessing appropriate immunostimulatory mechanisms is crucial in developing new cancer immunotherapy approaches. Toll-like receptors (TLRs) are a particular group of membrane receptor molecules that play the above-mentioned immunostimulatory functions in several innate immunity pathways (8). Consequently, TLRs are some of the most sought-after molecules used as vaccine adjuvants and in several immunotherapeutic approaches related to preventing and treating several infectious diseases, including cancer (8).

The inception of cancer immunotherapy dates back over a century, with the initial attempts involving using bacteria or bacterial products to activate the immune system (9–11). In 1891, William Coley pioneered the field of immunotherapy by administering a blend of heat-inactivated *Streptococcus pyogenes* (a Gram-positive bacteria) and *Serratia marcescens* (a Gram-negative bacteria) through intratumoral injections (9–11). This bacterial mixture became known as Coley's toxin later (11, 12). This approach by Coley achieved a robust immune response against sarcomas, resulting in reduced tumor growth and, in some cases, tumor elimination even though the inherent mechanism remained unclear at that time (10–12). Subsequent research elucidated this therapeutic response, unveiling the significance of unique signaling molecules like pattern recognition receptors (PRRs) and pathogen-associated molecular patterns (PAMPs), which serve as ligands or activators for PRRs (11, 13–15).

TLRs are a subclass of receptors from the PRR family and serve as central players in innate immune responses (16). TLRs are transmembrane domain proteins (type I) with tripartite motifs (16, 17). TLRs feature three distinct functional domains: an leucine-rich repeats (LRRs) containing amino (N)-terminal responsible for ligand binding (folded into a typical horseshoe-like structure), a transmembrane spanning region, and a carboxyl (C)-terminal cytoplasmic domain resembling the cytoplasmic region of globular Toll/interleukin-1 (IL-1) receptor (TIR) (16, 17). To date, ten human and thirteen murine TLRs have been identified (18). Based on their subcellular localization, TLRs are categorized into extracellular and intracellular groups (16, 19). TLRs such as TLR1, TLR2, TLR5, TLR6, and TLR10 are exclusively expressed on the plasma membrane and belong to the extracellular group; while TLR3, TLR7, TLR8, and TLR9 fall within the intracellular group, are expressed on the endosome and endoplasmic reticulum (16, 19). Only TLR4 is present in both intracellular components and the plasma membrane (16, 19). For each of the TLRs, there is a specific ligand(s) (Figure 1, Table 1). Every TLR with its ligand activates specific downstream signaling pathways either through myeloid differentiation primary response protein 88 (MyD88) and/or TIR-domain-containing adapter-inducing IFNβ (TRIF) (16, 20, 39–41). TLR-mediated signaling initiates the secretion of multiple cytokines that enhance the immune system's ability to combat external pathogens and infectious agents (16, 17, 39). Moreover, TLRs play a crucial role in activating and maturing various immune cells involved in innate and adaptive immune responses (16–18). We have listed the location of all the TLRs and their agonists in Figure 1. Moreover, we have provided a detailed classification, localization, and involved ligands of the TLRs in Table 1.

This review aims to consolidate the current strategies involving TLR agonists as potential therapeutics for cancer, either as standalone treatments, in combination therapies or as adjuvants for cancer vaccines. We also explore the supporting evidence for TLR agonists as adjuvants in cancer vaccines, promoting innate and adaptive immune responses against cancer cells, specifically focusing on the rWTC-MBTA autologous vaccine developed by our research group.

The roles of TLRs in various immune cell types and their impact on the regulation of cancer

It's crucial to note that TLRs are present in various types of cells, encompassing innate immune system components such as macrophages, neutrophils, dendritic cells (DCs), natural killer (NK) cells, and mast cells. They are also found in adaptive immune system elements like T and B lymphocytes, stromal cells, and various tumor cells. When TLRs engage with a ligand, they can significantly boost the expression of multiple costimulatory molecules on the cell membranes, activating cytokines and T-cell activation (16, 17). The following section briefly discusses how TLRs stimulate different immune cells and their role in regulating cancer immunity.

Dendritic cells

Dendritic cells (DCs) are widely recognized as the immune system's most efficient professional antigen-presenting cells (APCs) (42). DCs are also the most studied cells among all the TLR-expressing immune cells in the milieu of instigation of adaptive immunity (42). When faced with an infection or inflammation, immature DCs undergo a process of activation and transformation into mature DCs. These mature DCs are responsible for activating adaptive immune cells such as B and T lymphocytes (43). The

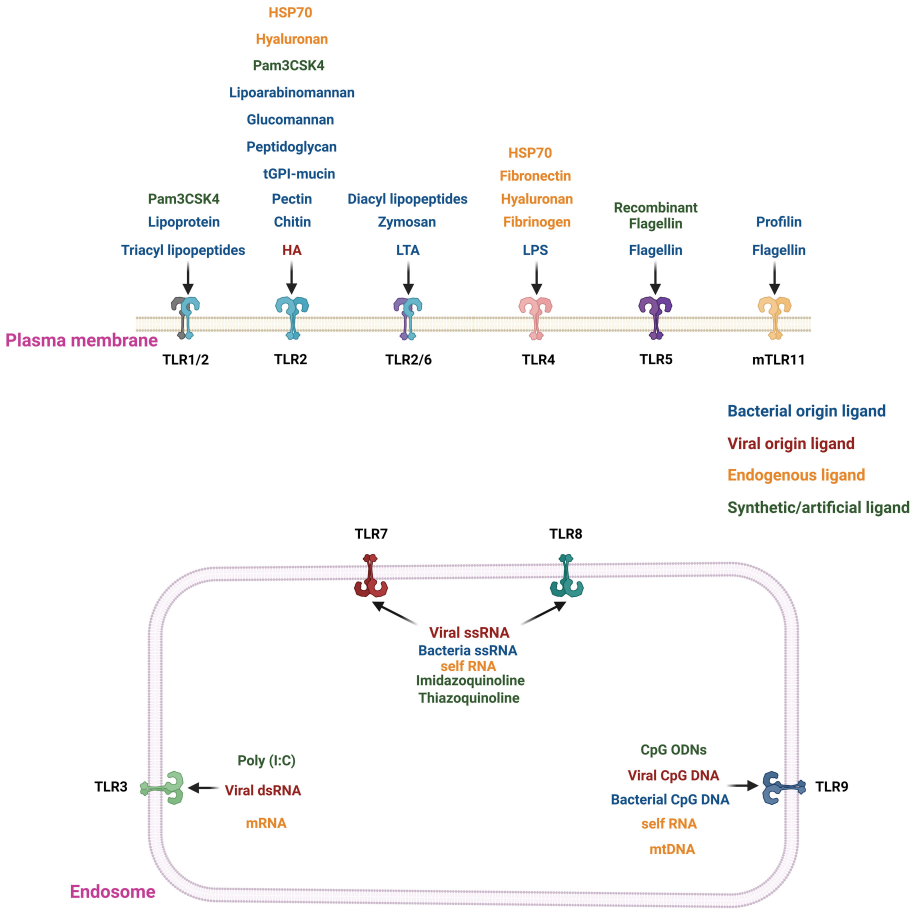

FIGURE 1
Location and agonists of different TLRs. TLRs 1/2, 2, 2/6, 4, and 5 are present in the extracellular region of the plasma membrane. In contrast, TLRs 3, 7, 8(only in humans), and 9 are localized on the endosomal membrane. The TLRs are stimulated by their specific ligand or agonists. The extracellular TLRs are mainly activated by exogenous agonists of bacterial, viral or pathogenic origin. The major exogenous ligands or microbial agonists are flagellin protein from bacterial flagella, lipoteichoic acid (LTA) and peptidoglycan (PGN) from Gram-positive bacteria, LPS from Gram-negative bacteria, lipoarabinomannan (LAM), lipopeptides, lipoglycans, and lipomannans from mycobacteria, zymosan from yeast (20, 21). There are synthetic TLR agonists like Pam3CSK4 or recombinant flagellin to stimulate the extracellular TLRs (20, 21). In contrast, nucleic acid ligands stimulate the endosomal TLRs 3, 7, 8, and 9. For example, TLR3 is stimulated by viral double-stranded RNA (dsRNA); TLR7 and 8 are triggered by viral and bacterial single-stranded RNA (ssRNA), and TLR9 recognizes CpG DNA from viruses and bacteria (20–25). There are also some endogenous ligands resulting from cellular injury, cell death, extracellular matrix components (e.g., hyaluronan, fibronectin, and fibrinogen), plasma membrane constituents, nuclear and cytosolic proteins and heat shock proteins, and elements of damaged/fragmented organelles such as mitochondrial DNA (mtDNA) (26, 27). TLRs 2 and 4 bind to most of the endogenous ligands resulting from cellular injury, cell death, and extracellular matrix components (27). The endogenous nucleic acid ligands like RNA or mtDNA bind with the endosomal ligands TLRs 3, 7, 8, and 9 (26, 27).

TABLE 1 Expression, localization, agonists/ligands of different TLRs.

TLR	Species	Localization	Microbial ligands	Microbes expressing TLR ligands	Endogenous ligands	Synthetic agonists	Ref.
TLR1	Human and mouse	Plasma membrane	Triacyl lipopeptides Bacterial lipoprotein	*Mycobacterium tuberculosis*	Unknown	Pam3CSK4	(20, 28)
TLR2	Human and mouse	Plasma membrane	Lipoproteins, zymosan, lipoarabinomannan, peptidoglycan, lipoteichoic acid	*Mycoplasma, Neisseria meningitides, Haemophilus influenzae, Leishmania major, Staphylococcus aureus*, Herpes simplex virus, Measles virus	Versican	Pam2CSK4, Pam3CSK4	(20, 28–32)

(Continued)

TABLE 1 Continued

TLR	Species	Localization	Microbial ligands	Microbes expressing TLR ligands	Endogenous ligands	Synthetic agonists	Ref.
TLR3	Human and mouse	Endosome	Viral dsRNA	Reovirus	mRNA	Poly(I:C), poly-ICLC, poly(I:C_{12}U) poly(A:U)	(20, 21, 33)
TLR4	Human and mouse	Plasma membrane and Endosome	LPS	*Escherichia coli, Pseudomonas aeruginosa*	Oxidized low-density lipoprotein, Amyloid-beta protein	Monophosphoryl lipid-A (MPL) derivatives	(20, 21, 33, 34)
TLR5	Human and mouse	Plasma membrane	Flagellin	*Salmonella* sp.	Unknown	Recombinant flagellin derivatives	(20, 21, 33)
TLR6	Human and mouse	Plasma membrane	Diacyl lipopeptides, lipoteichoic acid, zymosan	*Mycoplasma*, Hepatitis C virus (HCV), Cytomegalovirus	Oxidized low-density lipoprotein, Amyloid-beta protein, versican	Macrophage-activating lipopeptide 2, synthetic diacylated lipoproteins, Pam2CSK4	(20, 21, 29)
TLR7	Human and mouse	Endosome	Viral and bacterial ssRNA	Human immunodeficiency virus (HIV), HCV	Immune complexes, self-RNA	Thiazoquinoline and imidazoquinoline derivatives (e.g., resiquimod, imiquimod)	(20, 21, 33) (35, 36),
TLR8	Human and mouse	Endosome	Viral and bacterial ssRNA	Human immunodeficiency virus (HIV), HCV	Immune complexes, self-RNA	Thiazoquinoline and imidazoquinoline derivatives (e.g., resiquimod, imiquimod)	(20, 21, 33) (35, 36),
TLR9	Human and mouse	Endosome	Viral and bacterial CpG DNA, DNA: RNA hybrids	Human papilloma virus (HPV), Hepatitis B virus (HBV), Epstein-Barr virus (EBV), Polyomavirus	Chromatin-IgG-immune complexes, self-DNA	CpG Oligodeoxynucleotides (CpG ODNs)	(20, 33, 37)
TLR10	Human	Plasma membrane	Unknown		Unknown	Unknown	(20)
TLR11	Mouse	Endosome	Profilin and flagellin	*Toxoplasma gondii*	Unknown	Unknown	(38)
TLR12	Mouse	Endosome	Profilin		Unknown	Unknown	(20)
TLR13	Mouse	Endosome	Bacterial 23S ribosomal RNA (rRNA)		Unknown	23S rRNA-derived oligoribonucleotide	(20)

Adapted from "Toll-like receptors: Activation, signalling and transcriptional modulation." by De Nardo D. 2015, Cytokine. 74(2):181-9.

maturation of DCs involves a series of complex stages, including changes in the composition of receptors involved in endocytosis and phagocytosis, increased expression of co-stimulatory molecules like CD40, CD58, and CD86, alterations in morphology, and reorganization of lysosomal and MHC compartments (44). It's important to note that the DC population is highly diverse, consisting of various subtypes that exhibit differences in their functions, phenotypes, and distribution within the body (45). The two central populations of DCs found in the human immune system are lymphoid-derived plasmacytoid dendritic cells (pDCs) and myeloid-derived dendritic cells (mDCs) (45). Both pDCs and mDCs can activate the $CD4^+$ and $CD8^+$ T cells as well as facilitate the process of antigen cross-presentation to initiate the proliferation of $CD8^+$ T cells (46–48). Other phenotypes of DCs are monocyte-derived DCs (moDCs) and CD34+ cell–derived DCs (49). The activation status of dendritic cells is critical in determining how the immune system responds to a particular threat. All the subsets of DCs express distinctive TLRs, permitting themselves to generate a dedicated response against different pathogens (44). The major TLRs involved in DC maturation and function are TLR2, 3, 4, 5, 7/8, and 9 (50). TLR signaling is the key to DC-mediated cytotoxic T-cell activation (50). Previous studies demonstrated that TLR-mediated stimulation augments maturation and antigen presentation of murine DCs followed by induction of cytotoxic T cells (51, 52). Maturation of DC sub-populations and onset of cytotoxic $CD8^+$ T cells through IL-27-mediated signaling were reported after ligand mediated activation of TLR3 and TLR7 (51, 52). As suggested by the distinct Toll-like receptor (TLR) expression profiles in different DC subsets, the pDCs are primarily activated by viral pathogens, while mDCs primarily respond to fungal and bacterial antigens, and these

functional characteristics are exploited in DC-mediated vaccination and immunotherapy (53, 54). Similarly, the anti-tumor outcome of TLR7 activation was evident in central nervous system tumors, increasing maturation of DCs and activating tumor specific cytotoxic $CD8^+$ T cells (55). Another report demonstrated TLR mediated enrichment of the Th1 microenvironment and promoted activation of cytotoxic T-cells via IFN-λ-induced IL-12 released by breast cancer-associated dendritic cells (56). TLR4 activation also induced anti-colorectal cancer T cell response *in vitro* through DC maturation (57). Likewise, activation of TLR-4 and processing of tumor antigens stimulate DC maturation to markedly increasing *in vivo* $CD8^+IFN\gamma^+$ cytotoxic T cells (58). Interestingly, activating TLR7 and 8 was a crucial step in promoting the maturation of DCs isolated from AML patients and subsequently activating cytotoxic T cells *in vitro* (59). Interestingly, TLR7 signaling activated plasmacytoid dendritic cells (pDCs) leading to killing of murine melanoma cells through stimulation of NK cells and activating $CD8^+$ cytotoxic T-cells (60). Similarly, in ALL patients, activation of pDCs vial TLR9 molecules led to increased IFN production, which stimulated NK cells through TRAIL and CD69-mediated signaling (61). An earlier report about DC-targeted vaccines, demonstrated $CD8^+$ T cell response and better therapeutic efficacy after the activation of DCs through TLR7/8 and TLR3 mediated signaling (62). The immunosuppression present in the tumor microenvironment (TME) impedes the success of cancer immunotherapy, and DCs are extremely important in generating anti-tumor immunity inside the TME (42). Research has shown that the tumor microenvironment (TME) can hinder the growth and differentiation of mDCs (63). However, multiple studies demonstrated that TLR-mediated signaling has the potential to reactivate the immune functions of these inhibited dendritic cells, and this method could be beneficial to effectively counteract immunosuppression in the TME, offering a new arrow in the quiver of immunotherapy (64, 65).

Macrophages

Macrophages were the first immune cells identified to uphold tissue homeostasis, facilitate tissue repair, orchestrate immune responses, and combat pathogens (66, 67). Subsequently, it became evident that they also infiltrate and inhabit tumor sites and influence tumor development (66, 67). In addition, macrophages can alter their transcriptional profile, display remarkable cellular plasticity, and modify their functions in response to various inflammatory, tissue-specific, external pathogenic, and environmental stimuli, leading to anti-tumor and pro-tumor effects (67). In inflammatory conditions, classifying the tumor-associated macrophages (TAM) is still a complex task (66, 67). Classically, the macrophages were mainly categorized into two polarization states: M1, with pro-inflammatory traits, and M2, with anti-inflammatory characteristics (66, 67). M2 macrophages were considered to support tissue remodeling, tumor growth, and cancer-related processes, including cell proliferation, invasion, metastasis, and immune suppression; whereas, M1 macrophages were designated to drive immune responses, cause tissue damage, and inhibit tumor growth by enhancing anti-tumor responses of T cells and natural killer cells (66, 67). Macrophages are one of the most influential players in the TME, rendering them as a vital point for cancer immunotherapy (68). The anti-inflammatory M2 subtype of macrophages supports tumor growth and maintenance, but the pro-inflammatory M1 subtype promotes inflammation and tumoricidal properties (68). Switching the M2 subtypes to M1 in the tumor microenvironment by stimulants can promote tumoricidal activity (69). Regrettably, this simplified classification of macrophages into just the M1 or M2 category failed to define the diverse range of macrophage polarization states present within tumors or the TME (70), leading to a modern classification of TAMs where M1 and M2 represent the extremes of a spectrum with numerous intermediate subsets (66, 67). In relation to the complex interactions between different cell types within the TME, the TAMs are now considered into two main subtypes, M1-like (pro-inflammatory macrophages) and M2-like (anti-inflammatory macrophages) (67). Stimulation of Toll-like receptors (TLRs) in macrophages has been long recognized as a mechanism that drives macrophages toward a pro-inflammatory phenotype, and this renders TLR agonists particularly attractive in the context of cancer immunotherapy (71). It's noteworthy that since 2015, over 60 clinical trials have been initiated to assess the therapeutic potential of TLR agonists in treating various cancers (4). Activation of TLR3, recruits *in vitro* and *in vivo* IFN signaling cascade resulting in switching to M1 phenotype from M2 phenotype (69). The switching of M2 to M1 involves signaling associated with CD86, CD80, CD40, IL-12, IL-6, and TNF-α ensuing in enhanced antigen uptake by the macrophages and activation of T cells-mediated mice tumor growth regulation (72). Comparable anti-tumor results were detected in mice models of Lewis lung carcinoma and sarcoma following induction of TLR3 and TLR4 mediated signaling, respectively (73, 74). TLR4 was also suspected to promote the migration of macrophages through the upregulation of proinflammatory molecules like TNF-α, NF-κB, and VEGF (75). In a similar study, TLR-mediated signaling promoted the antitumor M1 phenotypes along with the upregulation of immunostimulatory cytokines like IL-18 (76). These immunostimulatory cytokines directed an antitumor collaboration between macrophages and NK cells *ex vivo* in ovarian cancer to stimulate IFN-γ secretion and Th1-type immune responses via NK cells (76). It is worth noting that TLR7/8 activation has been found to influence the differentiation of myeloid-derived suppressor cells (MDSCs) towards M1 phenotype within the tumor microenvironment, ultimately resulting in a regression of colorectal tumors in mice and a decrease in resistance to oxaliplatin (77). Oxaliplatin hindered the transformation of MDSCs into M1-like macrophages, but in combination with TLRs 7/8 agonist R-848, this hindrance was overcome (77). The addition of R-848 augmented the polarization of MDSCs to M1-like pro-inflammatory macrophages leading to increased apoptosis of the colorectal tumor cells (77). Furthermore, the stimulation of macrophages by TLR2/6 led to the activation of the NK cells and cytotoxic $CD8^+$-T cells in several tumors, including metastasis mice models and pancreatic cancer (78, 79). This was accompanied by increased immune surveillance in tumors

with concomitant increase of COX-2 expression in macrophages (78). COX-2 is the rate limiting enzyme of Prostaglandin E2 (PGE2) biosynthesis, and PGE2 is a strong suppressor of NK cells in the TME (78). Macrophage-activating lipopeptide-2 (MALP-2), a TLR2/6 agonist, enhances NK cell cytotoxicity towards the tumor cells, while the PGE2 mediated immunosuppression was blocked by COX-2 inhibitor (78).

NK cells

NK or natural killer cells are a group of lymphocyte, an indispensable component of the innate immune system, and they are best recognized for killing pathogen or virus infected cells and also responsible to detect and regulating initial signs of cancerous tissues (80). NK cells are termed as the first rank of defense against cancer cells, with the capability to kill the cancer cells without any prior activation or priming. That is why they are named "natural killers" (80). Multiple reports documented that depending upon originating population, NK cells express almost all types of TLRs (81). Amid all the TLR ligands TLR3, 7, 8, and 9 mediated signaling demonstrated a significant role in cancer biology. Human NK cell lines for instance YTC12, YTS, and NK92 expressed high amounts of activated TLR3, causing cytotoxic killing effects on K562 cancer cells (82). Furthermore, head and neck squamous cell carcinoma (HNSCC) cells are killed via IFNγ secreting NK cells activated through TLR3 (82, 83). TLRs like TLR7, 8, and 9 can sense foreign nucleic acids, and their subsequent activation on NK cells empowers anti-tumor immune responses (84, 85). Though the activation of this nucleic acid-sensing, NK cell-associated TLRs are mostly dependent on the signaling induced by other cells present in the associated tumor microenvironment (84, 85). While there is some argument concerning the expression of TLR7 and 8 on NK cells (84, 85), several reports depicted the activation and proliferation of NK cells by the cytokines secreted from neighboring cells of the tumor microenvironment (84, 85). In addition to TLR9 stimulated cytotoxicity of NK cells on B16 melanoma cells, the secretion of inflammatory cytokines as IFNγ and IL-12 was promoted via TLR7/8 activation, which in order aided the NK cells to eliminate the HNSCC cells and B16-F10 melanoma cancer cells (86–88). Interestingly, another report showed an acceleration of antitumor activity of HER2(human epidermal growth factor receptor 2)-targeting monoclonal antibodies both *in vivo* and *in vitro* after TLR2-mediated activation of NK cells (89).

B cells

B cells are the production house of antigen-specific antibodies and considered as the epicenter of the adaptive immune system (90). To date, several distinct B-cell subsets have been identified performing diverse functions in both adaptive and innate immune responses (90). B cells express an array of TLRs, whose signaling is collaborated with the B cell receptor signaling (91). Signaling from TLRs like TLR7 and TLR8 are well documented to augment the antibody and cytokine production from B cells (90). This TLR-mediated stimulation of B cells depicted increased expression of B7 costimulatory molecules and amplified survival as like B cell activation by CD40 (90). Activated B cells were reported to secrete multiple chemokines and cytokines after stimulation of TLR1/2, TLR7, and TLR9 (92). TLR-mediated signaling enhances cytokine secretion, promotes better antigen presentation from B cells along with overexpression of the costimulatory molecules, and, which sequentially augments the activation of helper T cells (91). Moreover, multiple reports demonstrated the activation of effector functions of B cells by TLR signaling, e.g., proliferation, antibody production, and immunoglobulin class switching (93–95). While B cells are known for their ample Toll-like receptor (TLR) expression and their critical role in humoral immunity and the adaptive immune response, their potential for TLR-mediated utilization in cancer immunotherapy remains relatively unexplored (91–93). Nevertheless, there have been a few instances where TLR-mediated activation of B cells has been applied in the context of cancer immunotherapy. B cells use TLRs to coordinate antibody responses during infection and autoimmune diseases, where the B cell receptors (BCR) and TLR7 or 9 are activated in response to self-antigens complexed with nucleic acids, such as RNA or DNA-containing immune complexes (96). This TLR-mediated stimulation can also be harnessed to generate tumor-specific antigen (TSA)-specific responses (44, 50). When high levels of antibodies are required for protection, be it infection or anti-tumor immunity, targeting TLRs on B cells can prove to be an effective strategy to enhance antibody production (97). The presence of tumor-specific antigens (TSAs) is essential for activating T cell and B cell immunity (98). Notably, B cells are the sole immune cells that consistently express TLR9 (97). Several studies have demonstrated that TLR9 agonists can induce significant anti-tumor immunity by activating B cells. TLR9 agonists endorse the differentiation of B cells into plasma cells and enhance antibody-dependent cellular cytotoxicity (ADCC) (99, 100). Brody et al. (101) reported clinically significant anti-B cell lymphoma responses following *in-situ* tumor vaccination with a TLR9 agonist. These studies underscore the efficacy and advantages of administering TLR agonists directly at the tumor site rather than systemically. TLR9 ligands like CpG-ODNs have shown great potential in stimulating B cell-mediated adaptive immunity (102–104). CpG-ODNs strongly induce B cell proliferation, activate plasmacytoid dendritic cells (pDCs) and monocyte maturation, stimulate natural killer (NK) cell activation, and trigger the production of inflammatory cytokines (102). B cell stimulation by CpG-ODNs increases their sensitivity to antigen stimulation and promotes their differentiation into antibody-secreting plasma cells, resulting in increased production of antigen-specific antibodies (103). TAC-001, an antibody-ODN conjugate consisting of a specialized TLR9 agonist (T-CpG) linked to an antibody against CD22 (a receptor restricted to B cells), is designed to deliver potent and targeted immune activation through systemic administration (104). *In vitro* stimulation of B cells with TAC-001 leads to increased expression of co-stimulatory molecules, immunoglobulin secretion, and cross-presentation, ultimately leading to T cell proliferation (104). TAC-001 has demonstrated efficient and durable single-agent anti-tumor activity in checkpoint inhibitor-resistant and

refractory murine tumor models (104). Systemic administration of TAC-001 in mice has resulted in increased B cell infiltration, enhanced T cell effector functions, modulation of myeloid-derived suppressor cells (MDSCs), and a significant decrease in IL-10+ regulatory B cells within the tumor microenvironment (104). Intravenous administration of TAC-001 in monkeys has shown favorable tolerability, pharmacokinetics, and pharmacodynamic profiles (104). Additionally, TLR9 activation in B cells leads to the expression of co-stimulatory molecules, enhancing cross-presentation, and allowing for the activation and proliferation of T cells, as well as the secretion of chemokines, cytokines, and immunoglobulins (3). Among other TLR9 ligands, Lefitolimod (MGN1703) has been utilized in several preclinical studies to assess B cell-mediated immunity. Multiple studies have demonstrated that MGN1703 significantly activates both innate and adaptive immune cells, including B cells, and induces the secretion of various inflammatory cytokines (IL-6, IL-8, IFN-α, and IFN-γ) and chemokines (CD40, CD69, CD86, CD169, and IP-10) from activated immune cells (105, 106). The combination therapy of TLR3 agonist with a TLR9 agonist (CpG: 5'-cytosine-phosphate-guanine-3') along with adoptive T cell transfer (ACT) has shown promise in increasing the abundance of various immune cell types, including B cells with $CD4^+$ and $CD8^+$ T cells, macrophages, neutrophils, and NK cells in tumor-draining lymph nodes (107). This combination therapy has augmented the elimination of murine melanoma cells and improved the survival of tumor-bearing mice, doubling their survival compared to untreated mice (107). Combination therapy involving TLR9 agonists and immune checkpoint inhibitors (ICIs) has also shown promising effects in clinical studies (108). For instance, Ribas et al. evaluated the safety and anti-tumor activity of co-treatment with intratumoral SD-101, a synthetic CpG oligonucleotide ligand for TLR9, and pembrolizumab in patients with melanoma (108). This combination therapy was well tolerated and improved overall survival, accompanied by a significant increase in B cells within the tumor microenvironment (TME), as well as other immune cell populations (108). These results indicate that combining SD-101 administration with PD-1 blockade potentially enhances clinical efficacy and reduces PD-1 blockade-related toxicity (108). Apart from TLR9, monophosphoryl lipid A (MPLA), a TLR4 ligand derived from the lipopolysaccharide (LPS) of Salmonella Minnesota, is used as an adjuvant in a prophylactic vaccine against human papillomavirus types 16 and 18, which are common causes of cervical cancer (109). As an adjuvant, MPLA enhances the antigen-presenting capabilities of macrophages and B cells, primes naive T cells, induces the maturation of dendritic cells, and stimulates antibody production (109).

Effector T cells

The effector T cells carry out multiple functions of the immune responses, like cytotoxicity, helper, and regulatory (110). Diverse types of effector T-cells express different TLRs, which can consequently regulate associated T-cell functions and antitumor immune activities (111). TLR1, 2, 5, 7, and 8 mediated signaling is identified to activate the proliferation of $CD4^+$ memory T-cells and upregulate accompanying cytokine secretion (112). For example, the presence of a higher amount of TLR5 agonists amplified $CD4^+$ T-cell population and concomitant expression of the cytokine IL2 (112). Activation of multiple TLRs like TLR2, 3, and 9 in purified B6 expressing CD4+ T cells provides costimulatory signals aimed at T cell receptor (TCR) activation. NF-κB signaling through TLR2-mediated signaling in $CD8^+$ T cells and TLR9 activation in $CD4^+$ T cells inhibits apoptosis and promotes survival (113). In a similar study, activation of TLR7 along with TLR8 on $CD4^+$ T-cells enhanced the secretion of IFNγ, IL-2, and IL-10; in addition to proliferation of T cells (114). Interestingly, the antitumor commotion of $CD8^+$ T-cells was promoted via glucose-uptake-dependent MyD88 and AKT-mTOR pathway through activation of TLR7 (115). It is well established that stimulation of immune cells like NK cells, DCs, and Tregs can control the $CD8^+$ effector T cell functions (51, 52, 82); similarly, multiple TLRs can control multiple functional characteristics of $CD8^+$ T-cells directly inside the tumor microenvironment (116). Activation of TLR1/2 promotes the effector activity of $CD8^+$ T cells in B16 melanoma cells both *in vivo* and *in vitro* through upregulation of perforin, Granzyme B, IFNγ and TNF-α (116). In addition, effector $CD8^+$ T cell functions along with increased IFNγ expression as a functional coactivator was also reported to be regulated by activation of TLR3 (117). Besides, transgenic OT-1 ($CD8^+$) T cells were stimulated through an antigen-independent manner after activation of TLR3, as measured by *in vitro* assays, leading to increased expression and robust expansion of immune-activation markers *in vivo* (118).

Regulatory T cells

The immunosuppressive activity of both human and murine regulatory T-cells (Tregs) can be modulated by some of the TLRs, and it is documented in multiple reports. TLR4 activation on Tregs enhanced their viability and immunosuppressive commotion (112). Also, a slight ligand-mediated activation of TLR5 increased the Treg marker FOXP3 on $CD4^+CD25^+$ Treg cells and increases their immunosuppressive aptitude slightly (112). There is also a contrasting report of reverting Treg's suppressive properties *in vivo* through the TLR8-MyD88-IRAK4 signaling cascade (119). There are some controversies regarding the reversion of suppressive activity of Tregs after TLR2 activation even though multiple reports depicted an increase in Treg proliferation after TLR2 activation (120, 121). For instance, activation of TLR2, inhibited the immunosuppressive activity of Tregs though it increased proliferation of Treg cells *in vivo* (122). In the tumor microenvironment (TME), activation of immunosuppressive cells like tolerogenic dendritic cells (DCs) and Treg cells is vital for establishing immunosuppression (123). Using antibodies to inhibit Treg cell function is an initial approach to enhance the effectiveness of cancer vaccines by reducing TME's immunosuppressive effects and boosting effector T cell function (124). Consistently, administering a DC vaccine with the TLR4 agonist LPS resulted in a notable increase in NK cells and a significant reduction in Treg cells within the tumor microenvironment in an ovarian cancer mouse model (125). TLR ligands can also trigger Th1 inflammatory

cytokines like IL-12, which facilitate the transition of $CD4^+$ T cells from Th2 to Th1 subtype, boost $CD8^+$ T cell responses, and suppress Treg cell function (126). TLR3 ligands were also reported to overturn the immunosuppressive TME towards anti-tumor immunity through modulation of the Treg cells (127, 128). TLR3 ligand poly A:U shifts the immunosuppressive tumor microenvironment towards anti-tumor immunity by altering the composition in favor of antigen-specific $CD8^+$ granzyme B^+ T cells, resulting in a lower Treg/$CD8^+$ cell ratio (127). Salazar et al. reported that administration of poly-ICLC induced *in situ* vaccination in a rhabdomyosarcoma patient induced local tumor inflammation and a systemic immune response, leading to a significant reduction in a facial tumor (128). Their research revealed that tumor regression was a result of the activation of both local and systemic anti-cancer immunity triggered by intratumoral and intramuscular poly-ICLC injections. Their findings suggest that intramuscular poly-ICLC maintenance therapy contributes to a systemic anti-tumor immune response through the induction of chemokines, co-stimulatory molecules, inflammasome formation, and an increase in the Teff/Treg cell ratio (128). In addition to TLR3, TLR7 agonists also inhibit Treg cell function, and activate NK cells, promoting anti-cancer immune responses (87, 129). Topical imiquimod application in a melanoma mouse model reduces Treg cell-related chemokine mRNA expression and increases cytotoxic molecules like granzyme B and perforin within tumors (130). Imiquimod also decreases Tregs and boosts $CD8^+$ cells in the tumor microenvironment (TME) (130). Intratumoral administration of SZU101(another TLR7 agonist) triggers a systemic anti-tumor response and alters the TME by increasing $CD4^+$ and $CD8^+$ cells while reducing Treg cells in a murine breast tumor model (131). Intraperitoneal injection of the TLR7 agonist resiquimod in mice with pancreatic ductal adenocarcinoma (PDAC) tumors reduces Tregs in the TME, enhances activation, infiltration, and cytotoxicity of $CD8^+$ T cells, suppressing tumor growth and improving survival (65). Combination therapy of radiation and imiquimod decreases Treg cells and MDSCs while increasing $CD4^+$ and $CD8^+$ T cell recruitment in the TME, commencing systemic anti-cancer responses and potentially limiting metastasis ultimately leading to increased survival (132). Administrating imiquimod as adjuvant preceding HPV vaccination enhances intratumoral $CD4^+$ and $CD8^+$ T cell infiltration while reducing Treg cells in the TME (133). Importantly, the effectiveness of the vaccination correlates with pre-existing and post-treatment (with imiquimod) Treg cell levels (133). Combining PD-L1 blockade with resiquimod reduces tumor size, activates DCs, diminishes Treg cells, and boosts the $CD8^+$ T cell/Treg cell ratio in the TME in mice tumor models (134). Furthermore, in the case of mice PDAC derived tumors, resiquimod elicited a robust immune response characterized by heightened immune complexity, reduced growth, enhanced infiltration of $CD8^+$ T cells, and a lowered frequency of intratumoral $CD4^+CD25^+FOXP3^+$ Treg cells (135). TLR9 ligands were also reported to modulate the TME via the suppression of Treg cells. CpG-A, the TLR9 ligand, induces IFNα and IFNβ production, promoting effector $CD4^+$ T cell proliferation by counteracting Treg cell suppression (119). In a mouse tumor model, adoptive transfer of Treg cells after pretreatment with poly-G10 (a TLR8 ligand) enhances antitumor activity and reduces Treg cell suppression (119). Remarkably, this study also suggests that Treg cells express TLR9 and can recognize CpG DNA molecules (119). Furthermore, CpG ODNs reduce Treg cell population in the draining lymph node (136). Local administration of CpG enhances OX40 expression, a TNF receptor, on both effector T and Treg cells in the tumor microenvironment (TME) (137). PF-3512676, one of the earlier synthetic TLR9 agonists to treat melanoma patients, increases pDC and mDC frequency, along with the release of inflammatory cytokines, while markedly reducing Treg cell population in the sentinel lymph nodes (SLN) (138). In addition, SD-101 (TLR9 agonist) treatment also reduces numbers of Treg cells and T follicular helper cells within tumors (139).

Application of TLR ligands/agonists in Cancer immunotherapy

With their ability to activate several innate immunity pathways, TLR ligands or agonists are considered compelling immunomodulators (44, 140, 141). Upon stimulation of TLRs by agonists, the downstream signaling also initiates enduring adaptive immune responses including cytotoxic NK cells, T-cells and maturation of DCs (140). Several TLR agonists demonstrated significant therapeutic efficacy against multiple ailments, including cancer (44, 141). Recent reports depicted improved efficacy of current immunotherapy approaches in cancer patients, such as cell-based immunotherapy combined with TLR agonists (19). TLR agonists are also known to sensitize cancer cells to conventional cancer therapies like radiation and chemotherapy (4, 140). Apart from combined therapy, TLR agonists are also administered as monotherapy in several malignancies (19). With growing information about several TLRs and involved TLR-agonists along with their downstream signaling pathways, several natural (resourced from microbes) or chemically synthesized TLR agonists, are being involved in cancer immunotherapy approaches (4, 140). But there are some early clinical setbacks in using TLR agonists as cancer therapeutics (142) because of the pro-tumorigenic nature of some TLRs in certain cancer types (44), and the activation of some of the TLRs led to an increase in tumor growth and metastasis (143). For this reason, it is necessary to determine the right tumor type and appropriate TLRs to be targeted and involved combinatorial approaches before treating any tumor with TLR-based immunotherapy. For the last two decades, TLR agonists have been used to stimulate and activate DCs in cancer immunotherapy (123). Moreover, in multiple vaccination strategies and immunotherapy approaches, TLRs can modify T-cell responses, which is revealed to be an excellent means to control and direct adaptive immunity (144, 145). One of the reasons for the growing popularity of TLR agonists for treating tumors is their aptitude to reinstate the activity of immunosuppressed DCs, which can be extremely useful for reversing the immunosuppressive atmosphere inside the TME (64, 65). TLR ligands have been widely utilized as adjuvants of anti-cancer vaccines, or in combination with other traditional standard of cares for cancer

(19, 44). Some TLR agonists have shown great promise at the clinical scenarios (19, 44). In recent years, against poorly immunogenic tumors, synthetic TLR agonists performed markedly better as adjuvants of cancer vaccines by enhancing the Th1 or Th2-mediated immune response (146). In Table 2, we have listed all the current clinical trials where TLR agonists are used as adjuvant(s) to cancer vaccines (3, 4, 6, 7, 90).

At the next section of this review, we are trying to present and discuss multiple clinical and preclinical pieces of evidence which demonstrates that TLR agonists can significantly improve the therapeutic outcome in different types of cancer, either in combined immunotherapy or as a cancer vaccine adjuvant.

Application of TLR agonists as adjuvants of cancer vaccine

TLR2/TLR4

Bacillus Calmette-Guerin (BCG) is the first successful TLR ligand/agonist approved for cancer treatment (147, 148). More than 40 years ago, BCG was first approved by the US Food and Drug Administration (FDA) to treat bladder cancer (147, 148). BCG wields its anti-cancer effect by the dual activation of TLR2, and TLR4 (147, 148). BCG as an adjuvant with whole cell vaccines also has been widely assessed in melanoma and colorectal cancer (CRC)

TABLE 2 Clinical Trials that are testing TLR agonists as adjuvants of cancer vaccines.

Target	Molecule	Indication	Status	Vaccine or co-therapy	Phase	NCT number
TLR2	BCG	Melanoma	Unknown	In combination with cyclophosphamide, IL-2 and a melanoma specific vaccine	II	NCT00477906
TLR3	Ampligen	Colorectal carcinoma	Withdrawn	In combination with DC-based vaccination, interferon-α2b and celecoxib	II	NCT02615574
TLR3	Hiltonol (poly (I:C))	Breast carcinoma	Active, not recruiting	In combination with a peptide vaccine and durvalumab	I	NCT02826434
TLR3	Hiltonol	Breast carcinoma	Active, not recruiting	In combination with a peptide vaccine and pembrolizumab	I	NCT03362060
TLR3	Hiltonol	Gynecological tumors	Active, not recruiting	In combination with a DC-based vaccine, guadecitabine and atezolizumab	I/IIb	NCT03206047
TLR3	Hiltonol	Lung cancer	Active, not recruiting	In combination with a MUC1-vaccine	I	NCT03300817
TLR3	Hiltonol	Solid tumors	Completed	In combination with a personalized vaccine	I	NCT02721043
TLR3	Hiltonol	Solid tumors	Withdrawn	In combination with bevacizumab and a peptide vaccine	I	NCT02754362
TLR3	Hiltonol	Multiple myeloma	Active, not recruiting	In combination with a peptide vaccine and durvalumab ± lenalidomide	I	NCT02886065
TLR3	Hiltonol	Glioma	Active, not recruiting	In combination with a cancer cell lysate vaccine before and after or only after surgery	I	NCT02549833
TLR3	Hiltonol	Glioma	Active, not recruiting	In combination with a peptide vaccine ± varlilumab	I	NCT02924038
TLR3	Hiltonol	Glioma	Active, not recruiting	In combination with a peptide vaccine	I	NCT02960230
TLR4	G100	Solid tumors	Terminated	In combination with a NY-ESO-1-targeting vaccine	I	NCT02387125
TLR8	Imiquimod	Cervical intraepithelial lesions	Unknown	In combination with a DNA-based vaccine	n.a.	NCT03206138
TLR8	Imiquimod	Cervical intraepithelial lesions	Active, not recruiting	Alone or in combination with HPV vaccination	II	NCT02864147
TLR8	Imiquimod	Genital warts	Completed	In combination with a DNA-based vaccine	II	NCT03180684
TLR8	Imiquimod	Chronic lymphocytic lymphoma	Completed	In combination with a peptide-based vaccine and lenalidomide	II	NCT02802943
TLR8	Imiquimod	NSCLC	Unknown	In combination with a DRibble-based vaccine, DC/CIK cells and GMCSF	I	NCT03057340

(Continued)

TABLE 2 Continued

Target	Molecule	Indication	Status	Vaccine or co-therapy	Phase	NCT number
TLR7/8	Resiquimod	Melanoma	Completed	Combined with a peptide-based vaccine	I	NCT01748747
TLR7/8	Resiquimod	Melanoma	Completed	Combined with a peptide-based vaccine	I	NCT00470379
TLR7/8	Resiquimod	Melanoma	Unknown	Combined with a peptide-based vaccine ± poly-ICLC	I/II	NCT02126579
TLR7/8	Resiquimod	Melanoma	Completed	Combined with a peptide-based vaccine	II	NCT00960752
TLR7/8	Resiquimod	NY-ESO-1+ tumors	Completed	Combined with a peptide-based vaccine	I	NCT00821652
TLR7/8	CV8102	Hepatocellular carcinoma	Completed	Combined with cyclophosphamide and a peptide-based vaccine	I/II	NCT03203005
TLR9	DUK-CPG-001	Hematological neoplasms	Withdrawn	In combination with a DC vaccine	II	NCT02115126
TLR9	Vidutolimod	Chronic lymphocytic leukemia	Recruiting	Multipeptide vaccine, XS15	I	NCT04688385

Adapted from.
1. "Trial watch: Toll-like receptor ligands in cancer therapy". By Le Naour J, and Kroemer G. 2023, Oncoimmunology. 12(1):2180237.
2. "Trial Watch: Toll-like receptor agonists in cancer immunotherapy". By Smith M, García-Martínez E, Pitter MR, Fucikova J, Spisek R, Zitvogel L, et al., 2018, Oncoimmunology. 7(12): e1526250.
3. "Trial watch: intratumoral immunotherapy". By Humeau J, Le Naour J, Galluzzi L, Kroemer G, and Pol JG. 2021, OncoImmunology. 10(1):1984677.
4. "Trial Watch: Immunostimulation with Toll-like receptor agonists in cancer therapy". By Iribarren K, Bloy N, Buqué A, Cremer I, Eggermont A, Fridman WH, et al., 2016, Oncoimmunology. 5 (3):e1088631.
5. "Trial Watch: experimental TLR7/TLR8 agonists for oncological indications". By Frega G, Wu Q, Le Naour J, Vacchelli E, Galluzzi L, Kroemer G, et al., 2020,OncoImmunology. 9(1):1796002.

(149, 150). In a randomized Phase III trial, Canvaxin, an allogeneic melanoma vaccine utilizing BCG as an adjuvant, failed to improve both overall and disease-free survival, despite showing promise in phase II (149). Interestingly, in the same trial with resected stage-III and stage-IV melanoma, monotherapy of BCG in patients demonstrated improved efficacy (149, 150). OncoVAX, an autologous colon cancer vaccine with BCG as an adjuvant, in a phase II study showed significant improvement in disease-free and overall survival (150, 151). Similarly, anti-tumor effect generated through activation of TLR2 and 4, by OM-174 (CXR-526), a lipid A (*Escherichia coli* origin) derivative, is currently being evaluated as a vaccine adjuvant for the treatment of melanoma in phase I/II trials, in addition to a phase I trial against solid tumors (152). The observed results from a few preclinical studies depict the increase of TNF-α, IFN-γ, and iNOS behind the therapeutic activity of OM-174 administration (152, 153). Another lipid A derivative, monophosphoryl lipid A (MPL), also an activator of TLR4, is also used in several vaccines as an adjuvant (153, 154). Stimuvax, the liposomal cancer vaccine against the MUC1 tumor antigen, uses MPL as an adjuvant (153). Stimuvax underwent phase III evaluation against advanced NSCLC but failed to add any marked therapeutic advantage (153). A cancer vaccine targeting the MAGE A3 tumor antigen utilizes a MPL containing special mixed adjuvant system (AS15, AS02b) (155). Other TLR4 activators like AS04 (MPL derivative, cervical cancer) and GLA-SE (lymphoma Merkel cell carcinoma) are also studied via preclinical and clinical studies (156–158). Meanwhile, lipoteichoic acids (LTA) from Gram-negative bacterial cell walls, responsible for the "endotoxin" of bacteria, can also act as an agonist of TLR2 receptors and trigger anti-tumor immune responses (11, 14).

TLR3

The activation of TLR3-mediated signaling by sense double-stranded RNA was first discovered by Alexopoulou et al. (159). Currently, the synthetic polynucleotide polyinosinic-polycytidylic acid or poly(I:C) is being used as a TLR3 agonist, and is known as a powerful activator of the innate immune responses (160). Poly(I:C) promoted the activation of DCs and subsequently enhanced antigen presentation for $CD8^+$ cytotoxic T cells (161). Additionally, after stimulation via poly(I:C), DCs can indirectly activate NK cells and T-cells, generating robust antitumor immune responses, and for this reason poly(I:C) is often employed in cancer vaccines (162). Because of the associated toxic effects and hasty degradation of poly (I:C) in the body, several stable derivatives or variants of poly(I:C) are established through experimental studies (163, 164). For example, Hiltonol or poly-ICLC is stabilized through the addition of poly-lysine and was assessed in several clinical trials involving different types of solid tumors (165, 166). Though these clinical studies didn't demonstrate significant anti-tumor efficacy but still it managed to be physiologically safe without any adverse side effects (165, 166). Additionally, rintatolimod or poly($I:C_{12}U$) (Ampligen), another poly(I:C) derivative, is stabilized by the substitution of cytidine with uridine and is approved for the treatment of pancreatic, triple-negative breast cancer, and brain tumors in combinatorial therapy with some vaccines demonstrated substantial efficacy (167–169). Poly(I:C) and all of its derivatives induce maturation of DCs, as well as intensify the expression of Th1-related cytokine, and currently evaluated in multiple clinical trials as potent vaccine adjuvants (170). In addition, poly-ICLC was moderately successful as combinatorial therapy with peptide or DC

vaccines in various advanced malignancies, including malignant glioma (136).

TLR5

TLR5 is activated by bacterial flagellum protein flagellin, and flagellin derivatives are evaluated for anticancer efficacy (171–173). The clinical efficacy of CBLB502 (natural flagellin/entolimod derived from natural *Salmonella* flagellin) is evaluated against squamous cell head and neck cancer and solid tumors in phase I clinical trials (174). Mobilan, a recombinant nonreplicating adenovirus encoding flagellin which is commercially available as M-VM3 is also has been studied for anti-cancer effects in prostate cancer (175). Treatment of breast cancer cells with the TLR5 agonist flagellin also reported to suppress cell proliferation and inhibiting anchorage-independent tumor growth (171). In another interesting *in vivo* study, the researcher demonstrated contrasting effects on tumor growth after TLR5 activation by flagellin. Activation of TLR5 by flagellin reduces the growth of strongly immunogenic tumors, but it failed to do the same for weakly immunogenic variants (172). These conflicting results were caused by the disproportionation between IFN-γ:IL-4 ratio and the concomitant number of $CD4^+CD25^+$ T regulatory cells (172). Also in the same study, early combinatory treatment of flagellin and CpG-containing oligodeoxynucleotides (CpG ODNs) completely inhibited tumor growth (172).

TLR 7/8

Among all the TLRs, ligands or agonists of TLR7 and 8 have shown the most promising immunomodulatory and anticancer effects, and many of them transitioned to the clinic (176). TLR7 and 8, both recognize ssRNA as ligands, and this property has been exploited to synthesize several types of TLR7/8 agonists that could achieve stimulation of these receptors simultaneously (176). Based on chemical structures, TLR7/8 agonists are organized into guanosine and adenosine analogs or imidazoquinoline derivatives with modified RNA sequences (176, 177). Dual agonists of TLR7/TLR8, resiquimod (R-848), and loxoribine (178) failed to enter phase III trials because they lacked significant efficacies (179). Initial studies attributed the lack of local immune activation by resiquimod to its property of solubility in body fluid and subsequent dispersion from the injection site (178). Resiquimod was thereafter administered as a dermal cream to counteract this problem (180). Resiquimod induces the expression of TNF-α, IFN-α, and other proinflammatory cytokines, via the initiation of the TLR7-MyD88-dependent pathway (22). Imiquimod, another imidazoquinoline marketed as Aldara (5% imiquimod cream), was approved by the European Medicines Agency and FDA in 1997 for treating human papillomavirus (HPV) induced genital warts (181). Later in 2004, imiquimod was also approved as therapeutics of primary skin malignancies like superficial basal cell carcinoma and premalignant actinic keratosis (182). Topical ointment of imiquimod is also used for the treatment of other local cutaneous tumors, including melanoma, and interestingly imiquimod exerts an impressive over 85% success rate while treating lentigo maligna melanoma (183, 184). Imiquimod also demonstrated significant efficacy in combinatorial therapies with other traditional anticancer therapies like chemotherapy or radiotherapy in multiple cancer types (180). Imiquimod has also shown promise in developing DC-based vaccines (6, 185). Imiquimod promoted the stimulation and maturation of immature DCs and their consequent migration to draining lymph nodes in cancer patients (185). Topical imiquimod ointment amplified the immunogenicity of the peptide vaccine for melanoma (185). In patients with resected melanoma, imiquimod as an adjuvant also augmented the immunogenicity of the NY-ESO-1 peptide vaccine, recruiting and activating pDCs and mDCs subcutaneously and in inflammatory infiltrates (6). In contrast to imiquimod's topical application, 852A (a TLR7 agonist) and VTX-2337 (a TLR8 agonist) are dispensed systemically, and their efficacy are under evaluation through multiple phase I/II clinical trials involving malignant breast, ovarian, endometrial, cervical, and head and neck cancers (186). 852A activates APCs and stimulate NK cells with increased secretion of IFN-α from plasmacytoid DCs in cancer patients (179, 187). In a phase II trial, 852A demonstrated safety and systemic immune activation in metastatic melanoma patients who had failed chemotherapy, leading to prolonged disease stabilization (188). While treating patients suffering from chronic hepatitis C virus (HCV) infection and cancer, ANA773- the orally administered TLR7/8 agonist, induced IFN-α, activated NK cells, and reduced serum HCV RNA levels (189). Lastly, 3M-052 (a lipid-modified imidazoquinoline derivative), was assessed as a cancer vaccine adjuvant demonstrating marked synergistic efficacy in tandem with checkpoint-blocking antibodies for CTLA4 and PDL-1 (190). This result highlighted the potential on the aspect of utilizing TLR7/8 agonists in combinatorial therapies with other immunotherapeutic agents like immune-checkpoint inhibitors (ICIs).

TLR9

Unmethylated cytidine phosphate guanosine (CpG) and oligonucleotides (CpG ODNs) are the main ligands or agonists for TLR9 receptors (191). Several CpG oligodeoxynucleotides are verified for their anticancer effects both *in vitro* and *in vivo* models of multiple cancers (192–194) and clinical trials (195). Some of the significant examples of TLR9 agonists undergoing clinical trials are IMO2055 (a CpG ODN-based oligonucleotide tested in advanced NSCLC), dSLIM (two single-stranded oligodeoxynucleotide loops connected with double-stranded oligodeoxynucleotide stem, currently tested in advanced colorectal cancer), MGN1703 (a natural DNA molecule assessed in small cell lung cancer and advanced solid tumors), CpG-7909 (a single-stranded CpG ODN, currently evaluated in melanoma, renal cell carcinoma, non-Hodgkin's lymphoma, glioblastoma, cutaneous T cell lymphoma, and NSCLC), KSK-CpG (phosphorothioated derivative of CpG ODNs, being evaluated in melanoma), SD-101 (tested in follicular lymphoma), ODN M362 (tested in hepatocarcinoma), and CpG-1826 (demonstrated amplified antitumor effect in glioma

xenografts) (106, 191, 196, 197). Even after promising preclinical studies, the administration of IMO2055 in combination with platinum-based drugs against recurrent and metastatic head and neck cancer, raised some safety issues in a phase II trial (142). Similar safety concerns were raised against CPG7909, in a phase III trial involving NSCLC (142). CpG ODNs blended (emulsified) with Montanide ISA 51, being used as an adjuvant with vaccines targeting cancer-testis antigens, demonstrated promising results by promoting pDC-mediated infiltration of lymphocytes at the site of vaccination (198). Therefore, the application of CpG ODN as an adjuvant of cancer vaccines or intratumoral injection could be a potential opportunity to direct effector lymphocyte-mediated response.

TLR ligands as adjuvants in autologous MBTA vaccine immunotherapy

Till now in the previous sections, we discussed the classification, the immunomodulatory functions of TLRs, and the administration of TLR agonists in immunotherapeutic strategies and cancer vaccines. We concisely described how different TLR agonists are employed as adjuvants to cancer vaccines in several preclinical and clinical studies. Most of the current immunotherapy trends are heavily oriented toward the onset of adaptive immunity via immunomodulators like TLR agonists. Here we present a new immunotherapeutic approach developed by our research group based on autologous tumor neoantigens and TLR agonists that are proficient in triggering both the innate and adaptive immune responses (199, 200). It's an autologous vaccine strategy that leverages the PRR assets of TLRs as well as fungal polysaccharides, and it has been tested in diverse types of mouse tumor models (11, 14, 199–201).

This vaccine is called rWTC-MBTA, comprising of irradiated autologous tumor cells (rWTC) mixed with mannan-BAM, TLR agonists, and anti-CD40 antibody (MBTA) (199–202). This vaccination strategy was initiated with the utilization of TLR agonists accompanied by concurrent labeling of tumor cells with phagocytosis-inducing ligands leading to enhanced recognition of the tumor cells by the different immune cells (203, 204). Mannan, a branched polysaccharide from the yeast *Saccharomyces cerevisiae*, is affixed to the cancer cell membranes through linkage with the hydrophobic BAM (Biocompatible Anchor for Membrane) anchor and serves as a PAMP, which in turn is recognized by the mannan-binding lectin complex (MBL) (11, 14) (Figure 2). Recognition of mannan-BAM by MBL activates the lectin pathway of complement activation and ultimately leading to iC3b-mediated opsonization and phagocytosis of tumor cells (11, 14, 201). To augment the vaccine-induced innate immune responses through the initiation of multiple inflammatory pathways, along with mannan-BAM, we use TLR ligands lipoteichoic acid (LTA)(agonist of TLR2), polyinosinic-polycytidylic acid (poly(I:C))(agonist of TLR3), and resiquimod (R-848)(agonist of TLR7/8) (11, 199–201) (Figure 2). Several previous reports from our group demonstrated the applicability of TLR ligands as adjuvants in rWTC-MBTA vaccines (11, 199–201). This vaccine strategy plays on stimulating the immune system on various stages, starting from primary activation of innate immunity trailed by concomitant activation of adaptive immunity (11, 14, 201). Each TLR ligands as adjuvants in the vaccine as unique function. The strongly immunogenic LTA, which is sourced from the Gram-Positive bacteria *Bacillus subtilis*, stimulates the TLR2-mediated inflammatory pathway, resulting in elevated secretion of TNF-alpha and heightened inflammatory response (205, 206). Poly(I:C) triggers TLR3-mediated signaling, leading to activation of antigen-presenting cells (APCs) and activates tumor associated macrophages (206–208). R-848 or resiquimod induces the activation of innate immune cells and the promotes Th1 cell-mediated immune responses (209, 210). In addition, anti-CD40 monoclonal antibodies in the vaccine preparation binds with the CD40L ligand to activate the $CD4^+$ T lymphocytes, permitting the dendritic cells to mediate the adaptive immune responses (199, 200) (Figure 2). To prepare rWTC-MBTA-Vax, (i) autologous or syngeneic cancer cells are irradiated so that it remains alive but non-replicative, (ii) irradiated cells are combined with mannan-BAM and TLR agonists, along with anti-CD40 antibody, to produce the effective vaccine, and (iii) the prepared rWTC-MBTA is injected peripherally over four weeks to propagate a tumor-specific immune response to inhibit tumor or cancerous growth, metastasis, and prevent recurrence (199, 200).

One of the foremost advantages of the MBTA vaccines or rWTC-MBTA is that it can affect the immunogenic status of the TME to facilitate the outcome of the immunotherapy. The "cold" TME of some solid tumors is a major barrier to cancer immunotherapy (211–213). The immunogenically cold TME status is associated with a lack of inflammatory T-cell infiltration and lower neoantigen presentation (214). TLR agonists can promote Th1(T helper) mediated inflammatory responses and activate APCs in the TME, facilitating tumor infiltration as well as improved functioning of the effector immune cells, like $CD8^+$ T cells and NK cells (212). When used as adjuvants, the TLR agonists augment the antigen presentation capacity of APCs and initiate the expressions of Th1 inflammatory cytokines along with increasing the expression of several co-stimulatory factors (126, 212, 215). The Th1 family of inflammatory cytokines endorse the switching of $CD4^+$ T cells from Th2 subtype to Th1 subtype, increase $CD8^+$ effector T-cell responses, and impede the immunosuppressive activity of Treg cells (126). The MBTA vaccine approach manipulates the TME, by the application of TLR agonists to turn the cold TME to hot, and it was evident by the efficacy of rWTC-MBTA on curbing immunogenically cold tumors like glioblastoma multiforme (GBM) (200) or triple-negative breast cancer (202).

Previous investigations involving intratumoral MBTA injections sustained a profound antitumor response, but patients are prone to secondary inflammatory damage or mass effect due to the *in situ* delivery of the vaccine (151, 216). Earlier studies of the MBTA anti-cancer therapeutics involved a unique combination of two different types of PAMPs, mannan-BAM serving as a tag for phagocytosis and soluble TLR agonist ligands as triggers of innate immunity (11, 14). This unique amalgamation of mannan-BAM and TLR agonists generates a robust infiltration of inflammatory cells toward the tumor. This led to reduction of tumor burden and even, in some experimental mice models, complete remission of the

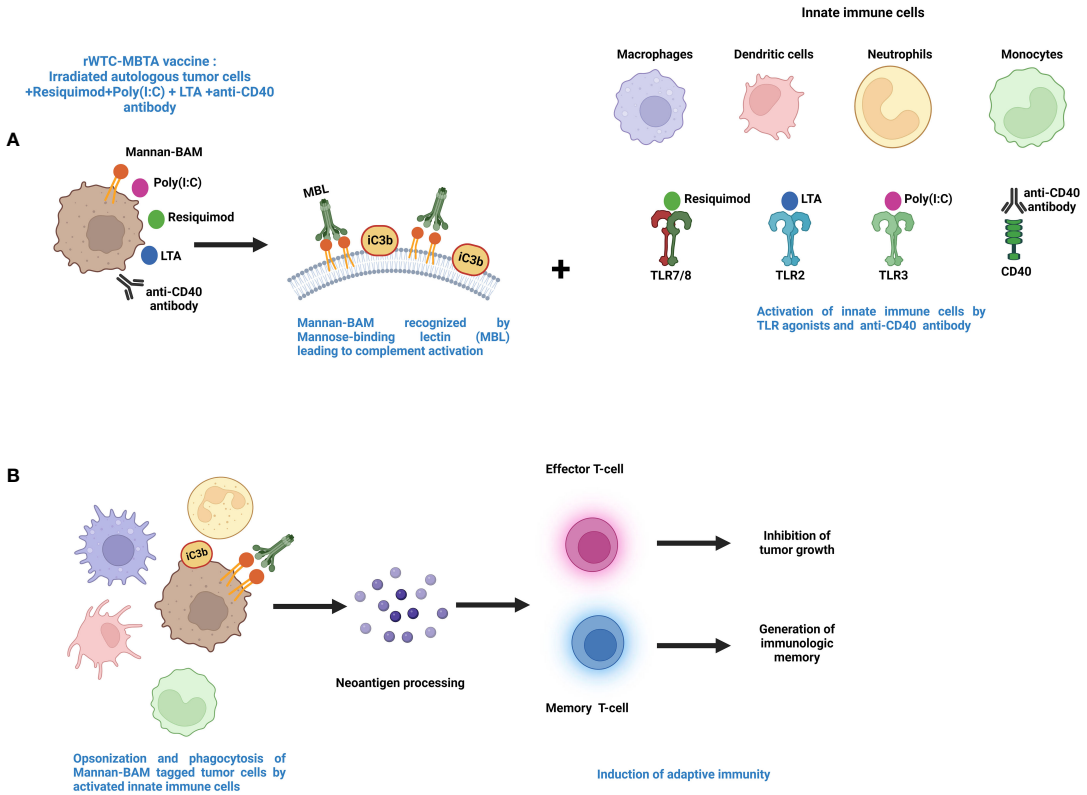

FIGURE 2
Mechanism of action for MBTA vaccine therapy. **(A)**. The MBTA vaccine consists of mannan-BAM tagged irradiated cancer cells mixed with TLR ligands resiquimod, poly(I:C), and LTA along with anti-CD40 antibody. The polysaccharide mannan is chemically linked with the hydrophobic lipid tail biocompatible anchor for membrane (BAM). The hydrophobic lipid tail enables the attachment of mannan to the plasma membrane of irradiated tumor cells. Mannan-BAM acts as a PAMP and exploits the pattern recognition properties of Mannose-binding lectin (MBL). This recognition of Mannan-BAM by MBL culminates into the activation of the lectin pathway of complement activation through the proteolytic cleavage of complement protein C3, and iC3b, the inactive cleaved form of C3 initiate the opsonization of the tumor cells. Concurrently, the three TLR ligands (resiquimod/R-848, poly(I:C), LTA) and anti-CD40-antibody act as adjuvants facilitate recruitment of the innate immune cells like macrophages, dendritic cells, neutrophils, and monocytes into the tumor (199–202). **(B)**. The TLR agonists activate the innate immune cells with augmented expression of inflammatory cytokines and chemokines that endorse maturation of APCs. The activated APCs opsonize and phagocytose the tumor cells and process tumor neoantigens. These activated APCs further internalize tumor antigens and display them to T cells in lymph nodes. This leads to the initiation of adaptive immune cells like effector T cells along with generation of immunologic memory through memory T cells (199–202).

tumor (11, 14, 203, 204). In our preceding study, in a colon carcinoma preclinical mouse model, compared to control or injecting irradiated whole tumor cells alone, we found that subcutaneous injection of the rWTC-MBTA vaccine (irradiated whole tumor cells mixed with MBTA) caused a substantial decrease in tumor volumes and improved overall survival (199). In one of our recently published manuscripts, we demonstrated that the rWTC-MBTA vaccine effectively inhibited the metastasis and impeded the growth of tumors in animal models of both breast cancer and melanoma (202). Additionally, in a therapeutically mimicking postoperative model of breast cancer, it prevented the metastasis of residual tumors and extended the survival (202). Our results also demonstrated that the rWTC-MBTA vaccine effectively prevented the growth of autologous tumors but rendered ineffective against allogeneic tumors (202). Mechanistic studies regarding the rWTC-MBTA vaccination revealed enhanced activation of APCs, heightened $CD4^+$ and $CD8^+$ T-cell mediated response, generation of immune memory along with tumor specific cytotoxicity (202). Moreover, we also proved rWTC-MBTA vaccine efficacy was T-cell dependent through T-cell depletion assay (202). With the surmounting preclinical evidence, we want to translate rWTC-MBTA to the clinic for further investigations, and altogether the efficacy of rWTC-MBTA is dependent on TLR agonists, and this can direct toward a new track of cancer immunotherapy.

Conclusions and future perspectives

TLR activation sparks immune responses against pathogens, making TLR agonists promising cancer immunotherapy. Targeting TLRs, alone or combined with other methods, offers a potential pathway to enhance the immune system and eradicate cancer cells. TLRs are crucial components of the immune system, playing a significant role in both innate and adaptive immunity. It's exciting to know that there are currently various TLR agonists being evaluated in both preclinical and clinical settings worldwide. However, there are some foremost expected roadblocks with the implementation of TLR agonists as therapeutic options. Toll-like receptors in cancer have a dual role; on one side, they activate innate immunity, recruiting immune cells to eliminate invasive pathogens

like tumor cells, but they can also contribute to chronic inflammation, driven by TLRs, resulting in anti-apoptotic effects through NF-κB and promoting tumor growth (217, 218). As TLRs regulate the stimulation of several immune cells of the human body, any improper tuning of the TLR agonists can trigger autoimmune diseases. There are also chances of the onset of chronic inflammatory side effects through uncalled activation of cytokines. Multiple examples of inflammatory side effects exist while using TLR ligands in immunotherapy (142, 217, 219, 220). Therefore, choosing the right TLR agonist for the treatment of a specific type of cancer is a vital issue to diminish the chances of post-therapeutic complications.

Both pre-clinical and clinical findings suggest that combining TLR agonists with antigens, immune modulators, or other treatments can enhance their effectiveness (19, 221). Therapies like chemotherapy or phototherapy release tumor antigens and cellular factors from dying cells, further activating dendritic cells and promoting cross-presentation to T cells (221). Current research highlights the potential of TLR-targeted drugs in cancer treatment. However, it's crucial to acknowledge that factors like tumor characteristics and the microenvironment can impact the clinical success of TLR-targeting immunotherapies. These variables should be carefully addressed, especially in preclinical animal studies. Recent data suggests that combining TLR antagonists with other immunotherapy approaches, like checkpoint inhibitors and cell-based treatments, could improve overall immunotherapy effectiveness (19). Current trends of using TLR agonists in clinical trials project them as a compelling booster of immune responses in combination with cancer vaccines or other therapeutic approaches, suggesting a more promising strategy (Table 2). Another challenge is the difficulty of translating many TLR agonists from animal studies to human applications due to significant species-specific differences in TLRs (97). For instance, murine TLR8 reacts differently to imiquimod and R848 compared to human TLR8 (97). This highlights the importance of assessing potential TLR agonists in appropriate animal models and considering species-specific variations when interpreting results. Despite the potential of TLR agonists to activate the immune system for anti-tumor effects, they face persistent limitations. For instance, small molecule TLR ligands often fail to accumulate adequately in lymph nodes to activate immune cells effectively, leading to drug resistance. Rapid dispersion of TLR ligands can also trigger the production of immunosuppressive factors and undesirable immune responses. Additionally, these agonists/ligands have a short *in vivo* lifespan, especially endosomal TLR ligands, which are vulnerable to nucleases (222). As a result, innovative and efficient delivery platforms like dendrimers, stimuli-responsive polymeric particles, liposomes, hydrogels, lipoprotein-based scaffolds, and complexes have been devised to address these challenges (222).

Here in this review article, we presented the immense therapeutic potential, background aspects, and key investigations of using TLR ligands or agonists as an emerging component of immunotherapy. We also review the current landscape of using TLR agonists in cancer immunotherapy, including ongoing clinical trials and their drawbacks. Moreover, we explored how TLR agonists can induce diverse components of the immune system and how they are or could be applied as adjuvants of cancer vaccines. Last but not the least, our research group implemented TLR agonists as adjuvants augmented the immunogenicity of the rWTC-MBTA whole-cell autologous cancer vaccine. By continuing further studies, we have confidence in TLR agonist-based immunotherapy, in combination with other conventional therapies like surgery, chemotherapy, and radiotherapy, can shift the much-needed paradigm in the treatment of cancer and confirm an improved quality of life (QoL) for cancer patients.

Author contributions

SC did the literature survey and wrote the article. JY, HW, MS, YZ, and XS contributed valuable inputs on the scientific contents. ZZ planned the sections of the article with SC. and gave scientific inputs. All authors have revised the manuscript and approved its submission.

Acknowledgments

This study was supported by the Intramural Research Program of the National Institute of Neurological Disorders and Stroke and the National Cancer Institute of the National Institutes of Health. The figures are created with BioRender.com.

Conflict of interest

Author SC is employed by NE1 Inc.

The remaining authors declare that the research was conducted in the absence of any commercial or financial relationships that could be construed as a potential conflict of interest.

Publisher's note

References

1. Ribas A, Wolchok JD. Cancer immunotherapy using checkpoint blockade. *Science* (2018) 359(6382):1350–5. doi: 10.1126/science.aar4060

2. Han D, Xu Z, Zhuang Y, Ye Z, Qian Q. Current progress in CAR-T cell therapy for hematological Malignancies. *J Cancer*. (2021) 12(2):326–34. doi: 10.7150/jca.48976

3. Le Naour J, Kroemer G. Trial watch: Toll-like receptor ligands in cancer therapy. *Oncoimmunology* (2023) 12(1):2180237. doi: 10.1080/2162402X.2023.2180237

4. Smith M, García-Martínez E, Pitter MR, Fucikova J, Spisek R, Zitvogel L, et al. Trial Watch: Toll-like receptor agonists in cancer immunotherapy. *Oncoimmunology* (2018) 7(12):e1526250. doi: 10.1080/2162402X.2018.1526250

5. Humeau J, Le Naour J, Galluzzi L, Kroemer G, Pol JG. Trial watch: intratumoral immunotherapy. *OncoImmunology* (2021) 10(1):1984677. doi: 10.1080/2162402X.2021.1984677

6. Iribarren K, Bloy N, Buqué A, Cremer I, Eggermont A, Fridman WH, et al. Trial Watch: Immunostimulation with Toll-like receptor agonists in cancer therapy. *Oncoimmunology* (2016) 5(3):e1088631. doi: 10.1080/2162402X.2015.1088631

7. Frega G, Wu Q, Le Naour J, Vacchelli E, Galluzzi L, Kroemer G, et al. Trial Watch: experimental TLR7/TLR8 agonists for oncological indications. *OncoImmunology* (2020) 9(1):1796002. doi: 10.1080/2162402X.2020.1796002

8. Iwasaki A, Medzhitov R. Toll-like receptor control of the adaptive immune responses. *Nat Immunol* (2004) 5(10):987–95. doi: 10.1038/ni1112

9. Coley WB. The treatment of Malignant tumors by repeated inoculations of erysipelas. With a report of ten original cases. 1893. *Clin Orthop Relat Res* (1991) 262):3–11.

10. Mellman I, Coukos G, Dranoff G. Cancer immunotherapy comes of age. *Nature* (2011) 480(7378):480–9. doi: 10.1038/nature10673

11. Uher O, Caisova V, Hansen P, Kopecky J, Chmelar J, Zhuang Z, et al. Coley's immunotherapy revived: Innate immunity as a link in priming cancer cells for an attack by adaptive immunity. *Semin Oncol* (2019) 46(4-5):385–92. doi: 10.1053/j.seminoncol.2019.10.004

12. Felgner S, Kocijancic D, Frahm M, Weiss S. Bacteria in cancer therapy: renaissance of an old concept. *Int J Microbiol* (2016) 2016:8451728. doi: 10.1155/2016/8451728

13. Akira S, Uematsu S, Takeuchi O. Pathogen recognition and innate immunity. *Cell* (2006) 124(4):783–801. doi: 10.1016/j.cell.2006.02.015

14. Caisová V, Uher O, Nedbalová P, Jochmanová I, Kvardová K, Masáková K, et al. Effective cancer immunotherapy based on combination of TLR agonists with stimulation of phagocytosis. *Int Immunopharmacol* (2018) 59:86–96. doi: 10.1016/j.intimp.2018.03.038

15. Chen GY, Nuñez G. Sterile inflammation: sensing and reacting to damage. *Nat Rev Immunol* (2010) 10(12):826–37. doi: 10.1038/nri2873

16. Lim KH, Staudt LM. Toll-like receptor signaling. *Cold Spring Harb Perspect Biol* (2013) 5(1):a011247. doi: 10.1101/cshperspect.a011247

17. Bowie A, O'Neill LA. The interleukin-1 receptor/Toll-like receptor superfamily: signal generators for pro-inflammatory interleukins and microbial products. *J Leukoc Biol* (2000) 67(4):508–14. doi: 10.1002/jlb.67.4.508

18. Wang Y, Song E, Bai B, Vanhoutte PM. Toll-like receptors mediating vascular malfunction: Lessons from receptor subtypes. *Pharmacol Ther* (2016) 158:91–100. doi: 10.1016/j.pharmthera.2015.12.005

19. Pahlavanneshan S, Sayadmanesh A, Ebrahimiyan H, Basiri M. Toll-like receptor-based strategies for cancer immunotherapy. *J Immunol Res* (2021) 2021:9912188. doi: 10.1155/2021/9912188

20. De Nardo D. Toll-like receptors: Activation, signalling and transcriptional modulation. *Cytokine* (2015) 74(2):181–9. doi: 10.1016/j.cyto.2015.02.025

21. Fitzgerald KA, Kagan JC. Toll-like receptors and the control of immunity. *Cell* (2020) 180(6):1044–66. doi: 10.1016/j.cell.2020.02.041

22. Hemmi H, Kaisho T, Takeuchi O, Sato S, Sanjo H, Hoshino K, et al. Small anti-viral compounds activate immune cells *via* the TLR7 MyD88-dependent signaling pathway. *Nat Immunol* (2002) 3(2):196–200. doi: 10.1038/ni758

23. Ayres JS, Schneider DS. Tolerance of infections. *Annu Rev Immunol* (2012) 30:271–94. doi: 10.1146/annurev-immunol-020711-075030

24. Hemmi H, Takeuchi O, Kawai T, Kaisho T, Sato S, Sanjo H, et al. A Toll-like receptor recognizes bacterial DNA. *Nature* (2000) 408(6813):740–5. doi: 10.1038/35047123

25. Hoebe K, Du X, Georgel P, Janssen E, Tabeta K, Kim SO, et al. Identification of Lps2 as a key transducer of MyD88-independent TIR signalling. *Nature* (2003) 424 (6950):743–8. doi: 10.1038/nature01889

26. Murad S. Toll-like receptor 4 in inflammation and angiogenesis: a double-edged sword. *Front Immunol* (2014) 5:313. doi: 10.3389/fimmu.2014.00313

27. Yu L, Wang L, Chen S. Endogenous toll-like receptor ligands and their biological significance. *J Cell Mol Med* (2010) 14(11):2592–603. doi: 10.1111/j.1582-4934.2010.01127.x

28. Takeuchi O, Sato S, Horiuchi T, Hoshino K, Takeda K, Dong Z, et al. Cutting edge: role of toll-like receptor 1 in mediating immune response to microbial lipoproteins1. *J Immunol* (2002) 169(1):10–4. doi: 10.4049/jimmunol.169.1.10

29. Kang JY, Nan X, Jin MS, Youn S-J, Ryu YH, Mah S, et al. Recognition of lipopeptide patterns by toll-like receptor 2-toll-like receptor 6 heterodimer. *Immunity* (2009) 31(6):873–84. doi: 10.1016/j.immuni.2009.09.018

30. Borrello S, Nicolò C, Delogu G, Pandolfi F, Ria F. TLR2: A crossroads between infections and autoimmunity? *Int J Immunopathol Pharmacol* (2011) 24(3):549–56. doi: 10.1177/039463201102400301

31. Leoni V, Gianni T, Salvioli S, Campadelli-Fiume G. Herpes simplex virus glycoproteins gH/gL and gB bind Toll-like receptor 2, and soluble gH/gL is sufficient to activate NF-κB. *J Virol* (2012) 86(12):6555–62. doi: 10.1128/JVI.00295-12

32. Moore CE, Segal S, Berendt AR, Hill AV, Day NP. Lack of association between Toll-like receptor 2 polymorphisms and susceptibility to severe disease caused by Staphylococcus aureus. *Clin Diagn Lab Immunol* (2004) 11(6):1194–7. doi: 10.1128/CDLI.11.6.1194-1197.2004

33. Jackson Hoffman BA, Pumford EA, Enueme AI, Fetah KL, Friedl OM, Kasko AM. Engineered macromolecular Toll-like receptor agents and assemblies. *Trends Biotechnol* (2023) 41(9):1139–54. doi: 10.1016/j.tibtech.2023.03.008

34. Ciesielska A, Matyjek M, Kwiatkowska K. TLR4 and CD14 trafficking and its influence on LPS-induced pro-inflammatory signaling. *Cell Mol Life Sci* (2021) 78 (4):1233–61. doi: 10.1007/s00018-020-03656-y

35. Heil F, Hemmi H, Hochrein H, Ampenberger F, Kirschning C, Akira S, et al. Species-specific recognition of single-stranded RNA *via* toll-like receptor 7 and 8. *Science* (2004) 303(5663):1526–9. doi: 10.1126/science.1093620

36. Zhang Y, El-Far M, Dupuy FP, Abdel-Hakeem MS, He Z, Procopio FA, et al. HCV RNA activates APCs *via* TLR7/TLR8 while virus selectively stimulates macrophages without inducing antiviral responses. *Sci Rep* (2016) 6:29447. doi: 10.1038/srep29447

37. Martínez-Campos C, Burguete-García AI, Madrid-Marina V. Role of TLR9 in oncogenic virus-produced cancer. *Viral Immunol* (2017) 30(2):98–105. doi: 10.1089/vim.2016.0103

38. Yarovinsky F, Hieny S, Sher A. Recognition of Toxoplasma gondii by TLR11 prevents parasite-induced immunopathology. *J Immunol* (2008) 181(12):8478–84. doi: 10.4049/jimmunol.181.12.8478

39. Akira S, Takeda K. Toll-like receptor signalling. *Nat Rev Immunol* (2004) 4 (7):499–511. doi: 10.1038/nri1391

40. Burns K, Janssens S, Brissoni B, Olivos N, Beyaert R, Tschopp J. Inhibition of interleukin 1 receptor/Toll-like receptor signaling through the alternatively spliced, short form of MyD88 is due to its failure to recruit IRAK-4. *J Exp Med* (2003) 197 (2):263–8. doi: 10.1084/jem.20021790

41. Cusson-Hermance N, Khurana S, Lee TH, Fitzgerald KA, Kelliher MA. Rip1 mediates the Trif-dependent toll-like receptor 3- and 4-induced NF-{kappa}B activation but does not contribute to interferon regulatory factor 3 activation. *J Biol Chem* (2005) 280(44):36560–6. doi: 10.1074/jbc.M506831200

42. Amon L, Hatscher L, Heger L, Dudziak D, Lehmann CHK. Harnessing the complete repertoire of conventional dendritic cell functions for cancer immunotherapy. *Pharmaceutics* (2020) 12(7). doi: 10.3390/pharmaceutics12070663

43. Banchereau J, Steinman RM. Dendritic cells and the control of immunity. *Nature* (1998) 392(6673):245–52. doi: 10.1038/32588

44. Javaid N, Choi S. Toll-like receptors from the perspective of cancer treatment. *Cancers (Basel)*. (2020) 12(2). doi: 10.3390/cancers12020297

45. Chiang CL, Kandalaft LE. *In vivo* cancer vaccination: Which dendritic cells to target and how? *Cancer Treat Rev* (2018) 71:88–101. doi: 10.1016/j.ctrv.2018.10.012

46. Fu C, Peng P, Loschko J, Feng L, Pham P, Cui W, et al. Plasmacytoid dendritic cells cross-prime naive CD8 T cells by transferring antigen to conventional dendritic cells through exosomes. *Proc Natl Acad Sci U S A*. (2020) 117(38):23730–41. doi: 10.1073/pnas.2002345117

47. Gutiérrez-Martínez E, Planès R, Anselmi G, Reynolds M, Menezes S, Adiko AC, et al. Cross-presentation of cell-associated antigens by MHC class I in dendritic cell subsets. *Front Immunol* (2015) 6. doi: 10.3389/fimmu.2015.00363

48. Tel J, Schreibelt G, Sittig SP, Mathan TSM, Buschow SI, Cruz LJ, et al. Human plasmacytoid dendritic cells efficiently cross-present exogenous Ags to CD8+ T cells despite lower Ag uptake than myeloid dendritic cell subsets. *Blood* (2013) 121(3):459–67. doi: 10.1182/blood-2012-06-435644

49. Shortman K, Liu Y-J. Mouse and human dendritic cell subtypes. *Nat Rev Immunol* (2002) 2(3):151–61. doi: 10.1038/nri746

50. Chen X, Zhang Y, Fu Y. The critical role of Toll-like receptor-mediated signaling in cancer immunotherapy. *Med Drug Discov* (2022) 14:100122. doi: 10.1016/j.medidd.2022.100122

51. Desch AN, Gibbings SL, Clambey ET, Janssen WJ, Slansky JE, Kedl RM, et al. Dendritic cell subsets require cis-activation for cytotoxic CD8 T-cell induction. *Nat Commun* (2014) 5:4674. doi: 10.1038/ncomms5674

52. Pantel A, Teixeira A, Haddad E, Wood EG, Steinman RM, Longhi MP. Direct type I IFN but not MDA5/TLR3 activation of dendritic cells is required for maturation and metabolic shift to glycolysis after poly IC stimulation. *PloS Biol* (2014) 12(1): e1001759. doi: 10.1371/journal.pbio.1001759

53. Boonstra A, Asselin-Paturel C, Gilliet M, Crain C, Trinchieri G, Liu Y-J, et al. Flexibility of mouse classical and plasmacytoid-derived dendritic cells in directing T helper type 1 and 2 cell development : dependency on antigen dose and differential toll-like receptor ligation. *J Exp Med* (2003) 197(1):101–9. doi: 10.1084/jem.20021908

54. Ito T, Amakawa R, Kaisho T, Hemmi H, Tajima K, Uehira K, et al. Interferon-alpha and interleukin-12 are induced differentially by Toll-like receptor 7 ligands in human blood dendritic cell subsets. *J Exp Med* (2002) 195(11):1507–12. doi: 10.1084/jem.20020207

55. Prins RM, Craft N, Bruhn KW, Khan-Farooqi H, Koya RC, Stripecke R, et al. The TLR-7 agonist, imiquimod, enhances dendritic cell survival and promotes tumor antigen-specific T cell priming: relation to central nervous system antitumor immunity. *J Immunol* (2006) 176(1):157–64. doi: 10.4049/jimmunol.176.1.157

56. Hubert M, Gobbini E, Couillault C, Manh TV, Doffin AC, Berthet J, et al. IFN-III is selectively produced by cDC1 and predicts good clinical outcome in breast cancer. *Sci Immunol* (2020) 5(46). doi: 10.1126/sciimmunol.aav3942

57. Fang H, Ang B, Xu X, Huang X, Wu Y, Sun Y, et al. TLR4 is essential for dendritic cell activation and anti-tumor T-cell response enhancement by DAMPs released from chemically stressed cancer cells. *Cell Mol Immunol* (2014) 11(2):150–9. doi: 10.1038/cmi.2013.59

58. Park HJ, Jang GY, Kim YS, Park JH, Lee SE, Vo MC, et al. A novel TLR4 binding protein, 40S ribosomal protein S3, has potential utility as an adjuvant in a dendritic cell-based vaccine. *J Immunother Cancer.* (2019) 7(1):60. doi: 10.1186/s40425-019-0539-7

59. Nourizadeh M, Masoumi F, Memarian A, Alimoghaddam K, Moazzeni SM, Yaghmaie M, et al. *In vitro* induction of potent tumor-specific cytotoxic T lymphocytes using TLR agonist-activated AML-DC. *Target Oncol* (2014) 9(3):225–37. doi: 10.1007/s11523-013-0285-6

60. Drobits B, Holcmann M, Amberg N, Swiecki M, Grundtner R, Hammer M, et al. Imiquimod clears tumors in mice independent of adaptive immunity by converting pDCs into tumor-killing effector cells. *J Clin Invest* (2012) 122(2):575–85. doi: 10.1172/JCI61034

61. Lelaidier M, Dìaz-Rodriguez Y, Cordeau M, Cordeiro P, Haddad E, Herblot S, et al. TRAIL-mediated killing of acute lymphoblastic leukemia by plasmacytoid dendritic cell-activated natural killer cells. *Oncotarget* (2015) 6(30):29440–55. doi: 10.18632/oncotarget.4984

62. Ramakrishna V, Vasilakos JP, Tario JD Jr., Berger MA, Wallace PK, Keler T. Toll-like receptor activation enhances cell-mediated immunity induced by an antibody vaccine targeting human dendritic cells. *J Transl Med* (2007) 5:5. doi: 10.1186/1479-5876-5-5

63. Zhong H, Gutkin DW, Han B, Ma Y, Keskinov AA, Shurin MR, et al. Origin and pharmacological modulation of tumor-associated regulatory dendritic cells. *Int J Cancer.* (2014) 134(11):2633–45. doi: 10.1002/ijc.28590

64. Mende I, Engleman EG. Breaking self-tolerance to tumor-associated antigens by in *vivo* manipulation of dendritic cells. *Methods Mol Biol* (2007) 380:457–68. doi: 10.1007/978-1-59745-395-0_29

65. Michaelis KA, Norgard MA, Zhu X, Levasseur PR, Sivagnanam S, Liudahl SM, et al. The TLR7/8 agonist R848 remodels tumor and host responses to promote survival in pancreatic cancer. *Nat Commun* (2019) 10(1):4682. doi: 10.1038/s41467-019-12657-w

66. Cassetta L, Pollard JW. A timeline of tumour-associated macrophage biology. *Nat Rev Cancer.* (2023) 23(4):238–57. doi: 10.1038/s41568-022-00547-1

67. Kerneur C, Cano CE, Olive D. Major pathways involved in macrophage polarization in cancer. *Front Immunol* (2022) 13. doi: 10.3389/fimmu.2022.1026954

68. Zeng Q, Jewell CM. Directing toll-like receptor signaling in macrophages to enhance tumor immunotherapy. *Curr Opin Biotechnol* (2019) 60:138–45. doi: 10.1016/j.copbio.2019.01.010

69. Sica A, Mantovani A. Macrophage plasticity and polarization: in *vivo* veritas. *J Clin Invest* (2012) 122(3):787–95. doi: 10.1172/JCI59643

70. Qian BZ, Pollard JW. Macrophage diversity enhances tumor progression and metastasis. *Cell* (2010) 141(1):39–51. doi: 10.1016/j.cell.2010.03.014

71. Cao X, Lai SWT, Chen S, Wang S, Feng M. Chapter Three - Targeting tumor-associated macrophages for cancer immunotherapy. In: Mariani SA, Cassetta L, Galluzzi L, editors. *International Review of Cell and Molecular Biology*, vol. 368. Academic Press (2022) 368 p. 61–108. doi: 10.1016/bs.ircmb.2022.02.002

72. Vidyarthi A, Khan N, Agnihotri T, Negi S, Das DK, Aqdas M, et al. TLR-3 stimulation skews M2 macrophages to M1 through IFN-αβ Signaling and restricts tumor progression. *Front Immunol* (2018) 9:1650. doi: 10.3389/fimmu.2018.01650

73. Huang Z, Yang Y, Jiang Y, Shao J, Sun X, Chen J, et al. Anti-tumor immune responses of tumor-associated macrophages *via* toll-like receptor 4 triggered by cationic polymers. *Biomaterials* (2013) 34(3):746–55. doi: 10.1016/j.biomaterials.2012.09.062

74. Müller E, Speth M, Christopoulos PF, Lunde A, Avdagic A, Øynebråten I, et al. Both type I and type II interferons can activate antitumor M1 macrophages when combined with TLR stimulation. *Front Immunol* (2018) 9:2520. doi: 10.3389/fimmu.2018.02520

75. Lee CH, Wu CL, Shiau AL. Toll-like receptor 4 signaling promotes tumor growth. *J Immunother* (2010) 33(1):73–82. doi: 10.1097/CJI.0b013e3181b7a0a4

76. Bellora F, Castriconi R, Dondero A, Pessino A, Nencioni A, Liggieri G, et al. TLR activation of tumor-associated macrophages from ovarian cancer patients triggers cytolytic activity of NK cells. *Eur J Immunol* (2014) 44(6):1814–22. doi: 10.1002/eji.201344130

77. Liu Z, Xie Y, Xiong Y, Liu S, Qiu C, Zhu Z, et al. TLR 7/8 agonist reverses oxaliplatin resistance in colorectal cancer *via* directing the myeloid-derived suppressor cells to tumoricidal M1-macrophages. *Cancer Lett* (2020) 469:173–85. doi: 10.1016/j.canlet.2019.10.020

78. Müller C, Tufa DM, Chatterjee D, Mühlradt PF, Schmidt RE, Jacobs R. The TLR-2/TLR-6 agonist macrophage-activating lipopeptide-2 augments human NK cell cytotoxicity when PGE2 production by monocytes is inhibited by a COX-2 blocker. *Cancer Immunol Immunother* (2015) 64(9):1175–84. doi: 10.1007/s00262-015-1723-3

79. Schmidt J, Welsch T, Jäger D, Mühlradt PF, Büchler MW, Märten A. Intratumoural injection of the toll-like receptor-2/6 agonist 'macrophage-activating lipopeptide-2' in patients with pancreatic carcinoma: a phase I/II trial. *Br J Cancer.* (2007) 97(5):598–604. doi: 10.1038/sj.bjc.6603903

80. Gang M, Wong P, Berrien-Elliott MM, Fehniger TA. Memory-like natural killer cells for cancer immunotherapy. *Semin Hematol* (2020) 57(4):185–93. doi: 10.1053/j.seminhematol.2020.11.003

81. Noh JY, Yoon SR, Kim TD, Choi I, Jung H. Toll-like receptors in natural killer cells and their application for immunotherapy. *J Immunol Res* (2020) 2020:2045860. doi: 10.1155/2020/2045860

82. Schmidt KN, Leung B, Kwong M, Zarember KA, Satyal S, Navas TA, et al. APC-independent activation of NK cells by the Toll-like receptor 3 agonist double-stranded RNA. *J Immunol* (2004) 172(1):138–43. doi: 10.4049/jimmunol.172.1.138

83. Xie L, Pries R, Kesselring R, Wulff S, Wollenberg B. Head and neck cancer triggers the internalization of TLR3 in natural killer cells. *Int J Mol Med* (2007) 20 (4):493–9. doi: 10.3892/ijmm.20.4.493

84. Gorski KS, Waller EL, Bjornton-Severson J, Hanten JA, Riter CL, Kieper WC, et al. Distinct indirect pathways govern human NK-cell activation by TLR-7 and TLR-8 agonists. *Int Immunol* (2006) 18(7):1115–26. doi: 10.1093/intimm/dxl046

85. Hart OM, Athie-Morales V, O'Connor GM, Gardiner CM. TLR7/8-mediated activation of human NK cells results in accessory cell-dependent IFN-gamma production. *J Immunol* (2005) 175(3):1636–42. doi: 10.4049/jimmunol.175.3.1636

86. Lester RT, Yao XD, Ball TB, McKinnon LR, Kaul R, Wachihi C, et al. Toll-like receptor expression and responsiveness are increased in viraemic HIV-1 infection. *Aids* (2008) 22(6):685–94. doi: 10.1097/QAD.0b013e3282f4de35

87. Ma F, Zhang J, Zhang J, Zhang C. The TLR7 agonists imiquimod and gardiquimod improve DC-based immunotherapy for melanoma in mice. *Cell Mol Immunol* (2010) 7(5):381–8. doi: 10.1038/cmi.2010.30

88. Sabel MS, Sondak VK. Pros and cons of adjuvant interferon in the treatment of melanoma. *Oncologist* (2003) 8(5):451–8. doi: 10.1634/theoncologist.8-5-451

89. Lu H, Yang Y, Gad E, Inatsuka C, Wenner CA, Disis ML, et al. TLR2 agonist PSK activates human NK cells and enhances the antitumor effect of HER2-targeted monoclonal antibody therapy. *Clin Cancer Res* (2011) 17(21):6742–53. doi: 10.1158/1078-0432.CCR-11-1142

90. Bishop GA, Hsing Y, Hostager BS, Jalukar SV, Ramirez LM, Tomai MA. Molecular mechanisms of B lymphocyte activation by the immune response modifier R-848. *J Immunol* (2000) 165(10):5552–7. doi: 10.4049/jimmunol.165.10.5552

91. Buchta CM, Bishop GA. Toll-like receptors and B cells: functions and mechanisms. *Immunol Res* (2014) 59(1-3):12–22. doi: 10.1007/s12026-014-8523-2

92. Agrawal S, Gupta S. TLR1/2, TLR7, and TLR9 signals directly activate human peripheral blood naive and memory B cell subsets to produce cytokines, chemokines, and hematopoietic growth factors. *J Clin Immunol* (2011) 31(1):89–98. doi: 10.1007/s10875-010-9456-8

93. Genestier L, Taillardet M, Mondiere P, Gheit H, Bella C, DeFrance T. TLR agonists selectively promote terminal plasma cell differentiation of B cell subsets specialized in thymus-independent responses. *J Immunol* (2007) 178(12):7779–86. doi: 10.4049/jimmunol.178.12.7779

94. Jiang W, Lederman MM, Harding CV, Rodriguez B, Mohner RJ, Sieg SF. TLR9 stimulation drives naïve B cells to proliferate and to attain enhanced antigen presenting function. *Eur J Immunol* (2007) 37(8):2205–13. doi: 10.1002/eji.200636984

95. Lin L, Gerth AJ, Peng SL. CpG DNA redirects class-switching towards "Th1-like" Ig isotype production *via* TLR9 and MyD88. *Eur J Immunol* (2004) 34(5):1483–7. doi: 10.1002/eji.200324736

96. Leadbetter EA, Rifkin IR, Hohlbaum AM, Beaudette BC, Shlomchik MJ, Marshak-Rothstein A. Chromatin-IgG complexes activate B cells by dual engagement of IgM and Toll-like receptors. *Nature* (2002) 416(6881):603–7. doi: 10.1038/416603a

97. Kaur A, Baldwin J, Brar D, Salunke DB, Petrovsky N. Toll-like receptor (TLR) agonists as a driving force behind next-generation vaccine adjuvants and cancer therapeutics. *Curr Opin Chem Biol* (2022) 70:102172. doi: 10.1016/j.cbpa.2022.102172

98. Wu H, Fu X, Zhai Y, Gao S, Yang X, Zhai G. Development of effective tumor vaccine strategies based on immune response cascade reactions. *Adv Healthc Mater* (2021) 10(13):2100299. doi: 10.1002/adhm.202100299

99. Hofmann MA, Kors C, Audring H, Walden P, Sterry W, Trefzer U. Phase 1 evaluation of intralesionally injected TLR9-agonist PF-3512676 in patients with basal cell carcinoma or metastatic melanoma. *J Immunother* (2008) 31(5):520–7. doi: 10.1097/CJI.0b013e318174a4df

100. Krieg AM. Toll-like receptor 9 (TLR9) agonists in the treatment of cancer. *Oncogene* (2008) 27(2):161–7. doi: 10.1038/sj.onc.1210911

101. Brody JD, Ai WZ, Czerwinski DK, Torchia JA, Levy M, Advani RH, et al. *In situ* vaccination with a TLR9 agonist induces systemic lymphoma regression: a phase I/II study. *J Clin Oncol* (2010) 28(28):4324–32. doi: 10.1200/JCO.2010.28.9793

102. Bode C, Zhao G, Steinhagen F, Kinjo T, Klinman DM. CpG DNA as a vaccine adjuvant. *Expert Rev Vaccines* (2011) 10(4):499–511. doi: 10.1586/erv.10.174

103. Bernasconi NL, Traggiai E, Lanzavecchia A. Maintenance of serological memory by polyclonal activation of human memory B cells. *Science* (2002) 298 (5601):2199–202. doi: 10.1126/science.1076071

104. Kuo TC, Harrabi O, Chen A, Sangalang ER, Doyle L, Fontaine D, et al. Abstract 1721: TAC-001, a toll-like receptor 9 (TLR9) agonist antibody conjugate targeting B cells, promotes anti-tumor immunity and favorable safety profile following systemic administration in preclinical models. *Cancer Res* (2021) 81(13_Supplement):1721. doi: 10.1158/1538-7445.AM2021-1721

105. Kapp K, Volz B, Oswald D, Wittig B, Baumann M, Schmidt M. Beneficial modulation of the tumor microenvironment and generation of anti-tumor responses by TLR9 agonist lefitolimod alone and in combination with checkpoint inhibitors. *Oncoimmunology* (2019) 8(12):e1659096. doi: 10.1080/2162402X.2019.1659096

106. Wittig B, Schmidt M, Scheithauer W, Schmoll H-J. MGN1703, an immunomodulator and toll-like receptor 9 (TLR-9) agonist: From bench to bedside. *Crit Rev Oncology/Hematol* (2015) 94(1):31–44. doi: 10.1016/j.critrevonc.2014.12.002

107. Amos SM, Pegram HJ, Westwood JA, John LB, Devaud C, Clarke CJ, et al. Adoptive immunotherapy combined with intratumoral TLR agonist delivery eradicates established melanoma in mice. *Cancer Immunol Immunother* (2011) 60(5):671–83. doi: 10.1007/s00262-011-0984-8

108. Ribas A, Medina T, Kummar S, Amin A, Kalbasi A, Drabick JJ, et al. SD-101 in combination with pembrolizumab in advanced melanoma: results of a phase ib, multicenter study. *Cancer Discov* (2018) 8(10):1250–7. doi: 10.1158/2159-8290.CD-18-0280

109. Fuge O, Vasdev N, Allchorne P, Green JS. Immunotherapy for bladder cancer. *Res Rep Urol* (2015) 7:65–79. doi: 10.2147/rru.S63447

110. Kaech SM, Wherry EJ, Ahmed R. Effector and memory T-cell differentiation: implications for vaccine development. *Nat Rev Immunol* (2002) 2(4):251–62. doi: 10.1038/nri778

111. Rahman AH, Taylor DK, Turka LA. The contribution of direct TLR signaling to T cell responses. *Immunol Res* (2009) 45(1):25–36. doi: 10.1007/s12026-009-8113-x

112. Crellin NK, Garcia RV, Hadisfar O, Allan SE, Steiner TS, Levings MK. Human CD4+ T cells express TLR5 and its ligand flagellin enhances the suppressive capacity and expression of FOXP3 in CD4+CD25+ T regulatory cells. *J Immunol* (2005) 175 (12):8051–9. doi: 10.4049/jimmunol.175.12.8051

113. Cottalorda A, Verschelde C, Marçais A, Tomkowiak M, Musette P, Uematsu S, et al. TLR2 engagement on CD8 T cells lowers the threshold for optimal antigen-induced T cell activation. *Eur J Immunol* (2006) 36(7):1684–93. doi: 10.1002/eji.200636181

114. Caron G, Duluc D, Frémaux I, Jeannin P, David C, Gascan H, et al. Direct stimulation of human T cells *via* TLR5 and TLR7/8: flagellin and R-848 up-regulate proliferation and IFN-gamma production by memory CD4+ T cells. *J Immunol* (2005) 175(3):1551–7. doi: 10.4049/jimmunol.175.3.1551

115. Li Q, Yan Y, Liu J, Huang X, Zhang X, Kirschning C, et al. Toll-like receptor 7 activation enhances CD8+ T cell effector functions by promoting cellular glycolysis. *Front Immunol* (2019) 10:2191. doi: 10.3389/fimmu.2019.02191

116. Asprodites N, Zheng L, Geng D, Velasco-Gonzalez C, Sanchez-Perez L, Davila E. Engagement of Toll-like receptor-2 on cytotoxic T-lymphocytes occurs in *vivo* and augments antitumor activity. *FASEB J* (2008) 22(10):3628–37. doi: 10.1096/fj.08-108274

117. Tabiasco J, Devêvre E, Rufer N, Salaun B, Cerottini JC, Speiser D, et al. Human effector CD8+ T lymphocytes express TLR3 as a functional coreceptor. *J Immunol* (2006) 177(12):8708–13. doi: 10.4049/jimmunol.177.12.8708

118. Salem ML, Diaz-Montero CM, El-Naggar SA, Chen Y, Moussa O, Cole DJ. The TLR3 agonist poly(I:C) targets CD8+ T cells and augments their antigen-specific responses upon their adoptive transfer into naïve recipient mice. *Vaccine* (2009) 27 (4):549–57. doi: 10.1016/j.vaccine.2008.11.013

119. Peng G, Guo Z, Kiniwa Y, Voo KS, Peng W, Fu T, et al. Toll-like receptor 8-mediated reversal of CD4+ regulatory T cell function. *Science* (2005) 309(5739):1380–4. doi: 10.1126/science.1113401

120. Oberg HH, Ly TT, Ussat S, Meyer T, Kabelitz D, Wesch D. Differential but direct abolishment of human regulatory T cell suppressive capacity by various TLR2 ligands. *J Immunol* (2010) 184(9):4733–40. doi: 10.4049/jimmunol.0804279

121. Sutmuller RP, den Brok MH, Kramer M, Bennink EJ, Toonen LW, Kullberg BJ, et al. Toll-like receptor 2 controls expansion and function of regulatory T cells. *J Clin Invest* (2006) 116(2):485–94. doi: 10.1172/JCI25439

122. Liu H, Komai-Koma M, Xu D, Liew FY. Toll-like receptor 2 signaling modulates the functions of CD4+ CD25+ regulatory T cells. *Proc Natl Acad Sci U S A.* (2006) 103(18):7048–53. doi: 10.1073/pnas.0601554103

123. Li K, Qu S, Chen X, Wu Q, Shi M. Promising targets for cancer immunotherapy: TLRs, RLRs, and STING-mediated innate immune pathways. *Int J Mol Sci* (2017) 18(2). doi: 10.3390/ijms18020404

124. Tang H, Qiao J, Fu Y-X. Immunotherapy and tumor microenvironment. *Cancer Lett* (2016) 370(1):85–90. doi: 10.1016/j.canlet.2015.10.009

125. Vindevogel E, Baert T, Hoylandt Av, Verbist G, Velde Gv, Garg Ad, et al. The use of toll-like receptor 4 agonist to reshape the immune signature in ovarian cancer. *Anticancer Res* (2016) 36(11):5781–92. doi: 10.21873/anticanres.11162

126. Mullins SR, Vasilakos JP, Deschler K, Grigsby I, Gillis P, John J, et al. Intratumoral immunotherapy with TLR7/8 agonist MEDI9197 modulates the tumor microenvironment leading to enhanced activity when combined with other immunotherapies. *J Immunother Cancer.* (2019) 7(1):244. doi: 10.1186/s40425-019-0724-8

127. Roselli E, Araya P, Núñez NG, Gatti G, Graziano F, Sedlik C, et al. TLR3 activation of intratumoral CD103+ Dendritic cells modifies the tumor infiltrate conferring anti-tumor immunity. *Front Immunol* (2019) 10. doi: 10.3389/fimmu.2019.00503

128. Salazar AM, Erlich RB, Mark A, Bhardwaj N, Herberman RB. Therapeutic *in situ* autovaccination against solid cancers with intratumoral poly-ICLC: case report, hypothesis, and clinical trial. *Cancer Immunol Res* (2014) 2(8):720–4. doi: 10.1158/2326-6066.CIR-14-0024

129. Hotz C, Bourquin C. Systemic cancer immunotherapy with Toll-like receptor 7 agonists. *OncoImmunology* (2012) 1(2):227–8. doi: 10.4161/onci.1.2.18169

130. Furudate S, Fujimura T, Kambayashi Y, Kakizaki A, Hidaka T, Aiba S. Immunomodulatory effect of imiquimod through CCL22 produced by tumor-associated macrophages in B16F10 melanomas. *Anticancer Res* (2017) 37(7):3461–71. doi: 10.21873/anticanres.11714

131. Diao Y, Wang X, Wan Y, Zhong J, Gao D, Liu Y, et al. Antitumor activity of a novel small molecule TLR7 agonist *via* immune response induction and tumor microenvironment modulation. *Oncol Rep* (2016) 35(2):793–800. doi: 10.3892/or.2015.4436

132. Cho JH, Lee HJ, Ko HJ, Yoon BI, Choe J, Kim KC, et al. The TLR7 agonist imiquimod induces anti-cancer effects *via* autophagic cell death and enhances anti-tumoral and systemic immunity during radiotherapy for melanoma. *Oncotarget* (2017) 8(15):24932–48. doi: 10.18632/oncotarget.15326

133. Daayana S, Elkord E, Winters U, Pawlita M, Roden R, Stern PL, et al. Phase II trial of imiquimod and HPV therapeutic vaccination in patients with vulval intraepithelial neoplasia. *Br J Cancer.* (2010) 102(7):1129–36. doi: 10.1038/sj.bjc.6605611

134. Nishii N, TaChinami H, Kondo Y, Xia Y, Kashima Y, Ohno T, et al. Systemic administration of a TLR7 agonist attenuates regulatory T cells by dendritic cell modification and overcomes resistance to PD-L1 blockade therapy. *Oncotarget* (2018) 9(17):13301–12. doi: 10.18632/oncotarget.24327

135. Lu R, Groer C, Kleindl PA, Moulder KR, Huang A, Hunt JR, et al. Formulation and preclinical evaluation of a toll-like receptor 7/8 agonist as an anti-tumoral immunomodulator. *J Controlled Release* (2019) 306:165–76. doi: 10.1016/j.jconrel.2019.06.003

136. Adams S. Toll-like receptor agonists in cancer therapy. *Immunotherapy* (2009) 1(6):949–64. doi: 10.2217/imt.09.70

137. Gallotta M, Assi H, Degagné É, Kannan SK, Coffman RL, Guiducci C. Inhaled TLR9 agonist renders lung tumors permissive to PD-1 blockade by promoting optimal CD4+ and CD8+ T-cell interplay. *Cancer Res* (2018) 78(17):4943–56. doi: 10.1158/0008-5472.CAN-18-0729

138. Molenkamp BG, van Leeuwen PAM, Meijer S, Sluijter BJR, Wijnands PGJTB, Baars A, et al. Intradermal cpG-B activates both plasmacytoid and myeloid dendritic cells in the sentinel lymph node of melanoma patients. *Clin Cancer Res* (2007) 13 (10):2961–9. doi: 10.1158/1078-0432.CCR-07-0050

139. Frank MJ, Reagan PM, Bartlett NL, Gordon LI, Friedberg JW, Czerwinski DK, et al. *In situ* vaccination with a TLR9 agonist and local low-dose radiation induces systemic responses in untreated indolent lymphoma. *Cancer Discov* (2018) 8(10):1258–69. doi: 10.1158/2159-8290.CD-18-0743

140. Keshavarz A, Pourbagheri-Sigaroodi A, Zafari P, Bagheri N, Ghaffari SH, Bashash D. Toll-like receptors (TLRs) in cancer; with an extensive focus on TLR agonists and antagonists. *IUBMB Life* (2021) 73(1):10–25. doi: 10.1002/iub.2412

141. Rostamizadeh L, Molavi O, Rashid M, Ramazani F, Baradaran B, Lavasanaifar A, et al. Recent advances in cancer immunotherapy: Modulation of tumor microenvironment by Toll-like receptor ligands. *Bioimpacts* (2022) 12(3):261–90. doi: 10.34172/bi.2022.23896

142. Guha M. Anticancer TLR agonists on the ropes. *Nat Rev Drug Discovery* (2012) 11(7):503–5. doi: 10.1038/nrd3775

143. Basith S, Manavalan B, Yoo TH, Kim SG, Choi S. Roles of toll-like receptors in cancer: a double-edged sword for defense and offense. *Arch Pharm Res* (2012) 35 (8):1297–316. doi: 10.1007/s12272-012-0802-7

144. Netea MG, van der Meer JW, Sutmuller RP, Adema GJ, Kullberg BJ. From the Th1/Th2 paradigm towards a Toll-like receptor/T-helper bias. *Antimicrob Agents Chemother* (2005) 49(10):3991–6. doi: 10.1128/AAC.49.10.3991-3996.2005

145. Re F, Strominger JL. IL-10 released by concomitant TLR2 stimulation blocks the induction of a subset of Th1 cytokines that are specifically induced by TLR4 or TLR3 in human dendritic cells. *J Immunol* (2004) 173(12):7548–55. doi: 10.4049/jimmunol.173.12.7548

146. Vaure C, Liu Y. A comparative review of toll-like receptor 4 expression and functionality in different animal species. *Front Immunol* (2014) 5:316. doi: 10.3389/fimmu.2014.00316

147. Morton DL, Eilber FR, Holmes EC, Hunt JS, Ketcham AS, Silverstein MJ, et al. BCG immunotherapy of Malignant melanoma: summary of a seven-year experience. *Ann Surg* (1974) 180(4):635–43. doi: 10.1097/00000658-197410000-00029

148. Silverstein MJ, DeKernion J, Morton DL. Malignant melanoma metastatic to the bladder. Regression following intratumor injection of BCG vaccine. *Jama* (1974) 229(6):688. doi: 10.1001/jama.1974.03230440046032

149. Morton DL, Mozzillo N, Thompson JF, Kelley MC, Faries M, Wagner J, et al. An international, randomized, phase III trial of bacillus Calmette-Guerin (BCG) plus allogeneic melanoma vaccine (MCV) or placebo after complete resection of melanoma metastatic to regional or distant sites. *J Clin Oncol* (2007) 25(18_suppl):8508. doi: 10.1200/jco.2007.25.18_suppl.8508

150. Vermorken JB, Claessen AM, van Tinteren H, Gall HE, Ezinga R, Meijer S, et al. Active specific immunotherapy for stage II and stage III human colon cancer: a randomised trial. *Lancet* (1999) 353(9150):345–50. doi: 10.1016/S0140-6736(98)07186-4

151. Uyl-de Groot CA, Vermorken JB, Hanna MG Jr., Verboom P, Groot MT, Bonsel GJ, et al. Immunotherapy with autologous tumor cell-BCG vaccine in patients with colon cancer: a prospective study of medical and economic benefits. *Vaccine* (2005) 23(17-18):2379–87. doi: 10.1016/j.vaccine.2005.01.015

152. D'Agostini C, Pica F, Febbraro G, Grelli S, Chiavaroli C, Garaci E. Antitumour effect of OM-174 and cyclophosphamide on murine B16 melanoma in different experimental conditions. *Int Immunopharmacol* (2005) 5(7-8):1205–12. doi: 10.1016/j.intimp.2005.02.013

153. Kroemer G, Zitvogel L, Galluzzi L. Victories and deceptions in tumor immunology: Stimuvax(®). *Oncoimmunology* (2013) 2(1):e23687. doi: 10.4161/onci.23687

154. MacLean GD, Reddish M, Koganty RR, Wong T, Gandhi S, Smolenski M, et al. Immunization of breast cancer patients using a synthetic sialyl-Tn glycoconjugate plus Detox adjuvant. *Cancer Immunol Immunother* (1993) 36(4):215–22. doi: 10.1007/BF01740902

155. Brichard VG, Lejeune D. GSK's antigen-specific cancer immunotherapy programme: pilot results leading to Phase III clinical development. *Vaccine* (2007) 25 Suppl 2:B61–71. doi: 10.1016/j.vaccine.2007.06.038

156. Bhatia S, Miller NJ, Lu H, Longino NV, Ibrani D, Shinohara MM, et al. Intratumoral G100, a TLR4 agonist, induces antitumor immune responses and tumor regression in patients with merkel cell carcinoma. *Clin Cancer Res* (2019) 25(4):1185–95. doi: 10.1158/1078-0432.CCR-18-0469

157. Lambert SL, Yang CF, Liu Z, Sweetwood R, Zhao J, Cheng L, et al. Molecular and cellular response profiles induced by the TLR4 agonist-based adjuvant Glucopyranosyl Lipid A. *PloS One* (2012) 7(12):e51618. doi: 10.1371/journal.pone.0051618

158. Lu H, Hewitt J, Meulen Jt. Abstract 4885: Intratumoral injection of G100 (TLR4 agonist glycopyranosyl lipid A) modulates tumor microenvironment and induces CD8 T cell-dependent, systemic anti-tumor immunity. *Cancer Res* (2016) 76 (14_Supplement):4885. doi: 10.1158/1538-7445.AM2016-4885

159. Alexopoulou L, Holt AC, Medzhitov R, Flavell RA. Recognition of double-stranded RNA and activation of NF-kappaB by Toll-like receptor 3. *Nature* (2001) 413 (6857):732–8. doi: 10.1038/35099560

160. Kato H, Takeuchi O, Mikamo-Satoh E, Hirai R, Kawai T, Matsushita K, et al. Length-dependent recognition of double-stranded ribonucleic acids by retinoic acid-inducible gene-I and melanoma differentiation-associated gene 5. *J Exp Med* (2008) 205 (7):1601–10. doi: 10.1084/jem.20080091

161. Datta SK, Redecke V, Prilliman KR, Takabayashi K, Corr M, Tallant T, et al. A subset of toll-like receptor ligands induces cross-presentation by bone marrow-derived dendritic cells1. *J Immunol* (2003) 170(8):4102–10. doi: 10.4049/jimmunol.170.8.4102

162. Perrot I, Deauvieau F, Massacrier C, Hughes N, Garrone P, Durand I, et al. TLR3 and rig-like receptor on myeloid dendritic cells and rig-like receptor on human NK cells are both mandatory for production of IFN-γ in response to double-stranded RNA. *J Immunol* (2010) 185(4):2080–8. doi: 10.4049/jimmunol.1000532

163. Jasani B, Navabi H, Adams M. Ampligen: a potential toll-like 3 receptor adjuvant for immunotherapy of cancer. *Vaccine* (2009) 27(25-26):3401–4. doi: 10.1016/j.vaccine.2009.01.071

164. Levy HB, Baer G, Baron S, Buckler CE, Gibbs CJ, Iadarola MJ, et al. A modified polyriboinosinic-polyribocytidylic acid complex that induces interferon in primates. *J Infect Dis* (1975) 132(4):434–9. doi: 10.1093/infdis/132.4.434

165. Isakoff SJ, Tolaney SM, Tung NM, Adams S, Soliman HH, Brachtel EF, et al. A phase 1b study of safety and immune response to PVX-410 vaccine alone and in combination with durvalumab (MEDI4736) in HLA-A2+ patients following adjuvant therapy for stage 2/3 triple negative breast cancer. *J Clin Oncol* (2017) 35(15_suppl): TPS1126–TPS. doi: 10.1200/JCO.2017.35.15_suppl.TPS1126

166. Karki NR, Bano K, Ramses S, Nayak A. A phase II trial of pembrolizumab and poly-ICLC in patients with metastatic mismatch repair-proficient colon cancer. *J Clin Oncol* (2021) 39(15_suppl):e15552–e. doi: 10.1200/JCO.2021.39.15_suppl.e15552

167. Matijevic Glavan T, Pavelic J. The exploitation of toll-like receptor 3 signaling in cancer therapy. *Curr Pharm Design* (2014) 20(42):6555–64. doi: 10.2174/1381612820666140826153347

168. Haddaoui H, Brood R, Latifi D, Oostvogels AA, Klaver Y, Moskie M, et al. Rintatolimod (Ampligen®) enhances numbers of peripheral B cells and is associated with longer survival in patients with locally advanced and metastasized pancreatic cancer pre-treated with FOLFIRINOX: A single-center named patient program. *Cancers* (2022) 14(6):1377. doi: 10.3390/cancers14061377

169. Gandhi S, Opyrchal M, Grimm M, Slomba R, Kokolus K, Battaglia S, et al. Abstract CT145: Systemic rintatolimod and interferon-α2b selectively reprogram local tumor microenvironment in patients with metastatic triple negative breast cancer for enhanced influx of cytotoxic T-lymphocytes but not regulatory T-cells. *Cancer Res* (2022) 82(12_Supplement):CT145–CT. doi: 10.1158/1538-7445.AM2022-CT145

170. Navabi H, Jasani B, Reece A, Clayton A, Tabi Z, Donninger C, et al. A clinical grade poly I:C-analogue (Ampligen) promotes optimal DC maturation and Th1-type T cell responses of healthy donors and cancer patients in vitro. *Vaccine* (2009) 27(1):107–15. doi: 10.1016/j.vaccine.2008.10.024

171. Cai Z, Sanchez A, Shi Z, Zhang T, Liu M, Zhang D. Activation of Toll-like receptor 5 on breast cancer cells by flagellin suppresses cell proliferation and tumor growth. *Cancer Res* (2011) 71(7):2466–75. doi: 10.1158/0008-5472.CAN-10-1993

172. Sfondrini L, Rossini A, Besusso D, Merlo A, Tagliabue E, Mènard S, et al. Antitumor activity of the TLR-5 ligand flagellin in mouse models of cancer. *J Immunol* (2006) 176(11):6624–30. doi: 10.4049/jimmunol.176.11.6624

173. Garaude J, Kent A, van Rooijen N, Blander JM. Simultaneous targeting of toll- and nod-like receptors induces effective tumor-specific immune responses. *Sci Transl Med* (2012) 4(120):120ra16. doi: 10.1126/scitranslmed.3002868

174. Burdelya LG, Krivokrysenko VI, Tallant TC, Strom E, Gleiberman AS, Gupta D, et al. An agonist of toll-like receptor 5 has radioprotective activity in mouse and primate models. *Science* (2008) 320(5873):226–30. doi: 10.1126/science.1154986

175. Mett V, Komarova EA, Greene K, Bespalov I, Brackett C, Gillard B, et al. Mobilan: a recombinant adenovirus carrying Toll-like receptor 5 self-activating cassette for cancer immunotherapy. *Oncogene* (2018) 37(4):439–49. doi: 10.1038/onc.2017.346

176. McGowan DC. Latest advances in small molecule TLR 7/8 agonist drug research. *Curr Top Med Chem* (2019) 19(24):2228–38. doi: 10.2174/1568026619666191009165418

177. Lan T, Kandimalla ER, Yu D, Bhagat L, Li Y, Wang D, et al. Stabilized immune modulatory RNA compounds as agonists of Toll-like receptors 7 and 8. *Proc Natl Acad Sci U S A.* (2007) 104(34):13750–5. doi: 10.1073/pnas.0706059104

178. Rodell CB, Ahmed MS, Garris CS, Pittet MJ, Weissleder R. Development of adamantane-conjugated TLR7/8 agonists for supramolecular delivery and cancer immunotherapy. *Theranostics* (2019) 9(26):8426–36. doi: 10.7150/thno.35434

179. Dudek AZ, Yunis C, Harrison LI, Kumar S, Hawkinson R, Cooley S, et al. First in human phase I trial of 852A, a novel systemic toll-like receptor 7 agonist, to activate innate immune responses in patients with advanced cancer. *Clin Cancer Res* (2007) 13 (23):7119–25. doi: 10.1158/1078-0432.Ccr-07-1443

180. Vasilakos JP, Tomai MA. The use of Toll-like receptor 7/8 agonists as vaccine adjuvants. *Expert Rev Vaccines* (2013) 12(7):809–19. doi: 10.1586/14760584.2013.811208

181. AG A, Tyring SK, Rosen T. Beyond a decade of 5% imiquimod topical therapy. *J Drugs Dermatol* (2009) 8(5):467–74.

182. Geisse J, Caro I, Lindholm J, Golitz L, Stampone P, Owens M, et al. Imiquimod 5% cream for the treatment of superficial basal cell carcinoma: results from two phase III, randomized, vehicle-controlled studies. *J Am Acad Dermatol* (2004) 50(5):722–33. doi: 10.1016/j.jaad.2003.11.066

183. Bong AB, Bonnekoh B, Franke I, Schön M, Ulrich J, Gollnick H. Imiquimod, a topical immune response modifier, in the treatment of cutaneous metastases of Malignant melanoma. *Dermatology* (2002) 205(2):135–8. doi: 10.1159/000063904

184. Wolf IH, Smolle J, Binder B, Cerroni L, Richtig E, Kerl H. Topical imiquimod in the treatment of metastatic melanoma to skin. *Arch Dermatol* (2003) 139(3):273–6. doi: 10.1001/archderm.139.3.273

185. Nair S, McLaughlin C, Weizer A, Su Z, Boczkowski D, Dannull J, et al. Injection of immature dendritic cells into adjuvant-treated skin obviates the need for ex vivo maturation. *J Immunol* (2003) 171(11):6275–82. doi: 10.4049/jimmunol.171.11.6275

186. Chi H, Li C, Zhao FS, Zhang L, Ng TB, Jin G, et al. Anti-tumor activity of toll-like receptor 7 agonists. *Front Pharmacol* (2017) 8. doi: 10.3389/fphar.2017.00304

187. Harrison LI, Astry C, Kumar S, Yunis C. Pharmacokinetics of 852A, an imidazoquinoline Toll-like receptor 7-specific agonist, following intravenous, subcutaneous, and oral administrations in humans. *J Clin Pharmacol* (2007) 47 (8):962–9. doi: 10.1177/0091270007303766

188. Dummer R, Hauschild A, Becker JC, Grob JJ, SChadendorf D, Tebbs V, et al. An exploratory study of systemic administration of the toll-like receptor-7 agonist 852A in patients with refractory metastatic melanoma. *Clin Cancer Res* (2008) 14 (3):856–64. doi: 10.1158/1078-0432.CCR-07-1938

189. Bergmann JF, de Bruijne J, Hotho DM, de Knegt RJ, Boonstra A, Weegink CJ, et al. Randomised clinical trial: anti-viral activity of ANA773, an oral inducer of endogenous interferons acting *via* TLR7, in chronic HCV. *Aliment Pharmacol Ther* (2011) 34(4):443–53. doi: 10.1111/j.1365-2036.2011.04745.x

190. Singh M, Khong H, Dai Z, Huang XF, Wargo JA, Cooper ZA, et al. Effective innate and adaptive antimelanoma immunity through localized TLR7/8 activation. *J Immunol* (2014) 193(9):4722–31. doi: 10.4049/jimmunol.1401160

191. Karapetyan L, Luke JJ, Davar D. Toll-like receptor 9 agonists in cancer. *Onco Targets Ther* (2020) 13:10039–60. doi: 10.2147/OTT.S247050

192. Baines J, Celis E. Immune-mediated tumor regression induced by CpG-containing oligodeoxynucleotides. *Clin Cancer Res* (2003) 9(7):2693–700.

193. Krieg AM. Antiinfective applications of toll-like receptor 9 agonists. *Proc Am Thorac Soc* (2007) 4(3):289–94. doi: 10.1513/pats.200701-021AW

194. Heckelsmiller K, Rall K, Beck S, Schlamp A, Seiderer J, Jahrsdörfer B, et al. Peritumoral CpG DNA elicits a coordinated response of CD8 T cells and innate effectors to cure established tumors in a murine colon carcinoma model. *J Immunol* (2002) 169(7):3892–9. doi: 10.4049/jimmunol.169.7.3892

195. Goutagny N, Estornes Y, Hasan U, Lebecque S, Caux C. Targeting pattern recognition receptors in cancer immunotherapy. *Target Oncol* (2012) 7(1):29–54. doi: 10.1007/s11523-012-0213-1

196. Cunningham D, Zurlo A, Salazar R, Ducreux M, Waddell TS, Stein A, et al. IMPALA, a randomized phase III study in patients with metastatic colorectal carcinoma: Immunomodulatory maintenance therapy with TLR-9 agonist MGN1703. *J Clin Oncol* (2015) 33(3_suppl):TPS791–TPS. doi: 10.1200/jco.2015.33.3_suppl.tps791

197. Houot R, Levy R. T-cell modulation combined with intratumoral CpG cures lymphoma in a mouse model without the need for chemotherapy. *Blood* (2009) 113 (15):3546–52. doi: 10.1182/blood-2008-07-170274

198. Valmori D, Souleimanian NE, Tosello V, Bhardwaj N, Adams S, O'Neill D, et al. Vaccination with NY-ESO-1 protein and CpG in Montanide induces integrated antibody/Th1 responses and CD8 T cells through cross-priming. *Proc Natl Acad Sci U S A*. (2007) 104(21):8947–52. doi: 10.1073/pnas.0703395104

199. Medina R, Wang H, Caisová V, Cui J, Indig IH, Uher O, et al. Induction of immune response against metastatic tumors *via* vaccination of mannan-BAM, TLR ligands and anti-CD40 antibody (MBTA). *Adv Ther (Weinh)* (2020) 3(9). doi: 10.1002/adtp.202000044

200. Lookian PP, Zhao D, Medina R, Wang H, Zenka J, Gilbert MR, et al. Mannan-BAM, TLR ligands, anti-CD40 antibody (MBTA) vaccine immunotherapy: A review of current evidence and applications in glioblastoma. *Int J Mol Sci* (2021) 22(7). doi: 10.3390/ijms22073455

201. Caisova V, Li L, Gupta G, Jochmanova I, Jha A, Uher O, et al. The significant reduction or complete eradication of subcutaneous and metastatic lesions in a pheochromocytoma mouse model after immunotherapy using mannan-BAM, TLR ligands, and anti-CD40. *Cancers (Basel)* (2019) 11(5). doi: 10.3390/cancers11050654

202. Ye J, Wang H, Medina R, Chakraborty S, Sun M, Valenzuela A, et al. rWTC-MBTA: autologous vaccine prevents metastases *via* antitumor immune responses. *J Exp Clin Cancer Res* (2023) 42(1):163. doi: 10.1186/s13046-023-02744-8

203. Janotová T, Jalovecká M, Auerová M, Švecová I, Bruzlová P, Maierová V, et al. The use of anchored agonists of phagocytic receptors for cancer immunotherapy: B16-F10 murine melanoma model. *PloS One* (2014) 9(1):e85222. doi: 10.1371/journal.pone.0085222

204. Waldmannová E, Caisová V, Fáberová J, Sváčková P, Kovářová M, Sváčková D, et al. The use of Zymosan A and bacteria anchored to tumor cells for effective cancer immunotherapy: B16-F10 murine melanoma model. *Int Immunopharmacol* (2016) 39:295–306. doi: 10.1016/j.intimp.2016.08.004

205. Seo HS, Michalek SM, Nahm MH. Lipoteichoic acid is important in innate immune responses to gram-positive bacteria. *Infect Immun* (2008) 76(1):206–13. doi: 10.1128/IAI.01140-07

206. Urban-Wojciuk Z, Khan MM, Oyler BL, Fåhraeus R, Marek-Trzonkowska N, Nita-Lazar A, et al. The role of TLRs in anti-cancer immunity and tumor rejection. *Front Immunol* (2019) 10. doi: 10.3389/fimmu.2019.02388

207. Bianchi F, Pretto S, Tagliabue E, Balsari A, Sfondrini L. Exploiting poly(I:C) to induce cancer cell apoptosis. *Cancer Biol Ther* (2017) 18(10):747–56. doi: 10.1080/15384047.2017.1373220

208. Steinhagen F, Kinjo T, Bode C, Klinman DM. TLR-based immune adjuvants. *Vaccine* (2011) 29(17):3341–55. doi: 10.1016/j.vaccine.2010.08.002

209. Rook AH, Gelfand JM, Wysocka M, Troxel AB, Benoit B, Surber C, et al. Topical resiquimod can induce disease regression and enhance T-cell effector functions in cutaneous T-cell lymphoma. *Blood* (2015) 126(12):1452–61. doi: 10.1182/blood-2015-02-630335

210. Wu JJ, Huang DB, Tyring SK. Resiquimod: a new immune response modifier with potential as a vaccine adjuvant for Th1 immune responses. *Antiviral Res* (2004) 64 (2):79–83. doi: 10.1016/j.antiviral.2004.07.002

211. Binnewies M, Roberts EW, Kersten K, Chan V, Fearon DF, Merad M, et al. Understanding the tumor immune microenvironment (TIME) for effective therapy. *Nat Med* (2018) 24(5):541–50. doi: 10.1038/s41591-018-0014-x

212. Duan Q, Zhang H, Zheng J, Zhang L. Turning Cold into Hot: Firing up the Tumor Microenvironment. *Trends Cancer*. (2020) 6(7):605–18. doi: 10.1016/j.trecan.2020.02.022

213. Liu Y, Guo J, Huang L. Modulation of tumor microenvironment for immunotherapy: focus on nanomaterial-based strategies. *Theranostics* (2020) 10 (7):3099–117. doi: 10.7150/thno.42998

214. Agrawal S, Kandimalla ER. Intratumoural immunotherapy: activation of nucleic acid sensing pattern recognition receptors. *Immunooncol Technol* (2019) 3:15–23. doi: 10.1016/j.iotech.2019.10.001

215. Wang D, Jiang W, Zhu F, Mao X, Agrawal S. Modulation of the tumor microenvironment by intratumoral administration of IMO-2125, a novel TLR9 agonist, for cancer immunotherapy. *Int J Oncol* (2018) 53(3):1193–203. doi: 10.3892/ijo.2018.4456

216. Koster BD, Santegoets SJAM, Harting J, Baars A, van Ham SM, Scheper RJ, et al. Autologous tumor cell vaccination combined with systemic CpG-B and IFN-α promotes immune activation and induces clinical responses in patients with metastatic renal cell carcinoma: a phase II trial. *Cancer Immunol Immunother* (2019) 68(6):1025–35. doi: 10.1007/s00262-019-02320-0

217. Gilliet M, Conrad C, Geiges M, Cozzio A, Thürlimann W, Burg G, et al. Psoriasis triggered by toll-like receptor 7 agonist imiquimod in the presence of dermal plasmacytoid dendritic cell precursors. *Arch Dermatol* (2004) 140(12):1490–5. doi: 10.1001/archderm.140.12.1490

218. Pradere JP, Dapito DH, Schwabe RF. The Yin and Yang of Toll-like receptors in cancer. *Oncogene* (2014) 33(27):3485–95. doi: 10.1038/onc.2013.302

219. Gearing AJ. Targeting toll-like receptors for drug development: a summary of commercial approaches. *Immunol Cell Biol* (2007) 85(6):490–4. doi: 10.1038/sj.icb.7100102

220. Tse K, Horner AA. Update on toll-like receptor-directed therapies for human disease. *Ann Rheum Dis* (2007) 66 Suppl 3(Suppl 3):iii77–80. doi: 10.1136/ard.2007.078998

221. Tran TH, Tran TTP, Truong DH, Nguyen HT, Pham TT, Yong CS, et al. Toll-like receptor-targeted particles: A paradigm to manipulate the tumor microenvironment for cancer immunotherapy. *Acta Biomater* (2019) 94:82–96. doi: 10.1016/j.actbio.2019.05.043

222. Jeong S, Choi Y, Kim K. Engineering therapeutic strategies in cancer immunotherapy *via* exogenous delivery of toll-like receptor agonists. *Pharmaceutics* (2021) 13(9):1374. doi: 10.3390/pharmaceutics13091374

frontiers | Frontiers in Immunology

TYPE Original Research
PUBLISHED 24 October 2023
DOI 10.3389/fimmu.2023.1190261

OPEN ACCESS

EDITED BY
Oliver Planz,
University of Tübingen, Germany

REVIEWED BY
Tünde Fekete,
University of Debrecen, Hungary
Przemyslaw Zdziarski,
Lower Silesian Oncology Center, Poland

*CORRESPONDENCE
Andrew R. Clark
a.r.clark@bham.ac.uk

†These authors contributed equally to this work and share first authorship

RECEIVED 20 March 2023
ACCEPTED 11 October 2023
PUBLISHED 24 October 2023

CITATION
O'Neil JD, Bolimowska OO, Clayton SA, Tang T, Daley KK, Lara-Reyna S, Warner J, Martin CS, Mahida RY, Hardy RS, Arthur JSC and Clark AR (2023) Dexamethasone impairs the expression of antimicrobial mediators in lipopolysaccharide-activated primary macrophages by inhibiting both expression and function of interferon β. *Front. Immunol.* 14:1190261. doi: 10.3389/fimmu.2023.1190261

Dexamethasone impairs the expression of antimicrobial mediators in lipopolysaccharide-activated primary macrophages by inhibiting both expression and function of interferon β

John D. O'Neil[1†], Oliwia O. Bolimowska[1†], Sally A. Clayton[1†], Tina Tang[1], Kalbinder K. Daley[1], Samuel Lara-Reyna[2], Jordan Warner[3], Claire S. Martin[4], Rahul Y. Mahida[1], Rowan S. Hardy[4], J. Simon C. Arthur[3] and Andrew R. Clark[1*]

[1]Institute of Inflammation and Ageing, University of Birmingham, Birmingham, United Kingdom, [2]Institute of Microbiology and Infection, University of Birmingham, Birmingham, United Kingdom, [3]School of Life Sciences, University of Dundee, Dundee, United Kingdom, [4]School of Biomedical Sciences, University of Birmingham, Birmingham, United Kingdom

Glucocorticoids potently inhibit expression of many inflammatory mediators, and have been widely used to treat both acute and chronic inflammatory diseases for more than seventy years. However, they can have several unwanted effects, amongst which immunosuppression is one of the most common. Here we used microarrays and proteomic approaches to characterise the effect of dexamethasone (a synthetic glucocorticoid) on the responses of primary mouse macrophages to a potent pro-inflammatory agonist, lipopolysaccharide (LPS). Gene ontology analysis revealed that dexamethasone strongly impaired the lipopolysaccharide-induced antimicrobial response, which is thought to be driven by an autocrine feedback loop involving the type I interferon IFNβ. Indeed, dexamethasone strongly and dose-dependently inhibited the expression of IFNβ by LPS-activated macrophages. Unbiased proteomic data also revealed an inhibitory effect of dexamethasone on the IFNβ-dependent program of gene expression, with strong down-regulation of several interferon-induced antimicrobial factors. Surprisingly, dexamethasone also inhibited the expression of several antimicrobial genes in response to direct stimulation of macrophages with IFNβ. We tested a number of hypotheses based on previous publications, but found that no single mechanism could account for more than a small fraction of the broad suppressive impact of dexamethasone on macrophage type I interferon signaling, underlining the complexity of this pathway. Preliminary experiments indicated that dexamethasone exerted similar inhibitory effects on primary human monocyte-derived or alveolar macrophages.

KEYWORDS

glucocorticoid, dexamethasone, macrophage, type I interferon, interferon β, innate immunity, virus, SARS-CoV-2

Introduction

Synthetic glucocorticoids are widely used in the treatment of both chronic and acute inflammatory pathologies (1), despite the fact that they can cause serious adverse effects, including immunosuppression (2). Both harmful and beneficial effects of natural and synthetic GCs are mediated by the GC receptor (GR), a member of a large family of ligand-activated transcription factors (3). Ligand-bound GR can either activate transcription (most often by binding as a dimer to palindromic GC response elements) or suppress transcription (for example via functional interference with the transcription factor NF-κB). It was initially thought that harmful effects of GCs were mediated by transcriptional activation, and beneficial anti-inflammatory effects by transcriptional repression (transrepression) (4). It is now increasingly recognized that this model is too simplistic. Instead, anti-inflammatory effects of GCs involve both transcriptional activation and repression (5, 6). For example, in several cell types GCs increase the expression of dual specificity phosphatase 1 (DUSP1), which exerts anti-inflammatory effects by inactivating mitogen-activated protein kinases (MAPKs) (7–11).

Monocyte-derived and tissue resident macrophages play central roles in both chronic inflammatory pathologies such as rheumatoid arthritis (12, 13) and acute inflammatory pathologies such as the viral sepsis that can be unleashed by the zoonotic pathogen SARS-CoV-2 (14, 15). Macrophages are important targets of the beneficial anti-inflammatory effects of endogenous and exogenous GCs (9, 16). To investigate how macrophages respond to GCs we and many others have used the Toll-like receptor 4 (TLR4) agonist lipopolysaccharide (LPS) as a stimulus. This reagent has some unique advantages as an experimental tool. When it engages TLR4 it initiates two distinct signaling responses that drive more or less discrete programs of gene expression (17). At the cell surface, TLR4 uses the adaptor molecule MyD88 (myeloid differentiation primary response 88) to activate NF-κB and MAPK cascades. These cooperate to drive rapid expression of several pro-inflammatory genes. Following internalization to endosomes, TLR4 also signals via the adaptor TICAM1 (TIR domain containing adaptor molecule 1) to activate TBK1 (Tank-binding kinase 1) promoting phosphorylation of the transcription factor IRF3 (interferon response factor 3), which in turn induces expression of the type I interferon IFNβ. Macrophages express the dimeric IFNβ receptor encoded by *Ifnar1* and *Ifnar2* genes, and can therefore respond in autocrine or paracrine fashion to secreted IFNβ. This causes activation of the tyrosine kinases JAK1 (Janus kinase 1) and TYK2 (tyrosine kinase 2), which then phosphorylate and activate the transcription factors STAT1 (signal transducer and activator of transcription 1) and STAT2. STAT1 can function as a homodimer to regulate transcription via palindromic GAS elements. STAT1 and STAT2 can also dimerize with one another and combine with a third protein, IRF9, to form the heterotrimeric transcription factor ISGF3 (interferon-stimulated gene factor 3), which binds to a distinct regulatory sequence known as an ISRE (interferon-stimulated response element) (18). ISGF3 and STAT dimers promote expression of hundreds of genes, many of which are mediators of antimicrobial defense, but some of which are pro-inflammatory cytokines and chemokines. A large part of the macrophage response to LPS is dependent on this positive feedback loop mediated by IFNβ (19–22). The use of LPS as a stimulus therefore allows researchers to examine a broad spectrum of pro-inflammatory and antimicrobial macrophage functions. Moreover, IFNβ serves as a generic alarm signal for the presence of intra- and extra-cellular pathogens, and evokes an antimicrobial state that is not highly pathogen-specific. Hence, many interferon-stimulated genes encode restriction factors that contribute to cell-intrinsic defense against diverse pathogens (23, 24).

Here we set out to investigate the impact of the synthetic GC Dexamethasone (Dex) on macrophage transcriptome and proteome responses to LPS. We also wanted to determine how the phosphatase DUSP1 contributed to effects of Dex. By serendipity, this study revealed an extremely broad effect of Dex on IFNβ signaling in primary mouse bone marrow-derived macrophages, including consistent suppression of many antimicrobial factors at both mRNA and protein levels. Dex inhibited both the LPS-induced expression of IFNβ and the regulation of gene expression by IFNβ, but neither of these effects could be explained by existing models of GC action. Our preliminary data indicated that at least some of these phenomena also occurred in primary human monocyte-derived or alveolar macrophages.

Results

Dexamethasone broadly inhibits IFNβ-dependent gene expression in LPS-treated macrophages

To investigate the impact of GCs on the macrophage response to LPS, primary mouse bone marrow-derived macrophages (BMDMs) were stimulated with LPS in the absence or presence of 100 nM Dex for four hours. This is similar to the mean serum concentration in healthy volunteers after 7.5 mg oral Dex, and can be considered a moderate dose (25). Steady state mRNA abundance was then assessed by microarray. The data were first filtered for robust gene induction by LPS (greater than five-fold increase of expression, $p < 0.05$), leading to the identification of 599 LPS-induced protein-coding transcripts. The responses of these transcripts to the addition of Dex were then assessed. As illustrated by volcano plot (Figure 1A), the effect of Dex was strongly dominated by inhibition, 169 transcripts being down-regulated and only 13 up-regulated (fold change > 2 and $p < 0.05$). Several LPS-induced genes were suppressed more than 80% by 100 nM Dex. Cooperative regulation of the *Lcn2* (lipocalin 2) gene by LPS and Dex was previously reported (28) and confirmed here (Figure 1A).

Gene Ontology (GO) analysis of GC down-regulated genes revealed highly significant enrichment of terms related to inflammation, cytokine production and responses to biotic stimuli (Figure 1B; Supplemental Table 1). Enrichment of such terms was predictable and uninformative, since the original set of 599 transcripts was selected on the basis of strong induction by LPS. We were interested by the gene sets "Response to virus"

10.3389/fimmu.2023.1190261

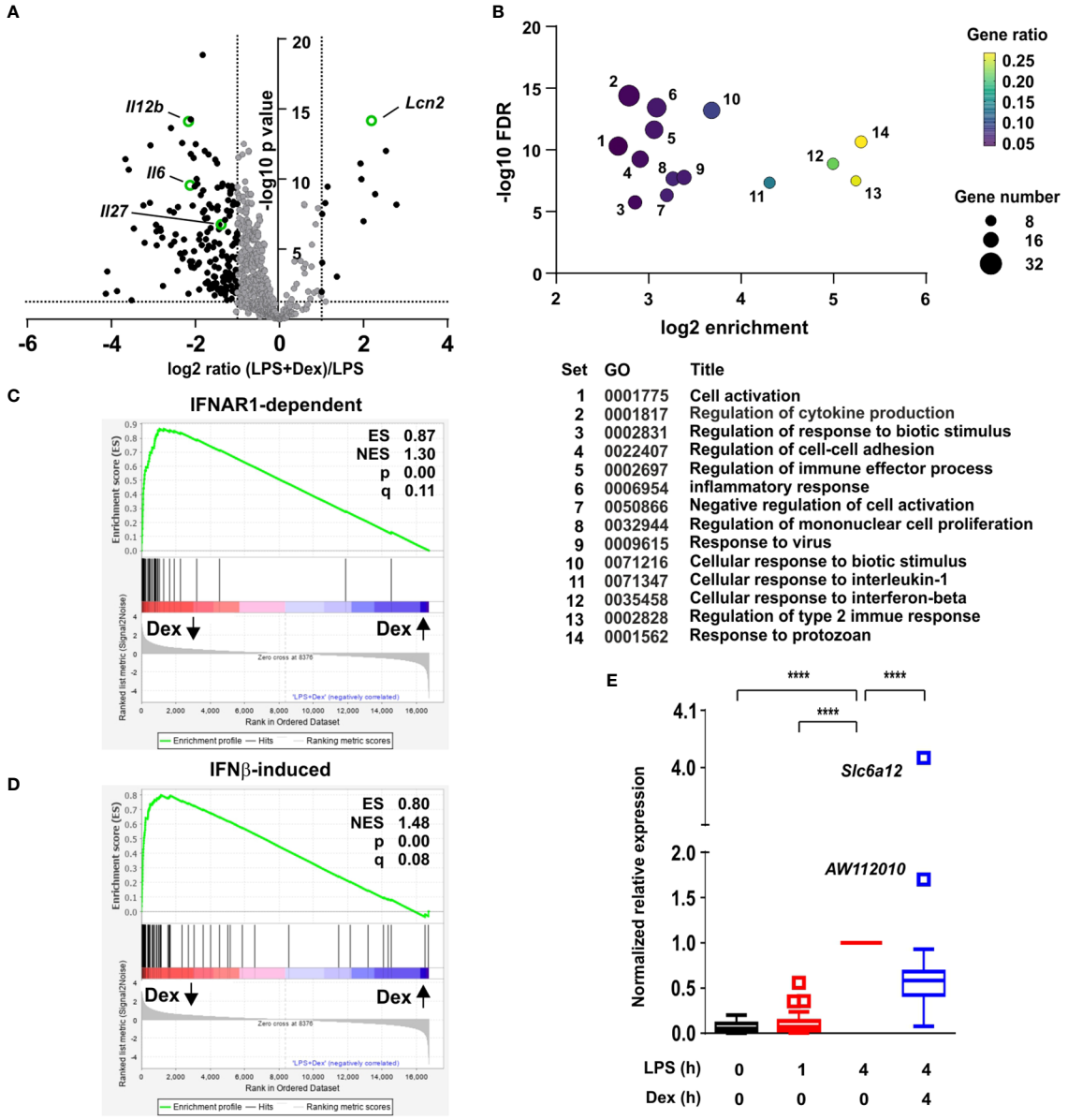

FIGURE 1
Dexamethasone broadly inhibits IFNβ-dependent gene expression in LPS-treated macrophages. **(A)** Mouse BMDMs (three independent isolates per condition) were treated with vehicle, 10 ng/ml LPS for 1 h or 4 h, or 10 ng/ml LPS + 100 nM Dex for 4 h. mRNA was harvested, quantified by microarray and analyzed using Partek. Transcripts robustly induced by LPS at 4 h (fold increase > 5, pAdj < 0.05) were identified and their responses to addition of Dex illustrated by volcano plot. Black dots represent LPS-induced transcripts whose expression was significantly altered by addition of Dex (fold change > 2, pAdj < 0.05). The transcripts highlighted in green are discussed in the text. **(B)** LPS-induced and Dex-suppressed transcripts (black dots in left quadrant of **(A)** were subjected to GO analysis using default parameters in Panther. Significantly enriched GO terms were filtered manually and using REVIGO to eliminate redundant terms. The top 14 remaining terms were plotted according to enrichment, FDR, gene number and gene ratio. **(C)** Gene set enrichment analysis was performed using the comparison of LPS vs. LPS + Dex as a quantitative data set, and the top 70 IFNAR1-dependent transcripts from (26) as a categorical gene list. Dex-inhibited transcripts are clustered at the left, and Dex-enhanced transcripts at the right. ES, enrichment score; NES, normalized enrichment score; q, false discovery rate. **(D)** Gene set enrichment analysis was performed as in C, except using the 93 most robustly IFNβ-inducible genes from (27). **(E)** For 96 genes that were robustly induced by LPS in our data set and interferon-regulated according to (26) or (27) gene expression was normalized to the 4 h value, and mean expression was plotted in Tukey box-and-whisker format. Outliers exceed the median by more than 1.5x interquartile range. ****, p < 0.001.

(GO:0009615; set 9 in Figure 1B), "Cellular response to interferon beta" (GO:0035458; set 12 in Figure 1B), and "Response to protozoan" (GO:0001562; set 14 in Figure 1B), which displayed 10.4-fold, 31.8-fold and 39.3-fold enrichment, respectively. Enrichment of these terms suggested that Dex inhibited expression of genes involved in antimicrobial responses (which are commonly regulated by IFNβ). However, there was no significant enrichment of GO terms specifically related to responses to intracellular bacteria.

Closer inspection of the microarray data revealed many interferon-stimulated genes (ISGs) amongst the LPS-induced genes that were significantly down-regulated by Dex. To explore

this in more detail we made use of two published data sets related to interferon-mediated gene regulation in primary murine macrophages (generated in a similar manner). First, a systems-based analysis of the macrophage transcriptome identified a large number of genes whose delayed induction by lipidA (a highly TLR4-specific LPS moiety) was dependent on autocrine signaling via the interferon receptor IFNAR1 (29). The top 70 IFNAR1-dependent genes from that study were used as a gene set for GSEA (gene set enrichment analysis) (Figure 1C). This confirmed extremely strong enrichment of IFNAR1-dependent genes amongst those negatively regulated by Dex in our own data set, with an enrichment score of 0.866 and p value 0.0. From a study of macrophage regulatory networks (26) we then identified genes robustly induced by treatment of BMDMs with IFNβ alone (fold change > 100 and $p < 0.05$), and used this list of 93 genes in GSEA (Figure 1D). Once again there was very strong enrichment of IFNβ-inducible genes amongst those suppressed by Dex in our microarray set, with enrichment score 0.800 and $p = 0.0$. Removal of genes common to the two lists reduced the enrichment score only marginally (ES = 0.775) and did not change the nominal p value of zero.

We generated a list of 96 genes that were robustly induced by LPS in our own data set and interferon-regulated according to one or both of the above-mentioned data sets (26, 29). Mean responses of these genes to LPS and/or Dex were then plotted (Figure 1E). The great majority were expressed in a delayed fashion, with little or no increase of expression 1 h after addition of LPS (Figure 1E). At the 4 h time point, expression of 86 out of 92 genes was significantly inhibited by Dex. Importantly, the inhibitory effect of Dex was not quite universal. The IFNβ-responsive gene *Acod1* (aconitate decarboxylase 1), previously known as *Irg1* (immune-responsive gene 1), mediates production of the anti-inflammatory metabolite itaconic acid (27, 30). The *Acod1* transcript was induced more than 1000-fold by LPS, and this response was spared from inhibition by Dex. Two IFNβ-responsive genes were significantly cooperatively regulated by LPS and Dex (the outliers *AW112010* and *Slc6a12* in Figure 1E: $p = 1.73 \times 10^{-4}$ and $p = 1.00 \times 10^{-7}$, respectively).

These data suggested that LPS treatment of BMDMs induced an antimicrobial state, likely involving autocrine signaling by IFNβ, and that this process was opposed by Dex. The nature of the antimicrobial state was difficult to define because of lack of knowledge of factors that restrict some pathogens, and because many antimicrobial factors are in fact not specific for pathogen class. We therefore focused on antiviral mediators, because many of these have been systematically identified and annotated on the basis of high throughput functional screens [for example (31)]. First we conducted a systematic screen of our microarray data, identifying genes that were induced by LPS ($\log_2$ fold change > 1, $p < 0.05$); expressed in a delayed manner (at least two-fold higher at 4 h than at 1 h); inhibited by Dex ($p < 0.05$); labelled as type I interferon-inducible in mouse according to the Interferome database (32); and had plausible roles in the regulation of viral life cycles (at least two supporting publications found in Pubmed using the systematic gene name and "antiviral" as search terms). This generated a list of 107 genes (Supplemental Table 2), which is likely to be under-inclusive because of the use of a single, relatively early time point for analysis of gene expression; shortcomings of the text-mining approach; or shortcomings in functional annotation of genes. For example, the poorly annotated gene *AA467197*, mouse ortholog of the human *C15orf48* gene, has only recently been identified as an interferon regulated gene and a putative antiviral factor (33, 34). It is also important to note that viruses may co-opt cellular antiviral machinery to gain a competitive advantage, therefore not all of the genes in the final list are unequivocally "antiviral" under all circumstances. However, many of these are known to contribute to cell-intrinsic defense against viral pathogens (23, 31). These genes belong to several classes including: GTPases or GTP-binding proteins, which contribute to antimicrobial defense via a number of mechanisms (23, 35) (*Gbp2*, *Gbp4*, *Gbp5*, *Gbp9*, *Gnb4*, *Iigp1*, *Irgm2*, *Mx1*, *Mx2*, *Tgtp1*, *Tgtp2*); PRRs involved in the recognition of intracellular pathogens and the initiation of antiviral responses (*Aim2*, *Ddx58* [RIG-I], *Dhx58*, *Eif2ak2* [PKR], *Ifi203*, *Ifi204*, *Ifih1* [MNDA-5], *Mndal*, *Nlrc5*, *Pyhin*); several members of the poly-ADP ribosyltransferase (PARP) and Schlafen (SLFN) families that contribute to antiviral defenses (36, 37); and diverse restriction factors that act at distinct points of infectious cycles to prevent entry, replication or exit of viruses (*Bst2* [tetherin], *Ch25h*, *Cmpk2*, *Herc6*, *Ifi35*, *Ifi44*, *Ifi47*, *Ifit1*, *Ifit2*, *Ifit3*, *Isg15*, *Isg20*, *Oasl1*, *Parp14*, *Rsad2* [viperin], *Trim21*, *Usp18*) (23, 24). Patterns of expression of the top 50 most Dex sensitive genes are illustrated in heatmap form in Figure 2A, whilst the full list is included in Supplemental Table 2.

An unbiased proteomic screen was then used to assess protein levels in BMDMs treated with vehicle, LPS or LPS + Dex for 24 hours. Depth of proteome coverage was good, with more than 6,000 proteins detected, and normalized protein concentrations were similar across conditions, indicating an absence of systemic bias (not shown). We identified proteins whose abundance was increased by LPS (> 1.5-fold increase, Padj < 0.05). The lower threshold for fold change was chosen because LPS-induced changes of abundance were generally lower at the protein than at the mRNA level. This generated a list of 410 LPS-regulated proteins, whose responses to Dex were then examined. According to volcano plot, the effect of Dex was again dominated by suppression (Figure 2B). 125 LPS-induced proteins were significantly negatively regulated by Dex, and 96 of these were identified as type I interferon-regulated genes in the Interferome database (32). Amongst these Dex sensitive targets, gene ontology analysis revealed very strong enrichment of terms related to type I interferons (response to interferon-beta, GO:0035456, fold enrichment 41.2, $p = 3.2 \times 10^{-19}$; cellular response to interferon-beta, GO:0035458, fold enrichment 40.9, $p = 9.3 \times 10^{-17}$). Gene set enrichment analysis also revealed exceptional enrichment of IFNAR-dependent genes that were negatively regulated by Dex at the protein level (Figure 2C). Where data were available in the proteomic data set, we examined the expression of individual protein products of the top 50 Dex-sensitive genes (Figure 2D). With a few exceptions, patterns of expression were similar at mRNA and protein levels, with significant increase in response to LPS and significant decrease in response to addition of Dex. The extent of agreement is striking given that mRNAs were sampled at 4 and proteins at 24 hours after stimulation. The selection of the 24 h time point for assessment of protein expression may have led us to miss or underestimate effects

10.3389/fimmu.2023.1190261

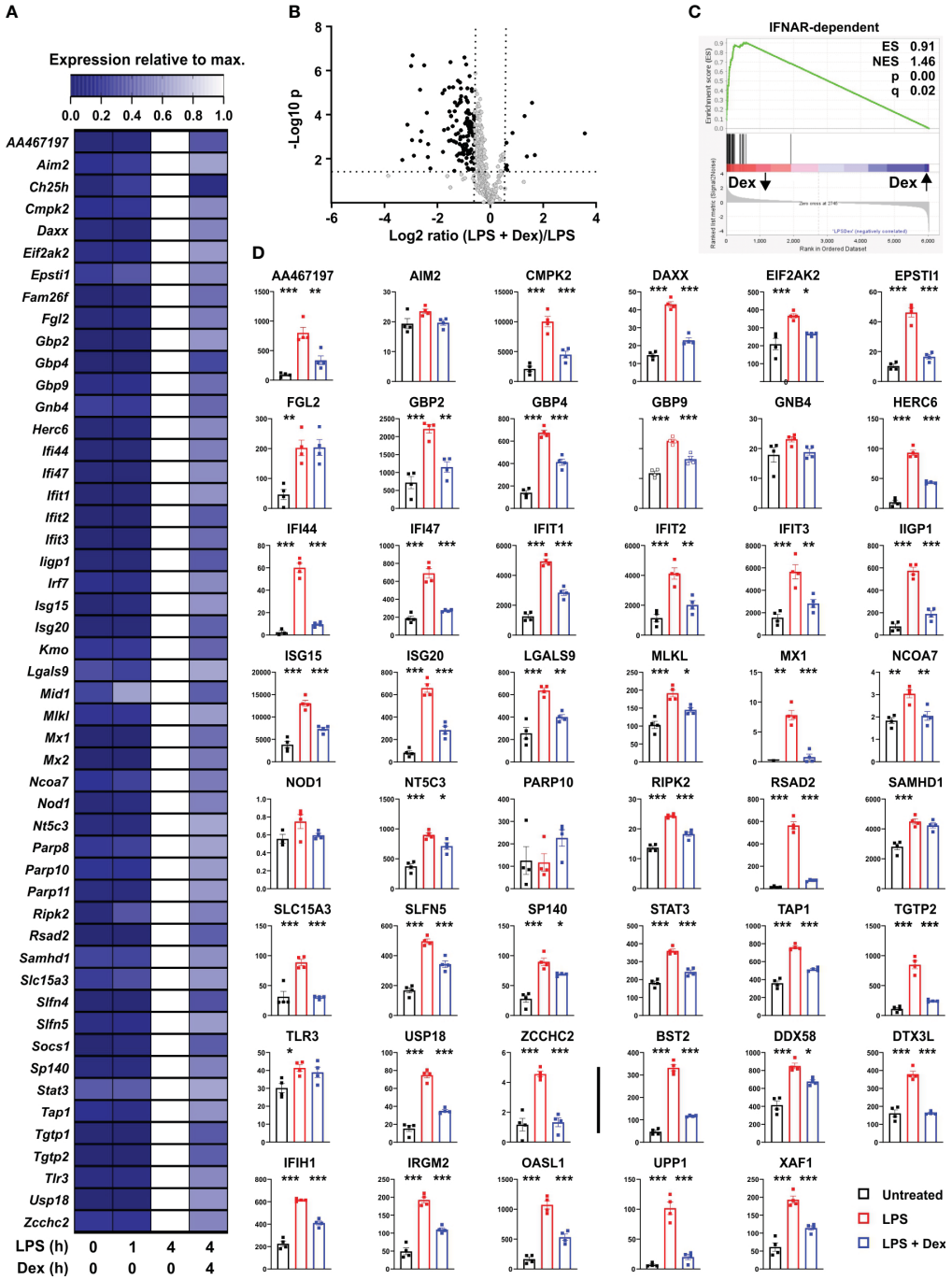

FIGURE 2
Dexamethasone inhibits expression of multiple antiviral mediators at both mRNA and protein levels. **(A)** To identify putative interferon-regulated antiviral mediators that are suppressed by Dex we filtered our data set for genes that were 1) well-annotated; 2) robustly induced by LPS (Log_2 FC > 1, padj < 0.05); 3) expressed in delayed manner (mean expression at least 2-fold higher at 4h than at 1 h); 4) significantly down-regulated by Dex (padj < 0.05); 5) annotated as type I interferon regulated genes according to the Interferome database (32); 6) with plausible evidence of a role in the regulation of viral life cycles (at least two supporting publications found by PubMed search with appropriate gene symbol and "antiviral"). For these 107 genes (See Supplemental Table 2), mean expression was normalized to expression after 4 h stimulation with LPS. The 50 most Dex-sensitive genes are illustrated in heat map format, ordered alphabetically. **(B)** Mouse BMDMs (four independent isolates per condition) were treated with vehicle, 10 ng/ml LPS or 10 ng/ml LPS + 100 nM Dex for 24 h. Protein lysates were generated and subjected to data independent acquisition-based quantitative proteomic analysis. The 410 proteins whose levels were increased by LPS treatment (> 1.5-fold change, padj < 0.05) are illustrated in volcano plot according to their response to addition of Dex. Black dots indicate proteins whose levels were significantly affected by Dex (> 1.5-fold increase or decrease, padj <0.05). **(C)** Gene set enrichment analysis was performed essentially as in 1C. Protein expression data were clustered according to response to Dex, with Dex-suppressed proteins on the left; protein accession numbers were substituted by corresponding gene symbols; and IFNAR-dependent genes from (26) formed the categorical list. **(D)** Where data were available from the proteomic study, levels of proteins corresponding to the genes listed in A were plotted. Numerical values are protein concentrations in nM. The last eight plots (after the vertical bar) show proteins of interest, whose corresponding transcripts were not in **(A)** *, $p < 0.05$; **, $p < 0.01$; ***, $p < 0.005$. Absence of symbol indicates lack of statistical significance.

10.3389/fimmu.2023.1190261

of both LPS and Dex in this experiment. Nevertheless, the emerging picture is one of strong and sustained GC-mediated suppression of antiviral programs. Note that some mediators of antiviral responses (e.g., STING1 and MAVS) were constitutively expressed at both mRNA and protein levels and neither up-regulated by LPS nor down-regulated by Dex (data not shown).

Several transcripts encoding secreted or cell-surface immunomodulatory factors were also expressed in delayed fashion, negatively regulated by Dex, and identified as ISGs according to the Interferome database (32) (Figure 3A). *Il12b*, *Il6* and *Il27* mRNAs were highlighted in Figure 1A. Levels of the corresponding proteins were measured in supernatants of BMDMs treated under the same conditions (Figure 3B). All of these cytokines displayed no increase of expression 1 h after an LPS stimulus, strong increase at 4h, and strong inhibition by Dex. Some of the immunomodulatory proteins were measurable in the unbiased proteomic screen, up-regulated by LPS and suppressed by Dex (Figure 3C). Here we also confirmed the strong induction of LCN2 protein by the combination of LPS and Dex (Figure 3C).

Dexamethasone strongly inhibits expression of IFNβ by LPS-activated BMDMs

ISGF3 plays a central role in the regulation of ISGs (18). Ligand-activated GR was reported to inhibit expression of ISGs by competing with ISGF3 for an essential transcriptional cofactor (38). To investigate the site of action of Dex we therefore used a mouse macrophage cell line stably transfected with an ISGF3-dependent reporter construct. This construct was strongly activated by either LPS or recombinant IFNβ, and in each case the response was ablated by the broad-spectrum JAK inhibitor Ruxolitinib, consistent with dependence on the phosphorylation of STAT1 and STAT2 (Figure 4A). LPS-induced activation of the reporter was dose-dependently inhibited by Dex, whereas the IFNβ-induced response was insensitive to even the highest dose of Dex used (1 μM), suggesting that Dex does not directly interfere with ISGF3 function.

IFNβ caused a rapid increase in the phosphorylation of STAT1, which was evident by 30 minutes and insensitive to Dex (Figure 4B). In contrast, LPS caused delayed STAT1 phosphorylation, which was not evident until 2 h, and was impaired by Dex, particularly at later time points. The delayed activation of STAT1 in response to LPS was dependent on IFNAR1-mediated signaling, and could be prevented by either an IFNAR1-neutralising antibody or treatment of cells with Ruxolitinib (Figure 4C). These observations suggest that Dex acts upstream of IFNβ biosynthesis to disrupt the IFNβ-mediated autocrine loop that controls macrophage functions. In fact, the *Ifnb1* gene appeared in several of the GO terms discussed above (Supplemental Table 1), and its expression was strongly inhibited by Dex in the microarray experiment (see below). Quantitative PCR confirmed rapid, strong and sustained induction of the *Ifnb1* gene following LPS

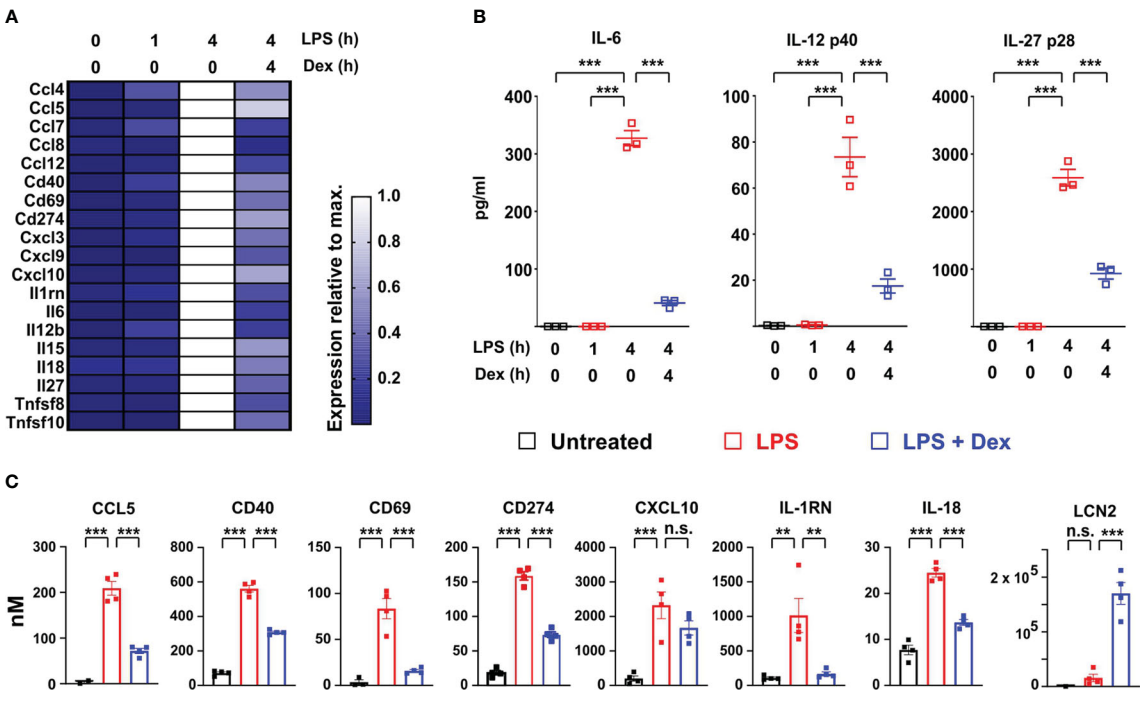

FIGURE 3
Dexamethasone inhibits expression of multiple cell surface and secreted immuno-modulators at both mRNA and protein levels. **(A)** Based on the same microarray data as analyzed in Figure 1, expression of selected interferon-regulated immuno-modulatory proteins is illustrated in heat map form as in Figure 2A. **(B)** In a separate experiment mouse BMDMs (three independent isolates) were treated as indicated, and secreted IL-6, IL-12 p40 and IL-27 p28 were measured in supernatants. ***, $p < 0.005$. **(C)**. Where data were available from the proteomic study, the expression of immunomodulatory proteins was plotted as in Figure 2D. **, $p < 0.01$; ***, $p < 0.005$; n.s., not statistically significant.

10.3389/fimmu.2023.1190261

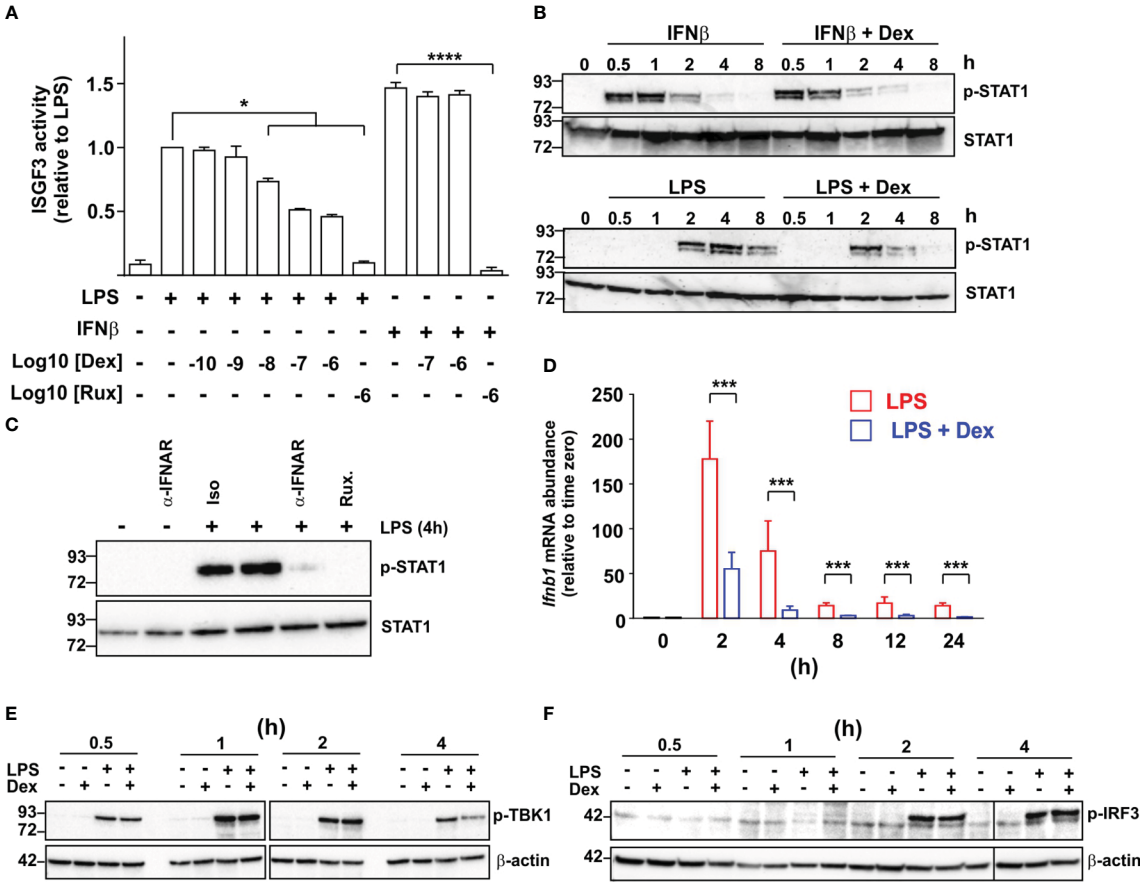

FIGURE 4
Dexamethasone inhibits expression of IFNβ in LPS-activated mouse macrophages via an unknown mechanism. **(A)** A RAW264.7 cell line stably transfected with an ISGF3-dependent SEAP (secreted alkaline phosphatase) reporter was treated with combinations of LPS (10 ng/ml), IFNβ (10 ng/ml), Ruxolitinib (Rux) and Dex as indicated for 24 h and reporter activity was assayed. The graph shows mean results from 3-6 independent experiments ± SEM, with normalization against reporter activity in the presence of LPS alone. *, $p < 0.05$ (Wilcoxon signed rank test); ****, $p < 0.001$ (ANOVA). **(B)** Mouse BMDMs were treated with combinations of LPS (10 ng/ml), IFNβ (10 ng/ml) and Dex (100 nM) as indicated. Cell lysates were generated and western blotted using antibodies against phosphorylated (Tyr 701) or total STAT1. Representative of three independent experiments. **(C)** Mouse BMDMs were stimulated with LPS for 4 h in the absence or presence of an IFNAR neutralizing antibody or isotype control (both 10 μg/ml). Cell lysates were prepared and western blotted as in **(B)** Representative of three independent experiments. **(D)** Mouse BMDMs were treated with LPS (10 ng/ml) or LPS + Dex (100nM) for the indicated times, and *Ifnb1* mRNA was measured by qPCR. Mean of three independent experiments ± SEM. ***, $p < 0.005$. **(E)** Mouse BMDMs were treated with combinations of LPS (10 ng/ml) and Dex (100 nM) for 0.5 – 4 h, cell lysates were prepared and blotted for phosphorylated (activated) TBK1 or β-actin. Representative of two independent experiments. **(F)** Mouse BMDMs were treated as in E and lysates were blotted for phosphorylated (activated) IRF3 or β-actin.

treatment of BMDMs (Figure 4D). Throughout a 24 h time course, this response to LPS was inhibited at least 70% by 100 nM Dex.

It was previously reported that pre-treatment of the myeloid cell line U937 with Dex impaired the LPS-induced phosphorylation and activation of TBK1 (39). We therefore considered the hypothesis that inhibition of TBK1 function explains the inhibitory effect of Dex on IFNβ-mediated feedback in primary macrophages. However, simultaneous treatment of primary BMDMs with LPS and Dex caused no impairment of early LPS-induced TBK1 phosphorylation under conditions that resulted in strong inhibition of both *Ifnb1* and ISGs (Figure 4E). Dex weakly but consistently reduced TBK1 phosphorylation at the four-hour time point. However, this late effect was unlikely to contribute to changes in expression of *Ifnb1*, which were strongly declining by four hours. Dex also had no effect on the phosphorylation of IRF3, which mediates the activation of *Ifnb1* transcription downstream of TBK1 (Figure 4F).

Glucocorticoids selectively inhibit the expression of certain pro-inflammatory genes by increasing and prolonging the expression of DUSP1 and inhibiting MAPK p38 (7–10). DUSP1 is a negative regulator of *Ifnb1* gene expression (40). Both serum IFNβ and hepatic IFNβ-dependent genes (including *Ifit2*, *Rsad2*, *Iigp1* and many more of the ISGs discussed here) were over-expressed in *Dusp1-/-* mice following infection with *E. coli* (41). These observations suggested the hypothesis that Dex impairs expression of IFNβ and IFNβ-dependent genes in LPS-activated BMDMs via the induction of DUSP1. This hypothesis was tested using macrophages generated from *Dusp1-/-* mice. IFNβ biosynthesis was elevated in *Dusp1-/-* BMDMs as previously reported (40), but similarly inhibited by Dex in *Dusp1+/+* and

Dusp1-/- BMDMs (Figure 5A: note different scales of y axes). A previous publication reported that Dex did not impair LPS-induced IFNβ expression in BMDMs (42). The reasons for this discrepancy are not clear, but may include different sources and doses of LPS or different duration of Dex treatment.

We then systematically examined the impact of DUSP1 depletion on the Dex sensitivity of IFNβ-regulated antiviral genes (Figure 5B, left) and immunomodulatory genes (Figure 5B, right). For the gene sets discussed above, Dex sensitivity was calculated as average ratio of expression under conditions (LPS + Dex/LPS). In plots of Dex sensitivity in *Dusp1+/+* (x axis) and *Dusp1-/-* (y axis) backgrounds the dotted diagonal line represents the null hypothesis that disruption of the *Dusp1* gene has no impact on responsiveness to Dex. For both gene sets, sensitivity to Dex was closely correlated in *Dusp1+/+* and *Dusp1-/-* BMDMs, supporting the null hypothesis and suggesting a minimal impact of DUSP1 depletion. However, there were several outliers whose response to Dex was altered by *Dusp1* gene disruption. Some of these are highlighted in Figure 5B, and primary data from the microarray experiment are illustrated in Figure 5C. In the cases of *Irf7*, *Bst2*, *Sp100* and *Cxcl3*, significant inhibitory effects of Dex were completely lost in the absence of DUSP1. We conclude that overall DUSP1 plays a minor and highly gene-specific role in the regulation of IFNβ signaling by Dex. Figure 5C also illustrates the behavior of the *Ifnb1* gene itself in the microarray experiment, confirming elevated expression in *Dusp1-/-* BMDMs and strong suppression by Dex in BMDMs of both genotypes.

Dexamethasone selectively inhibits IFNβ-induced gene expression in BMDMs

Collectively, these observations led to a clear and testable hypothesis: that Dex impairs the responses of macrophages to LPS by inhibiting the expression of IFNβ and disrupting the IFNβ-mediated autocrine feedback loop. We predicted that secondary genes, which are induced by LPS in an IFNβ-dependent manner, would be insensitive to Dex if activated directly by IFNβ, by-passing the site of GC action. To test this hypothesis, we first generated a panel of test genes comprising three intracellular antiviral effectors (*Ifit2*, *Rsad2* and *Iigp1*) and three secreted cytokines or chemokines (*Cxcl9*, *Il6* and *Il27*). IFNAR1

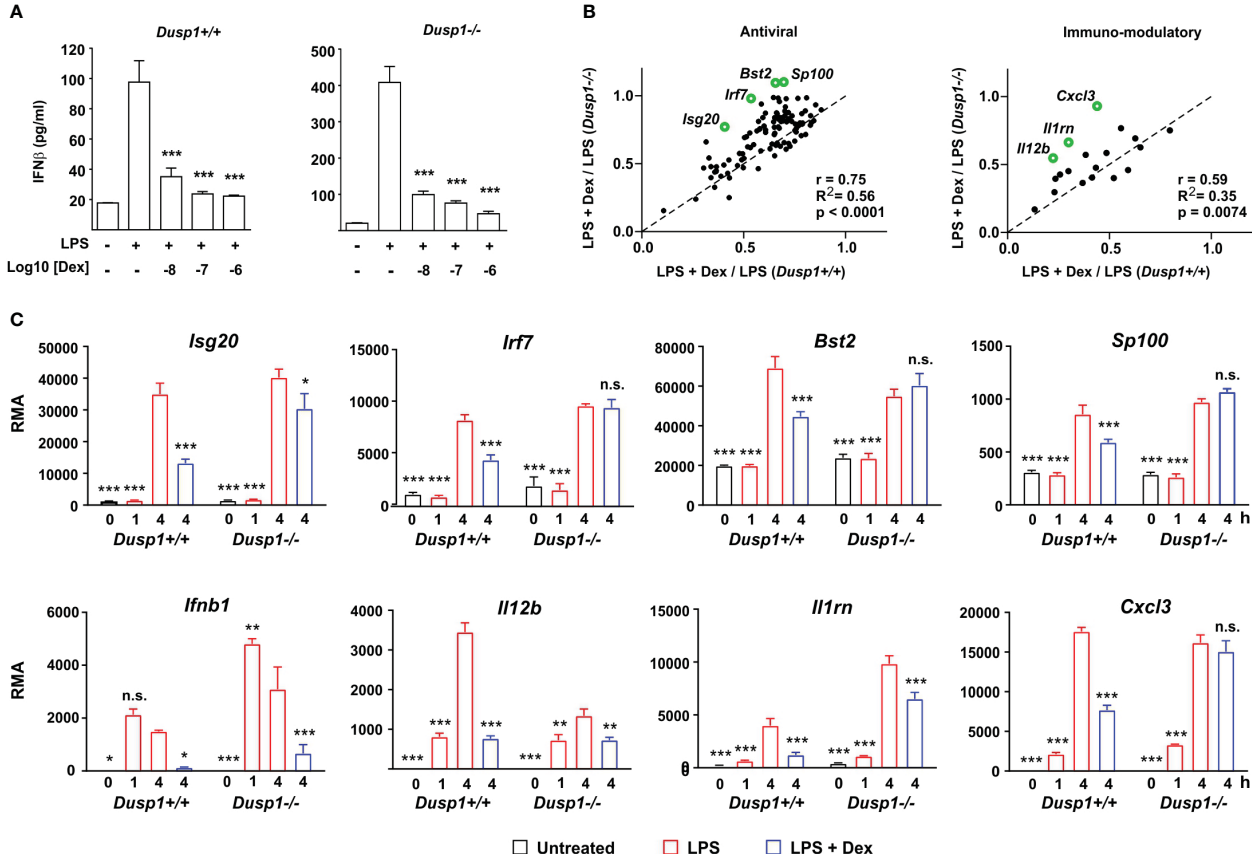

FIGURE 5
DUSP1 contributes to Dex-mediated suppression of ISGs. **(A)** *Dusp1+/+* or *Dusp1-/-* BMDMs (three independent isolates of each) were treated with LPS (10 ng/ml) for 4h with or without addition of Dex as indicated. IFNβ protein was measured by Luminex assay. The graph shows mean ± SEM, n = 3. ***, p < 0.005. **(B)** For each interferon-regulated gene of "antiviral" or "immmuno-modulatory" subsets (see Figures 2, 3), Dex sensitivity was calculated as the ratio of expression in the presence of LPS + Dex vs. expression in the presence of LPS alone. In the plot of Dex sensitivity in *Dusp1 +/+* and *Dusp1-/-* BMDMs, the dotted diagonal represents the null hypothesis, that effects of Dex are independent of *Dusp1* genotype. Selected outlier genes that do not fit the null hypothesis are highlighted. **(C)** Microarray-derived expression data for these outlier genes are illustrated. The pattern of expression of *Ifnb1* itself is also shown. n.s., not significant; *, p < 0.05; **, p < 0.01; ***, p < 0.005; all in comparison to 4 h LPS treatment.

10.3389/fimmu.2023.1190261

dependence of all of these genes was confirmed by reference to a published data-set (29); by our own experiments using *Ifnar1-/-* BMDMs (data not shown); and by use of an IFNAR1-blocking antibody (Figure 6A). We then tested the responses of all six genes to challenge with LPS or IFNβ in the absence or presence of Dex (Figure 6B). All three of the antimicrobial effector genes responded as predicted by the hypothesis: their expression in response to LPS was significantly impaired by Dex, whereas their expression in response to IFNβ was insensitive to Dex. Surprisingly, all three of the cytokine/chemokine genes were suppressed by Dex whether induced by LPS or IFNβ. Dex may therefore act both upstream and downstream of IFNβ to impair LPS responses of BMDMs. The IFNβ-induced expression of *Ifit2*, *Rsad2*, *Iigp1*, *Il6* and *Cxcl9* was very strongly dependent on ISGF3 (at least 100-fold lower expression in IFNβ-stimulated *Irf9-/-* BMDMs) (43). *Ifit2*, *Rsad2* and *Iigp1* were insensitive to Dex, whilst *Il6* and *Cxcl9* were suppressed by Dex in IFNβ-stimulated BMDMs. This confirms the conclusion from the reporter gene assay (Figure 4A); that Dex does not regulate IFNβ signaling in BMDMs via broad suppression of ISGF3 function.

Dexamethasone also acts both upstream and downstream of IFNβ in primary human macrophages

To investigate the same phenomena in human cells we generated monocyte-derived macrophages from peripheral blood of healthy donors and stimulated them with LPS in the absence or presence of 100 nM Dex. Surprisingly there was greater than ten-fold donor-to-donor variation in quantity of IFNβ secreted by LPS-activated MDMs (note logarithmic axis in Figure 7A). However,

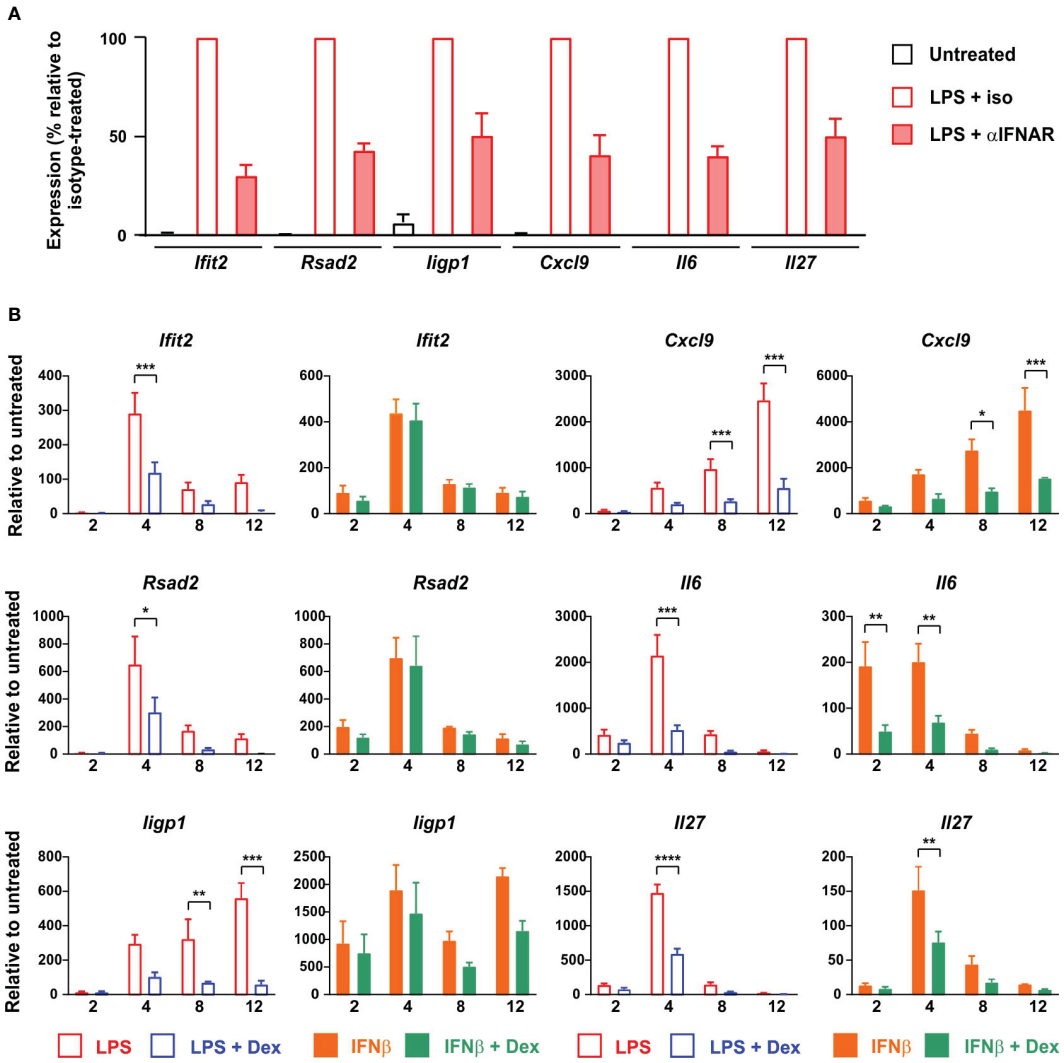

FIGURE 6
Dex regulates expression of ISGs both upstream and downstream of IFNβ in mouse BMDMs. **(A)** BMDMs (4-5 independent replicates) were treated for 4 h with vehicle, 10 ng/ml LPS + 10 μg/ml IFNAR neutralizing antibody, or 10 ng/ml LPS + 10 μg/ml isotype control. RNA was isolated and the indicated transcripts were measured by qPCR, with normalization against LPS + isotype control. **(B)** BMDMs (at least three independent replicates) were treated for 0 - 12 h with LPS (10 ng/ml) ± Dex (100 nM) or IFNβ (10 ng/ml) ± Dex (100 nM). Expression of selected genes was determined by qPCR. *, $p < 0.05$; **, $p < 0.01$; ***, $p < 0.005$; ****, $p < 0.001$; absence of symbol indicates lack of statistical significance ($p > 0.05$).

IFNβ release was consistently inhibited by 100 nM Dex (mean inhibition ± SEM 52% ± 6%, p = 0.001). Basal expression of some ISGs varied between donors by several hundred-fold (not shown), and magnitudes of response to both LPS and IFNβ were also highly variable (Figure 7B). This created a practical problem in generating adequate statistical power to investigate effects of Dex, power calculation suggesting that 100 or more individual donors would be needed for some ISGs. Nevertheless, a preliminary analysis using seven independent isolates of MDMs confirmed that Dex can inhibit expression of the ISGs *RSAD2* and *CXCL9* whether evoked by either LPS or IFNβ. In human alveolar macrophages the LPS-induced expression of *IFNB1* and *RSAD2* genes was consistently inhibited by Dex (Figure 7C); however, IFNβ protein was below the limit of detection in supernatants of these cells. Scarcity of samples, low yields of mRNA and lack of statistical power prevented us from carrying out an extensive survey of ISG expression. Yet these preliminary data suggest that Dex may also impair type I interferon signaling in alveolar macrophages.

Discussion

Glucocorticoids have been reported to impair type I interferon signaling in macrophages, but these studies tended to document expression of relatively few ISGs, at the mRNA level only (38, 39, 42, 44, 45). Here we describe a remarkably broad impact of Dex on the expression of ISGs by LPS-activated BMDMs, occurring at both mRNA and protein levels. Several mechanisms have been suggested to mediate inhibitory effects of GCs on type I interferon signaling, but none of them satisfactorily explain the observations described here. 1) Dex pretreatment impaired the LPS-induced phosphorylation and activation of TBK1 and IRF3 in a myeloid cell line (39). In our hands Dex did not affect LPS-induced TBK1 phosphorylation or downstream IRF3 activation under conditions where the expression of *Ifnb1* mRNA and IFNβ protein was strongly inhibited. In any case the impairment of IFNβ production only partially accounts for Dex-mediated impairment of ISG expression in LPS-treated BMDMs, because some ISGs were also sensitive to Dex when directly induced by IFNβ itself. 2) Downstream of the IFNβ receptor, Dex was reported to inhibit ISG expression by reducing the expression of STAT1 (44), or by up-regulating SOCS1 and inhibiting STAT1 phosphorylation (42). In the presence of either LPS or IFNβ, Dex did not influence STAT1 protein expression over 8 hours. Although Dex inhibited the LPS-induced phosphorylation of STAT1 this was almost certainly a consequence of impaired IFNβ secretion since IFNβ-induced STAT1 phosphorylation was insensitive to Dex. Furthermore, Dex reduced rather than increased the LPS-induced expression of *Socs1* mRNA (LPS alone, 17,621 ± 912; LPS + Dex, 6,278 ± 914). 3) Another proposed mechanism of action of glucocorticoids is the impairment of ISGF3 function, involving competition between GR and ISGF3 for the essential transcriptional cofactor NCOA2 (nuclear receptor coactivator A2) (38). Several lines of evidence argue against such a mechanism here. First, IFNβ-mediated activation of an ISGF3-dependent reporter construct was insensitive to Dex. In contrast the same reporter was sensitive to Dex when activated by LPS, presumably again due to impairment of IFNβ expression. Amongst our Dex-sensitive ISGs, just over half were reported to have ISGF3 binding sites in their vicinity in a previous study (43) (Supplemental Table 2). However, there was poor correlation between ISGF3-dependence in that study and Dex sensitivity in ours (R^2 = 0.09). The discrepancy is illustrated by the LPS-induced gene *Oas2* (oligoadenylate synthase 2), which was exceptionally dependent on ISGF3 (43) but unaffected by Dex in our study. Although we cannot rule out that Dex inhibits some ISGs via impairment of ISGF3 function, this mechanism cannot explain the broad impact of Dex. 4) We previously reported that Dex-induced expression of the phosphatase DUSP1 contributes to the suppression of certain LPS-induced genes in macrophages (7, 8, 10). However, the sensitivity of most ISGs to Dex was affected little by disruption of the *Dusp1* gene. In only a few cases was there a clear loss of sensitivity to Dex in *Dusp1*-/- BMDMs. If there is a unifying mechanism by which Dex controls the type I interferon response, it remains to be discovered. Any explanation of this phenomenon must account for its selectivity, and the escape of certain well-known ISGs such as *Acod1* and *Oas2* (46).

An important question is whether the same suppression of antimicrobial genes occurs in macrophages exposed to a viral mimetic such as poly(I:C), rather than the bacterial component LPS. Our preliminary data indicate that this is the case (data not shown) – as one would predict given that poly(I:C) also induces robust IFNβ expression in macrophages. A second important question is whether GCs similarly affect type I interferon-dependent antimicrobial programs in other cell types. In A549 airway epithelial cells stimulated for 18 h with IL-1β, the expression of 84 genes was significantly impaired by addition of Dex (fold decrease >2, p < 0.05) (47). The majority of these genes are interferon-regulated genes according to the Interferome database (32), and many are orthologs of genes that we found to be suppressed by Dex in LPS-treated BMDMs (e.g., *Cmpk2*, *Herc6*, *Ifi44*, *Ifih1*, *Ifit1*, *Ifit3*, *Isg15*, *Isg20*, *Usp18*). It is likely that Dex also disrupts IFNβ-mediated positive feedback loops in these cells. More than half of the ISGs discussed here were also induced by LPS in primary human alveolar macrophages, suggesting that antimicrobial responses of these cells are also governed by IFNβ-mediated feedback (48) (Supplemental Table 2).

The type I interferon pathway has been described as a two-edged sword in the battle between host and pathogen (49). On one hand interferons are critical for cell-intrinsic defenses against pathogens and initiation of adaptive immune responses to destroy pathogens and infected cells. On the other hand, they can contribute to pathogen-induced inflammatory pathology and consequent tissue damage in infectious diseases such as influenza and tuberculosis (50–52). GC treatment of infectious diseases also has highly variable consequences. In specific contexts or at specific stages of disease GCs may alleviate pathogen-induced inflammation, but otherwise they may exacerbate infection. In the majority of infectious diseases, the use of GCs is controversial, outcomes of clinical trials are often contradictory, and consensus on best practice is difficult to achieve. GC treatment of pandemic (H1N1) influenza was associated with increased mortality, increased length of stay in intensive care, and prolonged virus

10.3389/fimmu.2023.1190261

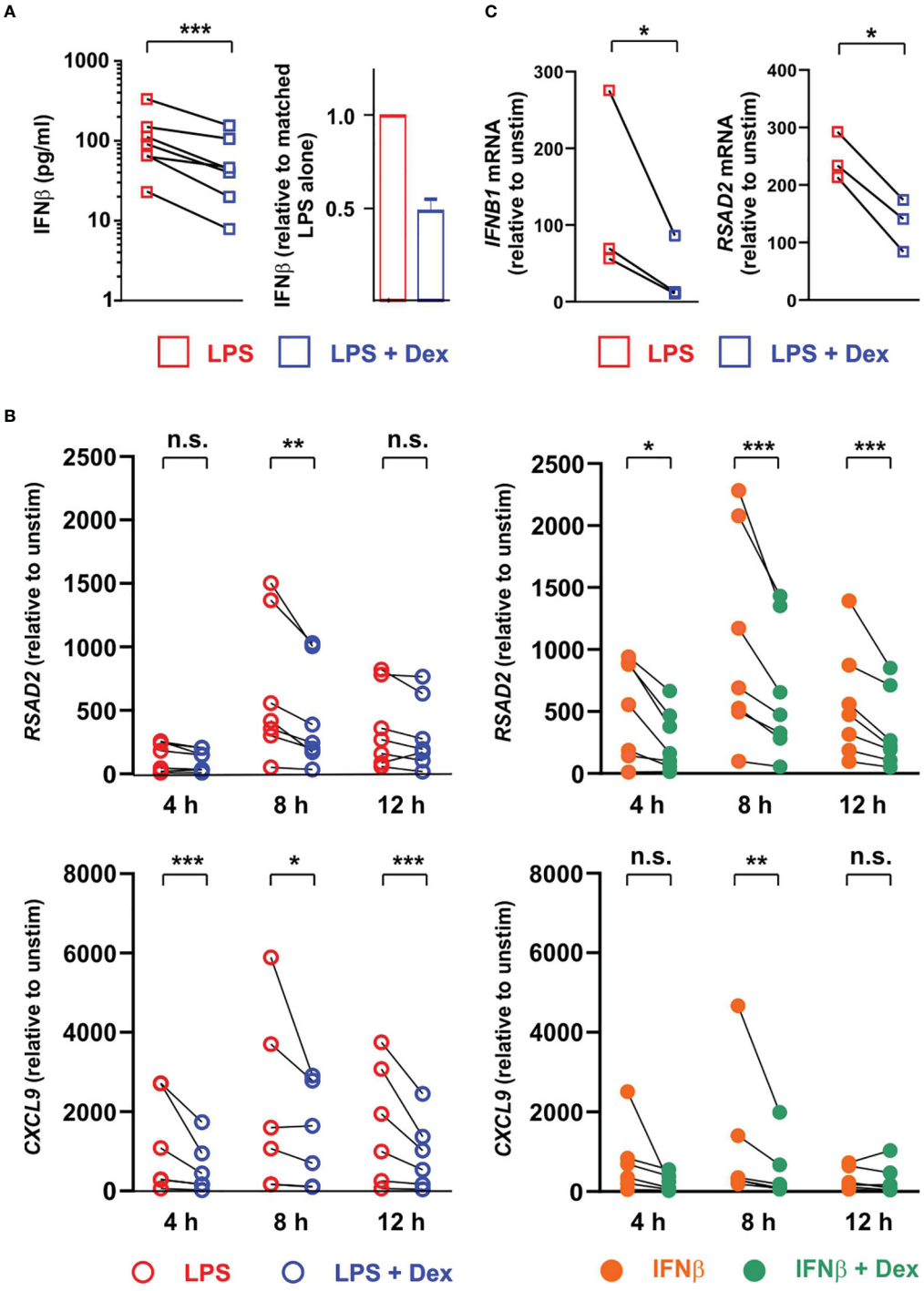

FIGURE 7
Dex regulates expression of ISGs both upstream and downstream of IFNβ in primary human macrophages. **(A)** Primary human monocyte-derived macrophages (n=7) were stimulated with 10 ng/ml LPS ± 100 nM Dex for 4 h, and IFNβ protein in supernatants was measured by Luminex assay. Right hand panel illustrates the same data with normalization to LPS alone. **(B)** Primary human monocyte-derived macrophages (n=7) were stimulated with 10 ng/ml LPS ± 100 nM Dex (left) or with 10 ng/ml IFNβ ± 100 nM Dex (right) for 4, 8 or 12 h. *Rsad2* and *Cxcl9* mRNAs were measured by qPCR, with normalization against untreated control for each individual macrophage culture. *, $p < 0.05$; **, $p < 0.01$; ***, $p < 0.005$; n.s., $p > 0.05$. C. Alveolar macrophages were isolated from histologically normal regions of lung resection tissue and treated with 1 μg/ml LPS ± 100 nM Dex for 12 h. *IFNB1* and *RSAD2* mRNAs were measured by qPCR, with normalization against untreated control for each individual sample. *, $p < 0.05$.

shedding (53–55). Deleterious outcomes may be related to the complex cross-talk between GCs and type I interferon signaling. For example, GC treatment of bronchial epithelial cells impaired the expression of selected ISGs and promoted infection by influenza A virus or rhinovirus. Treatment with a type I interferon reversed the pro-viral effect of GC treatment both *in vitro* and *in vivo* (56, 57), indicating that GCs can favor viral infections by suppressing the type I interferon pathway.

Several lines of evidence reveal the critical role of type I interferon signaling for host defense against the zoonotic coronavirus SARS-CoV-2. 1) Inborn and acquired defects of the type I interferon pathway are associated with increased susceptibility to infection (58). 2) Systematic screens and more targeted approaches have identified several ISGs as restriction factors that limit SARS-CoV-2 infection at different stages of the viral life-cycle (31). 3) Like other viruses (59), SARS-CoV-2 deploys several mechanisms to subvert the type I interferon-mediated defense machinery, both impairing the detection of virus and inhibiting the execution of antiviral programs of gene expression (60). 4) An early and robust type I interferon signature in circulating monocytes was associated with mild disease following SARS-CoV-2 infection (61). Likewise myeloid cell interferon responses correlated with viral clearance in an experimental model of COVID-19 (62). 5) Conversely, low expression of antiviral genes including *CMPK2*, *EPSTI1*, *HERC6*, *IFI44*, *OASL* and *RSAD2* in peripheral blood was associated with worse clinical outcomes in COVID-19 (63). On the other side of the equation, several components of the damaging SARS-CoV-2-induced cytokine storm are type I interferon-inducible factors that contribute to pathogenesis of COVID-19 (64).

Almost uniquely amongst infectious pathologies, severe COVID-19 is now routinely treated using GCs (65). This makes it an important context in which to discuss the crosstalk between GCs and type I interferon signaling, and the balance between beneficial and harmful effects of GCs. Beneficial effects of GCs in severe COVID-19 are thought to involve suppression of the pro-inflammatory cytokine storm (66), in which the inhibition of type I interferon signaling may play a part (67). For example, elevated levels of the interferon-regulated cytokines IL-27 and IL-6 contribute to a signature that is predictive of poor outcome in COVID-19 (68, 69). GC-mediated suppression of these factors may contribute to improved outcomes. On the negative side, endogenous GC excess is a risk factor for COVID-19 (70). Similarly, prolonged use of synthetic GCs for the treatment of immune-mediated inflammatory diseases both increases the likelihood of contracting COVID-19 and contributes to worse outcomes of the disease (71). Although GCs reduce mortality by approximately a third in patients suffering from severe COVID-19 and requiring respiratory support (72), in mild or early disease there is no evidence of benefit, and some suggestion of harmful effects including delays to viral clearance (72–74). We note that several of the ISGs that we found to be negatively regulated by Dex at mRNA and protein levels are known restriction factors for SARS-CoV-2 (31) (Supplemental Table 2). These include *DDX58* (RIG-I) and *IFIH1* (MDA5), which are essential for detection of intracellular SARS-CoV-2 (75) and are targeted by the virus as a means of evading interferon responses (76). We therefore hypothesize that GCs are able to promote SARS-CoV-2 infection by opposing type I interferon-mediated antiviral mechanisms. This hypothesis remains to be tested, and is the focus of our ongoing research.

There are clearly many unanswered questions about when and how best to use GCs against SARS-CoV-2 and other viral pathogens. Indeed, it has previously been argued that variable outcomes of GC trials in COVID-19 were related to inconsistent timing of delivery (77). The balance between the harm of suppressing antiviral mechanisms in early disease and the benefit of suppressing the cytokine storm in the later phase is precarious. The tipping point between harm and benefit may also differ between individuals. There is clearly a strong case for application of well-informed patient stratification in COVID-19 (78, 79). We argue that the effects of GCs on type I interferon-mediated host defenses should be part of such a precision medicine approach. Furthermore, there is urgent need for further research on the mechanistic basis of cross-talk between GCs and type I interferon signaling.

Materials and methods

Macrophage isolation and culture

All mice were maintained at the Biomedical Services Unit of the University of Birmingham. Animal care and experimental procedures were performed according to Home Office guidelines and approved by the University of Birmingham Local Ethical Review Committee. Bone marrow was isolated from the femurs of humanely culled 6–12-week-old wild type C57BL/6J mice, and BMDMs (bone marrow derived macrophages) generated essentially as described (80) by differentiation *in vitro* in RPMI 1640 medium with L-glutamine (Gibco Thermo Fisher Scientific 21875034) supplemented with 10% heat-inactivated fetal bovine serum (Sigma F0392) and 50ng/ml recombinant M-CSF (Peprotech 300-25) for 7 days. BMDMs were plated at a density of 1 x 10^6/ml in the appropriate cell culture plate at least 1 d prior to stimulation. This method generated primary mouse macrophages with purity approaching 99% as measured by flow cytometry using antibodies against F4/80, CD11b, CD14 and CD64 (Figure S1).

The *Dusp1-/-* strain was a generous gift from Bristol-Myers Squibb, and was back crossed to C57BL/6 for ten generations prior to experiments described here.

Human monocytes from healthy blood donors were isolated from leukapheresis blood cones supplied by the National Blood and Transplant Service (ethical approval ERN_16-0191). Monocytes were enriched by negative selection using StemCell RosetteSep Human Monocyte Enrichment Cocktail (StemCell 15068; 75µl per ml of blood) and Ficoll-Paque (VWR 17144003). Cells were differentiated for 7 days in RPMI 1640 medium with L-glutamine (Gibco Thermo Fisher Scientific 21875034) supplemented with 5% heat-inactivated fetal bovine serum (Biosera FB-1001) and 50ng/ml recombinant M-CSF (Peprotech 300-25). Differentiated macrophages were plated at a density of 1 x 10^6/ml in the appropriate cell culture plate at least 1 d prior to stimulation. In our hands this method generates primary human macrophages with purity >98% as measured by flow cytometry using antibodies against CD14, CD64 and CD206 (Figure S1).

Ethical approval was obtained to recruit adult patients scheduled for surgery to remove lung tissue as part of their clinical treatment plan (predominantly lobectomy for lung cancer) at the Thoracic Surgery Unit at the Queen Elizabeth Hospital Birmingham (REC 17/WM/0272). Lung tissue samples

distant from any tumor, without macroscopically evident pathology, and surplus to requirement for histopathology, were washed through with 500 ml of sterile 0.9% saline (Baxter, UK) using a 14-gauge needle (Vasofix ®). The washed through lavage fluid was collected and centrifuged at 4°C and 560g for 10 minutes. Cell pellets were resuspended in 10 ml of RPMI1640 containing 10% FBS, and overlaid onto 10 ml of Lymphoprep™ (StemCell) prior to centrifugation at 800g for 30 min at 4°C. The interphase layer containing mononuclear cells was aspirated into a sterile 50 ml tube containing PBS with 10% FBS, which was then centrifuged at 300g for 10 minutes at 4°C. AMs were resuspended in RPMI1640 containing 10% FBS, 100U/mL penicillin, 100µg/mL streptomycin and 2mM L-glutamine (Sigma-Aldrich), and plated. This method generates primary human alveolar macrophages with purity >98% as measured by a validated combination of cytospin and flow cytometry using antibodies against CD68 (81).

Stimulations were carried out in appropriate culture plates using the following reagents and concentrations unless otherwise stated: LPS (Enzo ALX-581-010-L002; 10ng/ml); recombinant human IFNβ (Peprotech 300-02BC; 10ng/ml); recombinant mouse IFNβ (BioLegend 581306; 10ng/ml); Ruxolitinib (Selleck S1378; 1µM); Dexamethasone (Sigma D8893; 100nM). Where stated, cells were incubated for 2 hours with an IFNAR1 blocking monoclonal antibody (Fisher Scientific MAR1-5A3; 10 µg/ml), or mouse IgG1 kappa isotype control, (Fisher Scientific P3.6.2.8.1; 10 µg/ml) prior to stimulations.

Quality control of primary macrophage populations

Upon harvesting of *in vitro*-differentiated cells for counting and seeding for experiments (mouse BMDMs day 7; human MDMs day 6), a fraction of the cell suspension was used for purity assessment by flow cytometry. Cells were stained with eFluor780 fixable viability dye (eBioscience 65-0865, 1/1000 in PBS) for 20min on ice to allow gating for live cells. Fc receptor blocking was performed for 5min prior to antibody staining using Mouse BD Fc Block (BD 553142) or Human BD Fc Block (BD 564220). Antibody staining was performed for 30min on ice in FACS buffer (PBS+2% FCS +1mM EDTA) using the antibodies and dilutions listed below. Cells were washed and resuspended in FACS buffer and run on a BD LSRFortessa X-20. Analysis was performed using FlowJo v10.

Mouse BMDM staining: PE rat anti-mouse F4/80 Antibody (Biolegend 123110, 1/50); PE rat IgG2a κ Isotype Control Antibody (Biolegend 400507, 1/50); FITC rat anti-mouse/human CD11b Antibody (Biolegend 101205, 1/100); FITC rat IgG2b Isotype Control Antibody (eBioscience 11-4031-82, 1/100); PerCP-eFluor710 rat anti-mouse CD14 Antibody (eBioscience 46-0141-80, 1/40); PerCP-eFluor710 rat IgG2a κ Isotype Control Antibody (eBioscience 46-4321-82, 1/40); APC rat anti-mouse CD64 Antibody (Biolegend 139305, 1/20); APC rat IgG1 κ Isotype Control Antibody (eBioscience 17-4301-81, 1/20).

Human MDM staining: PE mouse anti-human CD14 Antibody (Biolegend 367104, 1/100); PE mouse IgG1 κ Isotype Control Antibody (Biolegend 400113, 1/20); PerCP-eFluor710 mouse anti-human CD64 Antibody (eBioscience 46-0649-41, 1/20); PerCP-eFluor710 mouse IgG1 κ Isotype Control Antibody (eBioscience 46-4714-80, 1/20); APC mouse anti-human CD206 Antibody (Biolegend 321110, 1/20); APC mouse IgG1 κ Isotype Control Antibody (Biolegend 400119, 1/20).

Stable macrophage cell line ISGF3-dependent reporter assay

The RAW-Blue ISG macrophage cell line stably transfected with an ISGF3-dependent reporter construct was cultured and maintained according to the manufacturer's instructions (RAW-Blue ISG cells, Invivogen raw-isg). ISGF3 reporter activity was determined from cell culture supernatants using QUANTI-Blue detection reagents according to the manufacturer's instructions (Invivogen).

Measurement of mRNA

RNA was isolated from mouse BMDMs and human monocyte derived macrophages using Norgen Total RNA Purification Plus kit (Geneflow P4-0016) according to manufacturer's instructions. cDNA was synthesized using the iScript cDNA Synthesis Kit (Biorad 1708891). mRNA was detected by RT-qPCR using SYBR TB Green Premix Ex Taq (Takara RR820W) and primers supplied by Eurofins Genomics or Sigma Aldrich. UBC (human) or B2M (mouse) were used to normalize mRNA measurements via 2^-ΔΔCt method. Primers are listed in Table 1.

Microarray analysis and bioinformatics

Microarray analysis was performed using SurePrint G3 Mouse GE 8x60K slides (Agilent) and Partek Genomics Suite version 6.6, build 6.13.0315 (Partek) as previously described (82). For generation of volcano plots, transcripts were first filtered for significant upregulation in response to LPS (> 5-fold increase, adjusted p-value < 0.05) and weakly expressed transcripts were removed by application of an arbitrary filter of 200 RMA. Plots ($\log_2$ fold difference of expression vs $-\log_{10}$ ANOVA p-value) were constructed using Prism (GraphPad Software), with subset cut-offs at p-value < 0.05 and fold difference of expression > 2. Microarray data discussed in this paper were deposited at Gene Expression Omnibus (http://www.ncbi.nlm.nih.gov/geo/) with the accession number GSE68449.

Gene Ontology analysis was performed using the Panther v16 online toolset (83). Redundant GO terms were filtered using REVIGO (84). Gene Set Enrichment Analysis (GSEA) was performed using GSEA_4.1.0 (85).

Multiplex cytokine analysis

Conditioned medium samples from cultured macrophages were subjected to custom multiplex Luminex assay (Bio-Rad Custom Bio-

TABLE 1 PCR primers used in this study.

Gene name	Forward primer	Reverse Primer
Human PCR primers		
CXCL9	GAGAAAGGGTCGCTGTTCCT	TTTGGCTGACCTGTTTCTCC
IFNB1	ACGCCGCATTGACCATCTAT	GTCTCATTCCAGCCAGTGCTA
RSAD2	ATGTGGGTGCTTACACCTGC	GAGAGCTCAGAGGTTGCCTG
UBC	CGGGATTTGGGTCGCAGTTCTTG	CGATGGTGTCACTGGGCTCAAC
Mouse PCR primers		
B2m	CTGCTACGTAACACAGTTCCACCC	CATGATGCTTGATCACATGTCTCG
Cxcl9	TCGGACTTCACTCCAACACA	CCTTATCACTAGGGTTCCTCGAA
Ifit2	ACACAGCAGTCATGAGTACAACG	TCAGGATGCTGTTGCTGGAT
Iigp1	AGCACACTCAGAAGGGGAGA	ACTTCAAGCAATAAAGGCACAGA
Il6	ACTTCACAAGTCGGAGGCTT	ATTGCCATTGCACAACTCTTTT
Il27	TGTCCACAGCTTTGCTGAAT	GAAGGGCCGAAGTGTGGTAG
Rsad2	TGGCCGTGGTCAAGGAAAAA	TTAGGAGGCACTGGAAAACCTTC

Plex Assays), and Invitrogen ProcartaPlex Mouse or Human IFNβ simplexes, (EXP01A-26044-901 or EXP01A-12088-901, respectively), according to manufacturer's instructions.

Western blotting

For whole cell lysates, cells were harvested in RIPA buffer and samples passed through a Qiashredder column to disrupt genomic DNA (Qiagen 79656). Protein was quantified by Pierce BCA Assay (Thermo Fisher Scientific 23225). Laemmli or XT sample buffer was added and samples heated to 95°C for 5min. Western blotting was performed using Criterion TGX protein gels (BioRad) and Tris-Glycine SDS buffer (Geneflow B9-0032) or 4–12% Criterion™ XT Bis-Tris Protein Gels (BioRad) and XT MES running buffer (BioRad 1610789). Protein was transferred to BioRad Trans-Blot PVDF membranes (BioRad 1704157) using BioRad Trans-Blot Turbo transfer system. Blots were imaged using Clarity Western ECL Substrate (BioRad 1705061) and BioRad ChemiDoc MP Imaging System. Densitometry for Western blot quantification was performed using ImageJ. Antibodies used in western blotting are listed in Table 2.

Proteomic analysis

Following derivation and stimulation of mouse BMDMs (as described above) cells were washed with PBS and lysed in proteomic lysis buffer (5% SDS, 10mM TCEP, 50mM TEAB). Unbiased proteome analysis was carried out by data-independent acquisition (DIA) mass spectrometry proteomics utilizing S-Trap on-column digestion and purification, following the methods detailed by Baker et al. (86). Protein copy number was determined using Perseus software (86, 87) with normalization for histone protein content. Data were analyzed as described in the above methods for microarray analysis and bioinformatics.

Statistical analysis

GraphPad Prism software (Version 6) was used for statistical analysis. Mann Whitney U test was used for comparison of two groups. For analysis of multiple groups, ANOVA was used with Bonferroni correction for multiple comparisons. The following marks are used throughout: *,$p<0.05$; **,$p<0.01$;***,$p<0.005$; n.s., not statistically significant. N numbers specified in figure legends indicate biological replicates. In human alveolar macrophages, where expression of ISGs was highly variable between donors, ratio paired t test was used to test for consistent effect of Dex.

TABLE 2 Antibodies used in this study.

Antibody	Dilution		Company
pSTAT1	1:1000	58D6	Cell Signalling
Stat1	1:2000	(C-111) sc417	Santa Cruz
B-Actin	1:5000	A1978	Merck
pTBK1/NAK (S172)	1:1000	(D52C2) 5483S	Cell Signalling
TBK1/NAK	1:1000	(D1B4) 3504S	Cell Signalling
pIRF3 (S396)	1:1000	(D6O1M) 29047S	Cell Signalling
IFNAR1 Monoclonal Antibody Functional Grade	1:100 (10 ug/mL)	(MAR1-5A3), Cat: 16-5945-85	Fisher Scientific
Mouse IgG1 kappa Isotype Control	1:50 (10 ug/mL)	(P3.6.2.8.1) Cat: 14-4714-85	Fisher Scientific

Data availability statement

The datasets presented in this study can be found in online repositories. The names of the repository/repositories and accession number(s) can be found below: https://www.ncbi.nlm.nih.gov/geo/, GSE68449 https://www.ebi.ac.uk/pride/archive/, PXD041375.

Ethics statement

The studies involving humans were approved by West Midlands Research Ethics Committee. The studies were conducted in accordance with the local legislation and institutional requirements. The participants provided their written informed consent to participate in this study. Ethical approval was not required for the study involving animals in accordance with the local legislation and institutional requirements because bone marrow was obtained from mice after Schedule 1 procedure, not requiring ethical approval.

Author contributions

AC secured funding for the study and wrote the manuscript. AC, JO, RH and JA contributed to conception and design of the study. JO, OB, SC, TT, KD, SL-R, JW and CM performed experiments and analyzed data. RM provided essential clinical samples. All authors contributed to the article and approved the submitted version.

Funding

This work was supported by a Program Grant (21802) and Research into Inflammatory Arthritis Centre Versus Arthritis (22072), both from Versus Arthritis (UK). OB was supported by an MB-PhD studentship from the Kennedy Trust (UK).

Conflict of interest

The authors declare that the research was conducted in the absence of any commercial or financial relationships that could be construed as a potential conflict of interest.

Publisher's note

Supplementary material

The Supplementary Material for this article can be found online at: https://www.frontiersin.org/articles/10.3389/fimmu.2023.1190261/full#supplementary-material

References

1. Hillier SG. Diamonds are forever: the cortisone legacy. *J Endocrinol* (2007) 195 (1):1–6. doi: 10.1677/JOE-07-0309

2. Schacke H, Docke WD, Asadullah K. Mechanisms involved in the side effects of glucocorticoids. *Pharmacol Ther* (2002) 96(1):23–43. doi: 10.1016/S0163-7258(02) 00297-8

3. Cain DW, Cidlowski JA. Immune regulation by glucocorticoids. *Nat Rev Immunol* (2017) 17(4):233–47. doi: 10.1038/nri.2017.1

4. De Bosscher K, Vanden Berghe W, Haegeman G. Mechanisms of anti-inflammatory action and of immunosuppression by glucocorticoids: negative interference of activated glucocorticoid receptor with transcription factors. *J Neuroimmunol* (2000) 109(1):16–22. doi: 10.1016/S0165-5728(00)00297-6

5. Clark AR, Belvisi MG. Maps and legends: the quest for dissociated ligands of the glucocorticoid receptor. *Pharmacol Ther* (2012) 134(1):54–67. doi: 10.1016/j.pharmthera.2011.12.004

6. Oh KS, Patel H, Gottschalk RA, Lee WS, Baek S, Fraser IDC, et al. Anti-inflammatory chromatinscape suggests alternative mechanisms of glucocorticoid receptor action. *Immunity* (2017) 47(2):298–309.e5. doi: 10.1016/j.immuni.2017.07.012

7. Lasa M, Abraham SM, Boucheron C, Saklatvala J, Clark AR. Dexamethasone causes sustained expression of mitogen-activated protein kinase (Mapk) phosphatase 1 and phosphatase-mediated inhibition of mapk P38. *Mol Cell Biol* (2002) 22(22):7802–11. doi: 10.1128/MCB.22.22.7802-7811.2002

8. Abraham SM, Lawrence T, Kleiman A, Warden P, Medghalchi M, Tuckermann J, et al. Antiinflammatory effects of dexamethasone are partly dependent on induction of dual specificity phosphatase 1. *J Exp Med* (2006) 203(8):1883–9. doi: 10.1084/jem.20060336

9. Bhattacharyya S, Brown DE, Brewer JA, Vogt SK, Muglia LJ. Macrophage glucocorticoid receptors regulate toll-like receptor 4-mediated inflammatory responses by selective inhibition of P38 map kinase. *Blood* (2007) 109(10):4313–9. doi: 10.1182/blood-2006-10-048215

10. Joanny E, Ding Q, Gong L, Kong P, Saklatvala J, Clark AR. Anti-inflammatory effects of selective glucocorticoid receptor modulators (Sgrms) are partially dependent on upregulation of dual specificity phosphatase 1 (Dusp1). *Br J Pharmacol* (2011) 165 (4b):1124–36. doi: 10.1111/j.1476-5381.2011.01574.x

11. Wang X, Nelin LD, Kuhlman JR, Meng X, Welty SE, Liu Y. The role of map kinase phosphatase-1 in the protective mechanism of dexamethasone against endotoxemia. *Life Sci* (2008) 83(19-20):671–80. doi: 10.1016/j.lfs.2008.09.003

12. Udalova IA, Mantovani A, Feldmann M. Macrophage heterogeneity in the context of rheumatoid arthritis. *Nat Rev Rheumatol* (2016) 12(8):472–85. doi: 10.1038/nrrheum.2016.91

13. Kurowska-Stolarska M, Alivernini S. Synovial tissue macrophages in joint homeostasis, rheumatoid arthritis and disease remission. *Nat Rev Rheumatol* (2022) 18(7):384–97. doi: 10.1038/s41584-022-00790-8

14. Merad M, Martin JC. Pathological inflammation in patients with covid-19: A key role for monocytes and macrophages. *Nat Rev Immunol* (2020) 20(6):355–62. doi: 10.1038/s41577-020-0331-4

15. Knoll R, Schultze JL, Schulte-Schrepping J. Monocytes and macrophages in Covid-19. *Front Immunol* (2021) 12:720109. doi: 10.3389/fimmu.2021.720109

16. Fenton C, Martin C, Jones R, Croft A, Campos J, Naylor AJ, et al. Local steroid activation is a critical mediator of the anti-inflammatory actions of therapeutic glucocorticoids. *Ann Rheum Dis* (2021) 80(2):250–60. doi: 10.1136/annrheumdis-2020-218493

17. Amit I, Garber M, Chevrier N, Leite AP, Donner Y, Eisenhaure T, et al. Unbiased reconstruction of a mammalian transcriptional network mediating pathogen responses. *Science* (2009) 326(5950):257–63. doi: 10.1126/science.1179050

18. Platanitis E, Decker T. Regulatory networks involving stats, irfs, and nfκb in inflammation. *Front Immunol* (2018) 9:2542. doi: 10.3389/fimmu.2018.02542

19. Hirotani T, Yamamoto M, Kumagai Y, Uematsu S, Kawase I, Takeuchi O, et al. Regulation of lipopolysaccharide-inducible genes by myd88 and toll/il-1 domain

containing adaptor inducing ifn-beta. *Biochem Biophys Res Commun* (2005) 328 (2):383–92. doi: 10.1016/j.bbrc.2004.12.184

20. Karaghiosoff M, Steinborn R, Kovarik P, Kriegshauser G, Baccarini M, Donabauer B, et al. Central role for type I interferons and tyk2 in lipopolysaccharide-induced endotoxin shock. *Nat Immunol* (2003) 4(5):471–7. doi: 10.1038/ni910

21. Sheikh F, Dickensheets H, Gamero AM, Vogel SN, Donnelly RP. An essential role for ifn-beta in the induction of ifn-stimulated gene expression by lps in macrophages. *J Leukoc Biol* (2014) 96(4):591–600. doi: 10.1189/jlb.2A0414-191R

22. Thomas KE, Galligan CL, Newman RD, Fish EN, Vogel SN. Contribution of interferon-beta to the murine macrophage response to the toll-like receptor 4 agonist, lipopolysaccharide. *J Biol Chem* (2006) 281(41):31119–30. doi: 10.1074/jbc.M604958200

23. MacMicking JD. Interferon-inducible effector mechanisms in cell-autonomous immunity. *Nat Rev Immunol* (2012) 12(5):367–82. doi: 10.1038/nri3210

24. Fitzgerald KA. The interferon inducible gene: viperin. *J Interferon Cytokine Res* (2011) 31(1):131–5. doi: 10.1089/jir.2010.0127

25. Weijtens O, Schoemaker RC, Cohen AF, Romijn FP, Lentjes EG, van Rooij J, et al. Dexamethasone concentration in vitreous and serum after oral administration. *Am J Ophthalmol* (1998) 125(5):673–9. doi: 10.1016/s0002-9394(98)00003-8

26. Raza S, Barnett MW, Barnett-Itzhaki Z, Amit I, Hume DA, Freeman TC. Analysis of the transcriptional networks underpinning the activation of murine macrophages by inflammatory mediators. *J Leukoc Biol* (2014) 96(2):167–83. doi: 10.1189/jlb.6HI0313-169R

27. Mills EL, Ryan DG, Prag HA, Dikovskaya D, Menon D, Zaslona Z, et al. Itaconate is an anti-inflammatory metabolite that activates nrf2 via alkylation of keap1. *Nature* (2018) 556(7699):113–7. doi: 10.1038/nature25986

28. Yamazaki S, Akira S, Sumimoto H. Glucocorticoid augments lipopolysaccharide-induced activation of the Iκbζ-dependent genes encoding the anti-microbial glycoproteins lipocalin 2 and pentraxin 3. *J Biochem* (2015) 157 (5):399–410. doi: 10.1093/jb/mvu086

29. Tong AJ, Liu X, Thomas BJ, Lissner MM, Baker MR, Senagolage MD, et al. A stringent systems approach uncovers gene-specific mechanisms regulating inflammation. *Cell* (2016) 165(1):165–79. doi: 10.1016/j.cell.2016.01.020

30. Ferreira AV, Netea MG, Domínguez-Andrés J. Itaconate as an immune modulator. *Aging (Albany NY)* (2019) 11(12):3898–9. doi: 10.18632/aging.102057

31. Martin-Sancho L, Lewinski MK, Pache L, Stoneham CA, Yin X, Becker ME, et al. Functional landscape of sars-cov-2 cellular restriction. *Mol Cell* (2021) 81(12):2656–68.e8. doi: 10.1016/j.molcel.2021.04.008

32. Rusinova I, Forster S, Yu S, Kannan A, Masse M, Cumming H, et al. Interferome V2.0: an updated database of annotated interferon-regulated genes. *Nucleic Acids Res* (2013) 41(Database issue):D1040–6. doi: 10.1093/nar/gks1215

33. Clayton SA, Daley KK, MacDonald L, Fernandez-Vizarra E, Bottegoni G, O'Neil JD, et al. Inflammation causes remodeling of mitochondrial cytochrome C oxidase mediated by the bifunctional gene C15orf48. *Sci Adv* (2021) 7(50):eabl5182. doi: 10.1126/sciadv.abl5182

34. Sorouri M, Chang T, Jesudhasan P, Pinkham C, Elde NC, Hancks DC. Signatures of host-pathogen evolutionary conflict reveal mistr-a conserved mitochondrial stress response network. *PloS Biol* (2020) 18(12):e3001045. doi: 10.1371/journal.pbio.3001045

35. Rafeld HL, Kolanus W, van Driel IR, Hartland EL. Interferon-induced gtpases orchestrate host cell-autonomous defence against bacterial pathogens. *Biochem Soc Trans* (2021) 49(3):1287–97. doi: 10.1042/bst20200900

36. Kim ET, Weitzman MD. Schlafens can put viruses to sleep. *Viruses* (2022) 14 (2):442. doi: 10.3390/v14020442

37. Malgras M, Garcia M, Jousselin C, Bodet C, Lévêque N. The antiviral activities of poly-adp-ribose polymerases. *Viruses* (2021) 13(4):582. doi: 10.3390/v13040582

38. Flammer JR, Dobrovolna J, Kennedy MA, Chinenov Y, Glass CK, Ivashkiv LB, et al. The type I interferon signaling pathway is a target for glucocorticoid inhibition. *Mol Cell Biol* (2010) 30(19):4564–74. doi: 10.1128/mcb.00146-10

39. McCoy CE, Carpenter S, Palsson-McDermott EM, Gearing LJ, O'Neill LA. Glucocorticoids inhibit irf3 phosphorylation in response to toll-like receptor-3 and -4 by targeting tbk1 activation. *J Biol Chem* (2008) 283(21):14277–85. doi: 10.1074/jbc.M709731200

40. McGuire VA, Rosner D, Ananieva O, Ross EA, Elcombe SE, Naqvi S, et al. Beta interferon production is regulated by P38 mitogen-activated protein kinase in macrophages via both msk1/2- and tristetraprolin-dependent pathways. *Mol Cell Biol* (2017) 37(1):e00454-16. doi: 10.1128/mcb.00454-16

41. Kirk SG, Murphy PR, Wang X, Cash CJ, Barley TJ, Bowman BA, et al. Knockout of mapk phosphatase-1 exaggerates type I ifn response during systemic escherichia coli infection. *J Immunol* (2021) 206(12):2966–79. doi: 10.4049/jimmunol.2001468

42. Bhattacharyya S, Zhao Y, Kay TW, Muglia LJ. Glucocorticoids target suppressor of cytokine signaling 1 (Socs1) and type 1 interferons to regulate toll-like receptor-induced stat1 activation. *Proc Natl Acad Sci USA* (2011) 108(23):9554–9. doi: 10.1073/pnas.1017296108

43. Platanitis E, Demiroz D, Schneller A, Fischer K, Capelle C, Hartl M, et al. A molecular switch from stat2-irf9 to isgf3 underlies interferon-induced gene transcription. *Nat Commun* (2019) 10(1):2921. doi: 10.1038/s41467-019-10970-y

44. Ballegeer M, Van Looveren K, Timmermans S, Eggermont M, Vandevyver S, Thery F, et al. Glucocorticoid receptor dimers control intestinal stat1 and tnf-induced inflammation in mice. *J Clin Invest* (2018) 128(8):3265–79. doi: 10.1172/jci96636

45. Reily MM, Pantoja C, Hu X, Chinenov Y, Rogatsky I. The grip1:Irf3 interaction as a target for glucocorticoid receptor-mediated immunosuppression. *EMBO J* (2006) 25(1):108–17. doi: 10.1038/sj.emboj.7600919

46. Li Y, Gong W, Li W, Liu P, Liu J, Jiang H, et al. The irg1-itaconate axis: A regulatory hub for immunity and metabolism in macrophages. *Int Rev Immunol* (2023) 42(5):364–78. doi: 10.1080/08830185.2022.2067153

47. King EM, Chivers JE, Rider CF, Minnich A, Giembycz MA, Newton R. Glucocorticoid repression of inflammatory gene expression shows differential responsiveness by transactivation- and transrepression-dependent mechanisms. *PloS One* (2013) 8(1):e53936. doi: 10.1371/journal.pone.0053936

48. Pinilla-Vera M, Xiong Z, Zhao Y, Zhao J, Donahoe MP, Barge S, et al. Full spectrum of lps activation in alveolar macrophages of healthy volunteers by whole transcriptomic profiling. *PloS One* (2016) 11(7):e0159329. doi: 10.1371/journal.pone.0159329

49. Trinchieri G. Type I interferon: friend or foe? *J Exp Med* (2010) 207(10):2053–63. doi: 10.1084/jem.20101664

50. Wu W, Metcalf JP. The role of type I ifns in influenza: antiviral superheroes or immunopathogenic villains? *J Innate Immun* (2020) 12(6):437–47. doi: 10.1159/000508379

51. McNab F, Mayer-Barber K, Sher A, Wack A, O'Garra A. Type I interferons in infectious disease. *Nat Rev Immunol* (2015) 15(2):87–103. doi: 10.1038/nri3787

52. Moreira-Teixeira L, Mayer-Barber K, Sher A, O'Garra A. Type I interferons in tuberculosis: foe and occasionally friend. *J Exp Med* (2018) 215(5):1273–85. doi: 10.1084/jem.20180325

53. Gottlieb M, Seagraves T, Gore SR. Do corticosteroids benefit patients with influenza pneumonia? *Ann Emerg Med* (2020) 75(1):100–1. doi: 10.1016/j.annemergmed.2019.06.021

54. Lansbury L, Rodrigo C, Leonardi-Bee J, Nguyen-Van-Tam J, Lim WS. Corticosteroids as adjunctive therapy in the treatment of influenza. *Cochrane Database Syst Rev* (2019) 2(2):CD010406. doi: 10.1002/14651858.CD010406.pub3

55. Giannella M, Alonso M, Garcia de Viedma D, Lopez Roa P, Catalán P, Padilla B, et al. Prolonged viral shedding in pandemic influenza a(H1n1): clinical significance and viral load analysis in hospitalized patients. *Clin Microbiol Infect* (2011) 17(8):1160–5. doi: 10.1111/j.1469-0691.2010.03399.x

56. Marcellini A, Swieboda D, Guedán A, Farrow SN, Casolari P, Contoli M, et al. Glucocorticoids impair type I ifn signalling and enhance rhinovirus replication. *Eur J Pharmacol* (2021) 893:173839. doi: 10.1016/j.ejphar.2020.173839

57. Thomas BJ, Porritt RA, Hertzog PJ, Bardin PG, Tate MD. Glucocorticosteroids enhance replication of respiratory viruses: effect of adjuvant interferon. *Sci Rep* (2014) 4:7176. doi: 10.1038/srep07176

58. Zhang Q, Bastard P, Cobat A, Casanova JL. Human genetic and immunological determinants of critical Covid-19 pneumonia. *Nature* (2022) 603(7902):587–98. doi: 10.1038/s41586-022-04447-0

59. Zhu J, Chiang C, Gack MU. Viral evasion of the interferon response at a glance. *J Cell Sci* (2023) 136(12):jcs260682. doi: 10.1242/jcs.260682

60. Minkoff JM, tenOever B. Innate immune evasion strategies of Sars-Cov-2. *Nat Rev Microbiol* (2023) 21(3):178–94. doi: 10.1038/s41579-022-00839-1

61. Schulte-Schrepping J, Reusch N, Paclik D, Baßler K, Schlickeiser S, Zhang B, et al. Severe Covid-19 is marked by a dysregulated myeloid cell compartment. *Cell* (2020) 182(6):1419–40.e23. doi: 10.1016/j.cell.2020.08.001

62. Singh DK, Aladyeva E, Das S, Singh B, Esaulova E, Swain A, et al. Myeloid cell interferon responses correlate with clearance of Sars-Cov-2. *Nat Commun* (2022) 13 (1):679. doi: 10.1038/s41467-022-28315-7

63. Dong Z, Yan Q, Cao W, Liu Z, Wang X. Identification of key molecules in Covid-19 patients significantly correlated with clinical outcomes by analyzing transcriptomic data. *Front Immunol* (2022) 13:930866. doi: 10.3389/fimmu.2022.930866

64. Ramasamy S, Subbian S. Critical determinants of cytokine storm and type I interferon response in Covid-19 pathogenesis. *Clin Microbiol Rev* (2021) 34(3):e00299-20. doi: 10.1128/cmr.00299-20

65. Amati F, Tonutti A, Huston J, Dela Cruz CS. Glucocorticoid therapy in Covid-19. *Semin Respir Crit Care Med* (2023) 44(1):100–17. doi: 10.1055/s-0042-1759778

66. Kino T, Burd I, Segars JH. Dexamethasone for severe Covid-19: how does it work at cellular and molecular levels? *Int J Mol Sci* (2021) 22(13):6764. doi: 10.3390/ijms22136764

67. Kalinina O, Golovkin A, Zaikova E, Aquino A, Bezrukikh V, Melnik O, et al. Cytokine storm signature in patients with moderate and severe Covid-19. *Int J Mol Sci* (2022) 23(16):8879. doi: 10.3390/ijms23168879

68. Angioni R, Sánchez-Rodríguez R, Munari F, Bertoldi N, Arcidiacono D, Cavinato S, et al. Age-severity matched cytokine profiling reveals specific signatures in Covid-19 patients. *Cell Death Dis* (2020) 11(11):957. doi: 10.1038/s41419-020-03151-z

69. Ozger HS, Karakus R, Kuscu EN, Bagriacik UE, Oruklu N, Yaman M, et al. Serial measurement of cytokines strongly predict Covid-19 outcome. *PloS One* (2021) 16(12): e0260623. doi: 10.1371/journal.pone.0260623

70. Vogel F, Reincke M. Endocrine risk factors for covid-19: endogenous and exogenous glucocorticoid excess. *Rev Endocr Metab Disord* (2022) 23(2):233–50. doi: 10.1007/s11154-021-09670-0

71. Hasseli R, Mueller-Ladner U, Hoyer BF, Krause A, Lorenz HM, Pfeil A, et al. Older age, comorbidity, glucocorticoid use and disease activity are risk factors for Covid-19 hospitalisation in patients with inflammatory rheumatic and musculoskeletal diseases. *RMD Open* (2021) 7(1):e001464. doi: 10.1136/rmdopen-2020-001464

72. Horby P, Lim WS, Emberson JR, Mafham M, Bell JL, Linsell L, et al. Dexamethasone in hospitalized patients with Covid-19. *N Engl J Med* (2021) 384 (8):693–704. doi: 10.1056/NEJMoa2021436

73. Qiao W, Meng L, Zhang Y, Li D, Chen J, Wang J, et al. Safety and efficacy of glucocorticoids in the treatment of Covid-19: A meta-analysis of randomized control trials. *Expert Rev Respir Med* (2023) 17(1):81–96. doi: 10.1080/17476348.2023.2177155

74. Tang X, Feng YM, Ni JX, Zhang JY, Liu LM, Hu K, et al. Early use of corticosteroid may prolong Sars-Cov-2 shedding in non-intensive care unit patients with Covid-19 pneumonia: A multicenter, single-blind, randomized control trial. *Respiration* (2021) 100(2):116–26. doi: 10.1159/000512063

75. Yang DM, Geng TT, Harrison AG, Wang PH. Differential roles of rig-I like receptors in Sars-Cov-2 infection. *Mil Med Res* (2021) 8(1):49. doi: 10.1186/s40779-021-00340-5

76. Oh SJ, Shin OS. Sars-Cov-2-mediated evasion strategies for antiviral interferon pathways. *J Microbiol* (2022) 60(3):290–9. doi: 10.1007/s12275-022-1525-1

77. Cain DW, Cidlowski JA. After 62 years of regulating immunity, dexamethasone meets Covid-19. *Nat Rev Immunol* (2020) 20(10):587–8. doi: 10.1038/s41577-020-00421-x

78. Amati F, Dela Cruz CS. One size does not fit all: moving towards a personalized approach for steroids in Covid-19. *Chest* (2021) 159(5):1693–5. doi: 10.1016/j.chest.2021.01.043

79. Sinha P, Furfaro D, Cummings MJ, Abrams D, Delucchi K, Maddali MV, et al. Latent class analysis reveals Covid-19-related acute respiratory distress syndrome subgroups with differential responses to corticosteroids. *Am J Respir Crit Care Med* (2021) 204(11):1274–85. doi: 10.1164/rccm.202105-1302OC

80. Davis BK. Derivation of macrophages from mouse bone marrow. *Methods Mol Biol* (2019) 1960:41–55. doi: 10.1007/978-1-4939-9167-9_3

81. Mahida RY, Lax S, Bassford CR, Scott A, Parekh D, Hardy RS, et al. Impaired alveolar macrophage 11β-hydroxysteroid dehydrogenase type 1 reductase activity contributes to increased pulmonary inflammation and mortality in sepsis-related ARDS. *Front Immunol* (2023) 14:1159831. doi: 10.3389/fimmu.2023.1159831

82. Smallie T, Ross EA, Ammit AJ, Cunliffe HE, Tang T, Rosner DR, et al. Dual-specificity phosphatase 1 and tristetraprolin cooperate to regulate macrophage responses to lipopolysaccharide. *J Immunol* (2015) 195(1):277–88. doi: 10.4049/jimmunol.1402830

83. Mi H, Ebert D, Muruganujan A, Mills C, Albou LP, Mushayamaha T, et al. Panther version 16: A revised family classification, tree-based classification tool, enhancer regions and extensive api. *Nucleic Acids Res* (2021) 49(D1):D394–403. doi: 10.1093/nar/gkaa1106

84. Supek F, Bošnjak M, Škunca N, Šmuc T. Revigo summarizes and visualizes long lists of gene ontology terms. *PloS One* (2011) 6(7):e21800. doi: 10.1371/journal.pone.0021800

85. Subramanian A, Tamayo P, Mootha VK, Mukherjee S, Ebert BL, Gillette MA, et al. Gene set enrichment analysis: A knowledge-based approach for interpreting genome-wide expression profiles. *Proc Natl Acad Sci USA* (2005) 102(43):15545–50. doi: 10.1073/pnas.0506580102

86. Baker CP, Phair IR, Brenes AJ, Atrih A, Ryan DG, Bruderer R, et al. Dia label-free proteomic analysis of murine bone-marrow-derived macrophages. *STAR Protoc* (2022) 3(4):101725. doi: 10.1016/j.xpro.2022.101725

87. Tyanova S, Temu T, Sinitcyn P, Carlson A, Hein MY, Geiger T, et al. The perseus computational platform for comprehensive analysis of (Prote)Omics data. *Nat Methods* (2016) 13(9):731–40. doi: 10.1038/nmeth.3901

Frontiers in Immunology

Explores novel approaches and diagnoses to treat immune disorders.

The official journal of the International Union of Immunological Societies (IUIS) and the most cited in its field, leading the way for research across basic, translational and clinical immunology.

Discover the latest Research Topics

See more →

Frontiers

Avenue du Tribunal-Fédéral 34
1005 Lausanne, Switzerland
frontiersin.org

Contact us

+41 (0)21 510 17 00
frontiersin.org/about/contact